6th Asian Thermal Spray Conference

November 24-26, 2014, Hyderabad, India

PROCEEDINGS

atsc 2014
6th Asian Thermal Spray Conference

Organized by

ए आर सी आई
ARCI

International Advanced Research Centre for Powder Metallurgy & New Materials (ARCI)

In association with

ATSS
Asian Thermal Spray Society

Supported by

SAHTSE
Society for Advancement of Heat Treatment and Surface Engineering

LEADERS IN THERMAL SPRAY COATING AND SURFACE MODIFICATION TECHNOLOGIES

SAI SURFACE COATING TECHNOLOGIES

(AN ISO 9001:2008 Certified Company)

SURFACE MODIFICATION TECHNOLOGIES AVAILABLE

THERMAL SPRAY TECHNOLOGIES

DETONATION SPRAY PROCESS

HIGH VELOCITY OXY-FUEL (HVOF) PROCESS

PLASMA SPRAY PROCESS

WIRE ARC SPRAY PROCESS

FLAME SPRAY PROCESS

METALLIZING SPRAY PROCESS

SPRAY AND FUSE

HARD FACING

STELLITING BY TIG/PTA

COLOMONY BY TIG/PTA

NiCr BY TIG

TREATMENTS

PLASMA ION NITRIDING

HEAT TREATMENT

(CHAMBER/BOGIE/LOCALISED)

OTHER FACILITIES

FULLFLEDGE HEAVY & LIGHT DUTY MACHINE SHOP

CNC MACHINE SHOP

CHARACTERIZATION LABORATORY

(ALL COATING EQUIPMENTS EQUIPPED WITH ROBOTIC / PLC BASED MANIPULATORS)

TYPICAL APPLICATION AREAS :

- Aero-engine components, Gas Turbine Components, Nuclear, thermal, Hydel Turbine components, Rollers for Material Handling systems, Paper, Textile, Glass machinery components, Valves & Pistons, Pump sleeves etc., Compressor shafts, Automobile components, Wire and Cable Industry Components etc.

COATINGS UNDERTAKEN :

- Alumnia, Alumina-Titania, Chrome Oxide, Yitria Stabilized Zirconia, Abradable Coatings, WC, WC-Co, WC-CoCr., Cr3C2-NiCr,Stelliting, Ni Alloy among few.

Plot no: 17/A, Phase-III(Opp Export Zone)Pashamylaram, Patancheru(M), Medak Dist-502 307, (A.P). India
Tele /Fax : +91 – 8455- 223645 / 223646. E-mail: info@ssct.in

www.ssct.in

Proceedings

6th Asian Thermal Spray Conference

Organized by

ए आर सी आई
ARCI

INTERNATIONAL ADVANCED RESEARCH CENTRE
FOR POWDER METALLURGY & NEW MATERIALS (ARCI)

In association with

ATSS
Asian Thermal Spray Society

Supported by

SAHTSE
Society for Advancement of Heat Treatment and Surface Engineering

November 24-26, 2014
Hyderabad, India

CONTENTS

About ATSC

The Asian Thermal Spray Conference (ATSC), following concerted efforts by all segments of the thermal spray community in the member countries, has emerged as a flagship event in the Asia-Pacific region. The major objective of the event is to provide an attractive forum for all stakeholders (researchers from industry, R&D institutions and academia; thermal spray practitioners from service providers; capital installations; equipment and feedstock manufacturers as well as OEMs and users) from across the region to network in order to foster a fruitful interaction during and after the conference. The event is also expected to provide an ideal platform for researchers and engineers to familiarize themselves with recent advances in this rapidly evolving, yet industrially well-entrenched, broad-spectrum technology as well as for various companies to exhibit relevant products to a dedicated audience. The past editions of the event organized in Japan, Korea, Singapore and China were extremely successful in realizing the above objectives. The 6th edition of ATSC, to be held in India for the first time, will be organized in the city of Hyderabad during November 24-26, 2014.

www.atsc2014.in

About ATSS

The Asian Thermal Spray Society (ATSS) is a regional society with a mission to promote growth of research & development efforts and adoption of industrial applications of thermal spray technology in Asian countries. Through the ATSC series, ATSS has provided a forum to regularly share the latest advancements in the field of thermal spray technology.

www.asiantss.com

About ARCI

The International Advanced Research Centre for Powder Metallurgy & New Materials (ARCI) is an R&D institution of Department of Science and Technology (DST), Govt. of India specifically set-up with a mission to develop unique, novel and techno-commercially viable technologies in the area of advanced materials and subsequently transfer them to Indian industries. “Translating Research to Technology” has been ARCI’s motto and the institute has set for itself the task of striving to bridge the gap between conventional research institutes and laboratories and the high-technology industries.

A prominent thrust area at ARCI is surface engineering. ARCI has been playing a leading role in the development and demonstration of state-of-the-art surface engineering technologies of industrial relevance and is now recognized globally as a centre of excellence in the field. The Centre’s foremost accomplishments have included the successful transfer and implementation of Detonation Spray Coating (DSC), Micro-Arc Oxidation (MAO) and Electro-Spark Coatings (ESC) technologies. Signifcant progress has been made in taking the Cold Spray Coating (CSC) process closer to commercialization and interesting developments have also been made using the Solution Precursor Plasma Spray (SPPS) facility established recently. Electron Beam Physical Vapour Deposition (EBPVD), Cylindrical Rotating Cathodic Arc PVD (CAPVD) and Pulse Electrodeposition (PED) systems at the Centre have been utilized to initiate major programmes in the areas of thermal barrier coatings and nano composite wear resistant coatings, respectively.

www.arci.res.in

OUR SPONSORS

PLATINUM SPONSOR	MEC
OTHER SPONSORS	SSC sai surface coating technologies GE PRAXAIR SURFACE TECHNOLOGIES IPM A name you can trust
SUPPORTED BY	SAHTSE Society for Advancement of Heat Treatment and Surface Engineering iNSERB DIA BRNS DRDO CSIR

PROGRAM AT A GLANCE

Day / Time	08.00-09.00	09.00-09.15	09.15-09.30	09.30-10.30	10.30-11.15	11.15-13.00	13.00-14.00	14.00-15.00	15.00-15.45	15.45-17.30	17.30-19.00	19.00
November 24 Monday	Registration		Inaugural Function	Plenary Session-1 Seiji Kuroda Sanjay Sampath	Exhibition Inauguration + Tea Break	Parallel Technical Sessions • TBC-1 • Tribology • Cold Spray	Lunch	Plenary Session-2 William Clyne Christian Moreau	Exhibition/ Poster + Tea Break	Parallel Technical Sessions • TBC-2 • Erosion Resistant Coatings • Processing-Structure-Property Correlation	Exhibition/Poster and Networking	Dinner
November 25 Tuesday				Plenary Session-3 KA Khor Armelle Vardelle	Exhibition/ Poster + Tea Break	Parallel Technical Sessions • Processing of Novel Feedstock • Applications-1 • Splat formation studies		Plenary Session-4 Changhee Lee Richard Schmid	Exhibition & Tea Break	Parallel Technical Sessions • Hot Corrosion • Emerging Techniques • Applications-2		
November 26 Wednesday		Parallel Technical Sessions • Solution based Processes • Characterisation • Coatings for Energy Applications			Exhibition & Tea Break	Plenary Session-5 Chang-Jiu Li G Sundararajan Christopher Berndt	Wrap-up					

DETAILED TECHNICAL PROGRAMME

24th November 2014

08:00–09.15		**Registration**	
09:15–09.30		**Inaugural Function** ***Welcome*** **G Sundararajan – Chairman ATSC-2014** *ARCI, Hyderabad, India* ***Introduction to ATSC*** **M Fukumoto** *Toyohashi University, Japan* ***Opening Remarks*** **S V Joshi – Convenor ATSC-2014** *ARCI, Hyderabad, India*	**Shamshabad Ballroom**
	Plenary Session-1		**Shamshabad Ballroom**
09:30–10:00	**Seiji Kuroda** *National Institute of Materials Science, Japan*	Warm Spray Technology to Fill the Gap Between HVOF and Cold Spray	
10:00–10:30	**Sanjay Sampath** *Stony Brook University, USA*	Transforming Thermal Spray Technology through Interdisciplinary Research: From Protective Coatings to Functional Multilayers	
10:30–11.15		**Inauguration of Exhibition & Tea Break**	**Hyderabad Ballroom**
Parallel Technical Sessions 11:15-13:00		**Thermal Barrier Coatings-1**	**Shamshabad Ballroom I**
		Tribology	**Shamshabad Ballroom II**
		Cold Spray	**Hyderabad Ballroom III**
Thermal Barrier Coatings-1			**Shamshabad Ballroom I**
11:15-11.30	Processing, Microstructure and Thermo-physical Properties of Thermal Barrier Coatings Produced by Plasma Spray Physical Vapor Deposition Hongbo Guo, Lihua Gao, **Liangliang Wei,** Shengkai Gong, Huibin Xu *School of Materials Science and Engineering, Beihang University, China*		
11.30-11.45	Phase Retention of YSZ in Plasma Sprayed YSZ-CNT Reinforced Al_2O_3 Matrix Composites for Thermal Barrier Coating **Kantesh Balani,** Ariharan S, N. Balaji, S.T. Aruna *Indian Institute of Technology-Kanpur, Kanpur, India*		
11.45-12.00	Toughness Evolution of Zirconia Based Thermal Barrier Materials Upon High Temperature Exposure Archana Loganathan**, Ashutosh S. Gandhi** *Department of Metallurgical and Materials Engineering, Indian Institute of Technology- Madras, Chennai, India*		
12.00-12.15	Study on New Materials for High Temperature Gas Turbine Applications **Ramandeep Mandia,** B.K. Pant, P. Joshi, K.Vidyasagar *BHEL Corporate R&D, Hyderabad, India*		
12.15-12.30	Synthesis and Characterization of 25% Praseodymium Oxide Stabilised Zirconia Thermal Barrier Coating **R Rajeshwari,** Parvathi Ramasamy, R.Rajendran, L.Chandrasagar *Dr. Ambedkar Institute of Technology, Bangalore, India*		
12.30-12.45	Studies on the Mechanical and Oxidation Resistance Properties of CoNiCrAlY/Al_2O_3/YSZ Compositionally Graded Thermal Barrier Coating developed by Air Plasma Spraying **Subhasisa Nath**, Indranil Manna, Jyotsna Dutta Majumdar *Department of Metallurgical and Materials Engineering, Indian Institute of Technology, Kharagpur, India*		
12.45-13.00	Thermal Barrier Coating on Al-alloy 2024 for Protection Under Isothermal and Cyclic Heating Conditions **Dipak Kumar**, K.N.Pandey, Dipak Kumar Das *Department of Mechanical Engineering, Motilal Nehru National Institute of Technology, Allahabad, India*		

Tribology		Shamshabad Ballroom II
11:15-11.40	**Invited Talk** Driving Microstructural Optimization of Composite Coatings for Wear and High Temperature Applications **K. Anand**, Eklavya Calla, S.Hariharan, Prajina Bhattacharya, Paul Mathew, CH Sathisha, Biju Dasan, Kanchan Kumari, Dheepa Srinivasan, Tamara Muth, Dennis Gray, Todd Curtis *GE India Technology Centre, Power & Water – Materials, Bangalore, India*	
11.40-11.55	Deformation and Fracture Behavior of Chromium Carbide-nickel Chromium Wear Resistant Coating **S.S.K Balam**, M.Tamilselvi, J Chitra, V.U.Bagade, R.Rajendran *Gas Turbine Research Establishment, Bangalore, India*	
11.55-12.10	High Temperature Tribological Behaviour of Thermally Sprayed Wear Resistant Coatings **Vivek Arya**, Ramandeep Mandia, K. Vidyasagar *Surface Coatings and Treatment Laboratory, BHEL Corporate R&D Division, Hyderabad, India*	
12.10-12.25	Microstructure and Dry Sliding Wear Behavior of Atmospheric Plasma Sprayed Nanostrcutured 2024Al-15 wt.% SiC_p Composite Coatings Satish Tailor, R.M.Mohanty, **P.R. Soni** *Department of Metallurgical and Materials Engineering, MNIT Jaipur, India*	
12.25-12.40	Influence of Al_2O_3 Addition on the Wear and Corrosion Behavior of HVOF Sprayed WC-Co Coatings **R.P.S Chakradhar**, Meenu Srivastava, K Venkateswarlu *Surface Engineering Division, CSIR-National Aerospace Laboratories, Bangalore, India*	
12.40-12.55	Comparison of the Sliding Wear Behavior of Diffusion Treated M-50 NiL and Thermal Sprayed Coating on M-50 NiL Steel **Deepjyoti A. Shelwatkar**, S.V.Subba Rao, Manish Roy *Regional Center for Military Airworthiness, Kanchanbagh, Hyderabad, India*	
12.55-13.10	The Abrading Behaviors of Several Al-based Abradable Coatings Yueguang Yu**, Jianming Liu**, Jie Shen, Deming Zhang, Qiuyuan Lu,Tong Liu *Beijing General Institute of Mining and Metallurgy, China*	
Cold Spray		**Hyderabad Ballroom III**
11:15-11.40	**Invited Talk** Interface Behavior of Particles upon Impacting during Cold Spraying **Wen-Ya Li,** Kang Yang, Dongdong Zhang *Shaanxi Key Laboratory of Friction Welding Technologies, Northwestern Polytechnical University, China*	
11.40-11.55	Importance of Surface Activation for Cold Sprayed Particle Deposition Kazuhiro Ogawa, **Yuji Ichikawa**, Kentaro Hashimoto, Takehito Shimatsu *Tohoku University, Japan*	
11.55-12.10	Characterization of Cold Sprayed IN625 and NiCr Coatings **Dheepa Srinivasan,** Vighnesh Chandrasekhar, Y C Lau, Eklavya Calla *GE Power and Water, GE India Technology Center, Bangalore, India*	
12.10-12.25	Formation of Expanded Austenite on Cold-Sprayed AISI 316L Coating by Low-temperature Plasma Treatment **Shinichiro Adachi,** Nobuhiro Ueda *Technology Research Institute of Osaka Prefecture,Osaka, Japan*	
12.25-12.40	Effect of Oxyacetylene Flame Remelting on Wear Behavior of Supersonic Air-Plasma Sprayed NiCrBSi/h-BN Composite Coatings **Zhang Nannan,** Jiang Di, Zhang Guangwei, Li Deyuan, Zhang Yue *Department of Materials Science and Engineering, Shenyang University of Technology, Shenyang, China*	
12.40-12.55	Effect of Heat Treatment on the Mechanical Properties and Corrosion Performance of Cold Sprayed Tantalum Coating **S. Kumar**, V.Vidyasagar, A.Jyothirmayi, S.V.Joshi *International Advanced Research Centre for Powder Metallurgy and New Materials, Hyderabad, India*	
13:00–14:00	**Lunch**	
	Plenary Session-2	**Shamshabad Ballroom**
14:00–14:30	**William Clyne** *Cambridge University, UK*	Deposition of Volcanic Ash within Gas Turbine Aeroengines and Effect on the Thermo-mechanical Stability of Thermal Barrier Coatings
14:30–15:00	**Christian Moreau** *Concordia University,Canada*	Suspension Thermal Spraying: Opportunities and Challenges of an Emerging Coating Technology
15:00–15.45	**Exhibition/Poster & Tea Break**	

Parallel Technical Sessions 15:45-17.30	Thermal Barrier Coatings-2	Shamshabad Ballroom I
	Erosion Resistance Coatings	Shamshabad Ballroom II
	Processing-Structure-Property Correlation	Hyderabad Ballroom III

Thermal Barrier Coatings-2		Shamshabad Ballroom I
15:45-16.10	**Invited Talk** Suspension Plasma Sprayed Thermal Barrier Coatings **Per Nylen** *University West, Sweden*	
16.10-16.25	Study on the Chemical Compatibility of the Coating Interface Between Ce Modified $La_2Zr_2O_7$ and YSZ Qiong Wu, Xin Zhang, Haoran Peng, Xiaojuan Ji, Xianjing Ren, Yueguang Yu, **Jianming Liu** *Beijing General Research Institute of Mining and Metallurgy, Beijing, China*	
16.25-16.40	Anisotropy of Thermal Conductivity of Plasma Sprayed Thermal Barrier Coatings **Satoru Takahashi**, Yoshio Kobayashi, Megumi Akoshima *Department of Mechanical Engineering, Tokyo Metropolitan University, Hachioji, Japan*	
16.40-16.55	Spray Dried Yttria Stabilized Zirconia Powders from Fused and Crushed Powders and Evaluation of their Coatings Property for Thermal Barrier Coating Applications S.T.Aruna, **N. Balaji,** Prathap Kumar, Jinov J Kachappilly *Surface Engineering Division, Council of Scientific and Industrial Research-National Aerospace Laboratories, Bangalore, India*	
16.55-17.10	Deposition Technique using Atmospheric Plasma Spray and Performance of a Composite Thermal Barrier Coating **M. Sai Krishna Rao**, Vijay K Varma and B Venkataraman *Regional Centre for Military Airworthiness (Materials), CEMILAC, DRDO, Kanchanbagh, Hyderabad, India*	
17.10-17.25	Study of the Interdiffusion Behavior between NiCoCrAlYTa Coating and GH536 Superalloy Guo Donghai, Zhang Shuting, Li Jin, **Jianming Liu** *Beijing General Research Institute of Mining & Metallurgy, China*	
17.25-17.40	Metallurgical Evaluation of Thermal Spray Coatings used in Gas Turbines Hariharan S, Dheepa Srinivasan, **Murali Dontu**, Vighnesh Chandrasekhar *Ford Technologies Services India, Chennai, India*	

Erosion Resistance Coatings		Shamshabad Ballroom II
15:45-16.10	**Invited Talk** Cavitation Erosion Resistance Characteristics of HVOF and HVAF based 86WC-10Co-4Cr Hydro Turbine Coatings **M. Kamaraj** *Indian Institute of Technology Madras, India*	
16.10-16.25	Effect of Substrate on Erosion and Adhesion Behaviour of Detonation Gun Deposited Cr_3C_2-NiCr Coating **J.K.N. Murthy,** B. Venkataraman *Defence Metallurgical Research Laboratory, Hyderabad, India*	
16.25-16.40	Coatings for Protection Against Silt Erosion in Hydro Turbines **Rahul Sood** *Industrial Processors and Metallizers (P) Ltd., Delhi, India*	
16.40-16.55	Erosion Behaviour of Ni-based Alloys at High Temperatures **Manish Kumar,** S. Ashok, Krishna Praveen J, BH. Channabasappa *Hoganas India Private Limited, Pune, India*	
16.55-17.10	Air Jet Erosion of HVOF Sprayed Inconel 718-Titania Composite Coatings **C.S.Ramesh,** Sekhar N, Harsha R Gudi *PES University of Technology,Bangalore, India*	
17.10-17.25	Effect of Basalt Addition on Microstructural, Mechanical and Erosion Properties of NiCrSiB HVOF Coatings **A.Vallimanalan,** S.P.Kumaresh Babu, S.Natarajan, M.Kumarasamy, P.Veerabalu *National Institute of Technology, Tiruchirapalli, India*	
17.25-17.40	Solid Particle Erosion Behavior of Plasma Sprayed LaYSZ Nanocomposite Coatings S. Mantry, **B.B.Jha**, R. K Sahoo *CSIR-Institute of Minerals & Materials Technology, Bhubaneswar, India*	

Processing-Structure-Property Correlation		Hyderabad Ballroom III
15:45–16.00	Microstructure and Properties of HVOF Sprayed Nanostructured and Conventional WC-12Co Coatings **Wojciech Żórawski,** Merard Makrenek *Faculty of Mechatronics and Machine Building, Kielce University of Technology, Poland*	
16.00-16.15	Microstructural Characterization of Thermal Sprayed High Entropy Alloy Coatings **Ameey Anupam,** S. Praveen, R.S. Kottada, B.S. Murty, Andrew Siao Ming Ang, Chris Berndt *Indian Institute of Technology Madras, Chennai, India*	

16.15-16.30	Assessment of Microstructure and Mechanical Properties of HVOF Sprayed WC-Co-Cr Coatings **K. Murugan,** A.Ragupathy, V.Balasubramanian, K.Sridhar *Department of Mechanical Engineering, Annamalai University, Annamalai Nagar, India*
16.30-16.45	A Study on HVOF Process Parameter Optimization for Erosion Resistant WC-CoCr Nanostructured Coating **Lalit Thakur,** Navneet Arora *Mechanical Engineering Department, National Institute of Technology Kurukshetra, Kurukshetra, India*
16.45-17.00	Influence of Pulse Frequency on WC-Co and Al_2O_3 Coating Properties Obtained by Detonation Spray Coating Technique **D.Sen,** S.Nirmala, D.Srinivasa Rao *International Advanced Research Centre for Powder Metallurgy and New Materials, Hyderabad, India*
17.00-17.15	Wear and Oxidation Behaviour of CoNiCrAlY Coatings Sprayed with HVOF and CGDS **W.S.Rathod**, A.S.Khanna *VJTI, Mechanical Engineering Department, Mumbai, India*
17.15-17.30	Actual vs Measured Porosity in Thermally Sprayed TBC Coatings **Neha Kondekar,** Dheepa Srinivasan, Hariharan S *Department of Materials Engineering, Indian Institute of Science, Bangalore, India*
17.30–19.00	**Exhibition/Poster & Networking**
19:00	**Banquet Dinner**

25th November 2014

	Plenary Session-3	**Shamshabad Ballroom**
09:30–10:00	**KA Khor** *Research Support Office and Bibliometrics Analysis, Nanyang Technological University, Singapore*	Global Research Trends in Thermal Sprayed Coatings Technology Analysed with Bibliometrics Tools
10:00–10:30	**Armelle Vardelle** *University of Limoges, France*	Plasma Spray Torch Modeling: Issues and Practical Considerations
10:30–11.15	**Exhibition/Poster & Tea Break**	
Parallel Technical Sessions 11:15-13:00	**Processing Using Novel Feedstock**	**Shamshabad Ballroom I**
	Applications-1	**Shamshabad Ballroom II**
	Splat Formation Studies	**Hyderabad Ballroom III**

Processing Using Novel Feedstock	**Shamshabad Ballroom I**
11:15-11.30	Thermal Conductivity of the Atmospheric Aluminum Nitride Coatings *Mohammed Shahien,* ***Motohiro Yamada,*** Masahiro Fukumoto, Kazumi Egota, Kenji Okamoto *Department of Mechanical Engineering, Toyohashi University of Technology, Japan*
11.30- 11.45	Thermally Sprayed Fly-Ash Coatings on Mild Steel Substrates N.V.V.V.R. Rajesh, B. Pravallika, N.S. Karthiselva, K.Vasanthakumar, Debalina Bhattacharjee, M. Kamaraj, **Srinivasa Rao Bakshi** *Indian Institute of Technology Madras, India*
11.45-12.00	Hydroxyapatite/Graphene-nanosheet Composite Coatings Deposited by Vacuum Cold Spraying for Biomedical Applications **Yi Liu,** Jing Huang, Hua Li *Ningbo Institute of Materials Technology and Engineering, Chinese Academy of Sciences, Ningbo, China*
12.00-12.15	Effect of Processing Time on the Preparation of Natural Bovine Hydroxyapatite by using Transferred Arc Plasma Torch **C.P.Yoganand,** K.M. Paraskevopoulos, Dongfeng Xue *Department of Physics, Coimbatore Institute of Technology, Coimbatore, India*
12.15-12.30	Co-spraying of Lanthanum Phosphate-alumina: Coating Composition and Properties **Vandana Chaturvedi,** P V Ananthapadmanabhan, Y. Chakravarthy, A.Pragatheeswaran *Laser and Plasma Technology Division, Bhabha Atomic Research Centre, Mumbai, India*
12.30-12.45	Influence of Particle State Diagnostics on Microstructure of Plasma Sprayed Nanocomposite LaCeYSZ Coatings S. Mantry**, B. B. Jha**, R.Sahoo *CSIR-Institute of Minerals & Materials Technology, Bhubaneswar, India*
12.45-13.00	Development of a Novel Synthesizer for Antimicrobial Thermal Spray Coating for Food Processing Machineries/Equipments **Ramakrishna A** Defence Food Research Laboratory, Mysore, India

Applications-1		Shamshabad Ballroom II
11:15-11.40	**Invited Talk** Fabrication and Repair of Components by Cold Spray Process **J.Karthikeyan** *ASB Industries, USA*	
11.40-11.55	Development of Porous Plasma Sprayed Molybdenum Carbide-based Anode Layers with Various Metal Oxide Precursors for SOFC **Nadimul H Faisal,** Rehan Ahmed, Sai P Katikaneni, Stamatios Souentie, Mathues F A Goosen *School of Engineering, Robert Gordon University, Aberdeen, UK*	
11.55-12.10	Recent Development in HVOF System for ID Coating **Ankur Modi**, S C Modi, Rohit Upadhyaya *Metallizing Equipment Company Pvt. Ltd, Jodhpur, India*	
12.10-12.25	Thermal Spray Coatings for Blast Furnace Tuyere **Abhishek Pathak,** Debadutta Prusty, G. Sivakumar, J. Shalini, M. Dutta *Tata Steel Limited, Jamshedpur*	
12.25-12.40	An Approach for Selection and Validation of a Thermal Spray Coating for Repair of an Aero-Engine Component **P S Ashwin Kumar,** G Nithiyanantham, V Sambasiva Rao *Cyient Limited, Hyderabad, India*	
12.40-12.55	Thermal Spray Coatings and Laser Cladding for Oil & Gas and Steel Industry **Michael Breitsameter** *FW Gartner Thermal Spraying, Surface Technologies, USA*	
12.55-13.10	Effect of Colonization of Escherichia Coli on the Corrosion Behavior of Thermal Sprayed Al-based Coatings in Artificial Seawater **Leila Abdoli,** Yaling He, Hua Li *Key Laboratory of Marine Materials and Related Technologies, Chinese Academy of Sciences, Ningbo, China*	
Splat Formation Studies		**Hyderabad Ballroom III**
11:15-11.40	**Invited Talk** Control of Thermal Spray Process through Flattening Phenomenon of Individual Particles **M Fukumoto** *Toyohashi University, Japan*	
11.40-11.55	Splat Flattening Behavior and Coating Properties of NiCoCrAlYTa Powders Thermally Sprayed onto K4169 Substrates **Kun Yang,** Changguang Deng, Min Liu *Guangdong General Research Institute of Industrial Technology, Guangzhou, China*	
11.55-12.10	Critical Interface Temperature for Plasma Spray Ceramic Droplet to Form Bonding **Shu-Wei Yao,** Guan-Jun Yang, Cheng-Xin Li, Xiao-Tao Luo, Chang-Jiu Li *School of Materials Science and Engineering, Xi'an Jiantong University, Xi'an, China*	
12.10-12.25	Substrate Melting and Resolidification During Impact of High Melting Point Droplet Material on a Substrate Rajesh Kumar Shukla**, Arvind Kumar** *Department of Mechanical Engineering, IIT Kanpur, Kanpur, India*	
12.25-12.40	Structure-Property Correlation in Cold Sprayed Splats of Copper and Copper Alloys with Different Stacking Fault Energies (SFE) **Naveen Manhar Chavan**, Prita Pant, G. Sundararajan *International Advanced Research Centre for Powder Metallurgy and New Materials, Hyderabad, India*	
12.40-12.55	Correlation Studies Between In-flight Particle Characteristics, Splat Formation and Microstructure of Atmospheric Plasma Sprayed XPT 512 Powder **M.Jayamathy,** G.Sivakumar, S.V.Joshi, Vikram Jayaram *TVS Motor Company Limited, Hosur, India*	
13:00–14:00	**Lunch**	
	Plenary Session-4	**Shamshabad Ballroom**
14:00–14:30	***Changhee Lee*** *Hanyang University, Korea*	The Recent Developments and the Future of Kinetic Spraying
14:30–15:00	**Richard Schmid** *Oerlikon Metco, Switzerland*	Technologies to Address Today's Surface Solution Needs
15:00–15.45	**Exhibition & Tea Break**	

Parallel Technical Sessions 15:45-17:30	Hot Corrosion	Shamshabad Ballroom I
	Emerging Techniques	Shamshabad Ballroom II
	Applications-2	Hyderabad Ballroom III

Hot Corrosion		Shamshabad Ballroom I
15:45–16.10	**Invited Talk** Role of Oxide Dispersion on the Hot Corrosion Resistance NiCrAlY Bond Coat **V.S.Raja** *Indian Institute of Technology Bombay, India*	
16.10-16.25	Hot Corrosion Stability of Perovskites and Pyrochlores in Na_2SO_4+50 wt.% V_2O_5 and Na_2SO_4+10 wt.% NaCl at 900 ºC **Gosipathala Sreedhar,** T. Baskaran, S.B.Arya, L.John Berchmans *CSIR-Central Electrochemical Research Institute, Karaikudi, India*	
16.25-16.40	Improving Hot corrosion Reistance of Ti-31 Alloys by Thermal Spray Deposition N.Jegadeeswaran, M.R.Ramesh, **Udaya Bhat K** *Department of Metallurgy and Materials Engineering, NIT Surathkal*	
16.40-16.55	Corrosion Response of Cold sprayed IN625 and NiCr Coatings A S S Balan, Vighnesh Chandrasekhar, Dheepa Srinivasan, Y.C Lau, Eklavya Calla, **Vishwanathan Venkatachalapathy** *GE Power and Water, GE India Technology Center, Bangalore, India*	
16.55-17.10	High Temperature Exposure Studies of HVOF Sprayed Cr_3C_2-25(NiCr)/ (WC-Co) coatings **Manpreet Kaur,** Harpreet Singh, Satya Prakash *Baba Banda Singh Bahadur Engineering College, Fatehgarh Sahib, India*	
17.10-17.25	A study on Wear and Corrosion Resistant Cr_2O_3 – Al_2O_3 coating by Detonation Spray Technique **P.Suresh Babu,** D.Srinivasa Rao, D.Sen, S.V.Joshi *International Advanced Research Centre for Powder Metallurgy and New Materials, Hyderabad, India*	

Emerging Techniques		Shamshabad Ballroom II
15.45-16.10	**Invited Talk** Room Temperature Impact Consolidation (RTIC) of Fine Particles on Aerosol Deposition Process **Jun Akedo** *Advanced Industrial Science and Technology, Japan*	
16.10-16.35	**Invited Talk** Manufacturing of Thick Coatings by Very Low Pressure Plasma Spraying in a Reactive Mode: An Example with Aluminum, Titanium and Nitrogen **Ghislain Montavon** *University of Technology of Belfort-Montbeliard, France*	
16.35-16.50	Advancement in HP/HVOF Thermal Spray Equipment & Materials **Rakesh K Anand** *Praxair India Private Limited, Mumbai – 400093, India*	
16.50-17.05	Mechanisms Study of High Hardness Wear Resistant Coating onto Heat Susceptible Substrates Deposited by Low Power Microwave Plasma Spray **Ahmad Redza,** Toshiaki Yasui, Masahiro Fukumoto *Toyohashi University of Technology, Japan*	
17.05-17.20	High Performance Wear Resistance Titanium Coating on CFRP Materials Using High Pressure Warm Spray System **Amirthan Ganesan,** Okada Takuma, Motohiro Yamada, Masahiro Fukumoto *Department of Mechanical Eng.,Toyohashi University of Technology, Japan*	
17.20-17.35	Depositing Dense Ti and Ti6Al4V Coatings by In-situ Shot Peening Assisted Cold Spraying **Xiao-Tao Luo,** Ying-Kang Wei, Cheng-Xin Li, Guan-Jun Yang, Chang-Jiu Li *School of Materials Science and Engineering, Xi'an Jiantong University, China*	
17.35-17.50	Deposition of Nitrogen Doped Diamond/ Mo Hybrid Coating by APS with C_2H_2/O_2 Combustion Flame Assisted Ar/N_2 Plasma Jet **Yasutaka Ando,** Yoshimasa Noda *Ashikaga Institute of Technology, Japan*	

Applications-2		Hyderabad Ballroom III
15.45-16.10	**Invited Talk** Functional Coatings Formed by Gas Tunnel Type Plasma Spraying **Akira Kobayashi** *Osaka University, Japan*	
16.10-16.35	**Invited Talk** Novel Ceramic Coatings by Plasma Spray Deposition for Molten Metal Containment **P V A Padmanabhan** *Laser and Plasma Technology Division, Bhabha Atomic Research Centre, Mumbai, India*	
16.35-16.50	Adsorption of Alginate and Albumin Mediates Colonization of Escherichia-coli on Arc-sprayed Aluminum Coatings **Xiaoyan He,** Yi Liu, Hua Li *Ningbo Institute of Materials Technology and Engineering, Ningbo, China*	
16.50-17.05	Gas and Fuel Management in Thermal Spray Process **R.Bateriwala** *Keepsake Engineering Consultancy Pvt Ltd, India*	
17.05-17.20	Repair Development for a Thermal Spray Coated Component of an Aero-Engine **V Krishnakanth**, Ekshwaku N Srivastava, V Sambasiva Rao *CYIENT Limited, Hyderabad*	
17.20-17.35	Thermal Spray Coating on Geothermal Turbine Blades by High Velocity Oxy-Liquid Fuel Gun MJP-5000 for Corrosion Protection **Rohit Upadhyaya,** Sharad Shrivastava, S.C.Modi, A. Modi *Metallizing Equipment Company Pvt. Ltd, Jodhpur, India*	
17.35-17.50	Plasma Spray Coating as an Alternative Wear Resistance to Hard Chrome on Cast Iron Piston Ring Shailesh Mani Pandey, **Qasim Murtaza,** R. S Walia *Delhi Technological University, India*	
17.30–19.00	**Exhibition/Poster and Networking**	
19:00	**Banquet Dinner**	

26th November 2014

Parallel Technical Sessions 09:00-10:30	Solution Based Processes	Shamshabad Ballroom I
	Characterization of Thermal Spray Coatings	Shamshabad Ballroom II
	Coatings for Energy Applications	Hyderabad Ballroom III

Solution Based Processes		Shamshabad Ballroom I
09:00–09.25	**Invited Talk** Ceramic Films and Coatings Obtained by Solution Precursor Spray Techniques **Lech Pawlowski** *University of Limoges, France*	
09.25-09.50	**Invited Talk** Suspension Plasma-spray Fabrication of Nanocrystalline Titania Hollow Microspheres for Photocatalytic Water Disinfection **Hua Li,** Kun Ren *Ningbo Institute of Materials Technology and Engineering, Ningbo, China*	
09.50-10.05	Fabrication of Porous YSZ Coatings by Suspension Plasma Spray **Mohammed Shahien,** Masato Suzuki *Central Metallurgical Research and Development Institute, Egypt*	
10.05-10.20	Process Parameter Studies to Achieve Phase Pure α-Alumina Coatings during Solution Precursor Plasma Spraying **G.Sivakumar**, R.O.Dusane, S.V.Joshi *International Advanced Research Centre for Powder Metallurgy and New Materials, Hyderabad, India*	
10.20-10.35	Effects of Vanadates on High Temperature Degradation Behavior of Solution Precursor Plasma Srayed Thermal Barrier Coatings **A. Ajay,** V. S. Raja, G. Sivakumar, S. V. Joshi *Indian Institute of Technology Bombay, Mumbai, India*	

Characterization of Thermal Spray Coatings		Shamshabad Ballroom II
09:00–09.25	**Invited Talk** Influence of Intra-splat Cracks on Thermal and Mechanical Properties of Plasma-sprayed Ceramic Coatings **G.J.Yang** *Xi an Jiaotong University, China*	
09.25-09.40	Application of Instrumented Indentation and Scratch Methods for Characterization of Thermally Sprayed Coatings **Gregory Favaro,** Nicholas Randall, Jiri Nohava, Kapil Joshi, Hemant Gourkar, Shiva Tummalapalli *Anton Paar TriTec SA, Switzerland*	
09.40-09.55	Characteristics of Cold-sprayed Cu Coatings with Pretreated Feedstock **J.O.Choi,** K.H. Ko, H.Lee *Department of Energy Systems Research, Ajou University, Korea*	
09.55-10.10	Residual Stress Behaviour of Cold Sprayed IN625 Coatings **Chintala V Manikantha,** Dheepa Srinivasan *GE Power and Water, GE India Technology Center, Bangalore, India*	
10.10-10.25	Advanced Matallographic Sample Preparation Techniques for Thermal Spray Coatings **Patrick Voos** *Buehler, Germany*	
10.25-10.40	Quantification of Grit Entrapment in Thermal Sprayed Coatings **Hariharan S,** Dheepa Srinivasan, George Meng *GE Power and Water, GE India Technology Center, Bangalore, India*	
10.40-10.55	Oxidation and Protection of Graphite **Ariharan S,** Pradyut Sengupta, Ankur Agnihotri, N. Balaji, S.T. Aruna, Kantesh Balani *Indian Institute of Technology-Kanpur, India*	
Coatings for Energy Applications		**Hyderabad Ballroom III**
09:00–09.15	Evaluation of Air Plasma Sprayed Alumina Coatings for DC Conduction Pump **R.Krishnan** *Indira Gandhi Centre for Atomic Research, Kalpakkam, India*	
09.15-09.30	Plasma Sprayed Alumina Coating on Inconel 600 for Neutron Detector Application **A. Ravi Shankar,** K. Thyagarajan, Chandra Kant Upadhyay, C. Mallika, U. Kamachi Mudali *Indira Gandhi Centre for Atomic Research, Kalpakkam, India*	
09.30-09.45	Development of Tungsten Coating using Atmospheric Plasma Spraying for First Wall Applications in Fusion TOKAMAK **Shailesh Kanpara,** G. Sivakumar, Kedar Bhope, S.S. Khirwadkar, S.V.Joshi *Institute for Plasma Research, India*	
09.45-10.00	Application of Thermal Spray Coating in Fusion Reactor Components **Samiran Mukherjee,** Ranjana Gangradey, Jyoti Agarwal, Paresh Panchal, Pratik Nayak *Institute for Plasma Research, Bhat, Gandhinagar, India*	
10.00-10.15	Plasma Spray Coating of Yttrium Oxide Coating on Molybdenum and its Thermal Stability Studies up to 800°C **Y. Chakravarthy,** P V Ananthapadmanabhan, Vandana Chathurvedi, A Pragatheeswaran *Laser and Plasma Technology division, Bhabha Atomic Research Centre, Mumbai*	
10.15-10.30	Performance Evaluation of Yttria Coated High Density Graphite for Cathode Processor Applications **Ch. Jagadeeswara Rao,** E.Vetrivendan, A.Ravi Shankar, C.Mallika, U.Kamachi Mudali *Indira Gandhi Centre for Atomic Research, Kalpakkam, India*	
10.30-10.45	Microstructural Evolution of Stellite6 Coatings used in Gas Turbines after Service Exposure and Heat Treatment **Apaar Shanker,** Dheepa Srinivasan, Santhosh Bangera, Viswanathan Venkatachalapathy *Indian Institute of Science, Bangalore, India*	
10:30–11.15	**Exhibition and Tea Break**	
	Plenary Session-5	**Shamshabad Ballroom**
11:15–11:45	**Chang-Jiu Li** *Xi an Jiaotong University, China*	Understanding the Inter-Particle Bonding Formation in Thermal Spraying for the Design of Coating Microstructure
11:45–12:15	**G Sundararajan** *International Advanced Research Centre for Powder Metallurgy and New Materials, Hyderabad, India*	Assessment and Enhancement of the Integrity of Cold Sprayed Coatings
12:15–12:45	**Christopher Berndt** *Swinburne University of Technology, Australia*	The Grand Challenges for Thermal Spray that Lead to Industrial Outcomes
12:45–13:00	**Wrap-up**	
13:00–14:00	**Lunch**	

Plenary Lectures

Warm Spray Technology to Fill the Gap between HVOF and Cold Spray

Seiji Kuroda, Rafal Molak, Hiroshi Araki, Makoto Watanabe
High Temperature Materials Unit, National Institute for Materials Science, Tsukuba 305 0047, Japan
Hiroshi Katanoda
Department of Mechanical Engineering, Kagoshima University, Kagoshima 890-0065, Japan
Naoyuki Ohno and Hirotaka Fukanuma
Plasma Giken Co., Ltd., Saitama 369-1214, Japan.

Abstract
Since publication of our first papers on warm spraying (WS) in 2006, significant efforts have been made to understand its process fundamentals as well as to exploit the advantages of the process for potential industrial applications. More recently high-pressure WS has been developed by which particles velocity can reach a range comparable to these by He-driven cold spray. Coatings characteristics such as porosity and oxygen content of materials such as CP Ti and Ti6Al4V alloy as well as their mechanical properties have been investigated by using HP-WS, including the effects of post-spray heat treatment.

1 Introduction

High-velocity oxy-fuel (HVOF) spray has been highly successful in industry for production of wear resistant coatings such as WC-Co cermet owing to its capability to accelerate powder feedstock to relatively high velocity over 500 m/s. For more oxygen sensitive materials such as titanium, the process temperature is too high to avoid oxidation. Cold spray (CS), on the other hand, has emerged as a process to form thick and clean metallic coatings in the air atmosphere and has been successful for materials like Cu and Al. For materials with higher yield strength such as Ti- and Ni –based alloys, the process requires high pressure and high temperature of the propellant gas typically nitrogen or even helium. Warm spray has been developed since 2006 [1, 2] in order to fill the gap between HVOF and CS. Significant efforts have been made to understand its process fundamentals as well as to explore the advantages of the process for potential applications [3-6]. After a brief introduction of the WS process, its application to Ti6Al4V is discussed in detail in order to demonstrate the characteristics of coatings fabricated by this process.

2. Principles of warm spray

Figure 1 shows the schematic of WS process developed by NIMS, which is a modification from a commercial HVOF apparatus. Mixture of kerosene and oxygen is combusted continuously to generate a hot gas, into which nitrogen gas is injected inside the mixing chamber inserted between the combustion chamber and the converging-diverging nozzle. By adjusting the flow rate of the nitrogen gas injected, the flame temperature and concentrations of gas species can be controlled. The mixture ratio of kerosene to oxygen is usually set at the stoichiometric mixture ratio for complete combustion. Since the reaction rate of metallic powder with ambient gas such as oxygen and nitrogen increases dramatically once the particle is melted, it is of great advantage to avoid melting in order to control detrimental reactions during spraying. It has been widely recognized by CS research that solid metal particles need to exceed a critical velocity to form bonding with a solid target. Also the critical velocity can be significantly reduced by raising the temperature of solid impact. This has been shown by FEM calculation assuming the Johnson-Cook plastic deformation model; shear instability was regarded as the necessary condition for bonding to occur at the interface [2]. Lower critical velocity in WS implies higher deposition efficiency and denser coating structure.

Recently developed CS equipment is characterized by high gas pressure and temperature close to 5 MPa and 1,000°C, which is primarily effective to achieve high particle velocity. For metals with high critical velocity, He may be used as the propellant gas but its industrial usage will be limited due to its high cost. WS can be regarded as a more cost effective process when compared to such high pressure CS systems though the coating purity may be somewhat inferior.

More recently the combustion pressure of WS has been increased by some modification of the fuel injector and internal nozzle design modification. Gas dynamic simulation was fully utilized in the design change, whose results are summarized in Fig.2 for Ti powder of 20 μm diameter [6]. As can be seen, remarkable gain in velocity can be achieved by changing the propellant gas from nitrogen to helium while the temperature gain is rather modest. For warm spray, by increasing from 1 to 4 MPa, it has become possible to reach velocity range around 1,000 m/s while maintaining the temperature range significantly higher than CS.

3. Experimental

Commercially available powder of Ti6Al4V (Raymor Industries, Ltd., Que´bec, Canada) with D_{50} at 35 μm was used to form relatively thick coatings (3~4 mm) by using WS [7]. Both LP- and HP-WS were used with different nitrogen flow rates while the barrel length and the spray distance were fixed at 200 mm. Cross sections were observed by SEM to check the microstructure, and porosity was evaluated by image analysis while oxygen content was analyzed by the inert gas fusion method. Mini tensile specimens were cut out of the deposits to test the mechanical properties in the in-plane direction normal to the spraying direction. Effects of heat treatment at three different conditions were examined, i.e., mill annealing at 750 °C x 1 hr., recrystallization annealing at 940 °C x 4 hrs., and β annealing at 1025 °C x 1hr. + 760 °C x 2hr. in vacuum.

4. Results

Effects of nitrogen flow rate on the porosity and oxygen content in Ti6Al4V deposits formed by LP-(1MPa) and HP-

(4MPa) Warm Spray are shown in **Fig.3**. In spite of the trade-off relationships between the porosity and oxygen content, significant benefit was clearly observed by increasing the combustion pressure from 1 to 4 MPa.

Figure 4 shows measured engineering stress-strain curves of Ti6Al4V deposits formed by HP-WS with nitrogen flow rate of 1.0 m^3/min. As was the case for all the as sprayed deposits in this study, the deposit exhibited rather low failure stress around 200 MPa with almost no plastic elongation. With heat treatments, however, both the strength and elongation recovered, the degree of which sensitively depended on the WS condition. With this set of specimens, the strength recovered over 800 MPa with total elongation over 3 %.

While as sprayed deposits exhibited very fine microstructure with features due to severe plastic deformation resulting from high-velocity impacts of powder particles, mill annealed samples showed fine β phase in α phase matrix. The recrystallization annealed samples exhibited equaiaxed α and intergranular β, while the β annealed deposits showed acicular α and interagranular β phases.

5. Conclusions

Recent development of high-pressure warm spray (HP-WS) has made it possible to form dense coatings of high-strength alloys such as Ti6Al4V with reasonably low oxygen content. Due to this feature, it has become possible to recover its mechanical properties after proper heat treatment. Similar approach can be applied to other materials such as Ni-based alloys and carbide containing composites. The results suggest that the process can be used to reclaim damaged components made of such materilas.

Acknowledgements

This research was financially supported by the Organization for Small & Medium Enterprises and Regional Innovation, Japan.

References

[1] J. Kawakita et al., Surf. & Coat. Technol., 201 (2006) 1250-1255.
[2] K. Yokoyama et al., Mater. Trans., 47(2006) 1697-1702.
[3] M. Watanabe et al., J. Japan Inst. Metals, 71(2007) 853-859.
[4] J. Kawakita et al., Mater. Trans. 49 (2008) 317-323.
[5] S. Kuroda et al., Sci. & Technol. of Adv. Mater., 9(2008) 33002.
[6] S. Kuroda et al., J. Therm. Spray Technol. 20[4] (2011) 653-676.
[7] R.M. Molak et al., J. Therm. Spray Technol. 23[1-2] (2014)197-212.

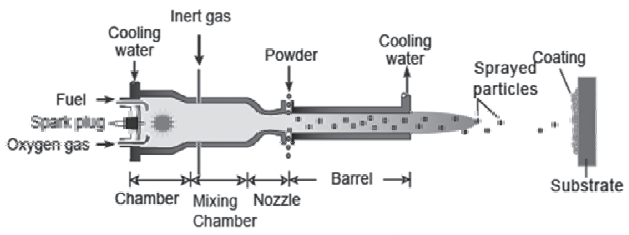

Fig.1. *Schematic of warm spraying apparatus.*

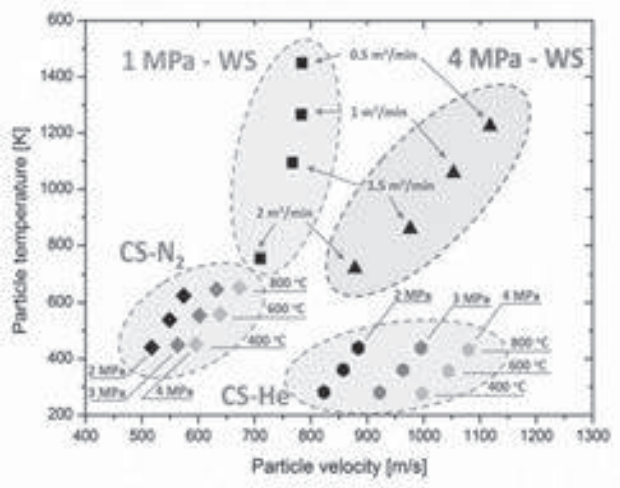

Fig.2. *Comparison of Warm Spray vs. Cold Spray in terms of particles temperature and velocity for Ti powder of 20 μm diameter* [6].

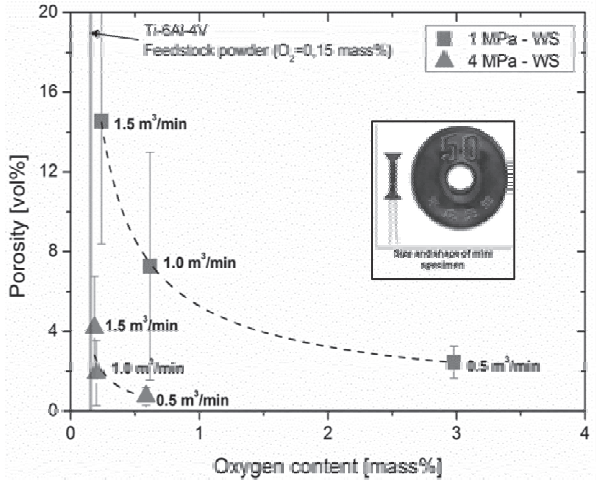

Fig.3. *Effects of nitrogen flowrate on the porosity and oxygen content in Ti6Al4V deposits formed by LP-(1MPa) and HP(4MPa)-Warm Spray* [7].

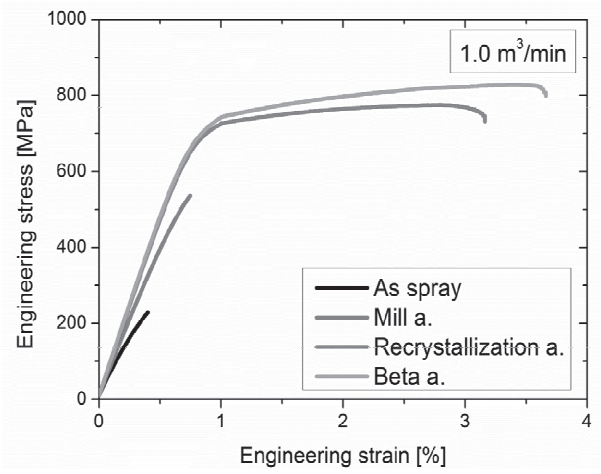

Fig.4. *Typical stress-strain curves obatined by mini-tensile specimens obatined by HP-WS with nitrogen flow rate 1.0 m^3/min.*

Transforming Thermal Spray Technology through Interdisciplinary Research: From Protective Coatings to Functional Multilayers

Sanjay Sampath
Center for Thermal Spray Research
Stony Brook University, State University of New York
Stony Brook, NY 11794-2275

Abstract
Thermal spray is a complex technology involving many sub-processes from thermo-fluids to mechanics to chemistry to materials science. Scientific and technological progress, including development of robust new applications, require multidisciplinary thinking and research consideration. This presentation will present examples of new results and outcomes enabled by such a research strategy.

1. Introduction

Thermal spraying is a directed melt spray deposition process, in which inorganic particles in the diameter range of 1-100 microns are heated, melted (in some cases partially), propelled and impacted onto a prepared substrate. Thermal spray has emerged as an innovative and multifaceted materials processing approach that extends well beyond the traditional application of protective coatings into the synthesis of functional surfaces and multilayer devices with complex chemistries, multiscale assemblage and defect dominated architectures. The principal materials processing advantages include: (1) Remarkable materials versatility (metals, ceramics and polymers on a wide range of substrates), (2) Cost-effective near-net-shape manufacturing of a range of materials at near ambient conditions, (3) Ability to synthesize specialized materials with novel structures and compositions, and (4) Flexible approaches to forming multilayered coatings and thick films. This versatility and flexibility with respect to materials and processes has enabled thermal spray to find wide-spread industrial applications. They are crucial to the economic and efficient operation of a range of engineering systems including gas turbines engines (for propulsion and energy), biomedical implants, industrial machinery, automotive components, heavy machinery reclamation/remanufacturing and semiconductor manufacturing.

During thermal spray processing, a rapid sequence of events occurs including: melting, impact (in some cases shock), spreading and rapid solidification, all of which take place in microsecond timescales, resulting in materials excursions from extreme conditions. The initial microstructure evolves within microseconds, whether process is based on powder melting, impact and solidification, or in more recent modifications involving thermal spraying of suspensions and liquid precursors. Thus, far-from equilibrium structures and compositions are common in thermal spray deposits, offering rich opportunities for fundamental materials research as well as extensive industrial applicability. Furthermore, thermal spray materials exhibit a hierarchy of microstructural features across a range of length scales: nano-elements, micron-sized grains contained within mesoscale splat structures and a variety of nano/micro/meso-scale defects such as voids, microcracks and oriented boundaries. Nanostructured materials rapid solidification processing, layered/graded architectures etc. - subjects of major excitement in contemporary materials research over the last two decades, entered the lexicon of thermal spray long before they were fashionable. In fact an exceptional confluence of science and engineering disciplines are engaged in thermal spray research across the globe yielding rich dividends in terms of both enhanced fundamental understanding and expanded applications.

In this context, over the last 15 years through support from the US- National Science Foundation, Center for Thermal Spray Research (CTSR) at Stony Brook University in New York USA has enabled a multidisciplinary group of investigators to critically examine the scientific underpinning behind thermal sprayed materials and unravel its complexity for enhanced utilization. Major advances have been made on a number of fronts including processing science, multi-scale characterization of complex defected structures, novel means of property extraction of layered materials and applications.

Key accomplishments include: (Detailed list of publications available at www.ctsr-sunysb.org)

- Advanced process diagnostics and physics based models providing insights into the process.
- Process maps: an intelligent approach to process optimization, coating design and reliability
- *In situ* methods to determine coating residual stresses including relations to deposit formation dynamics.
- Defect-property correlations and its relevance in design, performance and processing, including observation and quantification of non-linear phenomena resulting from layered coating assemblage.
- Multiscale methods for determining design relevant coating properties and relating to performance outcomes.

Figure 1 captures important developments in fundamental science enabled by interdisciplinary research.

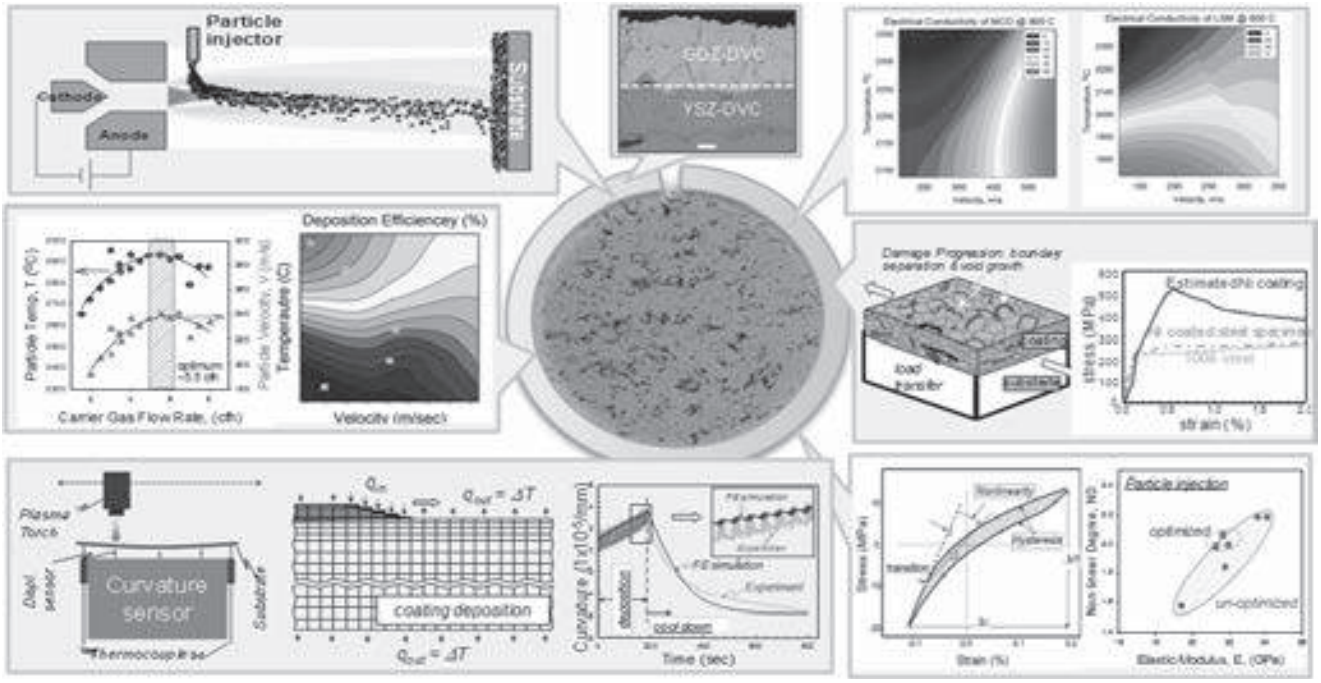

Figure 1: Illustration of research activities at the CTSR spanning from spray plume simulation and diagnostics to *insitu* curvature based coating property monitoring and resultant effects invest-igated through novel mechanical, thermal and electrical property assessment schemes. Integrated outcomes are represented through process maps which links process to properties for various materials and applications. (www.ctsr-sunysb.org)

These interdisciplinary studies have led to several important findings of direct relevance to coating design and industrial practice of thermal spray processing. This includes:

- Methodologies for integration of coating design, materials and process selection for given application
- Appropriate utilization of process sensors in industrial environment for enhanced reliability.
- New insights coating evolution dynamics through advanced coating monitoring sensors.
- Relevance of inelastic mechanisms in metals/cermets and non-linear properties of ceramics in design and fabrication of damage tolerant coatings
- Benchmarking process-property relationships with linkages to applications and manufacturing integration.
- Science based understanding and controlling process efficiency, coating reproducibility and reliability.

Major breakthroughs have been made on a number of fronts which has enabled new considerations of the process and materials technology towards synthesis of reliable, damage tolerant coatings for variety of applications. They have also yielded rich dividends to science, technology and human resources.

These accomplishments are now being transitioned to industrial practice through a pre-competitive knowledge transfer mechanism through the *Consortium for Thermal Spray Technology* comprising of some 35 leading companies (see Figure). The consortium allows application of the new methods to enhance efficiency, improve reliability and translate scientific knowledge developed at Center for industrial practice. The consortium brings together academia and industry in a pre-competitive setting to:

- Rapidly examine value proposition of new technology insertion across the supply chain to demonstrate business benefits(e.g. efficiency, reliability improvements)
- Enable identification of implementation issues / adaptation requirements for innovative new ideas and products
- Establish knowledge-technology connections through innovative field trip programs and workforce training on advanced concepts

This presentation will highlight past contributions and seek new opportunities in emergent coatings, synthesis and multiscale assembly of novel materials, and patterned functional devices.

Deposition of Volcanic Ash within Gas Turbine Aeroengines and Effect on the Thermo-mechanical Stability of Thermal Barrier Coatings

TW Clyne, M Shinozaki, C Taltavull & J Dean
Department of Materials Science, University of Cambridge, 27 Charles Babbage Road, Cambridge CB3 0FS

Abstract
Deposition of ingested volcanic ash has been studied in a turbojet aeroengine (using a borescope) and in a plasma torch-based set-up simulating a turbine combustion chamber (with the substrate being examined after removal from the set-up). Deposition in the engine mainly occurred on static components. Numerical modelling was used to predict particle flight histories. It was both observed and predicted that intermediate-size particles (~50-100 μm diameter) are more likely to adhere than smaller ones, since their greater inertia makes them more likely to impact on surfaces. While their impact temperature may be below that at which they become soft, the difference may be small (partly because such ashes often exhibit low T_g values). In conjunction with substrate temperatures often being higher than T_g, adhesion of such particles is a probable outcome. Particle size, T_g value and amorphous content are thus all of importance. Studies have also been made of the effect of deposited ash on sintering-induced spallation of plasma sprayed zirconia TBCs. It can induce various microstructural changes and accelerate sintering-induced stiffening. This raises the driving force for spallation from differential thermal contraction during cooling. It is shown that coating lifetime can be dramatically reduced via this mechanism.

1 Introduction

A key issue affecting the possibility of damage arising from ingestion of CMAS particles into gas turbines is the likelihood of them adhering to solid (hot) surfaces. This is of particular concern for volcanic ash (VA), which can soften, and perhaps melt completely, at relatively low temperatures. It's been demonstrated [1] that ingested VA particles can readily adhere to (static) surfaces within a small turbojet aeroengine, depending on their size and softening temperature. In general, intermediate-size particles are expected to adhere most readily, since large particles are unlikely to become sufficiently hot, while small ones will tend to be carried with the gas stream and avoid collision with any substrate. However, there is little information available about which size range is likely to be most problematic under given conditions.

If VA particles do adhere, they may cause two types of problem. Firstly, if they adhere in sufficient quantities, they may affect the gas flow through the engine and hence impair its operation - possibly even causing it to shut down. Previous work [1] has shown that there is a tendency for deposition to become concentrated in certain areas, which is likely to aggravate this problem. Secondly, if VA particles are deposited on ceramic coatings, such as zirconia-based TBCs, then they can cause [2] rapid spallation, probably by accelerating the sintering and stiffening processes, raising the driving force for interfacial debonding [3].

This paper outlines some work done both on the likelihood of VA particles adhering to solid surfaces and on the effect that such particles may have on the thermo-mechanical stability of TBCs. It is concluded that certain features of the ash, particularly the glass content and T_g value, can be important in determining the outcome.

2 Adhesion of VA Particles on Solid Surfaces

2.1 Stokes Number

The Stokes number (Fig.1) gives an indication of the likelihood of particle striking a solid surface (rather than being carried around it with the gas streamlines). It can be seen in the figure that particles above about 10 μm in diameter are likely to strike surfaces inside the turbine, although obviously this will depend on a number of factors.

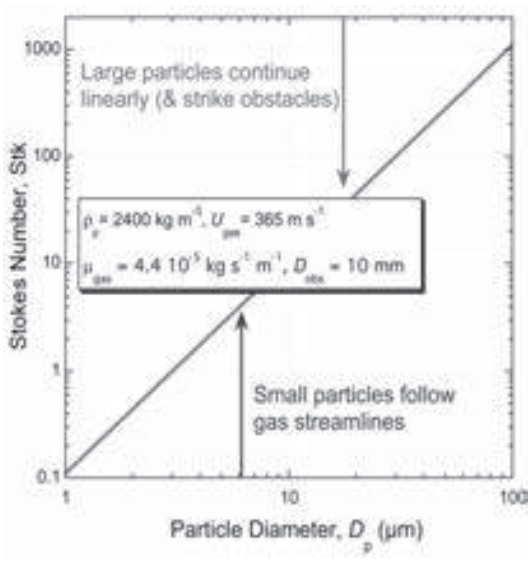

Fig. 1. *Plot of Stokes number (ratio of characteristic time for velocity change to that for flow past obstacles) against VA particle size, for conditions representive of a turbojet.*

2.2 Thermal Histories

Particles are naturally more likely to adhere to a solid surface on impact if their surfaces have reached higher temperatures, which in turn is affected by flight time, gas temperature and particle size (and, to a lesser extent, their conductivity, specific heat, latent heat, shape, interfacial heat transfer coefficient etc). However, also important are particle softening (and melting) temperatures. A significant characteristic of volcanic ashes is that they often have a relatively high glassy content (100% in some cases) and their T_g values (ie the temperature at which the glassy phase effectively becomes liquid) are often relatively low (<~800˚C). This is illustrated by the information in Fig.2, which demonstrates that VA samples will often become soft, if not liquid, at temperatures well below typical gas

temperatures within a turbine (~1000-1400˚C). This clearly makes them more prone to adhesion than more highly crystalline CMAS particles, such as sand.

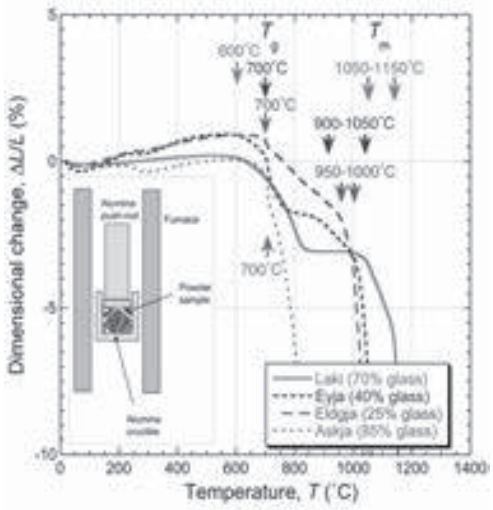

Fig. 2. *Assessment of T_g and T_m values for 4 (Icelandic) volcanic ashes, obtained using a dilatometry method.*

2.3 Adhesion Observations

Recent work has involved injection of VA powder into the region at the front of a plasma torch within a vacuum chamber (under controlled pressure). As can be seen in Fig.3, there is a tendency for an intermediate particle size (~60 μm in this case) to give the highest deposition rate, since these particles are large enough to strike the substrate, but sufficiently small to ensure that they reach temperatues at which they are suitably soft to adhere.

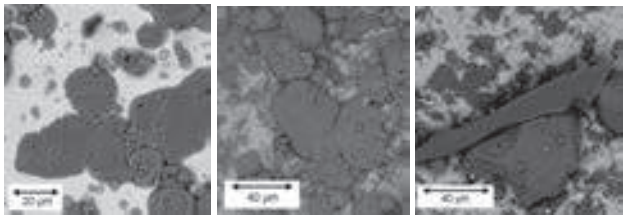

Fig. 3. *SEM micrographs of Laki ash particles splatted onto a steel substrate after injection into a plasma plume (with average gas temperature during flight ~1100˚C), for particle sizes (left to right) of 25 μm, 60 μm and 90 μm.*

3 Effect of VA Particles on TBCs

3.1 Sintering and Stiffening

If VA particles do adhere to a coating, such as a TBC, within a turbine, then they are likely to have a deleterious effect. At temperatures above about 800-900˚C, they tend to accelerate the sintering that occurs in service, by forming a liquid phase that enters the pores in the coating and/or by the atoms concerned migrating to the grain boundaries and promoting diffusion there. This sintering causes the coating stiffness to increase (Fig.4), which raises the driving force for spallation on cooling [3] - see §3.2.

3.2 Acceleration of Spallation

The main driving force for spallation (debonding) of TBCs arises during cooling, when differential thermal contraction between coating and substrate creates (in-plane) stresses in both constituents - mainly in the coating, which is normally both thinner and less stiff than the substrate. These stresses increase as the coating becomes stiffer (as a result of sintering). They give rise to a strain energy release rate (driving force) for debonding (allowing the stresses to be relaxed), which is proportional to the coating thickess (and to the square of the stress level).

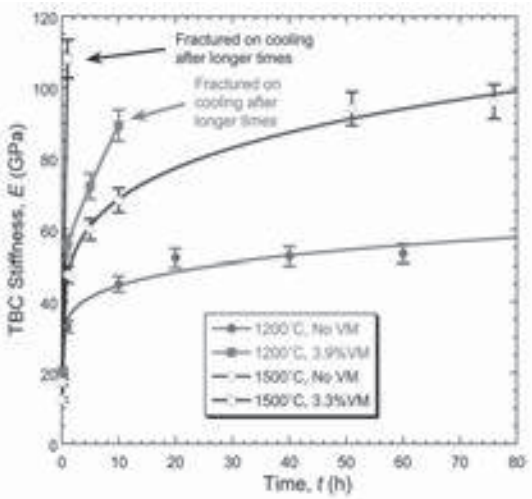

Fig. 4. *Effect of the addition of vermiculite (representative of VA) on the stiffening of plasma sprayed Yttria-Stabilized Zircona (YSZ) coatings during heat treatment.*

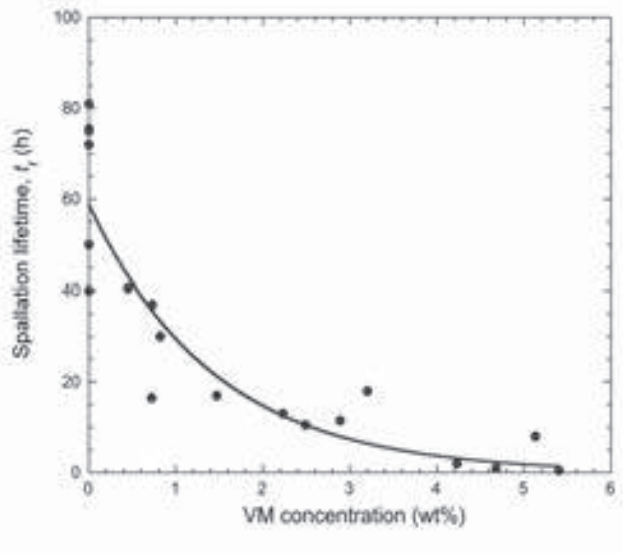

Fig. 5. *Effect of vermiculite on the spallation lifetime of plasma sprayed YSZ coatings (on alumina substrates) held at 1500˚C and quenched every hour to room temperature.*

If the strain energy release rate exceeds the fracture energy of the interface, then spallation is energetically favourable. Since the presence of VA on the surface (and subsequently in the interior) of a TBC accelerates stiffening (Fig.4), it also tends to promote debonding. This effect is illustrated in Fig.5, which shows how the spallation lifetime of a TBC can be sharply reduced by the presence of VA.

4 References

[1] M. Shinozaki, K. A. Roberts, B. van de Goor and T. W. Clyne: Adv. Eng. Mats. **15** (2013) 986-94.

[2] M. Shinozaki and T. W. Clyne: Surf. Coat. Techn. **216** (2013) 172-77.

[3] M. Shinozaki and T. W. Clyne: Acta Mater. **61** (2013) 579-88.

Suspension Thermal Spraying: Opportunities and Challenges of an Emerging Coating Technology

Christian Moreau [1], Fariba Tarasi[1]
[1] Department of Mechanical & Industrial Engineering, Concordia University, Montreal, Canada

Abstract
Over the last decade, extensive R&D efforts have been dedicated to the emerging technology of suspension thermal spray (STS). This technology has attracted much attention as it opens up a series of new opportunities but also a number of important challenges. In this presentation, an overview of the STS technology is provided with a summary of key opportunities in term of applications and research directions. Additionally, important challenges must be addressed to improve the control of the deposited coating properties and the process consistency for industrial implementation.

1 Introduction

Thermal spray processes have greatly evolved over the past decades in various domains. The driving force for such a remarkable evolution has mostly been economical, since it provides the means to modify the surface properties of critical and expensive parts by applying the materials interacting with the external environment only at the surface. In the meantime, the acquired knowledge of the improved properties of the nano-structured coatings urge the application of nano- to a few micron grain sized powder feeds in thermal spray systems aiming to achieve such microstructures.

For nearly one decade many efforts have been focused on spraying sub-micrometer or nanometer sized particles [1]. However, such fine particles are difficult to transport and inject in the plasma/flame jet. A high carrier gas flow rate is required to permit the fine particle to penetrate into the plasma/flame, often time with limited success and significant perturbation of the plasma/flame flow itself. Moreover, small particles, especially below 5µm, can readily agglomerate and result in rapid clogging of the flow paths toward injecting point. In suspension thermal spraying (STS), these small particles are suspended in a water or alcohol carrier liquid. SPS coatings are mostly produced using conventional air plasma spray (APS) or high velocity oxygen fuel (HVOF) processes. In some works, the torch design was modified to fulfill the specific STS technology requirements. The process ends with one or two orders of magnitude finer structures than those generated in conventional thermal spray. The grain size of the spray materials ranging typically between 30 to 100 nm provide unique characteristics to the deposited layers. Such a nanostructured layers result from the extremely rapid solidification rates of the few micron size molten particles upon impact on the substrate surface. Figure 1 shows a comparison of the in-flight particle sizes in both conventional and suspension plasma spraying (SPS).

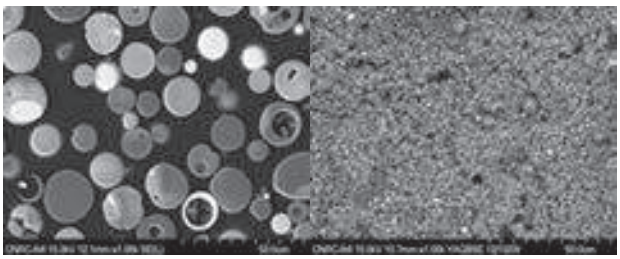

Fig. 1. *Alumina-zirconia particles collected in water as produced in conventional air plasma spray (APS) (left) and in suspension plasma spray (SPS) (right).*

Typical coatings like those shown in Figure 2, can present a wide range of microstructures from columnar, segmented, highly porous/high specific surface area or very dense. The technology can thus be promising for many applications. However, there is still numerous challenges that must be faced before reliable, reproducible and mass production of nano-structured coatings using suspension thermal spray can be achieved.

2 Challenges

In general, suspension thermal spray technologies are not yet sufficiently mature to satisfy the industrial standards and to be readily tailored to the needs of targeted applications. However, collaborative, multidisciplinary research has permitted during the last 15 years to improve the level of scientific understanding of the STS processes and will contribute in the coming years to the advancement of their technology readiness. A summary of research challenges was identified recently by a group of international experts in thermal spray science and technology including challenges facing the STS technology [2]. Accordingly, a series of research priorities were identified as summarized below:

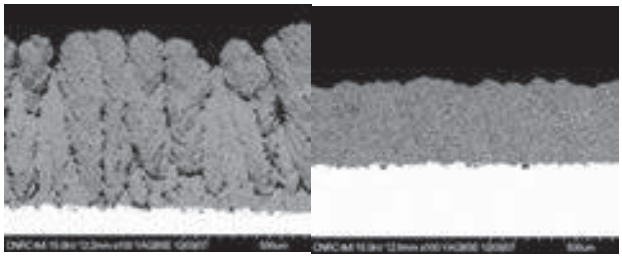

Fig. 2. *Typical coating microstructures that are produced in suspension plasma spray (SPS) under two different sets of spray condition*

2.1 Feed Stock

Suspension preparation and storage are basic but extremely important issues that must be addressed to better control the quality of the deposited SPS coatings.

- Formulation of stable suspensions :

Although fairly successful efforts have been dedicated to form stable suspensions of the industrially important ceramic oxides such as zirconia and titania, there is still a large group of materials for which forming a stable suspension is challenging. Some important examples are cermets like WC-Co or metals like Ni.

- Choice of the solid particle size and type:

Powder particles currently commercialized are manufactured in various size distributions and types/forms. They may be crushed, fused, sintered or not, synthesized from difference chemical/processing routes, constituted of agglomerates of different size and or shapes, etc. The appropriate choice of size and type of the solid particles must be identified for each targeted microstructure and service application.

• Handling and storage of suspensions:
Presently even for the most stable suspensions, there is a limited stability period. Changes in the suspension properties can lead to variations in the suspension droplet and molten particle sizes and, consequently, variations in the spray coating characteristics. Therefore, feed suspensions for industrial scale manufacturing have to be duly prepared and characterized. Accordingly, a procedure must be developed for adequately prepare, store for a specific period of time and use the spray suspensions.

2.2 Injection of suspension into the plasma/flame

The injection could be either radial or axial relative to hot gas flow direction. Radial injection normally imposes more complications in obtaining successful penetration of the feed material into the flame. The injection angle, flow rate and distance are parameters to control. Axial injection offers generally a better penetration of the suspension in the plasma/flame jet and a more uniform heating and acceleration of the spray materials. In axial injection, the suspension must be atomized at the injector tip. In the radial configuration, either atomizers or straight injection tubes can be used to feed the suspension into the plasma/flame jet.
Another difficulty in injecting the suspensions is the frequent clogging in the nozzle that urges appropriate combination of feeding line from the reservoir to the injection point, nozzle design and stable suspension.

2.3 Spray Process

• Design of stable spray guns:
The torches have to be adapted to the liquid feedstock. Typically torches used with suspensions are plasma torches including r.f. induction, axial and radial injection torches, cascaded torches as well as HVOF and detonation spray processes. Cold spraying of suspensions would most probably require in-flight heat treatment of the particles.
• Increase in stand-off distance:
The small molten particles formed in SPS have very low inertia and cool down rapidly. These facts dictate much shorter spray distances than the conventional powders (30–50 mm instead of 100–120 mm in conventional plasma spraying). The drawback of the short spray distance is the higher thermal load to the substrate and associated thermal stresses, oxidation, etc.
• Increase in deposition rate and efficiency:
Relative to conventional APS and HVOF processes, STS provides typically smaller deposition rates and relatively lower deposition efficiency of the small particles due to the deflection of their trajectory close to the substrate or in-flight evaporation.
• Complex surfaces:
Curved and sharp edges represent a challenge in most of thermal spray processes. The problem is even more acute in SPS as the in-flight particles have low inertia and their trajectories can be severely perturbed according to the actual shape of the substrate.

2.4 Process control to enhance reliability

• Development of sensors:
Sensors able to measure velocity, temperature and size of the STS particles must be developed to get a better understanding of the influence of the spray conditions on the in-flight particle and coating characteristics. Particle size measurement in STS is particularly important as the particle impact speed and angle depend on the particle size. Ensemble and individual particle sensors can provide complementary information about the spray particles.

• Modeling and simulation:
In order to gain an adequate knowledge of the transformations occurring in STS processes, development of modeling and simulation tools is essential. In particular, models of primary and secondary atomization, particle tracking in the plasma/flame and around the substrate, as well as coating buildup must be developed and validated to better control the spray process and the resulting coating characteristics.

3 Opportunities

STS can bridge the thicknesses of thin films deposited by vapor deposition (PVD) or chemical methods (CVD) to thick films deposited with conventional thermal spray processes. Accordingly a large variety of applications can be foreseen that will take advantage of the key characteristics of the STS processes. Potential applications include thermal barrier coatings with columnar or segmented structures with lower thermal conductivity for aerospace and gas turbines [3], low temperature solid oxide fuel cells manufactured potentially at lower cost as high temperature processing steps are avoided [4], environmental surfaces e.g. barriers against corrosion and wear, super-hydrophobic coatings, photo-catalytic surfaces, sensors manufacturing, anti-microbial coatings, and biomaterials.

4 References

[1] P. Fauchais, J.R. Heberlein, M. Boulos, in: Overview of Thermal Spray, Springer US, 2014, pp. 17-72.
[2] Thermal Spray White Paper - Addendum 4: Key Research Challenges in Thermal Spray Science and Technology, ASM Thermal Spray Society, 2014, http://www.asminternational.org/web/tss/technical/white-paper
[3] H. Kassner, R. Siegert, D. Hathiramani, R.Vassen, and D. Stoever, Application of Suspension Plasma Spraying (SPS) for Manufacture of Ceramic Coatings, J. Thermal Spray Technol., 17 (2008) 115-123
[4] R. Hui, J. Oberste Berghaus, C. Decès-Petit, W. Qu,S. Yick, J.-G. Legoux, C. Moreau, High performance metal-supported solid oxide fuel cells fabricated by thermal spray, J. Power Sources, V191 (2009) 371–376

Global Research Trends in Thermal Sprayed Coatings Technology Analysed with Bibliometrics Tools

K. A. Khor[1], L. G. Yu[1]

[1] Research Support Office and Bibliometrics Analysis, Nanyang Technological University, #B4-01, Block N2.1, 76, Nanyang Drive, Singapore 637331, Singapore

Abstract

In the past decades, thermal spray coating technology has experinced rapid scientific, technical and economic growth. In order to investigate the trends of scientific output, impact and collaboration on thermal spray technology, the global publications on thermal spray coating technology from 2000 to 2014 are extracted from Scopus database and the Web of Science Core Collection database, and studied using a bibliometric analysis method. Study focus on performances such as the annual scholarly outputs, the mainstream journals, leading countries and institutions, and research tendencies, as well as trends of collaborations. The results indicated that annual output of the related scientific articles increased steadily. Surface & Coatings Technology, Journal of Thermal Spray Technology, and Materials Science and Engineering A are three most common journals in thermal spray coating technology research. The USA took a leading position out of 83 countries/territories, followed by China, Japan, Germany and France.

1 Introduction

The significant growth of thermal spray technology research over the last several decades is driven by the industrial application needs, ease of implementation and the associated cost benefits [1, 2]. Research publication output and impact on thermal spray technology have also grown rapidly along with the technology growth.

In this report, research papers on thermal spray technology during the past 15 years (2000-2014) was extracted from SciVerse Scopus (Elsevier) and Web of Science (Thomson Reuters) databases, and analyzed to provide a basic understanding of the global research in this field. The annual scholarly outputs and impact, mainstream journals, leading countries and institutions are obtained from the analyses of the publication data.

2 Results and Discussion

2.1 Annual Scholarly Output and Inpact

Figure 1 provides the global annual numbers of publication on verious thermal spray coating technology. Thermal spray or plasma spray dominates the publications on thermal spray, and publications on cold spray inceases rapidly in the past 10 years.

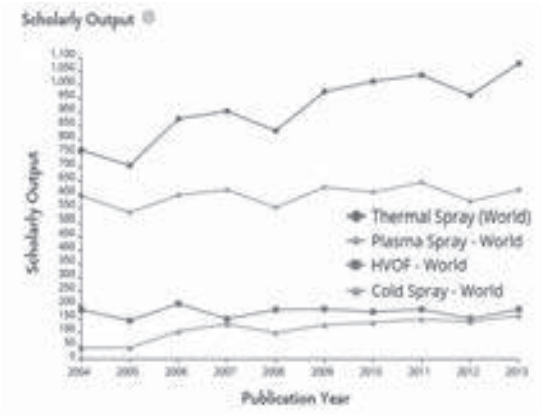

Fig. 1. *Global scholarly output searched by different spray technology as keywords in Elsevier SciVal*

Figure 2 and 3 shows the citations impact for the publications published in each year. One can found that publications on cold spray get higher citations per paper, although the annual number of publications on cold spray is significantly lower than that for plasma spray.

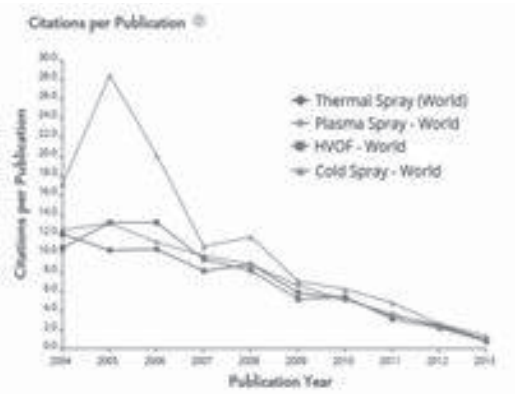

Fig. 2. *Citations per paper for different spray technology*

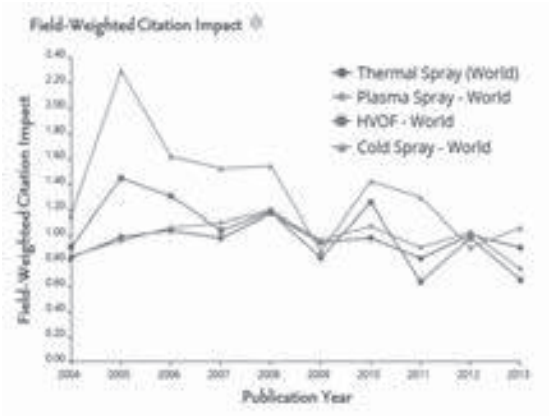

Fig. 3. *Field-Weighted Citation impact for different spray technology*

2.2 Leading Countries and Institutions

Figure 4 & 5 presented the top countries and institutions contributing to the publications on thermal spray coating technology. The USA took a leading position out the

countries/territories, followed by China, Japan, Germany and France.

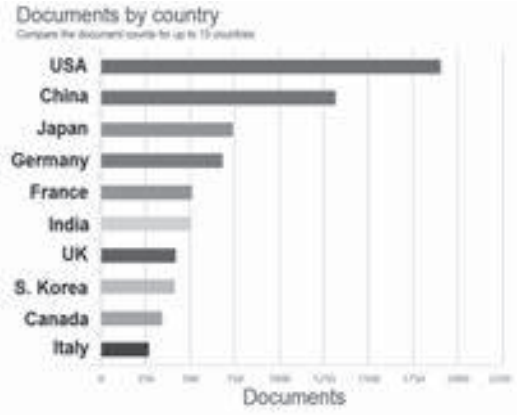

Fig. 4. *Top countries contributing to publications on thermal spray technologies(2000-2013)*

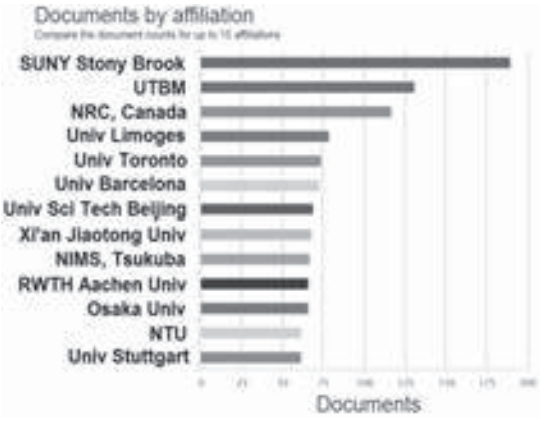

Fig. 5. *Top Institutions contributing to publications on thermal spray technologies(2000-2013)*

2.3 Mapping of leading Journals, Technical Terms and Institutions

Our analysis shows that, Surface & Coatings Technology, Journal of Thermal Spray Technology, and Materials Science and Engineering A are three most popular journals on thermal spray coating technology research.

Figure 6 (a) and (b) shows the research area trends by mapping the technical terms used in the titles and abstracts in the publications. Only terms occurred 20 times or more in the year are selected in the mapping. Terms like "cold spray" can be seen in the AD 2013 map while it cannot be seen in the AD 2000 map. And the spot for HVOF is relatively larger in the AD 2013 map than it in AD 2000 map.

Fig. 6(a). *Terms used in thermal spray coating technology publications published in Year 2000*

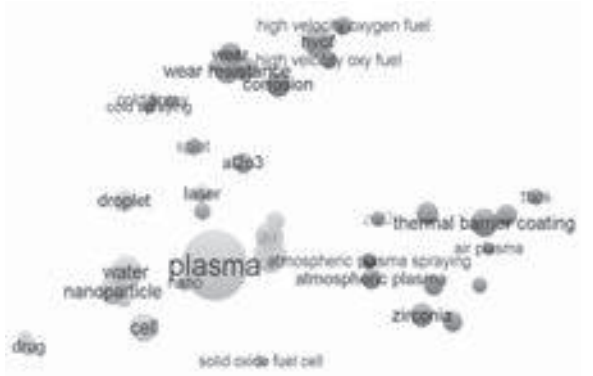

Fig. 6(b). *Terms used in thermal spray coating technology publications published in Year 2013*

Figure 7(a) and (b) shows the trends of publishing institutions on thermal spray technology and their collaborations, with SUNY Stony Brook dominating the publications in the years 2000 – 2003, and Chinese Academy of Science dominating the publications in the years 2012-2014.

(a) 2000-2003 (Institutions with 10 or more Papers)

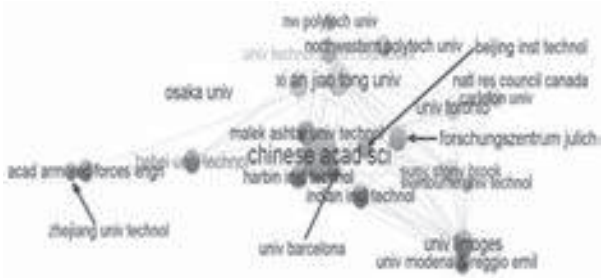

(b) 2012-2014 (Institution with 10 or more Papers)

Fig. 7. *Evolutiontrends of contributioninstitutions on thermal spray technology and their colaboration mapping*

3 Summary

In the past 15 years, the number of research publications on thermal spray technology grows steadily. The USA took a leading position in theremal spray technology research, and China is catching up fast, as indicated by the rapid rise of publications by Chinese Academy of Science and universities such as Xi'an Jiaotong University.

4 References

[1] S. Sampath: *Int. J. Materials and Product Technology*, Vol. 35, Nos. 3/4, (2009) 425-448.

[2] C. U. Hardwicke & Y.-C. Lau: *Journal of Thermal Spray Technology*, Vol.22(5) (2013) 564-576.

Plasma Spray Torch Modeling: Issues and Practical Considerations

Armelle Vardelle , Christophe Chazelas
" Sciences of Ceramic and Surface Treatment Processes Lab", European Ceramic Center, University of Limoges, Limoges, France

Abstract
Modeling of plasma torch operation has advanced greatly in the last fifteen years due to a better understanding of the underlying physics, development of commercial, open-source CFD software and, access to high performance and cloud computing. However, some phenomena, especially at the electrodes, need to be properly incorporated into the arc model. This presentation will discuss some of the main aspects involved in the modeling of plasma spray torches to achieve a predictive model, with a particular emphasis on the electromagnetic coupling between electrodes and plasma arc.

1 Introduction

The operation of the plasma torch determines to a large extent the overall performance of the plasma spraying process. It produces a processing medium with a high energy density (10^6 - 10^7 J/m^3) resulting in high temperatures (up to 15000 K) and heat flux (10^7 - 10^9 W/m^2) to the processed material injected in the plasma jet in the form of powder. Most of the plasma torches currently used in industry are characterized by a simple design involving a stick-type thermionic cathode located within a concentric anode. This apparent simplicity is in marked contrast to the intricate electromagnetic, thermal, acoustic and chemical phenomena that control the torch operation and give rise to two interlinked drawbacks; arc instability and electrode wear [1].

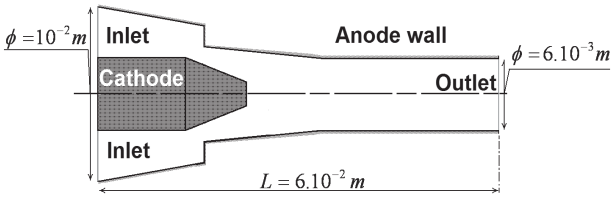

Fig. 1. *Typical inner geometry of mono-anode mono-cathode plasma torch*

Since the first reported plasma-sprayed metal coating in the 30's, many torch models have been proposed in the literature or patented with the objectives of improving plasma jet stability, reducing electrode erosion and increasing the enthalpy of the gas flow, the latter generally achieved by an increase in arc current [2,3]. However, these objectives can be conflicting; e.g., the anode erosion depends on the arc residence time and current density at the arc attachment and the maximum heat load to the anode wall is nearly proportional to the square of the arc current.
The designs of more advanced plasma torches involve forced rotational movement of the arc attachment, by means of vortex injection of the plasma-forming gas or external magnetic field; they also include multi-electrodes (cathode and/or anode) to divide the arc current, cascaded anode consisting of a stack of copper rings insulated from each other and ending to an anode-ring on which the arc attaches or magnetic stabilization of the arc.
Another essential issue in plasma spray torch design is the penetration of the coating powder into the plasma jet. While most plasma torches use powder injection close to the nozzle exit at angles nearly 90° to the plasma torch axis, a much more efficient configuration would be the axial injection in the hot gas. Because of the difficulty to avoid the clogging of electrode when using a hollow cathode, this type of injection is essentially realized by using converging or parallel independent plasma jets issuing from up to three plasma torches.
Modeling of the phenomena in mono-cathode mono-anode torches can be a very useful tool because (i) the torch design exaggerates the arc fluctuations and (ii) the actual behavior of the arc has been extensively studied which helps to determine whether the model is an accurate representation of the real world.

2 Plasma Spray Torch Model

Due to the stochastic movement of the arc anode attachment in a mono-anode mono-cathode plasma torch, the mathematical model must be time-dependent and tridimensional.

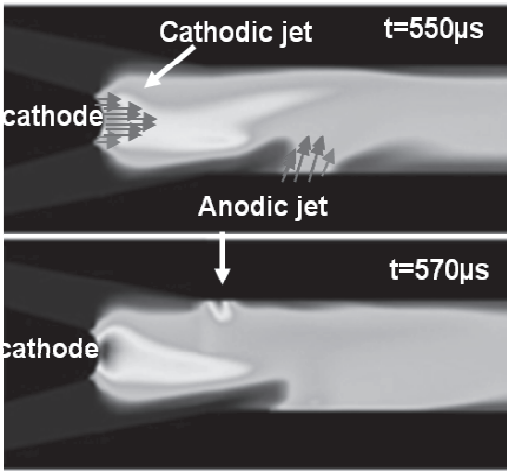

Fig. 2. *Arc dynamics*

2.1 Plasma Flow

The plasma flow within the torch is generally described by a fluid model consisting of the conservation equations of mass, momentum and energy, which are coupled with the Maxwell's equations. The latter describe the variation in space and time of the electromagnetic fields and are often expressed from the electric and magnetic vector potentials. The main assumptions needed to solve the set of mathematical equations deal with:

- the thermodynamic and chemical equilibrium prevailing in the various regions of the computer domain,
- the compressibility of the flow,
- its turbulence level,
- and everlasting electrodes.

- If the LTE (Local Thermodynamic Equilibrium) approximation is valid in the arc column where the electron density (10^{21} to 10^{24} m^{-3}) and collision frequencies between the plasma constituents are high, departures from LTE can occur in the regions of steep gradients, e.g. close to electrodes and walls and /or in high-velocity plasma jets. The kinetic energy of the plasma species cannot be characterized by a single temperature and the fluid is generally characterized by electron temperature and heavy species temperature [4]. This entails the computation of the non-LTE thermodynamic and transport properties of the plasma gas.
- It has been shown recently that acoustic resonance phenomena may take place inside the plasma torch due to compressibility effects of the plasma-forming gas in the cathode cavity [5]. These phenomena depend on the actual inner plasma torch geometry and may affect the anode arc attachment stability. Therefore, a predictive model of arc behavior should take into account the actual geometry of the plasma torch and the compressibility of the plasma gas. Furthermore, the fluid equations should be coupled with the wave equations.

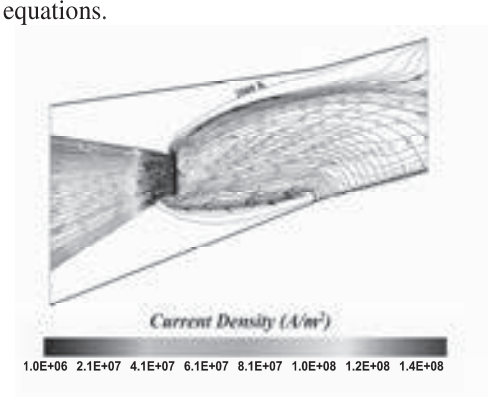

Fig. 3. *Current density distribution (vectors) close to the cathode tip with arc–cathode coupling.*

-The rapid heating of the plasma-forming gas (around 10^4 K/mm) passing through the arc causes a sudden expansion and acceleration that affect the stability of the flow and generate shear-layer turbulence. In addition, the electromagnetic field fluctuations need to be taken into account for modeling the flow turbulence. Therefore, direct numerical simulation (DNS) that makes it possible to solve the whole range of spatial and temporal scales of the turbulence should be used rather than standard turbulence models like the Reynolds-averaged-Navier-Stokes (RANS) models. However, DNS requires very fine grids to resolve the smallest of scales and calculations of the flow fields over long periods of time to delineate meaningful statistical averages and, to the best of the author's knowledge, DNS of the plasma flow within a DC plasma spray torch has not been performed yet.
- A useful output of a plasma torch model would be the predicted electrode erosion depending on the electrode materials, design and operating conditions. It is a very challenging issue; e.g., at the anode it requires (i) an accurate prediction of the location and residence time of the arc attachment and of the heat balance at the arc root, (ii) the implementation of phase change in the electrodes production of vapor from molten spots), (iii) the calculations of thermodynamic, transport and radiative properties of plasmas gas seeded by metal vapors and, (iv) in a final step, the implementation of surface wall modification, as the anode arc attachment is affected by the surface roughness resulting from erosion.
However, before tackling such piece of work, an issue that cannot be ignored is the interaction between the arc and electrodes.

2.2 Arc-Electrode Interaction

The zones close to the electrodes exhibit drastic variation in gas properties. They are characterized by non-equilibrium conditions and charge accumulation and give rise to an important voltage drop that cannot be calculated with magnetohydrodynamics model. They should be modeled by a non-continuum sheath model based on particle energy and charge conservation [6] but such a model entails a high computational cost. Since the sheath thickness is very small in comparison to the characteristic length of the flow (e.g. the torch diameter), the thermal and electromagnetic coupling of the arc and electrode are generally taken into account through boundary conditions at the electrode walls conditions involve parameters that affect the plasma flow fields and neglect physics phenomena at electrodes; e.g.; current density profile imposed at the cathode tip; artificially high electric conductivity value in a thin zone (about 100-µm thick) adjacent to the anode to allow the flow of the electric charges from the arc column to the wall. The latter condition brings about a sort of artificial flapping movement of the arc different from the actual reattachment process of an arc operating in the restrike mode.
The first step towards a consistent model of arc–electrode interactions could be to including the electrodes in the computational domain [7] and coupling the energy and electromagnetic equations in the electrodes to the Navier - Stokes and electromagnetic equation in the gas field (Fig.3).

4 Concluding Remarks

If the present models of plasma torch operation do not fully address the physics that control the dynamics of the arc, they are already useful tools for parametric studies and even geometry improvement. However, it is believed that the easier access to high performance computing resources has now open up the door to a comprehensive model of DC plasma torch operation that, in a reasonable time, will address fully the physics and help to improve the technology.

3 References

[1] J. P. Trelles, C. Chazelas, A. Vardelle and J. Heberlein, J. Thermal Spray Technol., **1**8 (2009) pp. 728-752
[2] I. Vladimirovich Zasypkin, M F Zhukov, Thermal Plasma Torches. (2006) Cambridge Int Science Publishing
[3] J.L. Marqués, G. Forster and J. Schein, The Open Plasma Physics Journal, **2** (2009) pp. 89-98
[4] J P Trelles, J V R Heberlein, and E Pfender, J P Trelles, J. Phys. D: Appl. Phys., **40** (2007), p. 5937
[5] V. Rat and J.F. Coudert, Appl. Phys. Lett. **96**, (2010) pp. 101503-101503-3
[6] M.S. Benilov J.Phys D: Appl. Phys., **41** (2008) pp. 144001-31
[7] M. Alaya, C. Chazelas, G. Mariaux, A. Vardelle**,** J. Thermal Spray Technol., **24,** (2015)

The Recent Developments and the Future of Kinetic Spraying

Changhee Lee*, Jaeick Kim, Hyungkwon Park
Kinetic Spray Coating Lab, Division of Materials Science and Engineering, Hanyang University, Seoul 133-791, South Korea, *E-mail: chlee@hanyang.ac.kr

The kinetic spraying, which produces the deposit by shooting the accelerated particles at supersonic velocity, has been developed continuously since the mid-1980s. As a result, the overall theoretical foundation of kinetic spraying has been established from the deposition mechanism to the gas dynamics, the relationship between process parameters and deposition behaviors, microstructural evolution, materials and etc. Also, kinetic spraying is practically used in various industrial fields in accordance with a number of researches about the industrial application of kinetic spraying. However, there are still a lot to investigate about the kinetic spraying, and, especially, in terms of materials, the researches about the kinetic spray are biased toward deformable metals. Therefore, the recent developments and the future of kinetic spraying will be considered and discussed taking this opportunity.

Technologies to Address Today's Surface Solution Needs

Dr. Richard K. Schmid, Dishant Mittal
Oerlikon Metco, Switzerland

Thermal Spray falls into a broad family of surface treatments available to customers to solve their surface improvement needs for increase machine performance and component life. The talk positions thermal spray within the relevant surface technology options. It then goes on to show important new developments in equipment and feedstock, and which applications these address.

Understanding the Inter-Particle Bonding Formation in Thermal Spraying for the Design of Coating Microstructure

Chang-Jiu Li, Shu-Wei Yao, Guan-Jun Yang, Cheng-Xin Li
State Key Laboratory for Mechanical Behavior of Materials, School of Materials Science and Engineering, Xi'an Jiaotong University

Thermal spray deposits are built up by layering fully molten or/and semi-molten thermal spray particles. The inter-particle bonding in the deposit determines their physical, thermal and mechanical properties and subsequently their performances. The formation of the inter-particle bonding upon spray particle impact depends primarily on the inter-reaction of impacting particle with the underlying substrate or previously deposited particles, which is influenced by the surface conditions of substrate and the parameters of spray particles. In this presentation, the effect of thermal spray conditions during plasma spraying on the interface bonding ratio of ceramic coatings will be reviewed to reveal the dominant factors controlling the bonding formation of inter-particles in terms of inter-splats for lamellar structured deposits. It will be demonstrated that the deposition temperature significantly influences the inter-splat bonding formation. The recent investigations showed that there is a critical deposition temperature for impacting molten droplet to form the bonding with the underlying identical substrate surface. The critical bonding temperature was found to be associated with the glass transition temperature of molten droplet. It will be demonstrated that the interface temperature between molten droplet and substrate prior to melt solidification controls the bonding formation and the bonding nature at the interface. Accordingly, the concept of microstructure design for thermal spray deposit from fully dense one to porous spherical skeleton will be introduced by controlled deposition of spray particles in different molten states.

Assessment and Enhancement of the Integrity of Cold Spray Coatings

G Sundararajan
International Advanced Research Centre for Powder Metallurgy and New Materials (ARCI) Hyderabad, India

Cold spray coatings of a variety of metals and alloys have been investigated extensively and several niche market applications have been established. In this context, the use of cold spray coatings for refurbishment of worn out components and for metal additive manufacturing has recently caught the attention of the thermal spray community. Cold spray coatings can qualify for such applications, only if they can mimic the bulk material behaviour in terms of their mechanical behaviour and performance. This in turn requires high level of coating integrity in terms of coating-substrate adhesion, porosity level in the coating and extent of inter-splat bonding. The residual stress and microstructure of the coating is also important. In the presentation, various techniques available to evaluate coating integrity will be presented and also the ways and means to enhance coating integrity and properties including post-coating treatment will be discussed.

The Grand Challenges for Thermal Spray that Lead to Industrial Outcomes

C.C. Berndt1,2, S.M. Ang1 and M.L. Sesso1
1 Swinburne University of Technology, Faculty of Science, Engineering and Technology, Hawthorn, VIC 3122 Australia
2 Adjunct Professor, Stony Brook University, Materials Science and Engineering, Stony Brook, 11794, NY-USA

Abstract

A Grand Challenge for science and technology may be defined as "The removal of one or more science or technology barriers to achieve a significant breakthrough in a particular area of science and technology". Thus, with regard to thermal spray, a Grand Challenge can be dictated in the following terms: "What is needed to discover, learn or understand so that thermal spray may advance beyond existing practices?"
This presentation will systematically classify thermal spray Grand Challenges under critical categories. As well as providing several Grand Challenges, there will also be an indication of the potential industrial and manufacturing outcomes that would arise if these unknowns became known. This approach is intended to be thought-provoking so that future R&D directions can become defined for the evolution of a guided and focused approach.

Key words: Grand Challenge, Scientific understanding, Knowledge-based discovery, Industrial outcomes, Future R&D focus.

1. Introduction

A search of the literature uncovers about 120 reviews on thermal spray in the areas of fundamental science, applied engineering and technology. Although informative, the majority of reviews are retrospective state-of-the-art contributions that do not reach far into the future. That is, they are not predictive concerning the barriers to thermal spray that limit growth. As well, these reviews are highly specialized by focussing on a specific aspect of thermal spray without any integration across these specializations.
One view is that the vision for thermal spray has not been articulated with the big picture in mind. There are pragmatic reasons for this approach since such strategic planning exercises are under the cloak of confidentiality for commercial reasons. Therefore, this current contribution is limited to sources that are available from the open literature as well as the opinions of the authors.

2. Topical Areas for Grand Challenges

The five areas of grand challenges that have been identified as being of distinct importance are discussed in this section. These five areas may be broadly based around the constituencies who have impact on the field of thermal spray; i.e., managers, scientists, engineers, national labs and institutes, companies and academic institutions.

2.1 The Science of Thermal Spray (Theory-based)

The critical question is How long does it take for any science-based accomplishment to become integrated into the practice of thermal spray and demonstrate substantial impact? It is suggested that the time scale for such an event would be of the order of more than 20 years; although examples may be available on a shorter time scale.

2.2 Engineering Thermal Spray (Applications-based)

The critical question is How long does it take for new applications to become accepted practice? It is suggested that the time scale is of the order of at least 5 years.

2.3 Technology of Thermal Spray (Equipment-based)

The critical question is If a new piece of equipment was available today, then how long would it take to have substantial impact? It is suggested that the time scale is of the order of at least 10 years.

2.4 Globalization to form a Community

If a decision was made today to establish a global institute of thermal spray, then it is suggested that it would take 12 or more years to bear substantial outcomes.

2.5 Who is Carrying the Torch? (Manpower-based)

How long does it take to cultivate and nurture the future leaders of thermal spray? More than 20-years would be a realistic time frame.
The integration of these 5 areas can be visualized in Figure 1 where the interdisciplinary and overlapping natures of these challenges are presented.

3. Some Grand Challenges

3.1 Creation of nano-Composites

Nanocomposites are multiphase materials that have at least one component within the nanoscale dimension. Such materials exhibit combinations of distinctive properties from each phase that are otherwise not achievable in conventional materials.
However, the upscale production of bulk nanocomposites due to the production costs of nanomaterials has rendered conventional approaches uneconomical. Nanocomposite coatings present an effective alternative to harness the unique properties of nanomaterials without bearing the production costs of full scale nanocomposites. Thermal spray technology presents a versatile approach for the deposition of nanocomposite coatings in relation to materials, deposition medium, and thickness, while offering advantages such as high deposition rates and low processing costs. Thermal sprayed nanocomposite coatings have been adopted commercially in many industries including the automotive, aerospace, marine, and medical fields, with potential in many others.

3.2 Suspension and Solution Plasma Spray

An emerging coatings research area concerns the development and deposition of liquid feedstock. The liquid feedstock can be in the form of a suspension, solution precursor or sol-gels; any of which may be deposited by plasma or combustion flame methods. These innovative coating technologies overcome the constraints of traditional thermal spray and permit the formation of nanostructured coatings from nano-sized primary particles.
Micron or nano-structured coatings have been deposited via solution plasma precursor spray (SPPS) or suspension plasma spray (SPS). SPS and SPPS require more energy per

deposited mass than conventional powder spraying because the liquid carrier must be vaporized before the plasma can interact with the coating material. The as-sprayed coatings of suspension plasma sprayed alumina, yttria stabilised zirconia (YSZ) and metal oxides have been reported to surpass the performance of conventional plasma spray deposits.

In all process arrangements, the powder port of the torch is modified to allow liquid feeding via a pneumatic or mechanical liquid pumping system while the other parts of the torch hardware remain relatively unchanged. Importantly, the potential hazards of handling nanoparticulate materials are reduced when they are contained within a suspension and the challenges of feeding fine grained powders into the combustion zones are eliminated. High deposition efficiencies and superior mechanical properties have been reported.

3.3 Prime Reliant Coatings and Near Net Shapes

The thermal spray family encompasses several processes, which, at their current stage in a technological evolution, all produce "coatings" in some form. The terminology of "coatings" is impeding the development of future applications for thermal spray since it imposes an artificial barrier to R&D.

Although the unique structures produced by the various thermal spray processes do not lend their use in areas where structural load is of importance, this should not rule them out for future applications. Technological developments of nano and composite materials, combined with new equipment and processes, could see the use of thermal spray as the major part of a structural component.

In other words, thermal spray methods can be considered as the matrix for a composite material system that is manufactured through the incorporation of thermal spray processes. As well, post processing technologies via sol-gel, laser treatment and other hitherto unexplored technologies can play important roles in modifying the microstructure for materials engineering advantages.

4. Concluding Remarks and "The Way Forward"

This presentation is designed to challenge the future directions of thermal spray and the associated technologies. It is not intended to present the known future, but to explore the process by which the global community of thermal spray interest groups can map out pathways to the future.

If there was one topic that is a pre-eminent Grand Challenge then it is "Globalization to form a Community" since such an accomplishment would reflect on all of the other proposed grand challenges.

Figure 1. The "BIG picture" approach for the formulation of potential grand challenge

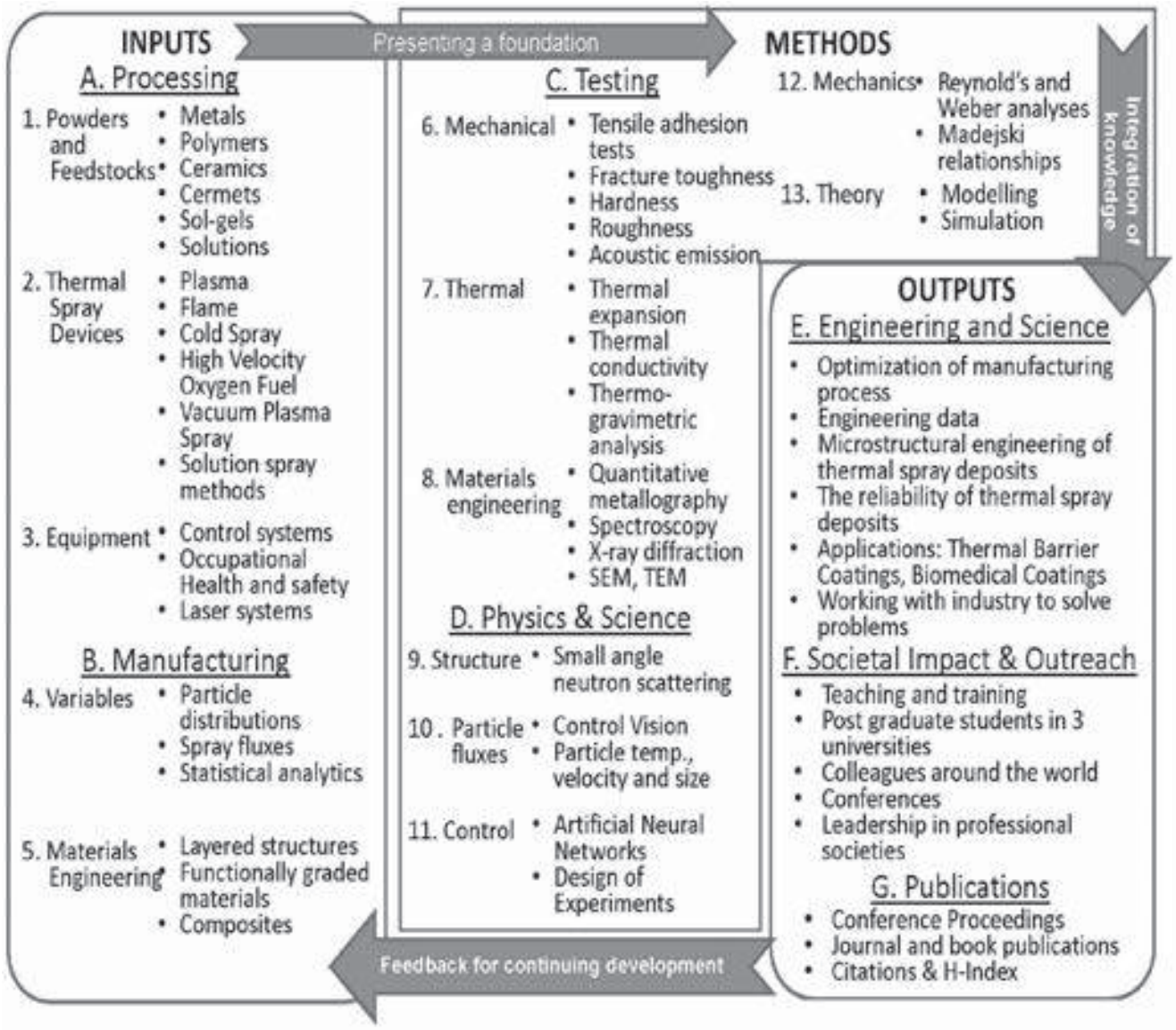

Invited Lectures

Driving Microstructural optimization of composite coatings for wear and high temperature applications

K. Anand[1], Eklavya Calla, S Hariharan, Prajina Bhattacharya, Paul Mathew, CH Sathisha, Biju Dasan, Kanchan Kumari, Dheepa Srinivasan, Tamara Muth[2], Dennis Gray, Todd Curtis[3]
[1]GE India Technology Centre, Power & Water – Materials, Bangalore, India
[2]GE Power & Water, Materials & Process Engg. Schenectady, US
[3]GE Global Research, Materials & Manufacturing Technologies, Niskayuna, NY, USA
e-mail: atsc2014@arci.res.in

Abstract
Wear phenomenaof multiphase particulate composite materials including erosion, abrasion and sliding are often controlled by the microstructural length scale of the material relative to the wear damage zone. Work on bulk sintered materials including cemented carbides have shown that it is possible alter wear mechanisms from the hard brittle phase dominated to the ductile binder phase by reducing hard particle sizes. This work describes translating these concepts in thermal sprayed coatings and improving wear properties through microstructural control.

1 Introduction

Mechanical behavior of composite materials is commonly evaluated under the framework of the rule of mixtures. However work done on erosion and abrasion behavior of particulate composites by Anand et.al [1,2] showed that it was possible to change the mechanism of wear damage from brittle to ductile even in 80-90 vol% brittle systems, by making the wear damage zone size much coarser than the feature size of the brittle phases. Figure1 shows an illustration of the role of the microstructural length scale on the mechanisms with SEM images of the damage zone. In such a situation the erosion rate could be reduced significantly because as nucleation and propagation could be avoided and the deformation response was heavily constrained by the WC hard particles; the erosion rate under the brittle regime was more than 10X higher than under the ductile regime. Similar findings were reported by Pugsley Allen et al. [3]. In order to leverage the full benefits of such a mechanism it was preferable to keep the hard particle sizes to less than a micron maintain high volume fractions of the hard phase (>80 vol%) [1-3].

Thermal spray technologies had steadily progressed by way offering both higher energy plasma spray systems and high kinetic energy combustion based processes that included D-Gun, Super D-Gun, HVOF and HVAF processes [6]. Carbide based multiphase coatings were deposited by both plasma spray and high kinetic energy combustion based processes.

Controlling the decarburisation [4] during the spray process through process selection as well as process parameter optimization to deposit a desired coating microstructure has been one of the main bodies of work by the above authors. The paper discusses some of the highlights of the work done to date and how optimzing microstructures impact erosion, abrasion and sliding response of multiphase coatings – consisting of a metal matrix with hard carbides dispersed within. This work primarily focuses on the WC-12 wt.%Co and WC-10wt.%Co-4wt.%Cr, and the CrC-20wt.%NiCr systems.

2.0 Experimental Work:

WC-Co,WC-Co10%4%Cr and CrC-20%NiCr systems were deposited through commercially available coating systems including HVOF, HVAF and pulsed detonation type systems from open domain vendors based on their best effort basis.

The coatings were subject to standard microstructural evaluation [1]. Palmquists indentation technique [1], which typically generates cracks between 10 to 100 microns, similar to what is typical in wear proces zone, was used to estimate indentation fracture toughness.

The deposited coatings were subject to erosion, abrasion and sliding wear tests using equipment customized to industrial environments. The results from such tests will be used to garner understanding of the relationshops between microstructure and wear mechanims.

3.0 Results and Discussions

Figure 2 shows typical microstructures of WC-10%Co4%Cr systems giving examples of high levels of decarburisation, and relatively lower levels of decarburisation. Figure 3 also shows two major types of crack propagation responses when the coating was subject to Palmquists indentation tests at 10 to 30N loads. When carbide grain size is relatively coarse, cracks generated at an indentor tip would travel along both the binder carbide interfaces and slice through the carbides. When the carbide grain size fell below a size threshold the cracks would hug the tortuous carbide binder interfaces and quickly die out, therefore the fracture toughness increased with decrease in spacing between carbides. Figure 4 shows the relationship between mean spacing between carbides and solid particle erosion rate. It is clear that even within the same composition of WC-10Co4Cr coatings the erosion rates can be decreased by a factor of three by leveraging on the changes in the crack propagation modes. Similar results were seen for Chromium Carbide NiCr coatings. The concepts are covered in patents already filed [5-7].

Abrasion tests were done using the ASTM G65 erosion test rig with 50 micron sized alumina as the abrasive media. Figures 5 shows the SEM images of abraded surfaces; with coarser carbide grains and wider dispersion between grains which would be typical of a decarburised coating the abrasive particle could dig into the binder phase preferentially exposing the carbides for easier removal. However when the carbide particles were finer and spaced lower than the typical scratch width produced by an abrasive media preferential removal of the binder phase was absent. The abrasion rate was therefore a function of the probability of abrasive particles digging between hard particles to preferentially wear the softer binder. Abrasion

rate under such a mechanism decreased by more than 4X with decrease in spacing between WC particles.

Carbide coatings are often used to combat sliding wear. Such systems work best when self mated coatings are used as hardness is well matched. However, in situations where due to cost or geometry considerations only one of the surfaces could be coated, then wear of the counterface by the carbides and preferential removal of the binder phase in the carbide-metal matricx coating is a concern. By keeping the spacing between carbides smaller than the asperity radius one can reduce wear significantly.

4.0 Conclusions:

1. By controlling the time-temperature exposure of feedstock in a high kinetic energy combustion based process one can reduce the degree of decarburisation.
2. Coatings with finer spacing between carbides show a change in crack propagation paths and produce coatimngs with higher fracture toughness.
3. Coatings with finer spacing between carbides show better erosion, abrasion and sliding wear properties.

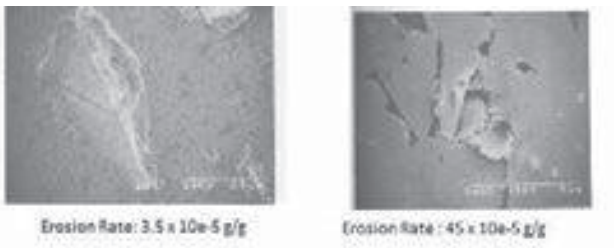

Figure 1: Effect of scale of impact damage zone relative to WC-6%Co sintered carbides and the 10X reduction erosion rate as the damage mechanism changes from brittle to ductile [1-2].

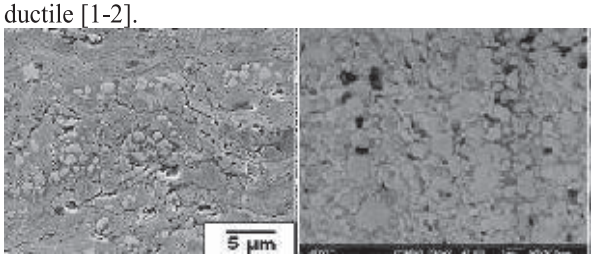

Figure 2. Examples of two tungsten carbide coatings with high (left) and low (right) levels of decarburisation.

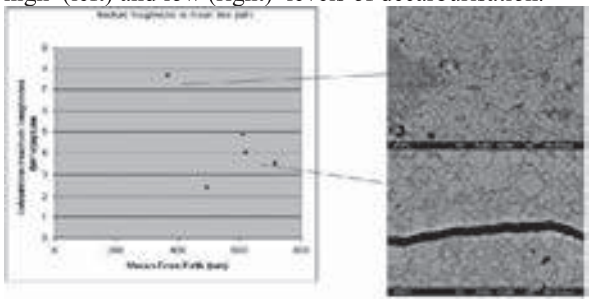

Figure 3. Indentation fracture toughness as a function of spacing between carbides [11].

Referennces

1. K. Anand, PhD Thesis, Materials Science & Engg, North Carolina State University, 1987
2. Wear of Materials, 1989, K. Anand, et.al pp 135-143, Vol 1, ed. K C Ludema

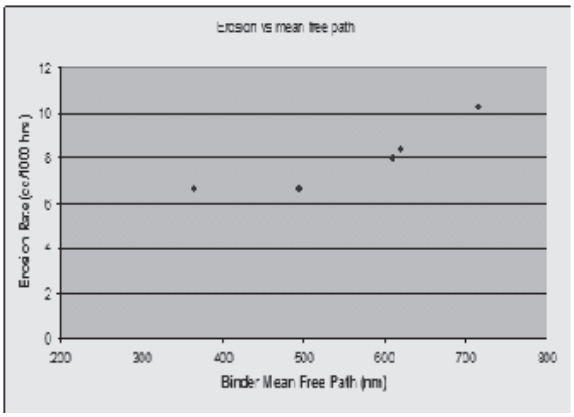

Figure 4. Erosion rate as a function mean free spacing between carbides [11].

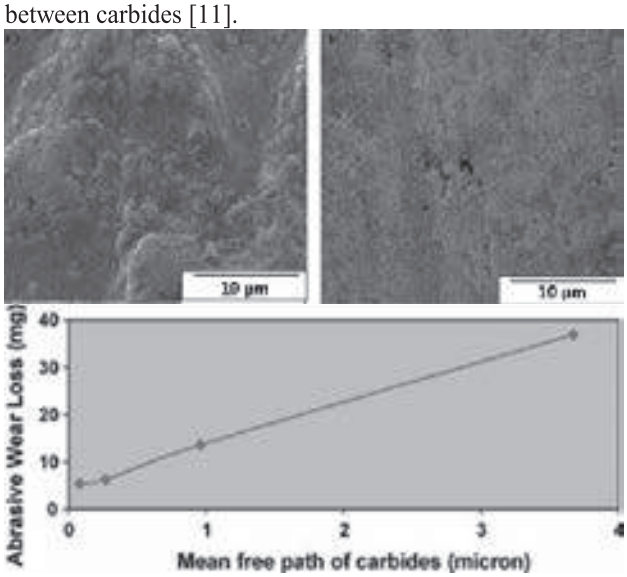

Figure 5. Preferential wear of the binder under abrasion.; wear depends on the spacing between carbides [12].

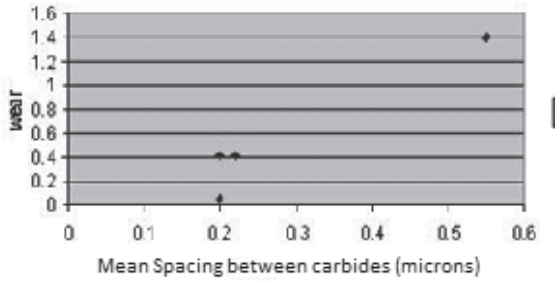

Figure 6. Reduced sliding wear with finely spaced carbides [13] .

3. Pugsley et. Al Wear, Volumes 225–229, Part 2, April 1999, Pages 1017-1024.
4. Qun Wang et. Al. Surface & Coatings Technology 218 (2013) 127–136
5. Patent #WO2005052210: Erosion resistant coatings and methods thereof
6. Patent# WO2005056879: Nano structured coating systems
7. Patent#US20070099027: Wear resistant coatings
8. K. Anand, et.al, Poster, Gordon Research Conference, 2006, Kilby, Maine 2006
9. Kanchan et.al Wear, Volume 268, Issues 11-12, 12 May 2010, Pages 1309-1319

Interface Behavior of Particles uponImpacting during Cold Spraying of Cu/Ni/Al mixture

Wenya Li [1] *, Kang Yang [1], Dongdong Zhang [1]

[1]State Key Laboratory of Solidification Processing, Shaanxi Key Laboratory of Friction Welding Technologies, Northwestern Polytechnical University, Xi'an 710072, P.R. China

Abstract

Cold spraying deposition completely depends on the particle interface behaviors during high velocity impacting. These phenomena will consequently influence the interface bonding. However, owing to the instantaneous impacting process (tens of nanoseconds), it is very difficult to observe and examine these interface behaviors. In this study, focused ion beam (FIB) was used to characterize the interface features of cold spray particles. Meantime, the developed Eulerian model was used to obtain the interface information during impacting. It was found that Al, Cu and Ni particles have different impacting behaviors during their impacting on a substrate and previously deposited particles.

1 Introduction

Cold spraying (CS) is a rapidly advancing coating technique on the basis of aerodynamics and high-speed impact dynamics. Investigations on bonding mechanism of CS have important theoretical significance, and help optimize process parameters to get high quality coatings. A few papers on CS of metal powder mixtures (such as Ni/Al [1], Ni/Cu [2]) indicated it is helpful to examine the particles interfaces bonding through CS composite powders and post-spray heat treatment. Therefore, this study investigated the deposition characteristics of cold-sprayed Cu/Ni/Al composite coating by experiments and numerical simulations.

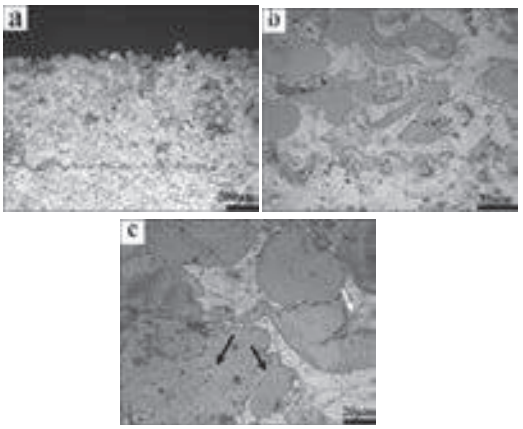

Fig. 1. Microstructure of the coating: (a) overview, (b) the bottom zone, (c) the inside of the coating.

2 Experimental procedure

The commercially available Cu, Ni and Al powders were used as the original feedstock and blended with a volume ratio of 1:1:1. FIB was used in this study to make particle cross-sections and the microstructures of the powders and as-sprayed coating were examined by OM, SEM and TEM. Numerical simulation was also used to investigate the impact.

3 Results and discussion

3.1 Microstructure of coating cross-section

Fig. 1a shows the cross-sectional microstructure of the as-sprayed Cu/Ni/Al composite deposit. Being the softest material among the three, the deformation of Al particle is the most severe. The bonding between the coating and substrate (Fig. 1b) seems close and wave and vortex-like features can be found at the interface. When observing the particle-particle interfaces, in some regions the local Al/Al interface seems to be folded as indicated by the white arrow in Fig. 1c. In addition, as shown by black arrows, some interfaces are not evident possibly due to the recrystallization of Cu. The results show a mixture of metallurgical bond and weak bonds or unbounded interfaces. So it is argued that mechanical interlocking is the main bonding mechanism in the

3.2 Bonding features between Cu/Al, Ni/Al and Ni/Cu

As for Cu on Al (Fig. 2a), it seems that deformation and spreading out of the Cu particle against the Al particle cause friction and heating of the thin Al layer adjacent to the surface [3]. Interaction of these layers with the surface results in the adhesion of the particles, and detachment from the bulk of the Al particle (as shown by black rectangular box in Fig. 2a). Small grains at the interface of Cu particle shown by the black circle in Fig.2a may suggest the recrystallization induced by impact. As for Ni on Al (Fig.

2b), there is no effective bonding in some places. The

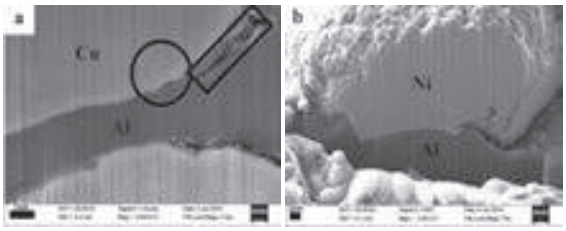

Fig. 2. Particle cross sections: (a) Cu on Al, (b) Ni on Al.

interface between particles is evident, thus again it is argued that the mechanical interlocking is the main bonding mechanism in this Cu/Ni/Al composite coating.

It is clear that the presence of an alignment of holes in the TEM sample is a sign for preferential etching of interparticle interfaces by ion milling. Some micropores observed within the structure (Fig. 3a) are possibly due to the weak grain boundaries or inner microvoids. Fig.3b shows a high dislocation density within Cu and this grain size is above 1μm. In Fig.3c, there are aligned and elongated grains in local region. In Fig.3d, the grains on both sides of the Cu/Ni interface show different appearances. In the Cu side, the nanometer grains near the interface are present compared to the inside grains which was resulted from recrystallization.

3.3 Simulation of particle interface features

The maximum plastic deformation and the temperature are concentrated at the surrounding of the contact zone rather than at the center point of initial impact. It is interesting to

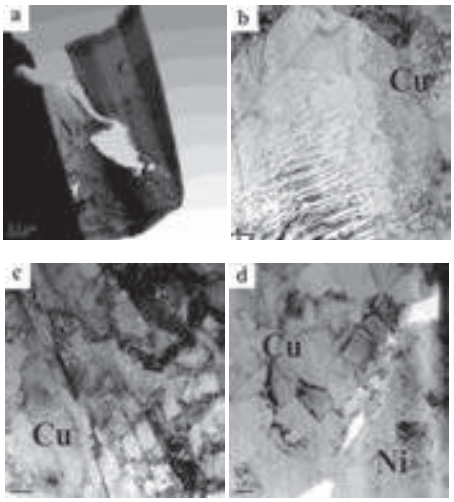

Fig. 3. TEM micrographs of (a) the Cu/Ni interface, (b) high dislocation density area, (c) elongated grains area, (d) high magnification of the Cu/Ni interface.

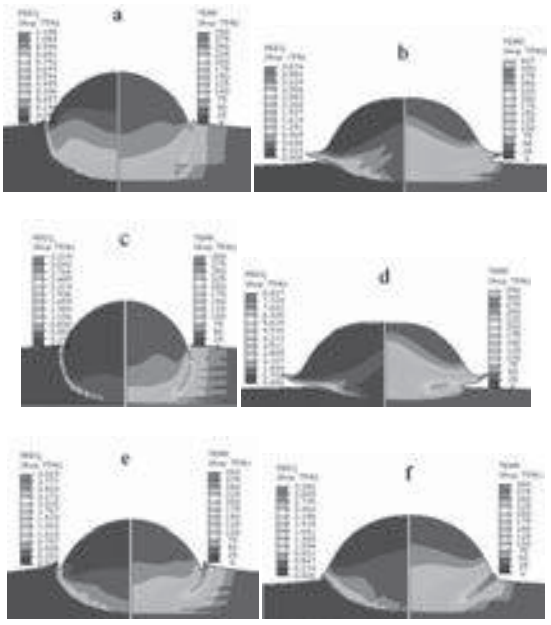

Fig. 4. Simulation results of: (a) Cu on Al, (b) Al on Cu, (c) Ni on Al, (d) Al on Ni, (e) Ni on Cu, (f) Cu on Ni.

find that the maximum interface temperature of Cu on Al is 204°C, of Cu on Al and 328°C of Cu on Ni which are higher than its recrystallization temperature (200°C) but far below its melting point (1083°C) indicating that recrystallization may happen in Cu particles which is consistent with the conclusion drawn before. The maximum temperatures of Ni and Al particles are below 280°C and 410°C respectively which are far below their respective recrystallization temperatures.

4 Conclusions

The as-sprayed Cu/Ni/Al composite coating presents a dense microstructure and the deformation of Al is the most severe; Recrystallization may has happened to Cu particle and gaps exist between the particles; The maximum plastic deformation and temperature are concentrated at the surrounding of the contact zone rather than at the center point of initial impact. From the simulation, recrystallization has happened to Cu rather than Ni or Al.

References

[1] H. Y. Lee, S. H. Jung, S. Y. Lee, K. H. Ko. Applied Surface Science. 253(2007) 3496-3502.

[2] H. Koivuluoto, J. Lagerbom, P. Vuoristo. Journal of Thermal Spray Technology. 16(2007) 488-497.

[3] P. C. King, S. H. Zahiri, M. Jahedi. Acta Materialia. 56(2008) 5617-5626.

Suspension Plasma Sprayed Thermal Barrier Coatings

Per Nylén, Nicholas Curry, Ashish Ganvir, Nicolaie Markocsan
University West, 46186 Trollhättan, Sweden

Abstract

Suspension plasma spray has become a promising technique for production of thermal barrier coatings. With the implementation of SPS using high power plasma guns, industrial application has become a reality. Particularly the use of axial feeding of the suspension as a number of drawbacks of radial feeding of the suspension.

Of particular interest in SPS spraying is the ability to generate structures that are difficult or impossible to generate via conventional powder spraying. In particular, the formation of segmented or fully columnar coatings is of great interest for TBC applications due to their inherent strain tolerance.

Columnar and segmented SPS coatings have been evaluated along with their conventional APS counterparts in both thermal shock and thermo-cyclic fatigue (TCF) testing. SPS coatings have demonstrated dramatically improved thermal shock performance and long TCF life. Thermal conductivity has been demonstrated to be in-line with or lower than conventional porous APS YSZ coatings and significantly below the dense vertically cracked APS competitor coatings.

Research is continuing into the appropriate bond coat preparation for SPS coatings; particularly as the columnar structured coatings are influenced by the underlying surface topography on which they are deposited.

Introduction

Development of Thermal barrier coatings (TBC's) have been in use for the protection of gas turbine hot section components for several decades [1],[2]. Traditionally, TBC ceramics have been applied either by air plasma spraying (APS) or electron beam physical vapor deposition (EB-PVD) [3]. Great strain tolerance and less thermal conductivity makes TBCs ideal for high temperature gas turbine application. EB-PVD can generate highly strain tolerant but higher as sprayed thermally conductivive TBCs than APS. SPS (Suspension plasma sparying) can put a siginificant balance between these two properties and hence becoming a great interest of study.

This study aims to outline the themal shock and thermal fatigue togetgher with caotings thermal properties of various SPS TBCs. However it also shows the influence of bond coat surafec roughness on the structure of axial SPS TBCs.

Experimental

Specifications of all samples produced in this work are listed in table 1 and table 2 for first and second part of this work respectively. First part of this work was dedicated to study the lifetime and thermal properties whereas in the last part dependence of microstructure on surface roughness of bond coat is discussed.

The suspension used for the first part of this study was 8 wt% yttria-stabilized zirconia (YSZ) material produced by Treibacher Industrie AG (Althofen, Austria). With a solid content of 25% by weight in ethanol and 50nm and 500nm median particle size for nano and submicron suspensions respectively. Whereas for the second part of this work the suspension used was 8 wt% yttria stabilized zirconia suspension (CrystalArc, Northwest Mettech Corp, Canada). The median particle size was 500 nanometers and solids loading of 10 wt% powder in ethanol.

Three different processes HVOF, Plasma and HVAF were used to generate different bond coat for lifetime and thermal property testing of SPS TBCs. Whereas for the surface roughness influence study only Plasma and HVAF were used. But Plasma sprayed bond coats were further modified by polishisng, grit blasting etc.

For SPS ceramic coatings deposited for thermal conductivity and lifetime purpose were sprayed using the 100HE Plasma system and the LiquifeederHE suspension feed system (Progressive Surface, Grand Rapids, MI, USA).Whereas for the surface roughness influence study they were deposited using the Axial III system (Northwest Mettech Corp, Vancouver, Canada) and Nanofeed 350 suspension feed system.

Table 1: *Different experimental TBCs systems generated for lifetime and thermal property study*

Coating ID	Bond coat method	Top coat feedstock	Top coat thickness (µm)	Surface Speed mm/s
H1	HVOF	Nano suspension	339	380
H2	HVOF		320	600
P1	Plasma		325	380
P2	Plasma		275	600
A3	HVAF	Sub-micron	303	1015
DVC	Plasma	Powder	444	

Table 2: *TBC systems generated to study the influence of bond coat surface roughness on top coat formation*

Coating ID	Surface Treatment	Surface Roughness Ra (um)	Bond coat thickness (um)
Plasma1	Polished	1-2	146
Plasma2	Polished & grit blasted	3-4	161
Plasma3	Grit Blasted	6-8	186
Plasma4	As-sprayed	11-12	183
HVAF	As-sprayed	8-9	211

The HVOF bond coats were sprayed using the gas-fuelled DJ-2600 hybrid gun (Sulzer Metco, Wohlen, Switzerland), and the air plasma spray bond coats were produced with a F4-MB gun (Sulzer Metco, Wohlen, Switzerland).The HVAF bond coat type was sprayed using the Uniquecoat M3 gun (Uniquecoat, Richmond, VA, USA).

Results

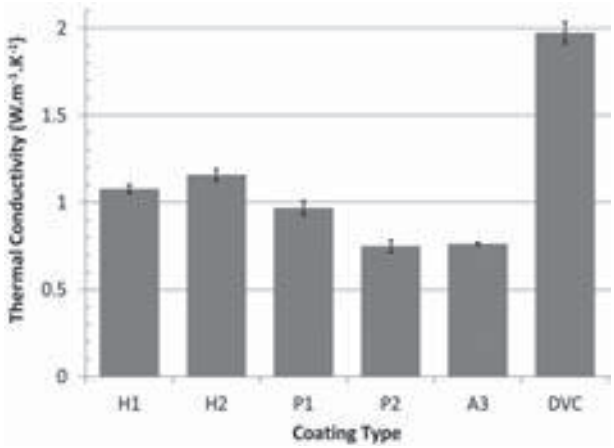

Figure 1: *Thermal conductivity of the TBC systems*

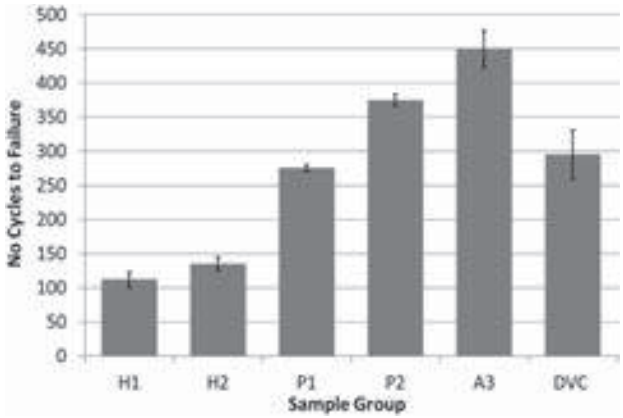

Figure 2: *Thermo-cyclic fatigue lifetime of coatings*

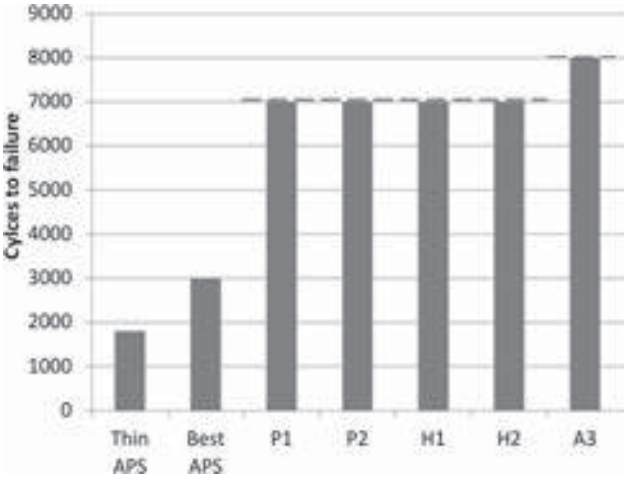

Figure 3: *Thermal shock testing data. The red dashed line indicates the number of cycles at which the test was halted*

It can be seen from figure 1, 2 and 3 that SPS TBCs have shown relatively similar thermal conductivity compare to plasma sparyed TBCs with significant porosity. Whereas it is much lower than APS sprayed DVC coatings. Since thermal fatigue failure is bond coat driven it can be seen from figure 2 that plasmasprayed and HVAF sprayed bond coat TBC system have much longer lifetime than HVOF sprayed bond coat TBC systems. However thermal shock test performance which is top coat driven failure analysis shows (figure 3) that SPS coatings have great performance compared to the APS coatings.

It can be observed from figure 4 that the greater the surface roughness of the underlying bond coat, the wider and more irregular the columns become in the SPS layer applied above. This can be correlated to the number of columns that can be observed in the top surface images. Higher density of column tops can be observed on bond coats with lower roughness.

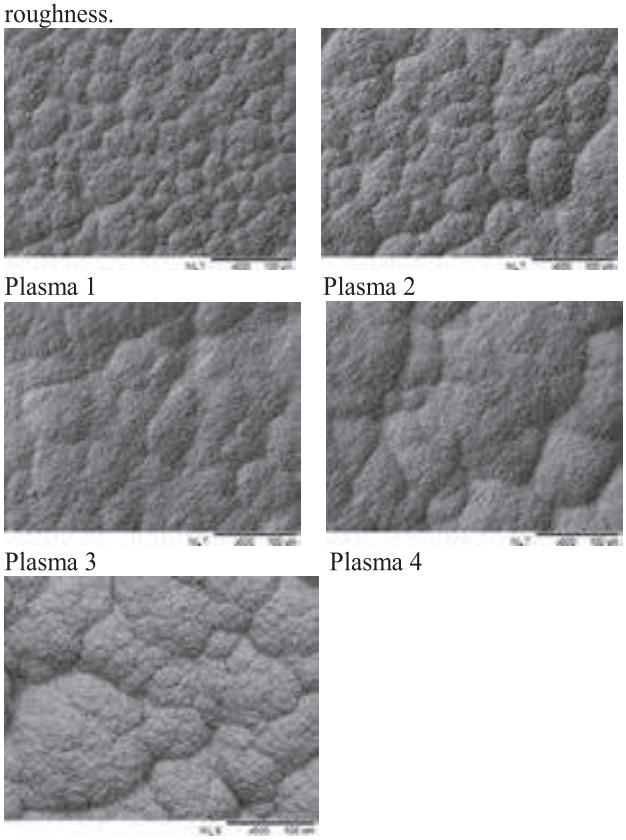

Figure 4: *Topographical top view of the SPS coatings showing the dependence of column width and randomness with surface roughness of bond coat*

Conclusion

First part of this work showed that SPS coatings have thermal conductivity in the similar ranges of APS coatings but have shown much better lifetime performance. Whereas in the second part of this work it was shown that increasing the surface roughness of the bond coat will decrease the column density and hence modifying bond coat surface roughness can influenec microstructure of SPS coatings and thus the thermal shock resistance. This relationship will be investigated in future work.

References

[1] F. O. Soechting, ―A Design Perspective on Thermal Barrier Coatings, J. Therm. Spray Technol., vol. 8, no. 4, pp. 505–511, Dec. 1999.

[2] R. Miller, ―Thermal barrier coatings for aircraft engines: history and directions, J. Therm. Spray Technol., vol. 6, no. 1, pp. 35–42, Mar. 1997.

[3] Schulz, U.; Leyens, C.; Fritscher, K.; Peters, M.; Saruhan-Brings, B.; Lavigne, O.; Dorvaux, J.-M.; Poulain, M.; Mévrel, R.; Caliez, M. Some recent trends in research and technology of advanced thermal barrier coatings. Aerosp. Sci. Technol. 2003, 7, 73–80.

Cavitation erosion resistance characteristics of HVOF and HVAF processed 86WC-10Co4Cr hydro turbine coatings

R.K.Kumar[1], M.Kamaraj[2], S.Seetharamu[1]

[1] Materials Technology Division, Central Power Research Institute, Bengaluru 560 080, India
[2] Department of Metallurgical and Materials Engineering, Indian Institute of Technology -Madras), Chennai 600 036, India

Abstract

The hydro plants utilizing silt-laden water for power generation suffers from severe metal wastage due to both particle induced erosion and cavitation. High Velocity Oxy-Fuel process (HVOF) based coatings is widely adopted to improve the erosion life. The High velocity Air Fuel (HVAF) technology, provides higher particle velocities and lower spray temperatures and gives dense and substantially non-oxidized coating. The cavitation resistance of 86WC-10Co4Cr type HVOF coating processed at 740m/s spray particle velocity has been compared with two HVAF coatings made at 895m/s and 1010m/s. The mechanical properties such as porosity, hardness, indentation toughness and cavitation resistance were investigated. The progress in the surface damage morphology during cavitation was analysed in SEM. The weight loss of cavitated surface was measured at different intervals. The homogeneity of the cohesion between different layers has been examined qualitatively through the measurement of scratch depth across the cross section. The HVAF coatings have shown lower porosity level, higher hardness and improved cavitation resistance. Both delamination and complete detachment of the WC grains was observed in HVOF coating while the volume of the affected area is considerably low in HVAF coating.

1. Introduction

The components of hydro plants utilizing silt-laden water for power generation suffers from severe metal wastage due to high velocity particle induced erosion and cavitation. Most of the service failures are attributed to the combined effect of cavitation and silt assisted erosion [1-2]. The phenomenon of cavitation erosion gets aggravated under high turbulent conditions of fluid flow containing the suspended particles [3-5]. The application of WC based hard coatings processed through HVOF is widely adopted to achieve improved service life. The cavitation resistance performance is readily affected by their hardness and toughness properties. The spray particles get heated up to a relatively higher temperatures and thus occurrence of W_2C phases due to decarburization is well known in HVOF coatings. The HVAF technology utilizes air–fuel mix combustion rather than oxygen-fuel mix, provides higher particle velocities coupled with lower spray temperatures... The potential of HVAF technology in terms of superior abrasion and slurry wear resistance has been well reported [6,7]. However, the cavitation resistance of WC-CoCr coatings is not widely reported.

2.0 Experimental program

2.1 Materials and coating preparation

Two HVAF coatings of 86WC-10Cr-4Co processed at particle velocities of 1010 m/s and 895 m/s and one HVOF coating at particle velocity of 740 m/s were made onto stainless steel substrate. The sintered and agglomerated type spray powder of 1.2µm carbide grain was used. The coating morphology, porosity, hardness and the indentation toughness of coatings was evaluated at a test load of 10 kg on the coating cross section. The cavitation erosion resistance was evaluated using a vibratory type cavitation test rig for duration of 10 hours. The diamond polished specimen of size 15x15x7 mm^3 was used.

2.2. Mechanical properties:

The Vickers hardness of the coating was measured on the cross section at a test load of 300gm and the porosity was measured on the polished surface of the coatings by metallography. The average of eight hardness readings was reported. The toughness of coatings were measured based on the crack length appeared under the test load of 10kg on the cross section and the fracture toughness was calculated according to Evans and Wilshaw equation.

Table-1: *Mechanical properties of coatings*

Coating	Spray gun / Nozzle	Hardness (HV0.3)	Porosity	Fracture toughness (MPa√m)
HVOF	JP-5000	1180±70	0.98	3.34±0.7
HVAF-1	AK-06/5L	1320±40	0.46	6.1±0.6
HVAF-2	AK06/5O	1473±40	0.42	7.1±0.5

The hardness of the HVAF coatings was comparatively higher than that of the HVOF coatings. The porosity of the coatings is also comparatively lower than that of HVOF.

2.2.1 Cavitation Erosion Resistance:

The cavitation erosion test was conducted using a commercial ultrasonic processor as per ASTM G32-03 [8]. Tap water was used as the solution. The test specimen of size 15 x 15 mm^2 was secured below the oscillating horn tip with a gap of 1 mm. The frequency of the oscillator was 20 kHz and the peak to peak amplitude was 100µm. The weight loss of coatings was recorded after every 1hr using an analytical balance with 0.01 mg resolution. Multiple specimens were used for varied exposure tests. The tests were continued upto10 hours until a steady rate of erosion loss was achieved. Fig.1 shows cumulative weight loss of all three coatings. All the coatings have shown progressive metal loss with cavitation time. The reduction in mass loss of HVAF coatings after 10 hr. cavitation is observed to be in the range of 4 to 8. The steady rate of metal loss due to

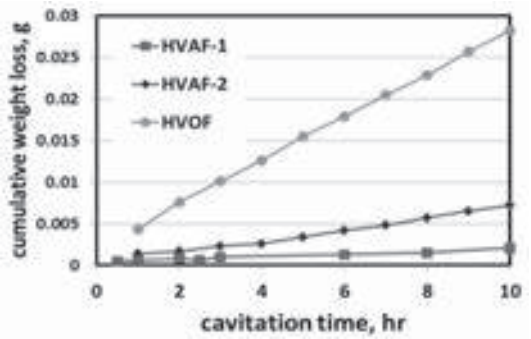

Fig. 1. *Weight loss of coating with cavitation time*

cavitation of HVAF is observed to be much lower (0.23 to 0.78mg/h) compared to 2.96 mg/h in HVOF coatings.

2.2.2 Scratch resistance measurements :

The measurement of interfacial cohesive strength of both HVOF and HVAF coatings was attempted qualitatively through scratch testing of the coatings on the cross section, under max. load of 200mN and the scratch velocity of 10µm/s in a G200 Nano Indenter. The Berkovich indentor was traversed from the interface to the surface as well as from surface to the interface and the scratch depth was monitored. Fig.2 shows the results of the scratch depth measurements.

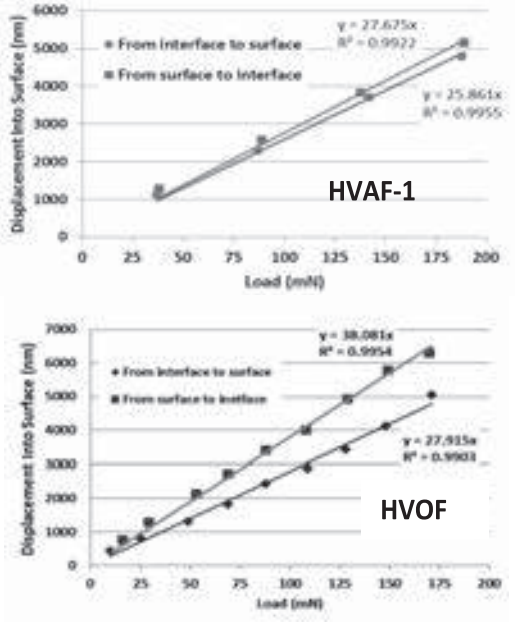

Fig. 2. *Scratch depth measurements of coatings*

It has been observed that the HVAF coatings show nearly a uniform increase in depth during both directional movements of the indenter. However, HVOF coatings show varied scratch depth with load indicating that the varied cohesive properties particularly at increased loads.

2.2.3 Surface damage profiles :

The evolution of surface damage during cavitation is observed through SEM and results are shown in Fig.3. The damage is observed to be initiated in the regions of porosity and progresses during continued exposure resulting in large craters in the affected areas. The HVOF coatings have shown formation of deep pits with evidence of delamination of coating layer. The HVAF coatings have exhibited comparatively flat macro-eroded surface with absence of deep pits and the volume of the affected area is considerably low.

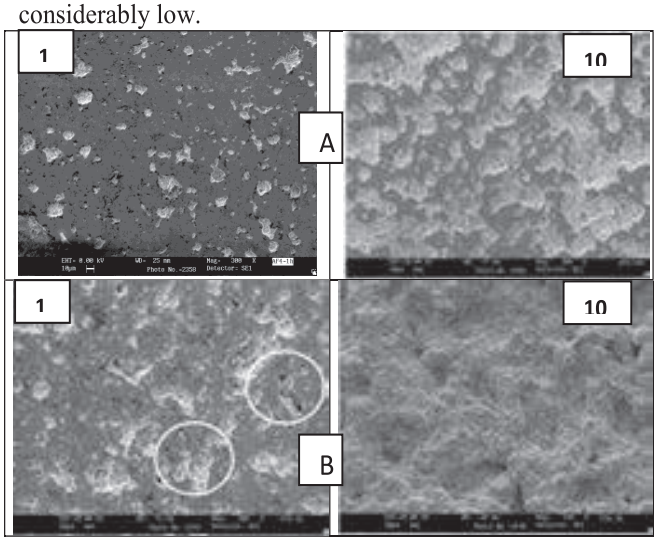

Fig.3. *Surface damage profiles of HVAF-1 (A) and HVOF Coatings (B) after 1h and 10h exposure*

Under the conditions of low cohesive strength of built-up layers in the coating coupled with localized bubble implosion pressures, delamination of the layers becomes the mode of metal removal giving rise to increased rate of metal loss. The higher particle impaction velocities achieved during the HVAF process provides improved cohesion properties and hence the cavitation resistance.

3.0 Conclusions:

The systematic study on the comparative cavitation resistance of both HVOF and HVAF processed tungsten carbide coatings indicate the following.

- HVAF coatings exhibit lower porosity, higher hardness and improved cavitation resistance compared to HVOF coatings. The higher toughness values and consistency in scratch depth results in HVAF coatings support this finding.
- Both delamination and complete detachment of the WC grains is observed in HVOF and the improvement factor in cavitation resistance of HVAF is up to 4.0.
- The particle velocity appears to play an important role achieving dense coating with lower porosity, improved cohesive strength and cavitation resistance in thermal spraying of 86WC-10Co4Cr powders
- Coating with combination of higher toughness and low porosity are considered important for achieving improved cavitation resistance.

4.0 References:

1. R.Singh, S. K. Tiwari, and S.K. Mishra, J. Mat.Engg. and Perf. 21.7 (2012), 1539-1551.
2. H.K.Sharma, J.K.Sharma, R.S.Chauhan, 3rd Intl. Conf. on Silting Problems in Hydro Power Projects, (2008), 27-28 Feb. 2008, New Delhi
3. T.Okada, Y. Iwai, K. Awazu, Wear 133(1989), 219-232
4. Y.Iwai, T.Okada, S. Tanaka, Wear 133 (1989), 233-243
5. C.Haosheng, L.Shihan, Wear 266.1 (2009), 69-75
6. L. Jacobs, M. Hyland, and M. De Bonte, J.Therm. Spray Technol., Vol.7 (No.2), 1998, 213-219.
7. Robert. J.K. Wood, Intl.Jl. of Refractory metals, 28 (2010), 82-94
8. ASTM Std.G32, Annual Book of AST Stds V3,(2003)

Fabrication and Repair of Components By Cold Spray Process

J. Karthikeyan and C. M. Kay

ASB Industries Inc., Barberton, OH 44203.

Cold sprayed coatings/freeforms have many advanced characteristics such as near theoretical density, phase purity, no grain growth, compressive residual strength, etc. Cold spray process has high deposition efficiency (60-95%) and deposition rate (40-65 g/min) with most metals, alloys and composites. Cold spray can produce well bonded ultrathick coatings on dissimilar materials with minimum masking and surface preparation requirements. Moreover, it imparts minimum heat input into the substrate. These unique advantages make cold spray process to be an ideal tool for both free form fabrication and component repair.

Various materials including pure metals (Cu, Ta), alloys (SS, Inconels) and composites (Al-B_4C, Mo-Ti) have been cold spray processed to obtain ultrathick coatings. Systematic spray experiments have yielded good quality coatings at acceptable DE and DR values. Coating characterization before and after post-spray heat treatment has resulted in a data bank that can be used for both component fabrication and repair.

Various shapes including flat plates, pipes, crucibles, etc have been fabricated for different industrial applications. Different surface finishes and features such as grooves, threads, etc have been machined onto the coatings to meet the application requirements of the components. At present, cold spray is also routinely used for repair/refurbishment of a large number of aerospace components and other industrial parts.

Control of Thermal Spray Process through Flattening Phenomenon of Individual Particles

Masahiro Fukumoto
Department of Mechanical Engineering, Toyohashi University of Technology, Toyohashi, Aichi 441-8580, Japan

Abstract
Several kinds of metallic and ceramic powder particles were thermally sprayed onto the mirror polished metallic substrate and the effect of both substrate temperature and ambient pressure on the splat shape of the particle has been systematically investigated. In the flattening of the sprayed particle onto the substrate surface, critical conditions were recognized both in the substrate temperature and ambient pressure. That is, the splat shape changed transitionally from splash type to disk one on that critical temperature and pressure range, respectively. A transition temperature, T_t, and transition pressure, P_t, were defined and introduced, respectively for those critical conditions. Correspondingly, the coating adhesion strength changed transitionally on that critical temperature and pressure range, respectively. Since an equivalency in both transitions was recognized, three dimensional transition curvature, given by combining the transition temperature and transition pressure dependence, was proposed as a practical and effective controlling principle for the thermal spray process. The fact that the dependence of both transition temperature and transition pressure on the sprayed particle material had similar tendency indicated that the dynamic wetting of the substrate by the molten particles thermally sprayed seemed to be a domination in the flattening.

1 Introduction

The reliability of the thermal spray process has not been always established due to its lower controllability. As a flattening of an individual particle on the substrate is a fundamental element for the coating formation, coating microstructure and corresponding properties, such as a porosity and adhesion strength, depend strongly on the flattening nature of an individual splat. Therefore, it is necessary to investigate in detail the nature on the flattening behavior of the sprayed particles, not only for scientific interest, but also for practical consequence. Up to today, effect of process factors on the flattening of an individual particle onto flat substrate surface has been investigated, through theoretical, numerical and experimental methods [1]. However, the splat formation nature of the particles is not fully understood yet.

In this study, the flattening nature of an individual thermal sprayed metallic and ceramic particle collected on the flat substrate surface with various temperatures and/or ambient pressures were investigated. In particular, the paper focused on the controlling principle for thermal spray process and splat formation mechanism through the observation on an individual splat.

2 Experimentals

Commercially available metallic and ceramic powders with diameter of several tens micrometers were used as feedstock materials. AISI304 stainless steel plates with dimensions of 25 mm×25 mm×6 mm finally polished with 0.3μm Al_2O_3 buff prior to spraying were used as substrates. Sprayed particles were collected on the substrate surface using atmospheric and low pressure plasma spray equipment. The number of the particles deposited onto the substrate in one passing of the shutter was around one hundred. The splat shape was cllassified and the number of both disk splat and splash splat were counted on every trial. The fraction of disk splat was defined as the ratio of the number of disk splat to the total splat. The cross section microstructure of the splat was observed using a scanning ion microscope, SIM and transmission electron microscope, TEM after cutting the splat by focused ion beam microscope, FIB.

3 Results and discussion

3.1 Transition in substrate temperature

The measurement results of the dependence both of the splat shape and coating adhesion strength on the substrate temperature in Ni is shown in Fig. 1. From the figure, a transition of the splat shape can be recognized, namely, while the splat on the substrate with room temperature range shows a splash shape, it undergoes a transition to a disk-shaped splat with the increase of the substrate temperature. Actually, most of the metallic and ceramic materials showed such transition by increasing the substrate temperature. The transition temperature, *Tt*, was defined as the critical temperature above which half of the splat had disk shaped. Meanwhile, the adhesion strength of the coating fabricated under the same process increased drastically and transitionally with the increase of substrate temperature clearly as shown in Fig. 1. Its dependence on the substrate temperature corresponds quite well to that of the splat shape, indicating that the flattening nature of the individual splat has a strong influence on the coating property.

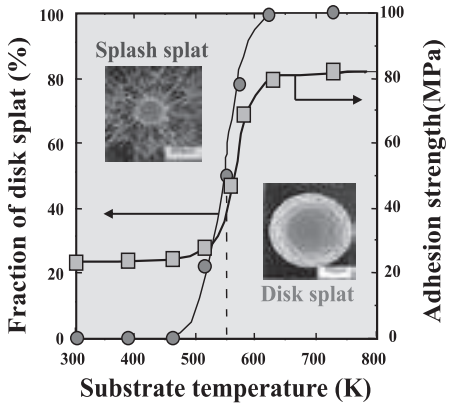

Fig. 1. *Dependence both of fraction of disk splat and adhesion strength on subsrtare temperature.*

3.2 3-D Transition curvature

Dependence of both individual splat shape and adhesion strength of the coating on the ambient pressure was also investigated systematically while keeping the substrate at room temperature. It was found that the splat shape changed

from splash type to disk one with decrease of ambient pressure. The adhesion strength changed correspondingly to the change of the splat shape with decrease of ambient pressure. The transition pressure, *Pt*, was defined as the critical pressure at which the fraction of disk splat exceeds 50% with reducing the ambient pressure. Common porous microstructure was observed on the bottom surface of the splash splat obtained at room temperature or at an atmospheric pressure condition, while the disk splat given at elevated temperature or reduced pressure condition had common dense microstructure entirely on its bottom surface. Namely, substrate temperature and ambient pressure have an equivalency on the transition in the splat formation.

By combining the dependence of fraction of disk splat both on the substrate temperature and the ambient pressure, a three-dimensional transition curvature concept was established. As a confirmation on this hypothesis, three-dimensional transition curvature for several kinds of metallic particles were measured based on the experimental data. Typical examples for Ni and Cu particles were shown in Fig. 2. Higher adhesion strength and the corresponding properties in the fabricated coating can be given by either substrate preheating or ambient pressure reduction in the thermal spraying. Hence, thermal spray process can be controlled more effectively by these curvature database.

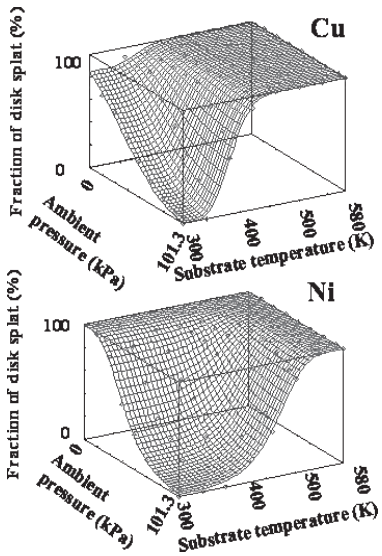

Fig. 2. *Experimental three dimensional transition curvature for Cu and Ni particles onto AISI304 substrate.*

3.3 Transition mechanism

To understand on the transition mechanism in the splat shape, solidification microstructure of thermally sprayed particle was observed both on the bottom surface and the cross section. On the bottom surface of the splat obtained at heated substrate or reduced pressure conditions indicated that ring shaped dense zone with fine microstructure was observed near peripheral zone. This fine microstructure near peripheral zone indicates that rapid solidification occurred at this region. To confirm the solidification inside of the splat and to elucidate the effect of rapid solidification on the flattening, cross section microstructure of the splat was precisely observed by SIM. The results are shown in Fig. 3. In the splat collected on the room temperature substrate under atmospheric pressure (Fig. 3(a)), coarser columnar grains perpendicular to the substrate surface are observed in whole part of the splat. On the other hand, in the splat collected on the heated substrate, more finer columnar grains inside of the splat are observed in whole part of the splat (Fig. 3(b)). Finer structure indicates that faster solidification occurred in this splat given on the heated substrate. However, since columnar solidification structure is generally formed after the flowing of the liquid, it is clear that the solidification inside of the splat never affect the flattening of the splat.

A layer composed with equiaxial fine grain, so-called chill crystal, exists near bottom part of the splat as shown in Fig. 3(a) and (b). Chill layer in the splat given on the heated substrate is much thicker than that on the unheated substrate, and the thickness of the layer increases gradually to the radial direction. Especially, this rapid solidified layer become thicker toward periphery of the splat, indicating that ultra rapid increase of the splat viscosity occurs near peripheral region and acts as the restrain for the splashing. This is exactly a new hypothesis established in this study. For the disk splat under reduced pressure condition, both similar fine columnar structured grain and the chill crystal layer near interface can be found at peripheral region (Fig. 3(c)). However, the fraction of the chill layer under low pressure condition is much smaller than that in the heated substrate.

The above hypothesis was verified on the ceramic materials. While chill structure was not observed in ZrO_2 disk splat, an amorphous layer was observed at bottom part of the Al_2O_3 splat near peripheral region. More precise, systematic observation has to be done in the future study.

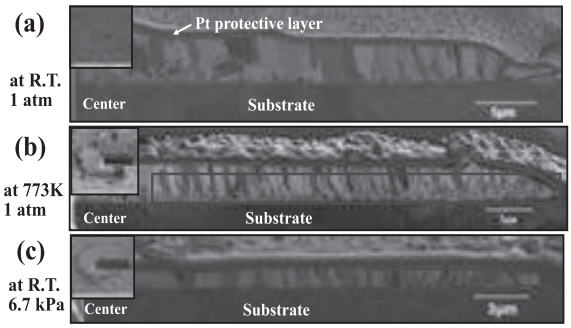

Fig. 3. *Cross section microstructure of Cu spltas obtained at each condition.*

4 Summary

By combining the transition curve both on the substrate temperature and the ambient pressure, a three-dimensional transition curvature was installed. Thermal spray process can be controlled more effectively by the 3-D curvature database. Chill crystal layer composed with equiaxial fine grain existed at bottom part of the splat. This rapid solidified layer become thicker toward periphery, indicating that ultra rapid increase of the splat viscosity occurs near peripheral region and acts as the restrain for the splashing.

5 References

[1] P. Fauchais, M. Fukumoto, A. Vardelle, and M. Vardelle: J. Therm. Spray Technol., **13(3)** (2004) 337-360.

Role of oxide dispersion on the high temperature oxidation and hot corrosion resistance of NiCrAlY bond coat

V.S. Raja, G. Sreedhar[#]
Department of Metallurgical Engineering and Materials Science, Indian Institute of Technology Bombay, Mumbai-400076, India
[#] Electropyro Metallurgy Division, CSIR-Central Electrochemical Research Institute, Karaikudi-630006, India

Abstract
Graded bond coatings of functionally graded thermal barrier coatings (TBCs) are meant to minimize coeffient of thermal expansion mismatch between bond coat and top coat for reducing thermal shock resistance of TBCs. However, oxide dispersion in graded bond coats can alter their high temperature oxidation resistance and hot corrosion. A systematic work was carried out in our laboratory to understand this aspect. Yttria stabilized zirconia (YSZ), magnesia stabilized zirconia (MSZ) and alumina (Al_2O_3) were taken as model oxides for dispersion whose effects were examined. Hot corrosion kinetics of these coatings showed that the oxide dispersion indeed is detrimental to high temperature chemical stability of the metallic phase of the graded bond coatings with respect to oxidation as well as hot corrosion, although there seems to exist threshold levels of dispersed oxides below which their detrimental effects are minimal. Thus, the work suggests the fact that it is possible to develop oxide dispersed bond coatings so as to have optimal service life aginst two different failures.

1. Introduction

Thermal barrier coatings (TBC) are used to protect hot section components of gas turbine engines [1]. A typical TBC applied on these components consists of a first layer of bond coat followed by a ceramic top coat. During service, a thermally grown oxide (TGO) forms *in-situ* between the bond coat and ceramic top coat offering protection against high temperature corrosion of the bond coat. However, occurrence of strains due to mismatch in thermal expansion co-eficient among these layers and thickening of TGO, spallation of the top (ceramic) coating occurs. In order to maximize the strain tolerance of the ceramic coat, research is focussed on newer coating coatings based on techniques like electron beam physical vapor deposition (EBPVD), solution precursor plasma spray (SPPS). But the coatings developed by these techniques lose-out on account of thermal conductivity which is one of the main requirements a top coat has to meet. Hence, there is a need to develope graded TBCs to lower thermal strains.

Only a few researchers have developed functionally graded coatings to enhance thermal cycle life of TBCs [2-5]. In such coatings, multilayered bond coats with increasing proportions of oxides from the bond coat to the ceramic top coat, have been applied as graded coating over the so called bond coat. By means of modelling, these coatings have been shown to exhibit very high resistance to thermal shocks over a large number of cycles [4,5]. While the oxide dispersion has been found to be beneficial towards tolerating thermal shocks, it should, however, be pointed that these studies did not take into account the role of oxide dispersants on high temperature oxidation and hot corrosion resistance of the oxide dispersed bond coatings. Hence a detailed study was undertaken in our laboratory to examine the role of these dispersed oxides on high temperature oxidation and hot corrosion. This paper outlines the important findings and suggests the limitations within which the graded coatings can be employed. More detailed work can be found in the references [6-8].

2. Experimental Methods

The experimental strategy employed to study the effect of oxide dispersion on high temperature oxidation and hot corrosion was as follows. Three different types of oxide powders, namely, 8% yttria partially stabilized zirconia (YSZ), magnesia stabilized zirconia (MSZ) and alumina (Al_2O_3) and NiCrAlY were used. Firstly, oxide-NiCrAlY powders of known proportions were first obtained by mixing appropriate proportions of oxides and NiCrAlY in a ball mill. Each of the mixtures were then applied as coating on Inconel 718 substrate using air plasma spray (APS) technique. All the faces of the substrate (Inconel 718) were covered with oxide-NiCrAlY powder coating. The kinetic parameters were obtained based on mass gain measurements. The formed oxides were examined using energy dispersive x-ray spectroscopy (EDS), scanning electron microscope (SEM) and x-ray diffraction (XRD). Further details of the experimental procedures employed can be obtained from the references [6-8].

2.1. Effect of YSZ dispersion on oxidation of NiCrAlY

Sreedhar [8] extensively investigated the role of YSZ content and alumina on the oxidation for his doctoral research. Typical weight gain plots of NiCrAlY with and without YSZ obtained at 800 ^{o}C is illustrated in Fig. 1a. Notably, in comparison with the plain NiCrAlY coating, its oxide dispersed counterpart was found to exhibit lower "apparent" weight gain (Fig. 1a) indicating that the oxide addition is beneficial in enhancing the oxidation resistance of the coating. However, the author noted that the oxide phase must be unaffected by high temperature exposure and hence must not contribute to the gross weight gain as brought out in plots of Fig. 1a. The true mass gain, occrued by the metallic phase was calculated by normalizing the apparent weight gain by the coating with respect to the volume fraction of the metallic component, namely, NiCrAlY.

The normalized data as brought out in Fig. 1b showed that the oxidation kinetics of the metallic component is accelerated due to the presence of oxides. Overall, the coatings exhibited rate constants in the range of 10^{-6} mg cm^{-4} s^{-1} with respect to their oxidation. Further, it was found that the beyond 57 vol.% of the oxides in NiCrAlY, the

oxidation tendency of the metallic phase tends to become quite high.

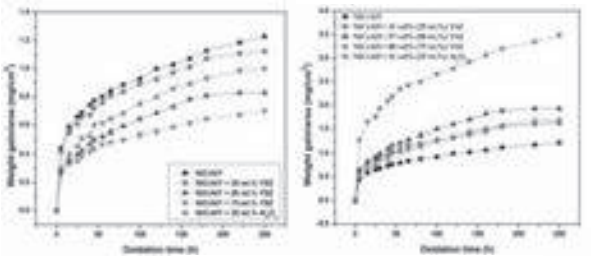

(a) (b)

Figure 1: (a) Weight gain and (b) normalized weight gain plots for coated specimens subjected to oxidation at 800 °C for 250 h [8].

2.2. Effect of YSZ dispersion on hot corrosion of NiCrAlY

Just to show the trend on the hot corrosion resistance of NiCrAlY with respect to oxide dispersion, normalized weight gain plots of weights gains of YSZ, alumina and MSZ dispersed NiCrAlY exposed to Na_2SO_4 + 50 wt% V_2O_5 salt at 800 ^oC are shown in Figure 2. Comparing the plots of Fig. 1b with those shown in Figs. 2 leads to the fact that high temperature oxidation is less severe than hot corrosion. Such a trend is in agreement with the fact that bond coatings are more prone to hot corrosion than high temperature oxidation [9]. It also looks that in the vanadate medium MSZ behaves almost similar to that of YSZ. The variation of rate constants with oxide contents in the case of YSZ and alumina in the vanadate salt is brought out in Fig. 3. The plot shows that there exists some threshold level of oxide dispersion beyond which they become responsible for very severe hot corrosion . Comparison of the rate constants (k_p) of the oxide dispered NiCrAlY in vanadate medium with those of the same coatings obtained obtained in air is imperative to get an idea of the severity of the two types of high temperature corrosion namely, hot corrosion and oxidation.

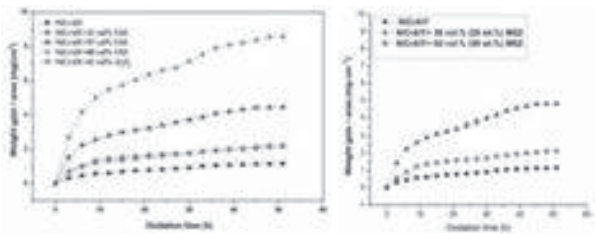

(a) (b)

Figure 2: Normalized weight gain plots corresponding to the hot corrosion tendency of (a) YSZ dispersed NiCrAlY and (b) YSZ dispersed NiCrAlY constituent of the coating at 800 °C [7,8].

Notably, the coatings showed k_p values in the range of 10^{-6} mg cm^{-4} s^{-1} with respect to their oxidation, while they showed rate constants in the range of 10^{-5}-10^{-4} mg cm^{-4} s^{-1} with respect to hot corrosion again suggesting that they coatings suffer more severe attack in molten salts (due to hot corrosion) than in air (high temperature oxidation). Examination of the cross-section of the coating (Fig.4) subjected to hot corrosion revealed that the splat boundaries suffered preferential corrosive attack due to hot corrosion. The degradation of t-ZrO_2 phase seems to accelerate spallation tendency of the oxide dispersed coating.

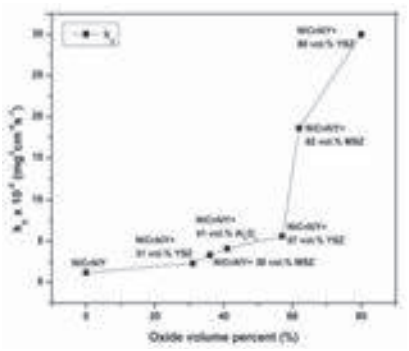

Figure 3: The rate constant (k_p) variation plot for to the hot corrosion of NiCrAlY at 800 °C with respect to oxide content in the coating [8].

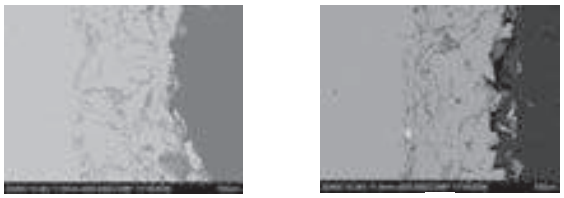

(a) (b)

Figure 4.: Back scattered cross-sections images of (a) plain NiCrAlY and (b) NiCrAlY + 75wt.% YSZ coatings exposed to Na_2SO_4 + 50 wt.% V_2O_5 environment at 800 °C [6].

3. Summary

The study shows that the oxide dispersion is detrimental to high temperature oxidation and hot corrosion of NiCrAlY. Between the two types of attack the latter is more aggressive. There seems to exist some threshold oxide level below which the oxide can cause less damage. This concept can be used to hornest the beneficial effects of oxides in developing graded TBCs.

References

[1] D.R. Clarke. C.G Levi, Annu. Rev. Mater. Res. 33 (2003) 383–417.

[2] Y.P. Wang, S. Sampath, V. Prasad, R. Williamson , J. R. Fincke. J. Mater. Process. Technol. 137 (2003) 110-116.

[3] J.H. Kim, M.C. Kim, C.G. Park. Surf. Coat. Technol. 168 (2003) 275-280.

[4] Zhihai Han, Bingshi Xu, Haijun Wang, Shikui Zhou. Surf. Coat. Technol. 201 (2007) 5253-5256.

[5] S. Rangaraj, K. Kokini. Surf. Coat. Technol. 173 (2003) 201-212.

[6] G. Sreedhar, M.D. Masroor Alam, V.S. Raja. Surf. Coat. Technol. 204 (2009) 291-299.

[7] G. Sreedhar, V.S. Raja. Corros. Sci. 52 (2010) 2592-2602.

[8] Sreedhar G., Doctoral thesis, Role of oxide dispersion on oxidation and hot corrosion behavior of NiCrAlY bond coat, Indian Institute of Technology Bombay, Mumbai, INDIA 2011.

[9] S. Mohsen, Afrasiabi Abbas, K. Akira. Transactions of JWRI, 36 (2007) 41-45.

Room Temperature Impact Consolidation (RTIC) of Fine Particles on Aerosol Deposition Process

Jun Akedo
[1] National Institute of Advenced Industrial Science & Technology (AIST), Tsukuba Ibaraki, Japan.

Abstract
A coating process such as Aerosol Deposition (AD) method and Cold Spray (CS) method, which is based on collision of particle materials, attracts attention recently. Those coating techniques deferent from conventional thermal spray method, among spray coating may use only mechanical impact pressure to form the material layer.
AD method is a unique approach for depositing films, where solid state submicron metal and ceramics particles (both oxide and non-oxide) are accelerated by gas flow up to 100 - 500 m/s and then impacted onto a substrate. It can form rapidly a thick, dense and hard metal and ceramic layer at room temperature without additional heating for solidifying starting powders, even in low vacuums, using relatively cheap and simple production facilities. We named this phenomenon "Room Temperature Impact Consolidation (R.T.I.C)". It is expected to reduce energy, cost, difficulty to fabricate the thin or thick film with complicate material compositions and the number of processes during fabricating electronic devices and others, as well as to improve their performances substantially.
In this presentation, the deposition mechanism of the AD process with RTIC phenomenon and comparison with other similar coating methods are explained. And its application to protection coating for erosion and weir of structural materials, energy related devices such as all solid state Li-ion battery (LIB), dye sensitized solar cell (DSC) etc., and its practical use example also are also introduced.

1 Introduction

Recently, Aerosol Deposition (AD) method has been made attention as room temperature ceramic coating technique. AD method is a unique approach for depositing ceramic films, where solid state submicron metal and ceramics particles (both oxide and non-oxide) are accelerated by gas flow up to 100 - 500 m/s and then impacted onto a substrate. It can form rapidly a thick dense, uniform and hard ceramic layer at room temperature without additional heating for solidifying starting powders, even in low vacuums, using relatively cheap and simple production facilities. This deposition phenomenon of solid state particles was called as Room Temperature Impact Consolidation (RTIC) [1]-[2]. It is expected to reduce energy, cost, difficulty to fabricate the thin or thick film with complicate material compositions and the number of processes during fabricating electronic devices and others, as well as to improve their performances substantially. In this presentation, the history of coating process based on collision of solid state particle, which include AD method is introduced. The difference between the AD method and the Cold Spray (CS) method, which is well known in the field of thermal spray coating technology as similar technique of AD method, and the future prospect of AD method will be presented.

1. Aerosol Deposition method

The AD method is based on shock-loading solidification due to the impact of ultrafine ceramic particles with a surface [1], [2]. First, particles are mixed with a gas to generate an aerosol. This aerosol is ejected through a nozzle at low pressure, and impacted onto a substrate to form a thin layer. During impact with the substrate, part of the particle's kinetic energy is converted into thermal energy that raises the temperature of the particle and promotes bonding between the substrate and the particles and also between multiple particles.

The AD apparatus is made up of two vacuum chambers connected by a tube. The first chamber is an aerosol-generation chamber, and the second chamber is a deposition chamber. The deposition chamber is used for the formation and patterning of layers.
The aerosol chamber has a carrier gas system and a vibration system to mix the powder with the carrier gas. The aerosol generated in the aerosol-generation chamber is delivered to the deposition chamber by a pressure difference between the two chambers. The deposition chamber contains a nozzle, substrate with heating system, and a mask alignment system, used for making patterned layers. A rotary vacuum pump coupled to a mechanical booster pump is used to evacuate this chamber to a pressure of about 1-50 kPa during deposition. The scale up of AD apparatus is easy because of a simple principle and low vacuuming condition.
Sintered, ceramic powders with a particle size range of about 0.08 – 2 μm are typically used as the deposition particles. After suspension in the carrier gas to form an aerosol, the aerosol is accelerated to several hundred m/sec though an orifice with diameter less than 1 mm. To form layers with acceptable density and material properties, particles with a particular size and morphology must be preferentially used.

2. Room Temperature Impact Consolidation (RTIC)

For the AD method, high-speed layer formation of ceramic layers at room temperature with high density and high transparency is possible by optimizing the particle diameter and deposition conditions. The result is a process that yields acceptable solidification without the need for high-temperature heat treatment. We call this process Room Temperature Impact Consolidation (RTIC) [1], [2].

The AD layer has high density and randomly oriented polycrystalline nano structures with crystallite size less than 20 nm. TEM and electron diffraction imaging did not show either amorphous layers or hetero structures at the boundary of crystal grains. XRD profiles confirmed that the spectral phases of the α-Al2O3 particles were retained in the deposited layer. However, broadening of the spectra and a slight shifting of the spectral angle were observed. The reason for the change between the spectra of the particles and the deposited layer may be due to reduction of the layer crystal size or distortion during deposition. The densification mechanism in detail was described in reference [1]. Clear lattice images in crystal grains less than 10 nm were observed, as well as uniform microstructures at the boundary between the substrate and the deposited layer. For α-Al2O3 layers deposited at room temperature, layer density was over 95% of theoretical density and Vickers hardness was over 1600 Hv. Such α-Al2O3 layers are acceptable for use as wear resistive coatings. The layer hardness increased with increasing particle-impact velocity, and sometimes was higher than that of the bulk material, which was sintered at a high temperature. The particle-impact velocity during deposition was estimated by newly developed measurement system based on combination of cutting a flow and ‘‘time-of-flight registration’’ measurements. Critical particle velocities for acceptable RTIC ranged from 100 - 500 m/sec, and the velocity needed to create layers with acceptable hardness tended to increase with increasing sintering temperature of a particular ceramic material.

The RTIC phenomenon was observed not only for oxide materials, but also for non-oxide materials. In either case, particles with diameter greater than 80 nm and with single crystal structure are needed to make layers with acceptable hardness. The crystal grain size of as-deposited layers was less than 50 nm, which was smaller than that of the starting particles. The reason for this is apparently that the starting particles break down during collisions and then each particle bonds together to form a nano-crystal layer.

3. Difference between AD method and CS methods

With AD method and CS method, highly dense and hard layers having a thickness of several mm can be obtained with relative ease. In addition, these methods seem to be very practical methods due to the simplicity of device structure. But, for the CS method, the formation of ceramic layers was not reported at all, though there were many reports for the formation of metal and metal alloy layers. In addition, for low melting point materials such as Al, Ni or Cu, the particle impact velocity to obtain the formation of a coating, known as critical velocity, was very high, ranging between 500 and 700 m/sec. In contrast, high temperature melting materials such as α-Al2O3 can be deposited at room temperature by the AD method. The particle impact velocity is low and ranging between 150 and 400m/sec. The deposition properties are different from that of the CS method. For the AD method, the kinetic energy, particle diameter and velocity of the particles are smaller than that in the CS method. These results can be explained by the two factors as follows. The first is that particle impact velocity on the CS method using the small particles less than 5μm in diameter is reduced by the reflection the jet flow and by resistance of the air layer near the substrate in atmospheric conditions. As a result, impact velocity and pressure in the CS method are not enough to produce the RTIC phenomenon, though the particle velocity just after ejection from the nozzle is very high. It is believed that a critical particle mass is necessary to overcome the slowdown resistance by the atmospheric layer near the substrate. Another factor to induce RTIC phenomenon of ceramic materials is required the small particle size less than 5μm. If the particle size becomes less than 1μm, plastically deformation of the particle is observed during the collision and obtains the dense film formation. Therefore, no reports on the deposition of pure dense ceramic coating with the CS method could be found. With the AD method, it is possible to deposit not only metallic materials but also ceramic materials. It is believed that the AD method and the CS method have RTIC phenomenon for solid state particles as common principle, as both deposition conditions and microstructures are comparable in the reported papers. However, it has to be pointed out that the AD method is different from the CS method because RTIC conditions for these two methods are very different.

4. Future prospects of AD method

For over 5 yerars, applications of AD method to micro devises such as micro actuators, RF-embedded passive components, high speed optial modulator etc, were developed on “Nano Structure Forming for Advanced Ceramic Integration Technology Project in Japan Nano Technology Program“. These microelectoric device applications were reported in reference 1. The most particular feature of AD process is that the RTIC phenomenon induces the room temperature coating for ceramic, metal, and polymer materials. It allows to make metal-ceramic and ceramic-polymer composite or gradient structured layer, which are also good candidates for fabrication of energy related devices such as a solar cell (DSC), an all solid state Li-ion battery (LIB), a fuel cell, heat, a heart dissipation module and so on. .

At the present state, the understanding of the deposition mechanisms due to the collision of solid state fine particles is insufficient. A more detailed understanding is necessary and will be needed to obtain and control above layer structure in a near future.

References

[1] J. Akedo, “Room Temperature Impact Consolidation (RTIC) of Fine Ceramic Powder by Aerosol Deposition Method and Applications to Microdevices”, (Invited Review Paper), JOURNAL OF THERMAL SPRAY TECHNOLOGY, Vol.17(2), pp.181-198 (2008)

[2]. J. Akedo, “CERAMIC INTEGRATION AND JOINING TECHNOLOGIES, Chap.16: Aerosol Deposition (AD) Integration Techniques and Their Application to Microdevices” Edt. by M. Singh et al., WILEY. (2012) pp489-520.

Manufacturing of thick coatings by very low pressure reactive plasma spraying: case of the Aluminum - Titanium – Nitrogen system

Béatrice Vautherin[1], Marie-Pierre Planche[1], Ghislain Montavon[1], Frédéric Lapostolle[1], Aurélie Quet[2], Luc Bianchi[2]
[1] IRTES-LERMPS, UTBM, 90010 Belfort cedex, France
[2] CEA, 37000 Monts, France

Abstract
The very low pressure plasma spraying in a reactive mode was investigated in view of manufacturing coatings made of condensed vapors and embedded nitrides formed *in situ* by reaction in between the metallic vapors and reactive gas species. The Titanium – Aluminum – Nitrogen system was considered. The long-term objective of this work is to develop capabilities to manufacture, by a thermal spray route, coatings made of materials exhibiting an incongruent melting behavior, such as most of the nitrides for example. Different physical mechanisms were identified for coating formation: the composition of the formed nitrides depends strongly upon their formation localization: $TiN_{0.3}$, TiN, AlN-β and $AlTi_3N$ are formed in-flight, Ti_2N is formed on the coating surface. Beside, the structural characterization of the coatings revealed an atomic percentage of Nitrogen varying from 5% to 25%, depending upon the operating parameters and the spray setup. The coatings, exhibiting a total void content of about 5% (with 80%, by volume, of the voids smaller than 2 µm, average diameter), are made of a mixture of a metallic matrix and nitrides. Coating microhardnesses up to 1300 $HVN_{0.25kg.f}$ were measured.

1 Introduction

One of the main limitations of the thermal spray processes relies in their inability, in most of the cases, or their poor capability, in some others, to process materials exhibiting an incongruent melting behavior. The incongruent melting behavior corresponds, in a first approximation, to the rejection of constituents upon melting: the material decomposition temperature is lower than or identical to its melting temperature. Most of the nitrides, numerous carbides and borides, etc., exhibit such a behavior. This limitation, intrinsic to the thermal nature of the spray processes, impedes the development of applications which require the implementation of thick (*i.e.*, from 80 to 300 µm) coatings made of such materials on large surface areas (*i.e.*, up to a few square meters), for high temperature corrosion resistant barriers, wear resistant coatings, etc., meanwhile such materials exhibit singular and peculiar properties (*e.g.*, [1-3]).

Researchers and engineers from the thermal spray community have developed, along the years, alternatives to circumvent this limitation. This concerns the manufacturing of cermet coatings following two routes. This first one considers a cermet feedstock, made of a metallic matrix and embedded reinforcing ceramic particles. The objective here is to thermally process the matrix at a temperature significantly lower than the degradation one of the ceramic particles. The resulting coatings exhibit a matrix with a dispersion of reinforcing ceramic particles. The main driving force of the development of the High-Velocity Oxy-Fuel (HVOF) thermal spray process by J. Browning in the early 80's was the manufacturing of such coatings [4]. Nevertheless, meanwhile a limited heat flux imparted by the high-energy flow to the ceramic particles, in-flight partial decompositions of ceramic phases are often observed and impede the coating functional properties in service (*e.g.*, see S. Rangaswamy and H. Herman [5] for one of the very first studies on this topic). Beside, such an approach does not allow manufacturing coatings fully made of the ceramic phase. Nevertheless, this technique is nowadays a standard to manufacture those coatings. The second route, mostly investigated by the scientific community during the late 80's and the early 90's, aims at producing *in situ* the ceramic phase, by a chemical reaction in between a metallic material and reactive gas species. The ceramic phases depend upon the nature of the reactive gas species: nitrides formed from Nitrogen species *via* a nitriding reaction, carbides from Carbon species *via* a carbonization reaction, etc. In such a case, the high-energy flow expands, at atmospheric pressure, in a shroud, into which the reactive gas species are injected to react with the molten metallic feedstock processed by the flow. Meanwhile this approach still arouses the interest of researchers *(e.g.*, [6-7] for recent studies), it never reaches a maturity high enough to envisage its industrial implementation. Indeed, this manufacturing route exhibits numerous drawbacks, among which the main ones are: **i**) the slow progress in the chemical reaction, since it occurs in between a liquid phase and a gaseous phase, together with a rather short interaction time (*i.e.*, in the order of 0.5 ms, maximum duration): this leads to partial / incomplete reactions and the resulting coatings are not fully made of ceramic phases; **ii**) the stoichiometry of the formed ceramic phases is difficult, if not impossible, to tailor; **iii**) oxidation occurs due to recirculation occurring at the extremity of the shroud; **iv**) clogging of molten particles in the shroud is often observed, etc.

The very low pressure (*i.e.*, in the range from 50 to 150 Pa) plasma spray (VLPPS) process is an emerging process that allows manufacturing metallic and ceramic coatings by condensation of vapors resulting from the vaporization of feedstock particles injected in the core of the plasma flow. The strong expansion of the plasma, under such a low pressure, allows carrying the formed vapors over long distances (*i.e.*, > 1 m). Sometimes designated PS-PVD process (plasma spraying – physical vapor deposition), it has been considered mostly, up to now, to manufacture cauliflower-like thermal barrier coatings (*e.g.*, [8-10]). Indeed, most of those works aim at developing an alternative process to APS (atmospheric plasma spraying) and EB-PVD (electron beam physical vapor deposition) technologies usually implemented.

This emerging process presents also a high potential for manufacturing coatings made of ceramics exhibiting an incongruent melting behavior, such as nitrides. Indeed, the

plasma state (with a rather high mass enthalpy, etc.), together with a long interaction time due to the plasma plume length (in the order of 1 m), can promote the chemical reactivity in between metallic vapors resulting from the vaporization of feedstock particles in the plasma core and reactive species, injected downstream in the plasma flow or issued from the plasma forming gases mixture itself.

This paper aims at presenting recent results with the primary goal of a better understanding of the mechanisms occurring during the reactive deposition process of Titanium (Ti), Aluminum (Al) and Ti-Al with Nitrogen.

2 Experimental protocols

2.1 Implemented strategy

The following three-step methodology was implemented:

1. identification of a set of spray operating parameters allowing manufacturing metallic matrices from the condensation of vapors made of pure Ti (T40), or Al (1050), or Ti-Al with different atomic ratios: 1/3, 1/2; 1/1 and 2/1, by implementing optical emission spectroscopy (OES);
2. identification of nitriding species in the plasma flow and the related excitation mechanisms, by implementing optical emission spectroscopy (OES);
3. manufacturing of coatings by very low pressure reactive plasma spraying and study of the coating formation mechanisms and the structures of the resulting coatings, by implementing X-ray diffraction (XRD), glow discharge optical emission spectrometry (GD-OES), microhardness (Vickers), nanohardness (Berkovich) and ultra-small angle X-ray scattering (USAXS).

2.2 Main operating parameters

After optimization, the main spray operating conditions used to carry-on this work are depicted in Table 1.

Table 1. *Main spray operating conditions.*

F4 (Sulzer) plasma torch anode diameter	6 mm
plasma gas total flow rate (Ar-N_2-H_2)	30-40 L.min-1
Nitrogen plasma gas ratio	75-80%
plasma gas mass enthalpy	20-40 $MJ.kg^{-1}$
chamber pressure (Argon)	150 Pa
spray distance	900 mm
plasma torch / substrate relative velocity	0.2 $m.s^{-1}$
substrate temperature during deposition	130-800°C
feedstock particle average diameter	15 µm
feedstock mass flow rate	1.5-3 $g.min^{-1}$
average thickness deposited per pass	1-2 µm

3 Main results

- Metallic matrices made of Ti, Al or Ti-Al exhibit structures characteristic of a dual deposition mode: condensed vapors and solidified lamellae, Fig. 1. The amount of solidified lamellae, resulting from non-vaporized or partially vaporized particles, depends upon the operating parameters. Vickers hardness average values of those sprayed matrices vary in between 110 $HVN_{25g.f}$ (pure Al) and 220 $HVN_{25g.f}$ (pure Ti).
- Coating total void contents, as quantified by USAXS, are in the 5% range. More than 75% of the voids, by volume, exhibit equivalent diameters smaller than 2 µm.
- Excited N_2 (wavelength: 380.5 and 891.2 nm), N_2^+ (wavelength: 391.4 nm) and N (wavelength: 575.3 nm) species have been identified as nitriding species in the plasma flow. The calculated N_2 rotational average energy is about 0.2 eV. Such a high rotational energy indicates that the excitation mechanism corresponds primarily to the transfer of charges with excited Ar I species (wavelengths: 483.6 and 458.9 nm) [11].
- AlN-β, $Ti_{0.3}N$, TiN and Ti_3AlN nitrides have been identified, by XRD analyses, in the sprayed coatings. The maximum amount of atomic nitrogen, as measured by GD-OES, is 5%. Vickers hardness average values of those sprayed coatings vary in between 341±164 $HVN_{25g.f}$ (Al-AlN system) and 1003±326 $HVN_{25g.f}$ (Ti-TiN system). Indeed, the deposited material incompletely reacts with nitriding species.
- Secondary injection of N species during deposition, close to the substrate, allows increasing the atomic nitrogen content, up to 25%, Fig. 2. Accordingly, this leads to the formation of additional nitrides and an increase in the coatings average hardness: *e.g.*, Ti_2N in the Ti-N system with a Vickers hardness average value of 1300±312 $HVN_{25g.f}$. With such a setup, the substrate temperature during deposition plays a relevant role in the nitriding mechanism.

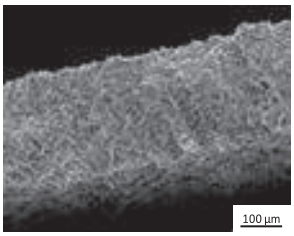

Fig. 1. *Metallic coating (Ti) manufactured by VLPPS.*

Fig. 2. *N atomic profile in a Ti-TiN VLPPS coating.*

4 References

[1] J. Lafait, J.-M. Behaghel, S. Berthier, J. Rivory: Journal de physique, Colloque C1, **42**, 1981

[2] S. Caron, F. Gitzhofer, J. Dhers, N. Goubot: 15th Int. Symp. on Plasma Chem. (CNRS, 2001) pp. 217-222

[3] M. N. Solovan, V. V. Brus, E. V. Maistruk, P. D. Maryanchuk: Inorganic Mat. **50** (2014) 40-45

[4] J.A. Browning: US patent # 4,416,421, November 1983

[5] S. Rangaswamy, H. Herman: 11th Int. Thermal Spraying Conf. (Welding Institute of Canada, 1986) pp.101-110

[6] C. Marchand, A. Maître, A. Grimaud, A. Denoirjean: Surf. and Coat. Tech. **201** (2006) 1988-1994

[7] S. Matthews: Surf. and Coat. Tech. **249** (2014) 56-74

[8] K. von Niessen, M. Gindrat, A. Refke: J. of Therm. Spray Tech. **19** (2010) 502-509

[9] G. Mauer, A. Hospach, R. Vaßen: Surf. and Coat. Tech. **220** (2013) 219–224

[10] M. Goral, , S. Kotowski, A. Nowotnik, M. Pytel, M. Drajewicz, J. Sieniawski: **237** (2013) 51–55

[11] D. H. Steman, D. W. Stetser: Prog. React. Kinet. **193** (1971)

Functional Coatings Formed by Gas Tunnel Type Plasma Spraying

Akira Kobayashi[1, 2]
[1] Graduate School of Engineering, Osaka University, Osaka 5650871, Japan
[2] Malaysia-Japan International Institute of Technology (MJIIT), UTM KL, Malaysia

Abstract
A high precise plasma system has been proposed for advanced thermal processing. The gas tunnel type plasma jet device developed by the author exhibits high energy density and also high efficiency. Among its various applications, one of the best applicability is the plasma spraying of ceramics such as Al_2O_3 and ZrO_2. The performances of these ceramic coatings are superior to conventional ones. Here the properties such as the mechanical and chemical properties, thermal behavior and high temperature oxidation resistance of the alumina/zirconia thermal barrier coatings (TBCs) are described and discussed. The ZrO_2 composite coating has a possibility for the development of high functionally graded TBC. The results showed that the alumina/zirconia composite system exhibited an improvement of mechanical properties and oxidation resistance. Another application of gas tunnel type plasma is for the surface modification of metals. For one example TiN films were formed in a short time of 5 s. And, the thick TiN coatings were easily obtained by gas tunnel type plasma reactive spraying.

1 Introduction

A plasma is one of the most superior heat sources, because of high temperature, high energy density, ease of control, etc. Therefore more precise plasma systems have been sought in order to establish smart thermal processing.
The gas tunnel type plasma system developed by the author has high energy density and also high efficiency[1,2]. Typical application is the plasma spraying of ceramics such as Al_2O_3 and ZrO_2. The characteristics of ceramic coatings by the gas tunnel type plasma spraying were superior to those by conventional jets. Usually, the Vickers hardness of this sprayed coating became 30% or more higher than that of conventional plasma sprayed coating. And, the porosity was only half of the value of the conventional ones [3].
By the gas tunnel type plasma spraying in detail in the previous studies [4,5], the Vickers hardness of ceramic coatings was increased with decreasing spraying distance, and a higher Vickers hardness could be obtained at a shorter spraying distance. At L=30 mm, the Vickers hardness of ZrO_2 coating was about Hv=1200 [6], which corresponds to the hardness of sintered ZrO_2. The ZrO_2 coating formed had a high hardness layer at the surface side, which showed the graded functionality of hardness[7].
Although zirconia coatings have been used in many applications, such as TBC for diesel engines [8], etc., the spallation problem due to the interface oxidation is still waiting to be solved under the extreme conditions such as high temperature and high corrosion environments. Alumina / zirconia composite coating was proposed as a potential candidate to improve the properties of thermal barrier coating systems due to alumina's low melting point and high hardness.
In this paper, typical application to plasma spraying of ceramics such as Al_2O_3 and ZrO_2 are described and its merit as TBC (thermal barrier coating) is discussed about high graded functionality etc. Other application of gas tunnel type plasma is the surface modification of metals. TiN films of 10 μm thickness are formed in a very short time of several seconds. The properties of thick TiN coatings by the gas tunnel type plasma reactive spraying are also described in this paper.

2 Experimental Procedure

The gas tunnel type plasma spraying torch used is shown in Fig.1. The experimental method to produce the ceramic coatings by means of the gas tunnel type plasma spraying is as follows. After igniting the plasma gun, the main vortex plasma jet is produced in the low pressure gas tunnel. The spraying powder is fed from the center inlet of the plasma gun. The coating is formed on the substrate traversed at the spraying distance of L.
The experimental conditions for the plasma spraying are as follows. The power input to the plasma torch was about P=25 kW which was supplied by the power supply PS-2. The spraying distance was short L= 40 mm. The working gas was Ar gas, and the flow rate for the gas tunnel type plasma spraying torch was Q=180 l/min, and gas flow rate of the carrier gas was 10 l/min. The powder feed rate of zirconia/alumina mixed powder was w=20~35 g /min. The traverse speed of the substrate was varied in value from v=25 to 1000 cm/min. Also the traverse number was changed 1-30 times.
The chemical composition of ZrO_2 and/or Al_2O_3 powder used in this study are; ZrO_2 powder was the commercially prepared type of K-90 (PSZ of 8% Y_2O_3), and Al_2O_3 powder was the type of K-16T. The substrate was SUS304 stainless steel (3x50x50), which was sand-blasted before use.

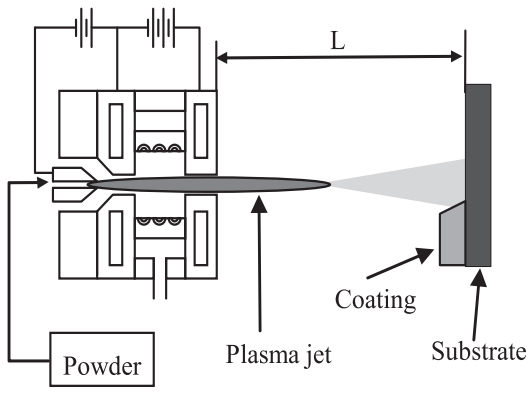

Fig.1. Schematic of the gas tunnel type plasma spraying torch. L: Spraying distance.

The Vickers hardness Hv_{100} of the sprayed coatings was measured at the non-pore region in the cross sections under the condition that the load weight was 100 g and its load time was 25s. The Vickers hardness: Hv_{100} was calculated as a mean value of 10 point measurements. The microstructure of the cross section of zirconia composite coating was observed by an optical microscope and SEM.

2 Results

2.1 Functionally graded ZrO_2 composite coating

The graded functionality of Vickers hardness of the ZrO_2 composite coating became much better, and the distribution of Vickers hardness was much smoother as the traverse number increased. This means that the structure at the surface of the coating was denser by the thermal process of the high energy plasma.

Then ZrO_2/Al_2O_3 coating was produced by the gas tunnel spraying on the fixed substrate for 3s spraying time. The microphotograph of the coating is shown in Fig.2. The thickness of the coating was about 250 μm, and white and gray layers were deposited alternately as shown in this photo.

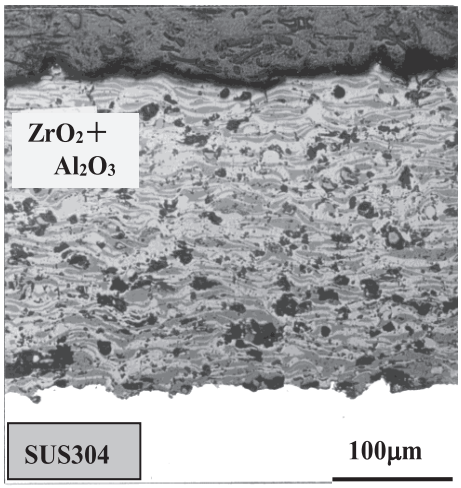

Fig.2. Typical ZrO_2/Al_2O_3 coating produced by the gas tunnel spraying on the fixed substrate for 3s spraying time.

The graded functionality of the structure is remarkable, and small pores are distributed disparately in the whole coating while larger pores exist near the substrate. The surface side has fewer pores and is dense, compared to the coating near the substrate. This was caused by the thermal process of the high energy plasma from the surface side of the coating. In this case, the Vickers hardness linearly decreased in the thickness direction towards the substrate side. This coating will be useful for high performance TBC.

2.2. Thick TiN coating by plasma reactive spraying

As other application of gas tunnel type plasma is surface modification of metals such as nitridation, carbonization, etc. For example the TiN films were formed in a very short time of 5 s by the irradiation of N_2 plasma jet. The thickness of the TiN film was 10 μm and the film is of high quality (homogeneous and high density). The Vickers hardness was about 1700 on the cross section of the film.

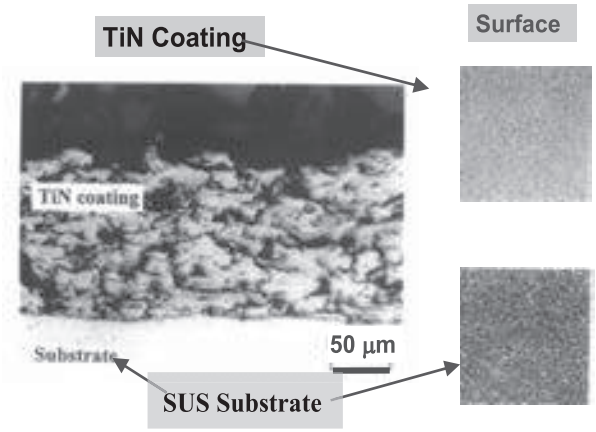

Fig.3. Cross section of typical TiN coating at P=25kW, L=60mm, t=5s and the surface view of the TiN coating (Hv=2000) and the substrate.

A new type of plasma reactive spraying was developed by using the gas tunnel type plasma spraying equipment. The thick TiN coatings were obtained by the gas tunnel type plasma reactive spraying [23]. Using this method it is easy to obtain thick TiN coatings in a short time of 10 seconds.

Figure 3 shows the cross section of typical TiN coatings and the surface view of the coating and the substrate. In this case, the spraying conditions of the gas tunnel type plasma reactive spraying were P=25 kW, L = 60 mm, and t = 4.8 s. The color of the TiN coating is gold and the Vickers hardness was about Hv= 2000.

4 Conclusions

The following results were obtained during the application of the gas tunnel type plasma system developed.

(1) Regarding the plasma spraying of ceramics such as Al_2O_3 and ZrO_2, the characteristics of those coatings were found to be superior to the conventional ones

(2) The ZrO_2 composite coating has graded functionality in terms of the hardness and porosity, and has the possibility of high performance TBC.

(3) The gas tunnel type plasma reactive spraying enable to make a thick TiN coating which color is gold and the Vickers hardness was about Hv= 2000 at P=25 kW.

References

[1] Y. Arata, and A. Kobayashi: *J. High Temp. Soc.* **11-3** (1984) pp.124-131.

[2] Y. Arata, and A. Kobayashi: *J. A. P.*, **59-9** (1986) pp.3038-3044.

[3] Y. Arata, A. Kobayashi, and Y. Habara,: *J. Applied Physics,* **62** (1987) pp.4884-4889.

[4] A. Kobayashi, S. Kurihara, Y. Habara, and Y. Arata: *J. Weld. Soc. Jpn.*, Vol.**8** (1990) pp.457-463.

[5] A. Kobayashi: *J. Thermal Spray Tech*. **5-3** (1996) pp.298-302.

[6] A. Kobayashi: *Surface and Coating Technology,* Vol.**90** (1997) pp.197-202.

[7] A. Kobayashi, T. Kitamura: *VACUUM*, Vol.**59-1** (2000) pp.194-202.

[8] D.N. Assanis: *Journal of Materials Processing Technology,* Vol. **4** (1989) p. 232.

Novel ceramic coatings by plasma spray deposition for molten metal containment

P V Ananthapadmanabhan
Laser and Plasma Technology Division, Bhabha Atomic Research Center, Trombay, Maharastra, India-400085
pvapadmanabhan@gmail.com

Abstract

Yttrium oxide and rare earth phosphates have thermal stability up to their melting point and are chemically inert in many reactive environments. These materials are stable in reducing environment and do not react with many molten metals. An overview of plasma sprayed coatings for applications as corrosion barrier against reactive molten metals would be covered in this lecture. The focus will be on recent developments on yttria and rare earth phosphate coatings for containment of reactive metals. Results indicate that plasma sprayed yttria and rare earth phosphates offer long-term solutions to handle molten uranium and its alloys.

1. Introduction

Plasma sprayed coatings of ceramic oxide materials are widely used for thermal barrier and corrosion barrier applications. The state-of-the-art coating for TBCs is Yttria stabilized zirconia (YSZ) containing 7-8 wt % of Y_2O_3. This material has been identified as the most preferred material after extensive research work [1,2]. However, stabilized zirconia cannot be used for corrosion protection of critical components handling reactive metals such as uranium.

Aluminium oxide has been used for short duration handling of molten uranium and also for high temperature processing of uranium alloys. However, aluminium oxide is not stable in vacuum, and under reducing atmosphere. In reducing environment and carbonaceous environment, alumina dissociates to its gaseous sub-oxides [3] such as AlO, Al_2O and Al vapour much below its normal melting temperature of 2323K. Further, aluminum oxide reacts with molten uranium, titanium and other reactive metals. Therefore, for applications involving containment of reactive molten metals such as uranium, coatings based on alumina and stabilized zirconia are not preferred.

2. Yttrium oxide coatings for corrosion barrier applications

The current research efforts are directed towards developing ceramic coatings with improved thermal shock resistance and high temperature phase stability for thermal barrier and high temperature chemical barrier applications. Recent studies show that yttrium oxide and the rare earth phosphates [4-6] are promising materials for thermal barrier coating applications and containment of reactive molten metals. Yttrium oxide has excellent thermal stability up to its melting temperature and also possesses superior resistance to aggressive chemical attack by molten metals, salts, slag and glass at high temperatures. By virtue of its high melting point and thermal stability, it is used in the form of sintered shapes and coatings for many high temperature corrosion applications. It is used for coating crucibles and moulds that handle highly reactive molten metals like uranium, titanium, chromium, beryllium and their alloys. A thin coating of Y_2O_3 is claimed to prevent corrosion of the substrate material by molten uranium and other reactive metals. It is also seen to be fairly stable with graphite up to 1600 ◦C.

Plasma sprayed yttrium oxide coatings have been successfully developed for barrier applications for processing of uranium and its alloys. Plasma spray deposited yttria coatings on various substrates have been found to offer very good protection [7] to the substrates against corrosive attack by molten uranium and uranium alloys.

3. Rare earth phosphates for molten metal containment

The use of rare earth phosphates coatings for corrosion barrier application is very recent. Thermal conductivity of $LaPO_4$ is much lower than that of YSZ. Further, it has a melting temperature (>2300 K) and higher thermal expansion coefficient. In addition, it has good corrosion resistance in environments containing sulphur and vanadium salts. In view of these properties, $LaPO_4$ is considered as a potential material for thermal insulation coating on Ni-super alloys. The use of $LaPO_4$ coatings for molten metal containment stems from the fact that it does not react with many molten metals.

Recent experiments on plasma spray deposition and spheroidization [6] show that lanthanum phosphate is a promising material for corrosion barrier experiments. Experiments with sintered lanthanum phosphate specimens and plasma spray deposited $LaPO_4$ coatings have shown that $LaPO_4$ offers adequate protection against corrosion by reactive molten metals including uranium. However, plasma spray deposition of $LaPO_4$ at high plasma power shows partial conversion of $LaPO_4$ to La-polyphosphate and La-oxyphosphate. On subsequent heat-treatment, the polyphosphate and oxyphosphate phases recombine to form the monazite phase. These phase instabilities, however, do not functionally impair corrosion resistance properties of $LaPO_4$. Another major problem with $LaPO_4$ coatings is the relatively low coating-substrate adhesion. This issue can be resolved to a certain extent by mixing rare earth oxides or rare earth phosphates.

Yttrium phosphate has high melting point (>2300K) and has thermal and chemical stability up to its melting point. Preliminary results show that plasma sprayed YPO_4 coatings

have better adhesion that $LaPO_4$ coatings and offer effective protection against molten metal corrosion. Results of recent studies show that rare earth oxide and phosphates are promising materials for molten metal containment and corrosion barrier applications.

4. Conclusion

Plasma sprayed aluminium oxide coatings are found to be suitable for short-term handling of reactive molten metal such as uranium. However, alumina coatings are not suitable for applications requiring long-term handling of molten uranium and other reactive metals. The new generation coatings developed for such applications are based on yttrium oxide and rare earth phosphates. Experimental results and coating evaluation studies have shown that plasma sprayed yttrium oxide coatings and rare earth phosphate coatings offer sufficient protection against corrosion by molten uranium and its alloys.

References

[1] . H.B. Guo, R. Vassen, D. Stover Surf & Coat. Techno 192 (2005) 48– 56

protection against molten metal corrosion. Recent

[2]. H.B. Guo, R. Vassen, D. Stover Int. J. Appl. Ceram. Technol., 1 4 (2004)351-61

[3] P.V. Ananthapadmanabhan, , T.K. Thiyagarajan, K.P. Sreekumar, N. Venkatraman, Scripta Materialia, 50 (2004) 143–147.

[4] Thiyagarajan T K, Ananthapadmanabhan P V, Sreekumar K P, Chakravarthy Y, Das A K, Gantayet L M, et al. Surf Eng **28** (2012) 646–56

[5] Alangi N, Mukherjee J, Anupama P, Verma M K, Chakravarthy Y, Padmanabhan P V A . J . Nucl Mater **410 (**2011) 39–45.

[6] P.V. Ananthapadmanabhan, K.P. Sreekumar, T.K. Thiyagarajan, R.U. Satpute, K. Krishnan, N.K. Kulkarni, T.R.G. Kutty, Materials Chemistry and Physics 113 (2009) 417–42.

[7] Y. Chakravarthy, Subhankar Bhandari, Vandana Chaturvedi, A. Pragatheeswaran, A. Nagraj, T.K. Thiyagarajan, P.V. Ananthapadmanaban, A.K. Das, Journal European ceramic society In Press, (2014)

Review of solution precursor spray techniques applied to obtain ceramic films and coatings

Lech Pawłowski[1]
[1] SPCTS, UMR CNRS 7315, 87068 Limoges, France

Abstract
The review describes the techniques of film and coatings deposition using solution as a feedstock. After a short description of the processes of: (i) spray pyrolysis; (ii) solution precursor plasma spray (SPPS); and, (iii) solution precursor high velocity oxy-fuel, some properties of solution feedstock are discussed. The properties include the chemical composition of solutions used to synthesize typical coatings, which determine the flow of solution in a pipeline and its injection to plasma or flame. The chemical and physical phenomena occurring at spraying are described including atomization in gas, heating and vaporization of solution, precipitation of solution and formation of solid and heating of this solid. The molten solid is then splashed onto substrate. Typical coatings formed using solution precursor spraying and the applications of solution precursor thermally sprayed coatings are reviewed.

1 Introduction

The spray pyrolysis started to be used as early as in the 60-ties of the last century [1]. The method was used to synthesize films of metal oxides, sulfides and selenides. The use of the torches generating combustion flames and plasma jets to process liquid solutions was first applied at the end of the 20th century [2]. The authors were inspired by the spray pyrolysis process. The torches generating high velocity flames have started to be used more recently [3]. The use of liquid feedstock in thermal spraying instead of usual solid powders was inspired by an interest in obtaining coatings having fine microstructure. Such coatings were easier to be sprayed with liquid feedstock (solution or suspensions) than with fine solid powders. In addition, thermal spraying is a well-established technology. The use of this technology for producing such coatings is industrially advantageous because of a dense network of job shops having expertise in coatings deposition, high productivity of coatings manufacturing and also a dynamic and well organized community of involved professionals.

2 Solution spray techniques

2.1 Spray pyrolysis

The technique of spray pyrolysis consists of atomizing the solution directed towards a hot substrate. The solutions of metal salts dissolved in organic or water are used generally to obtain coating of metal oxides. The atomized droplets impact the heated substrate to form lamellas and undergo a thermal decomposition. The substrate temperature is the main parameter, which influences the morphology and properties of coatings [4]. The final coating is a superposition of overlapping lamellas.

2.2 Solution precursor plasma spraying

The d.c. torches generate arc which heats working gases to form plasma jets. The jet's temperature, in a conventional plasma torch, reaches 14 000 K and its velocity on the nozzle exit reaches 800 m/s. The torches used in SPPS process [5]: (i) conventional, one cathode one having radial introduction of solution, (ii) three–cathode torch having axial introduction of solution; and (iii) segmented anode torches. The injection of solution can be made by an atomizer or by a nozzle. The working gases used to generate the plasma is usually argon with a molecular gas such as hydrogen or nitrogen. The molecular gases are added in order to increase the thermal conductivity of the plasma. The conventional one-cathode torches have important fluctuations and instabilities depending on kind of working gas [6]. The molecular gases contribute considerably the voltage arc fluctuations in the kilohertz frequency range. The use of three-cathode torches without the use of molecular gases maybe a solution of the fluctuation problem [7].

2.3 High velocity oxy-fuel spraying

The high velocity oxy-fuel torch is fuelled by a combustion hydrocarbon gases as ethylene, propylene and many others or hydrocarbon liquids as kerosene which is atomized prior to combustion. The combustion takes place in a chamber under high pressure, which varies from 0.3 to 4 MPa. The resulting jet issuing from a nozzle may reach temperature of about 3000 K and supersonic velocity by 2000 m/s. The solution can be injected radially, externally to the gun, directly into the HVOF flame or axially, directly into the combustion chamber [3].

3 Preparation of solutions

The precursors used for solution spraying of metal oxides films and coatings are generally the salts of metals and very frequently nitrates and acetates. In this way it is possible to obtain coatings of multi-oxide compound such as e.g. YBCO or YIG. Some authors, like [8], used the nitrates as the initial products to start sol-gel procedure to obtain fine particles. Such additives as acetic acid modify the chemistry of solution and influence the morphology of coatings. For example the structure of TiO_2 was changing from cracked to crack-free after the introduction of acetic acid into the solution [4]. The salts are used as solutions in water or in ethanol.

4 Phenomena occurring at spraying

The phenomena occurring during spray pyrolysis can be summarized by taking an example of spraying of metal salt solution onto a heated substrate. The most important of them is the deformation of the liquid into droplet and its thermal decomposition leading to the formation of the desired compound on the substrate [4]. The phenomena in-flight include mainly aerodynamic breakdown accompanied by the chemical reaction that occurs on the substrate.

The solution precursor thermal spraying includes more phenomena occurring in-flight occurring before the impact with the substrate (see Fig. 1):

a) aerodynamic break up;
b) heating, vaporization and internal precipitation;
c) internal pressurization and droplet breaking-up;
d) solid particle sintering, heating;
e) melting and evaporation from the melt.

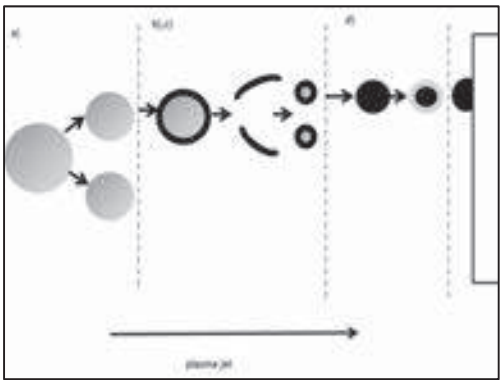

Fig. 1. *Phenomena which occur during a flight of a solution droplet in a high temperature gas jet [9].*

4.1 Injection

The solution may be transported to the injector with the use of a peristaltic pump or by a pneumatic transport. Its flow rate is controlled by the rotation of motor rollers or by the pressure acting on the fluid, respectively. The solution maybe atomized as in spray pyrolysis process or injected as a liquid stream to the jet or flame. The atomization is a process of which the external energy phase is needed to break up the liquid bulk.

The liquid stream undergoes an aerodynamic break up and the ligaments and large droplets are formed. Then, depending on the drag force acting on the droplet and their surface tension the large droplet may disintegrate into smaller ones. The process is called secondary break up [10]. This process leads to the formation of finer microstructure.

4.2 Physico-chemical phenomena

The droplets formed by successive break ups undergo rapid vaporization of solvent in hot temperature flame or jet. Consequently, the concentration of solute at the droplets surface increases, what may lead to precipitation in this region (because the concentration of solute reaches the super-saturation limit). The process is known as homogeneous precipitation [9] and was investigated for different thermal spray processes by e.g. [9, 11] and many others. The formation of solid crust outside of heated liquid leads to an increase in internal pressure inside a shell. Under the action of the pressure the shell may get fractured and smaller droplets of liquid get free and the process of precipitation and shell formation may be repeated. The processes may lead finally to the formation of solid particle as shows it Fig. 1.

The chemical phenomena occurring in flight of liquid droplet depend on the used metal salt precursor and on temperature. Generally, the sequence of chemical reactions includes evaporation of solvent, precursor pyrolysis and crystallization [12]

5 Possible applications of coatings

The solution precursor spray techniques including spray pyrolysis and thermal spray techniques are at present intensively explored. The potential advantage of these technologies can be related to the purity of the initial liquid precursors, which enable chemically pure coatings to be synthesized. The particularity of processing of small nano-particles renders it possible to obtain such phases as α-Al_2O_3, or TiO_2 crystallized as anatase obtained which are difficult to obtain using conventional thermal spray technique. Finely grained microstructure has another advantage, which is small thermal conductivity useful while synthesizing thermally insulating coating for TBCs.

The capacity to coat large surfaces must be also underlined. Not but not least, the possibility of obtaining columnar microstructure, is useful for enhancing the thermal shock resistance of coatings. The properties of solution precursor sprayed coatings have been tested by now for the following applications:

a) SOFC as electrodes, i.e. Ni-YSZ as anode, V_2O_5 as cathode and YSZ as solid electrolyte;
b) TBC made of YSZ and of $ZrO_2.La_2O_5$;
c) optoelectronic applications of Eu:Y_2O_3 or CZST coatings;
d) dielectric coatings in electronics made of α-Al_2O_3;
e) photocatalysis of TiO_2 coatings;
f) magnetic applications of YIG coatings;
g) biomedical coating of TiO_2 – rutile coatings.

The further perspectives of application these coatings in industry are related to the better control of the deposition process.

6 References

[1] M.S. Tomar and F.J. Garcia, F.J.: Prog. Crystal Growth Charact. **4** (1981) 221-48.

[2] J. Karthikeyan, C.C. Berndt, T. Tikkanen, J.Y. Wang, A.H. King,, and H. Herman: NanoStructured Materials **9** (1997) 137-40

[3] A. Killinger, R. Gadow, G. Mauer, A. Guignard, R, Vassen, and D. Stöver, D.) : J. Thermal Spray Technol. **20** (4) (2011) 677-95

[4] D. Perednis and L.J. Gauckler: J. Electroceram. **14** (2005) 103-11.

[5] P. Fauchais, A. Joulia, S. Goutier, C. Chazelas, M.Vardelle, A. Vardelle, and S. Rossignol: J. Phys. D: Appl. Phys. **46** (2013), 1-14.

[6] J.F. Coudert, and V. Rat: Surf. Coat. Technol. **205** (4) (2010) 949-53.

[7] R. Vassen, H. Kassner, G. Mauer, and D. Stöver: J. Therm. Spray Technol. **19** (1-2) (2010) 219-25.

[8] N. Sanpo, C.C. Berndt, A.S.M. Ang,, and J. Wang,: Surf. Coat. Technol. 232 (2013) 247-53.

[9] A. Saha, S. Seal, B. Cetegen, E.H. Jordan, A. Ozturk and S. Basu: Surf. Coat. Technol. **203** (2009), 2081-91.

[10] S. Basu, E.H. Jordan, and B.M. Cetegen: J. Thermal Spray Technol**. 17** (1) (2008) 60-72.

[11] A. Ozturk and B.M. Cetegen: Acta Materialia (2005) 5203-11.

[12] D. Chen, E.H. Jordan., and M. Gell: Surf. Coat. Technol. **202** (2008), 2132-8.

Suspension plasma spray fabrication of nanocrystalline Fe_3O_4-TiO_2 hollow magnetic microspheres for photocatalytic water disinfection

Hua Li*, Kun Ren
Key Laboratory of Marine Materials and Related Technologies, Ningbo Institute of Materials Technology and Engineering, Chinese Academy of Sciences, Ningbo 315201, China

Abstract
Bacterium-related environmental issues such as the drinking water problem due to the presence of microorganisms in water are gaining intensive worldwide concerns. Apart from its great potential for degrading toxic compounds, titania was evidenced to have antibacterial properties. Yet use of nanosized titania particles usually suffers from difficulties in removal after photocatalytic elimination of bacteria. Here we report nanocrystalline Fe_3O_4-TiO_2 hollow magnetic microspheres fabricated by suspension plasma spraying nanosized titania and ferriferrous oxide particles. Results showed that the as-sprayed microspheres with the size of 15~50μm in diameter have interior cavities with a mesoporous shell of 1~3μm in thickness. The spheres can be easily recycled through magnetic field collection after each time use. Formation mechanism of the spheres was discussed. And the ability of the hollow spheres to extinguish *E. coli* bacteria by their photocatalyitic properties was examined and elucidated.

1 Introduction

It was reported that about 80-90% of the water-related diseases are caused by contamination with pathogenic microorganisms, which has been a severe problem [1]. The United Nations identified improving water quality as one of the eight Millennium Development Goals (MDGs). To attain clean water, many disinfection processes have been developed, such as ozonation, chlorine dioxide treatment, advanced filtration, and germicidal ultraviolet radiation. Yet, the above traditional methods usually bear high cost, treatment complexity and detrimental byproducts, in turn restricting their potential applications. Novel water disinfection techniques are therefore to be developed.

Photocatalysis becomes a viable option by virtue of the use of sunlight to actuate the disinfection process and minimal hazardous disinfection byproducts. Among the possible semiconductor catalysts, titanium dioxide (TiO_2) is used extensively as photocatalyst to degrade organic compounds and microorganisms for the last 40 years. This is attributed to the favorable chemical stability, long durability, nontoxicity, low cost, and capability of repeated use without substantial loss of catalytic ability of titania [2, 3]. However, in a practical photocatalytic process, the separation of particle-type photocatalysts from the solution following the reaction can be very difficult and the tendency of the particles to agglomerate into larger particles effectively reduces the photocatalytic activity during the cycled use [4]. Hollow titania speres with magnetic feature could be a potential candidate to overcome the problems. Hollow sturcture offers the materials low density and large specific surface area. In addition, microspheres would not aggregate easily during service and magnetic separation has been a convenient approach for separating magnetized species easily and thoroughly by a simple magnetic device [5].

In this study, we proposed a suspension plasma spray approach for mass-production of titania hollow microspheres with magnetic properties. P25 titania (~20nm) and Fe_3O_4 (100~300nm) particles were used as the starting feedstock materials.

2 Experimental

2.1 Fabrication of Fe_3O_4-TiO_2 composite powder

19 g P25 (20 nm in diameter) and 1 g magnetic ferroferric oxide (100~300nm in diameter) powder was ultrasonically dispersed and mechanically stirred for 60 min in a 500 ml 20vol% alcoholic solution containing 4 g polyvinylpyrrolidone (PVP) and 1 g polyethylene glycol (PEG). The resultant slurry was then pumped at a speed of 60 mL/min to the plasma arc using peristaltic pump and home-made injection system. During the spraying, the slurry was propelled downwardly into the arc followed by atomization and evaporation of the water in the particles. The porous hollow spheres were collected in air by a container.

2.2 Microstructure characterization

Phase composition of the as-sprayed powder was analyzed by X-ray diffraction using CuKα radiation. Morphology of the powder was characterized using field emission scanning electron microscopy. Fourier transform infrared spectroscopy measurement and thermogravimetric analysis (TG) were also performed for the samples. The magnetic properties at room temperature were assessed with a vibrating sample magnetometer.

2.3 Photocatalytic disinfection testing

E. coli bacteria were cultivated in a shaker operated at 120 rpm for 24 h at 30 ^oC. They were havested by centrifugation at 2500 rpm and washed three times with 0.85% NaCl solution before being resuspended at a concentration of 5×10^7 CFU/ml in 0.85% NaCl solution. The concentration of the catalyst powder used was 1 g/L, and the powder was dispersed by sonication for 30 min in 0.85% NaCl solution. Afterwards 15 ml of the bacterial suspension and 15 ml of powder suspension was added into a Petri dish. During disinfection process, 100 μl sample was spread on agar plate after gradient dilution and incubated for 24 h at 37^oC in an incubator.

3 Results and Discussion

Hollow microspheres with the size of 15~50 μm in diameter were successfully fabricated by the suspension plasma spraying (Fig. 1). As noticed from both the topographical and crushed views of the powder particles, the big ferroferric oxide particles are clearly seen, which are dispersed in the composite structure. The interior cavities

with a mesoporous shell of 1~3 μm in thickness are demonstrated from the crushed spheres (Fig. 1b). The thickness of the wall is uniform for each hollow sphere. Spray parameters and organic content in the starting suspension play the key role in deciding the efficiency of accomplishing the hollow sphere structure. Further elucidation of the microstructure suggests the interior pressure generated by evaporating of the vapors of the droplets and the gases resulted from the organic decomposition is the crucial variable for making the hollow spheres.

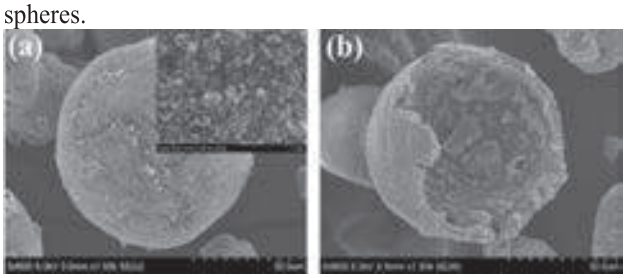

Fig. 1. *SEM images of the hollow spheres, (a) the surface view and (b) the view from a crushed sphere.*

After the spray processing, it is realized that minor transformation from anatase to rutile took place, as suggested by the XRD detection (Fig. 2). This is not surprising since ablation and evaporation of the solvent absorbs most of the heat exerted by the plasma arc. Trace of the magnetic ferroferic oxide in the composites is suggested by its weak XRD peaks, even though the dosage of the oxide is low. No spectra for ferric oxide or iron titanium oxide can be seen, suggesting negligible phase changes of Fe_3O_4 and mutual reaction between titania and Fe_3O_4 during the spraying. The saturation magnetization curve was acquired at room temperature for the as-sprayed hollow spheres. The hysteresis loop (the inset in Fig. 2) indicates that the as-sprayed powder could be considered as ferrimagnet. The saturation magnetization value of the Fe_3O_4-TiO_2 hollow spheres is 3.1 emu/g. And the residual magnetization and coercivity exhibit small values. In fact, preliminary testing already showed that the micron-sized spheres can be easily collected by external magnetic field (see the inset in Fig. 2). The spray processing permits most nano particles to retain their physiochemical properties in the resultant microspheres.

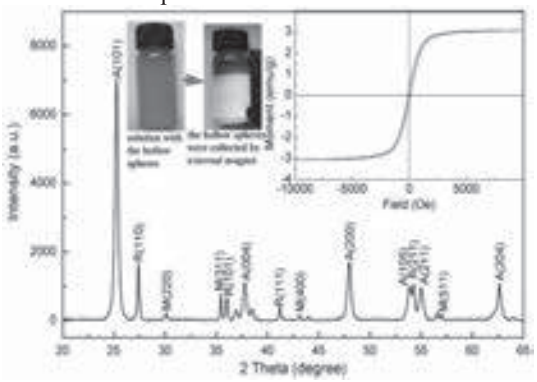

Fig. 2. *XRD spectrum and saturation magnetization curve of the as-sprayed hollow spheres.*

FTIR spectra of the hollow spheres evidences the presence of residual organics (Fig. 3). The broad band (400～800 cm^{-1}) is assigned to Fe-O, Ti–O and Ti–O–Ti skeletal frequency region. The peaks at 3400 cm^{-1}, 2349 cm^{-1} and 1656 cm^{-1} refer to the surface adsorbed water, hydroxyl group and the stretching vibration of C=O in CO_2. The peaks identified in Fig. 3(a) could be ascribed to the characteristic frequencies of residual PVP and PEG, which disappeared after calcination of the spheres at 600°C for 2 hours (Fig. 3b). This is consistent with the SEM observation from the surfaces of the spheres that remained binder is located in between individual titania/Fe_3O_4 particles (Fig. 1a). Our results showed that removal of the binder can be easily achieved by heat treating the spheres.

The TG/DTA curves (the inset in Fig. 3) of the as-sprayed hollow spheres can be divided into four stages, namely 30~250ºC, 250~360ºC, 360~600ºC and 600~800ºC. In the first stage, the mass loss is ~2%, which is likely caused by the elimination of adsorbed water in the microspheres. The mass loss of ~13.3% and ~13.7% in the second and third stage could be attributed to decomposition of residual organic compounds in the hollow spheres and oxidation of ferroferric oxide. After 600 ºC, no weight loss is seen, implying possible phase transformation alone.

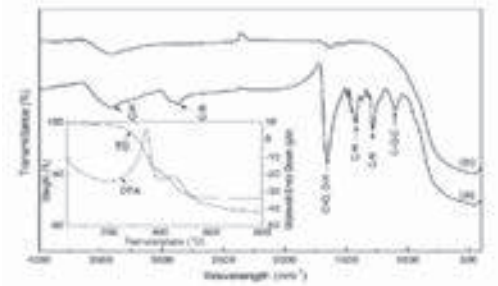

Fig. 3. *FTIR spectra and TG/DTA curves of the as-sprayed hollow spheres.*

Preliminary photocatalytic testing shows that after 5 hrs of UV irradiation of the solution containing both *E. coli* and the microspheres, ~90% bacteria were killed by the hollow microspheres. After the photocatalytic extinguishment, the spheres can be easily collected by external magnet for further use (see the inset in Fig. 2).

4 Conclusion

Fe_3O_4-TiO_2 hollow magnetic microspheres were fabricated by suspension plasma spray. Both the nano Fe_3O_4 and TiO_2 particles retain their physiochemical properties in the resultant microspheres. The spheres showed excellent capability of killing bacteria in solution and can be easily recycled by collecting them from the solution by external magnetic field.

References

[1] K. Backhaus, J. Marugan, R. van Grieken, and C. Sordo: Water Science & Technology. **61**(2010) 2355-2361.
[2] J. Gamage, and Z. Zhang: International Journal of Photoenergy. **2010**(2010) 1-11.
[3] K. Nakata, and A. Fujishima: Journal of Photochemistry and Photobiology C: Photochemistry Reviews. **13**(2012) 169-189.
[4] F. Ye, and A. Ohmori: Surface and Coatings Technology. **160**(2002) 62-67.
[5] M. Shokouhimehr, Y. Piao, J. Kim, Y. Jang, and T. Hyeon: Angewandte Chemie-International Edition. **46**(2007) 7039-7043.

Relationship between lamellar structure and elastic modulus of plasma sprayed ceramic coatings with intra-splat cracks

Guang-Rong Li[1], Bo-Wen Lv[2], Guan-Jun Yang[1*], Wei-Xu Zhang[2], Cheng-Xin Li[1], Chang-Jiu Li[1]
[1] State Key Laboratory for Mechanical Behavior of Materials, School of Materials Science and Engineering, Xi'an Jiaotong University, Xi'an, 710049, China
[2] State Key Laboratory for Strength and Vibration of Mechanical Structures, School of Aerospace, Xi'an Jiaotong University, Xi'an, 710049, China

Abstract
Elastic modulus of plasma sprayed ceramic coatings is often much lower than bulk material. For example, the coating elastic modulus in out-plane direction is only about 1/10 of bulk material, which is attributed to the limited inter-splat bonding. However, the lower elastic modulus in in-plane direction has not been well understood based on the lamellar structure of coatings. In this paper, a model taking both inter-splat pores and intra-splat cracks into account was proposed to comprehensively understand the correlation between lamellar microstructure parameters and the coating elastic modulus. In this model, the coating unit is the individual segment in a splat divided by the intra-splat cracks. Results show that the predicted values are well consistent with experimental results on coating elastic modulus in both in-plane and out-plane directions.

1 Introduction

Plasma sprayed (APS) yttria stabilized zirconia (YSZ) coatings are widely used as thermal barrier coatings (TBCs) in both aircraft engines and land-based gas turbines [1-3]. The inter-splat pores, intra-splat cracks and large globular pores are three major void systems existing in plasma sprayed lamellar structure [4], which leads to a low elastic modulus and high strain tolerance [5].

There have been several reported models to predict coating elastic modulus. Three types of voids (inter-splat pores, intra-splat cracks and globular pores) are inserted in dense material to predict elastic modulus[6]. A scatter for pore orientation is introduced in model to give a better explanation on the anisotropy of coating modulus [7]. However, both models disregard the connected role of inter-splat pores and intra-splat cracks. Finite element modeling (FEM) also represents an alternative method to predict elastic modulus [8], which captures the real microstructure and thus presents the interaction between different voids on coating properties. However, the limitation is that a sufficient large representative area with most large scale defects often neglects small and essential microstructural features. Li [9] developed a model based on lamellar structure and made a good prediction on elastic modulus in out-plane direction. However, it shows a higher in-plane elastic modulus than experimental data, and therefore needs further development.

In this work, a modified model based on lamellar structure with intra-splat cracks connected to inter-splat pores was developed with an aim at further comprehensively understanding the relationship between lamellar structure parameters and coating elastic modulus.

2 Model development

The essential features of APS ceramic coatings can be summarized as: (i) lamellar structure; (ii) connection between inter-splat pores and intra-splat cracks. A basic model shown in Fig.1a was adopted in this study [10]. The coating unit is not individual splats but the individual segments in a splat divided by the intra-splat cracks. The segments are connected layer by layer following cubic sequence. A circular bonding area is located at the bottom center of the segment as shown in Fig.1b. The calculation was carried out by Abaqus/CAE 6.11.

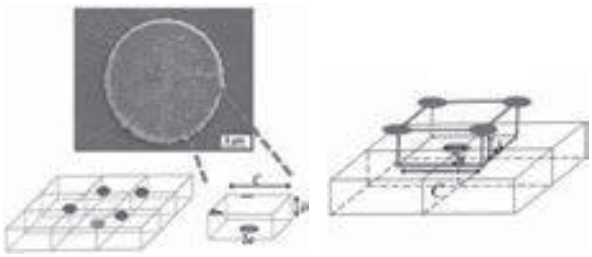

(a) (b)

Fig. 1. *Model description. (a) segments in a splat, (b) idealized model unit with bonding areas at bottom center.*

3 Results

3.1 Influence of segment structural parameters

Fig.2 shows the influence of segment structural parameters (ranges coming from reference [11]) on the elastic modulus in both directions. It can be seen that the thickening of splat segment leads to a decrease of elastic modulus in in-plane direction and an increase in out-plane direction (Fig.2a,b). On the contrary, the lengthening of splat segment results in an increase of elastic modulus in in-plane direction and a decrease in out-plane direction (Fig.2c,d). The elastic modulus in both directions becomes larger with the increase of inter-splat bonding ratio (Fig.2e,f).

3.2 Comparison with experimental results

Fig.3 shows the comparison between model prediction and experimental results from references [12-17]. It can be seen that the model captures the main range of elastic modulus of APS-YSZ in both in-plane direction and out-plane direction. Results obtained by resonant ultrasound spectroscopy [17], which is a non-destructive technique with excluding the effect of inelastic behavior caused by opening of cracks, agrees with this work. The Knoop indentation [12-15], whose scale is several times larger than the splat segment, yields a good consistence with this study. But some deviation still exists because the predicted results are based on the uniform distribution of bonding area, which results in the strongest connection between segments

and thereby a enhanced mechanical property. Therefore, it shows a little larger predicted values in in-plane direction and smaller in out-plane direction compared with Knoop indentation.

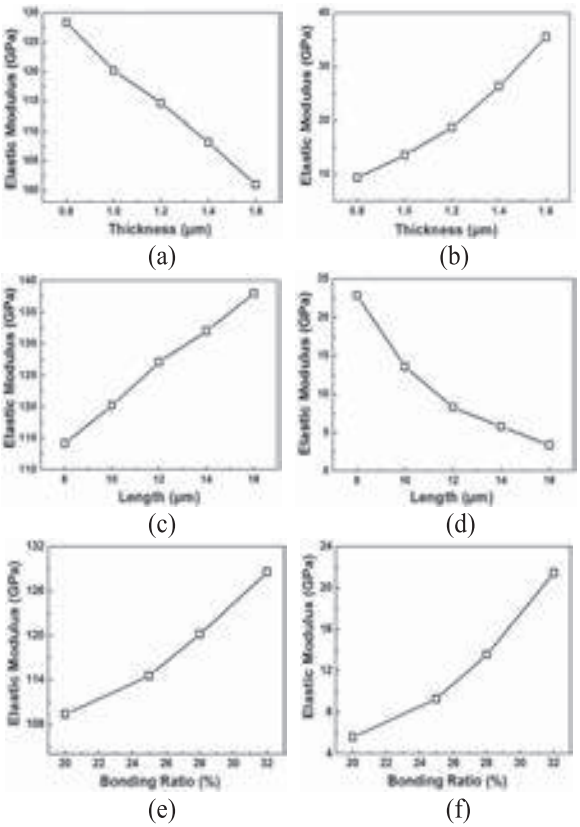

Fig. 2. *Effect of structural parameters on elastic modulus in in-plane direction (a,c,e) and out-plane direction (b,d,f).*

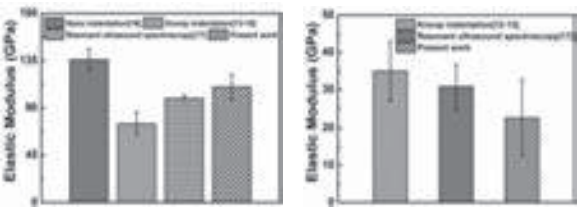

Fig. 3. *Comparison between model prediction and experimental results from references [12-17]. (a) in-plane direction; (b) out-plane direction.*

3.3 Comparison between models

Fig.4 shows the in-plane direction elastic modulus of model results normalized by Knoop indentation(the red solid horizontal line)[18]. It can be found that the model based on the lamellar structure with connected inter-splat pores and intra-splat cracks predicts a more rational results compared to the experimental results measured by Knoop indentation.

4 Conclusions

A modified model based on lamellar structure with connected inter-splat pores and intra-splat cracks was developed to predict elastic modulus in different directions of APS ceramic coatings. A good consistence between model prediction and experimental data was obtained for the elastic modulus in both out-plane and in-plane directions. Compared to reported models, this work emphasizes the connection of intra-splat cracks and inter-splat pores. It contributes to further comprehensively understanding of the dependence of anisotropic elastic modulus of APS coatings on lamellar structure.

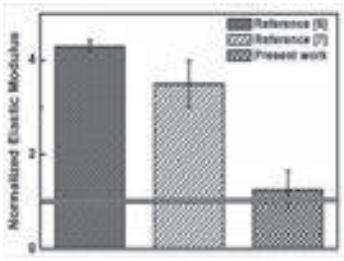

Fig. 4. *The in-plane direction elastic modulus of model results normalized by Knoop indentations (red solid line).*

5 References

[1] V. Teixeira, M. Andritschky, W. Fischer, H.P. Buchkremer, D. Stover: Surf. Coat. Technol. 120-121(1999)103.
[2] N.P. Padture, M. Gell and E.H. Jordan: Science 296(2002)280-284.
[3] A. Portinha, V. Teixeira, J. Carneiro, M.G. Beghi, C.E. Bottani, N. Franco, R. Vassen, D. Stoever and A.D. Sequeira: Surf. Coat. Technol. 188-189(2004)120-128.
[4] A. Cipitria, I.O. Golosnoy and T.W. Clyne: Acta Mater. 57(2009)981.
[5] J.S. Wallace and J. Ilavsky: J. Therm. Spray Technol. 7(1998)521-525.
[6] F. Kroupa and J. Dubsky: Scripta Mater. 40(1999)1249-1254.
[7] I. Sevostianov and M. Kachanov: Acta Mater. 48(2000)1361-1370.
[8] J.-H. Qiao, R. Bolot and H.-L. Liao: Surf. Coat. Technol. 220(2013)170-173.
[9] C.-J. Li, A. Ohmori and R. McPherson: J. Mater. Sci. 32(1997)997-1004.
[10] H. Xie, Y.-C. Xie, G.-J. Yang, C.-X. Li and C.-J. Li: Journal of Thermal Spray Technology. 22(2013)1328-1336.
[11] C.-J. Li and A. Ohmori: J. Therm. Spray Technol. 11(2002)365-374.
[12] D.-M. Zhu and R. A. Miller: J. Therm. Spray Technol. 9(2000)175-180.
[13] H.-J. Kim and Y.-G. Kweon: Thin Solid Films. 342(1999)201-206.
[14] R.S. Lima, A. Kucuk and C.C. Berndt: Surf. Coat. Technol. 135(2001)166-172.
[15] S.-H. Leigh, C.-K. Lin and C.C. Berndt: J. Am. Ceram. Soc. 80(1997)2093-2098.
[16] J.A. Thompson and T.W. Clyne: Acta Mater. 49(2001)1565-1575.
[17] Y. Tan, A. Shyam, W.B. Choi, E. Lara-Curzio and S. Sampath: Acta Mater. 58(2010)5305-5315.
[18] M. Vilemova, J. Matejicek, R.Musalek and J. Nohava: J. Therm. Spray Technol. 21(2012)372-382.

Contributory Oral Presentations

Processing, microstructure and thermo-physical properties of thermal barrier coatings produced by plasma spray physical vapor deposition

Hongbo Guo*, Lihua Gao, **Liangliang Wei,** Shengkai Gong, Huibin Xu

School of Materials Science and Engineering, Beihang University, No. 37 Xueyuan Road, Beijing 100191, China

*To whom all correspondence should be addressed. E-mail address: guo.hongbo@buaa.edu.cn.

Thermal barrier coatings (TBCs) produced by electron beam physical vapor deposition (EB-PVD) or plasma spray (PS) have been extensively used to protect hot components in turbine engines from harsh environment. Recently, plasma spray physical vapor deposition (PS-PVD) has attracted increasing attention because it allows designing of new microstructure architecture achieved by combination of liquid droplets, vapor phases and nano-clusters. In this work, yttria stabilized zirconia (YSZ) thermal barrier coatings were produced by PS-PVD and the microstructures were characterized by SEM/EDS and TEM. The spray distance, powder feed rate and rotation speed of sample holder had significant effect on the coating microstructure. The coating sprayed at 1.9 m with a rotation speed of 2 r/min revealed feather-like columnar structure, as shown in Figs. 1a and b. The thermal conductivity was determined by laser flash to be in a level of ~1.0 W/mk at 1200 °C, around 40 % lower than that of the coatings produced by EB-PVD. The thermal shock testing was performed in a gas burner in which the TBC samples were heated to a coating surface temperature of ~1200 °C while the substrate temperature was kept at 1000~1050 °C. The PS-PVD YSZ TBCs had a life of ~2000 cycles, which was comparable to that of EB-PVD TBCs, exhibiting an excellent thermal shock resistance.

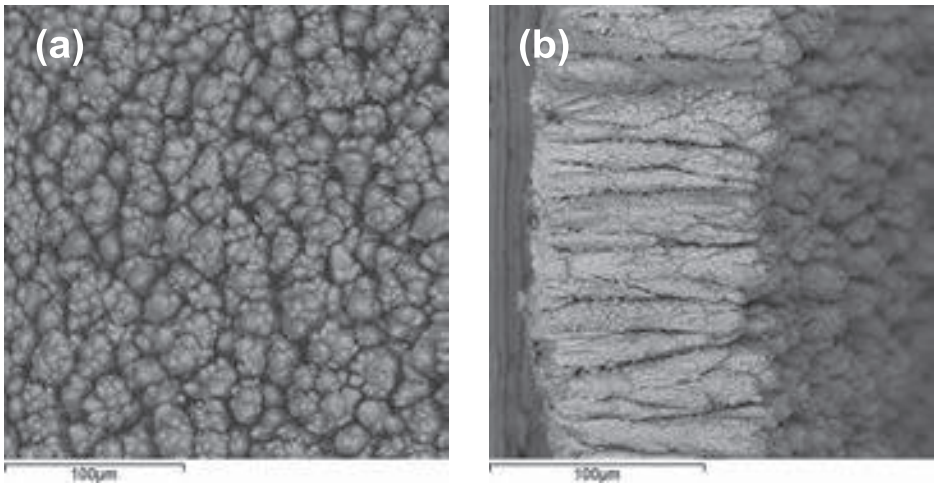

Fig. 1 SEM micrographs of YSZ coating produced by PS-PVD: (a) surface; (b) cross-section.

Keywords: Thermal barrier coatings (TBCs); Plasma spray physical vapor deposition (PS-PVD); Electron beam physical vapor deposition (EB-PVD); Thermal conductivity; Thermal shock.

Phase Retention of YSZ in Plasma Sprayed YSZ-CNT Reinforced Al2O3 Matrix Composites for Thermal Barrier Coating

Kantesh Balani, Ariharan S. N. Balaji, S.T. Aruna

Indian Institute of Technology Kanpur, National Aerospace Laboratory Bangalore,National Aerospace Laboratory Bangalore, Indian Institute of Technology Kanpur

Yttria stabilized zirconia (YSZ) is widely used as thermal barrier coating (TBCs) for gas turbine engines blades due to its low thermal conductivity (1.8-2.2 W/mK) and comparable thermal expansion coefficient (~7x10-6 K-1) with that of nickel substrate. But, the coating failure occurs mainly due to its poor fracture toughness and development of residual stresses. In the present research, Al2O3 was blended with 0, 3 and 8 mol.% Y2O3 doped zirconia and deposited on Inconel 718 alloy. Further, 4vol.% multiwall-carbon nanotubes (CNTs) are reinforced to enhance the fracture toughness of plasma sprayed coatings. Complimentary spark plasma sintering technique is also utilized to produce bulk YSZ-CNT composites. Phase retention has been analyzed using x-ray diffraction, transmission electron microscopy and Raman spectroscopy. The retention of ~26% transformable tetragonal ZrO2 phase is believed to play a major role in imparting enhanced fracture toughness (by 28%, from ~4.3 MPa.m1/2 to ~5.4 MPa.m1/2), whereas, CNTs have shown to provide synergistic toughening (from ~5.2 to ~5.9 MPa.m1/2). Thus, synergistic toughening can render enhanced damage resistance and provide prolonged life to thermal barrier coatings.

Toughness Evolution of Zirconia based Thermal Barrier Materials upon High Temperature Exposure

Archana Loganathan, **Ashutosh S. Gandhi**
Department of Metallurgical and Materials Engineering, Indian Institute of Technology Madras, Chennai – 600036, India

Abstract
Turbine blades at high temperature operation are protected by thermal barrier coatings (TBCs) and in turn these coatings enhance the performance of gas turbine engines. At present, the top coat (yttria stabilized zirconia, YSZ) with *t*□ phase transforms to *t* + *c* upon high temperature exposure. The yttria-depleted tetragonal phase may transform to the monoclinic phase. The effect of high temperature on the *t′* phase and toughness in zirconia with 8 mol% $REO_{1.5}$ (RE = Y and Gd) were studied. Dense compacts were prepared by pressureless and spark plasma sintering were subjected to prolonged thermal exposure at 1250°C up to 192 h. As-sintered pellets of GdSZ comprising of the *t*□ phase exhibited higher initial indentation toughness of 117 ± 8 Jm^{-2} than YSZ (98 ± 9 Jm^{-2}). Cubic phase precipitation was observed in GdSZ in the early stage of exposure, similar to YSZ. Upon thermal exposure, toughness decreased initially and then increased gradually. After 96 h, GdSZ showed higher toughness than in the as-sintered condition. The changes in the indentation toughness are analysed in terms of ferroelastic toughening and transformation toughening.

1 Introduction

High temperature metallic components of the gas turbine engines are insulated by thermal barrier coatings (TBCs) which in turn enhance the durability of the components and energy efficiency of the engines. Currently, ZrO_2 with 6-8 mol% $YO_{1.5}$ (YSZ) with non-transformable tetragonal (*t′*) phase is used as TBCs [1]. They are deposited by either air plasma spraying (APS) or electron beam physical vapor deposition (EBPVD). The long lifetime of *t′* YSZ is ascribed to high fracture toughness due to ferroelastic toughening. Different types of failure occur in the thermal barrier coating system. For example, the delamination of the top coat is caused by stresses developed during thermal cycling (intrinsic failure) or penetration of molten dust, erosion or foreign object damage (extrinsic failures) [2]. During cooling, the stress in the TBC increases due to mismatch in thermal expansion coefficient with the underlying layer (thermally grown oxide, TGO). This actuates crack nucleation at the TGO/TBC interface and it propagates further through the interface leading to failure of the system. Higher fracture toughness of the TBC material is imperative to render longer lifetime during service. Therefore, enhancing the inherent fracture toughness of the TBC material and monitoring its variation with thermal exposure is the focus of this study.

2 Experimental Details

Zirconia stabilised with 8 mol% $REO_{1.5}$ (RE = Y and Gd) were synthesized by reverse co-precipitation. Pyrolysed powders were compacted using pressureless sintering (PS) for YSZ and spark plasma sintering (SPS) for GdSZ [3, 4]. Ceramographic polishing was carried out for the dense compacts and it was cut into small samples. Phase stability of the sintered pellets were studied by thermal exposing them at 1250°C from 0 to 192 h. The corresponding room temperature indentation toughness was measured by Vicker's hardness tester (Wolpert Wilson 4325VA) and 3 kg load was optimized for the measurements. Using critical strain energy release rate (Γ), the toughness was measured,

$$\Gamma = 2\varsigma^2 P\left(\frac{d^2}{c^3}\right)$$

where the toughness (Γ) is in Jm^{-2}, load (P) is in N, the geometry factor (ζ) is ~ 0.016, d (half the diagonal length of the indent) and c (crack length from the indent center) are measured using scanning electron microscopy [5, 6].

XRD patterns were collected in the 2θ range of 20 - 80° in steps of 0.01° with 4's dwell time for the as-sintered and thermal exposed specimens. Raman spectra were obtained from the Horiba Jobin Yuvon HR 800 UV spectrometer (He–Ne laser, λ=632.8 nm). The monoclinic phase fraction (f_m) from the crack end was calculated using the peak intensity corresponding to the monoclinic (182 and 191 cm^{-1}) and tetragonal (148 and 263 cm^{-1}) phases [7].

3 Results and Disscussion

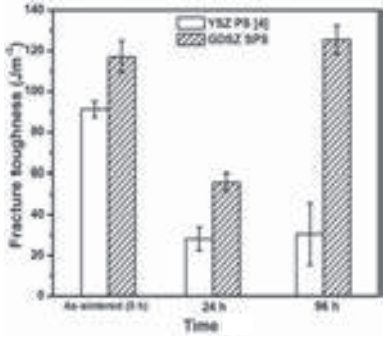

Fig. 1. *Change in fracture toughness upon thermal exposure*

As-sintered GdSZ exhibited higher fracture toughness compared to YSZ, **Fig. 1**. Upon thermal exposure, the toughness dropped initially around 6 h for both the compositions and later, the toughness increased gradually. After thermal exposed for 96 h, GdSZ showed an increase in toughness around ~125 ± 7 Jm^{-2} and crack propogation was not observed in the 192 h sample. However, significant increase in toughness was not observed for the YSZ exposed for 96 h and after 192 h showed around ~1.5 times

increase in toughness. Raman studies for the GdSZ sample comprised of monoclinic phase at the crack end from 24 h and at the free surface it was observed around 96 h respectively. However, monoclinic phase was not observed in the free surface of YSZ up to 192 h. Around 40 vol% of monoclinic phase was observed in the crack end for the 192 h YSZ [4]. After the initial drop, the increase in toughness can be attributed to ferroelastic toughening. Transformation toughening gets activated around 24 h for GdSZ, compared to 192 h for YSZ [4]. This was evident from the presence of monoclinic phase at the crack end (not shown here). Additionally, phase transformation studies were carried out to validate the toughening mechanism.

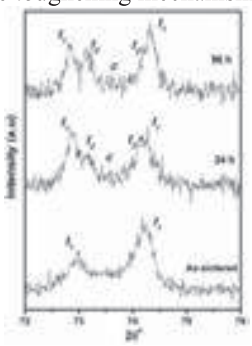

Fig. 2. *XRD pattern for GdSZ before and after thermal exposure*

Phase transformation for the GdSZ sample exposed at 1250°C was recorded using XRD as shown in, **Fig. 2.** Using XRD and Raman spectroscopy, the as-sintered compact was confirmed to be *t′* phase. With increase in thermal exposure time, the *t′* phase transformed into $t_1 + c$ around 6 h for GdSZ and YSZ. Another tetragonal phase (t_2) was observed in samples exposed from 24 h for GdSZ and second tetragonal phase was not observed in case of YSZ up to 192 h [4]. From XRD patterns, monoclinic phase was not observed for YSZ till 192 h, but for GdSZ, monoclinic phase was observed from 24 h of thermal exposure (**Table.1**). The above results are in accord with the literature, where GdSZ is more susceptible to monoclinic formation compared to YSZ [8, 9]. During thermal exposure at 1250°C, Raman peak shifts were observed for both the compositions which signifies the inducement of strain due to phase transformation [10]. With increase in thermal exposure time, continuous increase in crystallite size was observed for all the phases. Also, bimodal microstructure consisting of nano and micro sized grains were observed in the samples upon prolonged exposure as observed earlier by Ren et al. [11].

Table.1. *Phase evolution and tetragonality (c/a ratio) for YSZ PS and GdSZ SPS*

Composition	Phase evolution			c/a ratio	
	0 h	24 h	96 h	0 h	96 h
YSZ	*t*□	$t_1 + c$	$t_1 + c$	1.012	1.015
GdSZ	*t*□	$t_1 + t_2 + c + m$	$t_1 + t_2 + c + m$	1.014	1.018

The tetragonality of the as-sintered YSZ sample was lower than as-sintered GdSZ, **Table.1.** This was observed even after 96 h of exposure. The tetragonality increased constantly with increase in exposure time. From the interplay of toughness and phase transformation, high initial toughness is related to the *t′* phase which facilitates the ferroelastic toughening. The initial drop in toughness upon thermal exposure can be correlated to the increase in crystallite size. After the initial drop, the gradual increase in toughness is related to the increase in tetragonality [12]. For the GdSZ 24 h and 96 h, and YSZ for 192 h, the toughness increased and this is ascribed to the role of both transformation and ferroelastic toughening. The final toughness was higher than the as-sintered toughness, in case of GdSZ. On the other hand, the final toughness of YSZ was lower than the as-sintered toughness. This concludes that the transformation toughening is the dominant mechanism after 24 h in GdSZ.

4 Conclusions

As-sintered GdSZ samples showed higher indentation toughness than YSZ. For both the compositions, toughness drops initially upon thermal exposure and then gradually increases. GdSZ shows higher toughness than YSZ around 96 h of thermal exposure at 1250°C. Monoclinic zirconia was observed in the indentation crack tips after 24 h for GdSZ, compared to 192 h for YSZ. Early cubic precipitation was observed for GdSZ around 6 h. The t_2 phase was observed around 24 h for GdSZ, whereas no second tetragonal phase was observed up to 192 h in YSZ. The onset of transformation toughnening was observed along with ferroelastic toughening for GdSZ at 24 h. As a concluding remark, ferroelastic toughnening plays a predominant role in GdSZ up to 12 h, compared to 96 h in YSZ. Subsequently, transformation toughening emerges as the operative toughening mechanism.

5 References

[1] N.P. Padture, M. Gell, E.H. Jordan, Science **296** (2002) 280-284.
[2] A.G. Evans, D.R. Clarke and C.G. Levi, J. Eur. Ceram. Soc. **28** (2008) 1405-1419.
[3] A. Loganathan and A.S. Gandhi, Trans. IIM **64** (2011) 71-74.
[4] A. Loganathan and A.S. Gandhi, Mater. Sci. Eng. A: **556** (2012), 927–935
[5] C. Mercer, J.R. Williams, D.R. Clarke, A.G. Evans, Proc. R. Soc. A **463** (2007) 1393-1408.
[6] T.A. Schaedler, R.M. Leckie, S. Kramer, A.G. Evans, C.G. Levi, J. Am. Ceram. Soc., **90** (2007) 3896-3901.
[7] V. Lughi, D.R. Clarke, Surf. Coat. Technol. **200** (2005) 1287-1291.
[8] N.R. Rebollo, Ph.D. Dissertation, University of California, Santa Barbara, 2005.
[9] L. Archana, M.S. Thesis, Indian Institute of Technology Madras, Chennai, 2012.
[10] A.M. Limarga, J. Iveland, M. Gentleman, D.M. Lipkin, D.R. Clarke, Acta Mater., **59** (2011) 1162-1167.
[11] X. Ren and W. Pan , Acta Mater., **69** (2014) 397-406.
[12] A.G. Evans, J. Am. Ceram. Soc., **73** (1990) 187-206.

Study of new TBC materials for high temperature Gas turbine applications

Ramandeep Mandia, B. K. Pant, P. Joshi, K. Vidyasagar
Centre of Excellence - Surface Engineering, BHEL R&D, Hyderabad 500093, India

Abstract

At present thermal barrier coating systems are based on Yttria stabilized zirconia. These coatings are stable up to working temperatures of 1473K and are not suitable for long term application at higher temperatures. For applications beyond 1473K alternate materials like Lanthanum phosphate ($LaPO_4$), Lanthanum Zirconate ($La_2Zr_2O_7$) and Lanthanum Cerium Oxide($La_2Ce_2O_7$) were selected because of their better thermal and physical properties. Lanthanum Zirconate and Lanthanum Cerium oxide was synthesized using precursor powders (La_2O_3, ZrO_2, and CeO_2) and spray dried to obtain sprayable size and shape. The powders were plasma sprayed on SS samples individually as well as multi-layered coating. The coating properties were investigated for microstructure, SEM analysis, porosity, thermal cycling, thermal conductivity, bond strength.

1 Introduction

Thermal barrier coatings (TBC) are used in Gas turbine(GT) hot gas path components to reduce the surface temperature, thus increasing the life of the component, increase efficiency by operating at higher temperature and also reduce the cooling air requirement.

At present, Yttria stabilized Zirconia (YSZ) is used as the TBC material. The thermal expansion coefficient of YSZ (10.7×10^{-6} K^{-1}) being close to that of substrate material ($12X10^{-6}$ K^{-1}) makes it's the top contender of choice for the ceramic top coats of high temperature components. A major disadvantage of YSZ is the limited operation temperature (<1473 K) for long term application. At higher temperatures, phase transformations from t'-tetragonal to tetragonal and cubic (t + c) and then to monoclinic (m) occur giving rise to the formation of cracks in the coating. On the other hand, these coatings possess a high concentration of oxygen vacancies, which at high temperature assist oxygen transport and the oxidation of the bond coat at the ceramic – bond coat interface, namely the formation of TGO on the bond coat surface.

2 New Materials – potential candidates for high temperature TBC application

The three selected candidates were:

i) $LaPO_4$ (Lanthanum Phosphate - LP),
ii) $La_2Zr_2O_7$ (Lanthanum Zirconate - LZ),
iii) $La_2Ce_2O_3$ (Lanthanum Cerium Oxide - LC),

each having some advantages/ limitations over the others.

LC and LZ are not commercially available. So they are to be prepared from Lanthanum oxide, zirconia and cerium oxide by solid state reactions in high temperature furnaces.

Synthesis of $La_2Zr_2O_7$ and $La_2Ce_2O_3$ by solid state reaction involved mixing of precursor powders (La_2O_3 + ZrO_2, La_2O_3 + CeO_2) in pot mill, followed by sintering at 1673K, and spray drying to get optimum size of powder. The plasma spray coating parameters were optimized for each powder, to obtain the best possible coating.

A comparison of advantages and disadvantages of LZ, LC, LP with YSZ is given in **Table. 1**.

Table. 1. *Characteristics of TBC materials*

	Advantages	Disadvantages
7-8 YSZ	- High Thermal expansion co-efficient - Low thermal conductivity - High Thermal shock resistance	- Sintering above 1473K - Phase transformation (1443K) - Corrosion, Oxygen-transparent
La2Zr2O7	- Very high thermal stability - Low thermal conductivity - Low sintering - Not oxygen-transparent	- Relatively low Thermal expansion co-efficient
La2Ce2O7	- High Thermal expansion co-efficient - Low thermal conductivity - High corrosion resistance - Less phase transformation upto 1650K - High thermal shock resistance	- High sintering rate - CeO2 precipitation - CeO2 evaporation while spraying if powder not prepared properly
LaPO4	- High thermal expansion co-efficient - Low thermal conductivity - High temperature stability - Good corrosion resistance in salty environments	- Poor adhesion

3 Results Achieved

- Synthesis of the LZ and LC from the precursor powders was done as per procedure. XRD analysis of the powder confirms the desired composition i.e. $La_2Zr_2O_7$, $La_2Ce_2O_3$.
- Granulation of the powder was done after optimizing the parameters to get maximum amount of required size powder using spray dryer. The powder sieved after spray drying gave about 50-60% of the required size (i.e., 40-120 μm) powder. SEM images of the spray dried powders display the spherical shape of the powders. The SEM image of LP after spray drying is shown in **Fig 1**.

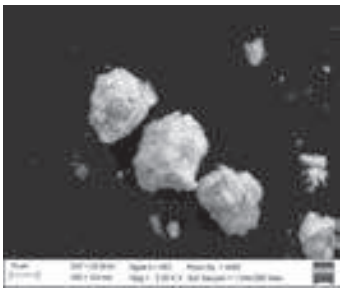

Fig. 1. *LP after Spray drying at 2.5KX*

The spray drying parameters of each powder is listed below in **Table. 2**.

Table. 2. S*pray drying parameters for LP, LZ and LC*

Parameters	LP	LZ	LC
%PVA(binder) in 25% solution	8%	7%	7%
Blower rpm	2031	1800	1800
Pump rpm	220	150	150
Chamber Temperature (K)	472	423	423
Outlet Temperature (K)	473	423	423
Inlet Temperature (K)	623	633	633

- LP gave the best flow rate, deposition rate as compared to LZ and LC. Many difficulties were faced while coating LC on the substrate, but eventually obtained successful coating.
- Microstructure of all the three powders coated with plasma spray is shown in **Fig. 2, 3 and 4**.

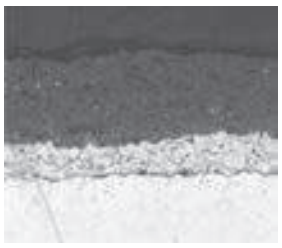

Fig.2. *LP top coat*

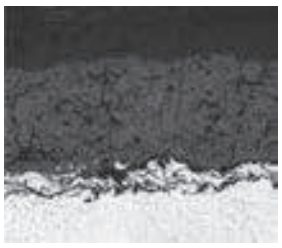

Fig.3. *LZ topcoat*

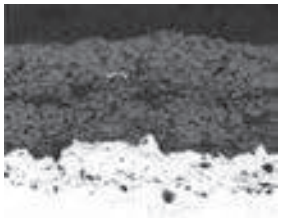

Fig. 4. *LC topcoat*

- XRD results of the coated sample when compared to the powder before coating, shows no phase change.
- Porosity results for these coatings showed satisfactory results as depicted in **Table. 3**.

Table. 3. *Porosity values of coatings*

TBC Material	Average porosity
LP	10.59
LZ	12.33
LC	8.85

- Bond test results are shown below:
  LP - Coating failed at 1300 psi
  LZ – Coating failed at 2200 psi.
- Thermal cycling carried out on LP and LZ for 50 cycles. Each cycle comprising 30 min soaking at 1073K followed by 15 min air quenching. The results showed no spalling or any visual detrimental effect on coatings. Thermal cycling of coating at 1273K is in progress, results will be obtained after a minimum no of 100 cycles.
- Thermal conductivity results are yet to come. The thermal conductivity values till 1273K will be obtained.

4 Conclusions

- Successful synthesis of Lanthanum zirconate and lanthanum cerium oxide powders.
- Successfully coated Lanthanum Phosphate (LP), Lanthanum Zirconate (LZ) and Lanthanum Cerium oxide (LC) by atmospheric plasma spray process.
- Preliminary investigation with respect to microstructure/porosity, thermal cycling. bond test, phase analysis of coatings show promising results.

5 References

[1] X.Q. Cao , R. Vassen, D. Stoever, Ceramic materials for thermal barrier coatings, Journal of the European Ceramic Society, 24(1), 2004, P 1–10.

[2] Henry Lehmann, Dieter Pitzer, Gerhard Pracht, Robert Vassen, and Detlef Stöver, Thermal Conductivity and Thermal Expansion Coefficients of the Lanthanum Rare-Earth-Element Zirconate System, Journal of the American Ceramic Society, 2003, 8(13), p 1338–1344.

[3] Dongming Zhu and Robert A. Miller, Development of Advanced Low Conductivity Thermal Barrier Coatings, International Journal of Applied Ceramic Technology, 2004, 1(1), 86–94.

[4] X. Cao, R. Vassen, W. Fischer, F. Tietz, W. Jungen and D. Stöver, Lanthanum–Cerium Oxide as a Thermal Barrier-Coating Material for High-Temperature applications, Advanced Materials, Journal of the European Ceramic Society, 2003, 15(17), p 1438–1442.

[5] X.Q. Cao, R. Vassen, F. Tietz, D. Stoever, New double-ceramic-layer thermal barrier coatings based on zirconia–rare earth composite oxides, Journal of the European Ceramic Society, 2006, 26(3), P 247–251.

Synthesis and Characterization of 25 % Praseodymium Oxide Stabilized Zirconia Thermal Barrier Coatings

[1]R. Rajeshwari, [4]Dr. Parvati Ramaswamy, [3]Dr. R. Rajendran, [2]Dr.L.Chandrasagar

[1]Asst.Professor and Research Scholar, Dr.Ambedkar Institute of Technology, Bangalore, India
[2]Professor, Dr.Ambedkar Institute of Technology, Bangalore, India
[3] Scientist F, Gas Turbine Research Establishment, Bangalore, India
[4] Consultant, R&D, Dr.Ambedkar Institute of Technology, Bangalore, India

ABSTRACT

Thermal barrier coatings (TBCs) are essential materials in aerospace-related applications such as gas turbine engine blades, combustion chambers etc.; for their dynamic capabilities to protect the metal components from oxidation during high-temperature operations. Typically a two-layered TBC system comprises of a ~250 µm ceramic layer over a ~100 µm metallic "bond coat" on the e.g. the turbine superalloy component. The superalloys have typical melting points of 1230-1315°C in turbine applications, depending on specific compositions. Even a 5% reduction in the component temperature during operation brings in enormous benefit in terms of life of component and performance of the system. Ceramic materials are optimal for TBCs due to their high melting points and good insulation characteristics. Zirconia-based ceramics are the most suited TBC materials and oxides of Y, Ce, Mg, Ca etc. are used to stabilize zirconia to improve its thermo-mechanical characteristics: the dopant character and percentages form important parameters in stabilizing the crystal structural phases of zirconia. Related with this subject of TBCs, important findings from a study on the suitability of a newer compound - i.e. Praseodymium Oxide (Pr_6O_{11}) and its effects on stabilization of the cubic/tetragonal phases of zirconia with optimization of % stabilizer, technique to prepare free-flowing plasma sprayable powders, spray powder characteristics (crystallographic phases, chemical composition, flowability, particle size & distribution, tap density, deposition efficiency etc.), preparation of thermal barrier coatings(TBCs) from the prepared powder, sprayed-coating characteristics (thermal insulation, stability, adhesion, and shock resistance characteristics, microstructure etc) have been presented in this paper. Optimization parameters are discussed with respect to the factors that contribute to the diversity of results obtained.

Introduction

High temperature coatings are used to restrict surface degradation or to thermally insulate the material against the hot environment. Coatings which are used for thermal insulation purposes, called thermal barrier coatings (TBC), are typically made of thermally insulating e.g. ceramic materials and especially partially/fully (PSZ/FSZ) stabilized zirconias. Plasma sprayable powders of desired composition are commercially made by sol-gel/fusion sintering methods. Microwave sintering is used to prepare plasma sprayable powders for time/energy efficiency.

Plasma spray powder compositions& initial processing-XRD patterns of powder compositions shown below

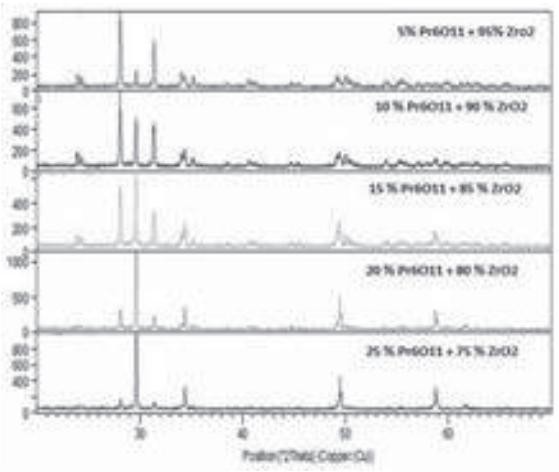

The spray coat powder compositions and %stabilization of Praseodymium Oxide (Pr_6O_{11}) in (ZrO_2, $(Pr_6O_{11})_x(ZrO_2)_{1-x}$ (x = 0.05, 0.10, 0.15, 0.20, & 0.25 is shown below

Compositions	% m- ZrO_2	% c/t- ZrO_2
5%Pr_6O_{11} –ZrO_2	85	15
90%ZrO2+10	62	38
85%ZrO2+	44	56
80 %ZrO2+20	22	78
75%ZrO2+25%Pr6O11	20	80

Each composition was ball milled, subjected to microwave sinter at high temperature (~1600°C) and evaluated for structural phases (c/t ZrO_2). 25% Pr_6O_{11} was the most suitable composition. (80% C/t ZrO2) to be made into plasma sprayable powder.

Plasma sprayable TBC powder preparation

The microwave sintered composition and ball milled material (1-2 µm particle size) was agglomerated by 10% PVA binder and granulated and segregated to obtain spray powder particle sizes between 45 and 90µm.

- **Studies on 25%Pr_6O_{11}-ZrO_2TBC spray powder** Structural Phase (XRD) - c/t phase 83%
- Flowability – 36 g/min
- Particle size- suitable for plasma spray
- Tap density- 2.85g/cc

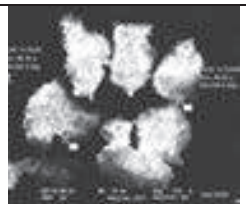

Microstructure analysis via SEM/EDS-

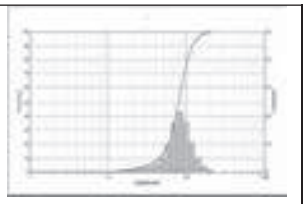

Particle size analysis

Characterization of Thermal barrier coating

- Adhesive strength (ASTM C633-69) – 24 Mpa
- Thermal shock (simulated burner rig): 1200^0C/1 min heat and 1 min cool: 730 cycles to fail (cohesive)
- Structural phase(XRD): c/ t ZrO_2: 100% (as sprayed)
- Structural phase(XRD) thermal shock tested:failed: c/ t ZrO_2: 83%
- Structural phase(XRD): thermal shock tested, failed, extent of destabilization to monoclinic -ZrO_2: 17%

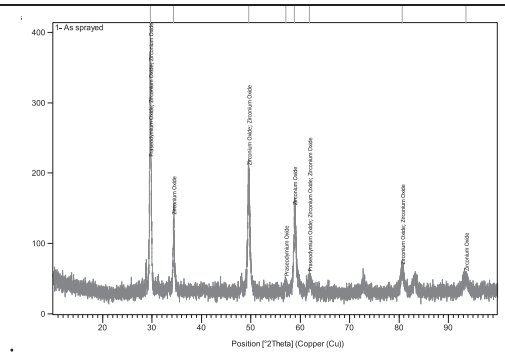

XRD,Pr_6O_{11}-ZrO_2: As sprayed surface

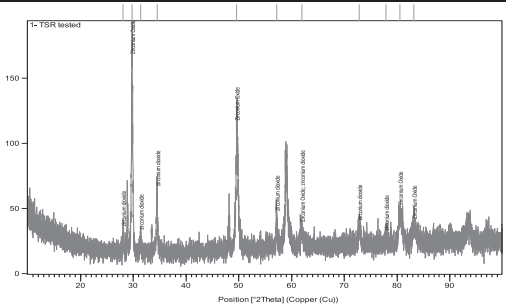

XRD, Pr_6O_{11}-ZrO_2: thermal shock, 730 cycles (Fail)

Cross Section Microscopy (SEM)

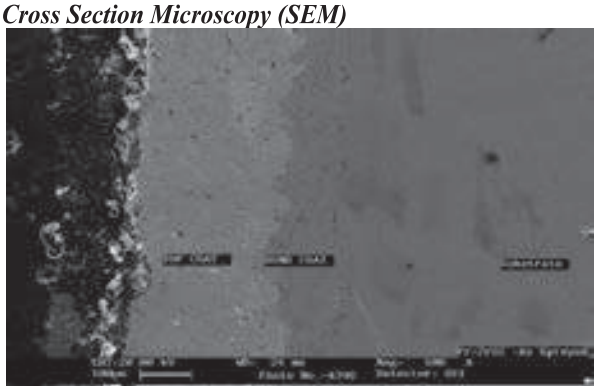

Cross section of coating – as sprayed

Around 300 microns top coat, ~75 microns bond coat, smooth ceramic bond coat interface were the characteristics of the as sprayed coating, viewed in mounted and polished cross section. EDS analysis showed presence of suitable quantities of Pr in the as sprayed coating material.

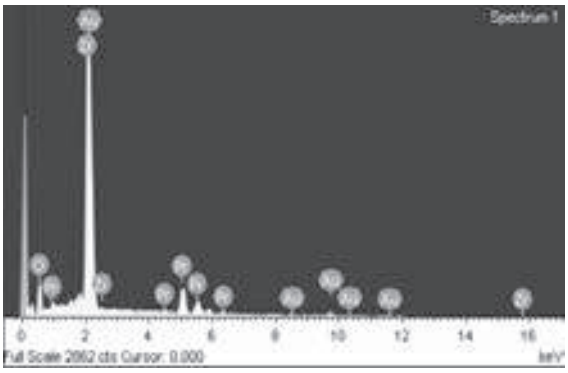

The failure of the top-coat, cohesive in nature, when viewed in cross section, revealed delamination of the top coat layers. The bondcoat -ceramic interface was intact, confirming the failure mechanism due to destabilization of the top most ceramic layers when exposed to high temperature

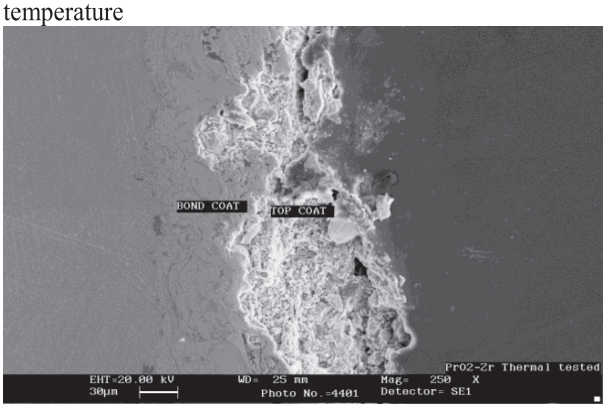

Coating cross section – failed after thermal shock test

Concluding summery

The present study involving preparation of plasma sprayable powder using microwave sintering process has been established in our laboratory and which has been presented. However, while praseodymium oxide allows itself to stabilize ZrO_2 to cubic/tetragonal phase, the Pr_6O_{11}-ZrO_2 system does not appear to be a promising candidate for TBC applications due to the destabilization it undergoes to monoclinic ZrO_2, when exposed to high temperatures of the order of 1200^oC. Other applications of this process (microwave sintering) and coating material will be explored further

.

Typical literatures Reviewed

Preparation and characterization of photoluminescent praseodymium-doped ZrO2 nanostructured powders, Journal of Physics, 37 (2004) L1–L4 SICS,

Relation between structural properties of Pr^{3+}-doped yttria-stabilized zirconia nanopowders and their luminescence efficiency, Journal of Scripta Materialia, Volume 61, Issue 4, August 2009, Pages 415–418

Mesoporous structure of praseodymium-stabilized zirconia, Journal of Materials Letters, Volume 61, Issue 1, January 2007, Pages 192–195

Synthesis Mechanism of Low-Voltage Praseodymium Oxide Doped Zinc Oxide Varistor Ceramics Prepared Through Modified Citrate Gel Coating , International Journal of Molecular Sciences2012, 13, 5278-5289

Studies on the Mechanical and Oxidation Resistance Properties of CoNiCrAlY/Al_2O_3/YSZ Compositionally Graded Thermal Barrier Coating Developed by Air Plasma Spraying

Subhasisa Nath[1], Indranil Manna[1,2], Jyotsna Dutta Majumdar[1]
[1] Department of Metallurgical & Materials Engineering, Indian Institute of Technology, Kharagpur 721302, India
[2] Indian Institute of Technology, Kanpur 208016, India

Abstract
The service life of thermal barrier coating (TBC) is determined by it's mechanical properties like Young's modulus and toughness and high temperature oxidation resistance (under isothermal condition). Conventionally, TBC is composed of Yttria stabilized Zirconia (YSZ) top coating applied on MCrAlY bond coat. Alumina is also a promising diffusion barrier coating which has improved performance against high temperature oxidation and hot corrosion. However, large probability to sintering, high Young's modulus and low coefficient of thermal expansion are the drawbacks associated with application of alumina as the thermal barrier coating. The present study concerns development of a compositionally graded CoNiCrAlY/Al_2O_3/YSZ thermal barrier coating by thermal spray deposition route and a detailed investigation of mechanical (Young's modulus, hardness and fracture toughness) and high temperature oxidation resistance properties (under isothermal condition) of the compositionally graded TBC and its comparison with conventional CoNiCrAlY/YSZ duplex TBC. The properties achieved in the graded coating are analyzed and compared with the duplex coating.

1 Introduction

Ceramic insulating materials are applied as thermal barrier coating, on to the surface of metallic components which operates in high temperature environment to limit the heat transfer towards the substrate [1]. The dominant failure mechanisms usually observed in conventional duplex TBCs are due to the stress generated because of (a) thermal expansion mismatch between the ceramic top coat and metallic bond coat and (b) growth of TGO during oxidation of bond coat [1]. The oxidation of bond coat occurs by the diffusion of oxygen through the ceramic top coat and the growth rate of TGO is influenced by the partial pressure of O_2 (P_{O2}) available at the bond coat and top coat interface. Hence, application of oxygen diffusion barrier coating between the top coat and bond coat has been helpful in lowering the TGO growth rate [2]. In the present study, a detailed investigation of isothermal oxidation behavior of compositionally graded CoNiCrAlY/Al_2O_3/YSZ TBC has been undertaken (kinetics and mechanism) and compared with conventional duplex TBC of CoNiCrAlY/YSZ.

2 Experimental

In the present study, Ni-based superalloy (Inconel 718) of 20 mm × 20 mm × 5 mm dimensions are used as substrate. CoNiCrAlY bond coat is deposited on sand blasted Inconel 718 superalloy substrate using high velocity oxy-fuel spray (HVOF) technique. The details of parameters used for the developemnt of duplex and compositionally graded TBC have been reported elsewhere [3]. The composition of the compositionally graded CoNiCrAlY/Al_2O_3/YSZ TBC consists of the mixture of CoNiCrAlY and Al_2O_3 in the ratio of 70:30, 50:50, 30:70, and 0:100 applied onto the surface of 100% CoNiCrAlY followed by a coating mixture of Al_2O_3 and YSZ in the ratio of 70:30, 50:50, and 30:70 on top of already developed 100% Al_2O_3. Isothermal oxidation studies of the coated samples are undertaken by holding the samples isothermally in air at temperatures ranging from 900 °C to 1000 °C and subsequently, measuring the weight change at regular interval from 1 hour to 96 hours. Microstructural analysis of the coating is carried out by field emission scanning electron microscope. Phase and residual stress are measured by x-ray diffraction technique. Indentation fracture toughness is measured by indenting at the bond coat and top coat interface with Vickers indenter at 5 Kgf and 10 Kgf load and holding at the maximum load for 10 s. The indentation fracture toughness (K_{IC}) of the interface is obtained using the following equation [4]:

$$K_{IC} = 0.016\left(\frac{E}{H}\right)^{1/2}\frac{P}{c^{3/2}}$$

Where, P is the applied load in Kgf, c is the crack length in μm, E is the Young's modulus in GPa and H is the hardness in GPa.

3 Results & Discussion

3.1 Microstructural Characterization

The cross-sectional microstructure of (a) CoNiCrAlY/YSZ duplex and (b) CoNiCrAlY/Al_2O_3/YSZ compositionally graded TBC deposited by plasma spraying technique is shown in **Fig. 1**. Heterogeneous distribution of microstructural defects (globular porosities/voids, intralamellar cracks, and interlamellar pores) is evident from **Fig. 1**. Improper melting of the powder particle, entrapment of carrier gases, and poor intersplat bonding between the splats cause the formation of these defects [5]. Though, these defects act as paths for the diffusion of oxygen, however, the presence of the defects increases the strain tolerance capacity of the TBC system as well as reduces thermal conductivity effectively by acting as phonon scattering centers [6].

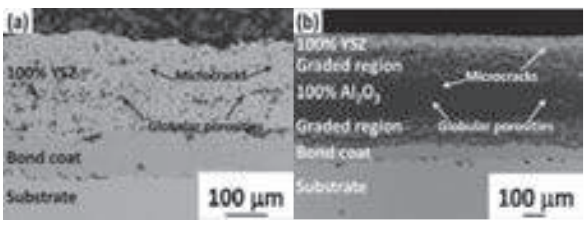

Fig. 1. *Microstructure of cross-section of (a) duplex CoNiCrAlY/YSZ TBC and (b) compositionally graded CoNiCrAlY/Al_2O_3/YSZ TBC.*

3.2 Isothermal Oxidation

Isothermal oxidation results are shown in **Fig. 2**. The mass gain per unit area in compositionally graded TBC is higher than that in duplex TBC both at 900 °C and 1000 °C. In the case of oxidation carried out at 950 °C, no significant difference between the mass gain curves for duplex and graded TBC is observed, initially, up to 24 hour of oxidation beyond which the mass gain in graded TBC shows a decreasing trend with increase in oxidation temperature. At 1000 °C, the severity of oxidation in graded TBC is more severe. The higher mass gain in graded TBC as compared to duplex TBC is attributed to the rapid oxidation of metallic elements present in the graded regions due to the spallation of coating.

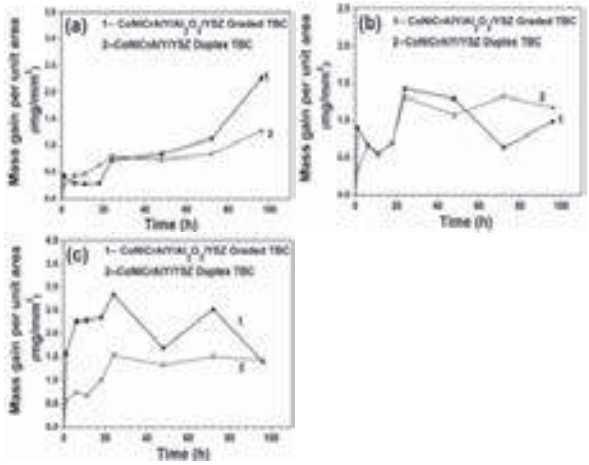

Fig. 2. *Kinetics of isothermal oxidation in compositionally graded (plot 1) and duplex (plot 2) TBC at (a)900 °C, (b) 950 °C, and (c)1000 °C.*

3.3 Post-oxidation Analysis

The post oxidation microstructural analysis of graded TBC and duplex TBC after oxidation at 900 °C up to 96 hour is shown in **Fig. 3**. Formation of TGO at the interface between top coat and bond coat is evident from **Fig. 3a**. The formation TGO is the result of oxidation metallic elements present in the bond coat to that of atmospheric oxygen. The graded TBC shows complete spallation after thermal exposure for 96 hour as observed from **Fig. 3b**. The spallation is observed at the interface between 100% Al_2O_3 and 70% Al_2O_3 + 30% CoNiCrAlY coating layers. The spallation in the graded TBC is observed during cooling period which indicates that the failure in graded TBC is attributed to the developemnt of large residual thermal stress.

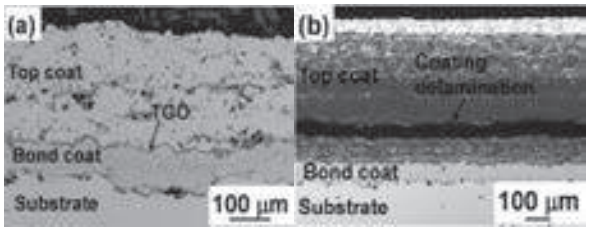

Fig. 3. *Microstructure of cross-section of (a) duplex CoNiCrAlY/YSZ TBC and (b) compositionally graded CoNiCrAlY/Al_2O_3/YSZ TBC after isothermal oxidation at 900 °C for 96 hour.*

3.4 Indentation Fracture Toughness

Indentations are made at the interface between 100% Al_2O_3 and 70% Al_2O_3 + 30% CoNiCrAlY layers and 30% Al_2O_3 + 70% CoNiCrAlY and 100% CoNiCrAlY layers as shown in **Fig. 4**. The fracture toughness at the interface between 100% Al_2O_3 and 70% Al_2O_3 + 30% CoNiCrAlY layers and 30% Al_2O_3 + 70% CoNiCrAlY and 100% CoNiCrAlY layers are measured to be 0.42 MPa.$m^{-1/2}$ and 8.2 MPa.$m^{-1/2}$, respectively. The maximum crack length of 644 µm is observed at the interface between 100% Al_2O_3 and 70% Al_2O_3 + 30% CoNiCrAlY layers with an applied load of 5 Kgf, whereas a crack length of 234 µm is obtained at the interface between 30% Al_2O_3 + 70% CoNiCrAlY and 100% CoNiCrAlY coating with an applied load of 10 Kgf. From the results, it is observed that the at the interface with 100% Al_2O_3, the fracture toughness is inferior which resulted in spllation of the coating.

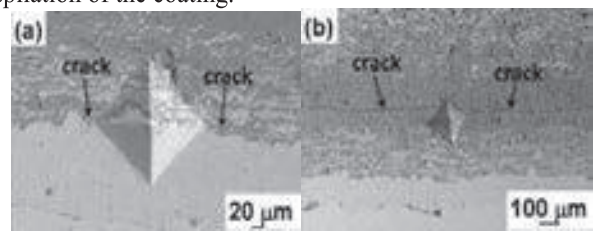

Fig. 4. *Microstructure of cross-section showing indentataion at the interface between (a) 70% CoNiCrAlY and 100% CoNiCrAlY layers and (b) 100% Al_2O_3 and 70% Al_2O_3 + 30% CoNiCrAlY layers.*

4 Conclusions

The following conclusions may be drawn from the present study:

1. The graded CoNiCrAlY/Al_2O_3/YSZ TBC shows inferior oxidation resistance as compared to duplex TBC. Complete spallation of the graded coating is observed at the early stage of oxidation.
2. The fracture toughness of the interface close to Al_2O_3 layer shows the lowest value which is the main reason for the complete spallation of graded TBC.

5 References

[1] W. R Chen, X. Wu, B. R. Marple and P. C. Patnaik: Surf. Coat. Technol. 197 (2005) 109-115.

[2] W.Y. Lee, D.P. Stinton, C.C. Berndt, F. Erdogan, Y.D. Lee and Z. Mutasim: J. Am. Ceram. Soc. 79 (1996) 3003-3012.

[3] S. Nath, I. Manna and J. Dutta Majumdar: J. Therm. Spray. Technol. 22 (2013) 901-17.

[4] G.R. Anstis, P. Chantikul, B.R. Lawn and D.B. Marshall: J. Am. Ceram. Soc. 46 (1981) 533-542.

[5] L. Pawlowski: The science and engineering of thermal spray coating. 2nd ed. England: John Wiley and Sons Ltd; 2008.

[6] A.A. Kulkarni, A. Goland, H. Herman, A.J. Allen, J. Ilavsky, G.G. Long, C.A. Johnson and J.A. Ruud: J. Am. Ceram. Soc. 87 (2004) 1294–1300.

Thermal barrier coating on Al-alloy 2024 for protection under isothermal and cyclic heating conditions

Dipak Kumar[1], K.N.Pandey[2], Dipak Kumar Das[3]
[1,2] Department of Mechanical Engineering, Motilal Nehru National Institute of Technology, Allahabad 211004, India
[3] Defence Metallurgical Research Laboratory, Hyderabad-500057, India

Abstract

Yttria stabilized zirconia (YSZ) thermal barrier coatings (TBCs) are being used on several Al-alloys for automotive applications. Evaluation of TBC coated Al-alloys such as AA 2024 under thermal cycling conditions at temperatures up to 700°C has been reported. In the present study, the microstructural aspects of air plasma sprayed 7% YSZ (7YSZ) coating on alloy AA 2024 has been examined under both isothermal and cyclic loading conditions at 600 and 700°C. The purpose of testing the coated Al-alloy at the above temperatures was to check the ability of 7YSZ coating in providing thermal insulation to this alloy. The extent of cracking in the coating, as observed on the sample surface, increased with increase in cycling temperature. Localized through-thickness cracks were found at the corners of the square-shaped specimens and the extent of such cracking also increased with increase in cycling temperature. The above localized cracking led to rapid delamination of the coating at the sample corners. Under isothermal loading, however, the coating spallation occurred over the entire sample surface, which was unlike the localized spallation observed under thermal cycling.

1. Introduction

Thermal barrier coatings (TBCs) are used as thermal insulating materials to improve the in-service performance of high temperature exposed components such those in as gas turbines and internal combustion (IC) engines. IC engine components such as pistion head, fire decks and exhaust manifolds are provided with a TBC for reducing cylinder heat rejection and thermal fatigue protection of the metallic parts [1-3]. Typicically, a TBC consists of an outer yttria stabilized zirconia ceramic coating for sustaining high temperature gradients and an inner MCrAlY (M = Co/Ni or both) bond coat (BC). The bond coat provides oxidation resistance at high temperatures and also aids in the adhesion of the TBC to the substrate [4,5]. The primary objectives of applying a TBC on a piston surface are to decrease heat flux into the piston, to provide it protection against thermal stresses, and fuel-related corrosion and also to reduce vehicular emissions [6-8]. Top surface of the piston near the crevice is specifically chosen as the place for TBC deposition to decrease the risk of knocking in SI gasoline [9].

Keeping in view the application of aluminium alloys in IC engines, the present study examines the microstructural aspects of 7% yttria stabilized zirconia (7YSZ) thermal barrier coating on an automotive grade Al-alloy AA 2024-T351 under isothermal and thermal cycling loads at temperatures of 600^0C and 700^0C.

2. Experimental Details

Specimens prepared from Al-alloy AA 2024-T351 and having dimensions of 25×25×6 mm were used for coating deposition. The chemical composition of the above alloy is given in Table1. The specimens were first blasted using alumina grits (of size 125 μm) to remove surface scales. Subsequently, a CoNiCrAlY bond coat of 150 μm thickness was deposited on their surfaces by air plasma spray (APS) method. Subsequently, a 7YSZ top coat with an approximate thickness of 250 μm was also sprayed on the bond coated specimens by APS technique. Coatings were done at Sai Surface Coatings and Technology, Patencheru (Hyderabad) India. Parameters used for BC and 7YSZ coating deposition are provided in Table 2 and 3, respectively.

Table.1: *Chemical Composition of AA2024-T351*

Elements	*Cu*	*Mg*	*Si*	*Zn*	*Mn*	*Al*
Compositions (%)	*4.7*	*1.4*	*0.5*	*0.25*	*0.5*	*Balance*

Table.2: *Spraying Process Parameters for bond coat*

Current (A)	*Voltage (V)*	*Pr.gas,Ar (l/min)*	*Sec.gas,H_2 (l/min)*	*Powder feed rate (g/min)*	*Spray dist. (mm)*	*Power (kW)*
550	*67*	*43*	*9.5*	*20*	*102*	*37*

Table.3: *Spraying Process Parameters for YSZ coating*

Current (A)	*Voltage (V)*	*Pr.gas,Ar (l/min)*	*Sec.gas,H_2 (l/min)*	*Powder feedrate (g/min)*	*Spray dis.(mm)*	*Power (kW)*
600	*71*	*44*	*13*	*20*	*102*	*42.6*

The schematic of the thermal cycling test set-up used in this study is shown in Fig.1 (a) and one typical thermal cycle in Fig. 1(b). Cycling of coated specimens was carried out at 600 and 700°C. When more than about 30% of a coating developed visual cracks during cycling, the coating was considered to have failed..

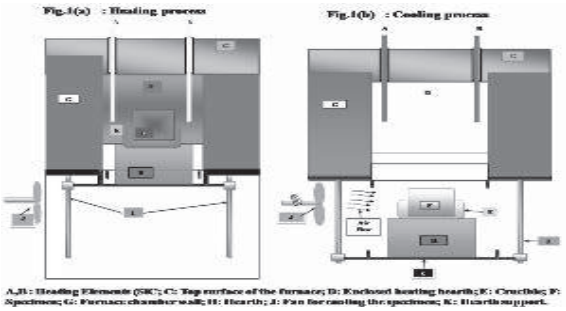

Fig.1(a)Heating stage of thermal cycle,(b)Cooling stage of thermal cycle.

Isothermal test of the coated samples was conducted at 700^{0}C for 4 hours. The same criterion, as mentioned above, was used for deciding the failure of the ceramic coating of the TBC under isothermal loading..

3. Results and discussion

Figure 2 shows the as-sprayed YSZ coating surface which revealed the typical presence of porocity and some micro-cracks in the coating. However, during thermal cycling, the ceramic coating developed a network of cracking in a mud-crack patteren, as shown in Fig. 3, after 97 cycles at 600^{0}C. Such damage to the coating can be ascribed to the thermal stresses that were generated in the YSZ layer due to cyclic heating and cooling. The coated specimens did not show drastic weight changes during cycling till the spallation of the YSZ layer began after about 95 cycles (Fig. 4). Similar observations were also made in case of samples cycled at 700°C, although the extent of cracking was higher for 700°C. The coating cracking and failure primarily began at the sharp corners and edges of rectangular specimens,refers to Fig.5.

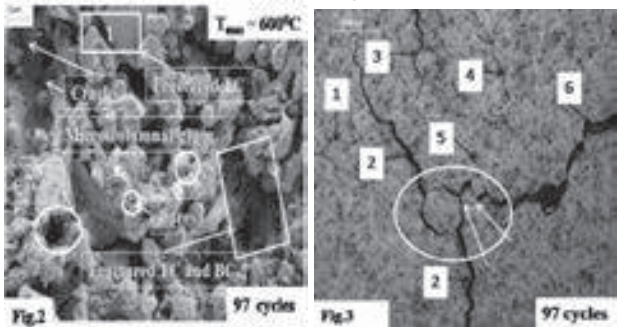

Fig.2.SEM image of TF coatings, and Fig.3. OM image of TF coatings at maximum thermal cyclic temperatures of 600^{0}C.

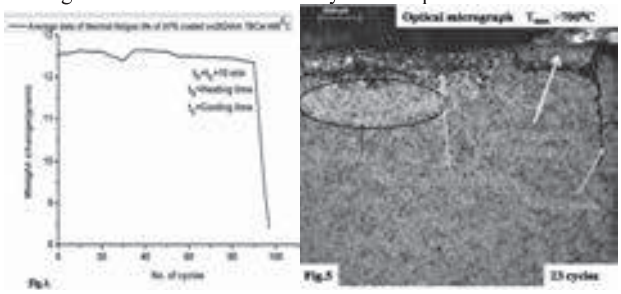

Fig.4.Weight change with thermal cycles, and Fig.5.Optical Microscopic (OM) image of TF coating at maximum thermal cyclic temperature of 700^{0}C.

In case of specimens that underwent isothermal exposure at 700°C for 4 h, the YSZ coating splalled at various locations over the entire specimen surface (Fig.6). There was no preference for cracks to develop at the sharp corners of the specimens, as observed under thermal cycling.

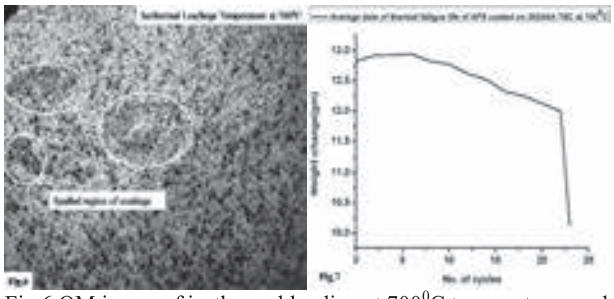

Fig.6.OM image of isothermal loading at 700^{0}C temperatures,and Fig.7. Weight change with thermal cyclic temperature at 700^{0}C.

Fig.7 shows the thermal degradation phenomenon due to weight loss/gain of TBCs sample subjected to thermal cyclic loading test at 700^{0}C.

Failure of the 7YSZ layer of the TBC under both cycling and isothermal loading with or without development of cracking/spallation is expected to have been caused by the thermal stresses arising from the thermal expansion mixmatch between the YSZ layer and the bond coated metallic AA 2024 alloy. Coating failure started from the comparatively high stressed areas such as edges or corners [10] because of the singularity of thermal residual stresses at such locations [12]. Subsequently, the failure propagated to adjacent areas of the coating. In all cases, damage of the YSZ coating occurred progressively starting with microscopic cracks within the coating, which ultimately induced fracture through in-plane crack propagation with or without spallation.

4. Conclusions

- In both cyclic and isothermal loadings, failure of the YSZ coating of the TBC occurred by the initiation of cracks at the high stress regions such as edges/corners of the rectangular specimens.
- The extent of cracking in the coating, as observed on the sample surface, increased with increase in cycling temperature.
- The above localized cracking led to rapid delamination of the coating at the sample corners.

References

[1] C.R.C.Lima and J.M. Guilemany: Surf.Coat.Technol. 201 (2007) 4694–4701.
[2] D. W.Parker: Mater.Des.13 (1992)345-351.
[3] M.B. Beardsley, P.G. Happoldt, E .F. Rejda and D.F. Socie: High Eff. Diesel Engine Applications,1999.
[4] A. Gilbert, K. Kokini and S. Sankarasubramanian: Surf.Coat.Technol.203(2008) 91-98.
[5] A.Gilbert, K. Kokini and S. Sankarasubramanian: Surf. Coat. Technol. 202 (2008) 2152-2161.
[6] T. Hejwowski and A. Weronski:Vacuum65 (2002)427-432.
[7] E. Buyukkaya: Surf.Coat.Technol.202(2008)3856-3865.
[8] E. Buyukkaya and M. Cerit : Surf.Coat.Technol. 202 (2007) 398-402.
[9] M. Cerit, V. Ayhan, A. Parlak and H. Yasar: Appl. Therm. Eng. 31(2011)336-341.
[10] C. Giolli, A. Scrivani, G. Rizzi, G. Bolelli and L. Lusvarghi: J. Therm. Spray Technol.18 (2009) 223–230.
[11] R. Ghasemin, R. Shoja-Razavi, R. Mozafarinia and H. Jamali: Ceram. Int. 40 (2014) 347 – 355.

Deformation and fracture behaviour of chromium carbide-nickel chromium wear resistant coating

S.S.K.Balam, M.Tamilselvi, J.Chitra, V.U. Bagade, R.Rajendran
Gas Turbine Research Establishment, CV Raman Nagar, Bangalore 560093, India

Abstract
Compressor disc of higher stages of an aero engine experiences a temperature of around 600 degree centigrade during operation. While in rotation, this disc comes in contact with the stator blade due to close clearance between these two components. As the disc is not expendable and is therefore to be protected, stator blades are permitted to undergo rub and wear. This is achieved by protecting the disc with hard high temperature wear resistant coating. As hard coatings are brittle in nature, it is of interest to know the mechanical behaviour of them. Chromium carbide-nickel chromium powder was thermally sprayed through high velocity oxy fuel (HVOF) process to characterize for microstructure and hardness. Instrumented tensile test was carried out on coated specimens by fixing T-rosettes at the front and rear side of the coated specimen, with one axis of the rosette element aligned to the loading axis. Longitudinal and transverse strains were recorded with increasing axial load. elastic modulus and Poisson's ratio of the coating were estimated from the recorded data. Segmented cracks have initiated and propagated across the width of the coating.

1 Introduction

Study of mechanical behavior of wear resistance coating is of interest as it can generate input for component design. Several techniques were in use to measure these properties namely, Nano indentation, Impulse excitation and Bend test [1]. But these techniques have inherent limitations like probing small volumes, difficulty in evaluating fracture strains and Poisson's ratio. Tensile testing can overcome these diffuclties in a single test but the real challenge would be the experimenation on the coating–substrate composite specimen to extract coating properties. Similar exepriments were done earlier on film coatings[2]. In the present investigation an attempt was made through instrumented tensile test to evaluate the mechanical properties of the Chromium carbide-nickel chromium coating.

2 Experimental

2.1 Coating

Chemically clad Cr_2C_3-20(Ni20Cr) cermet powder with typical particle size disribution of -45 +5.5 µm was HVOF sprayed onto oneside of a SU-718 alloy tensile test specimen. The tesile test specimen was manufactured as per ASTM E8 with a thickness of 2.03 mm, guage length 50 mm and guage width 12.5 mm. Thickness of the coating was 604±9 µm and the microstructure is shown in Fig. 1.

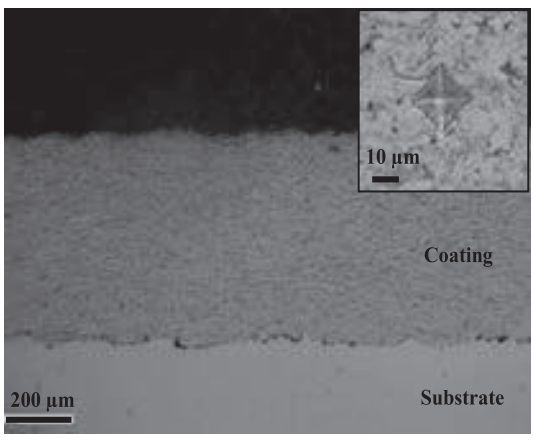

Fig. 1. *Microstructure of the coating. Inset shows its quality at higher magnification and microindentation.*

Porosity in the coating measured through image analyis was less than 1% and the measured microhardenss was 934±27 $HV_{0.3}$.

2.2 Mechanical testing

Two Vishay make T-rosette (guage factor 2.11, guage resistance 350 Ω) were fixed at the center of the guage length on both sides of the tensile test specimen using epoxy adhesive M Bond 610. This specimen was tested using a MTS universal testing machine with constant cross head velocity of 0.05 mm/min. During testing, strain guage signal was collcted by a data aquisition system through Vishay 2310 signal conditioner. An in-situ microscope was used to continously record the events during testing. Typical mechanical testing setup is shown in Fig. 2.

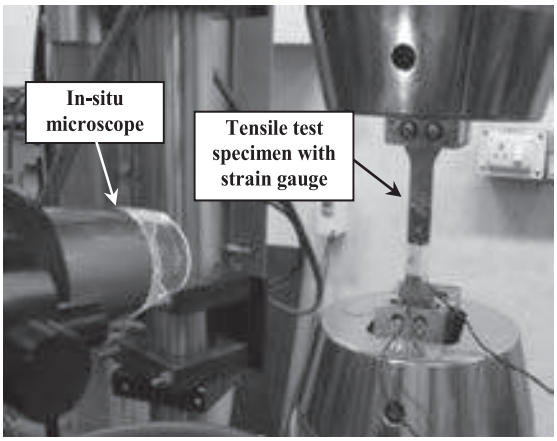

Fig. 2. S*etup for mechanical testing.*

3 Results & Discussion

3.1 Deformation response

The axial and transverse strain response on the coated and bare surface of the specimen is shown Fig. 3. It's clearly seen from Fig. 3 that the strain response on both sides of the specimen were identical up to an axial strain of 1068 µε. The strain response on the coated surface becomes non linear beyond this strain due the reason that micro cracking intiated in the coating. This was corroborated by a clear

distinguishable crackle sound. The immediate decrese in the axial strain rate is attributed to change in the compliance of the coating. The following steep raise is attributed to crack opening below the strain guage. The coating delamination from the substrate was observed at nearly 3,100kgf.

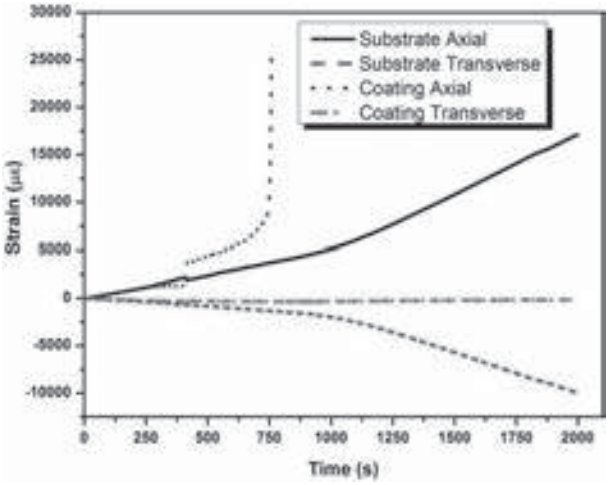

Fig. 3. *Strain response of the coated test specimen*

3.2 Coating elastic modulus

Considering coating and substrate as a composite assemly, elastic moduls for the coating (E_c), is derived from the composite specimen and is given as

$$E_c = \frac{\frac{P}{\varepsilon} - E_s A_s}{A_c} \qquad (Eq.1)$$

Here, P and ε are respectively the load and strain of the coatig-substrate composite specimen. E and A are the elastic moduls, area respectively and the subscripts c and s represent corresponding properties for coating and substrate.

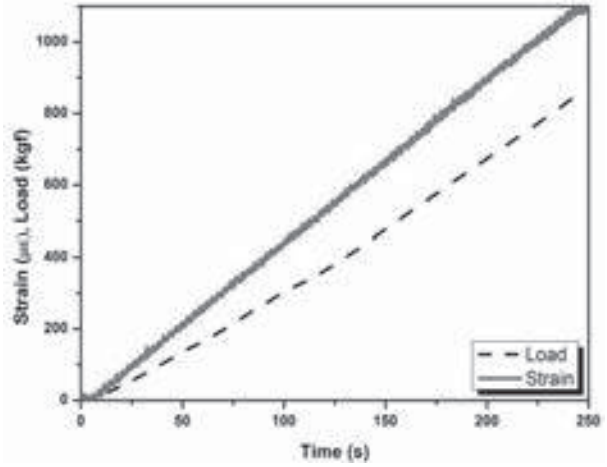

Fig. 4. *Load and strain data for the coated test specimen.*

The intial time response of load and strain for the coated tensile test specimen is shown in Fig. 4. Elastic modulus of the coating calculated using Eq.1 and linear fits of the of the Fig. 4. yielded a value of 332 GPa. This value is inline with expected values for Cr_2C_3-20(Ni20Cr) cermet [3].

3.3 Coating Poisson's ratio

Strian gauge signals for the axial and transverse direction on the coated surface are shown in Fig. 5. Composite Poisson's ratio calculated from the slopes of the linear fits gave a value, 0.25.

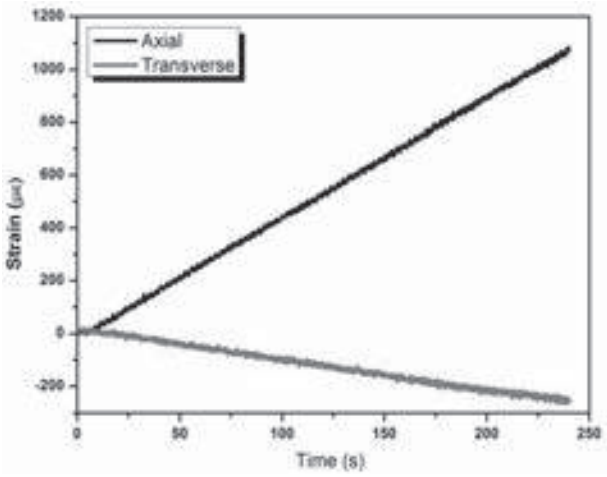

Fig. 5. *Axial & Transverse strains on the coated surface.*

Considering the composite Poisson's ratio as the mean of coating and substrate, the coating Poisson's ratio was found to be 0.18 using substrate poisson's ratio of 0.32 [4]. This in good correlation with reported literature value of 0.2 [3].

3.3 Fracture response

Fracture stress of the coating is estimated from fracture strain of 1068 με as 354 MPa.

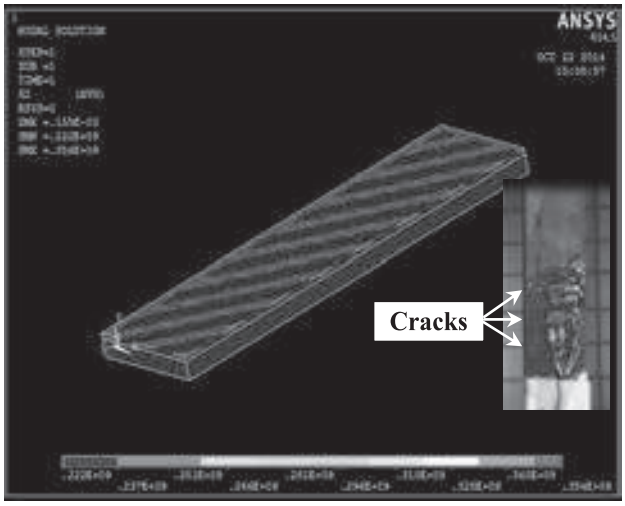

Fig. 6. *Stress contour of the coating. Inset shows coating fragmentation observed on the test specimen.*

Finite element analysis using ANSYS gives the stress pattern on the coating as shown in Fig. 6. Stress contour of the coating indicates fracture pattern that correlates well with the experiment. Similar fracture pattern was observed earlier on Al_2O_3 coated Al-5%Mg substrate [2].

3 References

[1] W. Tillmann, U. Selvadurai, and W. Luo: Journal of Thermal Spray Technology. **22(2-3)**（2013）290-298.

[2] C. Xie, W. Tong: Acta Metall. **53**（2005）477-485

[3] M. Antonov and I. Hussainova: Proc. Estonian Acad. Sci. Eng. **12(4)** (2006), 358-367

[4] R. Rajendran, V. Petley and B.Rehmer:Proc. Imech E Part L: J Materials:Design and Applications. **227(3)** (2012), 243-249

High temperature tribological behaviour of thermally sprayed wear resistant coatings

Vivek Arya, Ramandeep Mandia and K. Vidyasagar
Surface Coatings and Treatment Laboratory, BHEL Corporate R&D Division, Vikasnagar,
Hyderabad-500093, India. email: vivek@bhelrnd.co.in

Abstract
Friction and wear studies are major concerns in the performance and reliability of components where sliding contacts are involved. Various thermally sprayed wear resistance coatings have been studied in earlier studies which are used for many industrial applications. At high temperature, importance of tribological studies of these wear resistant coating are more significant due to change in its wear resistance, seizure resistance and thermal compatibility with the mating substrate. The development of high-quality piercing plug is one such example in the production of seamless steel pipe. The piercing plug contact directly with high-temperature steel and is subjected to great friction in the process of piercing. At the same time, the piercing plug experiences mechanical and thermal shock leading to failure such as nasal cavity collapse, deformation, steel plating and cracking. Chromium carbide, alumina titania based wear resistant coatings by HVOF/D-gun/plasma processes is potential candidates for such high temperature applications. In this study, these thermally sprayed coating are deposited on steel substrate and their tribological behaviour are studied. Wear behaviour of these coatings is analysed using high temperature pin-on-disk experiments. The sliding wear characteristics of these coating under various test conditions are discussed and reported in this paper.

1 Introduction

Tribology deals with phenomena related to wear and friction. Wear can be defined as the progressive loss of material form the surface of the body due to relative motion of the surface with respect to another body. The components that are subjected to frictional contact are prone to wear in some or other way. The tribological behaviour of the surface is governed by numerous factors and it is not unique to any particular material or coating and largely controlled by the complete tribo system, which consists of the materials, surface properties, interaction mode like sliding or impacting, interaction condition like presence of lubrication, temperature etc. [1].

Piercing plugs are used in the process of rolling seamless steel pipe for piercing and rolling at high temperature into hollow billets for further rolling into tubes. The piercing plug contacts directly with high-temperature steel in the production of seamless steel pipe and bear a great friction in the process of piercing. The life of plugs is matter of concern as the average wear out rate of piercing plug is 120 grams per ton of production. The piercing plug goes through severe cycles - thermal fatigue, high temperature metal to metal wear, galling, oxidation besides softening after some service. These piercing plugs are made of alloy steel and a suitable coating is required to take care of all these aspects. Chromium carbide, alumina titania based wear resistant coatings by HVOF/D-gun/plasma processes are potential candidates for this application.

Yougquang Guo studied in-situ synthesized TiC reinforced Ni based composite coatings by laser cladding for piercing plug application [2]. Friction and wear behaviour of various coatings such as chromium carbide, chromium oxide, chromium oxide +titania+silica, NiCrAlY and Al_2O_3 + NiCr deposited by plasma spray and D-gun was studied at high temperature of 550^oC for steam turbine valve spindle application [3]. Chromium carbide coating deposited by plasma spraying has been identified as the most suitable coating for this application. Alumina-titania, titania, chromia and chromia-titania coatings are being used for many industrial applications [4-8]. Yesim et.al. studied these coatings with atmospheric plasma-spray coating techniques (APSCTs) on a low-frequency reciprocating-sliding tribometer. The denser Cr_2O_3 coatings showed a higher wear resistance than the more porous Al_2O_3-TiO_2 and TiO_2 coatings. Cr_3C_2-NiCr coating is reported to be used for good oxidation, abrasion, particle erosion, fretting, cavitation resistance and hot gas corrosion resistant up to 870^oC. Al_2O_3 + TiO_2 coating are also used as corrosion, abrasion, erosion and sliding wear resistant coatings up to temperature of 1100^0C. In the present study, characterisation and evaluation of the sliding wear behaviour of Al_2O_3 + TiO_2 and Cr_3C_2-NiCr coating under various test conditions are carried out.

2 Experimentation

2.1 Sample preparation

Suitable samples have been made from alloy steel as per the drawing, **Fig 1**. These disc samples are needed to carry out high temperature tribological studies.

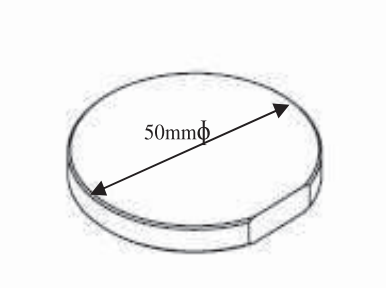

Fig. 1. S*ample disc for high temp tribological studies*

The samples were first girt blasted using alumina grit to achieve optimum surface finish before coating. This is important to get proper adhesion of coating with base material. Al_2O_3 + TiO_2 (ALT) coating was carried out by D-gun process. A bond coat of NiAl is given before Al_2O_3 + TiO_2 coating. Cr_3C_2-NiCr (CRC) coating was carried out by liquid fuel HVOF system on the steel samples. These coating were carried out by already established process parameters explained elsewhere [3].

2.2 Characterisation

These coating were characterised for its micro-hardness, microstructure, thickness etc. The coated samples have been cut in the slow cutting machine and then mounted in bakelite. The mounted specimen is polished to see the microstructure. Optical micrographs were taken using Image analyser at a magnification of 100X to see coating microstructure and interface between top coat, bond coat and base material. **Fig 2 (a & b)** shows the micrograph of Al_2O_3 + TiO_2 and Cr_3C_2-NiCr coatings respectively. The micrographs clearly show that these coating are uniform and interfaces are free from any defects.

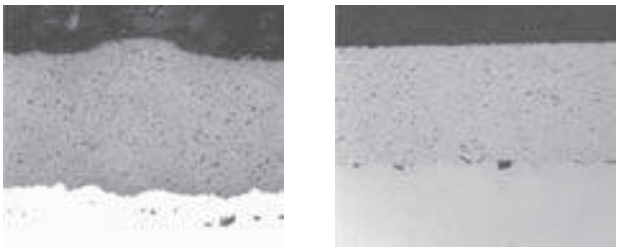

a) Al_2O_3 + TiO_2 coating *b) Cr_3C_2-NiCr coatings*

Fig 2: *Optical micrograph of each coating at 100x*

Cr_3C_2-NiCr coatings were found to be more dense (porosity ~ 0.5%) than Al_2O_3 + TiO_2 coatings (porosity ~ 2%). Coating thickness was in the range of 300-400 microns for both the coating. The surface finish achieved on the test specimen was Ra 5-6 µm. The Vicker's micro hardness was measured using Tukon 2100 Macro/Micro hardness tester by applying a load of 300 gm with a dwell time of 13 seconds. The surface hardness was in the range of 780 $HV_{0.3}$ for Al_2O_3 + TiO_2 and 1100 $HV_{0.3}$ for Cr_3C_2-NiCr coatings.

2.3 Evaluation

These coating were evaluated using high temperature Pin-on-disc tribometer. High temperature tribometer (with pin-on-disk / ball-on-disk friction) is intended for determining tribological properties of engineering materials and lubricants used for sliding contacts to determine the wear resistance and friction coefficient for a pair of materials, depending on sliding velocity, applied load, presence and kind of a lubricant, temperature in the test chamber, kind of a gas in the test chamber and other factors. The Tribometer consists of the stationary pin (ball) pressed at the required load against the disk rotating at the defined speed. The friction couple is inserted in the insulated test chamber equipped with the heater, which enables to raise the temperature and keep it constant. It is possible to control the atmosphere by introducing a gas into the test chamber. The measured values are displayed on the monitor screen and saved on the computer disk.

Al_2O_3 + TiO_2 and Cr_3C_2-NiCr coatings are tested against steel balls under reciprocating motion by varying loads (20N and 60N) at RT as well as high temperature of 750°C. The contact mechanism consists of steel ball over coated disc without any lubrication moving in cyclic motion of straight line. The wear in terms of depth of erosion is recorded along with friction data. These data were compared for each coating.

The wear pattern on coated disc is also analysed using optical profilometer. An optical profilometer is a white light interferometer that creates sub nm resolution images widely used to measure surface roughness, step height, film thickness etc.

The test at room temperature shows that coefficient of friction is constant for each material irrespective of load. The COF for Al_2O_3 + TiO_2 coatings is in the range of 0.1-0.2 whereas COF for Cr_3C_2-NiCr coatings is in the range of 0.4-0.5. This may be due to the fact that Cr_3C_2-NiCr coating is harder than Al_2O_3 + TiO_2 coating and apply more resistance in sliding movement. The Cr_3C_2-NiCr (CRC) coating shows more wear resistance than Al_2O_3 + TiO_2 (ALT) coating particularly at higher load, **Fig.3**. The wear pattern obtained by optical profilometer also confirms the finding of tribometer data. The high temperature studies are in progress and results will be presented in the conference.

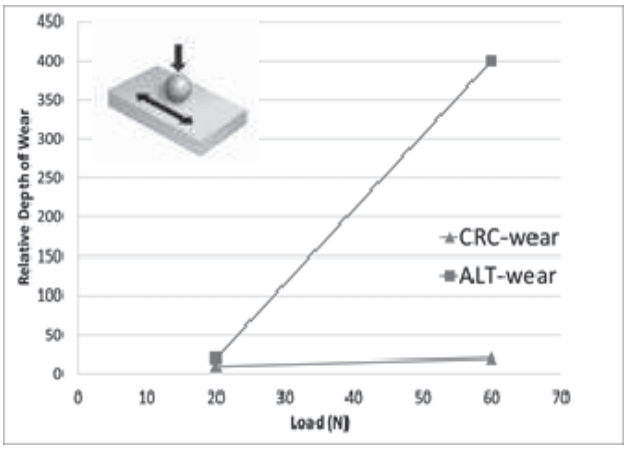

Fig3: *Wear behaviour of coatings at room temperature*

3 Conclusion

Initial studies at room temperature show that Cr_3C_2-NiCr coatings are better wear resistant than Al_2O_3 + TiO_2 coating. However coefficient of friction is less in the later. The high temperature tribological studies will determine the exact behaviour of both the coatings in actual application that will be discussed in details during presentation.

4 References

[1] B. Venkatraman: Proc. of DAE-BRNS workshop on Plasma Surface Engineering (September 2004) 217-235.

[2] Yongqiang Guo: Modern Applied Science vol.3 no.3 (March 2009) pp. 6469.

[3] B.S. Mann & Braham Prakash: Wear 240(2000) pp. 223-230.

[4] Yesim Sert, Nil Toplan: Materials and technology 47 (2013) 2, 181–183

[5] H. S. Ahn, O. K. Kwon, Wear, 225–229 (1999), 814–824

[6] V. P. Singh, A. Sil, R. Jayaganthan, Wear, 272 (2011), 149–158

[7] S. Tao, Z. Yin, X. Zhou, C. Ding, Tribology International, 43 (2010), 69–75

[8] S. T. Aruna, N. Balaji, J. Shedthi, V. K. W. Grips, Surface & Coatings Technology, 208 (2012), 92–100.

Microstructure and Dry Sliding Wear Behavior of Atmospheric Plasma Sprayed Nanostructured 2024Al-15 wt.% SiCp Composite Coatings

Satish Tailor[1], RM Mohanty[2] and P. R. Soni[3]

[1]National University of Science and Technology " MISIS", (Moscow Institute of Steels & Alloys) Moscow, Russia.
[2]Council of Scientific and Industrial Research, CSIR-HQS, Rafi Marg, New Delhi, India.
[3]Department of Metallurgical and Materials Engineering, Malaviya National Institute of Technology, Jaipur, India.

1. Introduction

Al-based metal matrix composites (MMCs) are one of the most widely used metal based composites which have attracted much attention of researchers and industries so that a large number of studies have been carried out in the field of Al-MMCs [1, 2]. Due to the low density of 2024Al alloy (as a matrix) have long being used in synthesis of composite [3-4]. But the major drawback of 2024Al is its low wear resistance. Numerous attempts have been made to overcome this draw back. Ceramic reinforced Al-MMCs have collected significant attention due to the integration of their tribological properties without dropping the corrosion properties of Al-alloys [5-6]. Al_2O_3 [7], TiN [8], B_4C [9], SiC [10] MgO [11], $MoSi_2$ [12], etc are the mostly used ceramic particles used in producing Al-MMCs. But the specific properties of SiC i.e. high melting point (2,730 °C), high modulus (250 GPa), good thermal stability, good hardness, high wear and impact resistance and high chemical resistance make it an appropriate reinforcing material for producing Al-MMCs.

The objective of the present work was to investigate the properties of SiC reinforced 2024 aluminum alloy matrix coatings developed by using mechanical alloying (MA) technique for preparing the feedstock powder and the atmospheric plasma spray (APS) process. The mechanical and wear properties of 2024Al coatings, thus produced were evaluated.

2 . Experimental

2.1 *Materials*

2024Al alloy powder, supplied by the M/S ECKA Granulate Velden GmbH, Germany, with a particle size of <71μm, and silicon carbide powder of <40μm were used in these investigations. Scanning electron micrographs of as-received materials are shown in Fig 1.

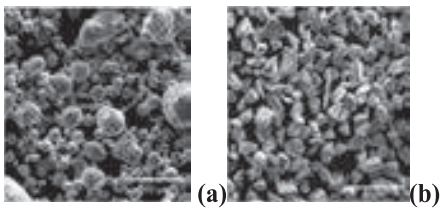

(a) (b)

Figure 1: Scanning electron micrographs of as-received powders (a) 2024Al and (b) SiC

2.2 *Feedstock powder preparation and APS processing*

The 2024Al and 15 wt. % SiC powder particles were mechanically alloyed in an indigenous high-energy attrition ball mill, in purified nitrogen (99.99 %) atmosphere for 8 h. The milling media consisted of 12.2 mm size hardened steel balls. Ball to powder weight ratio and rotational speed were 10:1 and 350 rpm, respectively. The composite powder mixture was processed in a batch size of 100 g along with 1 wt% Acrawax carbon (supplied by Lonza Inc., NJ.) as process control agent (PCA). The MA powder was then degassed for one hour at 200^0C in a vacuum of 1×10^{-2} torr. The MA composite powder was deposited on the grit-blasted weathering steel (Cor-Ten A242) substrates using Sulzer Metco plasma spray equipment with 3 MB gun. APS coatings of as-received 2024Al and blended 2024Al-SiCp powders were also applied on to the substrate for comparison purposes. A coating of about 250 μm thickness was applied in all the cases. The spray parameters are presented in Table 1.

Table 1: Plasma Spray Parameters

Parameters	Values
Current, A	500
Voltage, V	50
Primary gas, Ar, SCFH*	70
Secondary gas H_2, SCFH*	10
Carrier gas Ar, SCFH	20
Powder feed rate,(gm/min)	36
Spray distance, mm	100

*SCFH: Standard cubic feet per hour

3.Results and Discussion

It can be seen (Fig.2a) that SiC_p particles are uniformly distributed and the initial spherical shape of the 2024Al powder particles has become flake-like and irregular. The SiC particles (smaller as well as larger) distribution in the Al matrix powder was confirmed by back scattered X-ray mapping of SiC_p using EDX (Fig. 2b).

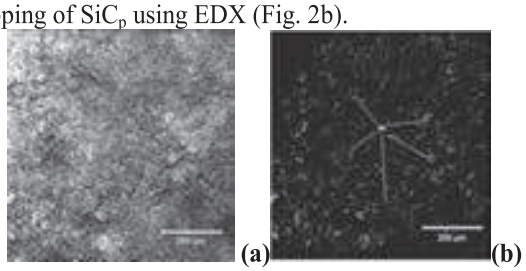

(a) (b)

Figure 2: SEM showing (a) powder morphology and (b) distribution of SiC particles in MA 2024Al-SiCp

A decrease in peak intensity (Fig.3) may be attributed to embedment of SiC_p in the 2024Al matrix after MA processing.

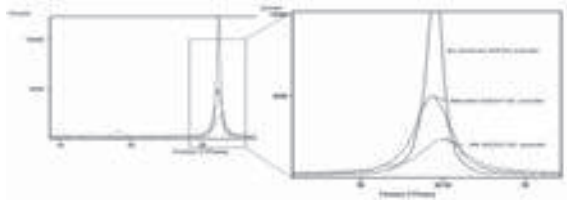

Figure 3: XRD patterns of as-received 2024Al, blended 2024Al-SiCp and MA 2024Al-SiCp powders

The crystallite size of the coatings were calculated from broadening of XRD peaks (Fig 4) using the Williamson-Hall method. The results showed that the crystallite size decreased to 17 nm for MA 2024Al-SiCp coating.

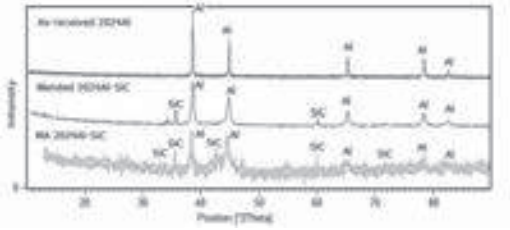

Figure 4: XRD patterns of as-sprayed APS coatings

Table 2: SiC_p fraction, porosity, crystallite size and microhardness in the coatings

Material	SiC fraction	Porosity (%)	Crystallite size (nm)	Microhardness (MPa)
as-received 2024Al	------	5% ± 3	50 ± 9	137
blended 2024Al-SiC_p	35%	4% ± 2	45 ± 5	245
MA2024Al-SiC_p	35-45 %	1-2% ± 1	17 ± 2	328

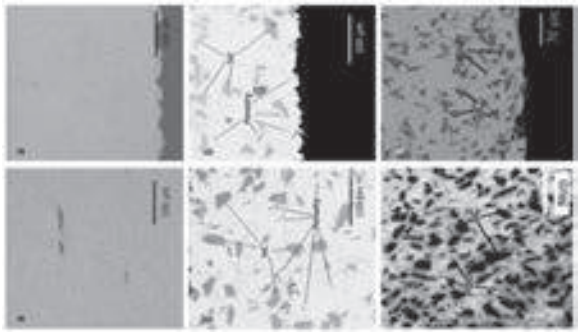

Figure 5: The microstructure of top and cross sectional view of coatings (a) as-received 2024Al (b) blended 2024Al-SiCp and (c) MA 2024Al-SiCp

Table 3: Adhesion Strength of Different Coatings

Applied load / Coating Material	0.98 N	1.96N	2.94N	3.92N
as-received 2024Al		✓		
blended 2024Al-SiC_p			✓	
MA 2024Al-SiC_p				✓

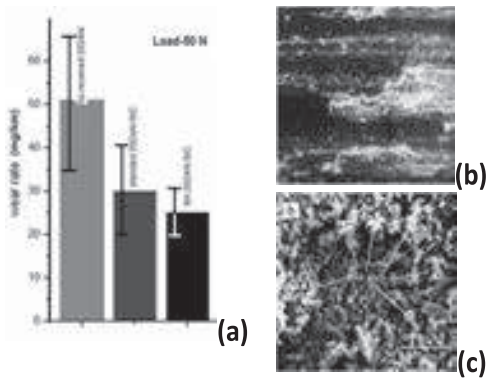

Figure 6: (a) Histograms of the wear rates of as-sprayed coatings; Scanning electron micrographs of worn surface (b) and corresponding debris (c) of MA 2024Al-SiCp at the load of 50N

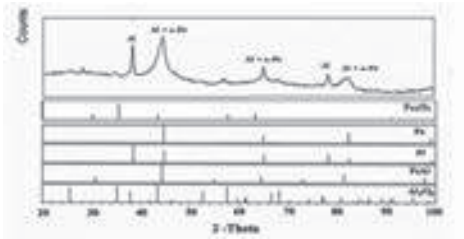

Figure 7: XRD analysis of the wear debris of 2024Al-SiC formed at the load of 50N. (The bottom shows the standard XRD spectra for different phases)

4. Conclusions

Microstructural studies confirmed that is a uniform distribution of SiC-reinforced particles in the coating. The coating was found to have 35-45 % fraction of SiC particles, low porosity level of about 1-2%, hardness to the level of 328 MPa. Adhesion strength of the coating with the substrate was also excellent due to increased degree of diffusion at the interface. The wear rate in the coatings was found to decrease by 60% as compared to the 2024Al matrix. The wear mechanism in the coating was found to be delamination and oxidative type.

4. References

[1]. J. Onoro, M. D. Salvador and L. E. G. Cambronero, 'High-temperature mechanical properties of aluminum alloys reinforced with boron carbide particles', *Mater Sci Eng A.,* 2009, 499, 421–426.

[2]. S. Mula, P Padhi, S. C. Panigrahi, S. K. Pabi and S. Ghosh, 'On structure and mechanical properties of ultrasonically cast Al–2% Al_2O_3 nanocomposite', *Mater. Res. Bull,.* 2009, 44, 1154–60.

[3].J. Dutkiewicz, L. Litynska, W. Maziarz, K. Haberko W. Pyda, and A. Kanciruk, 'Structure and properties of nanocomposites prepared from ball milled 6061aluminium alloy with ZrO2 nanoparticles', *Cryst Res Technol.*, 2005, 44, 1163–69.

[4]. J. M. Torralba, C. E. Costa and F. Velasco, 'P/M aluminum matrix composites: an overview', *J. Mater Process Technol.*, 2003, 133, 203–06.

[5].J. A. Hookery and P. J. Doorbar, 'Metal matrix composites for aero engines', *Mater. Sci. Technol.*, 2000, 16, 725–31.

[6].F. H. Froes, 'Advanced metals for aerospace and automotive use', *Mater. Sci. Eng. A,* 1994, 184, 119–33.

[7].M. Alizadeh and M. Mirzaei Aliabadi, 'Synthesis behavior of nanocrystalline Al–Al_2O_3 composite during low time mechanical milling process', *J Alloys Compd.,* 2011, 509, 4978–86.

[8].J. L. Ortiz, V. Amigo, A. Manzano and M. A. Perez, 'Mechanical properties of composites made of an aluminum alloy matrix reinforced with titanium nitride particles, consolidated by powder extrusion'. *Metall Mater Trans B.*, 2007, 38, 1–4.

[9].B. Yao, B. Simkin, B. Majumdar, C. Smith, M. Bergh, K. Cho, et al., 'Strain-induced grain growth of cryomilled nanocrystalline Al in trimodal composites during forging', *Mater Sci Eng A,* 2012, 536 , 103–9.

[10].Satish Tailor, R. M. Mohanty, V. K.Sharma and P. R. Soni, 'Fabrication and Wear Behaviour of Nanostructured Plasma Sprayed 6061Al-SiCp Composite Coating', *J. Thermal Spray Tech-JTST.* 2014 (**Online first published**) DOI: 10.1007/s11666-014-0065-6.

[11].M. A. Baghchesara and H. Abdizadeh, 'Microstructural and mechanical properties of nanometric magnesium oxide particulate-reinforced aluminum matrix composites produced by powder metallurgy method', *J Mech Sci Technol.*, 2012, 26 , 367–72.

[12].J. Corrochano, M. Lieblich and J. Ibanez, 'The effect of ball milling on the microstructure of powder metallurgy aluminum matrix composites reinforced with MoSi2 intermetallic particles', *Composites A.*, 2011, 42, 1093–99.

Influence of Al_2O_3 addition on the wear and corrosion behaviour of HVOF sprayed WC-Co coatings

R.P.S Chakradhar[a], Meenu Srivastava[a], K Venkateswarlu[b]
[a]Surface Engineering Division, [b]Materials Science Division
CSIR-National Aerospace Laboratories, Bangalore -560017, India.

Abstract

WC-12Co and 30wt.% of Al_2O_3 powder mixture was sprayed on EN-24 steel using high velocity oxy fuel (HVOF) method. The chemical, mechanical and tribological performances of WC-12Co and WC-12Co-Al_2O_3 coatings have been evaluated. XRD analysis clearly showed the presence of WC, and Al_2O_3 peaks in WC-12Co-Al_2O_3 coating. The FESEM studies showed a homogeneous microstructure with low amount of porosity in WC-12Co-Al_2O_3 samples as compared to WC-12Co coatings. An improved hardness of 1100 Hv was observed with the addition of Al_2O_3 content compared to 950 Hv (WC-12 Co). The 3D roughness profiles show a higher roughness of R_a ~ 7.6µm for Al_2O_3 incorporated coatings when compared to WC-12Co coating (R_a ~ 6.5µm). Wear results of WC-12Co-Al_2O_3 coating exhibited higher wear resistance as compared to WC-12Co coating. This is probably due to low porosity levels and good metallurgical bonding between the EN24 substrate and the coating. Electrochemical impedance spectroscopy (EIS) studies showed better corrosion resistance for WC-12Co-Al_2O_3 coatings (I_{corr}=0.1µA, R_p= 2010Ω) as compared to WC-12Co (I_{corr}=0.9µA, R_p=406 Ω) coating. It is concluded that WC-12Co-Al_2O_3 coating exhibited better chemical, mechanical and tribological properties compared to WC-12Co coating under identical HVOF coating conditions.

1. Introduction

Thermal spray coatings using high velocity oxy-fuel (HVOF) process is highly promising due to the benefits of lower cost, tribologically superior, and well adhering metallic and composite cermet coatings whose thickness ranges from several micrometers to tenths of a millimeter to a great variety of metallic surfaces [1-3]. The HVOF process has been very successful in spraying wear resistant WC-Co coatings with higher density, superior bond strengths and less decarburization than many other thermal spray processes [4-6]. It has become a reliable alternative to electrolytic hard chrome coating in the aeronautical industry to coat and repair landing gear and worn components [7]. The main goal of this paper is to study the influence of Al_2O_3 addition on the corrosion and tribological behaviour of HVOF sprayed WC-Co coatings sprayed from conventional powders.

2. Experimental

WC-12Co and fused Al_2O_3 powders with an average particle size of 16µm and 26µm respectively was used for spraying on an EN24 steel using the conventional HIPOJET 2700 gun. The phase purity of the coatings was examined by XRD (Bruker D8 Advace). The morphology of the coatings, microstructure were examined by means of a scanning electron microscope FESEM (model Carl Zeiss Supra 40 VP). The 3D roughness profile was measured using 3D profilometer (model Nano Map 500LS USA). The micro hardness of the coatings was measured by using a Knoop's indenter (Buehler Microhardness tester Micromet 100) employing a load of 0.05kgf. The wear behaviour was studied using tribotester. The corrosion behavior of the composite coatings was studied using potentiodynamic polarization and electrochemical impedance studies (EIS). The measured current-voltage data are plotted as Tafel plot in the form of potential vs. log(i). From the Tafel curve, corrosion potential $E_{corr,}$ corrosion current I_{corr} and polarization resistance R_p were obtained. Potentiodynamic polarization tests were performed using a CHI042D instrument.

3. Results and discussion

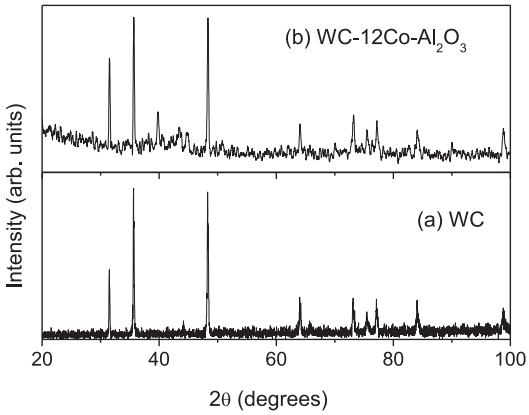

Fig. 1 XRD pattern of (a) WC-12Co and (b) WC-12Co- Al_2O_3 coatings.

In the XRD the distinct diffraction peaks at 2θ= 31.54, 35.70 and 48.28 degrees are indexed as the (001), (100), (101) planes of hexagonal WC phase. The XRD analysis clearly showed the presence of WC, Al_2O_3 peaks in WC-12Co-Al_2O_3 coating. The studies also indicated the presence of

a small amount of W_2C, but did not reveal any cobalt containing sub carbides.

Fig. 2 shows the FE-SEM micrographs for (a) WC-12Co (b) WC-12Co-Al_2O_3 coatings. The FESEM studies show a homogeneous microstructure in WC-12Co- Al_2O_3 coatings as compared to WC-12Co coatings. From the microstructure, it is observed that Al_2O_3 is diffused in the WC-12Co matrix. The 3D roughness profile measurements indicated a higher roughness of R_a ~ 7.6 μm for Al_2O_3 incorporated coatings when compared to WC-12 Co coating (Ra ~ 6.5 μm) respectively.

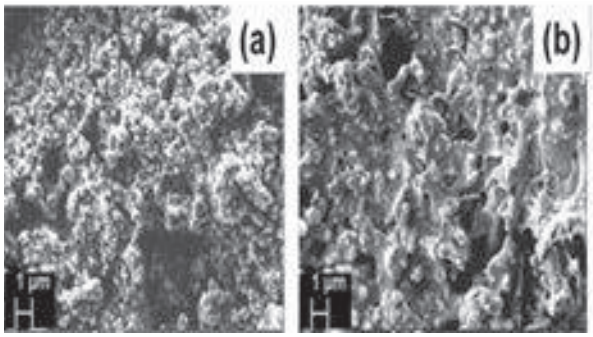

Fig.2 FE-SEM microstructures for (a) WC-12Co (b) WC-12Co-Al_2O_3

The indentation microhardness of WC-12Co and WC-12Co- Al_2O_3 coatings was measured by using a Knoop's indenter employing a load of 0.05kgf and a relaxation time of about 15 s. It was observed that an improved hardness from 950 Hv (for WC-12 Co) to 1100 Hv is achieved with the addition of Al_2O_3 content. The increase in hardness may be due to the microstructural changes with the addition of Al_2O_3. The wear studies showed that WC-12Co-Al_2O_3 coating exhibited better resistance compared to WC-12Co coating.

Fig. 3(a) shows the Nyquist plot of WC-Co and Al_2O_3 modified WC-12Co coatings in 3.5% NaCl solution at their respective open circuit potential. The plot shows a semicircle for both the coatings. In principle, bigger is the diameter of the semicircle, higher is the corrosion resistance. Thus, modified WC-Co coating displays better corrosion resistance due to the larger size of the semicircle. The Tafel curves obtained for WC-12Co and Al_2O_3 modified WC-12Co coatings are displayed in Fig. 3(b). The corrosion current (Icorr), corrosion potential (Ecorr), polarization resistance (rp), were obtained from the Tafel plots. It is seen that, the Al_2O_3 modified WC-Co coatings show less corrosion current density, icorr values (0.1μA/cm^2) compared to WC-Co coating (0.91μA/cm^2). This indicates that, the modified coating possesses better corrosion resistance compared to the unmodified coating.

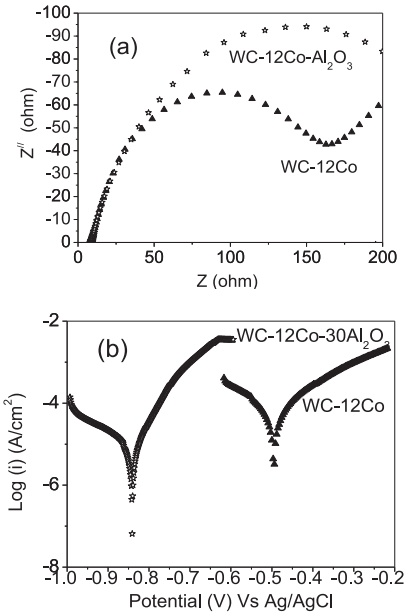

Fig.3 (a) Nyquist and (b) Tafel plot of WC-12Co and WC-12Co-Al_2O_3 coatings

The polarization resistance Rp is higher for the Al_2O_3 modified WC-12Co coating (2010Ω) compared to WC-12Co coating (406Ω). The higher polarization resistance affirms the above results that the modification of WC-12Co coating with Al_2O_3 helps to improve the corrosion resistance of the coating. Thus it can be inferred from the above studies that addition of Al_2O_3 enhanced the corrosion and wear behaviour of WC-12Co coating.

4. Acknowledgements

The authors would like to thank Director, NAL and Head, SED for the permission to carry out and publish this work. A special thanks to Mr.Siju for recording the FESEM and Mr. G. Prasad for the assistance in the HVOF coatings.

References

[1] J. Matejicek, S. Sampath, Acta Mater. 49 (2001) 1993-1999

[2] J. Rodriguez, A. Martin, R. Fernandez, J.E. Fernandez, Wear 255 (2003) 950 - 955

[3] T. S.Sidhu, S. Prakash, A.D. Agarawal, J. Mater. Sci. 41 (2005) 805 - 823

[4] H. Chen, C. Xu, Q. Zhou, I. M. Hutchings, P.H. Shipway, J. Liu, Wear 258 (2005) 333-358

[5] S. Sampath, J. Materials and Product Technology,35 (2009) 425 448

[6] T. Sahraoui, S. Guessasma, N.E. Fenineche, G. Montavon, C. Coddet, Mater. Lett., 58 (2014) 654-660

[7] K. Raghu Ram Mohan Reddy, N. Ramanaiah, M.M.M. Sarcar, Procedia Engineering 64 (2013) 888 – 895

Comparison of the sliding wear behavior of diffusion treated M-50 NiL and thermal sprayed coating on M-50 NiL steel

Deepjyoti A. Shelwatkar[1], S.V.Subba Rao [1], Manish Roy[2]

[1]Regional Center for Military Airworthyness Kanchanbagh, Hyderabad: 500058, India

[2]Defence Metallurgical Research Laboratory Kanchanbagh, Hyderabad: 500058, India

M-50 Nil is a low carbon bearing steel having high toughness. This steel is normally used in carburized condition. In the present investigation, an attempt has been made to compare and contrast the sliding wear behavior of diffusion treated M-50 Nil steel and thermal sprayed coating on M-50 Nil steel. The micro structural features and mechanical properties of the diffusion treated surface and the thermal sprayed coatings are evaluated using optical microscope, scanning electron microscope and micro indenter. Sliding wear test on both modified surfaces are carried out for different applied load. The results show that both modified surfaces have comparable wear properties. However, at higher load improved performance of the thermal sprayed coating is observed. The detail result will be presented.

The Abrading Behaviors of Several Al-based Abradable coatings

Yueguang Yu[1, 2], Jianming Liu[1, 2], Jie Shen[1], Deming Zhang[1], Qiuyuan Lu[1], Tong Liu[1]
[1] Beijing General Research Institutes of Mining and Metallurgy, Beijing, 100160, China
[2] North East University, Shenyang, 110819, China

Abstract
The abradability and the coating adhesive transfer rubbed against titanium blades of five aluminum based abradables were studied under the simulated engine conditions. The influence of coating chemical composition, filler type anddistribution as well as the testing temperature, blade tip velocity and incursion rates were analyzed. It is found that the abradability and adhesive transfer was significantly affected by the coating matrix metal and the second phase filler type and content.

1 Introduction

In order to reduce the clearance between the rotor and stator of aero-engines the abradable coatings are widely used. In the medium and low temperature sections of the engine compressor, the blades are made of titanium alloys which are not so hard as the superalloys and need a relatively softer abradable coating to be easily rubbed in. Aluminium based abradable coatings with lower E modlous and lower melting point than the Ti alloy at ambient and service temperatures[1] are the best choice for the Ti blades up to now. The Al-based abradable which is abradaed by plastic deformation has a drawback of adhesive transfer to the blade and the transferred material which is highly work hardened will damage the seal itself[2].

Many approaches has been made to reduce the tendency of adhesive transfer including the use of AlSi alloy and the addition of second phase fillers based on different design principle or experience. The modified coatings do show lower tendency of adhesive transfer but in some service conditions high adhesive transfer is reported[3].

To obtain a deeper understanding of the influence of coating comoposition and microstructure on the abradability, the in-service and trial Al-based abradable coatings with different composition and microstructure were evaluated by the high speed and high temperature abradability testing rig which can simulate the coating-blade scratching under engine conditions.

2 Experiment

2.1 Materials

Five Al-based coatings were choosen and Table 1 gives the main coating information. The AlSi is an alloy coating, and the rest is mechanical compositions of the metal matrix and the second phase fillers. The Al/hBN and AlSi/hBN has the same filler type and fraction but with different matrix metal and different filler size and distribution. The Al/hBN has a pure aluminium matrix and a fine hBN filler minus 10μm which surrounding the Al matrix splats while the AlSi/hBN has an eutectic Al-12Si matrix and a coarse hBN filler between 80~200μm which surrounded by the fine AlSi matrix splats and both of coatings have been used in the engines for years. The AlSi/PHB has the Al-12Si matrix metal and a similar microstructure to the AlSi/BN but with a higher filler fraction and the coating is considered to be the most successeful abradable for engine sections below 325℃. The Al-AlSi/BN is the only trial coating and has a similar structure to the Al/BN coating but half of the Al matrix is replaced by the AlSi. All coatings were air plasma sprayed to the hardness of 50~80 HR15Y. Figure 1 gives the SEM pictures of coating microstructures.

Table 1. Main composition of the Al-based abradables

Coating Name	Naminal composition	Status
AlSi	Al-12%Si	In Service
Al/hBN	Al-20%hBN	In Service
AlSi/hBN	AlSi-20% hBN	In Service
AlSi/PHB	AlSi-40%Polyester	In Service
Al-AlSi/hBN	Al-40%AlSi-20%hBN	Trial

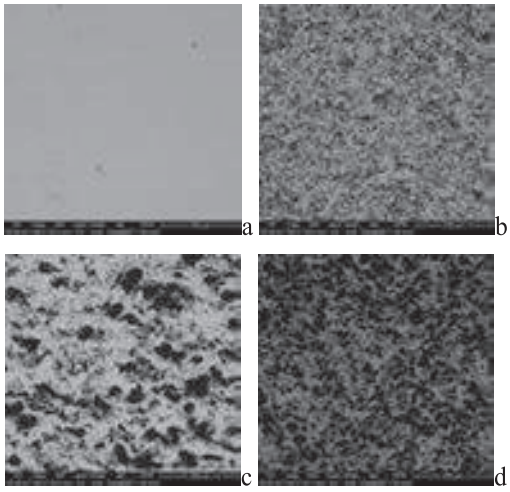

Fig. 1. *SEM pictures of coating microstructures,a:AlSi, b:Al/hBN, c:AlSi/hBN, d:AlSi/PHB, and the Al-AlSi/hBN is the same as the Al/BN.*

2.2 Testing rig and testing parameters

Abradability tests were carried out on the BGRIMM BKY-HVT300/800 abradablity test rig. This rig is capable of operating at up to 800 °C. Blade tip speeds can be adjusted from 100 to 350 m/s with corresponding incursion rate settings ranging from 5 to 1000 μm/s.

Table 2 gives the testing parameter. The abradability testings were done both at room temperature and the coating maximum service temperatures. Some of the tests were repeated to verify the acuracy of the testing rig.

All coatings were rubbed by the Ti-6Al-4V dummy blades with a tip thickness of 0.7 mm. The blade height is recorded before and after the test to caculate the height change and when there is coating adhesion on the blade tip the blade height change is marked as minus. The coating scratch depth is caculated geometrically using the scratch length. The blade wear ratio is used as the indicator of coating abradability and it is defined as the percentage of the blade height change to the coating scratch depth. If the blade

height is reduced the wear ratio is marked as positive and if the blade height is increased the wear ratio is marked as minus.

Table 2. Abradablity testing parameters

Coati -ng	Blade tip velocity (m·s-1)	Incursion rate (μm·s-1)	Temperat -ure(℃)	Blade tip wear ratio(%)
AlSi	300	5	25	90.4
		5	450	26.7
		50	450	-3.57
		480	450	-26.2
Al/BN	300	5	25	6.33
		5	450	1.34
		5	450	-8.2
		50	450	2.89
		480	450	7.66
AlSi/ BN	300	5	25	47.6
		5	450	26.8
		50	450	2.6
		480	450	2.41
AlSi/ PHB	300	5	25	1.56
		5	325	1.45
		50	325	1.54
		480	325	7.27
Al-AlSi/ hBN	300	5	25	4.33
		5	450	5.37
		5	450	4.38
		50	450	3.08
		50	450	2.76
		480	450	1.45
		480	450	2.35

2.3 Results and discussion

Figure 2. gives the wear ratio of five coatings both at room temperature(RT) and maximum service temperatures(ET). At room temperature and low incursion rate(5μm/s), the AlSi alloy coating without second phase wears the blade heavily and the AlSi/hBN coating with a coarse second phase is just a little better than the AlSi coating. The other three coatings exhibit good abradability and only slight blade wear occured.

At the maximum service temperatures and low incursion rate(5μm/s), the blade wear is reduced for the AlSi but is still higher than the other coatings except the AlSi/hBN whose abradability is similar to that of AlSi. The Al/BN with pure Aluminum matrix is the only coating increased the blade height which means coating transfer to the blade tip occured. As the incursion rate increases at elevated temperaturee, the AlSi began to transfer heavily to the blade tip and no other coating transfer happened including the AlSi/BN and Al/BN.

In all conditions the AlSi/PHB and the Al-AlSi/hBN exhibit excellent abradablity while the Al-AlSi/hBN can withstand higher temperature upto 450℃.

Pure aluminum coating is reportly not abrasive to the Ti-6Al-4V blade both at room and the elevated temperatures[1], but with a high tendency of adhensive transfer to the blade tip. The eutectic Al-12Si alloy is believed to reduce the adhensive transfer of pure aluminum, it is true at the low temperature and low incursion rates but with a drawback that the AlSi alloy is abrasive to the Ti blade. At elevated temperature and high incursion rates the adhesive transfer of coating to the blade still exists. It means that only the AlSi alloy can not solve the problem properly.

The test results show that the addition of second phase fillers can improved the coating abradabilty and the quantity

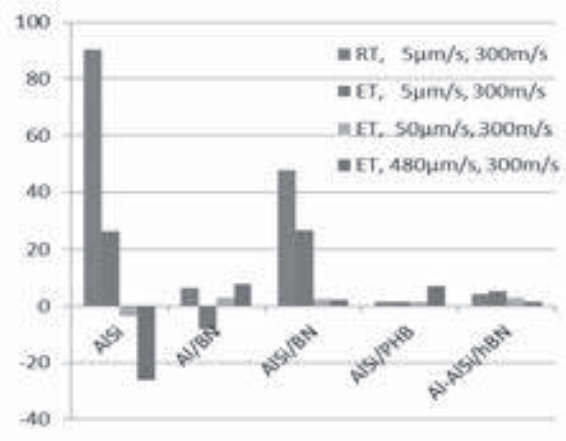

Fig. 2. *Blade tip wear ration of five coatings at room and maximum service temperatures.*

and distribution of second phase fillers are the key influencing factors.

To compare the AlSi, AlSi/hBN and the AlSi/PHB we can see that the addition of second phase filler hBN does restain the coating transfer to the blade in all test conditions. And it can reduce the blade wear ratio but can not change the abrasive nature of AlSi alloy matrix to the Ti blade unless the filler content is high enough.

Al/hBN has a pure aluminium matrix which ensures that the coating is not abrasive to the Ti blade. Although there is not pure aluminium coating test results in hand, Al/hBN results prove that the addition of second phase filler hBN to Al coating can enhance coating abradability to an acceptable level. While there still is Al/hBN coating transfer to the blade in the low incursion rate. The trial coating Al-AlSi/hBN is designed to reduce the adhensive transfer by replacing 50% of the aluminium matrix with AlSi. The trial coating is proved to be successful in the test conditions. The reason is infered as such: the Al matrix has a tendency of adhesive transfer at low incursion rates and it is neutralized by the AlSi matrix which is abrasive at low incursion rates, and the tendency of adhesive transfer of AlSi matrix at high incursion rates is neutralized by the Al matrix.

2.4 Conclusions

Al-based abradables were tested with simulating engine testing rig and the primary analysis show that the coating abradability is significantly affected by the coating matrix metal and the second phase fille. The blade wear and coating adhesive transfer to the blade can be restrained by ajusting the matrix metal and the second phase filler.

More tests and investigation are undergoing in BGRIMM to reveal the abrading mechanism of Al-based abradables.

3 References

[1] R. C. SCHWAB:*Program To Develop Sprayed, Plastically Deformable Compressor Shroud Seal Materials*(1979)NAS3-20054, CR159741.

[2] Richard .K. Schmid: *New High Temperature Abradables for Gas Turbines* (Diss. ETH No. 1223, 1997), pp.83-89.

[3] N. Fois, Stringer, M.B. Marshall: *Adhesive Transfer in aero-engine abradable lings contact*, Wear 304（2013）pp.202-210.

Importance of Surface Activation for Cold Sprayed Particle Deposition

Kazuhiro OGAWA, Yuji ICHIKAWA, Kentaro HASHIMOTO, Takehito SHIMATSU

Tohoku University, Japan

Cold spray (CS) technique is a technology for making thick deposition by solid particle impingement onto a substrate at high velocity. It can be said the adhesion principle is the bonding of activated surfaces which exposed by large deformation during particle impingement. Although many researches have been discussing how to expose activated surfaces, there is few consideration of the bonding mechanism of activated surfaces itself. On the other hand, there is another bonding technology, which has similar bonding principle to the CS, namely surface activation bonding (SAB) technique. The SAB activates solid surfaces by removing the oxide layer by using a fast atom beam (FAB), and joins activated surfaces at room temperature. From the bonding point of view, it is easy to understand the bonding mechanism and importance of surface activation rather than that of the CS. Therefore, in this study, several metal combinations were bonded by the SAB, and dominant factor and the bonding mechanisms were discussed from the results of bonding experiments and observation of the interface structures.

Characterization of Cold Sprayed IN625 and NiCr Coatings

Dheepa Srinivasan[1], Vighnesh Chandrasekhar[2], Y.C. Lau[3] and Eklavya Calla[1]

[1] GE Power and Water, GE India Technology Centre, Bangalore 560066, India
[2] Tata-AIG General Insurance Company, Mumbai 400012, India
[3] GE Power and Water, Schnectady - 12345-6000, New York, USA

The Cold spray method of material deposition is widely used for surface enhancement, to improve properties such as corrosion and wear. A detailed microstructural analysis of cold sprayed Ni based coatings (IN625 (Inconel 625 is a Trademark of Huntington alloys corporation) and NiCr), using the transmission electron microscope, and orientation imaging and Electron probe microanalysis, revealed the origin of two distinct types of microstructures in the as sprayed condition. Region I comprised very fine grains, in both the 625 as well as the NiCr, which upon heat treatment, revealed a fine grained recrystallized structure (50-100 nm) in IN625, whereas the NiCr had recrystallized into much larger grains (> 1 μm). A detailed characterization of the interface chemistry and the nature of bonding, metallurgical vs mechanical interlocking, was carried out via carrying out systematic in-situ heat treatments and mapping the diffusion kinetics along the interface. The bonding mechanism of the intersplat boundaries as well as the coating-substrate interaction was studied in detail and able to reveal some insights about the compressibility as well as interfacial behavior, on a 4130 steel substrate.

1. Introduction

Inconel 625 (IN625) is a well known Ni based superalloy used for corrosion propection applictions [1]. It exhibits excellent corrosion behaviour in severe environments, with outstanding creep properties, and is a popular alloy used as a cladding on to low alloy steels in several Oil and Gas and petrochemical industry applications. A γ′′ precipitation hardened alloy [2], it is used as a weld overlay used on low alloy steels. In recent times, the cold spray coating technology has been utilized for surface enhancements such as protection against wear, erosion and corrosion, as well as alternatives to bulk forms, especially in applications involving metal build up during repair and refurbishment [3-5]. In particular, the use of cold spray alternatives are attractive in the area of repair of components, from a stand point of cost as well as productivity of repair, not to mention the quality of the repaired component. This study comprises characterization of IN625 (a precipitated hardened alloy) and Ni20wt%Cr (NiCr-a solid solution), cold sprayed coatings, on a low alloy steel, AISI 4130. This was part of the effort to explore cold spray as a possible alternative to weld cladding, in different applications. A detailed analysis of the microstructure and residual stress is presented in this study.

2. Experimental Details

Powders of IN625 and NiCr were cold sprayed on to a low alloy steel AISI 4130 steel substrate with a hardness of ~220 Hv, using, CGT Kinetics 8000 (IN625) and Kinetics 4000/47 (NiCr), using Helium (He) as the process gas, at 30 bar pressure (500-600°C, gas temperature). The nominal coating thickness was ~500 μm. The coatings were characterized using a Nikon Eclipse MA 200 optical microscope, Shimadzu microhardness tester (0.3 $H_{v)}$, SEM (Carl Zeiss EVO18) with EDS (Oxford, Link), TEM (JEOL, 2000FXII, 200 KV), EPMA (JEOL-JXA 8530 F, 15KV), EBSD (FEI-Quanta 200, TSL-OIM-EDAX), X-ray residual stress ($Sin^2\psi$-$CrK_{\alpha,}$ λ=2.284°) analyzer. The coatings were heat treated at 650°C, for 2.5 h, in a Lindberg furnace, in air, to study the coating thermal response.

3. Results and Discussion

Fig. 1 (a-b) shows representative SEM micrographs of the cold spryaed IN625 and NiCr coatings, revealing a nearly 100% dense coating. Table 1 lists the measured coating thickness, porosity and microhardness, in the as sprayed condition and after heat treatment (HT). Both the coatings measure a hardness of 500-520 H_v in the as sprayed condition. After heat treatment at 650°C (2.5 h), the IN625 coating sees ~12% increase in the hardness(600H_v), while NiCr, measures a ~20% drop (400 Hv). Fig. 2(a-d) are representative TEM bright field (BF) micrographs, from IN625 and NiCr, in the as sprayed condition and after HT. The coating microstructure reveals a severely deformed structure, in both the coatings. Upon heat treatment, the NiCr coatings (Fig. 2d) undergo complete recovery, and have strain free grains (~1-2μm), whereas the IN625 coatings undergo partial recovery, having many regions of the coating with a deformed structure and other locations of the coating with recrystallized, 50-200 nm grains. Detailed analysis of the as sprayed coating microstructure and recovery is presented in [5]. The increase in hardness of the IN625 coating is partly attributed to the occurrence of < 200 nm grains in this coating. Fig.3 shows the through thickness residual stress of the as sprayed coating vs the heat treated coatings. The compressive stress in both the coatings, is seen to completely recover to nearly zero stress, at 650°C. Amongst the two, the NiCr is seen with a higher stress as compared to the IN625, in the as coated condition. The coating substrate interface was examined, in detail, via an EBSD scan, as shown in Fig. 5 for the IN625 coating. The extent of substrate deformation has been quantified, as shown in the inset in Fig.5a.

Table 1: *IN625 and NiCr cold sprayed coating properties*

Substrate	Coating	Coating thickness (μm)	Condition	Coating Porosity (%)	Microhardness (H_v0.3)
4130 Steel	IN625	525	As Sprayed	< 0.2%	530
			650°C, 2.5h	0.4%	600
	NiCr	490	As Sprayed	0.5%	514
			650°C, 2.5h	0.8%	400

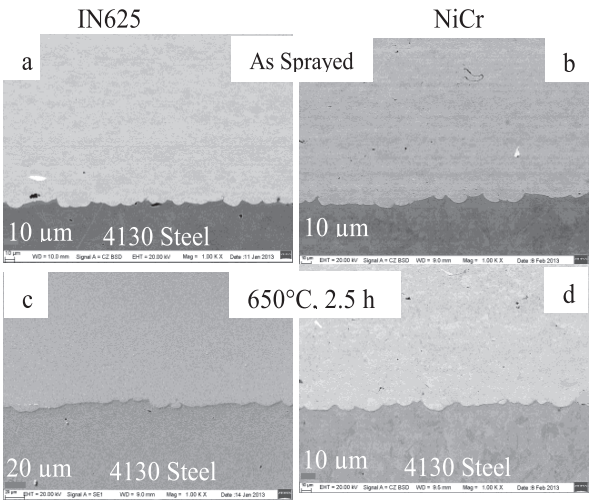

Fig. 1 : *SEM micrographs, (a-b) As sprayed, vs (c-d) Heat treated, coatings, of IN625 (a-c) and NiCr (b-d.)*

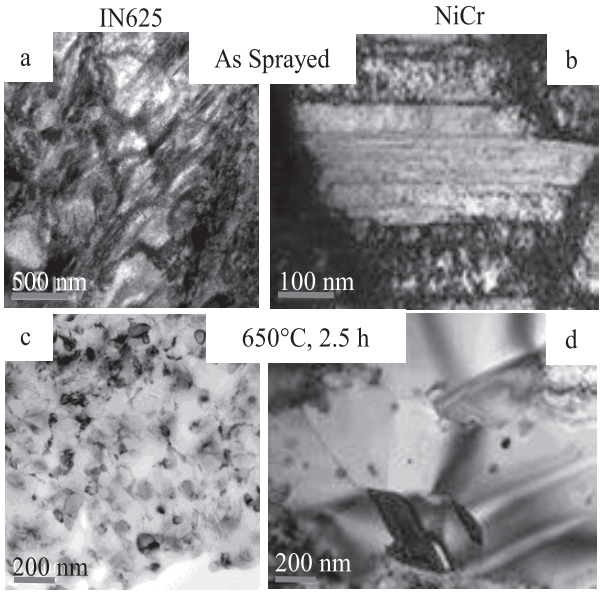

Fig. 2 *: Repesentative TEM (BF) micrographs from, (a-b) As Sprayed, (c-d) Heat treated, coaitngs, (a,c) IN625 and (b,d) NiCr.*

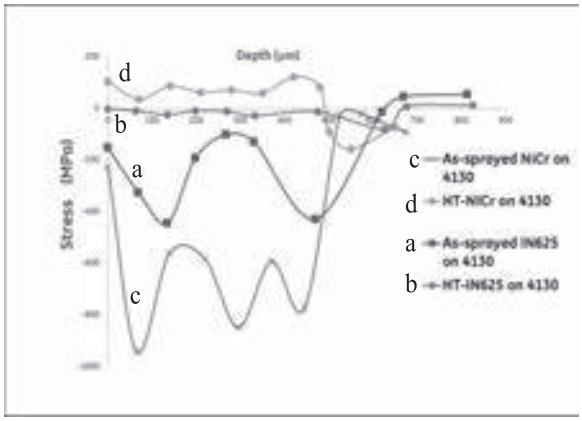

Fig. 3 : *Through thickness residual stress comparison of the IN625 (a-b) and NiCr (c-d)coating and substrate, in the as sprayed (a,c) vs the heat treated(b,d), condition.*

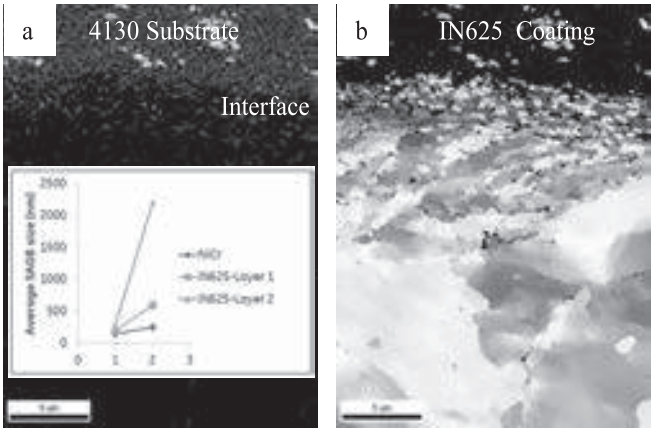

Fig. 5 : *EBSD scans from the, (a) IN625 coating, (b) 4130 substrate, in the as sprayed condition. Inset : Comparison of the average small angle grain boundary in the substrate, near the coating substrat, in IN625 and NiCr.*

4. Conclusions :

Dense IN625 and NiCr (0.5 mm) cold sprayed coatings were obtained using He as the process gas, on 4130 steel substrates. Both types of alloy coatings measured between 500-520 H_v in the as sprayed condition. The however, varied in their response to heat treatment at 650°C, 2.5 h. The NiCr coating was found to show a decrease in the hardness, while the IN625, was found to get hardner after the HT. The coating relaxation mechanism was monitored via TEM microstructures and residual stress behaviour. Detailed phase analysis of the coating structure reveals the strain free grains, some of which have undergone grain growth in the NiCr coating, while the IN625 coating displays remnance of partial recovery, with nanocrystalline grains in the IN625 coating, with heat treatment. The substrate deformation (up to 50µm), for the IN625 coatings revealed a two distinct regions with small angle grain boundaries with rampant grain rotation, indicative of a much higher deformation with IN625 as compared to NiCr. Residual stress behaviour indicated the NiCr to be a more compressive coating as compared to IN625, with the heat treatment at 650°C, annealing out the stresses in both the coatings.

5. Acknowledgements :

This work was carried out as part of the Oil and gas coatings program, financial support from the program manager, Mr. Adam Drufke, is gratefully acknowledged. Dr. Sundar Amancherla, Mr. Christopher Thompson and Dr. Kathleen Morey, GE Power and Water, are acknowledged for their support of this work.

6. References

[1] Inconel 625, Special Metals Publn. wspecialmetals.com
[2] H.L. Eiselstein, D.J. Tillack, in E.A. Loria (Ed.), Superalloy 718. 625 and various derivatives, (1991) 1-11.
[3] A.N. Papyrin, Cold spray technology, Elsevier, 2007.
[4] R. Morgan, P. Fox, J. Pattison, C. Sutcliffe, W. O'Neill, Mater. Lett., **58** (2004) 1317-1320.
[5 M. Hassan, M.Tech thesis, Univ. Of Waterloo, Canada, 2011.
[6] D. Srinivasan and R. Amuthan, *Superalloys* 718, 625 and 706 conference proceedings, Sept 2014.

Formation of Expanded Austenite on Cold-Sprayed AISI 316L Coating by Low-temperature Plasma Treatment

Shinichiro Adachi, Nobuhiro Ueda
Technology Research Institute of Osaka Prefecture, Ayumino 2-7-1, Izumi, Osaka, Japan

Abstract

Cold sprayed austenitic stainless steel coatings include little oxide compared with thermally sprayed coatings, therefore the sprayed coatings have a possibility of excellent corrosion property. However, it is difficult to produce a dense austenitic steel coating, because work hardening occurs during the cold spraying process. Then, a laser post-treatment was examined for cold sprayed AISI 316L coating. The porous microstructure was modified to be a dense microstructure, like a bulk steel plate. Besides, the AISI 316L coatings are relatively low hardness compared with ordinary hard coatings, ceramics and cermet coatings, etc. Then, the low-temperature plasma nitriding and carburizing at treatment temperature of 400 ℃ and 450 ℃, were applied for the cold sprayed AISI 316L coating. The surface hardness was recognized to enhance over 1000 HV. The carburizing layer thickness was thicker than the nitriding one, but the nitriding layer was higher hardness.

1 Introduction

Cold-sprayed austenitic stainless steel coatings include little oxide, however, it is difficult to produce a dense coating, because work hardening occurs easily when the sprayed particles are stacked onto the substrate; this then inhibits plastic deformation of the sprayed particles and leads to a porous microstructure [1].

A laser post-treatment has been reported to reduce the porosity and gives a dense microstructure by modifying cold-sprayed coating texture through fusing and cooling [2].

In addition, the surface hardness of the cold sprayed austenitic stainless steel coatings is about 300 HV, not sufficient to apply under severe friction conditions. It is reported that low-temperature nitriding and carburizing at treatment temperatures below 450 ℃ can improve the surface hardness of austenitic stainless steel by producing an expanded austenite (known as S-phase). The S-phase has high hardness and superior wear resistance, and contains little Cr nitride or Cr carbide; thus it shows excellent corrosion resistance, similar to that of ordinary austenitic stainless steels [3,4].

We have previously examined plasma-sprayed austenitic AISI 316L stainless steel coatings and shown that the surface hardness can be enhanced by low-temperature plasma nitriding and carburizing to be over 1000 HV [5,6]. However, the plasma-sprayed austenitic stainless steel coatings included oxide layers, these layers deteriorated the corrosion resistance considerably.

In the present study, AISI 316L stainless steel coatings were fabricated by the cold spray technique, and densified by the laser post-treatment. Subsequently, the coatings were treated by low-temperature plasma nitriding and carburizing to improve their wear resistance.

2 Experimental procedure

2.1 Cold spraying

AISI 316L spraying powders, with particle diameter of -45/+10 μm or -20 μm, were used and cold spray was performed with a CGT Kinetics 4000 (Winterthur, Switzerland) by using spray gas of N_2 with spray distance of 15 mm. Conditions for the spray gas pressure and temperature were 3 MPa・700 ℃ (-45/+10 μm powder) and 3.5 MPa・800 ℃(-20 μm powder).

The substrate was an AISI 316L steel plate.

2.2 Laser post-treatment

A semiconductor laser system, LDL160-1000 (Laserline, Mulheim-Karlich, Germany), was used at a laser power of 0.5 kW, and scan speed of 12 mm/s. In addition, Ar gas (20 L/min) was blown across the laser spot to prevent oxidation of the sprayed AISI 316L coating.

2.3 Low-temperature plasma treatment

Before plasma treatment, the surfaces of the sprayed coatings were polished using metallographic 3 μm diamond pastes to flatten the surface. Low-temperature plasma treatment was performed using a laboratory-type DC plasma ion treatment machine (FECH-1N, Fuji Electronics Industry Co, Ltd., Osaka, Japan). The specimen was placed on a holder in the chamber, and the holder was connected to the cathode. The plasma gas was nitriding of N_2:H_2=80:20, and carburizing of CH_4:Ar:H_2=5:50:45 at a flow rate of 1 L/min, and the pressure in the chamber was maintained at 667 Pa. The treatment temperature was 400 ℃ or 450 ℃, and treatment time was 4 h.

Overall experimental procedure was as follows;

・Cold sprayed AISI 316L stainless steel coating
↓
・1st treatment Post laser remelting (Skipped)
↓
・2nd treatment Low-temperature plasma nitriding or carburizing.

3 Results and discussion

3.1 Coating structure and formation of S-phase

Figure 1 shows the cross-sectional micrographs of the AISI 316L coatings with or without the laser post-treatment, and subsequently nitriding or carburizing at 450 ℃. Interconnected pores and cracks were clearly observed at as-sprayed coatings. The nitrided coatings were seems to be large grain size compared with the carburized coatings, since the nitrided coatings were sprayed by using -45/+10 μm powder and the carburized coatings by using -20 μm powder. In contrast, the laser remelted coatings were far fewer pores and cracks, and the boundaries of the sprayed

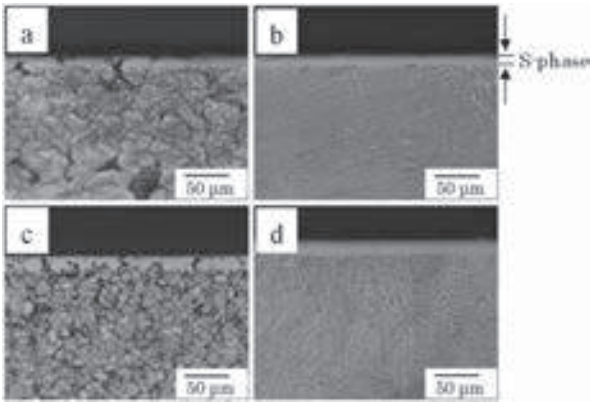

Fig. 1. *Cross-sectional micrographs of the cold sprayed AISI 316L coating with plasma treatment at 450℃; (a) as-sprayed nitrided coating, (b) laser remelted nitrided coating, (c) as-sprayed carburized coating, (d) laser remelted carburized coating.*

particles also vanished; instead, a columnar dendrite structure was observed.

The lighter region at the surface of the coating was nitride or carburized layer. The average thicknesses of the nitride layer were 3 μm at a nitriding temperature of 400 ℃ and 9 μm at 450 ℃, and those of the carburized layer were 7 μm and 13 μm respectively. The carburized layer was thicker than the nitride layer, because the diffusion rate of carbon in austenite is faster than that of nitrogen [7].

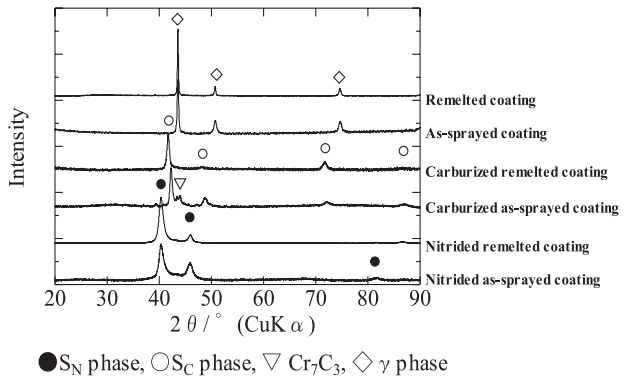

Fig. 2. *X-ray diffraction patterns of the as-sprayed AISI 316L coatings and laser remelted AISI 316L coatings with nitrided or carburized at 450 ℃.*

X-ray diffraction patterns in Figure 2 suggested that the γ(111) and γ(222) peaks were shifted toward lower angles by the plasma treatment, suggesting the FCC lattices of the austenite were expanded by dissolving nitrogen or carbon atoms, and confirming that the nitride layer and carburized layer could be considered as S-phase.

The peaks of the nitride layer were shifted lower angles than those of the carburized layer. This means that the nitride layer contained higher content of dissolved atoms than the carburized layer.

3.2 Wear resistance

The Vickers hardness was measured with test load of 10 g, and the wear test was performed by using alumina ball on

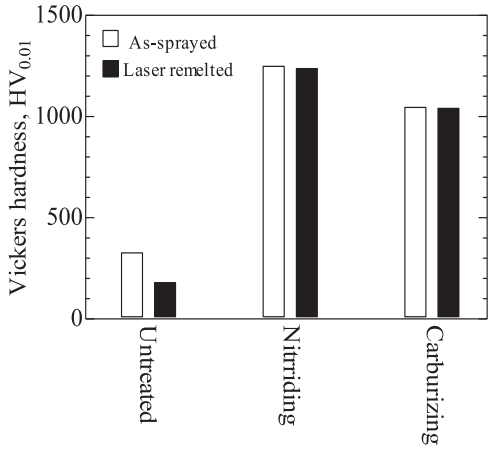

Fig. 3. *Vickers hardness of the as-sprayed AISI 316L coatings and laser remelted AISI 316L coatings with nitriding or carburizing at 450 ℃.*

disk wear test machine with test load of 200 g. The as-sprayed AISI 316L coating (-45/+10 μm powder) without plasma treatment had a hardness of 326 HV in figure 3 and the specific wear amount of 7×10^{-13} m^2/N; those of the laser remelted coating were 179 HV and 4×10^{-13} m^2/N, respectively. The reason for the higher hardness of the as-sprayed AISI 316L coating is the work hardening when the sprayed particles stacked on the substrate. In contrast, the laser remelted AISI 316L coating has been recrystallized, which decreases the hardness.

The Vickers hardness of the nitrided coatings at 450℃ were 1200 HV,the nitrided specific wear amounts were 2×10^{-15} m^2/N, the specific wear amount improved by two orders of magnitude. Meanwhile, the both carburized coatings at 450 ℃ were about 1000 HV and a wear amount of 1.5×10^{-14} m^2/N.

4 Conclusion

Sprayed AISI 316L coatings by cold spray technique were porous microstructure, however, it was recognized that the laser post-treatment modified the coating microstructure to be a dense.

The low-temperature plasma treatments enabled the surface hardness of the cold sprayed AISI 316L coatings to enhance over 1000 HV. The carburizing layer thickness was thicker than the nitriding one, but the nitriding layer was higher hardness and superior wear resistance.

5 References

[1] K. Spencer, M.-X. Zhang: Surf Coat Technol. **205** (2011) 5135-5140.
[2] T. Marrocco, T. Hussain,D. G. McCartney, P. H. Shipway: J. Therm. Spray Technol. **20** (2011) 909-917.
[3] Z. L. Zhang, T. Bell: Surf. Eng. **1** (1985) 131-136.
[4] Y. Sun, X. Li, T. Bell: Surf. Eng. **15** (1999) 49-54.
[5] S. Adachi, N. Ueda: Thin Solid Films. **523** (2012) 11-14.
[6] S. Adachi, N. Ueda: Advanced Powder Technol. **24** (2013) 818-823.
[7] Y. Sun: Mater. Sci. Eng. **A 404** (2005) 124-129.

Effect of Oxyacetylene Flame Remelting on Wear Behavior of Supersonic Air-Plasma Sprayed NiCrBSi/h-BN Composite Coatings

Zhang Nannan, Jiang Di, Zhang Guangwei, Li Deyuan, Zhang Yue
Department of Materials Science and Engineering, Shenyang University of Technology, Shenyang 110870,China

Abstract
NiCrBSi/h-BN composite coatings have been successfully prepared on a cast-ironsubstrate by supersonic air-plasma sprayed technology. The phase constitution, microstructure characterization and microhardness of the coatings before and after oxyacetylene flame remelting were investigated by means of X-ray diffraction(XRD), scanning electron microscopy(SEM) and energy dispersive analysis of X-rays(EDAX) techniques, respectively. The wear resistance of composite coatings was also tested in this paper. It was found that the microstructure was well refined by remelting treatment and the wear resistance property of the coating has been improved. The evenly distributed ultra-micro h-BN particles played a dispersion lubrication role in the coating.

1 Introduction

Coating materials such as Fe-, Ni- and Co-based alloys have been widely used in many industries to protect critical components from wear, corrosion and oxidation [1]. The Ni-based alloy is one of the coating materials that performs well in abrasive and sliding wear, and Ni-based coatings produced by cladding processes, like spraying, surfacing and laser cladding, are suitable for preparing relatively thick coatings, which possess the properties of both abrasion and corrosion resistance [2,3]. Among of them, from the point of view of economy and fast deposition, thermal spraying technology has been successfully applied in many industrial sectors. Recent years, some studies were focus on mixinglubricant like MoS_2, WS_2, CaF_2, PbO and h-BN for preparing self-lubricating coatings [4]. While the others reported research work has been focused on WC, TiC and Cr_3C_2 particle reinforced coatings for their high hardness, high wear resistance and good metallic properties [5].

In this paper, hexagonal boron nitride (h-BN) was selected as a self-lubricating, which has the equivalent in structure of graphite. Its plate like microstructure and layered lattice structure give it good lubricating properties. S. Zhang studied the influence of h-BN content for laser cladding Ni-based coating and found that the addition of BN could increase the hardness of coating and decrease the friction coefficient [6]. However, there is still little publication on the plasma sprayed NiCrBSi/h-BN composite coatings, especially for the structure and performance of remelting coating in surface modification technology. Thus in the present work, the authors investigate the influence of h-BN and oxyacetylene flame remelting treatment for the composite coatings.

2 Experimental

In our experiments, the plasma was generated by means of a DC plasma torch SG-100 (Praxair, Cincinnati, OH, USA). The powder used for the experimentation was NiCrBSi (Hongsheng Inc, Hebei, China) having particle size in the range of 50-150 μm. SEM photos of the powders, which were carried out using the S-3400N (Hitachi Inc, Japan),are shown in Fig. 1.

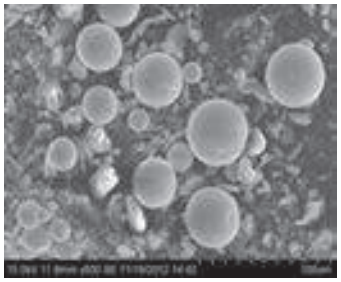

Fig. 1. *SEM photos of the powders*

3 Results and discussion

3.1 X-ray Diffraction

X-ray diffraction pattern of the coating is shown in Fig. 2. It reveals that the microstructure of the coating consists mainly of γ-(Ni,Fe) which was presented as Fe_3Ni. It has no distinct difference with or without h-BN from the results. After remelting process, the phase constituents in the coating include some small peaks like CrB, CrB_2 and CrB_4. Owing to the decomposition of BN in high temperature, a large number of active B combine with Cr in the formation of stable phase CrB_x. The compound CrB_2 is in equilibrium with a solid solution of chromium in ß-rhombohedral boron and determined a temperature of the peritectic decomposition of 1870°C .

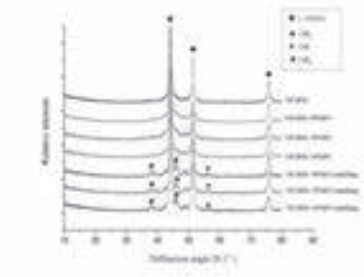

Fig. 2. *X-ray diffraction pattern of NiCrBSi/h-BN coating*

3.2 Microstructure

Figure 3 shows the typical microstructure of NiCrBSi/h-BN. It can be clearly seen the interface between the coating and substrate showing that the coating adhesion is good.

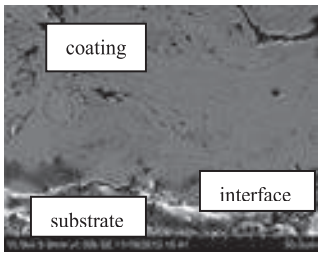

Fig. 3. *Microstructure of NiCrBSi/h-BN coatings*

In Fig.4, it can be found small dendritic crystals in the coating. With increasing of h-BN content, the distribution of dendritic crystals became more and more. However, different from laser cladding technology, these crystal textures appeared dispersedly and locally. It is also found that a mass of finer white particles are dispersed within the metallic matrix.

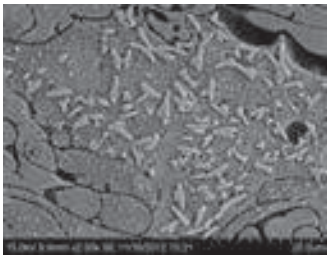

Fig. 4. *SEM photograph of fine dendrites in the coating*

A microstructure of the NiCrBSi/h-BN composite coating prepared by oxyacetylene flame remelting process is presented in Fig.5(a). The boundaries between the coating and the substrate could be observed significantly. The coating is look identical, and large dendrites organization mixed white phase lie in cross section of plasma spray coating, as shown in Fig.5(b).

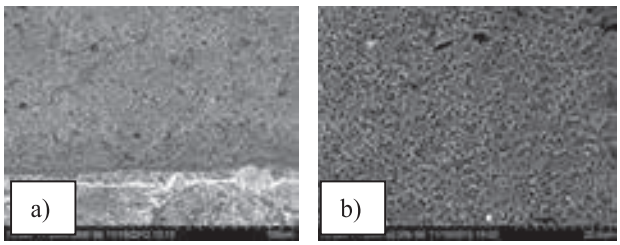

Fig. 5. *SEM photograph of remelting coating*
a) Coating and substrate b) partial enlarged view

3.3 Microhardness

The micro-hardness distributions with three h-BN powder ratios 10%, 20%, 30% are shown in Fig.6. It can be concluded that the hardness of plasma spraying coating layer with h-BN is a little higher than NiCrBSi coating. But the difference of h-BN content has no large effect on the hardness in this experiment. The authors also studied on spraying NiCrBSi /WC composite coating, and found that the hardness of coating increased obviously (about 600 HV), especially after oxyacetylene flame remelting process the hardnesscan be over 1000 HV.

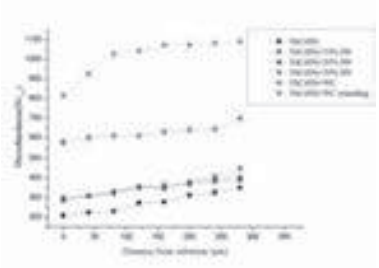

Fig. 6. *Microhardness distribution of composite coating*

3.4 Abrasion Test

Figure 7 shows the wear volume loss of NiCrBSi coating with three h-BN powder ratios 10%, 20%, 30% under the condition of dry grinding, 5 minutes wear time, and 200 N test load. It could be found that the wear weight of original NiCrBSi/h-BN coating is larger than that of after remelting treatment.

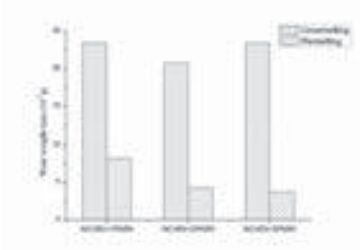

Fig. 7. *Wear weight loss of the coating*

4 Conclusions

(1) The microstructure was well refined by remelting treatment. In the composite layers, a mass of finerh-BN particles was uniformly distributed within the metallic matrix.

(2) The addition of h-BN has no remarkable effect on the coating hardness.The microhardness of the NiCrBSi/h-BN composite coating reaches only 300-400 HV which is far from the NiCrBSi/WC composite coating.

(3) Friction and wear tests without oil lubricant show that the wear weight loss of remelted coating is little than the unremelted one. The wear resistance property of the coating improves with the increase of ultramicro h-BN content which play a dispersion lubrication role in the coating.

5 References

[1] Z.Q.Zeng, H.C.Wang, H.F.Wang, and Y.Wang:Journal of Wuhan University of Technology.27(2012)389-393.

[2] Z.Y. Zhang, Z.P.Wang, and B.N.Liang: Journal of Materials Processing Technology.209(2009)368-374.

[3] R.L. Sun, W.X.Lv, and X.J.Yang:Journal of the Chinese Ceramic Society.33(2005) 1448-1452.

[4]J.X.Yang, D.H.Liu, X.Ding, L.Lei, and T.C.Zuo: Metal Science and Heat Treatment.35(2010)22-26.

[5] H.T.Wang, S.Q.Zhang, J.Zhu, J.H. Huang, H.Y.Liu, and H. Zhang: Journal of Thermal Spray Technology. 18 (2009) 103-109.

[6] S.T. Zhang, J. S. Zhou, B.G. Guo, H.D.Zhou, Y.P. Pu, and J.M.Chen :Material Science and Engineering A. 491 (2008) 47-54.

This work was financially supported by the National Natural Science Foundation, No. 51301112

Effect of heat treatment on the mechanical properties and corrosion performance of cold sprayed tantalum coatings

S.Kumar, V.Vidyasagar, A.Jyothirmayi, S.V.Joshi
International Advanced Research Centre for Powder Metallurgy and New Materials, Hyderabad- 500 005, India

Abstract

Cold spray is a thermal spray variant in which high velocity micron-sized particles are impacted onto a substrate / previously deposited layers to form a coating by strain induced adiabatic heating accompanied by shear instability. It is of significant interest to deposit refractory metals with relatively high melting point through cold spray technique for a variety of high performance applications. In the present study, mechanical properties of cold sprayed tantalum coatings heat treated at different temperatures were studied using micro-tensile testing, scratch testing and nanoindentation. Corrosion performance of the heat treated coatings in 1M KOH solution was determined and potentiodynamic polarization as well as impedance spectroscopy studies were also carried out. The property – performance correlation was investigated by evaluating the microstructure, porosity, inter splat bonding state etc. and attempting to relate them to the mechanical and corrosion properties of the heat treated cold sprayed tantalum coatings. Performance of coatings annealed at 1500^0C (~T_{Rx}) was observed to closely match that of bulk tantalum.

1 Introduction

Cold spraying has emerged as a popular coating technique for deposition of high density metallic coatings for a variety of potential applications. A wide variety of metals and alloys have already been successfully deposited using cold spray technique. The bonding process in cold spray is unique among all the thermal spray variants in that the feedstock is in fully solid state at the moment of impact with the substrate, or the already deposited layer, and does not undergo any thermal degradation in flight. Inter-particle/splat bonding in the above circumstances is governed by localized severe plastic deformation induced adiabatic shear instability, which can be correlated with abnormal temperature / strain growth and flow stress collapse at the impacting interface. This bonding process can be compared with the well established techniques such as explosive cladding and explosive powder compaction. It is of significant interest to deposit refractory metals with relatively high melting temperature through cold spray process. Use of air as process gas for the above purpose is particularly attractive from a commercial standpoint. The mechanical properties of cold sprayed coatings can be investigated by different approaches, which include direct determination of stress-strain curves. It is well known that the post heat treatment process not only relieves the residual stress and decreases the porosity in the coatings but also increases the inter-splat bonding, which can enhance the mechanical/corrosion performance of the coatings. Tantalum is a promising material for various high temperature mechanical applications. Also tantalum is gaining increasing attention due to its superior corrosion resistance when exposed to acids, salts and organic materials even at elevated temperatures. In the present work, tantalum coatings deposited using a cold spray system were heat treated and characterized. The effect of heat treatment temperature on the mechanical properties and corrosion performance is reported herein.

2. Experimental

A cold spray system was used to deposit tantalum coatings employing compressed air as the process gas as well as the powder carrier gas. Commercially available tantalum powder having a size range of 15-45 µm (Inframat, USA) was used as feedstock. All the coatings were deposited at 20 bar stagnation pressure and 450ºC preheat temperature. Sectioned samples were heat treated at five different temperatures (500º C-1500ºC) in a vacuum furnace for two hours. As coated and heat treated samples were mounted and polished using colloidal silica for microstructure characterization using Scanning electron microscopy (Hitachi-S-4300N, Japan). The coated specimens were also subjected to microhardness measurement (UHL VMHT), porosity measurement (Image Pro Plus, Media Cyber Netics, USA), scratch testing (MTS System Corporation, USA) and nanoindentation measurement (CSM). A set of coated samples were sectioned at the coating interface in order to get freestanding sheets which were used for micro tensile and corrosion tests. Potentiodynamic polarization and impedance spectroscopy tests were carried out in 1M KOH solution.

3. Results and Discussion

Figure.1a shows the morphology of the starting tantalum powder feedstock while Fig. 1b reveals the typical microstructure of cold sprayed tantalum. The coatings are noted to be dense, with little porosity being discernible. The porosity in the coating was found to reduce drastically as a function of heat treatment temperature. Coatings heat treated at 1500ºC showed porosity as low as ~ 0.1%.

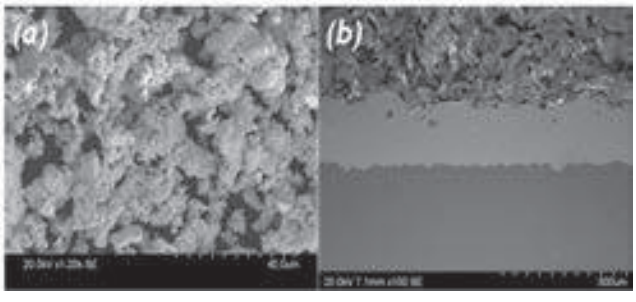

Fig.1. Scanning electron micrographs of (a) Ta powder and (b) cross section of cold sprayed Ta coating.

Figure.2 summarizes the results of mechanical property assessment of the cold sprayed tantalum coatings. It is clear from the data that increasing heat treatment temperature decreases the microhardness (Fig.2a) but increases the critical load for debonding under scratch test (Fig.2c). It is clear from Figures 2a and 2c that the coatings heat treated at 1250ºC show a drastic improvement in mechanical properties. This observation can be attributed to the fact that heat treatment above the recrystallization temperature of tantalum, which corresponds to 1200ºC ($0.4T_m$), helps in fusing majority of the inter-splat boundaries.

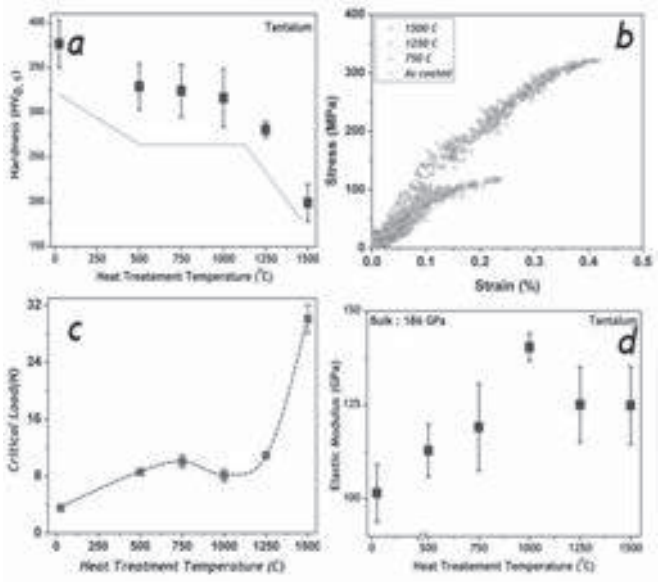

Fig.2.Effect of heat treatment on (a) microhardness, (b) stress-strain behaviour as determined from micro-tensile testing, (c) critical load and (d) elastic modulus of cold sprayed tantalum coatings.

Figures 2b and 2d show micro-tensile testing and elastic modulus results. It is clear that increasing the heat treatment temperature increases the ductility and elastic modulus of the coatings (indentations were conducted at 500g load so that the indent can cover a large number of splats in the coatings). Examination of the fractured surface revealed a ductile mode of fracture, with dimples at the inter-splat boundaries being seen in Figure. 3.

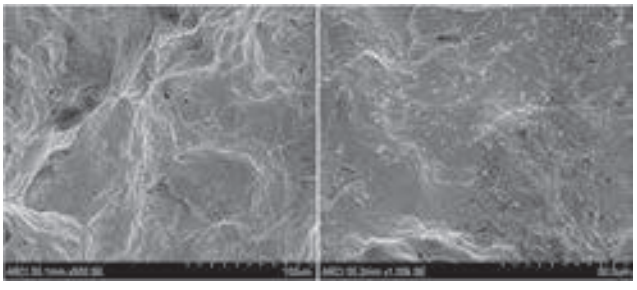

Fig.3. Fracture surface of Ta coating heat treated at 1500ºC

The potentiodynamic polarization plots of the as-deposited and heat treated coatings, along with the bulk tantalum performance, are shown in Figure. 4a. The current density and potential indicate that heat treatment enhances the corrosion resistance of the coatings. The corrosion rate for as-deposited coatings and those heat treated at 1500ºC were found to be 10.1 MPY and 0.9 MPY, respectively, indicating the vastly superior performance of the latter. The above value compares well with that of the bulk, which was found to be 0.7 MPY. The corrosion potential of the coatings heat treated at 1500ºC was found to be actually better than that of bulk tantalum, even though it exhibited lower passivity. It is also interesting to note that, in all the heat treated coatings, the current density during reverse polarization was lower than that during forward scan, which is an indication of effective re-passivation.

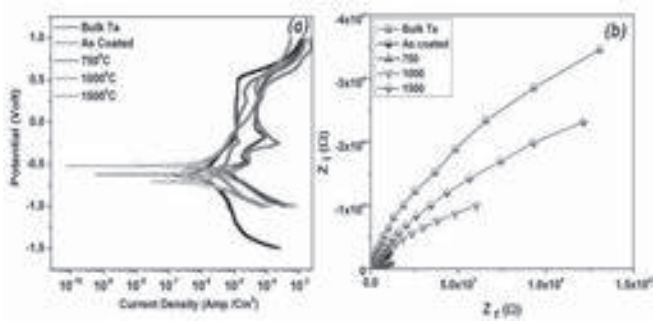

Fig.4. (a) Polarization plot and (b) Nyquist plot of the tantalum coating in as-deposited and heat-treated conditions.

Except for bulk tantalum, all Nyquist plots showed two time constants indicating the influence of defects in the coatings. However, with increase in the heat treatment temperature, the total impedance offered by the coatings was also found to increase.

4. Conclusion

Heat treatment of cold sprayed tantalum coating enhances the mechanical properties and corrosion resistance performance. Coatings heat treated at above the recrystallization temperature of tantalum showed vastly improved functional properties, which were comparable with those of bulk Tantalum.

Acknowledgement

Authors acknowledge the support of Dr.G.Ravichandra for Micro tensile experiments and Dr.Nitin Wasekar for use of Nanoindentation facilities.

References

[1]. Wen-Ya Li, Chang-Jiu Li, Hanlin Liao, C.Coddet, App.Surf.Sci., 253, 2007, 5967.
[2]. P. S.Phani, D.S.Rao, S.V.joshi, G.Sundararajan, J. Therm.Spray Technol., 16(3) 2007,425.
[3]. Koivuluoto et.al, J.Therm.Spray Technol., 18(1), 2009, 75.
[4]. N M Chavan, M.Ramakrishna,P.S.Phani, D.S.Rao, G.Sundararajan, Surf.Coat.Technol., 205 (2011) 4798.
[5]. H Koivuluoto, G Bolelli, L Lusvarghi, F Casadei, P Vuoristo, Surf.Coat.Technol., 205(2010), 1103.
[6]. S.Kumar, G.Bae, K.Kang, S.Yoon, C.Lee, J.Phy.D. Applied Physics, 42(7), 075305.

Study on the chemical compatibility of the coating interface between Ce modified $La_2Zr_2O_7$ and YSZ

Qiong Wu, Xin Zhang, Haoran Peng, Xiaojuan Ji, Xianjing Ren and Yueguang Yu

Sub-Institute of Metal Materials, Beijing General Regearch Institute of Mining and Metallurgy, Beijing 100044, China

Abstract

In this paper, the phase stabilities of powder mixtures and coating interfaces of different Ce modified $La_2Zr_2O_7$ and yttria-stabilized zirconia (YSZ) after heat-treated at 1300°C for 10h was investigated by X-ray diffraction (XRD) and scanning electron microscope. The experimental results showed that due to the cerium and yttria ion diffusion, the $La_2(Zr_{0.3}Ce_{0.7})_2O_7$ would react with YSZ, the chemical compatibility between them is poor. While $La_2Zr_2O_7$(LZ) and $La_2(Zr_{0.7}Ce_{0.3})_2O_7$ showed good chemical compatibility with YSZ.

1 Introduction

The development of a new generation of high-performance aircraft engine requires advanced thermal barrier coatings (TBC) withstand higher temperatures. Lanthanum zirconate ($La_2Zr_2O_7$, LZ) material with pyrochlore structure (($A_2B_2O_7$) has good high temperature phase structure stability, and is one of the most promising new TBCs. However, the LZ has the shortcomings about the thermal conductivity does not fully meet the requirements of thermal insulation at high temperature, and relatively lower thermal expansion coefficients (TECs)[1] and low fracture toughness[1]. Cerium (Ce) occupies Zr position after Ce were doped into LZ (LZC). The Ce-doping can increase the oxygen vacancies and defects, resulting in a decrease of the thermal conductivity of the material through increasing the phonon scatterings [2]. The Ce-doping also decrease the B-O bond energy in $A_2B_2O_7$, which increase the TECs [3]. However, the over-doping of Ce can decrease the B-O bond energy greatly, which decrease the structure stability of LZC, and the high temperature stable phase would transform from pyrochlore to fluorite structure, which decreases the TECs[4]. The double-layer structured TBCs, such as YSZ/$La_2Zr_2O_7$, YSZ/$Gd_2Zr_2O_7$[5], YSZ/$La_2Hf_2O_7$ [6], have been proven to exhibit prolonged thermal cycling life compared with traditional monolayer TBCs.

In the present work, different amounts of Ce modified $La_2Zr_2O_7$ and YSZ double layered coatings were prepared by atmospheric plasma spraying method. The chemical compatibility of the coating interface was studied. The results were verified by phase and crystallographic analyses. The interdiffusion behaviors of YSZ and LZC coatings with different amounts of Ce were compared.[1]

2 Experimental procedure

The original LZC powders were prepared by co-precipitation method. The powders were then spraying-dried to granulated powder with good bulk density and mobility. (powder grades KF-237, KF-238, Beijing General Research Institute of Mining and Metallurgy production). The coatings were prepared using atmospheric plasma spray system (GTV-MF-P-HVOF-K-ARC, Germany). The YSZ and LZC coatings were prepared by F6 gun. The NiCoCrAlY coating were prepared using HVOF gun K2. (NiCoCrAlY powder grades KF-309, Beijing General Research Institute of Mining and Metallurgy production). The matrix material is a nickel-based superalloy.

The cross-sectional microstructures of the coatings were observed using a scanning electron microscope. The powder phase structure were analysed by an X-ray diffractometer (Shimadzu SHIMADZU-6000 type).

3 Results and discussion

3.1 The lattice model of Ce-modified lanthanum zirconium

XRD results of $La_2Zr_2O_7$(LZ), $La_2(Zr_{0.7}Ce_{0.3})_2O_7$(LZ7C3), $La_2(Zr_{0.3}Ce_{0.7})_2O_7$(LZ3C7) powders are shown in Fig.1. The $La_2Zr_2O_7$ and $La_2(Zr_{0.7}Ce_{0.3})_2O_7$ powder shows pyrochlore structure, and $La_2(Zr_{0.3}Ce_{0.7})_2O_7$ shows fluorite structure. As the Ce content increases, the XRD peak shifts to the left, indicating that Ce doping increases the lattice constant.

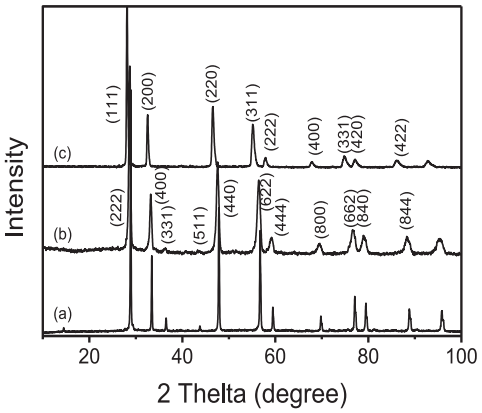

Fig. 1 *XRD results of (a) $La_2Zr_2O_7$, (b) $La_2(Zr_{0.7}Ce_{0.3})_2O_7$, (c) $La_2(Zr_{0.3}Ce_{0.7})_2O_7$ powder*

3.2 The chemical compatibility of Ce modified $La_2Zr_2O_7$ and YSZ powders

Due to the pyrochlore structured coatings were often applied in double-ceramic-layers, the study of chemical compatibility of pyrochlore and YSZ is very important. Phase compositions of the new ceramic powder and the mixed powders of the new ceramic and YSZ powders after heat-treated at 1300°C for 10h were shown in Fig. 2 and Fig. 3, respectively. Fig. 2 shows that the LZ and LZ7C3 powders still show single pyrochlore structure, while the fluorite structure peak of LZ3C7 shows some sub-peak, which means phase transition occurred in LZ3C7. The over Ce doping decreased the phase structure stability of LZ. Fig. 3 shows the mixed YSZ and (a)LZ, (b) LZ7C3, (c) LZ3C7 powders after heat-treated at 1300°C for 10h. There are no

[1] Corresponding author. Tel.: +8601058915101; fax: +8601058915130.
E-mail address: queong@126.com (Qiong Wu).
This work is supported by National Key Technology R&D Program of P.R. China under the contract of 2012BAE02B00.

new phases formed between YSZ and LZ, YSZ and LZ7C3, which demonstrated that YSZ has good chemical compatibility with them. While pyrochlore structure fomed in LZ3Z7 and YSZ mixed powder after heat-treated at 1300°C for 10h, and the pyrochlore structure is much more obvious than single LZ3C7 powder after heat-treated at 1300°C for 10h. It demonstrated that YSZ accelerated the phase transformation of LZ3C7. The reaction equation can be written as: $La_2(Zr_{0.3}Ce_{0.7})_2O_7 \rightarrow La_2Zr_2O_7+La_2Ce_2O_7$.

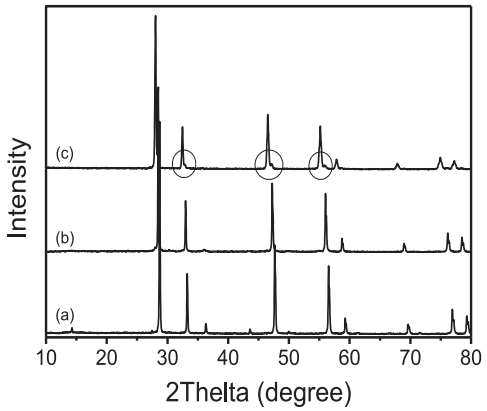

Fig. 2 *XRD results of (a) $La_2Zr_2O_7$, (b) $La_2(Zr_{0.7}Ce_{0.3})_2O_7$, (c) $La_2(Zr_{0.3}Ce_{0.7})_2O_7$ powder after heat treated at 1300°Cfor 10h.*

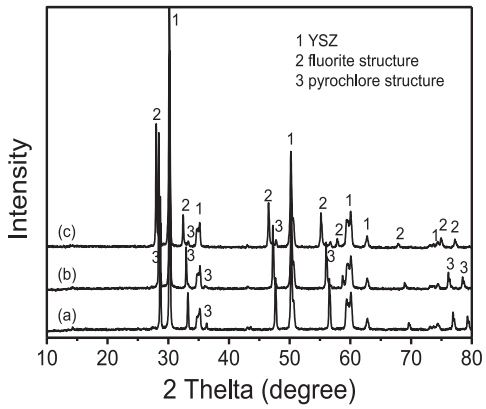

Fig. 3 *XRD results of mixed YSZ and (a) $La_2Zr_2O_7$, (b) $La_2(Zr_{0.7}Ce_{0.3})_2O_7$, (c) $La_2(Zr_{0.3}Ce_{0.7})_2O_7$ powders after heat treated at 1300°Cfor 10h.*

3.3 The chemical compatibility of the coating interface between Ce modified $La_2Zr_2O_7$ and YSZ

Fig. 4 shows the as-deposited double layered LZC/YSZ coatings, The interfaces of LZC/YSZ were very clear. Fig. 5 shows the cross-section microstructure of the LZC/YSZ coatings after heat-treated at 1300°C for 10h. The LZ/YSZ interface was very clear in Fig. 5(a), shows no interaction happens between them. The LZ7C3/YSZ interface was a little indistinct. A diffusion zone about ~7μm formed at the

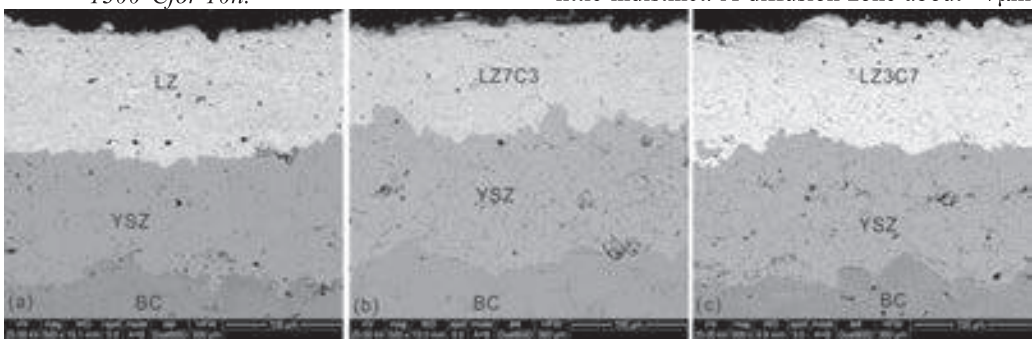

Fig. 4 *The polished cross-section of the as-deposited (a) LZ/YSZ, (b) LZ7C3/YSZ, (c) LZ3C7/YSZ coatings*

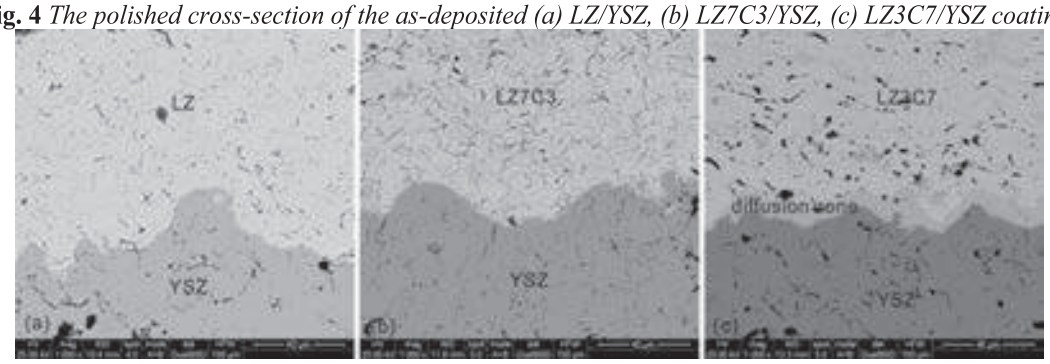

Fig. 5 *The cross-section of the (a) LZ/YSZ, (b) LZ7C3/YSZ, (c) LZ3C7/YSZ coatings after heat treated at 1300°C for 10h.*

LZ3C7/YSZ interface. EDS shows the diffusion zone mainly contents La, Ce, Zr and Y, which means the Ce in LZ3C7 moved interward to YSZ, and Y in YSZ moved into LZ3C7. The specific diffusion mechanisms will be discussed in the full paper.

4 Conclusions

The chemical compatibility of YSZ/LZC powders and YSZ/LZC coating interfaces were studied. The experimental results shows that $La_2(Zr_{0.7}Ce_{0.3})_2O_7$ and $La_2Zr_2O_7$ has good chemical compatibility with YSZ. While $La_2(Zr_{0.3}Ce_{0.7})_2O_7$ would react and interdiffuse with YSZ, and shows poor chemical compatibility with YSZ.

5 References

[1] K. Shimamura, T. Arima, K. Idemitsu, et al., International Journal of Thermophysics 28 (2007) 1074-1084.

[2] H. Zhou, D. Yi, Z. Yu, et al., Journal of Alloys and Compounds 438 (2007) 217-221.

[3] N.P. Bansal, D. Zhu, Materials Science and Engineering: A 459 (2007) 192-195.

[4] X. Cao, J. Li, X. Zhong, et al., Materials Letters 62 (2008) 2667-2669.

[5] R. Vassen, H. Kassner, A. Stuke, et al., Materials Science Forum 631 (2010) 73-78.

[6] R. Vaßen, M.O. Jarligo, T. Steinke, et al., Surface and Coatings Technology 205 (2010) 938-942.

Anisotropy of Thermal Conductivity of Plasma Sprayed Thermal Barrier Coatings

Satoru Takahashi[1], Yoshio Kobayashi[1], Megumi Akoshima[2]
[1] Department of mechanical Engineering, Tokyo Metropolitan University, Hachioji, 192-0397, Japan
[2] National Metrology Institute of Japan (NMIJ), AIST, Tukuba, 305-8563, Japan

Abstract
Thermal conductivities of a through-thickness and a in-plane directions in a top-coat (TC) for thermal barrier coatings (TBCs) were investigated in order to clarify an influence of its microstructure on the thermal conductivity. Several kinds of free-standing TCs were produced by plasma spraying methods. Their thermal conductivities were determined according to calculation using the thermal diffusivities, the specific heat capacities, and the bulk densities. The thermal diffusivities of the through-thickness and the in-plane directions were measured in air at room temperature using a laser flash method and a micro-spot heating angstrom method, respectively. It was found that the plasma sprayed TCs have a significant anisotropy in the thermal conductivity, and the thermal conductivity of the in-plane direction is higher than that in the through-thickness direction. The anisotropy in the thermal conductivity depends on the porosity, the size of splats and the microcracks between splats in the TC.

1 Introduction

Thermal barrier coatings (TBCs) are an indispensable technology for hot-section components of advanced industrial gas turbines. A TBC consists of a metallic bond-coat and a ceramic top-coat (TC) on a superalloy substrate. A thermal barrier function of the TBC depends strongly on the thermal conductivity of a through-thickness direction in the TC. Under an actual operating environment of gas turbines, a hot-spot occurs on the surface of the hot-section component, which induces a spallation of the TC. Therefore, an in-plane thermal conductivity of the TC related to temperature distribution on its surface is also important. However, the thermal conductivity of the in-plane direction in the TC has been hardly reported.

In the present study, the thermal conductivities of the through-thickness and the in-plane directions in the TC were investigated. The influence of its microstructure on the thermal conductivities were discussed in some detail.

2 Experimental

2.1 Preparation of TC specimen

Four kinds of free-standing TCs were manufactured and their process conditions are summarized in Table 1. Hollow spherical powders (HOSP) or angular powders that were made by fusing and crushing (F&C) of 7-8 mass % Y_2O_3 stabilized ZrO_2 (YSZ) were deposited by an atmospheric plasma spraying (APS) or a water plasma spraying (WPS). Flat disk specimens of 10 mm in diameter and 1 mm in thickness were prepared for measuring the thermal conductivity of the through-thickness direction. For measuring the thermal conductivity of the in-plane direction, flat thin square plate specimens of 10 mm in length and 0.25 mm in thickness were used. Some specimens were subjected to the heat treatment in air at 1373 K for 100 h. Figure 1 shows the typical cross-sectional microstructures of as-sprayed TCs. While the YA1 had a relatively dense microstructure, the YA3 had a porous microstructure.

Table 1 *Coating process of various TCs.*

Code	Powder	Spray process
YA1	YSZ (F&C, -45+10 μm)	APS
YA2	YSZ (HOSP, -125+11 μm)	APS
YA3	YSZ (HOSP, -106+11 μm) + 10 %Polyester	APS + 1073 K x 2h in air
YW	YSZ (F&C, -106+45 μm)	WPS

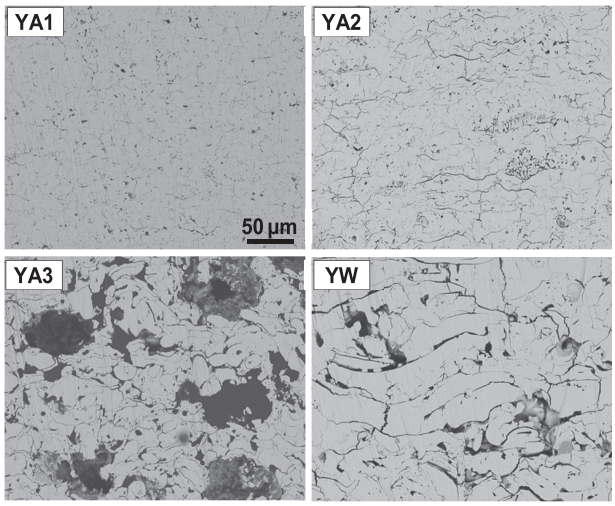

Fig.1 *Typical cross-sectional microstructures of TCs.*

2.2 Measurement of thermal conductivity

The thermal diffusivities, the specific heat capacities, and the bulk densities of these TCs were measured, and finally the thermal conductivities were determined. The thermal diffusivity of the through-thickness direction was measured using a laser flash method according to ISO 18755 [1]. The thermal diffusivity of the in-plane direction was measured using a micro-spot heating angstrom method, as shown in Fig. 2. The small area of 0.15 mm in diameter around the center of the specimen surface was heated by a modulated laser beam of 1 Hz in frequency (f) and 0.15 mm in diameter. The heat modulating with the frequency diffuses hemispherically from the heated spot. The modulated heat in a area of 0.15 mm in diameter at the position of distance (l) away from the heating spot in the rearface was observed as the temperature oscillation by an infrared sensor. The temperature phase delay (θ) between the modulated laser beam and the temperature oscillation is negatively proportional to the distance from the heated spot (l), and the thermal diffusivity (α) of the in-plane direction in the TC can be determined by the following equation (1), when $l >> d$ [2]. Here, d is thickness of the specimen.

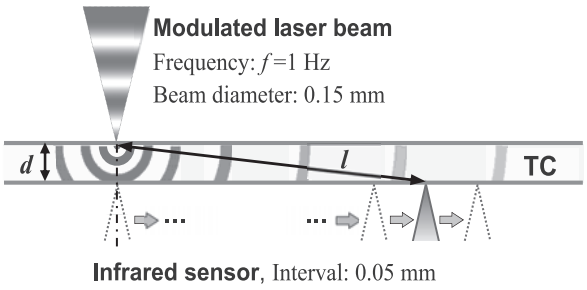

$$\theta = -\sqrt{\frac{\pi f}{\alpha}} \cdot l \qquad (1)$$

Fig.2 *Schematic illustration of micro-spot heating angstrom method.*

The measurements were carried out in air at room temperature. Prior to the measurement, both surfaces of the TC were vapor-deposited with a gold, and also were painted with a graphite. The specific heat capacities and the bulk densities obtained by the previous study [3] were used.

3 Results and discussion

3.1 Thermal diffusivities of through-thickness and in-plane directions of TCs

Figure 3 shows the temperature-rise curves of as-sprayed TCs obtained by the laser flash method. Depending on the TC, a significant change was observed in their curves. The half raise-time became long in order of the YA1, the YA2, the YW and the YA3. In any TCs, the half raise-time after the heat treatment was shorter than that of the as-sprayed TC. Figure 4 shows the typical temperature phase delay diagram

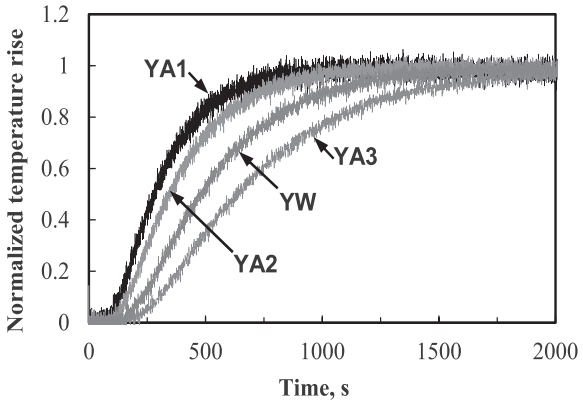

Fig.3 *Temperature-rise curves of as-sprayed TCs.*

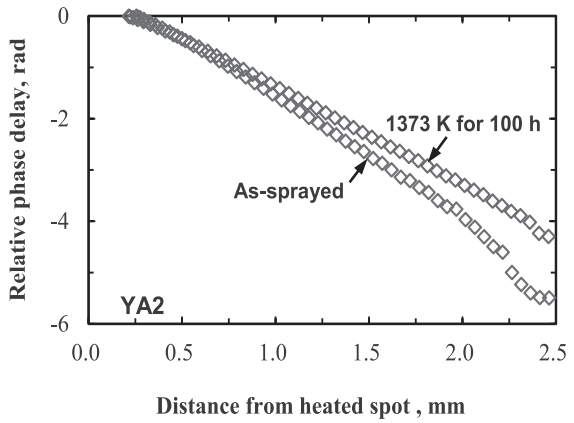

Fig.4 *Typical temperature-phase delay diagram of TC.*

of the TC before and after the heat treatment. The phase delay decreased linearly with increasing the distance from the heated spot. After the heat treatment, the slope of its linear range was decreased. This means the increase of the thermal diffusivity by the heat treatment.

3.2 Thermal conductivities of through-thickness and in-plane directions of TCs

Figure 5 shows the thermal conductivities of the through-thickneess and the in-plane directions of the TCs. It was found that the plasma-sprayed TCs have a significant anisotropy in the thermal conductivity. In any TCs, the thermal conductivity in the plane direction is higher than that of the through-thickness direction regardless of the heat treatment. The anisotropy is attributed to the TC microstructure . Since the YA1 has small splats and the dense microstructure, the anisotropy is low. The YA3 and the YW, on the other hand, have a porous microstructure including many pores and many microcracks between splats. Such microcracks act as a barrier of the thermal conduction and decrease the thermal conductivity of the through-thickness direction. As the results, the anisotropies of the YA3 and the YW become high. Accordingly, the anisotropy in the thermal conductivity depends strongly on the porosity, the size of splats and the microcracks between splats in the TC.

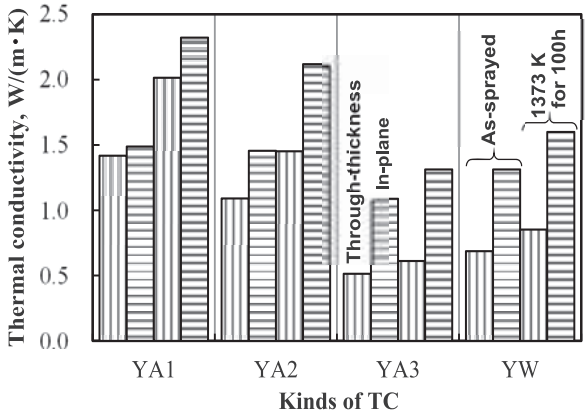

Fig.5 *Thermal conductivities of through-thickness and in-plane directions in TCs.*

4 Conclusions

1) The TCs have the anisotropy in the thermal conductivity. The thermal conductivity of the in-plane direction is higher than that in the through-thickness direction.
2) The thermal anisotropy depends strongly on the porosity, the size of splats and the microcracks in the TC.

Acknowledgments

The authors wish to acknowledge Dr. Takashi Yagi of NMIJ for measuring the thermal diffusivity of the in-plane direction and discussions. A part of this study was supported by Ministry of Economy, Trade and Industry of Japan.

References

[1] ISO 18755:2005 Determination of thermal diffusivity of monolithic ceramics by laser flash method.
[2] W. Nakano, K. Morishita, G, Matsui, T. Yagi, H. Ohta: Proc. 31st Jpn. Symp.Thermophys. Prop. (2010) B304.
[3] Y. Kobayashi, S. Takahashi, M. Akoshima: Netsu Bussei (2014) in press.

Spray dried yttria stabilized zirconia powders from fused and crushed powders and evaluation of their coatings` property for thermal barrier coating applications

S.T. Aruna[1*], N. Balaji[1], Prathap Kumar[2], Jinov J Kachappilly[2],
[1]Surface Engineering Division, Council of Scientific and Industrial Research-National Aerospace Laboratories, HAL Airport Road, Bangalore 560 017, Karnataka, India
[2]Carborundum Universal Limited, Plot No 7, CSEZ, Kochi 682 037. India

Abstract

Plasma sprayed yttria stabilized zirconia is the most widely used topcoat thermal barrier coating (TBC) system that is universally used in the aerospace and automotive industries. The properties of ceramic layers obtained from plasma spray technique depend strongly on the properties of the powders used. For plasma spray applications, the YSZ powder should possess good flowability. The main aims of the present study were (i) preparation of plasma sprayable spherical YSZ powders from fused and crushed YSZ powders using spray drying process and (ii) evaluation of the properties of plasma sprayed YSZ coating for TBC application. The spray drying process parameters were optimized to get powders with a flowability of 80 sec/50 g and average agglomerated particle size of 40 μm. The spray dried YSZ powder was plasma sprayed using two different plasma powers (37.5 and 42 kW) and the coating obtained with lower plasma power had higher porosity and lower thermal conductivity (0.84 W/m.K) at 900°C. The coatings were subjected to thermal cycles and they exhibited good spallation resistance. During thermal cycles, a thin layer (<10 μm) of thermally grown oxide (TGO) was formed. The microstructure and phases of the coatings were evaluated before and after thermal cycles.

Introduction

Thermal barrier coatings (TBCs) perform the important function of insulating components, such as gas turbine and aeroengine parts, operating at elevated temperature [1]. TBCs are characterised by their very low thermal conductivity, the coating bearing a large temperature gradient when exposed to heat flow [2]. The most commonly applied TBC material is yttria stabilized zirconia (YSZ) which exhibits resistance to thermal shock and thermal fatigue up to 1150°C [3]. YSZ is generally deposited by plasma spraying and electron beam physical vapour deposition (EBPVD) processes [4]. The properties of plasma sprayed YSZ coating depends on the spraying conditions and the feedstock material. For plasma spraying application, powders should be larger in size and possess flowability. Plasma sprayable powders are being prepared by a variety of techniques like fusion and crushing, spherodization, co-precipitation, spray drying, sol–gel, milling and sintering etc. Among these techniques, spray drying is a very effective, promising technique that can be industrially scaled up. Spray drying involves evaporation of moisture from an atomised feed by mixing the spray and then drying by air [5].There are a few papers that describe the spray drying of YSZ powders and none of the papers evaluate the properties related to TBCs completely [5]. The main aims of the present study are (i) preparation of plasma sprayable spherical YSZ powders from fused and crushed YSZ powders using spray drying process and (ii) evaluation of the properties of plasma sprayed YSZ coating for TBC application.

Experimental

The slurry for spray drying was prepared from fused and crushed YSZ powders (M/s CUMI). The slurry was prepared using a water soluble binder followed by milling and sieving the slurry to remove the aggregates present in the slurry. During spray drying (laboratory type tall type spray dryer, SM Scientech), the slurry was continuously stirred using a magnetic stirrer at a low speed to avoid the settling of particles. The composition of the slurry and the spray drying parameters were optimized to get the maximum yield of flowable powder. After spray drying the powder was sintered in a muffle furnace at 1200°C. The sintered powder was then sieved according to the requirements. After spray drying the YSZ powder was characterized for flowability, particle size, phase and morphology. The phases present in the powder was confirmed by X-ray diffractometry (Bruker D-8 Advanced). Particle size distribution of the spray dried powder was determined using particle size analyser (Mastersizer 2000). Flowability of the powder was measured using a Hall flow meter (ASTM B213-97). The morphology of the powder and surface and cross-sectional microstructures of the coatings were examined using field emission scanning electron microscope (FESEM, Carl Zeiss). The spray dried YSZ powder was plasma sprayed on a bond coat (Amdry 962 from Sulzer Metco) using air plasma spraying system (Sulzer Metco-9M). Deposition was performed using argon and hydrogen as plasma-forming gases. The coatings were fabricated on SS 304, aluminium and super Ni alloy substrates for XRD, thermal conductivity and thermal cycling studies respectively. Prior to plasma spraying, the substrates were grit blasted with alumina grits (45 μm) and then cleaned with compressed air and acetone. The plasma spraying of the spray dried YSZ powder was carried out at 37.5 and 40 kW and the obtained coatings were designated as P-YSZ-1 and P-YSZ-2 respectively. Thermal conductivity of the coatings was measured at 900°C using thermal conductivity set-up (Flashline 4010, Anter Corpn,). The thermal cycling experiments were conducted for 100 cycles (60 min ramp to 1200 °C, 60 min isothermal hold at 1200 °C, and forced air cooling to room temperature 20 min) using thermal cycling furnace (DUCOM, TM-1200). The TBC coated disc specimens were placed inside the pallet with coatings facing upward during thermal cycling.

Results and Discussion

The powder XRD pattern of as received YSZ powder was purely tetragonal and after spray drying and sintering the powder showed the presence of tetragonal zirconia along with traces of monoclinic zirconia (Fig.1).

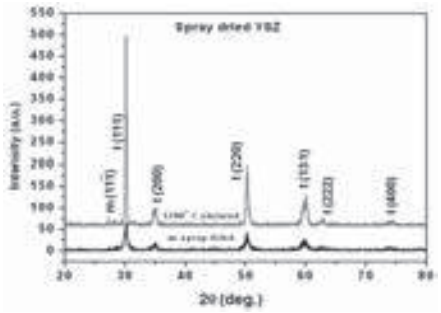

Fig.1. *Powder XRD patterns of spray dried YSZ powders*

The particles exhibited average agglomerated particle size (d_{50}) of ~ 40 µm (Fig.2a) and flowability of the powder was found to be 80 sec/50gms. During spray drying, the blocky angular shaped fused and crushed YSZ powders transformed to spherical particles with a circularity value of 0.946 (Fig.2b).

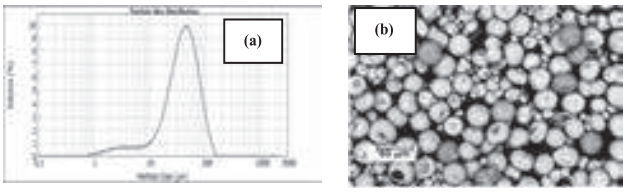

Fig. 2. *(a) Particle size distribution curve and (b) scanning electron microscope image of spray dried YSZ powder*

FESEM images of the surface and cross sections of P-YSZ-1 coating showed fully melted and unmelted regions (Fig. 3). The cross-section of the coating clearly showed the presence of bond coat (~50 µm thickness) and ~ 100 µm thick YSZ topcoat. P-YSZ-1 and P-YSZ-2 coatings exhibited a total porosity of 16 and 15% respectively.

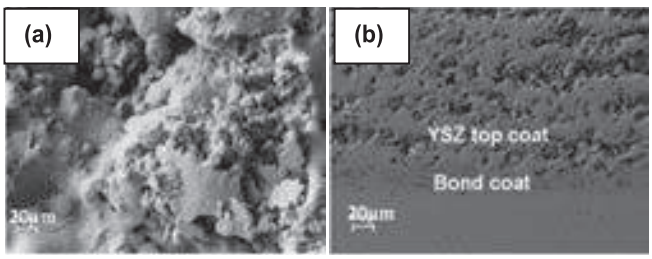

Fig. 3. *FESEM images of the (a) surface and (b) cross-sections of P-YSZ-1 coating*

Thermal conductivity of PYSZ-1 and PYSZ-2 coatings at 900°C were respectively 0.84 and 0.97 W(m.K) which is suitable for TBC application. The coatings withstood 100 thermal cycles without any spallation (Fig.4). However, there were some minor phase changes in the YSZ coating during thermal spraying. A small percentage of cubic zirconia was formed and there was a reduction in the percentages of monoclinic and tetragonal phases as revealed by the Rietveld analysis. During thermal cycles, a thin layer (<10 µm) of thermally grown oxide (TGO, Al_2O_3) which provides oxidation protection was formed (Fig.5).

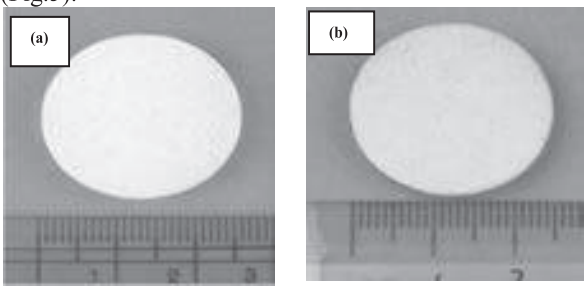

Fig.4. *Photographs of P-YSZ-1 coatings (a) before (b) after 100 thermal cycles*

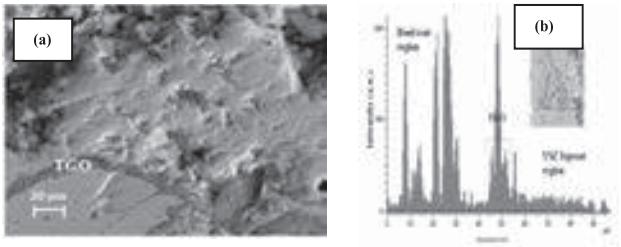

Fig.5. *(a) FESEM image of P-YSZ-1 coating after 100 thermal cycles (b) EDX line scan spectrum of aluminium along the cross-section of the coating after thermal cycles.*

Conclusions

Fused and crushed tetragonal YSZ powder was transformed to spherical shaped particles by spray drying process. The spray dried parameters were optimised to get spherical powders with an average agglomerated particle size of 40 µm and a flowability of 80 sec/50 gms. The spray dried powder was plasma sprayed using two different plasma powers and the coatings obtained with lower power had larger porosity and lower thermal conductivity (0.84 W/m.K) at 900°C. The plasma sprayed YSZ coatings showed spallation resistance and withstood 100 thermal cylces at 1100°C. During thermal cycles, a thin layer (<10 µm) of thermally grown oxide (TGO) was formed and there were some minor phase changes in the YSZ coating. The developed spray dried YSZ powders can be used for TBC applications.

References

[1] R.S. Lima and B.R. Marple: J Therm Spray Technol. **16** (2007) 40–63.

[2] D. R. Clarke and S. R. Phillpot: Mater Today **8** (2005) 22–29.

[3] C.G. Levi: Curr. Opin. Solid State Mater Sci. **8** (2004) 77–91.

[4] M.J. Kelly, D.E. Wolfe, J. Singh, J. Eldridge, D-M. Zhu and R. Miller: Int J Appl Ceram Technol. **3** (2006) 81–93.

[5] G. Bertrand, P. Bertrand, P. Roy, C. Rio, R. Mevrel: Surf Coat Technol. **202** (2008) 1994–2001.

Deposition Technique Using Atmospheric Plasma Spray and Performance of a Composite Thermal Barrier Coating

M. Sai Krishna Rao[1] Vijay K Varma[2] and B Venkataraman[3]
[1]Regional Centre for Military Airworthiness (Materials), CEMILAC, DRDO, Kanchanbagh, Hyderabad – 500 058
[2]Centre for Military Airworthiness and Certification (CEMILAC), DRDO, Marathahalli Colony, Bangalore – 560 037
[3]Defence Metallurgical Research Laboratory, DRDO, Kanchanbagh, Hyderabad – 500 058

Abstract
The spallation failures in conventional Thermal Barrier Coatings (TBC) are mainly due to the stresses arising as a result of mismatch in coefficient of thermal expansion and interfacial oxidation. In the present work, a composite layer has been introduced in between the metallic bond coat and the ceramic top coat in a conventional TBC system to delay the onset of failure. For the purpose, one of the variables namely the injector angle has been varied while keeping all other parameters constant during atmospheric plasma spraying. Four injector angle combinations (bond coat-top coat) namely 90^0-90^0, 75^0-90^0, 100^0-105^0 and 90^0-105^0 have been chosen for the deposition of composite layer by in-situ method. Properly mixed composite layer has been achieved with an injector angle combination of 90^0-105^0.The differential densities of the NiCrAlY and YSZ are found to play a crucial role in deciding the injector angle combination for the deposition of well mixed composite layer. This paper discusses the results of variation of particle injector angle on the nature of the composite layer. Finally, the results obtained on isothermal oxidation studies have been compared with conventional duplex TBC and presented.

1Introduction

The problems of failure in a thermal barrier coating system occurring either due to the stresses arising out of mismatch of thermal expansion or due to interfacial oxidation can be addressed by deposition of functionally graded TBCs wherein *in-situ* mixing and deposition is carried out by the use of twin powder particle feeders with a single plasma torch [1-3]. However, optimizing and control of process parameters in this method is a challenge. Further, the available literature is also rather scanty on this technique [4-5]. Accordingly, there is a technology gap in thorough understanding of this technique and implementation in the field. Further studies are, therefore, needed to understand the oxidation behavior of these FGTBCs to have reliable coatings in many oxidizing environments [6]. The present work partly addresses this aspect and aims to deposit a composite layer in between the bond coat and the ceramic top coat in order to provide a gradual transition of thermal expansion mismatch. Four injector angle combinations (bond coat-top coat) namely 90^0-90^0, 75^0-90^0, 100^0-105^0 and 90^0-105^0 have been chosen for the deposition of composite layer by in-situ method. The results obtained are presented and discussed.

2Experimental Work

2.1Materials

25.0 mm diameter and 1.20 mm thick discs of cold rolled and solution treated Nickel base wrought super alloy Superni 263A (Ni-20Cr-19Co-5.9Mo-2.1Ti-0.4Al) sheet have been chosen as the substrate for the present study. NiCrAlY coating powder (AMDRY 962) and YSZ coating powder (METCO 204NS) have been used as bond coat and top coat respectively.

2.2 Coating Technique

A robotized Atmospheric plasma spray (APS) facility with METCO F4 gun has been used for deposition of the coatings. The coating technique employed for the deposition of conventional thermal barrier coating system and composite layered thermal barrier coating system is detailed in the following paragraphs. Prior to deposition, the substrate surfaces were alumina grit blasted, acetone cleaned and dried. Conventional thermal barrier coating system consisting of substrate, bond coat and top coat as well as substrate with bond coat have been deposited using single powder particle feeder. The powders were deposited using 90^0 injector angle (shown schematically in Figure 1.0 (a). Initially, bond coat (AMDRY 962) has been and subsequently, top coat (METCO 204NS) has been deposited.

The powder feeding for deposition of composite layered TBC system has been done through specially designed twin powder particle feeders (shown schematically in Figure 1.0 (b). The deposition of composite layer has been experimented using combination injector angles viz., 90^0 – 90^0, 100^0 - 105^0, 90^0 – 105^0, and 75^0 - 90^0. The former one is for the deposition of the NiCrAlY powder and the later one is for the deposition of YSZ powder. Initially, the injector holder with an injector angle of 90^0 has been fixed on to the nozzle assembly and bond coat powder (NiCrAlY) has been deposited. After this, each combination of injector angles (90^0 – 90^0, 100^0 - 105^0, 90^0 – 105^0, and 75^0 - 90^0) has been fixed on to the nozzle assembly and the powder feeder lines have been attached to this combination injector holder and the deposition has been carried out *in-situ*. Finally, the injector angle of the injector holder has been changed to 90^0, powder feeder line of YSZ connected and the top coat has been deposited.

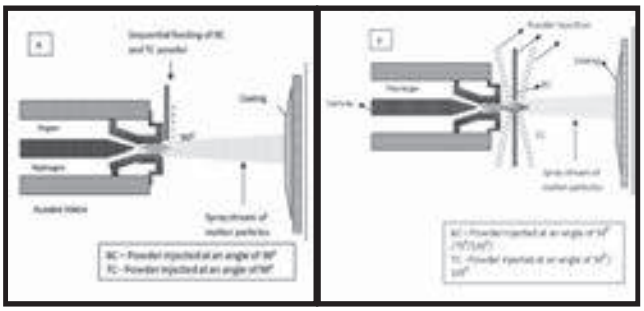

Figure 1.0: Schematic of the experimental set up for deposition of (a) conventional TBC and (b) composite layered thermal barrier coating (BC – Bond coat; TC – Top coat)

2.3 Isothermal Oxidation

Isothermal oxidation studies were conducted in a muffle furnace at a temperature of 1000^0C ($\pm 5^0$C). Four specimens of each category namely bare substrate, substrate with bond coat, conventional TBC and composite layered TBC after initial weight measurements have been loaded in the furnace at room temperature and the chamber was heated at a rate of 20^0C/min up to 1000^0C. The specimens were then held isothermally at that temperature for a continuous period of 500 hours. Weight gain/ loss measurements were made with an accuracy of 0.01 mg.

3.0 Results and Discussion

3.1 Deposition of conventional thermal barrier coatings

The SEM image showing transverse section of the typical microstructure of as-sprayed conventional thermal barrier coating system is shown in Figure 2.0 (a).

The microstructure shows a distinct separation of the bond coat and the ceramic top coat. The coating exhibited a lamellar structure typical of plasma sprayed coatings.

3.2 In-situ co-deposition of composite thermal barrier coatings

The present study involves mixing the powder in-situ during the deposition process. The SEM image showing transverse section of the typical microstructure of as-sprayed composite thermal barrier coating system with an injector angle combination of 90^0 – 105^0 is shown in Figure 2.0 (b). As could be seen, the composite layer consisted a well mixed microstructure. The ratio of NiCrAlY: YSZ: Porosity was 53.0: 42.6: 4.1.

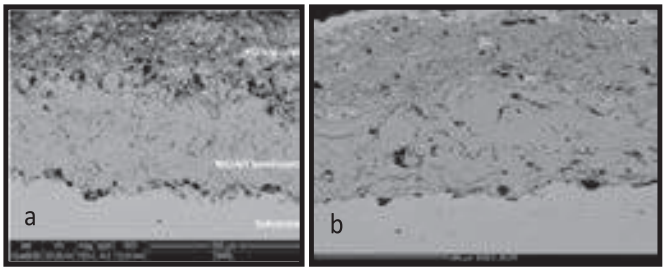

Figure 2.0: SEM image of the (a) conventional thermal barrier coating and (b) composite thermal barrier coating

3.3 Isothermal oxidation studies

Specimens have been exposed for a longer duration of up to 500 hours. Figure 5 shows the specific weight gain. As seen, the specific weight gain of conventional TBC system is marginally higher as compared to bare NiCrAlY specimen. This data suggests that the NiCrAlY bond coat although gains weight initially, starts losing the weight beyond a critical time of exposure. On the other hand, the composite layered TBC system keeps gaining the weight progressively.

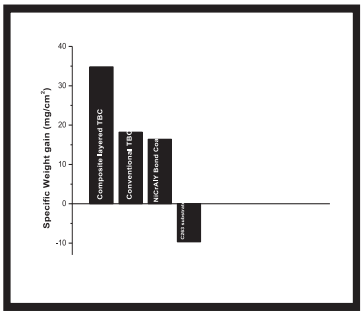

Figure 3: Isothermal oxidation behaviour of the conventional TBC system and composite layered TBC system exposed for a period of 500 hours

Conclusion

Properly mixed composite layer can be achieved with an injector angle combination of 90^0-105^0. The differential densities of the NiCrAlY and YSZ powders are found to play a critical role in deciding the injector angle combinations for the deposition of well mixed composite layer.

The oxidation rate of composite layered TBC was higher as compared to conventional TBC. Nevertheless, the bond coat below the composite layer was un-affected during oxidation as the oxidation was within the composite layer itself. On the contrary, the bond coat in conventional TBC was severely oxidized. Thus the composite layered TBC provides enhanced oxidation protection to the bond coat.

References

[1] Parameswaran V and Shukla A, (1998) "Dynamic fracture of a functionally gradient materials having discrete property variation", Journal of Material Science, Vol.33,pp 3303-3311

[2] Jamarani F, Korotkin M, Lang R V, Ouellette M F, Yan K L, Bertram R W, and Parameswaran V R, (1992) "Compositionally graded thermal barrier coatings for high temperature aero gas turbine components"; Surface & Coatings Technology, Vol. 54-55,pp 58-63.

[3] Khor K A, Gu Y W , and Dong Z L., (1999) "Plasma spraying of functionally graded thermal barrier coatings". Material letters , Vol.38, pp 437- 444

[4] Demirkiran A S, Celik E, Yargan M, and Avci E, (2001) "Oxidation behavior of functionally gradient coatings including different composition of cermets". Surface & Coatings Technology, Vol.142-144, pp551-556.

[5] Saeedi B, Sabour A, Ebadi A and Khoddami A M (2009) "Influence of the thermal barrier coatings design on the oxidation behaviour". Journal of Material Science and Technology, vol.25, No.4, P 499-507.

[6] Kawasaki A and Watanabe R, (2002) "Thermal fracture behavior of metal/ceramic functionally graded materials". Journal of Engineering fracture Mechanics 69; pp 1713-1728

Study of the Interdiffusion Behavior Between NiCoCrAlYTa Coating and GH536 Superalloy

Guo Donghai[1,2], Zhang Shuting[1,2], Li Jin[1,2]
[1] Beijing General Research Institute of Mining & Metallurgy, Beijing 100 160, China
[2] Beijing Engineering Research Center on Surface Strengthen and Restoration of Industrial Parts, Beijing 102 206, China

Abstract
The NiCoCrAlYTa coatings were prepared on Ni-based superalloy GH536 by Air plasma spraying (APS). For the oxidation time of 0, 100, 300h and 500h at 1273K, the interdiffusion law and microstructural evolution were analyzed by SEM and XRD. The results indicate that The elemental interdiffusion between the coatings and the substrate occurs as Al ,Ta, Co diffuse inward from the coating to the substrate and Fe, Mo diffuse outward from the substrate to the coatings. As the oxidation time extended, the interface of NiCoCrAlYTa coatings were enriched of Ta-rich phase, a diffusion barrier was formed, that prevent Al in the coatings spread to the oxidation layer and substrate; meanwhile the Fe in substrate diffusion into coating was slowed. Meanwhile, phase transition of β → γ' → γ happened in coatings, the β phase in coatings were on the decrease, and the γ', γ phase were increased as the degree of oxidation.

1 Introduction

GH536 alloy is a nickel-based superalloy containing solid solution strengthening elements like Co, W, Cr and Mo. It has good oxidation resistance and corrosion resistance, therefore, it is applying in aeroengine combustion chamber components and other high-temperature parts used under 900℃[1]. With the development of aviation industry, the oprating temperature of turbine blade in aircraftengine is higher, in order to improve the oxidation and corrosion resistance of alloy substrate, it is a good choice of using high temperature protective coatings[2].

MCrAlY coatings (M = Ni, Co) have excellent performance of high temperature corrosion resistance, as one of MCrAlY coatings, NiCoCrAlYTa coating is widely used for high temperature protection on the blade of aircraft engine. However, Al, Cr in the coating spreading to the substrate, and Ti, W, Mo diffused into coatings from substrate continuously in high temperature environment, this results in premature degradation failure[3-4]. Therefore, to control the element interdiffusion between coatings and substrate, NiCoCrAlYTa coatings were prepared on GH536 by air plasma spraying (APS) technology, the microstructural evolution and nterdiffusion behavior between coatings/ GH536 at 1000℃ were studied in this article.

2 Experimental

2.1 Materials

The GH536 alloy were machined into substrates discs (Φ23mm×5mm), then polished and ultrasonic cleaning in acetone. The NiCoCrAlYTa powder produced by Sulzer Metco(Armdy 997), thickness of coatings about 2mm were prepared on the discs. The chemical composition of GH536 substrate and Armdy 997 powder were shown in Table. 1.

Tab. 1. *Composition of substrate and coating(in wt.%)*

Sample	Ni	Co	Cr	Al	Y	Ta	Mo	Fe
GH536	Bal.	2	21	≤0.5	--	--	9	19
Coating	Bal.	23	20	8.5	0.6	4	–	–

2.2 Methods

The element diffusion experiments between coating and the substrate were carried out in muffle furnace at 1000 ℃ for 500h, samples were taken at 100h, 300h, 500h respectively. Then the samples were electro-discharge machined into halves lengthwise and polished, the HITACHI S-500 scanning electron microscope (SEM) and energy dispersive spectroscopy (EDS) were used to morphology and composition analysis of coating and substrate.

3 Discussion

3.1 Elemental analysis of APS samples

The microstructure (Figure. 1.) of NiCoCrAlYTa coating indicates that coating thickness was uniform, the boundry betwen coating and GH536 substrate was clear and joined well.

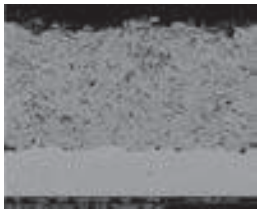

Fig. 1. *SEM Morphology of cross-section of NiCoCrAlYTa coating*

Contrast the chemical composition of coating with substrate, the content of Al, Fe, Ta, Co in them were very different, analysis of EDS line scanning was carried out from top of coating to about 0.2mm depth in the substrate, the result was shown in Figure. 1. The curves stated that content of Co, Fe and Al had an abrupt change from the coating to substrate, meaning that speed of element interdiffusion was very low in process of coating preparation, elements content in each parts were not change compared to the coating had not yet prepared. Because of the content of Y in the coating was too little to detect, so there was no significant difference between the coating and substrate.

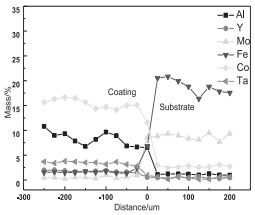

Fig. 2. *Element concentration along the coating and substrate*

3.2 Behavior of element interdiffusion

After oxidation for 100 h at 1000℃, Fe was found in the coating near the interface, and the content in β phase lower than in γ' phase, was 1.47%, 4.95% respectively, as the A and B point shown in Figure. 3. But in the central area of coating, there was no Fe detected, and so it was in the coating which oxidation for 300h as well. After 500h, about 2.86% Fe was found in the central area, but the Fe still didn't diffuse to top of coating from the substrate.

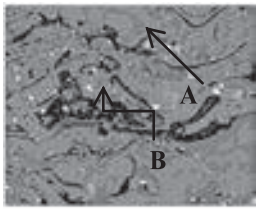

Fig. 3. *Morphologies of coatings for oxidation time of 100h*

The coating was comprised of oxide phase and gray β phase before oxidation, the content of Al in β phase was about 8% -10%. With the oxidation time increased, the amount of poor aluminum phase (γ' and γ phase) and oxide phase increased, the aluminum-rich phase (β) was on the decrease. In the samples which oxidation for 300h and 500h, Al was detected in substrate close to the coating/substrate interface (limited to 50 microns), as shown in Figure. 4. The content of Al in point A and B were 2.08% and 3.25%, but there was no presence of Al in the area where far away from the interface.

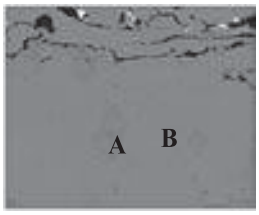

Fig. 4. *Morphology of substrate close to the interface*

In the process of this experiment, Ta was not found in the substrate, the distribution characteristics of Ta in coating as described below: Ta was uniformly distributed in the coating without oxidation, but the content of Ta exited in γ phase was significantly higher than in β phase after samples oxided; more and more white CoCrTa phase(Ta-rich phase) appeared in the coating close to the interface of enrichment in the coating substrate, a diffusion barrier was formed (Figure. 5.), this barrier would help slowing down the element interdiffusion between coating and substrate.

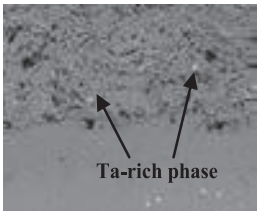

Fig. 5. *Ta-rich phase in the coating*

3.3 Microstruture evolution of coating

With the extention of oxidation time, Al in the dark gray β-NiAl phase was consumed, light grey γ'-Ni3Al phase was formed. As the consume of Al, β-NiAl and γ'-Ni3Al phase were replaced by γ phase, after oxidation for 500h, distribution of each phase in coating shew in Figure. 6.

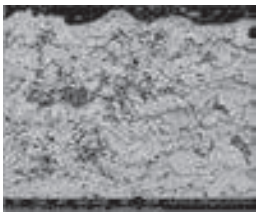

Fig. 6. *The distribution of each phase in NiCoCrAlYTa coating by oxidation of 500h*

4 Conclusions

1) With the growth of oxidation time at 1000℃, the rate of interdiffusion between NiCoCrAlYTa coating GH536 alloy substrate increased. Co, Al in coating diffused to substrate and Fe, Mo diffused to the coating from the substrate. Y and Ta were not detected in substrate, but there were plenty of Ta-rich phase with size of 5μm along the interface in the coating, the diffusion barrier was formed by Ta-rich phase slowed down the element interdiffusion between coating and substrate.

2) With Al consumed after NiCoCrAlYTa coating was oxided, the phase transformation process of β→γ'→ γ was occured. After oxidation for 500h, poor aluminum area which mainly comprised of γ phase were formed close to the oxide layer on the top of coating and the interface between coating and substrate. The matrix phase in coating was γ phase, γ' and little of β phase scattered in the matrix, almost all of the Ta-rich phase existed in γ phase closed to the coating/substrate interface.

5 References

[1] W. H. Wei, S. Yang and E. P. Chen: Iron and Steel. **17**（1994）47-51.

[2] N. P. Padture, M. Gell and E. H. Jordan: Science. **296**（2002）280-284.

[3] Y. H. Sohn, E. Y. Lee and B. A. Nagaraj: Science. **296**（2002）280-284.

[4] N. P. Padture, M. Gell and E. H. Jordan: Surface & Coatings Technology. **146**（2001）132-139.

Metallurgical Evaluation of Thermal Spray Coatings used in Gas turbines

Hariharan S[1], Dheepa Srinivasan[1], Murali Dontu[2] and Vighnesh Chandrasekhar[3]
[1] GE Power and Water, GE India Technology Centre, Bangalore 560066, India
[2] Ford Technologies Services India, Chennai 600096, India
[3] Tata-AIG General Insurance Company, Mumbai 400012, India

Abstract
Preparation and evaluation of thermal spray coatings poses several challenges to a metallographer. The microstructure is particularly sensitive to coating artifacts, such as oxide pull outs along the particle boundaries, or eroding away material between particles and causing excessive porosity. In fact a very careful selection of the media (grinding and polishing papers), is needed in order to reveal what is truly representative of these coatings, which typically comprises, materials that have vastly differing mechanical properties, on a more ductile metallic substrate. In many a case, the coatings are bi-layered, having a more brittle top coat, on top of a ductile underlying bond coat, which makes it challenging to grind and polish using one single set of metallographic parameters. For instance, in a HVOF Cr_3C_2-NiCr coating, smearing of the ductile phase during grinding, could lead to an apparent low porosity, whereas in the case of the APS, YSZ-TBC, grinding could lead to unanticipated pull out of the brittle phase, especially along regions that have not seen a good binder. This paper will illustrate some aspects of proper vs improper metallography in the evaluation procedure for different coatings, MCrAlY, Cr_3C_2-NiCr, Stellite6, FSX414, YSZ-TBC, and DVC-TBC (dense vertically cracked), sprayed using the HVOF and APS thermal spray processes.

1 Introduction

Over 15-16 different types of thermally sprayed coatings, both metallic and ceramic, are used in a modern gas turbine, both industrial as well as aero engines, serving as thermal, oxidation, wear and corrosion protection coatings. Ascertaining the quality of these coatings via metallography is an important aspect of the coatings process cycle, in order to ensure that the coatings can be effective in lasting through a cyle of engine operation. There are very few other ways of determining accurately, the coating thickness, porosity, oxides, coating-substrate interface grit contamination and chemistry, in determining the overall uniformity of the coating, including the soundess of any metallurgical diffusion bonding. However, owing to the vastly different nature of the coating and substrate characteristics, ceramic coating on a metallic Ni based superalloy substrate (eg. a thermal barrier coating (TBC) on a MCrAlY bond coat (BC)), or a metallic coating of high hardness (Stellite6) on top of a Ni based alloy substrate, the sample preparation poses serious challenges, leading to artefacts that may end up erroneously, disqualifying the coating process. This paper presents some of the artefacts during metallographic sample preparation of 6 types of coatings, to look for, and means to eliminate these artefacts to obtain a more representative micrograph of the coating.

2. Experimental Details

Table 1 presents the list of thermally sprayed coatings, that were metallographically evaluated, along with their corresponding coatng process. The standard metallorgraphic process, starting with 1“x1“(25.4 mm) square coupons were cut, mounted, ground and polished, using the standard metallographic equipment, listed in Table 2. The coating microstructures were examined using a Nikon Eclipse MA 200, attached with a Clemex image analysis system.

3. Results and Discussion

Fig. 1 illustrates the some of coating artefacts that could arise during each step of metallography, starting with, cutting, mounting, polishing and imaging, for porous and dense vertically cracked TBC, ceramic coatings. Included in Fig. 1d and 1h, are the representative proper images from both the coatings. Figs. 1a and 1e, show an example of using very high cutting speed vs not mounting the cutting such that it is compressive to the coating, thereby resulting in cutting cracks, in both the porous-TBC and DVC-TBC. Fig. 1b and 1f, illlustrate the result of using hot mounting and improper grinding, resulting in excessive pull outs in both the coatings. In particular, the DVC-TBC coating, shows several additional horizintal cracks generated during grinding adn polishing. Fig. 1c and 1g, show how image analysis can be manipulated to indicate excessive porosity, not belonging to coaitng, which can end up rejecting the coating. Fig. 1d and 1g, are examples of proper microstructures for both types of TBC-ceramic coatings, revealing no cutting cracks, proper filling of the pores during mounting, the right process steps for grinding and the right image analysis to detect the % porosity (inset). These have been obtained after careful optimizing the cutting speed, mounting cmpound and time, grinding and polishing load and time, to result in good quality images that are representative of the coating process parameters.

Table 1 : Coatings used for metalllography with the process

Coating Type	Coating	Process
Metallic	MCrAlY	HVOF
	Stellite6	HVOF
	FSX414	HVOF/APS
Ceramic	TBC-porous	APS
	TBC-DVC	APS
	$Cr_{23}C_6$	APS

Table 2 : Flow chart for coating metallography

Step	Equipment	Type
1	Cutting	Low Speed vs High Speed saw
2	Mounting	Cold vs Hot Mount
3	Grinding	80 upto 600 grit
4	Polishing	Diamond and colloildal silica
5	Imaging	Porosity, Thickness, Grit entrapped

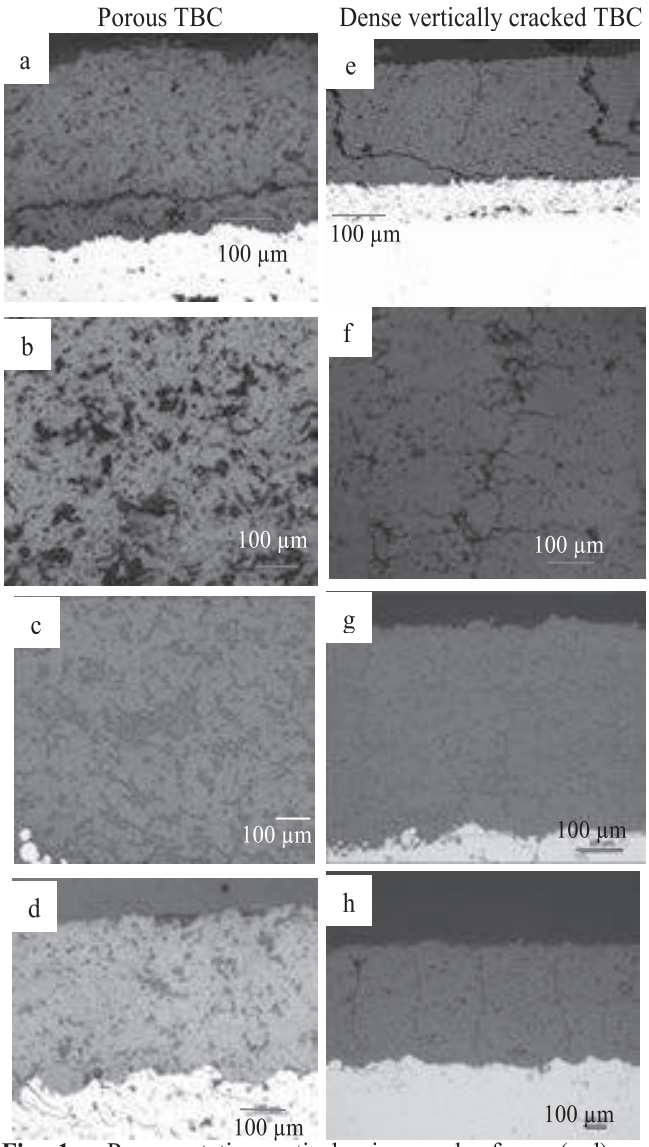

Fig. 1 : Representative optical micrographs from, (a-d) Porous TBC, and (e-h) Dense vertically cracked TBC, showing, (a,e) Cutting cracks, (b,f) Pull outs during grinding, (c,g) high porosity from image analysis, (d,h) proper images, of the TBC top coating.

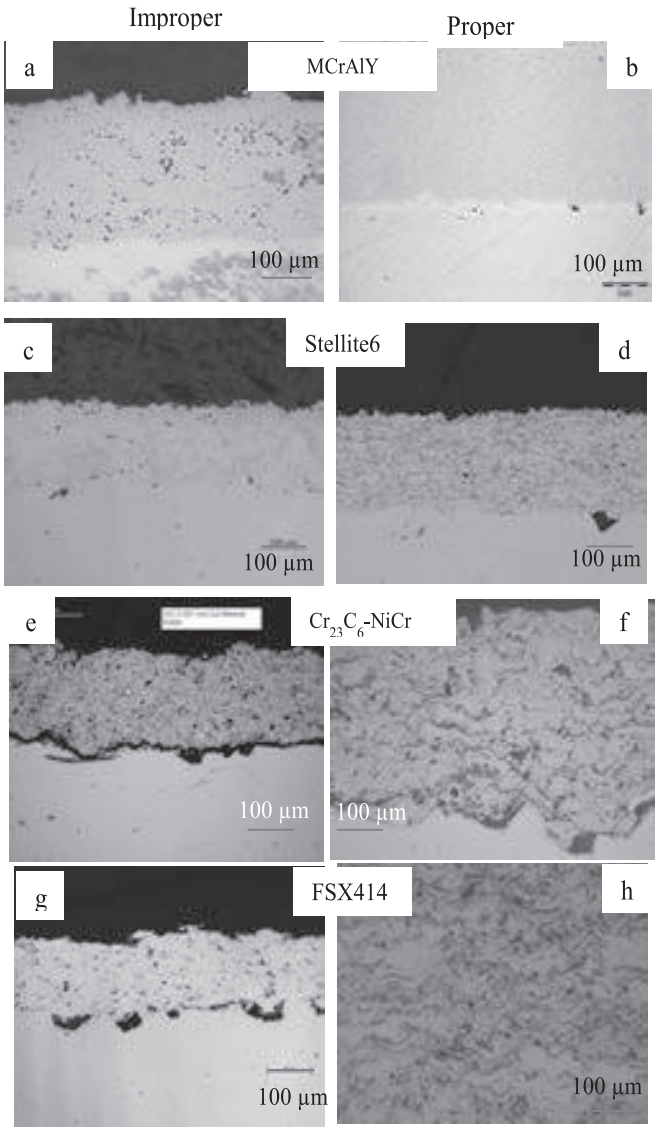

Fig. 2 : Representative optical micrographs from coatings, (a-b) MCrAlY, (c-d) Stellite6, (e-f) $Cr_{23}C_6$, (g-h) FSX414, illustrating an example of, Proper (b,d,f,h) vs Improper (a,c,e,g) metallography.

In Fig. 2, a comparison of good microstructure with the improper ones has bene made for different metallic coatings, that serve as oxidation (MCrAlY) and wear protection coatings, Stellite6, FSX414 and a carbide, $Cr_{23}C_6$ coating. Fig. 2a shows the excessive pull outs in a MCrAlY-HVOF coating, along with stains that could arise in the fine polishing step, owing to lack of lubricants. Fig. 2c, 2e and 2f illustrates the effect of, lack of proper grinding, very aggressive cutting and excessive grit entrapment, in Stellite6, $Cr_{23}C_6$ and FSX414, respectively. The corresponding good micrographs after correcting these metallographi process methods, have been shown in Figs. 2b, 2d, 2f and 2f, respectively. Optimized grinding and polishing parameters were evaluated for each type of coating, keeping in mind the hardness, porosity, brittleness of the coating with respect to the substrate, while at the same time, optimizing for one sequence of polishing operation that combines the metallic substrate, metallic coatings or a metallic bond coat (as applicable) for the ceramic top coat.

4. Summary

The metallorgaphic proceedures have been optimized for several metallic and ceramic thermal spray coatings. 6 different coatings were illustrated in this study, illustrating the defects that could result in improper coating microstructure at each step of the sample preparation process, from cutting until image analysis.

6. Acknowledgements

This program was support by GE, Power and Water, Repair Development Centre, as part of the shop optimization program. Mr. Christopher Thompson and Dr. Sundar Amancherla, GE Power & Water, are acknowledged.

7. References

1. A.K. Ray, Mater. Charac. **57** (2006) 199-209.
2. G. Moskal, B. Witale, A. Rozmyslowska, Arch. Mater. Sci. Engg., **39** (2009) 53-60.3.
3. B. Schorr, **42** (1999) 93-100.
4. D.G. Puerta and G. Blann, Researchgate publ. unknown.

Effect of Substrate on Erosion and Adhesion Behaviour of Detonation Gun Deposited Cr_3C_2-NiCr Coating

J.K.N. Murthy, B. Venkataraman
Defence Metallurgical Research Laboratory, Kanchanbagh.P.O., Hyderabad-500 058

Abstract
Thermal spray Cr_3C_2-NiCr coatings are in practice deposited on engineering components of different materials to combat wear and corrosion. However, studies mostly have been done using steel as substrate material. In the present work, SS304, IMI834 and IN718 were chosen as substrate materials and Cr_3C_2-20(Ni20Cr) coating was deposited by D-gun spray (DS) process to study its erosion performance and adhesion behaviour. The coating on different substrate materials were first characterized in the as-sprayed and annealed conditions (600 °C) to determine the microstructure, phases and residual stresses. The particle erosion was done using silica sand and the coating adhesion strength was determined by the pull-off test method. The results show that erosion rate and adhesion of the coating are significantly affected by substrate materials. The coating on IMI834 gave the lowest erosion resistance, while the coating on SS304 substrate provides best erosion resistance. The coating adhesion with SS304 substrate was found to be better than the other two substrate materials. Annealing, in general, was found to improve both erosion resistance and adhesion of the coating. The residual stresses induced in the coating are found to play an important role, particularly, with respect to erosion.

1 Introduction

Chromium carbide-nichrome based thermal spray coatings in actual practice are deposited on engineering components of different materials such as steel, aluminium alloys, titanium alloys and nickel alloys. However, most of the studies on these coatings have been done using steel as the substrate material. In the present work, three different substrate materials namely steel (SS304), Ti alloy (IMI834) and Ni alloy (IN718) were chosen for depositing Cr_3C_2-Ni20Cr coating by detonation gun spray (DS) process. The aim of the work was to study the effect of the substrate material on: a) coating adhesion and b) solid particle erosion.

2 Experimental

Cr_3C_2-20(Ni20Cr) coating was deposited on test samples of different substrate materials mentioned above by DS process using standard deposition parameters. The test samples of dimensions 30 mm x 30 mm and 4-5 mm thick were cleaned and grit blasted to prepare the surface prior to coating deposition. The thickness of the coating deposited was 200-250 μm. Some of the coated samples were annealed at 600 °C for 90 mins. The coatings on different substrates were then systematically characterized to obtain the microstructure and phases in the as-sprayed and annealed conditions by scanning electron microscopy and X-ray diffraction. The surface residual stresses in the coating on different substrate materials were determined by XRD technique using $Sin^2\psi$ method. The coating adhesion strength was obtained by the pull-off adhesion test method as per ASTM standard C-633. The solid particle erosion was carried out using angular silica particles (180-300μm size) impinging at 30° impact angle and a particle velocity of 45 ms^{-1} in ambient atmosphere. The tests were done until steady state was attained to determine steady-state erosion rate.

3 Results and Discussion

The as-sprayed Cr_3C_2-20(Ni20Cr) coating on steel, Ni alloy and Ti alloy substrates had similar microstructure and phases. A typical microstructure is shown, **Fig. 1a.** The microstructure revealed primary carbides that were uniformly distributed in the binder. The binder had varying grey scale due to differential dissolution of some carbides in the NiCr binder during thermal spraying process [1]. The XRD patterns showed a broad hump on the binder phase spectra indicating the presence of amorphous / nanocrystalline phase. The main peaks identified were Cr_3C_2, Cr_7C_3 and Ni. Upon annealing at 600 °C, major changes take place as secondary carbides precipitate within the super-saturated binder, **Fig. 1b**. The XRD peaks become sharp and the phases identified are similar as in as-sprayed coating. The TEM studies confirm the binder to be largely amorphous in the as-sprayed coating and after annealing at 600 °C the binder becomes crystalline [2].

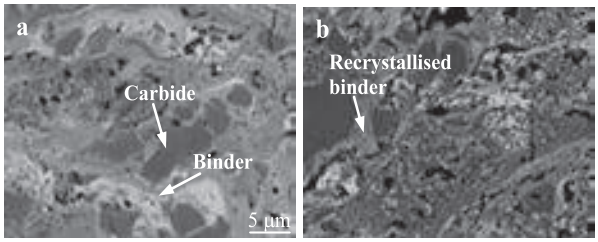

Fig. 1. *SEM micrographs of DS Cr_3C_2-20(Ni20Cr) coating, a) as-sprayed and b) annealed at 600 °C.*

The surface residual stresses induced in the as-sprayed coating on different substrate materials is shown, **Table. 1**. The residual stresses in the coating were compressive for SS304 and IN718 substrates while tensile in case of IMI834 substrate. The difference in residual stresses arises largely due to mismatch in the coefficient of thermal expansion (CTE) between the coating material, α_c (12 x 10^{-6} K^{-1}) and the substrate material, α_s. Higher CTE mismatch induces higher residual stresses, **Table. 1.** The residual stresses in the coating on different substrates after annealing is also given in the table. For the Ti alloy and steel substrates, the surface residual stresses after annealing became increasingly tensile and compressive, respectively, in the coating. These stresses were generated due to thermal mismatch between the substrate and the coating as they cooled from the annealing temperature (600 °C). However,

in case of Ni alloy substrate the residual stress in the coating only marginally decreased after annealing. These results may indicate that the stress relaxation mechanisms in the coating like plastic deformation, microcracking and creep were negligible. This is possible as stresses induced in the coating were low. Further, the binder that was largely amorphous in the as-sprayed coating transforms to a crystalline phase upon annealing. The change in phase (with possibly difference in values of α in amorphous and crystalline phases) and the inter-splat bonding may have also influenced the residual stress in the annealed coating.

Table. 1. *Residual stress in the coating on different substrate materials.*

Substrate		Surface Residual Stress, MPa	
Material	CTE, 10^{-6} K^{-1}	As-sprayed	Annealed
SS304	17	-295	-360
IN718	13	-145	-120
IMI834	10.6	60	210

The adhesion strength of as-sprayed DS Cr_3C_2-20(NiCr) coating varies with different substrate materials, **Fig. 2**. The coating on SS304 substrate gave the highest average bond strength value (65 MPa) while the coating on IMI834 and IN718 substrates the bond strength value was nearly same (46 MPa). Factors like mechanical mixing, particle embedment and possibly metallurgical bonding that occur during splat formation may affect the coating adhesion. Annealing resulted in a change in coating adhesion strength. The coating adhesion strength increased in case of Ni and Ti alloy substrates while with steel adhesion strength was found to decrease. The interfacial elemental diffusion and residual stresses may influence adhesion in the annealed coating.

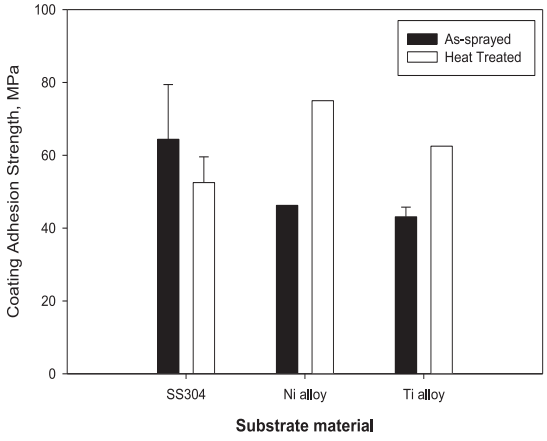

Fig. 2. *Coating adhesion strength in DS Cr_3C_2-20(Ni20Cr) coating deposited on different substrate materials.*

The steady-state erosion rate of as-sprayed DS coating deposited on different substrate materials is not same, **Fig. 3**. The coating deposited on IMI834 showed slightly higher erosion rate compared to the same coating on other substrates. Annealing, in general, resulted in improving the erosion resistance of the coatings on different substrates. Significant improvement occurred in the annealed coating on IMI834 substrate. Though the coating appeared to be similar in microstructure (both as-sprayed and annealed) significant differences were observed in the erosion rate when deposited on different substrates. Such a variation in the erosion rate may be due to the presence of residual stress in the coating [3,4].

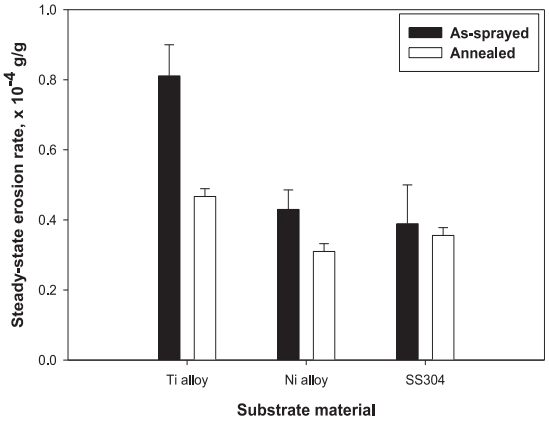

Fig. 3. *Steady state erosion rate of DS Cr_3C_2-20(Ni20Cr) coating deposited on different substrate materials.*

A graph of steady-state erosion rate vs residual stress was plotted, to understand the influence of the residual stress state, **Fig. 4**. The presence of tensile stress resulted in a higher erosion rate whereas compressive stress in the coating could reduce the erosion rate in general. The presence of tensile residual stress in the as-sprayed coating (IMI834) may have caused early crack initiation and its propagation due to erodent particle impact leading to higher erosion rate. These events would have been delayed with other substrates due to compressive residual stresses. In the annealed coating better inter-splat cohesion, fine carbide precipitates, higher volume fraction of carbides and binder ductility improves erosion resistance and also compensates for the tensile stresses.

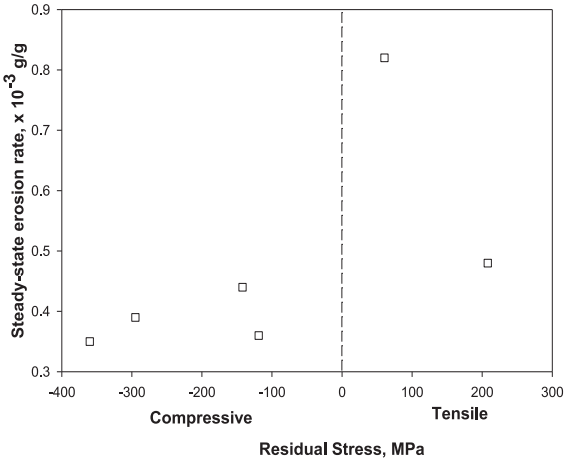

Fig. 4. *Steady-State Erosion Rate of DS Cr_3C_2-20(Ni20Cr) Coating vs Residual Stress in the Coating.*

4 References

[1] S. Zimmerman and H. Kreye: Proc. 9th Nat. Conf. on Thermal Spray, (ASM International, 1996) pp. 147-152.
[2]J.K.N.Murthy, S.Bysakh, K. Gopinath and B.Venkataraman: Surf. Coat. Technol. **202** (2007) 1-12.
[3] D. A. Stewart, P.H. Shipway and D.G. McCartney: Surf. Coat. Technol. **105** (1998) 13-24.
[4] J. K. N. Murthy, D.S. Rao and B. Venkataraman: Wear, **249** (2001) 592-600.

Coatings for Protection Against Silt Erosion in Hydro Turbines

Rahul Sood

Director, Industrial Processors & Metallizers (P) Ltd., Delhi, India.

Synopsis

We at IPM, study the phenomena of erosion at silt-affected power stations, in order to have an in-depth understanding of the problem and then offer our customer a suitable repair & coating solution. This approach, adopted by us, has given very promising results to our esteemed customers, which include 1500MW Nathpa Jhakri Hydro Electric Power Station as well as other silt affected power stations, operating in the Himalayan region. It has not only considerably extended the life of the underwater parts and increased the power generation but also increased the capacity index of these power plants.

In this paper, through a case study, we will be discussing how thermal spray coating has provided by IPM, have helped silt affected power stations to manage their erosion problem and improve their over all performance and profitability.

Erosion behaviour of Ni-based alloys at high temperatures

Manish Kumar[1], S. Ashok[1], Krishna Praveen J[1], BH. Channabasappa[2]

[1] Höganäs India Private Limited, Pune 411001, India

[2]Ducom Instruments Private Limited, Bangalore 560058, India

ABSTRACT

There are several industrial applications where materials are subjected to erosion at high temperatures which often leads to accelerated degradation. To overcome these industrial problems, coating of the exposed surface is a cost effective solution. This paper discusses, two coating techniques, High velocity oxy fuel (HVOF) and Plasma spraying, which were used to deposit Ni-based powder with WC-Co. Particle erosion tests have been conducted on the coated samples as per ASTM standards at various temperatures. Microstructure and the wear properties have been correlated.

INTRODUCTION

High temperature erosion is a major problem in industries such as oil and gas refinery and coal based power station. Erosion of components which are exposed to high temperature conditions are degrading at high rate by silica and alumina or some hard particles which are present in raw materials. Sever erosion happens especially in carrying pipes and at elbow where these particles impinge or impact on surface. Replacement of this erode components usually are very high capital intensive, so therefore Ni-based coating of such components is economically feasible solutions for erosion issues as this coating gives good resistance to erosion at high temperature.

Surface coating with some harder materials is a potential solution for wear. There are several methods for depositing such coating. Some of them are plasma based, laser based and mechanically bonded based. In Present studies, two techniques has been used which are Plasma Spraying and HVOF Spraying. For deposition, Höganäs's powders have been used in mixture (20:80) form of 1616-02 with 46712-12 powders on mild steel substrate. Chemistry and particles sizes are tabulated in Table 1 and 2.

EXPERIMENTAL PRCEDURE

Mild steel substrates were made in dimensions 15x15x5 mm^3 on which coating to be done. Plasma and HVOF Coating were performed on this substrate. Figure 1 showing Plasma and HVOF coated samples.

a b

Figure 1: Plasma sprayed(a) and HVOF sprayed(b) sample

Table 1: Chemistry and particle size for Ni-based powder,

Powder	Particle Size (µm)	C (%)	Si (%)	B (%)	Fe (%)	Cr (%)	Ni (%)
1616-02	20-53	0.2	1.0	Nil	0.5	20.0	Bal.

Table 2: Chemistry and particle size for WC-Co powder,

Powder	Particle Size (µm)	C (%)	Co (%)	W (%)
46712-12	10-53	5.4	12.2	Bal.

Coating of samples has been characterized using optical microscope to see interface of coating before perform any erosion test at Ducom's test rig. Erosion testing conditions have been summarized in Table 3.

Table 3: Erodent velocity and flow for testing,

Erodent Velocity	30 m/s
Flow of Erodent	2 ± 0.5 g/s
Erodent Average Size	50 µm
Test Temperatures	25, 250, 750 °C

After high temperature erosion testing erodes samples were again analysed with the help of optical microscope.

RESULTS AND DISCUSSION

In Fig. 2 is showing initial microstructure of coated samples, it is also indicating that good coating has been done on substrate because on interface not much porosities are present. Coating thickness for Fig. 1(a) is around 0.3 mm and Fig. 2(b) is around 0.4 mm for respective cases.

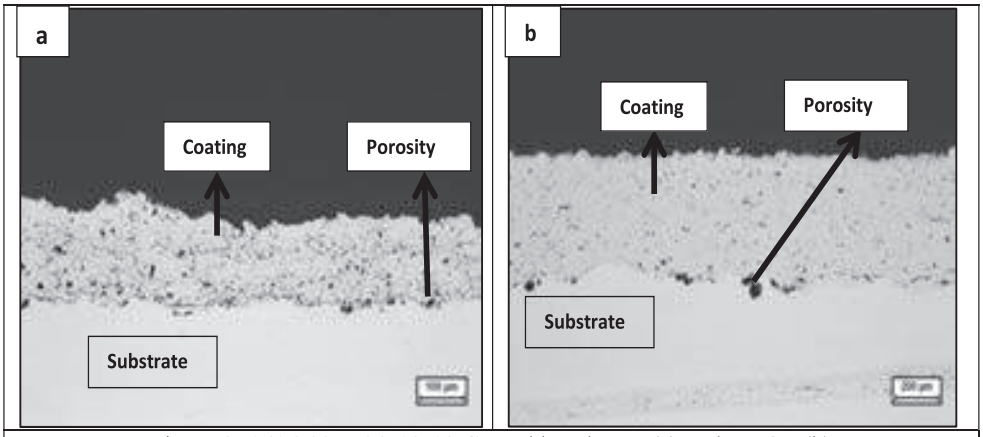

Figure 2: 1616-02 + 46712-12 Coated by Plasma (a) and HVOF (b)

Effect of Temperature and Coating Techniques on Erosion Rate

Figure 3 shows the effect of temperature on erosion rate of coating. It has been observed that coating of 1616-02 + 46712-12 by HVOF coated samples shows good resistance to erosion wear at high temperature than plasma and also signifying that both coating have good resistance to erosion till 250 °C. Erosion rate is much higher for plasma coated samples at 750 °C.

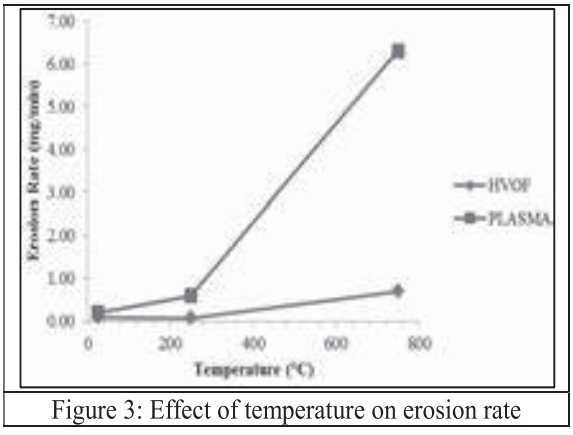

Figure 3: Effect of temperature on erosion rate

Erosion scars on HVOF coated samples are shown in Fig. 4. It is clearly visible, sample which are tested at elevated temperature (750 °C) has deeper scar than else samples.

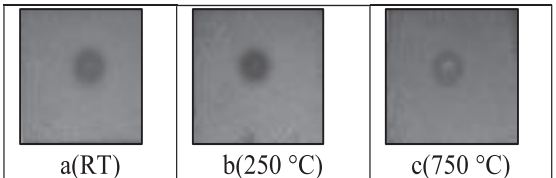
a(RT) b(250 °C) c(750 °C)

Figure 4: Erosion scar mark on HVOF coated sample a, b and c after 10 minute of testing

CONCLUSIONS

In present studies is signifying following conclusions,

1. 1616-02 + 46712-12 mix coated by HVOF shows better erosion resistance properties than plasma coated.
2. Plasma coated surface is uneven than HVOF coated surface which is again a reason for much erosion wear for plasma coated surface.
3. At high temperature (greater than $0.5T_m$) there is always chance for oxidation of substrate/coating. So, exact initial mass calculation is still a challenge.

SCOPE OF FUTURE WORK

At high temperature erosion, many phenomena are involved such as oxidation of substrate/coating and coating softening. So, there are many areas where work could be done,

1. Erosion tests need to be done at differential temperature interval with small gap for more precise study.
2. Exact mass should be calculated at testing temperature.
3. Carbide contain should be varied to examine effect of carbide.

REFERENCES

[1] Standard Test Method for Conducting Erosion Tests by Solid Particle Impingement Using Gas Jets: ASTM International G 76, (2007).

[2] L. Yourong, T. E. Fischer, A. Dent: Surface and Coating Technology, 167(Issue 1), (2003) 68 – 76.

Air Jet Erosion of HVOF Sprayed Inconel 718-Titania Composite Coatings

C.S. Ramesh1*, Sekhar N, Harsha R Gudi
[1]Professor, Department of Mechanical Engineering, PES Institute of Technology, 100ft Ring Road, BSK 3rd Stage, Bangalore-560085, India. E-mail: csr_gce@yahoo.co.in *Corresponding author
[2]PhD Scholar, Visveswariah Technological University, Belgaum, India. E-mail: sekharn1947@gmail.com
[3]Assistant Professor, Department of Mechanical Engineering, BMS College of Engineering, Bangalore-560019, India.
E-mail: harsha.gudi@gmail.com

Abstract
Composite coatings are currently the most sought after owing to their surface hardness coupled with good wear and corrosion resistance. These composites are finding applications in boilers where the failure is mainly by erosion mode of wear. Currently, Nickel based coatings containing 20% Chromium are the most popular ones to combat erosion and corrosion.
Titania is an oxide which is the most popular HVOF spray material possessing high hardness and excellent corrosion resistance. Inconel 718 having major alloying elements such as Ni, Cr, Co & Fe possess high hardness coupled with good corrosion resistance.
In light of the above, this paper focuses on the assessment of air jet erosion behaviour of HVOF thermally sprayed Inconel 718-Titania composite coatings. Titania content has been varied between 5-15 weight percentages. Air jet erosion has been carried out using sand as erodent at different impact angles varying between 60-90 degrees in steps of 15 degrees. The test duration was varied from 5-30minutes in steps of 5minutes.It is observed that under all the identical test conditions Inconel 718 by 85% wt&15%wt of Titania coatings exhibits the best erosion wear resistance, Further, SEM and confocal image studies have been carried out on eroded surfaces to investigate the mechanism of material removal.

1. Introduction
Many of the engineering problems like friction, wear, slurry erosion, corrosion are all surface phenomenon. Extreme importance is given to the modification of the surface properties of industrial structures to overcome the ill effects of aforementioned problems. Thermal spray coating is one of the oldest methods used for obtaining a protective layer on surfaces and reclamation of damaged components in all major sectors of engineering. Of all the thermal spraying techniques, high velocity oxy fuel (HVOF) coating process is recognised as one of the novel methods owing to its ease of operation, high quality of end product, reduced thermal damages of substrates and excellent adhesive strength which directly enhances the durability of coating. Coatings developed from the HVOF process possess excellent corrosion and erosion resistance, low porosity, reduced oxide content and high bond strength [1][2].
Extensive research is going on in the field of HVOF coatings upon various substrates for numerous industrial applications. Inconel 625 alloy was coated on different metallic substrates to study the fatigue and corrosion behaviour of coatings [1].
Ramesh et al. have studied on slurry erosive wear behaviour of Inconel-718 sprayed coatings on mild steel substrates; they have reported that the slurry erosive wear resistance of developed coatings is superior than uncoated mild steel substrate in all the cases studied.
Hadad et al. [3] have concluded that WC-Cr-Co coatings deposited by thermal spray methods on steel substrate exhibited improvement in slurry erosive wear resistance.

2. Experimental Details

2.1 Materials
TiO_2 and Inconel 718 feed stock powders are mixed together to have different proportions by weight (Titania 5-15%). In the present study, mild steel was selected as substrate considering its numerous applications in various industrial sectors. The HVOF coating was carried out at

M/S Metallising Equipment Company. The HVOF coating system selected was MEC Hipojet 2100 Hybrid modified version (water cooled) with KUGA robot (two axes, x-y movements). In the present study, HVOF system with gas fuelled gun is used for coating trials (HVOGF).

2.2 Thermal spraying
The obtained TiO_2 and Inconel 718 powders were preheated to 800ºC and pre agitated to improve its flowability during coating trials. The mild steel substrate was cut into 75 mm × 25 mm × 8 mm size and was thoroughly milled and ground to obtain dimensional equilibrium. Further, the substrate samples were cleaned using acetone and shot grit blasted to attain proper roughness of the surface. The coating trials were carried out using the above said HVOF system with typically 20 to 25 microns of coating deposition at the end of each cycle. Optimum and uniform coatings were obtained at a standoff distance of 187.5 cm with the optimised process parameters.

2.3 Characterisation
The above developed coatings were subjected to air jet erosion using sand as erodent at different impact angles varying between 60 to 90 degrees in steps of 15 degrees, with a test duration of 5 to 30 minutes in steps of 15 minutes.

3. Results and Discussions
It is observed that under all the identical test conditions Inconel 718 by 85% wt&15%wt Titania exhibits better erosive wear resistance. Further from Fig 1 and Fig 2 Inconel 718 by 85% wt&15%wt Titania coatings of 200 microns thickness showed a best resistance to erosion wear when compared with 100 microns thickness.

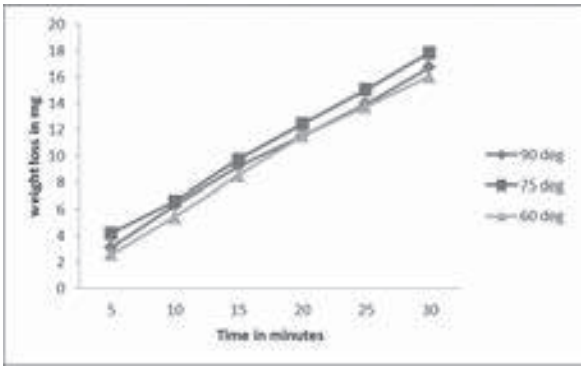

Fig 1: *Air Jet Erosion at different angles on Inconel 718 (85%) Titania (15%), Thickness 200 Microns*

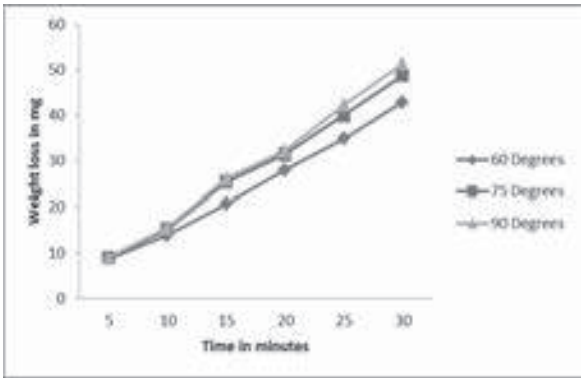

Fig 2: *Air Jet Erosion at different angles on Inconel 718 (85%) Titania (15%), Thickness 100 Microns.*

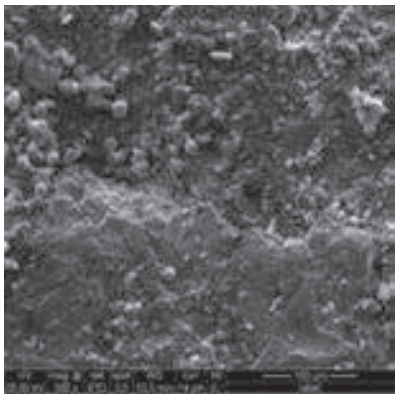

Fig 3: *SEM image of the worn surface at 300X*

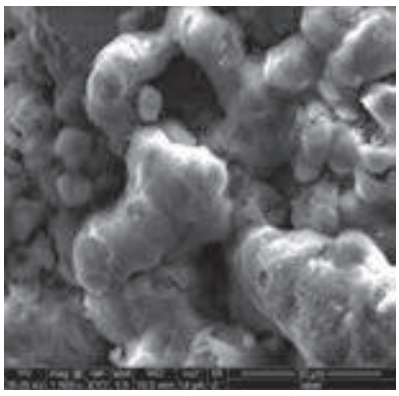

Fig 4: *SEM image of worn surface at 1500X*

4. Conclusion

A large number of minor cracks and craters have been observed which are mainly caused by the impingement of erodent particles. Further, the coating remains intact after the test, with very few erosion cracks observed. Very few flakes and craters have been observed, which are mainly caused by the impinging sand particles, justifying the abrasive wear mechanism. (Refer Fig. 3 and Fig. 4)

5. References

[1] Al-Fadhli, H.Y., Stokes, J., Hashmi, M.S.J. and Yilbas, B.S. (2006) 'HVOF coating of welded surfaces: fatigue and corrosion behaviour of stainless steel coated with Inconel-625 alloy', *Surface Coating & Technology*, Vol. 200, Nos. 16–17, pp.4904–4908.

[2] Boudi, A.A., Hashmi, M.S.J. and Yilbas, B.S. (2004) 'HVOF coating of Inconel 625 onto stainlessand carbon steel surfaces: corrosion and bond testing', *Journal of Material Processing,Technology*, Vols. 155–156, No. 30, pp.2051–2055.

[3] M. Hadada, R. Hitzekb, P. Buerglerb, L. Rohra, S. Siegmanna"Wear performance of sandwich structured WC–Co–Cr thermally sprayed coatings using different intermediate layers", *Wear*, Volume 263, Issues 1–6, 10 September 2007, Pages 691–699.

[4] Ramesh, C.S., Devaraj, D.S., Keshavamurthy, R. and Sridhar, B.R. (2011) 'Slurry erosive wear behaviour of thermally sprayed Inconel-718 coatings by APS process', *Wear*, Vol. 271, Nos. 9–10, pp.1365–1371.

Effect of basalt addition on Microstructural, Mechanical and Erosion properties of NiCrSiB HVOF coatings

A.Vallimanalan[1], S.P.Kumaresh Babu[1], S.Natarajan[1], M.Kumarasamy[2], P.Veerabalu[2]
[1] Department of and Materials Engineering, National Institute of Technology, Tiruchirapalli, India
[2] CARD, Neyveli Lignite Corporation, Neyveli, India

Abstract
Basalt and products made out of them are known to provide substantial wear resistance and resistance to chemical attack, especially in acidic environment. Its mechanical strength, low density, high hardness and superior corrosion resistance makes it a reliable addition to High Velocity Oxygen Fuel sprayed coatings. The aim of the present work is to study the effect of basalt addition on the microstructure, mechanical and slurry erosion properties of HVOF sprayed NiCrSiB Coating on IS3589 Fe410 grade carbon steel substrate. Effect of addition of different volume percentages of basalt to HVOF sprayed NiCrSiB coatings are studied using XRD, Optical and Scanning Electron Microscopy. The chemical composition of the coated substrate is confirmed with Optical Emission Spectroscopy. The slurry erosion resistance exhibited by each coating is compared using Waterjet Erosion tester with 10 m/s, 15 m/s and 20 m/s velocity at 30, 60 and 90 degrees. Corrosion resistance to pH is tested at different pH levels.

1 Introduction

IS3589 Fe410 grade carbon steel is used in liginite mines as dewatering pipelines. These pipelines are prone to erosion and corrosion mainly owing to the acidic nature of water being transported.

Surface protective coatings by thermal spray technique is a common method used to increase wear and corrosion resistance of these pipelines. Basalt, a volcanic rock, is a glass-ceramic with high hardness and low density. It is a naturally occuring raw material having superior wear, abrasion, chemical and thermal resistance[1]. Coating basalt onto a steel substrate results in a basalt-steel composite material as the melting temperature of basalt is similar to steel [2]. Basalt added NiCrSiB was sprayed on steel substrate to increase the erosion and corrosion resistance, effectively reducing the cost of coatings.

The present study analyses the impact of mixing basalt with HVOF sprayed NiCrSiB. It compares the microstructural and mechanical properties of different coatings, along with their erosion and corrosion resistance.

2 Material and Experimental Procedure

2.1 Materials

HIPOJET 2700 HVOF spray equipment of Metallizing Equipment Co. Pvt. Ltd, Jodhpur, was used for deposition of coatings on 8mm thick substrate. Coating thickness of around 200-230 µm was achieved. **Table.1.** gives the, **coating parameters**, used.

Table.1. *Coating Parameters*

Oxygen Flow	270 SLPM
LPG Flow	50-55 SLPM
Air Flow	550 SLPM
Nitrogen Flow	20 SLPM
Spray distance	7 inch
Powder feed rate	40g/min
Particle velocity	300-350 m/s

Basalt rocks were crushed using Jaw Crusher and sieved to 45 and 38 µm. **Table. 2.** gives the, **chemical composition of the substrate**, used.

Table. 2. *Chemical composition of substrate*

Element	C	Mn	S	P	C Eq.
wt% (max)	0.2	1.3	0.04	0.04	0.45

ICP-OES was used to determine the chemical composition of powders and substrate. **Table. 3.** gives the, **chemical compostion of the powder**, used.

Table. 3. *Chemical composition of Basalt powder*

Compound	wt%
SiO_2/Al_2O_3	51.62/13.64
Fe_2O_3/MgO	13.16/5.77
CaO/Na_2O	9.15/2.98
TiO_2/K_2O	0.978/0.87
MnO/ P_2O_5	0.20/0.13
LOI	1.502

NiCrSiB alloy powder, supplied by Metallizing Equipment Co Pvt Ltd, Jodhpur, was mixed with 15, 20 and 25 volume % of basalt using High Energy Planetary Ball-mill.

The basalt content in the powder mixture and its presence on the coated substrate was confirmed using SEM. **Fig. 1.** shows, **SEM image of the powder and coated substrate**.

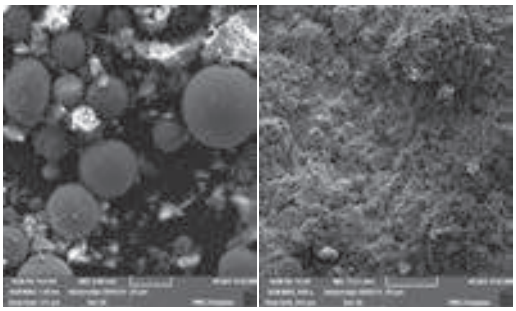

Fig. 1. *SEM of Powder(L) and Coated Substrate (R)*

2.2 WaterJet Erosion Test

Waterjet erostion tester (ASTM G105) was used to conduct erosion resistance test of the coated samples. The experiment was conducted both on NiCrSiB coated subtrates and basalt added NiCrSiB coated substrates. The

coated surface of the substrate was exposed to the jet at velocities 10 m/s, 25 m/s and 20 m/s at angles 30, 60 and 90 degrees. The acidity of the erodent medium used was varied at 3, 5 and 7 pH levels. The slurry concentration was maintained at 2 wt% at all velocities. **Fig. 2.** shows, **the effect of the individual parameters on the mass loss of NiCrSiB coated subtrated**.

.

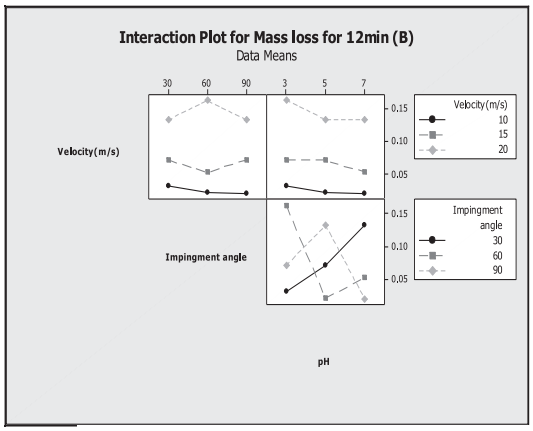

Fig. 2. *Erosion effect on NiCrBSiFe coated substrate*

Weight loss of the samples at regular time intervals were noted. The experiment was designed to run in L9 orthogonal array and analysed using minitab. **Fig. 3.** shows, **the effect of the individual parameters on the mass loss of 25 vol% basalt added coating.**

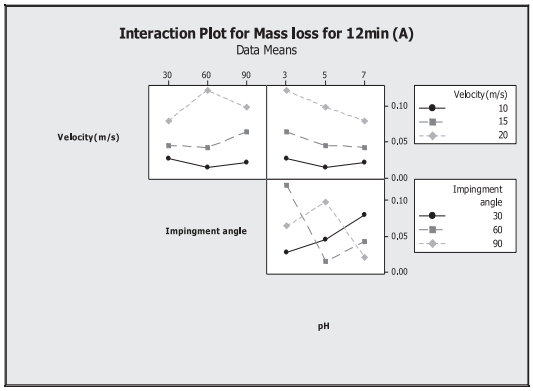

Fig. 3. *Erosion effect on Basalt added NiCrSiB Coated Substrate*

2.3 Corrosion Test

Corrosion test was conducted using an electrochemical workstation of ACM Gill model 1762. Potentiodynamic polarization (PDP) was used to evaluvate corrosion behaviour under different pH (mine water) of 3.33,5.08 and 8.42. The Ecorr and Icorr values were noted and were used to find the corrosion rate of 25 Vol% basalt added NiCrSiB.

3 Results and Discussion

Basalt added NiCrSiB, in all volume percentages showed increased coating hardness, surface roughness and better bond strength. The addition also showed slight increase in porosity of the coating which may be due to the milling technique used for powder preparation [3].

Velocity and pH of the liquid medium played the major role in eroding the samples at all angles. The weight loss of basalt added NiCrSiB was found to be higher in the initial stages of erosion which later almost matched the NiCrSiB coating. Increased weight loss can be attributed to the porosity of the coating. The optimum levels of the factors for maximum weight loss of basalt added NiCrSiB was found to be at 20 m/s velocity and 3pH. The maximum weight loss occurs at 90° because of the brittle nature of the coating. The most encouraging result was obtained with 25 vol% basalt addition.

Fig. 4. Shows, **corrosion behaviour of 25 vol% basalt added NiCrSiB coating**, on the substrate.

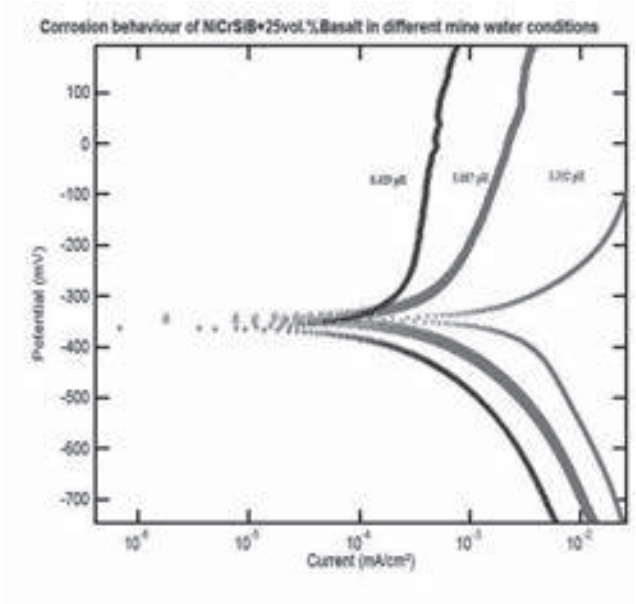

Fig. 4. Tafel curve 25 vol% basalt NiCrSiB coating

The corrosion rate of 25 vol% basalt added NiCrSiB coating was found to be 0.01347 mm/year, 0.00018 mm/year and 0.00077 mm/year at 3.33 pH, 5.08 pH and 8.42 pH respectively. **Table. 4.** shows the, **Ecorr and Icorr values,** obtained.

Table. 4. *Ecorr and Icorr values of coating*

pH	3.332	5.087	8.429
Ecorr	(-)347.12 mV	(-)347.12mV	(-) 363.94mV
Icorr	0.0010529	0.0001438	5.988×10^{-5}
β_A	91.256	94.964	99.997
B_C	90.66	68.169	67.813

It is seen that erosion and corrosion resistance of 25 vol% basalt added NiCrSiB coating is substantially better than the resistance offered by bare substrate in mining condition.

4 References

[1] S.Shrestha, T.Hodgkiess and A.Neville: Wear. 259 (2005) 208- 218.

[2] Makism Antonov, Andrei Surzenkov, Irina Hussainova, Dmitri Golkandin and Valdek mikli: Estonian Journal of Engineering. 18 (2012) 211-220

[3] I.A. Kalashnikova and A.V. Kalashnikov: Welding International. 24 (2010) 301-303

[4] Senol Yilmaz, Gunhan Bayrak, Saduman Sen and Ugur Sen: Materials and Design. 27 (2006) 1092-1096

Solid Particle Erosion behavior of Plasma Sprayed LaYSZ Nanocomposite Coatings

S. Mantry[1], B.B.Jha[1], R.K Sahoo[1]*
[1]CSIR-Institute of Minerals & Materials Technology, Bhubaneswar 751013, Odisha, India
[*]*Corresponding Author: bbjha59@yahoo.com*

Abstract—
Thermal barrier coatings (TBC) are more susceptible to erosion because their microstructure contains many crack-like features. This article presents the solid particle erosion response of plasma sprayed La_2O_3 doped nanostructured YSZ coatings on Inconel 718 substrates. The influence of five operating parameters i.e. impact velocity , erodent size, erodent temperature, impingement angle and stand-off distance with four different level each, on performance output (i.e. erosion rate) are studied using Taguchi's L_{16} orthogonal array design. Out of the five parameters, impact velocity has been found to be most significant factor followed by erodent temperature and impingement angle influencing erosion. The morphology of the worn out surface also showed micro-cracks and small crater formation in the surface caused by the repetitive impacts of erodents. The reason of higher wear resistance in case of LaYSZ composite coatings may be attributed to embedded toughened nano-zones and compact structure of the coating.

Keywords- *plasma spraying, nano-zones, Erosion wear, Taguchi's experimental design*

INTRODUCTION

Thermal spray coatings obtained from nano structured powders exhibits such outstanding properties. Erosion of plasma sprayed ceramic coatings due to solid particles has been a serious concern in recent engineering applications that needs high temperature resistances. Thermal barrier coatings (TBC) are more susceptible to erosion because their microstructure containing many crack-like features. Thus, erosion rates are expected to be higher for TBC than for their bulk ceramic counterparts. Plasma sprayed coatings have found applications in engineering as well as structural components, where erosion occurs frequently. Due to severe dusty working environments, the study of solid particle erosive analysis of these coatings on these components becomes highly relevant [1,2].

There are quite a few reports available regarding erosion behavior of plasma sprayed YSZ coatings [3]. But solid particle erosion response of nanostructured YSZ based coatings has not been reported in recent times. To reduce wear, all process parameters need to be understood, so as to carry out suitable steps in designing of substrates and coating materials [4]. As the number of such process parameters is too large, statistical techniques such as Taguchi experimental design could be employed for identification of significant process parameters for optimization [5]. In this work, this method has been adopted to investigate the influencing parameters like impingement angle, impact velocity, erodent size, erodent temperature and stand-off distance on the erosion wear rate.

Synthesis of nanostructured powders by sol-gel route

The nanostructured YSZ powders employed in this study were synthesized through sol-gel technique [6]. Commercial nano La_2O_3 of particle size ~ 10-30 nm obtained from M/s Sky spring Nanomaterials, Inc.USA. Both the powders were mixed and heated at 1400 ^oC. The calcined powders were taken as the raw ingredients for the plasma spray process.

Coating material

Nano-sized powder of 5LaYSZ [YSZ (5.4 wt. % Y_2O_3–ZrO_2) + 5 wt. % La_2O_3] was plasma sprayed on to Inconel 718 substrates. The finely dispersed nano particles were made agglomerated to a size of ~ 30–100 µm as required for plasma spraying. The nano particles were agglomerated by the spray drying technique. The process is described elsewhere [7]. The final product is a feedstock of size ~50 µm spherical agglomerates containing nano grains of size 20-30 nm as shown in Fig.1.

Fig.1. *FESEM micrograph of spray dried LaYSZ particles*

Development of coatings

The coating process was carried out at CSIR-IMMT, Bhubaneswar using an 80 kW plasma spray system supplied by M/s Metallization, U.K. The process parameters are listed in Table 1. The number of passes was kept constant for each sample in order to make thickness of all coatings (~150 µm) within similar range.

Table 1. *Operating Parameters for Plasma spraying process*

Parameter	Operating Range
Operating Power	38 kW
Current	865 amps
Primary gas (Argon) flow rate	40 lpm
Secondary gas (Hydrogen) Flow rate	0.5 lpm
Carrier Gas flow rate	5 lpm
Nozzle to substrate distance	80 mm
Powder feed rate	25 g/ min

Erosive wear analysis using DOE

The solid particle erosion tests were carried out using a standard air-jet erosion test rig (M/s Ducom, TR-600) as per ASTM G76. The compressed and dried air is mixed with the erodent particles in the mixing chamber and then accelerated via a convergent nozzle at different impingement angles ranging from 15-90°. The control factors with their selected levels are shown in Table 2.

Table 2 . *Control factors with their selected levels*

Control Factor	Levels				Units
	I	II	III	IV	
A: Impact Velocity	33	47	57	68	m/s
B: Stand-off distance	10	20	30	40	mm
C: Erodent Size	100	200	300	400	µm
D: Impingement Angle	30	45	60	90	deg.
E: Erodent Temperature	25	200	400	600	^{0}C

The test results of the erosion wear of the nanostructured YSZ coated substrate according to L_{16} orthogonal design along with their corresponding signal-to-noise (S/N) ratio is shown in Table 3. S/N ratios were calculated for minimum erosion rate under "smaller is better" characteristics as a logarithmic transformation of loss function, given by

$$S/N = -10 \log 1/n (\sum y^2) \quad [1]$$

Where 'n' represents the number of observations and 'y' represents the observed data.

Table 3. *L_{16} Orthogonal array design with output and S/N ratio*

Sl No	Impact Velocity	Stand-off Distance	Erodent Size	Impingement angle	Erodent Temp.	Erosion rate	S/N Ratio
1	33	10	100	30	25	14.6567	-25.8307
2	33	20	200	45	200	14.3937	-23.1996
3	33	30	300	60	400	20.1759	-26.0539
4	33	40	400	90	600	24.0345	-27.6167
5	47	10	200	60	600	26.1667	-28.3550
6	47	20	100	90	400	19.0769	-25.6102
7	47	30	400	30	200	29.2986	-29.3369
8	47	40	300	45	25	20.5643	-26.2623
9	57	10	300	90	200	18.5769	-25.3795
10	57	20	400	60	25	17.3564	-24.7892
11	57	30	100	45	600	18.0917	-25.1496
12	57	40	200	30	400	25.1987	-28.0276
13	68	10	400	45	400	33.8709	-30.5965
14	68	20	300	30	600	42.3926	-32.5458
15	68	30	200	90	25	19.5674	-23.2672
16	68	40	100	60	200	32.0714	-30.1224

Table 4. *Response Table for Signal to Noise Ratios under Smaller is better characteristics*

Level	A	B	C	D	E
1	-25.03	-26.90	-26.04	-28.29	-25.04
2	-27.39	-26.54	-26.35	-26.30	-27.01
3	-25.84	-26.59	-27.56	-27.33	-27.57
4	-29.77	-28.01	-28.08	-26.11	-28.42
Delta	4.74	1.47	2.05	2.19	3.38
Rank	**1**	**5**	**4**	**3**	**2**

In this study impact velocity having higher delta value (as shown in Table 4) was found to be the most significant factor followed by the erodent temperature on the erosion wear rate of the as-sprayed nanostructured YSZ coatings. Fig. 2 shows the main effect plot for S/N ratios of individual control factors. From the graphical analysis of this figure it was concluded that a minimum wear could be obtained with the combination of A1, B2, C1, D4 and E1.

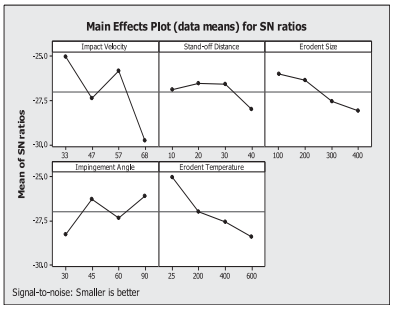

Fig. 2 . *Main effect plot for S/N ratio of individual control factors.*

Surface morphology:

The eroded coating micrograph showing worn surface indicates cracks, crater formation etc. as shown in Fig.3 (a-b). At low impact velocity of erodent, the particle impinge on the surface having less kinetic energy , hence less lateral cracks as shown in Fig. 3(a). But at higher impact velocity and at impingement angle 90°, high impact energy of particles leads to more plastic deformation and this in turn should result in more material being displaced from the coating surface during impact , shown in Fig. 3 (b). However the craters are relatively smaller in size in case of nanostructured YSZ coatings. This may be attributed to high toughness and presence of adherent nano-zones of the coating.

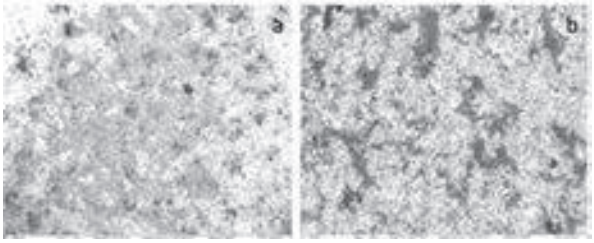

Fig. 3 . *SEM micrographs of eroded nano LaYSZ coatings*
(a) at impact velocity of 33 m/sec and impingement angle of 30°
(b) at impact velocity of 68 m/sec and impingement angle of 90°

Conclusion:

From the Taguchi design method, impact velocity is found to be the most significant factor followed by erodent temperature, impingement angle and erodent size, influencing the erosion wear rate of LaYSZ nanocomposite coatings. The enhanced erosion wear resistance of as-sprayed coatings may be attributed to compact structure, high toughness due to presence of nanozones in the molten matrix.

Reference:

1. Finnie, Wear, 1 (1995), 186–187
2. S. Usmani, S. Sampath, JOM, 48 (11) (1996) 51-54
3. B.Z. Janos, E. Lugscheider, P. Remer, Surface and Coating Technology 113 (1999) 278–285
4. Thomas H, Kosel. ASM Inter Hand book Comm., 18 (1992); 371–372
5. S. Mantry, R. Sahoo, B. B. Jha et al, J Engineering Tribology, 228(8),(2014), 872-880
6. R.E. JuaÂ rez, D.G. Lamas, G.E. Lascalea et al., J Eur ceramic Soc, 20 (2000), 133-138
7. S, Mantry, A. Mandal, D.K Mishra et al., J Therm spray Technol., 23(7), (2014), 1073-1080

Microstructure and properties of HVOF sprayed nanostructured and conventional WC-12Co coatings

Wojciech Żórawski[1], Merard Makrenek[2]
[1] Faculty of Mechatronics and Machine Building, Kielce University of Technology, Poland
[2] Faculty of Management and Computer Modelling, Kielce University of Technology, Poland

Abstract
Nanostructured and composite WC-12Co coatings were prepared by means of the supersonic spray process (HVOF). The microstructure and composition of WC-12Co nanostructured powder were analyzed by scanning electron microscope (SEM) and transmission electron microscope (TEM). Investigations revealed nano grains of WC with the size on the range of 50-500 nm. The nanostructured sprayed coating was analysed by SEM and phase composition was investigated by X-ray diffractometer (XRD). A denser coating structure with higher hardness was observed compared to conventional coating with a small amount of W_2C, WC_{1-x}, W and some amorphous phase. Young's modulus and hardness were determined by depth sensing indentation in HVOF sprayed WC-12Co nanostructured coatings. Results were compared to conventional coatings and the relevance of the nanostructure was analyzed. An indentation size effect was observed on the polished surface of both coatings. Data provided by indentation tests at maximum load allow to estimate hardness and elastic modulus. Enhanced nanomechanical properties of nanostructured coating in comparison to conventional one were observed.

1 Introduction

Nanostructured materials provide new possibilities, which enable creating composite structures with much better properties than composites obtained from conventional materials. Tungsten carbide is the material used for numerous applications. Taking its high level of hardness into consideration, it is most often used material in the form of sinter with cobalt, which guarantees its high durability. Its outstanding wear resistance contributed to the use of WC-Co to increase durability of various machine parts [1,2]. The structure of the sprayed coatings is composed of hard WC grains deposited in a cobalt matrix. Today HVOF spraying is currently used for WC-Co application because athmosferic plasma spraying (APS) with higher temperature of the process leads to its decomposition, decarburization and oxidation what significantly decreases properties of coatings. Higher velocity and lower temperature of HVOF process allow to form very dense coatings with larger fraction of retained WC and excellent adhesion to the substrate. Moreover such coatings are environment friendly and can replace galvanic chrome plating coatings [3,4].
In the present paper, WC–12Co nanostructured and conventional coatings were prepared by means of liquid-fuel HVOF spraying technology to investigate the microstructure of and the nanomechanical properties of the deposited coatings.

2 Experiment

Nanostructured WC-12Co, with a granularity of -45 +5μm (Infralloy S7412) and conventional WC-12Co (Amperit 519.074, with a granularity of -45 +5.5μm were HVOF sprayed. The size and shape of powder grains are shown in Figure 1a and 1b respectively. The nanostructured powder and coating was denoted as WC-12Co (N), the conventional materials were denoted as WC-12Co (A). The coatings were deposited by means of TAFA JP-5000 system with kerosene as a fuel with spraying parameters: an oxygen flow rate – 890 l/min, a kerosene flow rate – 22.7 l/min, a barrel length – 150 mm, a spray distance – 380 mm.

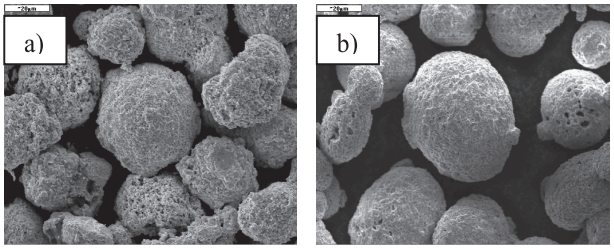

Fig. 1. *Powder grains: a) WC-12Co (N), b) WC12Co (A)*

The structure and chemical composition of the powders and the coatings were analyzed using the following scanning microscopes: JSM–5400 with an ISIS 300 Oxford (EDS) microprobe and FEI Nova™ NanoSEM 200. Their phase composition was studied using a Bruker D8 Advance diffractometer with Co-Kα radiation of wavelength λ = 1.78897 Å.
An Nanovea nanoindenter was applied to analyse the nanohardness and Young's modulus of the resultant polished coating with a calibrated Berkovich indenter. The reference material for nanointender calibration was sample of silica. The indentations were performed at constant depth 0.1 μm.
The samples for indentation were prepared in plan view from the as sprayed coatings. The topography of the coatings after polishing was analyzed by means of a Talysurf CCI-Lite non-contact 3D profiler [5].

3 Results and discussion

The microstructures of both HVOF sprayed coatings are presented in Fig. 2. Metallographic images of the two WC12Co coatings showed that there were some small undeformed tungsten carbide grains embedded in the cobalt matrix. From the EDS microanalysis, it was clear that the coating content was different in each zone. The light-coloured grains in the WC12Co coatings confirm a high amount of tungsten, whilst the dark-coloured matrix is an area with a high content of cobalt and a low content of

tungsten. Different sizes of tungsten carbide grains were visible in both coatings.

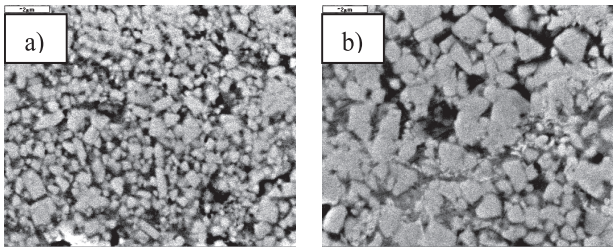

Fig. 2. *Cross-section of HVOF sprayed coatings: a) WC-12Co (N), b) WC12Co (A)*

The coating deposited using the nanostructured powder had a finer-grained structure with unmodified nanocrystals. It exhibited lower porosity, despite the fact that the nanostructured powder contained larger grains. The coating produced from the conventional powder, on the other hand, had higher porosity, resulting from the higher porosity of the grains, which can be seen in the metallographic images. Microstructure in bright field (BF) and related electron diffractions from an area with grains of different Co content are shown in Fig. 3. In the area with enhanced Co content, an amorphous structure occurs, and crystallite grains possess a hexagonal WC structure. The dimensions of WC grains are in the range of 200-500 nm.

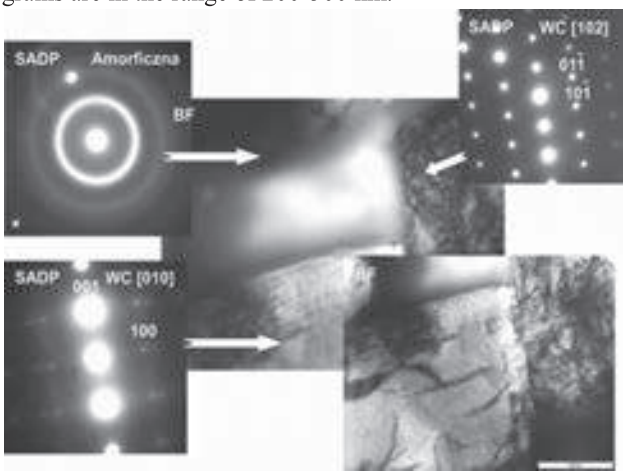

Fig. 3. *Microstructure of HVOF sprayed WC-12Co (N) coating*

Analysis of the powder diffraction patterns showed that the WC grains in the nanostructured powder were half the size of those in the conventional powder. The diffraction patterns revealed the presence of WC and Co both in the WC-Co powder and in the deposited coating. The new phases that appeared in both coatings, i.e. W_2C, WC_{1-x} and W, were attributable to the prior disintegration of WC in the spray stream. The diffraction lines of the phases after spraying were considerably wider. This testified to a significant degree of elastic and plastic deformation, i.e. a high level of energy stored in the form of network defects; this particularly in the case of the Co phase [6].

The hardness and Young's modulus of the investigated microstructures were analysed using a square grid of 150 nanoindentation tests on the sample in plan view from the as-sprayed coatings. The arithmetic mean of the surface height Sa of the polished coating was slightly higher for the WC–12Co (N) coating than for the conventional coating; it was 8.030 nm and 7.723 nm, respectively. The distance between each nanoidentation was changed by nanointender as 1 μm. The distributions of the nanomechanical properties were as then plotted as histogram distributions and maps of surface in which each hardness and Young's modulus result was showed on the charts with the same dimensions and locations as in the investigated areas. Histograms and probability distributions of the hardness and Young's modulus of the WC-12Co (N) coating is shown in Fig. 4 and Fig. 5 respectively.

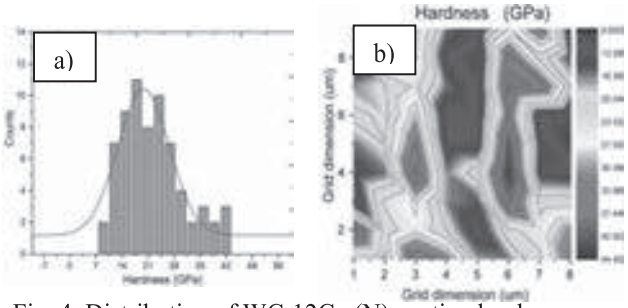

Fig. 4. Distribution of WC-12Co (N) coating hardness : a) histograms and probability, b) map

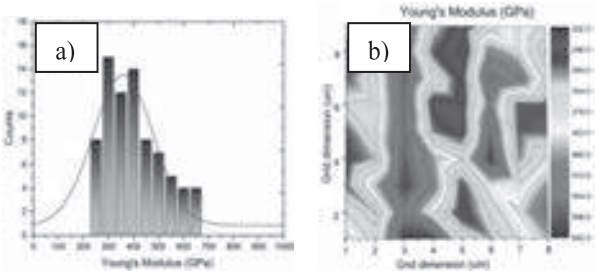

Fig. 4. Distribution of WC-12Co (N) coating Young's modulus: a) histograms and probability, b) map

Nanohardness of the WC-12Co (A) sample point to the dominant value of ~ 6 GPa, and this value corresponds to the probability density distribution, which is indicated on the graph a red line. The distribution of Young's modulus is most common value of ~ 150 GPa, but the match probability density curve shows a slight shift towards higher values. For the sample WC-12Co (N) the dominant value of the hardness is 20 GPa, and the most likely value of Young's modulus is 350 GPa.

The present work is supported by project no: WND-POKL.08.02.02-26-001/12.

4 References

[1] L. Pawlowski: *The science and engineering of thermal spray coatings,* J.Willey & Sons Ltd, Chichester, II ed. 2008.

[2] Chang-Jiu Li, Guan-Jun Yang: Int. J. Refr. Met. Hard Mat. **39** (2013) 2-17.

[3] P. Fauchais, G. Montavon, G. Bertrand: J. Therm. Spray Technol. **19** (1-2) (2010) 56-80.

[4] Qun Wang, Jing Xiang, Genyu Chen, Yingliang Cheng, Xinqi Zhao, Shiqi Zhang: J. Mat. Proc. Tech. **213** (2013) 1653-1660.

[5] S. Adamczak, D. Janecki, K. Stępień, Measurement, **44** (1) (2011) 164.

[6] W. Żórawski: Surf. Coat. Technol. **220** (2013) 282-289

Microstructural characterization of thermal sprayed high entropy alloy coatings

Ameey Anupam, S. Praveen, R.S. Kottada, B.S. Murty,Andrew Siao Ming Ang, Chris Berndt

IIT Madras, Chennai, India,Swinburne University of Technology, Melbourne, Australia

High entropy alloy powders of XCoCrFeNi (X = Al, Mn), synthesized by mechanical alloying route were coated on mild steel substrate by plasma spray coating technique. Mechanically alloyed powders and plasma sprayed coatings were characterized by XRD, SEM and Vickers hardness. Major FCC phase and minor BCC phase were observed in powders of MnCoCrFeNi whereas major BCC phase and minor FCC phase were observed in AlCoCrFeNi. After coating, FCC phase was observed as a major phase in both the alloys with minor fraction of oxides. Formation of Al-rich oxide in AlCoCrFeNi coating suggests that depletion of Al from major BCC phase of powder may be responsible for the manifestation of FCC phase as major phase in the coating. Hardness of 430 + 10% HV0.5 and 450 + 10% HV0.5 were observed for AlCoCrFeNi and MnCoCrFeNi coatings, respectively.

Assessment of Microstructure and Mechanical properties of HVOF sprayed WC–Co-Cr coatings

K.Murugan[1], A.Ragupathy[1],V.Balasubramanian[2],K.Sridhar[3].
[1] Department of Mechanical Engineering, Annamalai University, Annamalainagar 608002, India
[2] Centre for Materials Joining and Research (CEMAJOR), Department of Manufacturing Engineering, Annamalai University, Annamalainagar 608002, India
[3] Naval Materials Research Laboratory (NMRL), Ambernath India

Abstract
Among versatile thermal spray techniques, the high velocity oxy-fuel (HVOF) spray which involves burning a certain kind of gaseous or liquid fuel with a large quantity of oxygen has become one of the most advanced processes for producing high performance cermet or alloy coatings. HVOF spray techniques can produce cermet coatings for applications that require corrosion and erosion resistant surfaces. Commercially available WC-10Co-4Cr powder was thermally sprayed by HVOF process. The investigation was carried out to determine the influence of operating parameters on the evolution of microstructure and mechanical properties of the coatings in order to have a better understanding of the interaction between the particle and the flame jet. Properties of the sprayed coatings were examined in terms of microstructure, porosity level and tensile bond strength. The results show that the microstructure and tensile bond strength depends strongly on the oxygen flow rate. The variation of the methane flow rate has a less obvious influence on the bond strength of coating than that of the oxygen. The changes of porosity and bond strength of deposited coatings are discussed corresponding to the variation of fuel and oxygen flow rates.

Keywords: *HVOF spraying, WC-Co-Cr coatings, Porosity, Tensile bond strength*

1. Introduction

The high-velocity oxyfuel (HVOF) process is widely used in product design to enhance functional performance and in repair applications to extend product life and reduce maintenance costs. WC- based cermet coatings are widely used against wear and corrosion in gas and oil industries. The flame-particle interaction during the particle in-flight and the formation of the coatings particle by particle involve complex physical-chemical interactions. In order to fundamentally understand the relationships between process parameters and the coating adhesion strength, establishment of relationships between controllable process parameters, in-flight properties of the injected powder. and microstructure properties is important. The bond strength is one of most important properties to a thermally sprayed coating [1]. It is generally believed that high velocity and temperature improved spray particle melting, which benefit the adhesion of a coating to a substrate. High velocity oxy-fuel (HVOF) is characterized by high flame velocity up to 2000 m/s. Such high velocity flame consequently results in the formation of spray particle stream with high velocity compared to conventional flame spraying and plasma spraying. Accordingly, HVOF spray process is a promising thermal spray process to deposit coatings with low porosity, and consequently high density and high bond strength. In this work, Design of Experiments (DoE) was used to establish relationships between process parameters, microstructure properties, and coating adhesion strength. DoE is a standard statistical approach conventionally used to study relationships between process parameters and coating microstructure in thermal spray [2].

2. Experimenal

WC-Co-Cr feedstock powder was deposited on naval brass substrates using a MEC HVOF HipoJet-2700 gun. Substrates with standard cylindrical geometry (25.4 mm in diameter and 25 mm thick for metallographic obbservations and tensile bond tests) were degreased and grit blasted to coating deposition. The coating thickness was kept constant to a thickness of 300 µm. Experiments were conducted by varying oxygen flow rate and fuel flow rate at five levels.The spray parameters used in this study are shown in Table 1. Spray parameter combinations and experimental results are presented in Table 2.

Table: 1 *HVOF spray parameters and their levels*

No	Factors	Units	Levels				
			-1.4	-1	0	1	1.4
1	Oxygen flow rate (O)	lpm	242	246	250	254	258
2	LPG flow rate (L)	lpm	52	56	60	64	68

Table: 2 Design matrix and experimental results

Sl.No	Oxygen flow rate (O), lpm	Fuel flow rate (F), lpm	Porosity, (vol. %)	Tensile bond strength (MPa)
1	246	56	3.54	56
2	254	56	2.18	64.5
3	246	64	2.98	60.1
4	254	64	2.2	63
5	242	60	3.42	57.7
6	258	60	2.1	65.1
7	250	52	3.43	57
8	250	68	2.21	63
9	250	60	1.63	67
10	250	60	2.1	65
11	250	60	1.55	68
12	250	60	1.61	67.7
13	250	60	1.63	67.1

According to the ASTM B 276 standard, the porosity measurement was carried out on the metallographically prepared cross sections of the coating, using optical microscope (Make: MEIJI; Japan, Model: MIL-7100) equipped with an image analyzing software (MetalVison version.6). The procedures prescribed in ASTM- C633 standard was used to evaluate for adhesion bond strength of as sprayed coatings..

3. Results and Discussion.

3.1 Bonding mechanisms of HVOF sprayed WC-Co-Cr coatings for low porosity coating

The adhesion between the coating and the substrate primarily depends on the mechanical interlocking which is mainly related to the substrate surface roughness and the solidification of impacting droplets [3]. Figure 1 (a-d) shows formation of bonding, i.e., coating powder impacts on a substrate surface subsequently spreads over the rough surface. Figure. 1 confirms that there is a good mechanical interlocking between the coatings and the substrate.

3.2 Effect of oxygen flow rate on coating porosity and adhesion strength

When oxygen flow rate (O) increases, the porosity decreases and hardness increases. This situation may be due to the fact that oxygen flow rate (O) which is the main factor affects the thermal energy of the coating powder particle. As the oxygen gas flow rate increased, to provide the in-flight particle with more heat, gas enthalpy increases and enhances the gas thermal conductivity. Higher oxygen flow rate led to higher particle velocity and particle temperature and also to the lower coating porosity, increases coating bond strength [4]. Fig. 1 shows the optical micrograph of the HVOF sprayed WC-Co-Cr coatings deposited at various levels.

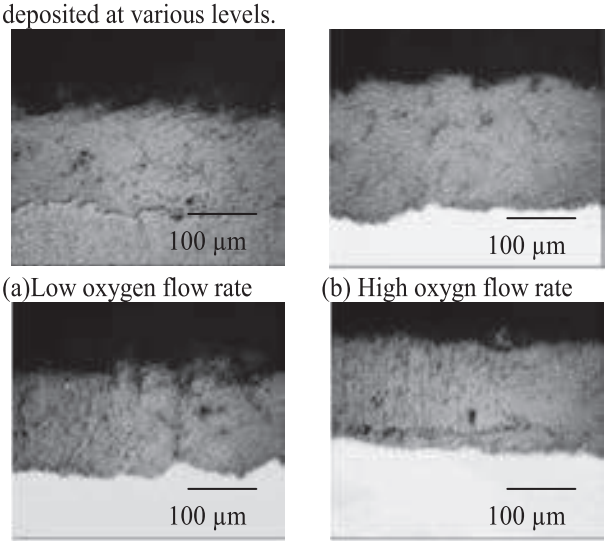

(a)Low oxygen flow rate (b) High oxygn flow rate

(c) Low fuel flow rate (d) Higher fuel flow rate

Fig. 1 *Microstrucutres of WC-Co-Cr coatings*

3.3 Effect of Fuel flow rate on coating porosity and adhesion strength

At lower LPG flow rate, the flame temperature decreases and less amount of heat generation is utilized for melting the powders. Owing to this condition, in-flight particle oxidation needs to be considered. Oxide phase fraction was increased with the increase of stoichiometric ratio [4].

From the figure, it can be seen that at lower and higher LPG flow rates, the percentage of porosity is greater compared to the intermediate level of LPG flow rate; Similarily increasing the LPG flow rate, will increase the flame temperature thus help the particle to recrystallize by the flame.

Fig. 2 *Photograph of Tensile bond tested sprecimens*

At higher fuel flow rate, the powder melting is lower owing to less amount of heat utilized since the increase in LPG flow rate increase the total gas flow rate subsequently increases the particle velocity, reducing the residence time of the particle into the flame, and consequently decreasing the particle. This may be the reason for the increase in the percentage of porosity at higher LPG flow rate and reduced tensile bond strength of the coating. Figure 4 shows the tensile bond tested specmens shows adhesive/cohesive pattern of failure irrespective of the coating bond strength.

3.3 Relationship between coating microstructure and adhesion strength.

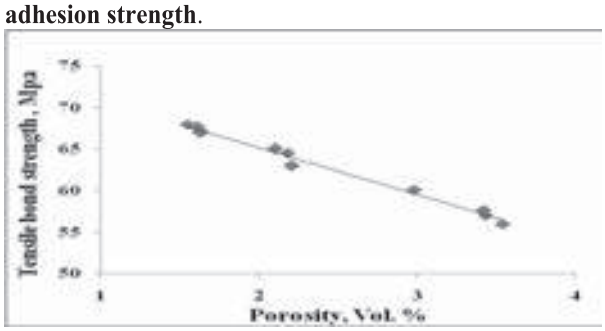

Fig. 3 *Relationship between porosity and tensile bondstrength*

From the correlation graph (Fig. 3), it is inferred that higher the porosity and lower the tensile bond strength vice versa.

4. Conclusions

1) From the experimental results,coating porosity decreases with increasing oxygen content leads to effective melting of the powder particles.

2) Increase in fuel flow rate increases porosity and decreases coating bond strength, due to increased momentum of the particles.

Acknowledgements

The authors wish to express their sincere thanks to the Naval Research Board (NRB), DRDO, New Delhi for the financial support to carry out this investigation through the sponsored project No. DNRD/05/4003 NRB/212 dated 25.07.2011 and the Department of Manufacturing Engg., Annamalai University for extending necessary facilities to carry out this investigation.

References

[1] A. Scrivani, S. Ianelli, A. Rossi, R. Groppetti, F. Casadei, G. Rizzi: Wear 250 (2001) 107–1137.

[2] P.K. Aw, B.H. Tan: J. Mat. Pro. Technol. 174 (2006) 305–311.

[3] W. Fanga, T.Y. Choa, J.H. Yoona, K.O. Songa, S.K. Hura, S.J. Younb and H.G. Chun: J. Mat. Pro. Technol. 2 0 9 (2 0 0 9) 3561–3567.

[4] Lidong Zhao, Matthias Maurer, Falko Fischer, Robert Dicks and Erich Lugscheider: Wear. 257 (2004) 41–46.

A study on HVOF process parameter optimization for erosion resistant WC-CoCr nanostructured coating

Lalit Thakur[1], Navneet Arora[2]
[1] Mechanical Engineering Department, National Institute of Technology Kurukshetra, Kurukshetra, Haryana 136119, India
[2] Mechanical and Industrial Engineering Department, Indian Institute of Technolog Roorkee, Uttarakhand 247667, India

Abstract
In the present study, a highly erosion resistant WC-CoCr nanostructured coating has been obtained by HVOF process parameters optimization. The optimization has been done by using a standard L9 (orthogonal array) Taguchi experimental plan. During the coating deposition the temperature and velocity of in-flight powder particles were also recorded for each set of process parameters. Coating properties like hardness, porosity, and as-sprayed surface roughness has been calculated for 9 sets of parameters given in Taguchi design matrix. Solid particle erosion testing was conducted at room temperature using 50-µm Alumina (Al_2O_3) particles impacting the coated surface at 90° impact angle. The coatings were developed using the powders feedstocks having nano-scale WC particles mixed with CoCr binder material. Finally a set of optimized parameters for nano-WC-CoCr coating has been obtained. At this parameter set coating had shown highest wear resistance due to its improved properties. Further this coating was subjected to lower impact angle and finally the wear mechanisms have been studied and discussed with the help of SEM images of worn surfaces. In this study the conventional coating was also deposited with same optimized parameters and its performance was compared with nano-WC-CoCr coating.

1 Introduction

The main problem associated with WC-Co based material is the decomposition of WC phase during thermal spray coating deposition. During the high velocity oxy-fuel (HVOF) coating deposition several detrimental phases are evolved such as W_2C, W, WC_{1-x}, Co_3W_3C, and Co_6W_6C [1, 2]. The decomposition of WC phase is severe in case nano-structured WC-Co based materials when deposited by same process parameters as used for conventional material, due to large surface-area-to volume ratio of nano-WC grains in feedstock powder particles [3-5]. Therefore, there is a great need for the optimization of HVOF spray process parameters in case of nanostructured coating and very few studies have been conducted in this area [6-8].
In the present research work, the nanostructured WC-Co-Cr coating has been deposited with minium decomposed WC phase. This has been achieved by optimizing the main parameters of HVOF process using Taguchi method. The solid particle erosion behaviour of optimized nanostructured WC-Co-Cr coating has been studied and compared with conventional coating.

2 Experimental procedure

2.1 Materials

In this study, WC-10Co-4Cr cermet material in powder form has been used for HVOF coating deposition over a grit blasted AISI 304 stainless steel substrate (Ra≈5-8 µm). The nanostructured powder is composed of WC grains in the size range of 50-300 nm whereas the size of WC grains in conventional powder is about 2-5 µm.

2.2 HVOF coating deposition and Taguchi method

In the present study, HVOF coating deposition has been done by kerosene fuelled JP-5000 gun, equipped with in-flight particle state measurement sensor (Accuraspray, Tecnar, Canada). Prior to the deposition of nanostructured WC-10Co-4Cr material, an in-flight particle diagnostic was performed to obtain the ranges of process parameters. The process parameters are optimized by using a standard L9 Taguchi test design matrix as shown in Table. 1.

Table. 1. *Taguchi design matrix for coating deposition*

S.No	Fuel flow rate *FFR* (l/hr)	Oxygen flow rate *OFR* (lpm)	Standoff distance *SOD* (Inch)	Powder feed rate *PFR* (gm/min)	Wt. loss (x10-3 gm)
NC 1	18	800	13	60	66.8
NC 2	18	900	15	90	67.2
NC 3	18	1000	17	120	69.8
NC 4	20	800	15	120	65.5
NC 5	20	900	17	60	66.8
NC 6	20	1000	13	90	63.3
NC 7	22	800	17	90	55.5
NC 8	22	900	13	120	59.3
NC 9	22	1000	15	60	62.2
ONC	**22**	**800**	**13**	**90**	**54.9**
CC	**22**	**800**	**13**	**90**	**97.5**

It is well known fact that Taguchi method is normally used to reduce a large number of experiments, but it is most suitable for the optimization of single objective function [7]. In case of thermal spray hard coatings, the wear resistance is mainly represented by volume or weight loss during the test. Therefore, in the present study average weight loss of three samples during solid particle erosion (SPE) at 90° impact angle is taken as an output response for each parameter combination set, listed in Taguchi design matrix. SPE testing was conducted with alumina erodent of size 50 µm and impingement velocity of 60 m/s, at 30° and 90° impact angles in an air-jet erosion test rig.

3 Results and discussion

Fig. 1., represents scanning electron microscopy (SEM) images of conventional (CC) and nanostructured WC-10Co-4Cr (NC) powders. The influence of process parameter on weight loss of coating is shown in Fig. 2. It can be observed that weight loss is minimum at parameter setting 'ONC'. During the coating deposition the in-flight particle states were recorded for all the combination sets listed in Table. 1. Important properties such as microhardness, porosity, as-sprayed roughness of all the nine coatings were calculated, and presented in Table. 2.

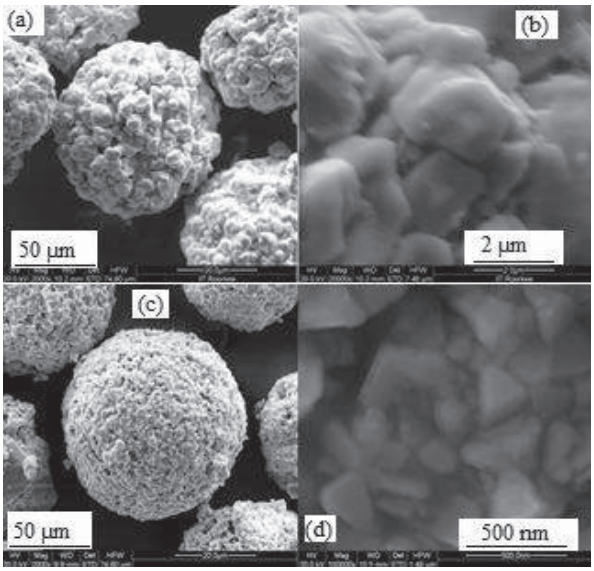

Fig. 1. *(a-b) conventional (c-d) nanostructured powder*

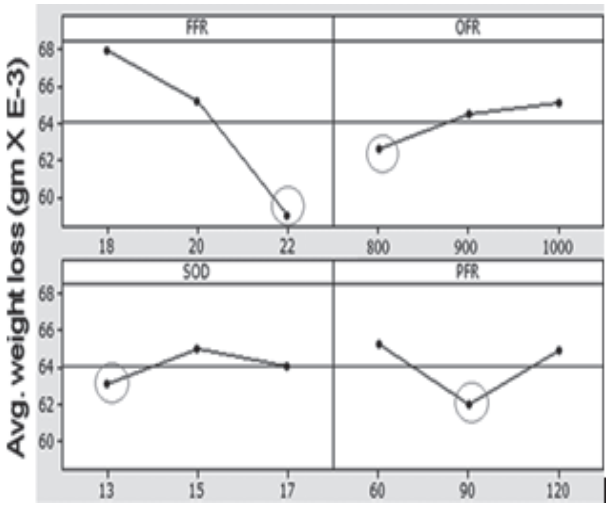

Fig. 2. *The influence of parameters on coating weight loss*

Table. 2. *Coating properties and in-flight particle states*

S.No	Micro-hardness (300Hv)	%age Porosity	Roughness (Ra, µm)	Temp. (°C)	Vel. (m/s)
NC 1	1236±93	1.59±0.18	3.27±1.17	1871	647
NC 2	1180±79	1.80±0.04	2.97±1.18	1843	643
NC 3	1208±88	1.91±0.27	3.20±1.16	1796	637
NC 4	1247±87	1.63±0.31	3.08±0.78	1873	638
NC 5	1239±59	1.61±0.08	3.18±1.35	1867	669
NC 6	1154±66	1.98±0.17	3.59±0.89	1853	708
NC 7	1473±50	1.22±0.25	2.69±1.26	1903	664
NC 8	1598±44	1.09±0.16	2.69±1.11	1897	706
NC 9	1200±56	1.55±0.12	2.88±1.22	1886	731
NC	1665±66	0.62±0.22	2.54±1.15	1915	698
CC	1147±50	0.81±0.19	4.8±0.6	1768	739

Finally the nanostructured WC-10Co-4Cr (NC) powder was deposited with parameter setting 'ONC' and further subjected to SPE testing. It was observed that optimized NC coating exhibit enhanced erosion resistance as compared to other coatings listed in Taguchi design matrix. The CC coating was also deposited with same ONC parameter setting and its erosion resistance was compared with NC coating. The erosion resistance of NC coating was found to be higher than CC coating in both the impact angles.

In Fig. 3(a-b), the material has been removed from the surface of CC coating in the form of pulllout of WC grains. Craters are surrounded by 'lips' which represents the strain hardening of CoCr binder material. At some locations, deformed and fractured WC grains can be seen and some cracks are propagating into the matrix. On repeated impacts these cracks can be expected to grow and join together resulting in material removal. The eroded surface of NC coating revealed a similar mechanism of material removal but at relatively smaller level as compared to CC coating, shown in Fig. 3(c-d). It can also be seen that cracks have propagated but they are arrested at nano-scale feature due to higher fracture toughness and it may be attributed to large number of grains boundaries and fine dispersion of WC grains in binder matrix. This enhanced erosion resistance of NC coating may be attributed to improved mechanical properties.

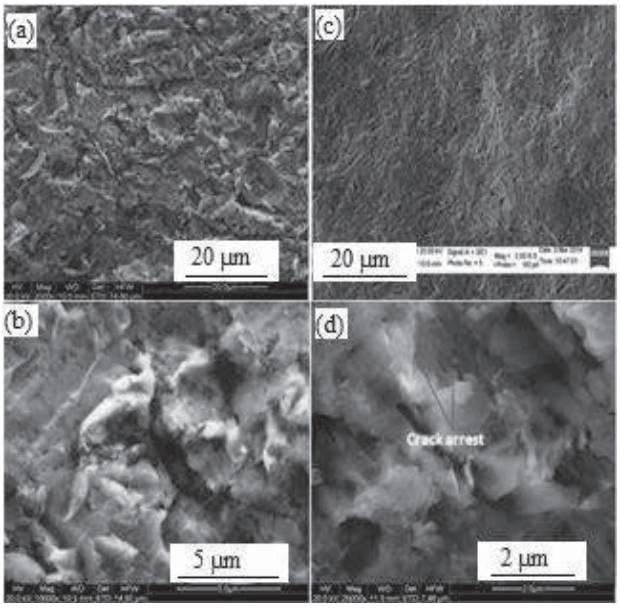

Fig. 3. *Worn surfaces of (a-b) CC (c-d) NC coating*

3 References

[1] G. Barbezat and A. R. Nicoll: Wear 162-164 (1993) 529-537.

[2] H. J. Kim, Y.G. Kweon and R. W. Chang: J. Therm. Spray Technol. 32(2) (1994) 169-178.

[3] D. A. Stewart, P. H. Shipway and D. G. McCartney: Acta Mater. 48 (2000) 1596-1604.

[4] B. H. Kear, G. Skandan and R. K. Sadangi: Scripta Mater. 44 (2001) 1703-1707.

[5] Y. Qiao, T. E. Fischer and A. Dent: Surf. Coat. Technol. 172 (2003) 24-41.

[6] B. R. Marple and R. S. Lima: J. Therm. Spray Technol. 14(1) (2005) 67-76.

[7] W. Fang, T. Y. Cho, J. H. Yoon, K. O. Song, S. K. Hur, S. J. Youn and H. G. Chun: J. Mat. Proc. Tecnol. 209 (2009) 3561-3567.

[8] Q. Wang, Z. Chen, L. Li and G. Yang: Surf. Coat. Technol. 206(8-9) (2012) 2233-2241.

Influence of Pulse Frequency on WC-Co & Al_2O_3 Coating Properties Obtained By Detonation Spray Coating Technique

D.Sen*, S. Nirmala and D. Srinivasa Rao

International Advanced Research Centre for Powder Metallurgy and New Materials,Hyderabad-500005,India
Ph: +91 40 24452342, Fax: +91 40 24442699, Email: dsen@arci.res.in

Abstract:
Successful technology transfer and implementation of indigenously built DSC systems to different private entrepreneurs in India and considering further demand for DSC technology, ARCI has decided to improve the existing DSC system's design by replacing mechanically moving devices with electrical/electronic systems to automate the gases and powder injection with an objective to simultaneously enhance firing frequency such that coating productivity and efficiency could be improved. In view of above, the gas mixing chamber responsible for four steps of operation to obtain a detonation wave has been redesigned and controlled the gas mixing using electronically controlled solenoid valves. Present investigation reports the salient outcome of coatability studies and eventually compare the quality of the coatings in terms of microhardness, micro porosity and microstructure in comparison with conventional 3Hz system. The tribological properties like sliding wear (pin-on-disc test), abrasion wear, erosion wear were also evaluated. The scientific outcome of above study has been reported.

1. Introduction

Thermal spray coating represents an important and costeffective technique for tailoring the surface properties of engineering components with a view to enhancing their durability and performance under a variety of operating conditions[1–3]. Among the commercially available thermal spraycoating techniques, detonation spray (DS) and high velocityoxy fuel (HVOF) spray are the best choices to obtain hard, dense and wear resistant coatings [4]. In continuation to the Successful technology transfer and implementation of indigenously built DSC systems to different private entrepreneurs in India and considering the further demand for DSC technology, ARCI has decided to improve the existing DSC system's design by replacing mechanically moving devices with electrical/electronic systems to automate the gases and powder injection with an objective to simultaneously enhance firing frequency such that coating productivity and efficiency could be improved. In view of the above, the gases mixing chamber responsible for four steps of operation to obtain a detonation wave has been redesigned with precise valves for controlling the gas feeding such that several mechanical parts those undergo wear damage during prolonged operation periods like cams, gears, carbon seals, piston, rollers, bearings, rings were completely replaced. Graphite seal assemblies in existing system causes extensive heat generation due to graphite seals expansion and being in continuous contact with piston and seal leads to seizer of piston assembly in turn. The redesigned mixing assembly is expected to minimize the heat generation during continuous operation.

2. Experimental Details

The new DSC gas mixing system has been fabricated with electronically controlled solenoid valves and gas mixing chamber. The main function of solenoid valves is to maintain the pre-set valve opening time controlled through Labview software. Exact time required to fill the oxy-fuel gas in the new mixing chamber has been calculated based on the cam profile used in conventional DSC system. After integrating the new gas mixing mechanism with the existing spray system and successful coating trial runs with regard to overall function of the DSC system, the essential coating characterization studies were carried out and compared with the coating properties of conventional DSC system.

The mild steel test specimens were used of different sizes (75x25x12 mm^3 - abrasive wear, 30x30x5 mm^3 - erosive wear, 6 mm dia x 30 mm length - sliding wear and 15x10x4 mm^3 – metallography and microhardness evaluation) were fabricated. All the substrates were grit blasted using alumina grit of 30mesh size, cleaned with acetone and coating experiments were carried out using conventional and modified DSC systems for obtaining WC-17Co and Al_2O_3 coatings.

3. Results and Discussion:

The reengineeed DSC system employed in the present study eliminates several mechanical parts which are commonly used in the conventional system as the parts such as cams, gears, carbon seals, piston, rollers, bearings, rings undergo wear and tear process during the operation. The assembly has been reengineered in such a way that it minimizes the heat generated during continuous operation of the DSC system (with increased pulse frequency). In particularl the graphite seal's expansion due to its continuous contact with the piston causes increase in friction between the cylinder internal surface and outer surface of graphite seal thereby accumulated leads to seizer of piston assembly. Further, the newly designed and fabricated gas mixing mechanism as shown in Fig.1 do not requires regular maintenance work and replacement of worn out spare parts and hence, the overall productivity of the DSC system can be enhanced without the maintenance interruption.

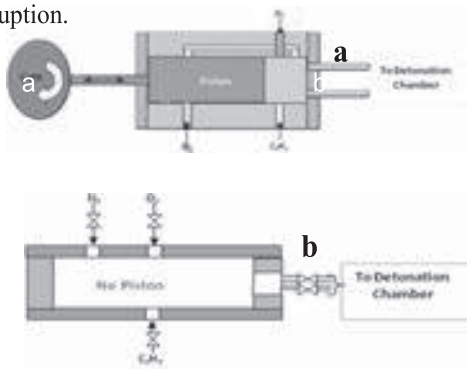

Fig.1 (a) Conventional and (b) Advanced DSC mixing chambers

It may be explicitely noted that the new DSC gas mixing system has only electronically controlled solenoid valves and gas mixing chamber without any mechanically moving parts. The main function of solenoid valves is to regulate the valve opening timing through Labview software controlled computer online connected to the DSC system. Exact time required to fill oxy-fuel gas in the new mixing chamber has been recalculated utilizing the design of cam profile used in conventional DSC system. The quality of the coatings in terms of microhardness, porosity and microstructure are very similar or slightly better as shown in Fig.2. The DSC system with new gas mixing chamber has also been subjected to continuous operation to assess the performance and to find any one the above mentioned technical issues like either overheat or seizure. The major breakthrough and achievement is the new DSC system can be operated continuously without any interruption for providing the DSC coatings on larger sizes of the parts thereby increasing the efficiency and productivity of the coatings.

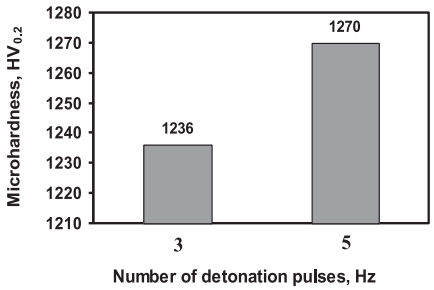

Fig.2 Microhardness value of WC-17Co DSC coatings deposited at two-different pulse frequencies

Typical cross-sectional view of the detonation sprayed WC-Co and Al_2O_3 coatings with frequency 3shot/sec and 5 shot/sec are illustrated in Fig. 3 (a-b) and (c-d) respectively. The coatings have been carried out for a fixed time of 35 sec for both coatings and at both pulse frequencies. The coatings appear dense and the coating- substrate interface is clean and devoid of cracks, indicating excellent coating adhesion with the substrate. The thickness of the coatings in normal frequency (3 shot/sec) is around 120-150 micron where as at higher frequency (5 shot/sec) is in the range of 200-250 micron. Further, upon comparing Fig.3 (a-d), it may also be noted that the above observation is valid for both WC-Co and Al_2O_3 coatings.

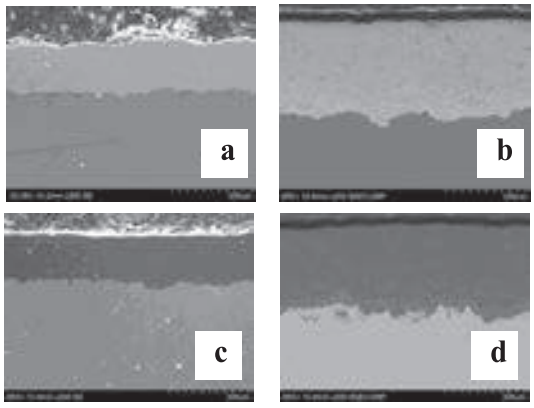

Fig.3 Cross-sectional microstructures of (a-b) WC-17Co and (c-d) Al_2O_3 coatings obtained at (a,c) 3Hz and (b,d) 5Hz DSC systems

The average hardness and pososity values for WC-Co and Al_2O_3 coatings at both pulse frequencies namely 3 shot/sec & 5shot/sec are almost similar or marginally better in the case of coatings obtained higher frequencies. Under the sliding wear mode at identical test conditions, the coatings obtained at higher frequencies (5shot/sec) as shown in Fig.4 exhibits significantly better wear resistance. It is further necessary to undertake the exercise forward to explore the possibilities to further enhance the pulse frequency such that the deposition efficiency and higher throughput can be simultaneously achieved.

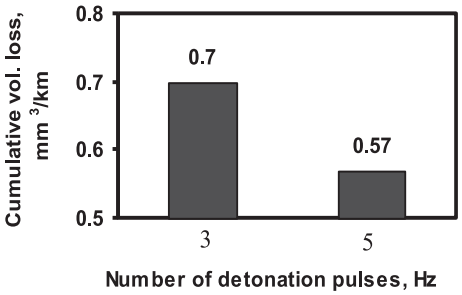

Fig.4 Cumulative sliding wear volume loss as suffered by the WC-17Co detonation spray deposited coatings at 50N load and 5.2 m/s sliding velocity

4. Conclusions :

i) Higher frequency cycles are posssible in advance DSC system where as conventional system operates at ≤ 3 shot/sec pulse frequency.

ii) In advance DSC system, absence of misfiring and only moderate heat generation of the mixing chamber after continous operation of 5000 cycles indicate that the technological modifications incorporated into the advance system are fully functional and capable of delivering high throughput in the industrial mode of working.

iii) Metallugical and tribological properties are found to be similar or marginally better for the coatings deposited utilizing the advanced DSC system at higher frequencies compared to the coatings obtained at lower frequencies.

Acknowledgements:

Authors of this article are grateful to Dr. G. Sundararajan, Director, ARCI and Dr. S.V. Joshi, Additional Director, ARCI for their valuable suggestions and guidance during the reported work.

References:

1. L. Pawlowski, The Science and Engineering of Thermal Spray Coatings,Wiley, UK, 1995.

2. P. Fauchais, A. Vardelle, B. Dussoubs, Quo Vadis Thermal Spraying, J. Thermal Spray Technol. 10 (2001) 44-66

3. R. Knight, R.W. Smith, Thermal Spray Forming of Materials, Vol. 7, ASM Handbook, 1998.

4. Y. Wang, Friction, Wear performances of detonation gun and plasma sprayed ceramic and cermet hard coatings, Wear 161 (1993) 69-78.

Wear and oxidation behavior of CoNiCrAlY coatings sprayed with HVOF and CGDS

W.S.Rathod[1], A.S.Khanna[2]
[1] VJTI, Mechanical Engg.Dept., Matunga, Mumbai, India
[2] Department of Metallurgical Engineering, IIT, Bombay, Powai, Mumbai, India
Corresponding Author (wsrathod@vjti.org.in)

Abstract

High Velocity Oxy Fuel (HVOF) and cold spray techniques have been used to form oxidation resistant hard coatings for bond coat application for gas turbine blades. Though, both techniques accelerate powder particles with high kinetic energy, the coatings formed, differ considerably in their microstructures. In the former, high pressure is created by burning gases such as acetylene, propane or kerosene at high pressure and generating high temperature (3500 to 4500 ^{0}C) in the gun. This gives high acceleration to powder particles which melt and deposit on substrate layer by layer with splat cool mechanism. On the other hand, large Kinetic energy (KE) is generated in Cold Spray by passing carrier gases such as He or N_2 through a converging-diverging nozzle, with a lower gun temperature of around 500 ^{0}C. In this work, CoNiCrAlY powder was used. Presence of Al creates suitable deformation properties on impact. The powder was deposited on 316L SS substrate using HVOF and also by Cold Gas Dynamic Spray (CGDS) deposition process. In the latter, there are two processes, which give two different kinetic energies, depending upon the gas used, nitrogen or helium. Latter gives much higher KE. The deposited coatings were, characterized and the subjected to wear and oxidation studies. One of the interesting results was that the oxidation resistance of CGDS coating was much superior to that HVOF coated stainless steel with low wear rate and better friction behavior.

Keywords: Cold Gas Dynamic Spray (CGDS), High velocity oxygen-fuel (HVOF), bond coat.

Introduction

In the last three decades, extensive research has been undertaken to improve the efficiency, durability and overall performance of gas turbine engines. To protect hot- sections of power generation components of gas turbine engine, thermal barrier coatings (TBCs) are widely used. Conventional TBCs consist of a MCrAlY alloy (where M stand for Co, Ni) bond coating for oxidation resistance and a ceramic top coating for thermal insulation (mainly YSZ) [1, 2]. The oxidation resistance of the coating depends not only on the chemical composition of the coating but also on the technique used to deposit the bond coat. CoNiCrAlY superalloy is typically coated by VPS (Vacuum plasma spraying), APS (Air-plasma spraying), LPPS (Low pressure plasma spraying) and HVOF (High velocity oxygen-fuel spraying) [3,4]. The main limitation of these techniques is that their inherent elevated temperature, which often leads to changes in the alloy phases. APS gives a coating which has porosity and oxide inclusions. VPS represents the state of the art technology for the bond coat deposition, but the cost is relatively high due to vacuum operation. Shibata et al., [5] deposited CoNiCrAlY bond coat using APS, LPPS and HVOF and the extent of oxide contamination was 1.8, 0.16 and 0.94 wt. % respectively. Tang et al., [6] deposited CoNiCrAlY coating by HVOF and reported the surface oxidation, during deposition, which is detrimental to the TGO growth mechanism. Richer et al.,[7] deposited CoNiCrAlY coating using CGDS operated with He gas, and reported the formation of an oxide scale composed of alumina, without the presence of NiO or spinel-type mixed oxides. Zhang et al., [8] studied oxidation behavior of NiCrAlY coatings deposited using CGDS technique. They reported the formation of (α-A_2O_3) at 900 ^{0}C and 1000 ^{0}C. The main objective of this work is to compare the properties of the bond coat formed using CGDS with HVOF in terms of porosity, hardness, wear and friction and also its oxidation kinetics.

1. Results and Discussion

1.1 Oxidation study

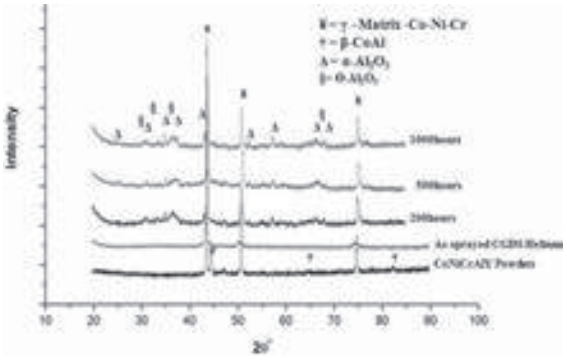

Fig.1 XRD results of the oxidized CGDS coating sprayed with He gas at the temperature of 900 ^{0}C for 200, 500 and 1000h exposure

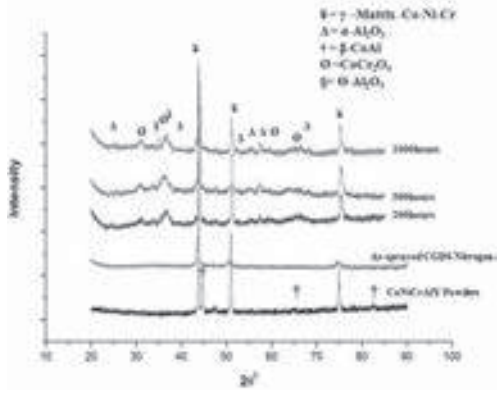

Fig. 2 XRD patterns of oxidized CGDS coating sprayed with N_2 gas at the temperature of 900 ^{0}C for 200, 500 and 1000h exposure

Fig. 1 shows the oxide layer consisting of a mixture of θ-Al_2O_3, and α-Al_2O_3 right from the initial stages of oxidation, dominated by θ-Al_2O_3 in the initial stages and almost fully covered by α-Al_2O_3 at longer duration of 1000h. Fig. 2 shows formation of θ-Al_2O_3, in the initial stages of oxidation, followed by α-Al_2O_3 domination after longer hours of exposure. XRD results also shows the presence of CoCr spinel formation ($CoCr_2O_4$ spinal-type oxide) during longer exposure along with α-Al_2O_3. This confirms slightly higher oxidation rate of CGDS coatings

deposited N_2 as carrier gas as compared to CGDS with He gas.

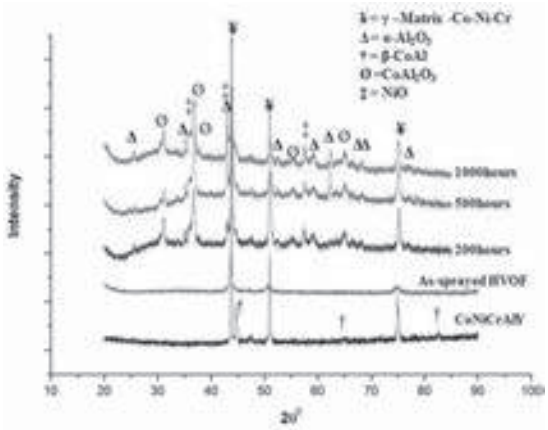

Fig. 3 XRD results of oxidized HVOF coating at the temperature of 900 ^{0}C for 200, 500 and 1000h exposure

The HVOF coating is mostly covered with an oxide scale composed of alumina, NiO and spinel-type oxides. This is confirmed by XRD results that the coating, consists of NiO oxides, spinel oxide of $CoAl_2O_3$, NiO and α-Al_2O_3 confirming still higher oxidation rate of HVOF coated stainless steel.

1.2. Wear study

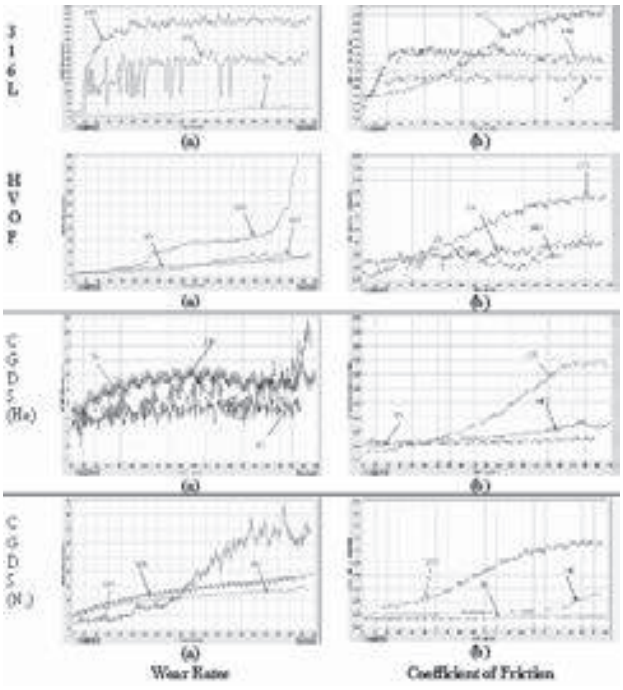

Fig. 4 Wear rates and coefficient of friction values for the uncoated 316L SS and that coated with CGDS and HVOF deposited method

From Fig.4**.** The wear rate falls drastically after 316L SS is coated with CoNiCrAlY coating. The reduction is almost 40% for HVOF coating and 85% in case of CGDS with He and about 60 % in case of coating deposited by CGDS with N_2 as carrier gas. Effect of load is quite alarming. The wear rate is quite high at higher load of 15N. The wear rate is negligible of the coated specimens up to 10N, especially for the CGDS coated samples. There is also a change in the mechanism of wear which changes from ploughing to adhesive wear at higher loads.The coefficient of friction variation is also very significantly improved at low loads, however at higher load of 15N, there appears to be no improvement.

Conclusions

Bond coats deposited by CGDS technique was harder, denser and had almost no oxide inclusions, while bond coat formed using HVOF technique has higher porosity, lower hardness and several oxide impregnations. Oxidation kinetics of CGDS was an order of magnitude lower than that HVOF. HVOF shows the presence of sublayer of α-Al_2O_3 and upper layer of (Ni,Co) (Al,Cr) $_2O_4$ spinal-type oxides suggests that the coating is nearing the end of its Al-rich lifecycle. CGDS processed with helium display low wear rate and better friction behavior when compared to that of coatings processed HVOF and CGDS sprayed with N_2 as carrier gas.

Regferences

[1] Wright PK, Evans AG, Mechanisms governing the performance of thermal barrier coating. Current opinion in Solid State and Mater Sci: 1999:4: 255-265.

[2] Bhattacharyya D, Targa M, Nicholls JR, Surface Eng: 2012:28: 2:122-128.

[3] Evans AG, Mumm DR, Hutchinson JW, Meier GH, and Pettit FS, Mechanisms controlling the durability of thermal barrier coatings: Progress in Mater. Sci: 2001: 46 (5):505-553.

[4] Messaoudi K, Huntz AM, and Lesage B, Diffusion and growth mechanism of Al2O3 scales on ferritic Fe-Cr-Al alloys. Mater Sci. and Eng A.1998: 247 (1-2):248-262.

[5] Shibata M, Kuroda S, Murakami H, Ode M, Watanabe M, Sakamoto Y, Comparison of microstructure and oxidation behavior of CoNiCrAlY bond coating prepared by different thermal spray process: Mater Trans. 2006 (47) 7:1638-1642.

[6] Tang F, Ajdelsztajn L, Kim GE, Provenzano V, Schoenung JM, Effects of surface oxidation during HVOF processing on the primary stage oxidation of a CoNiCrAlY coating: Surf and Coating Techno, 2004:185:228-233.

[7] Richer P, Yandouzi M, Beauvais L, and Jodoin B, Oxidation behavior of CoNiCrAlY bond coats produced by plasma, HVOF and cold gas dynamic spraying: Surf CoatingsTechno, 2010:204:3962-3974.

[8] Zhang Q, Li CJ, Li Y, Zhang S, Wang XR, Zhang Q, Yang GJ and Li CX, Thermal failure of nanostructured thermal barrier coatings with cold-sprayed nanostructuredNiCrAlY bond coat: J Thermal Spray Techno, 2008:17(5-6):838-845.

Actual vs Measured Porosity in Thermally Sprayed TBC Coatings

Neha Kondekar[1], Dheepa Srinivasan[2] and Hariharan S[2]
[1] Department of Materials Engineering, Indian Institute of Science, Bangalore 560 012, India
[2] GE Power and Water, GE India Technology Centre, Bangalore 560066, India

Abstract
Thermal barrier coatings sprayed using the air plasma sprayed coating process, are designed to have porosity in the as coated condition. The porosity is an integral part of functioning of the coating, in terms of providing strain tolerance, during service operation and hence determines the life of the coating and the reliability of the part. The current practice of establishing the porosity is via destructive metallography, via cutting, grinding, polishing, and evaluating the coating cross section. This technique, however, poses severe challenges in terms of determining the exact porosity, to the metallographer. Given the vastly different materials, ductile ceramic, on a dense metal, that is being used for obtaining metallographic samples, this can end up in causing pull outs in the TBC, and hence read an exaggerated porosity. This paper attempts to determine the actual porosity in a free standing TBC using Pycnometry and compares it with the porosity measured using metallographic samples, and brings out the possible standard deviations that could be associated with practical means of measuring porosity.

I Introduction

Thermal barrier coatings (TBC) used in gas turbines, comprise an architecture, that has a ceramic coat, alongwith a metallic MCrAlY bond coat, on top of the Ni based superalloys substrate [1-3]. The ceramic top coat, is usually a porous coating, that is able to accommodate the thermal fatigue (strain tolerance) that is experienced by the hardware and the coatings during gas turbine operation. Owing to the complex nature of the TBC coating architecture on a gas turbine hot gas path component, including a brittle ceramic coating (TBC), with a metallic bond coating (BC), on a metallic substrate, it is imperative to have a robust way to measure the TBC porosity. The porosity measurement is usually done via destructive metallurgical analysis, that involves cutting a cross section of the coating(s) on the substrate, mounting and polishing, followed by image analysis, and measuring the porosity using image analysis (as shown in Fig, 1a and 1b. However, this method is usually fraught with erros that creep up due to over grinding, improper impregnation of the mounting compound leading to excessive pull outs, that could end up over estimating the porosity. This study presents an analysis of accurately determining the TBC's porosity via pycnometry, and comparing the same with the metallographic estimation of porosity.

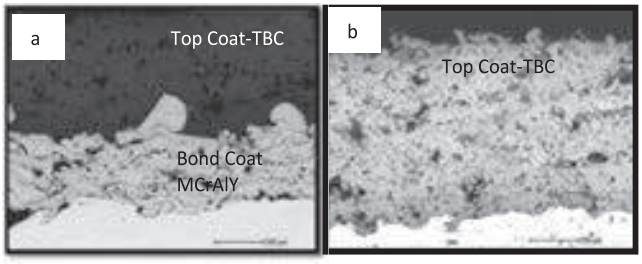

Fig. 1 : *Representative Optical micrograps at 200X showing, (a) the TBC-BC-substrate , (b) TBC-Top Coat.*

2. Experimental Details

Two sets of TBC samples, with varying porosity were deposited as free standing films, on to 2.5 x 2 cm substrates, (a) with and (b) without, a metallic bond coat and grit blasting, via an APS (Air Plasma Spray) process, in a GE service centre, as shown in Fig. 2. The nominal TBC coating thickness was ~ 350 µm. The regular TBC coatings (with the BC), were sectioned, and taken through a standard proceedure for polishing TBC's on a substrate, to obtain metallorgraphic samples. These were imaged using a Nikon, Eclipse, Optical micrscope, at 200 X. The coating porosity was measured using a Clemex image analysis attached to the microscope, from an average of 4-5 frames. The porosity in the free standing TBC films were analysed using Pcynometry, in accordance with ASTM 373-14 [4]. The coatings were weighed using a microbalance, in air (D= Dry weight) and in water (S=suspended weight). Deionised waer was brought to boiling condition after ensuring that the samples were fully submerged and a ratio of 3:1 was maintained with respect to the weight of water and the weight of the samples. After continuouly boiling for ~ 5h, the specimens were left to soak in the water overnight, and the suspended mass (S) in water was measured. Thereafter, the free standing coating was dried such that excess water on the surface is removed and the saturated weight (open+ interconnected pores with filled water) was measured (M). Fig. 3 is a schematic showing a possible configuration of various pores (C-closed, O- open, and I-Interconnected and open), in the TBC. Using these the measurements, the exterior volume (V), volume of open pores (V_{op}), volume of impervious-closed and interconnected pores (V_{IP}) , the apparent porosity (P) and the bulk density B, are calculated, as illustrated in Table 2.

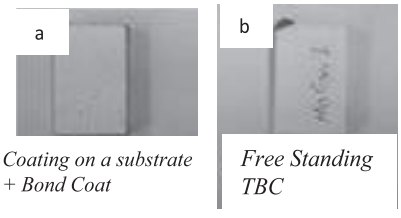

Fig. 2 : *Macrophotograh of the, (a) Coating on the substrate with a bond coat, and (b) free standing coating*

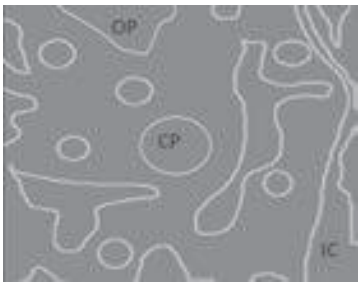

Fig. 3 : *Schematic of the different pore configurations in the TBC, O-open pore, C-closed pore, IP-Interconnected*

3. Results :

(i) TBC porosity using Pycnometry :

Table 1 lists the all the measurements carried out on 6 different free standing TBC coatings, and Table 2 includes an estimation of the porosity.

Table 1 : *Measured weights of the free standing TBC film (ρ_{H2O} = 1 g/cc)*

Sample No.	D (mg)	S (mg)	M (mg)	V = (M-S)/ρ (cc)
1	1274.0	926.2	1331.70	405.50
2	1068.5	889.4	1114.00	224.60
3	770.1	640.9	798.40	157.50
4	544.4	451.2	563.50	112.30
5	462.4	383.3	477.60	94.30

Table 2 : *Average porosity (%) in the free standing film using Pycnometry*

V_{OP} = (M-D)/ρ (cc)	**V_{IP} = (D-S)/ρ (cc)**	**B = D/V (mg/cc)**	**% P = (V_{OP} /V)*100**
57.70	347.80	3.14	14.23
28.30	129.20	4.89	17.97
19.10	93.20	4.85	17.01
15.20	79.10	4.90	16.12

(ii) TBC porosity using Image Analysis :

Figs. 4a and 4b show optical micrographs, at 50X and 100 X, from sample A, to reveal the coating thickness of the top coat and bond coat, along with the corresponding image. Figs. 4c and 4d, show a representative region in the TBC, taken at 200 X and the corresponding grey scale threshold that reveals the porosity in that location. Table 2 lists the measurements carried out on three different samples and lists the average porosity in the coating, measured via optical image analysis. Also listed in Table 3, are the coatings thickness of the top coat and bond coat.

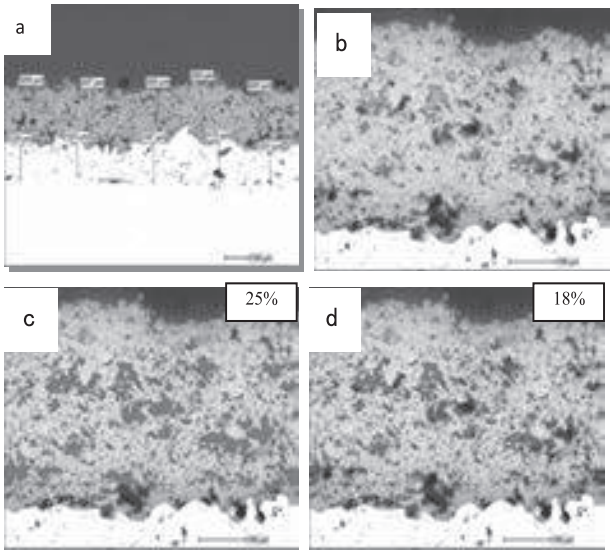

Fig. 4 : *Representative optical images (a) Top and Bond Coat thickness at 50X, (b) revealing the TBC at 200X,(c-d) different image analysis, with and without pull outs.*

Table 3 : *Average porosity measured using image analysis*

	Sample1	Sample 2	Sample 3
Topcoat Thickness (μm)	356.52	345.33	348.12
Bond Coat Thickness (μm)	138.4	89.2	123.6
% Porosity (including the pull outs)	21	21	26
% porosity (excluding the pull outs)	18	17	18

4. Summary and Conclusions :

The average porosity measured using pycnometry, ranges between 16-17%, while that using image analysis, via sectioning of the coating, lies between 21-25%, if the image is processed without excluding the pull outs. A careful delineation of the pull outs based on visual examination is then essential in order to estimate the porosity (which lies between 17-18%, Fig.4d). It can be seen that there is a 4-5% enhanced porosity measured using the image analysis, as compared to the pycnometry. In addition, the standard deviation in the measurements are also higher using image analysis (3%) as compared to pycnometry (0.5). It may not always be practical to obtain free standing films of the coating, during normal production runs of the TBC coatings, and estimate the porosity in a precise manner using pcynometry. However, in order to ascertain the porosity in a new coating or in a new process or during spraying of a new component, it is recommended that the actual porosity be ascertained using pycnometry, in order to define the allowable tolerances, while defining the subsequent process specifications.

6.Acknowledgements

The coatings were sprayed in Gulf Turbine Service Centre, Abu Dhabi. The authors would like to thank Ms. Suleiman Fatima and Mr. Ahmed Behri for their help with the TBC coatings. Dr. Sundar Amancherla and Mr. Christopher Thompson, GE Power & Water, are gratefully acknowledged for their support of this work. The pycnometry experiments were carried out at Prof. Rajiv Ranjan's laboratory at the Indian Institute of Science, Banglore.

7. References

1. D.R. Clarke, O. Matthias Oechsner and N. P. Padture, MRS Bull., **37** (2012) 891-893.
2. D. R. Clarke and S. R. Phillpot, Materials Today, **8** (2005) 22-23.
3. F.H. Yuan, Z.X. Chen, Z.W. Huang, Z.G. Wang a, S.J. Zhu, **50** (2008) 1608-1610.
4. ASTM 373-14, Standard Test Method for Water Absorption, Bulk Density, Apparent Porosity, and Apparent Specific Gravity of Fired Whiteware Products, Ceramic Tiles, and Glass Tiles.

Thermal Conductivity of the Atmospheric Aluminum Nitride Coatings

Mohammed Shahien[1,3], Motohiro Yamada[1], Masahiro Fukumoto[1], Kazumi Egota[2], Kenji Okamoto[2]
[1] Department of Mechanical Engineering, Toyohashi University of Technology, Toyohashi 441-8580, Japan
[2] Fuji Electric Co.,Ltd., Hino 191-8502 , Japan
[3] Currently Central Metallurgical Research and Development Institute, CMRDI, Helwan 11421 Cairo, Egypt

Abstract
Reactive plasma spraying (RPS) is a promising technology for *in-situ* formation of aluminum nitride (AlN) thermal spray coatings. Recently, thick AlN/Al_2O_3 (Alumina) composite coatings were successfully fabricated through RPS of Al_2O_3/AlN mixture powders in N_2/H_2 plasma under the atmospheric ambient. This study will focus on the evaluation of the thermal conductivity of the fabricated AlN coatings. The thermal conductivity of the caotings were low compared to the AlN value. It is related to the phase composition of the coatings, oxide content and porosity. Thus, the presence of Al_2O_3, Al_5O_6N and the high coating porosity decreased the thermal conductivity. Furthermore, the coating density is lower than the AlN value, which suppressed the coatings thermal condutivity. In addition, although the N_2 gas flow improved the nitride content, it suppressed the thermal conductivity gradually, due to the further decrease in the coating density and increasing its porosity with the N_2 gas.

1 Introduction

Aluminum nitride (AlN) is outstanding ceramic material for several electrical and electronic applications. It is attributed to its high thermal conductivity, dielectric properties and unique mechanical properties [1]. On the other hand, thermal spraying is a versatile technique for producing abradable and protective thick ceramic coatings. However, it has been impossible to fabricate AlN coating by conventional thermal spray processes directly from AlN feedstock powder due to the thermal decomposition of AlN particles during spraying without a stable melting phase.
In order to fabricate AlN thermal sprayed coatings, the solution was using the reactivity of thermal plasma which is usually used to melt and accelerate the spray materials. Reactive plasma spraying (RPS) has been considered as a promising technique for *in-situ* formation of AlN thermal sprayed coatings [2-4]. The process is based on the reaction of molten particles (metallic or non-metallic materials) with the surrounding active species in the plasma such as atom, ion and radical. In our previous studies [4], it was possible to fabricate AlN based coatings with high nitride content through the RPS of Al_2O_3/AlN mixture and controlling the reaction process. This study will focus on the evaluation of the thermal conductivity of the reactive plasma sprayed AlN coatings and studying the effect of process parameters on the thermal conductivity.

2 Experimental Procedures

All the spray experiments were carried out by the atmospheric plasma spray system (APS: 9MB, Sulzer Metco, Switzerland), using N_2 and H_2 as plasma gasses. The spray conditions are shown in details in the previous sudy [4], the flow rate of the N_2 plasma gas varied from 100 to 160 SCFH (standard cubic feet per hour) with keeping its pressure at the standard conditions of 330.9 kPa. The H_2 plasma gas was kept at the standard condition of 5 SCFH and 344.7 kPa. The spray distance was kept at 150 mm from the gun exit. The feedstock powder is spray-dried fine 60 wt.% Al_2O_3 and 40 wt.% AlN mixture, its details are described before [4].
The thermal conductivity sample was prepared on pure copper (Cu) substrate, in a disk shape with a diameter of 10 mm and thickness about 0.5 mm. The thermal conductivity, thermal diffusivity and specific heat of the coatings were measured by Laser Flash method using the LFA 447 Nanoflash® instrument, (NETZSCH, Inc., Germany). Figure 1 shows the schematic diagram of the measurement process. The measurement is basically done through the following equation:

$$\lambda = \alpha \rho Cp \quad (1)$$

where:
λ= thermal conductivity (W/m.K), ρ= density (Kg/m^3)
α = thermal diffusivity (m^2/s), Cp = specific heat (J/Kg.K)

The specific heat capacity or specific heat, Cp, was measured using a differential scanning calorimeter (Perkin-Elmer Co., DSC-7) comparative method, in the temperature range of 100-1000 ºC with increasing rate of 10 ºC/min in dry N_2 atmosphere. The specific heat of the material is defined as:

$$Cp = Q/m\Delta T \quad (2)$$

Where: Cp = specific heat (J/Kg.K),
m = mass, ΔT = change in the temperature.

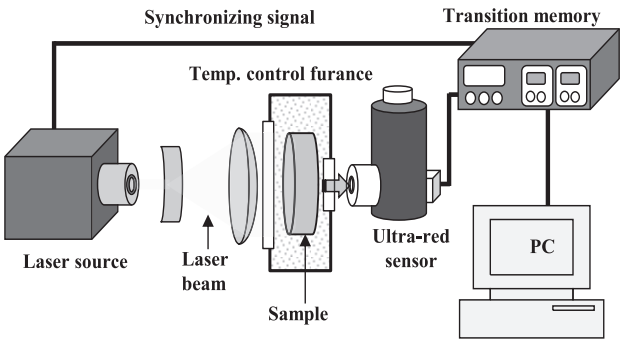

Fig. 1. *Thermal conductivity measurment sketch.*

The specific heat was measured by comparing the temperature rise of the sample to the temperature rise of a reference sample (sapphire: α-Al_2O_3) of known specific heat tested under the same conditions. The sample bulk density is normally calculated from the measured sample volume (calculated from the measured sample dimensions) and mass by using the Shimadzu Co. electronic balance (AuW120D) at 25ºC. The phase compositions of the fabricated coatings were verified by X-ray diffraction

(XRD: RINT-2500, Rigaku, Japan). A scanning electron microscope (SEM: JSM-6390, JEOL, Japan) was used to observe the cross-section microstructure of the fabricated coatings. The coating porosity was estimated by image analysis of SEM cross-sections.

3 Results and Discussion

Figure 2 shows the thermal conductivity and density of the fabricated coatings as function of the N_2 plasma gas flow rate. It is clear that, the thermal conductivity of the coatings is very low compared to the AlN sintered compacts. Moreover, the further increase in the N_2 gas flow rate suppressed the coatings thermal conductivity. The low thermal conductivity of the fabricated coatings is mainly attributed to several factors; the coating phase composition, oxide content and porosity. Thus, the fabricated coating consists of cubic-AlN (*c*-AlN), hexagonal-AlN (*h*-AlN), aluminum oxynitride (Al_5O_6N), γ-Al_2O_3 and small content of α-Al_2O_3 phases as shown in details in the previous study [4]. The presence of such large amount of alumina significantly lowered the AlN thermal conductivity due to its low conductivity. Furthermore, the formation of relatively large amounts of oxynitride phase in the Al_2O_3-AlN system, which has lower thermal diffusivity compared even with the Al_2O_3 itself, leads to further decrease in the fabricated coating thermal conductivity. Thus, the presence of oxygen is the principle impurity in the AlN industry, which may leads to phonon scattering and therefore a decrease in thermal conductivity of the polycrystalline AlN.

Furthermore, Fig.2 also shows the measured values of the coatings density. It is clear that, the values are lower than the AlN value (3.16 g/cm^3) and gradually decreased with the N_2 gas flow. This can also clarify the extreme low thermal conductivity of the fabricated RPS AlN coatings and its further decrease with the N_2 gas flow rate.

On the other hand, Figure 3 shows the the SEM cross-section microstructure of the fabricated coating at N_2 gas flow of 100 SCFH. It is clear that, the coating is approximately 500 μm thick with a uniform and porous structure. The porosity of the coating was estimated by image analysis of SEM cross-section. The coating has about 20 % porosity, which led to further decrease in the coating thermal conductivity.

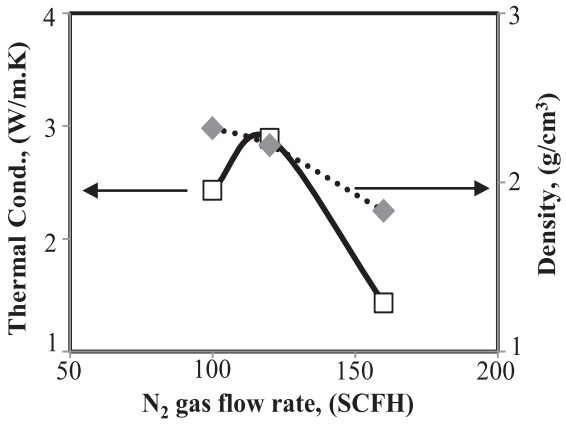

Fig. 2. *Thermal conductivity and Density Vs N_2 gas flow.*

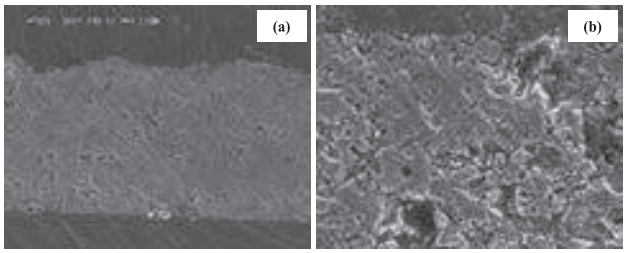

Fig. 3. *The fabricated coating cross-section microstructure.*

Thus, it is well known that, the plasma sprayed coating thermal conductivity is significantly lower than that of the corresponding bulk material. It is attributed to, the higher thermal resistance due to interlamellae boundaries, porosity, and microcracks parallel to the coating plane. Thus, the plasma sprayed coating consists of highly anisotropic layered structure with individual splats oriented parallel to the substrate surface, which lowered the thermal conductivity. It is related to the interfacial thermal contact caused by pores or secondary phases. Thus, the crystal lattice wave and heat wave are the main media through which the heat is transported in the ceramic materials, and dispersion as well as interference of the wave result from the pores and cracks in the coating lower its thermal conductivity.

The further decrease in the coatings thermal conductivity with increasing the N_2 gas flow rate can be explained as follow: Although the N_2 gas flow improved the nitriding conversion and therefore the AlN content in the coatings [3, 4], the coating porosity gradually increases with increasing N_2 gas flow rate, as shown before [4]. Therefore, the thermal conductivity decreased with the further increase in N_2 gas flow rate. Increasing the porosity with the N_2 gas is related to the increasing particle velocity with the N_2 gas. Thus, increasing particle velocity shortened the particle residence time in the plasma and leads to worse melting behavior of the powder in the plasma, which significantly affects the coating porosity. Besides that, increasing the N_2 gas flow in the RPS process enhanced the reaction tendency between the particles and the surrounding plasma, which leads to increasing the coating porosity. Further studies are under progress to increase the coating thermal conductivity based on theses current results.

4 Conclusions

The RPS AlN coating thermal conductivity was investigated as function of the N_2 plasma gas. It was clear that, not only the AlN content and its distribution are the required to get high thermal conductivity coatings. But also adjusting the oxide content and the coating porosity are required.

5 References

[1] H. O. Pierson, *Handbook of Refractory Carbides and Nitrides*, Noyes Publications, New Jersey, USA, 1996, pp. 237-239.

[2] M. Shahien, M. Yamada, T. Yasui and M. Fukumoto: J. Therm. Spray Technol. **20-3** (2011) 580-589.

[3] M. Shahien, M. Yamada, T. Yasui and M. Fukumoto: Surface and Coatings Technol. **216** (2013) 308-317.

[4] M. Shahien, M. Yamada, T. Yasui and M. Fukumoto: J. Therm. Spray Technol. **22-8** (2013) 1283-1293.

Thermally Sprayed Fly-Ash Coatings on Mild Steel Substrates

N.V.V.V.R. Rajesh, B. Pravallika, N.S. Karthiselva, K.Vasanthakumar, Debalina Bhattacharjee, M. Kamaraj, Srinivasa Rao Bakshi

Indian Institute of Technology Madras

Fly-ash generated in coal fired thermal power plants is an industrial waste and environmental pollutant. There has been much emphasis on the usage of fly-ash as a potential material outside of construction industry in the last few years. Therefore, an attempt has been made to use coal fly-ash to develop coatings on mild steel substrates for enhanced wear and erosion resistance. Some studies exist on utilization of fly-ash for wear resistant coatings but the results were not encouraging. Characterisation of the fly-ash powder classified into various size ranges is carried out and compared with that of as received sample prior to coating. Plasma spraying and High velocity oxy fuel (HVOF) spray coating were used to synthesize the coatings. Microstructure and phase characterizations of the two coatings are done using SEM. Hardness measurements were carried out using nanodentation. Slurry erosion studies showed that Plasma sprayed coatings had poor wear resistance while the HVOF coatings had slightly better wear resistance than the steel substrate. In corrosive and erosive environment, it is believed that the HVOF coatings may perform better.

Hydroxyapatite/graphene-nanosheet composite coatings deposited by vacuum cold spraying for biomedical applications

Yi Liu, Jing Huang, Hua Li*
Key Laboratory of Marine Materials and Related Technologies, Ningbo Institute of Materials Technology and Engineering, Chinese Academy of Sciences, Ningbo 315201, China

Abstract
Discovery of novel biocompatible nanomaterials has given bright insights into their possible biomedical applications. Recent exciting findings of the biological properties of graphene have shed light on potential biomedical applications of graphene-containing composites. Here we report hydroxyapatite (HA) and HA-graphene nanosheet (GN) composite coatings deposited by vacuum cold spraying at room temperature. The HA-GN composite coatings retained intact nano-structural features of both HA and GN. Significantly enhanced fracture toughness and elastic modulus has been revealed. *In vitro* cell culture assessment showed that filopodia of osteoblast cells inclined to move towards and got anchored by GN. Further observation by electron microscopy of adsorption of fibronectin on GN showed fast adsorption of fibronectin. This presumably accounts for the enhanced spreading and subsequent proliferation of the cells on the GN-containing coatings. The strategy of depositing the novel HA-GN composite coatings sheds some light on potential biomedical applications of the composites.

1 Introduction

Demand for biomedical implants to correct skeletal defects or substitute for load bearing hip, knee and dental endoprosthetic is constantly increasing. Development of novel biomaterials with improved lifetime, reliability and bioactive functions is high up on the agenda of worldwide research. Thermal sprayed in particular plasma sprayed hydroxyapatite (HA) coatings are routinely applied on metallic implants to promote fast fixation with bony tissues after surgery [1]. Furthermore, despite its excellent biological properties, the inherent brittleness of HA restricts its application in many load-bearing situations [2]. Therefore, incorporating second phase reinforcements into HA coatings as toughening component was developed [3]. Graphene has been attracting intense attentions due to its unique structural features and exceptional mechanical properties [4]. Exciting findings of the biological performances of graphene reported in recent years [5] further imply the possibility of it being used as additives in HA for load-bearing biomedical applications. In addition, it is well established that among the crucial variables that decide the quality of the biomedical coatings are purity (phase composition), crystallinity, Ca/P ratio, grain size, porosity, surface roughness, thickness, and surface texture etc [6]. Nanostructured HA exhibit further enhanced biocompatibility when compared to their conventional counterparts [7]. Vacuum cold spray (VCS) is a promising spray technique based on shock-loading solidification, enabling deposition on various substrates such as metals, ceramics and plastics. Owing to the room-temperature deposition, VCS offers the advantages of efficient transferring the microstructure of feedstock powder to the as-deposited coating without remarkable crystal grain growth or structural changes [8]. In this paper, we report novel nano-HA - graphene-nanosheet (GN) composite coatings deposited by VCS, giving insights into their potential biomedical applications for repair/replacement of hard tissues.

2 Results and discussion

2.1 Microstructure characterization

The as-synthesized GN shows wrinkled-paper-like morphology (Fig. 1a). AFM measurements suggest the uniform height of the nanosheets of 0.8-1.1 nm and the lateral dimensions ranging from a few hundred nanometers to ~4 μm (Fig. 1b). In accordance with previous reports and TEM observation , the GNs are interpreted to be single-layered sheets. Further TEM characterization reveals that rod-like HA nano grains evenly attach on graphene flakes with an intimate contact (Fig. 1c). HA grains have the size of ~20-45 nm in length and ~10 nm in diameter.

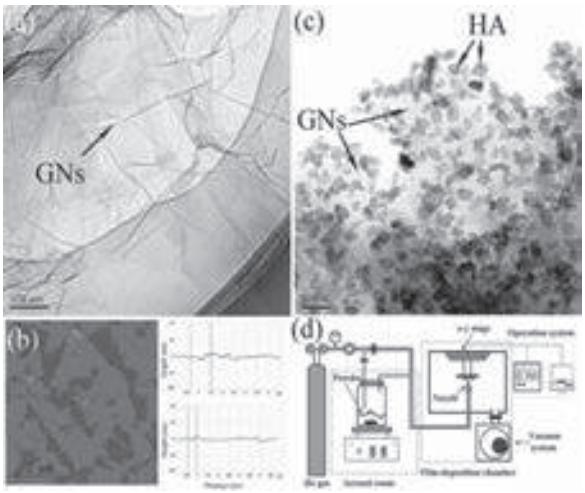

Fig. 1. *Characterization of the GNs and HA-GN composites powder (a,b,c) and schematic depiction of the VCS system.*

Nanostructured HA and HA-GN coatings were successfully deposited by the VCS. As noticed from the TEM images of the coatings (Fig. 2), randomly oriented small HA crystallites in the size of <20 nm can be clearly seen, which are identical to the starting rod-like HA feedstock. Graphene flakes are homogeneously dispersed in HA matrix in the coatings. The cross-sectional morphologies of the coatings show dense microstructure.

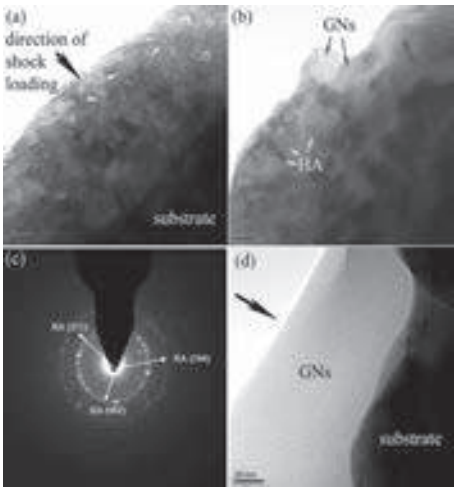

Fig. 2. *TEM images of the HA-1.0wt.%GN coatings*

Unlike other surface coating techniques, VCS offers the advantages associated with room-temperature processing, for example non-changes of the phases in the coatings compared to the starting feedstock (data not shown). Almost identical XRD peaks have been detected from the coatings and the feedstock powder.

2.2 Mechanical properties of the composite coatings

The adhesion of biomedical coating to substrate is one of the crucial factors that affect its long-term functional service after surgery. The adhesive strength of the VCS coatings was assessed by the MST approach. The average normal force ranges from 20 to 45 N, showing irrelevance of adhesion to content of GN in the coatings. On the other hand, the microhardness and elastic modulus of the coatings are improved by the addition of GN. The fracture toughness (K_{IC}) of the HA-1.0 wt.% GN composite reaches 0.42 MPa·$m^{1/2}$, showing ~280% improvement compared to the pure HA coating of 0.11 MPa·$m^{1/2}$. The microhardness and elastic modulus of the HA-1.0wt.%GN coating are 0.22 GPa and 4.25 GPa, respectively, showing marked increase compared to the pure HA coating, 0.17 GPa and 3.05 GPa. An appropriate elastic modulus for the implant is crucial in order to avoid stress shielding and bone resorption, and it also determines the fatigue behavior of the coatings under cyclic loading. The elastic modulus of the HA-GN coating is closer to that of human skeletal bone (~10 GPa).

2.3 In vitro biocompatibility of the composite coatings

To gain clear insight into effect of the addition of GNs on cell responses, the cytotoxity and biocompatibility of the HA-GN coatings were examined by MTT assay. Uncoated Ti samples were used as the control group for this experiment. SEM observation of the cells on the sample surfaces after the incubation time of 3 hrs, 1 day, 3 days, and 5 days suggests that the cells exhibit faster spreading and better stretching state on the HA-based coatings than on bare Ti (data not shown). And more GN in the HA-based coatings resulted in faster recruitment of the cells. The HA-1.0wt.%GN composite coating shows the highest cell proliferation rate (Fig. 3a), suggesting consistent results that GN enhance cell behaviors, apart from their exciting toughening effect on HA. The enhanced spreading of the cells on the GN-containing coatings possibly indicates more adhesion sites on the surfaces of the coatings. In fact, further examination of the spreading of the cells on the HA-GN coatings suggested preferential stretching of the cells to GNs (Fig. 3b). Interestingly, it is noted that filopodia of the cells incline to approach GN, i.e. the filopodia extend primarily all the way to graphene sheets and get anchored by the sheets.

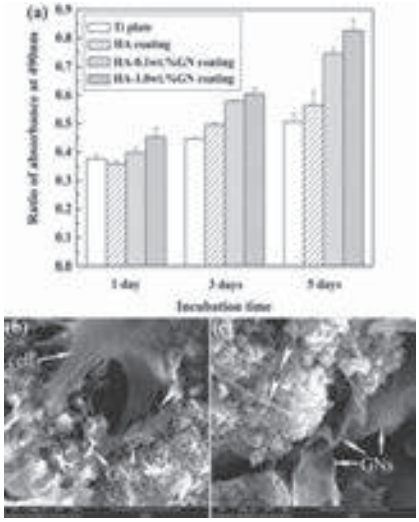

Fig. 3. *Cell culture results for the composite coatings*

3 Conclusions

We successfully deposited HA-GN composite coatings by VCS operated at room temperature. The coatings are uniform in tailorable thicknesses and showed competitive adhesive strength and fracture toughness. Comprehensive microstructural characterization showed that the physical characteristics of the starting feedstocks were completely inherited by the as-deposited coatings without detectable crystal grain growth or phase changes. The GN-containing HA coatings markedly enhanced attachment and proliferation of the osteoblast cells. The fabrication of the novel HA-GN composite biomedical coatings by the cold vacuum spray approach could open doors for processing new nanostructured biomaterials with exceptional properties.

4 References

[1] R.G.T. Geesink, K. de Groot, and C.P. Klein: J. Bone Joint Surg. **70B** (1988) 17-22.
[2] Y.W. Gu, N.H. Loha, K.A. Khor, S.B. Tor, and P. Cheang: Biomaterials **23** (2002) 37-43.
[3] D. Zhang, C. Yi, J. Zhang, Y. Chen, X. Yao, and M. Yang: Nanotechnology **18** (2007) 475102-475110.
[4] K.S. Novoselov, D. Jiang, F. Schedin, T.J. Booth, V.V. Khotkevich, S.V. Morozov, and A.K. Geim: Proc. Natl. Acad. Sci. USA **102** (2005) 10451-10453.
[5] C. Chung, Y.K. Kim, D. Shin, S.R. Ryoo, B.H. Hong, and D.H. Min: Acc. Chem. Rre.(2013), DOI: 10.1021/ar300159f
[6] S. Limin, C.B. Christopher, A.G. Karlis, and K. Ahmet: J. Biomed. Mater. Res. (Appl. Biomater.) **58** (2001) 570-592.
[7] Webster TJ, Siegel RW, Bizios R: Biomaterials **20** (1999) 1221-1227.
[8] J. Akedo: J. Therm. Spray. Techn. **17** (2008) 181-198.

Effect of processing time on the preparation of natural bovine Hydroxyapatite by using Transferred arc plasma torch

C.P.Yoganand[1], K.M. Paraskevopoulos[2] and Dongfeng Xue[3]

[1]Department of Physics, Coimbatore Institute of Technology, Coimbatore-14, India.
[2]Department of Physics, Aristotle University of Thessaloniki, 54124 Thessaloniki, Greece.
[3]State Key Laboratory of Rare Earth Resource Utilization, Changchun Institute of Applied Sciences, Chinese Academy of Sciences, Changchun 130022, China.

Abstract

Hydroxyapatite HA ($Ca_{10}(PO_4)_6(OH)_2$) is well known material which is of considerable interest in dental and medical research. The present methods of preparation of hydroxyapatite range from conventional wet synthesis, solid-state reaction, hydrothermal exchange process and calcination of animal skeletal bone etc. In this work, Natural Hydroxyapatite was derived from skeletal bovine bones by Transferred arc plasma (TAP) processing at 5 kW in argon plasma for different processing times (i.e. 30, 45, 60, 90 and 120 seconds). The Phase and Microstructural characterizations were done by XRD, FT-IR, SEM-EDX and TG-DTA analysis. The effect of TAP processing time on the preparation of organic free HA from skeletal bovine bone was studied. The results indicated that organic free bovine HA was prepared within short time duration (90 seconds) by TAP process.

1 Introduction

Hydroxyapatite (HA), is currently used as biomaterial for many applications in both dentistry and orthopedics, because they it form a real bond with the surrounding bone tissue when implanted. Variety of calcium phosphate-containing materials has been investigated extensively for application in the field of bone repair and regeneration because of their bioactivity to form a bond to living bone for load-bearing positions [1,2]. HA can be produced chemically or from natural resources like corals and bovine bones. Recently, annealing method (i.e. heat treatment) has been suggested as an alternative technique to produce HA from bovine bones. At the material level, bovine bone is composed of organic and inorganic components. The organic part contains mainly collagen and proteins, whereas the inorganic component is mainly HA with a small percentage of other elements being incorporated in the structure such as carbonate, magnesium and sodium. More over the presence of these elements in the HA produced from bovine bones is absent in the case of synthetic HA. The presence of trace elements is very important and plays a vital role in bone metabolism process. The annealing method of HA synthesis usually takes a few to many hours of thermal treatment during which the organic materials in the bovine bones gets removed leaving pure inorganic HA as the residue [3,4]. The present study was aimed at preparing HA from bovine bone through transferred arc plasma processing method within short time duration. Besides that, in this study it was also attempted to determine the effect of different processing times. Our observations based upon the studies of the process are presented and discussed.

2 Methodology

HA was obtained by plasma processing of the natural bovine bones. The bones were deproteinized with reagent grade NaOH treatment (1 hour) and were cut into pieces (lxb~2cmx1cm) was used for plasma processing at 5 kW of plasma power in argon plasma for different processing times. A dc transferred arc plasma torch which can be operated at a maximum power of 10 kW was used for the purpose (Figure.1).

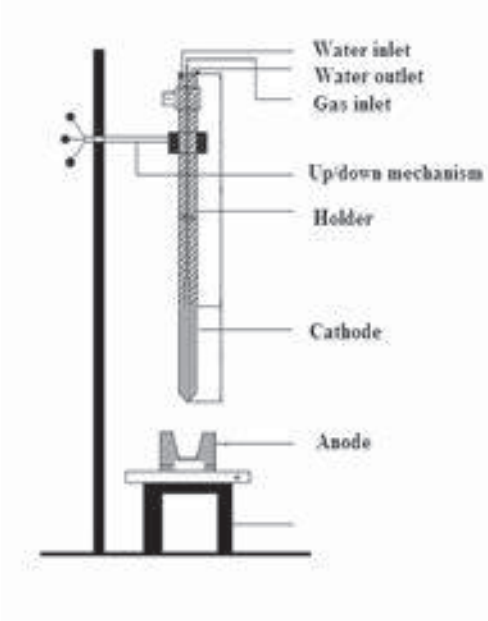

Figure.1:Schematic of TAP torch.

The arc is typically struck between the cathode and the anode by applying a high current arc between the cathode and the anode (at an electrode gap of about 25mm) and the desired power level was maintained by controlling the flow rate of the plasma gas and the arc current. Plasma was generated and the bovine bone was processed by varying the melting times for 30, 45, 60, 90 and 120 seconds respectively. The effect of TAP processing time on the formation of HA from organic bovine bone was studied. The operating parameters are given in Table 1.

Torch type:	Tranferred arc
Input power:	5 kW dc
Plasma Gas and flow rate:	Argon; 10 lpm
Cooling water flow rate:	12 lpm
Processing time:	30,45,60,90&120 seconds
Quenching medium:	air

Table.1: Operating parameters.

.

The samples were characterized by Fourier transform infrared spectroscopy (FTIR), Scanning electron microscopy with Energy dispersive X-ray spectroscopic analysis (SEM-EDX), Thermo gravimetric differential thermal analysis TG-DTA and X-ray diffractometry.

3 Results and discussion

A direct observation was made upon TAP processing for different processing time, there was colour change of the sample with respect to processing time. The colour of the as-prepared bovine bone was light yellow. Upon TAP processing for 30, 45, 60, 90 and 120 seconds the colour of the samples changed from yellow to grey and then to white. This series of colour change is believed to be associated with the burn out process of organic matrix (e.g. protein and collagen) in the bovine bone. The darker colours observed for samples at 30 and 45 seconds of TAP processing indicated incomplete removal of organic compositions [5]. However, for more than 60 seconds of plasma processing, the samples were white in colour, suggesting complete removal of organic substances. The XRD pattern of the samples processed at 45, 60, 90 and 120 seconds exhibited a substantial increase in peak height and a decrease in peak width, thus indicating an increase in crystallinity.

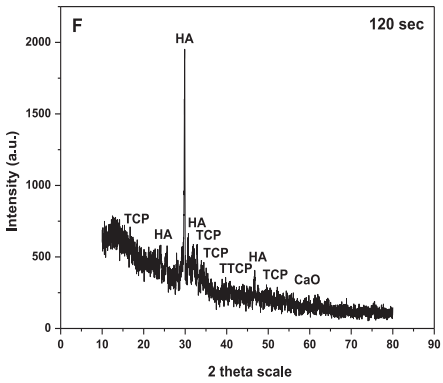

Figure.2:XRD pattern of 120 seconds TAP processed bovine bone.

However, the XRD pattern of the 120 seconds processed sample (Figure.2) showed the diffraction peaks of tricalcium phosphate (TCP), tetracalcium phosphate (TTCP) and CaO, respectively [6]. This may be due to the chemical transformation involved due to the prolonged TAP processing. From the FTIR spectra in general it was noticed that a large number of bands in all the spectra's corresponded to the standard spectral range (3571–3572 cm^{-1}, 3422.3–3425.1 cm^{-1}, 2072 cm^{-1}, 2002 cm^{-1}, 1411–1457 cm^{-1}, 1044–1049 cm^{-1}, 959– 962 cm^{-1}, 631 cm^{-1}, 601–601 cm^{-1}, 568–571 cm^{-1}, 472–473 cm^{-1} and 425–426 cm^{-1}) and matches with the bands in the HA reference spectrum [7]. The EDX analysis results indicated that the inorganic phases of all the samples were mainly composed of Ca, P and O as the major constituents with some minor components like Na, Mg, Al, Si, S, Cl and K.

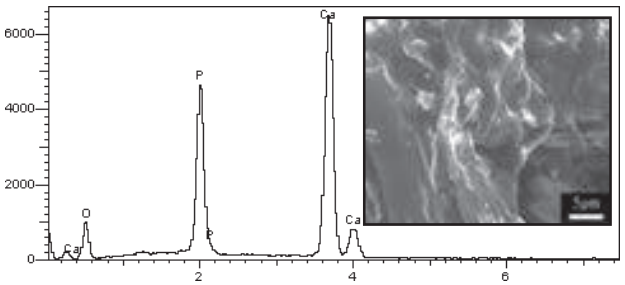

Figure.3:EDX and SEM image of 90 seconds TAP processed bovine bone.

The DTA of HA produced by TAP method (90 seconds) confirm its thermal stability and formation. It is observed in SEM that the microstructure of raw bone is highly dense which may be due to the presence of organic components. The processed samples exhibited almost much similar micromorphology (Figure.3). The EDX study indicated that 90 seconds of TAP processing was more beneficial in HA production with a Ca/P ratio of 1.93 which was well in accordance with the commercially available natural HA-Endobon powder [8].

4 Conclusion

The study indicated that 90 seconds of TAP processing was much beneficial in production of phase pure HA from the bovine bone and the method suggested production of HA from natural resources. Further the processed HA powder was powdered by using mechanical milling and seiving which could enable it to be used as a feed stock powder for thermal spraying for biomedical implant applications.

5 References

[1] Tadashi Kokubo: Biomatenals.12 (1991)155-163.
[2] S.W.K. Kweh, K.A. Khor and P. Cheang: J. Mater. Technol. 89 (1999) 373-377.
[3] G. Goller, F.N. Oktar, L.S. Ozyegin, E.S. Kayali, E. Demirkesen: Mat. Lett. 58 (2004) 2599-2609.
[4] M.R. Mucalo, D.L. Foster, B. Wielage, S. Steinhaeuser, H. Mucha, D. Knighton and J.Kirby: J. Appl. Biomater. Biomech. 2 (2004) 96-104.
[5] C.Y. Ooi , M. Hamdi and S. Ramesh: Ceram. Int. 33 (2006) 1171–1177.
[6] K.A. Gross and C.C. Berndt: J. Biomed. Mater. Res. 39 (1998) 580–587.
[7] S.Joschek, B.Nies, R.Krotz and A.Gopferich: Biomaterials. 21(2000)1645-1658.
[8] J.R.Sharpe, R.L.Sammons and P.M. Marquis: Biomaterials.18 (1997)471-476.

Co-spraying of lanthanum phosphate- alumina: coating composition and properties

Vandana Chaturvedi[1], P.V.Ananthapadmanabhan[1]*, Y.Chakravarthy[1], A .Pragatheeswaran[2].
[1]Laser and Plasma Technology Division, Bhabha Atomic Research Center, Trombay, Maharastra, India-400085
[2]Department of Physics, Karunya University, Coimbatore, Tamilnadu, India-641114
*Corresponding author. Tel.: +91-22-25595107; *E-mail address:* pvananth@barc.gov.in (P.V. Ananthapadmanabhan).

Abstract
Plasma-sprayed coatings of lanthanum phosphate–alumina (60:40 & 80:20 by weight) have been prepared under different operating parameters. The coatings have been characterised with respect to chemical composition, phase composition, adhesion strength and microhardness. Hardness of the plasma sprayed coatings was found to increase with power and wt% of alumina. XRD shows increase in alumina in the coatings with plasma input power. Partial conversion of $LaPO_4$ to La-polyphosphate and La-oxy phosphates was also observed in the coatings. SEM of the coating cross section shows no detachment of the coating from the substrate. EDX results show the segregation of phases in the coating. By choosing the proper combination of power and weight ratio, the spray process can be optimised to obtain a targeted coating composition. Adherent coatings of $LaPO_4$-Al_2O_3 could be deposited onto substrates by atmospheric plasma spray technique.

1. Introduction:

By virtue of its thermal stability, high thermal expansion coefficient and low thermal conductivity, $LaPO_4$ is considered as a potential material for thermal barrier coating applications. It has also good corrosion resistance in environments containing sulphur and vanadium salts and is reported to be non-reactive with many molten metals [1]. In radioactive waste disposal, RE phosphates are considered as potential matrices for the specific conditioning of separated long-lived radionuclides, such as trivalent actinides [2]. Plasma spraying involves injection of metallic or ceramic particles into the plasma jet, where they undergo rapid melting and are accelerated to high velocities. These molten droplets moving at velocities exceeding 100 m/s impact on the surface of the substrate, forming an adherent coating [3,4]. We need to ensure that all the particles injected into the plasma stream penetrate the plasma and are completely molten. However, the particle size distribution of the feedstock powder makes it difficult to achieve this. Powder blend spraying often leads to particle segregation due to the differences in thermo-physical properties, particle diameter, density, etc. This can lead to poor coating properties. We need to control the process parameters and powder characteristics to obtain the required coating composition and properties.

The present study was carried out to illustrate the use of a mixed coating of $LaPO_4$-Al_2O_3 in preference to pure lanthanum phosphate. However, due to the differences in the melting point, specific heat and latent heat of fusion of lanthanum phosphate and alumina as well as the difference in their particle sizes, the chemical composition of the coating can be significantly different from that of the starting material, leading to undesirable coating characteristics.

2. Experimental methods

The powders ($LaPO_4$-Al_2O_3) were mixed in appropriate amounts to give two compositions consisting of 20 wt.% Al_2O_3 and 40 wt.% Al_2O_3 respectively. A 40 kW DC plasma torch was used for coating. Free flowing $LaPO_4$-Al_2O_3 powder, prepared as described above, was stored in a powder feeder and injected into the plasma jet by means of a carrier gas. The powder was injected through a side port on the torch nozzle.

Table1: *Operating parameters for plasma spray*

Parameter	Value
Torch input power (kW)	16 and 20
Plasma gas (Ar) flow rate (SLPM)	30
Secondary gas ($_{N2}$) (SLPM)	3
Powder feed rate (g/min)	10
Powder carrier gas flow rate (SLPM)	8
Torch–base distance (mm)	100

3. Characterization: X-Ray diffraction was used to identify the different phases present in the coatings. The microhardness of the coatings was measured using a standard Vickers hardness tester. SEM and EDX were also done to see the microstructure and composition.

4. Results and Discussion

4.1 X-Ray diffraction

Figure 1 shows the x-ray diffraction patterns of the starting powder and the coated specimens. The XRD profile of the feedstock powder corresponds to lanthanum phosphate (monoclinic phase) and alpha alumina. On the other hand, the coatings showed $LaPO_4$ (monazite) as the major phase. However, partial conversion of $LaPO_4$ to La-polyphosphate and La-oxy phosphates was also observed in the coatings. As compared to the feedstock powder pattern, alumina peak intensity was found to be lower for both 20 wt% alumina and 40wt % alumina samples deposited at 16 kW. However, at 20 kW alumina peak intensity was found to increase. The deposition efficiency of feedstock powder mainly depends on the melting point, specific heat, particle size distribution and input plasma power. The results here show that a significant fraction of unmelted alumina particles, which bounce off the substrate surface at lower power levels, leading to enrichment of lanthanum phosphate in the coating.

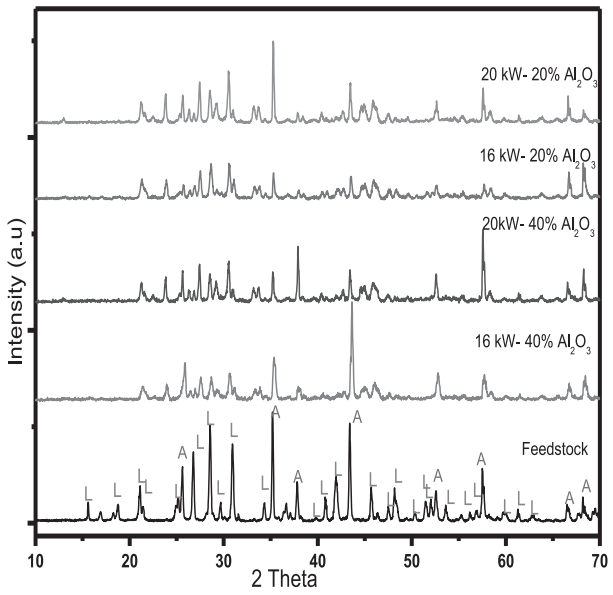

Fig 1. *XRD of feedstock powder and plasma deposited $LaPO_4$-$Al_2O_3$with JCPDS cards LaPO4 (84-0600) and Al_2O_3 (89-7716).*

4.2 Scanning Electron microscopy (SEM)

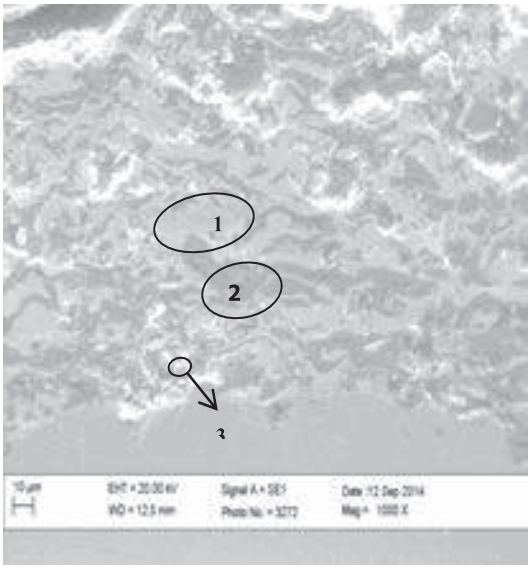

Fig 2. *Cross section SEM image of plasma spray deposited at 20 kW (20 wt % alumina*)

The microstructure of sample with 20 wt% alumina deposited at 16 kW is shown in figure 2.There is no detachment or de-lamination between the substrate and coating and the microstructure indicates good coating adhesion with the substrate. The microstructure across the coating cross-section shows fully molten lamellae, un-melted particles and molten spherical particles characteristic of plasma spray deposited coatings. The molten lamellae of $LaPO_4$ and Al_2O_3 are identified in conjunction with EDX. The molten lamella of $LaPO_4$ (bright, maked as 1.) and Al_2O_3 (dark, marked as 2) were evenly distributed across the microstructure. The SEM image also shows alumina spherical particles (marked as 3) trapped between lamellae. These inter-lamellar spherical deposits did not have sufficient velocity to flow and spread. The figure also shows that there is no such spheroidized $LaPO_4$ particle.

5. Conclusions:

Adherent coatings of $LaPO_4$-Al_2O_3 could be deposited on stainless steel substrates by plasma spray technique. The coatings were found to consist of $LaPO_4$ (monazite) and alumina along with La- polyphosphate and La-oxy phosphates in minor amount. Hardness of the plasma sprayed coatings was found to increase with power and wt% of alumina. SEM analysis of the coatings showed microstructures typical of plasma sprayed coatings with molten, partially molten lamellae and porosity. EDX results show the segregation of phases in the microstructure.

Acknowledgement

The authors express their gratitude to Dr. L.M. Gantayet, Group director, BTDG and Dr. K Dasgupta, Head, L&PT Division, BARC for their constant support.

References

[1] X.Q. Cao, R. Vassen, D. Stoever, J. Eur. Ceram. Soc. 24 (2004) 1-10.

[2] J. McCarthy, W.B. White, D.E. Pfoertsch, Mater. Res. Bull. 13 (1978) 1239–1245.

[3] R.B. Hiemann, Plasma-Spray Coating—Principles and Applications,VCH Publishers Inc, New York, USA, 1996.

[4] D. Matejka, B. Benko, Plasma Spraying of Metallic and Ceramic Materials, John Wiley & Sons Ltd, Chichester, UK,1989.

Influence of particle state diagnostics on microstructure of Plasma Sprayed nanocomposite LaCeYSZ coatings

S. Mantry[1], *B.B.Jha*[1*], *R.K Sahoo*[1]
[1]CSIR-Institute of Minerals & Materials Technology, Bhubaneswar 751013, Odisha, India
[*]*Corresponding Author: bbjha59@yahoo.com*

Abstract—

This article describes the effect of controlling in-flight hot particle characteristics on properties of plasma sprayed nanostructured yittria stabilized zirconia (YSZ) coatings doped with $La_2Ce_2O_7$. This article reports the dependence of properties of as-sprayed coatings on in-flight particle temperature and velocity prior to impact the substrate. Particle temperature measurement is based on two-colour pyrometry and particle velocities are measured from the length of the particle traces during known exposure times. The properties which depend on the microstructure are studied in detail. The adhesion strength is measured at different particle states and the effect on microstructure is presented. FESEM results revealed that morphology of coating exhibits bimodal microstructure consisting of nano-zones reinforced in the matrix of fully-melted particles. Maximum adhesion strength of 43.73 MPa has been experimentally found out by selecting optimum levels of particle temperature and velocity. The enhanced bond strength of as-sprayed nanocomposite coatings may be attributed to higher interfacial toughness due to cracks being arrested by embedded nano-zones.

Keywords- *Nanozones, Spray diagnostics, Plasma Spraying, Adhesion*

INTRODUCTION

Plasma sprayed coatings based on yttrium stabilized zirconia (YSZ) are considered to be best suitable for thermal barrier applications due to its low density, high hardness, low thermal conductivity [1]. All above properties are depending upon the microstructure of the ceramic system. Hence it is very much important to have a control over the particle state to achieve the required microstructure and properties in coatings by identifying the particular process parameters, so that reproducibility of the same microstructure and properties can be achieved. The important control parameters in plasma spraying are the flow rates of plasma and powder carrier gas, torch input power, dwell time and powder feed rate. There have been a few reports regarding the studies on structural, micro-structural, thermal and mechanical properties by controlling particle velocity and temperature [2]. However, an optimum condition is not set properly to have a better understanding to control all those control parameters. Amongst the parameters of utmost interest are the particle temperature and velocity distributions, size distribution of particles prior to the impact on the substrate. These parameters play an important role in enhancement of interfacial bond strength of nanostructured coatings as compared to conventional coatings. The presence of dense nano zones will have an important influence on their mechanical properties and the microstructure depends on particle temperature and velocity. In this article, an attempt has been made to address the effect of controlling in-flight hot particle characteristics (monitored by CCD camera) on adhesion strength of as-sprayed $La_2Ce_2O_7$ doped YSZ coatings on Inconel 718 substrates.

Synthesis of nanostructured powders by sol-gel route

The nanostructured YSZ and $La_2Ce_2O_7$ powders employed in this study were synthesized through a sol-gel technique [3]. Both the powders were mixed and heated at 1400 ^oC. The calcined powders were taken as the raw ingredients for the plasma spray process.

Coating material

Nano-sized powder of 8LaCeYSZ [YSZ (5.4 wt. % Y_2O_3–ZrO_2) + 8 wt. % $La_2Ce_2O_7$] was plasma sprayed on to Inconel 718 substrates. The finely dispersed nano particles were made agglomerated to a size of ~ 30–100 µm as required for plasma spraying. The nano particles were agglomerated by the spray drying technique. The process is described elsewhere [4]. The final product is a feedstock of size ~50 µm spherical agglomerates containing nano grains of size 20-30 nm as shown in Fig.1.

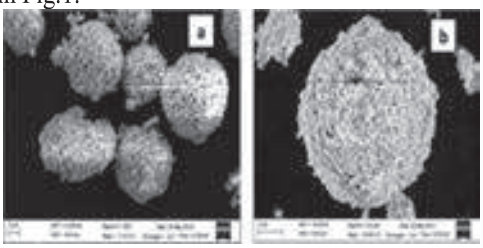

Fig.1. *FESEM micrograph of spray dried LaCeYSZ particles*

Development of coatings

The coating process was carried out at CSIR-IMMT, Bhubaneswar using an 80 kW plasma spray system supplied by M/s Metallization, U.K. The process parameters are listed in Table 1. The number of passes was kept constant for each sample in order to make thickness of all coatings (~150 µm) within similar range.

Table 1. *Operating Parameters for Plasma spraying process*

Parameter	Operating Range
Operating Power	38 kW
Current	865 amps
Primary gas (Argon) flow rate	40 lpm
Secondary gas (Hydrogen) Flow rate	0.5 lpm
Carrier Gas flow rate	5 lpm
Nozzle to substrate distance	80 mm
Powder feed rate	25 g/ min

Adhesion Strength

To evaluate the coating adhesion strength, universal testing machine (make: INSTRON 8801) was used. The test was conducted by the pull-out method (shown in Figure 2) as per ASTM C633 standard using two cylindrical specimens.

Fig.2. *Plasma spraying torch with particle diagnostics and adhesion test set-up as per ASTM C-633 standard*

Online Particle Diagnostics

Online diagnostics using Spray watch 2i equipment were carried out at different spray conditions to measure the particle velocity and temperature. Distance of the camera from the spray gun was kept between 150 and 200 mm. Particle temperature determination is based on the two-color pyrometry and in-flight particle velocities are measured from the length of particle traces during known exposure times using a single high speed CCD camera [5]. The average particle temperature is 2650 ± 50 °C and velocity prior to impact is 200 ± 50 m/sec, which is below the melting point of YSZ.

Adhesion Test Results

Adhesion strength for as-sprayed coatings with the variation of particle temperature and velocity is shown in Fig. 3 (a & b), keeping other process parameters constant. It is found that bond strength increases from 2550± 50 °C to 2650± 50°C and then decreases after 2700°C (~ melting point of feed stock). Similarly it is maximum at particle velocity of 240 m/sec and seems to attain minimum value at 220 m/sec (may be fully melted) and 280 m/sec (may be un-melted). A series of coating are developed in the broad range of temperature and velocity. The maximum adhesion strength of LaCeYSZ nanocomposite coating is found to be 43.73 MPa at 40 kW torch input power corresponding to particle temperature of 2686 °C and velocity of 241.6 m/s. The test results for the adhesion of the APS nano YSZ-coated substrate using Taguchi's L_{16} orthogonal design along with the corresponding S/N ratios is described elsewhere, where maximum adhesion strength is found to be 40.56 MPa [6]. The enhancement of adhesion strength compared to nano YSZ coatings is attributed to the compactness and uniform microstructure of as-sprayed coatings and formation of La and Ce diffusion layers within the splats.

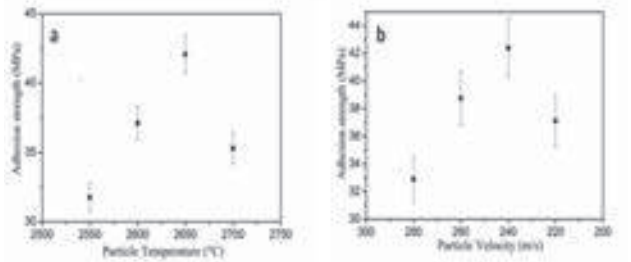

Fig.3 (a &b) *Variation in adhesion strength with Temperature & velocity of agglomerates prior to impact on the substrate*

Surface Morphology Analysis

The field emission scanning electron micrographs of YSZ-$La_2Ce_2O_7$ nanocomposite coatings are shown in Fig.4, which represents bimodal microstructure consisting of dense and smooth zones, indicating good molten state of particles and the rough and porous zones, indicating unmolten or semi-molten state of particles (Fig. 4a).

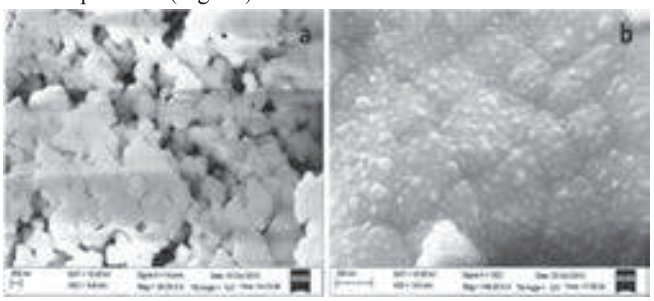

Fig.4. *FESEM micrographs of LaCeYSZ nanocomposite coatings (a) at particle temperature 2500 ± 50 °C and particle velocity 280 m/sec , (b) at particle temperature 2650±50 °C and particle velocity 240 m/sec*

The micrographs (Fig.4 a, b) show densely packed nanograins having average grain size of ~ 90-120 nm. The grains are very closely packed with development of distinct grain boundaries without having any voids and porous structure (Fig. 4b). In Fig. 4b, it is found that, the grains are clearly visible and suggests presence of nanozones on the surface, but micro-pores are present, indicating the presence of some amount of unmolten particles.

4. Conclusions:

Successful coating deposition of nanocomposite LaCeYSZ powder by plasma spraying route is possible on Inconel 718 substrates. Particle temperature and velocity seems to be most significant parameter affecting adhesion. Optimum adhesion strength of 43.73 MPa has been experimentally found out at 40 kW torch input power corresponding to particle temperature of 2686 °C and velocity of 241.6 m/sec. Micrograph of surface reveals the average grain size to be in the range of ~90-120 nm. The grains are very closely packed with distinct grain boundaries. The grains are interconnected with tetragonal grain boundary junctions. In summary the enhancement of adhesion strength may be attributed to compact structure and high toughness of embedded nanozones.

Reference:

1. Michael R. Winter and David R. Clarke, J. Am. Ceram. Soc., 90 (2) (2007), 533–540.
2. J.R. Fincke, D.C.Haggard and W.D. Swank, J. Therm. Spray. Technol, 10(2) (2001), 255-266
3. R.E. JuaÂ rez, D.G. Lamas, G.E. Lascalea et al., J Eur ceramic Soc, 20 (2000), 133-138.
4. S, Mantry, A. Mandal, D.K Mishra et al., J Therm spray Technol., 23(7), (2014), 1073-1080
5. J. Vattulainen, E. Ha¨ma¨la¨inen, R. Hernberg, P. Vuoristo, T. Ma¨ntyla, J.Therm. Spray Technol., 10 (1) (2001), 94-104
6. Sisir Mantry, B. K.Mishra, M. Chakraborty, The Scientific world journal, (2013), Article No: 527491.

Development of a Novel Synthesiser for Antimicrobial Thermal Spray Coating for Food Processing Machineries/Equipments

Ramakrishna A

Head (RA), Defence Food Research Laboratory, DRDO, Mysore-570 011, INDIA

Antimicrobial surface coated food processing machineries/equipments is a promising field for all food processing industries from small to medium to automated MNC's, and to be one of the novel approaches to prevent contamination of bacteria on the surface of food processing machineries . An ideal solution to the food industry for food safety and environment problems is to incorporate antimicrobial coatings into the food contact surfaces of the machineries. An effort has been made to develop synthesiser for production of antimicrobial agents and thermal spray coated on the surfaces and were shown to inhibit the food spoilage bacteria. The chemical composition, microstructure, and surface morphology of composite silver and copper coatings were characterized TEM and SEM. Determination of thickness; adhesions, scratch resistance and porosity of the coating were investigated. The antibacterial property of composite coatings was analyzed by both gram negative and gram positive organisms. The antibacterial performance of coatings was compared to that of stainless steel 304, 316L and commercially available materials. Results indicated that the thermally sprayed composite coatings have excellent antibacterial behaviour compared to stainless steel and are discussed.

Development of porous plasma sprayed molybdenum carbide-based anode layers with various metal oxide precursors for SOFC

Nadimul H Faisal[1,2*], Rehan Ahmed[2,3], Sai P Katikaneni[4], Stamatios Souentie[4], Mathues F A Goosen[5]
[1] School of Engineering, Robert Gordon University, Garthdee Road, Aberdeen, AB10 7GJ, UK
[2] College of Engineering, Alfaisal University, P.O. Box 50927, Riyadh 11533, Saudi Arabia
[3] School of Engineering and Physical Sciences, Heriot-Watt University, Edinburgh, EH14 4AS, UK
[4] Research & Development Center, Saudi Aramco, Dhahran 31311, Saudi Arabia
[5] Office of Research & Graduate Studies, Alfaisal University, P.O. Box 50927, Riyadh 11533, Saudi Arabia

Abstract
Air plasma sprayed (APS) coatings provide an ability to deposit a range of novel fuel cell materials at competitive costs. This work therefore develops three different types of composite porous anodes (Mo-Mo_2C/Al_2O_3, Mo-Mo_2C/ZrO_2, Mo-Mo_2C/TiO_2) using a combination of APS process parameters within the identified range on Hastelloy®X interconnect substrates for potential application in intermediate temperature range proton conducting solid oxide fuel cells (PC-SOFC). Commercially available carbide of molybdenum powder catalyst (Mo-Mo_2C) and three metal oxide precursors (e.g., Al_2O_3, ZrO_2, TiO_2, all beneficial for catalyst stability) were used to prepare three composite feedstock powders (Mo-Mo_2C/Al_2O_3, Mo-Mo_2C/ZrO_2, Mo-Mo_2C/TiO_2) to fabricate three different anodes. Each of the modified composition anode feedstock powders included a stoichiometric weight ratio of 4:1. We report herein that an optimized anode layer of 200 µm to 250 µm thickness and a porosity as high as 20% are controllable by a selection of the APS process parameters with no addition of a sacrificial pore forming material. The morphological features, crystallinity, and the phases of the powders and developed coatings were characterized by scanning electron microscopy (SEM) and energy dispersive X-ray spectroscopy (EDS) of relevant surfaces were performed to determine the material properties.

1 Introduction

The development of low-cost fuel cell materials with high durability and lower operating temperatures is the key technical challenge facing solid oxide fuel cell (SOFC) technology. The future of SOFC technology depends upon the development of new materials (electrode, electrolyte, interconnects) which can be used to manufacture SOFC's in a cost effective manner. SOFC present a number of inherent challenges. Low mechanical strength, slow start-up time (i.e. in minutes), and serious anode deterioration represent some of these inherent challenges. The high operating temperatures (600-1000 ^oC) place additional durability requirements on SOFCs materials [1-4]. The development of low-cost materials with high durability at lower operating temperatures is the key technical challenge facing SOFC technology. Reducing the operating temperature to intermediate range can lower the cost but also reduce the reaction rate [3]. Some of the recent articles [4-8] summarize most of the known SOFC materials (electrodes, electrolytes, interconnects) and their manufacturing alternatives, relevant to modern requirements. However, the scope of this work is to present a development of air plasma sprayed (APS) new anode materials for SOFC systems.

2 Materials

Hastelloy®X: The Hastelloy®X material was chosen as a disc substrate (interconnect in SOFC). The disc substrates (20 mm diameter and 4.76 mm thick) were supplied by Haynes International Limited, Manchester, UK.
Mo-Mo_2C: The Mo-Mo_2C feedstock powder material (Fig. 1) was an agglomerated and sintered spheroidal powder designed for coating application using atmospheric plasma spray (APS). This powder material (Metco 64) was supplied by Sulzer Metco, Germany. It consists of Molybdenum and Mo_2C with nominal particle size distribution of -90+38 µm. It produces coatings that are harder and more resistant to abrasion while maintaining many of the useful properties of pure molybdenum coatings, such as high scuff resistance, low frictional characteristics and high toughness.

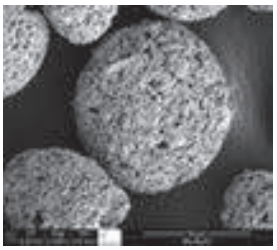

Fig. 1. *Agglomerated/sintered Mo-Mo_2C powder showing high porosity and surface area [50 µm scale marker]*

Al_2O_3: The white alumina (Al_2O_3) feedstock powder material was available in a wide variety of shapes (fused and crushed) and sizes with angular and blocky morphology. Alumina is a hard, wear resistant material that is chemically inert and stable at high temperatures. In addition, the high purity grades exhibit excellent electrical insulation (dielectric characteristics) and thermal conductivity. This powder material (METCO-105SFP) was supplied by Sulzer Metco, Germany. Alumina can improve electrical properties by grain boundary modification.
ZrO_2: The Zirconia (ZrO_2) feedstock powder material was available in a wide variety of shapes and sizes. Zirconia is stable in oxidizing and mildly reducing atmospheres. It reacts with carbon, nitrogen and hydrogen at temperatures above 2200 °C. It is inert to acids and bases at room temperature with the exception of HF and does not react with the refectory metals up to 1400 °C. This powder material (40453) was supplied by Alfa Aesar, UK. which consists of Zirconium(IV) oxide, calcia stabilized, 99.4% (metals basis excluding Hf). Stabilized zirconia is used in

oxygen sensors and fuel cell membranes because it has the ability to allow oxygen ions to move freely through the crystal structure at high temperatures. This high ionic conductivity (and a low electronic conductivity) makes it one of the most useful electroceramics.

TiO_2: The dark grey to black titanium oxide (TiO_2) feedstock powder material was available in a wide variety of shapes (fused and crushed or agglomerated and sintered) and sizes with angular, blocky or spheroidal morphology. Titanium oxides are used for a wide variety of applications that include wear resistant coatings and electrically conductive coatings. This agglomerated/sintered and spheroidal powder material (METCO-6231A) was supplied by Sulzer Metco, Germany. The addition of TiO_2 can improve electrical properties by grain boundary modification. This powder can be designed to produce coatings with low electrical resistivities and potentially superior tribological properties.

3 Air plasma spraying of SOFC anode layers

The carbide of molybdenum powder catalyst (Mo-Mo_2C) and three metal oxide precursors (e.g., Al_2O_3, ZrO_2, TiO_2, all beneficial for catalyst stability) were used to prepare three composite feedstock powders (Mo-Mo_2C/Al_2O_3, Mo-Mo_2C/ZrO_2, Mo-Mo_2C/TiO_2) to fabricate three different anodes. Each of the modified composition anode feedstock powders included a stoichiometric weight ratio of 4:1. The substrate (Hastelloy®X) was grit blasted using 100-250 µm size quartz particles. Coating process parameters which have greater influence on coating thickness, coating hardness, porosity level coating withstanding capability were identified from published literature. Various experiments were conducted to determine working range of above factors. Three controllable parameters namely angle, current, hydrogen flow, spray distance and feed rate were indentified and air plasma spraying was carried out by varying the parameters as prescribed by the design matrix and coatings were produced over Hastelloy®X substrate. Plasma spray deposition was carried out using an APS system (Metco 3MB gun and the nozzle used is a 3M 7A GP, Sulzer Metco). The powders were directly sprayed on to the grit blasted substrate and bond coat was not used. Different combinations of APS process parameters were used to carry out the trial runs. To fix the limits of the considered factors, a key criteria that the anode layer must have high porosity were adopted. Finally, an optimised process parameters chosen for each anode layers (Mo-Mo_2C/Al_2O_3, Mo-Mo_2C/ZrO_2, Mo-Mo_2C/TiO_2) are (current: 500 A, auxiliary H_2 gas flow: 60%, spray distance: 4 inch, powder feed rate: 70 $g.min^{-1}$, spray angle: 30°).

4 Results and discussion

In scanning electron micrographs (Fig. 2) the presence of high surface connected porosity was observed. An elemental analysis was performed on the coating surface in order to determine the distribution of the elements in different region of the coatings. We report herein that an anode layer of 200-250 µm thickness and volumetric porosity as high as 18-20% for Mo-Mo_2C/Al_2O_3 and Mo-Mo_2C/TiO_2 and around 16% for Mo-Mo_2C/ZrO_2, all controllable by a selection of the APS process parameters with no addition of a sacrificial pore-forming material. The reduced thickness (e.g. 250 µm through thermal spraying as opposed to high thickness due to casting) and high porosity of anode layer can potentially lead to an increment of gas permeability and it can also results in a high flux of fuel to the anode/electrolyte interface and of the produced H_2O away from this interface [2,4]. Hence, pore structure and permeability factor are very important for the proper operation of the anode and the whole of SOFC [5-8]. For that reason, further characterisation of the combined microstructure and its parameters, e.g. total porosity, open porosity, pore size distribution, as well as gas permeability can be used as control parameters for the development of highly permeable anode material.

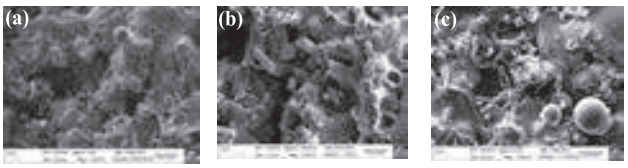

Fig. 2. *APS coated anode layers: (a) Mo-Mo_2C/Al_2O_3, (b) Mo-Mo_2C/ZrO_2 and (c) Mo-Mo_2C/TiO_2 [10 µm each scale marker]*

5 Conclusions

Thermal spraying process can enable the control of porosity in SOFCs which can be used to control gas permeability in anode layer. This investigation indicates that the Mo-Mo_2C/Al_2O_3 and Mo-Mo_2C/TiO_2 anode layer of 250 µm thickness and volumetric porosity as high as 20% is controllable by a selection of the APS process parameters with no addition of a sacrificial pore-forming material. The process parameters developed through this work paves a way for further development of other composite layers. The microstructures and basic electrochemical properties of the anode coatings were analyzed which showed features consistent with the desired properties.

6 Acknowledgement

This work has been supported by the project titled "Advance anode materials for direct hydrocarbon proton conducting solid oxide fuel cell (PC-SOFC) in auxiliary power unit", funded by Saudi Aramco (Contract number 6000074197).

7 References

[1] Hydrogen & Fuel Cells: Review of National R&D Programs, International Energy Agency, 2004.

[2] S. McIntosh and R.J. Gorte, Chem. Rev. **104** (2004) 4845-4865.

[3] Z. Shao, S.M. Haile, J. Ahn, P.D. Ronney, Z. Zhan and S.A. Barnett, Nature **435** (2005) 795-798.

[4] F. Tietz, H.P. Buchkremer and D. Stöver, Journal of Electroceram **17** (2006) 701-707.

[5] R. Hui, Z. Wang, O. Kesler, L. Rose, J. Jankovic, S. Yick, R. Maric and D. Ghosh, Journal of Power Sources **170** (2007) 308-323.

[6] K.C. Wincewicz and J.S. Cooper, Journal of Power Sources **140** (2005) 280-296.

[7] S.M. Haile, Acta Mater. **51** (2003) 5981-6000.

[8] B.D. White, O. Kesler and L. Rose, Journal of Power Sources **178** (2008) 334-343.

Recent Development in HVOF system for ID Coating

Ankur Modi, S.C Modi, Rohit Upadhyaya

Metallizing Equipment Company Private Limited, Jodhpur

Thermal spraying, a group of coating processes in which finely divided metallic or nonmetallic materials are deposited in a molten or semimolten condition to form a coating. The coating material may be in the form of powder, ceramic-rod, wire, or molten materials. Thermal spray processes are classified into four major categories – flame, plasma arc, electric arc and cold spray-with many of their subsets

Thermal spraying operations are normally executed with 90° spray angle. It is easy to apply the thermal spray coating on regular shape or flats plates. But actual industrial component like hydro plant are large and the runner blades or buckets, helicopter component are not flat, it is therefore difficult to do coating. However, only a few studies of spraying system on complex geometries without changing the microstructure, mechanical, physical and chemical properties of coatings.

The following section is a brief review of the previous investigations carried out in this field with special attention being paid to the investigation carried out on thermal spray coating parametric, microstructural, gun, wear and corrosion experimental studies.

Thermal Spray Coating For Blast Furnace Tuyere

Abhishek Pathak[1], Debadutta Prusty[1], G. Sivakumar[2], J. Shalini[2], M Dutta[1]
[1] Research & Development, Tata Steel Ltd., Jamshedpur 831 001, India
[2] Center of Engineered Coatings, ARCI, Hyderabad 500 005, India.

Abstract
Blast furnace tuyeres are exposed to extreme service conditions like thermal damage (by splashing of molten metal/slag), erosive damage (by falling burden material) and the damage due to ensuing corrosive gases which collectively reduce tuyere life which could lead to explosion in blast furnace. Recently, thermal spray coatings by air plasma and detonation spray have emerged as effective solutions to mitigate the damage caused by the operating challenges. In the present work, five different ceramic coatings deposited on copper substrate are assessed. Investigation consisted of thermal cycling, hot corrosion, ΔT (temperature drop) test, porosity, erosion and microhardness. Amongst the coatings tested, detonation sprayed Alumina-Zirconia coating demonstrated best microhardness, thermal cycling, hot corrosion and wear resistance properties, with moderate thermal conducitivity and porosity making it a suitable coating for blast furnace tuyere coatings.

1 Introduction

Blast furnace tuyere is used for injecting hot air (~1200°C) and pulverized coal into the furnace. It is typically manufactured from high thermal conductivity copper and is necessarily, water cooled. It operates under severe working conditions and combustion temperature near the tuyere is around 2200°C [1,2]. Although it is provided with extensive water cooling arrangements to avoid any thermal damage, there are possibilities of severe thermal damage due to sudden rise in temperature on account of premature combustion of fuel inside the tuyere[1,2]. Erosive impact from molten slag and falling burden (coke, iron ore, sinter, pellets, etc.) material causes mechanical damage to tuyere [3]. Further damage can also be attributed to the corrosive gases (mainly sulphur and chlorine) emited during the burning of coal [4].

In the present work, thermal barrier coatings deposited using Detonation Spray Coating (DSC) and Air Plasma Spray (APS) on copper substrate are evaluated for properties such as porosity and microhardness, erosion etc. Erosion test was conducted at two impact angles to simulate wear caused by falling burden material. High temperature service conditions were simulated by performing hot corrosion, thermal cycling and ΔT measurement tests.

2 Experimental Work

2.1 Coating Synthesis

Pure copper (99.9%) was used as substrate. Square shaped specimens of length 30 mm and thickness 5 mm were fabricated for property evaluation. Five different types of coatings systems and the optimum spraying parameters for Detonation Spray Coating (DSC) and Air Plasma Spraying (APS) are shown in Table 1 and Table 2.

Table. 1. *Optimum DSC parameters*

Powder	O_2, slph	C_2H_2, slph	Spray distance, mm	N_2, slph
Al_2O_3-ZrO_2	4960	2000	200	720
Mullite	4800	1920	170	720
Mullite+YSZ	4800	1920	200	720
Cr_3C_2-NiCr	2800	2240	170	720
NiCoCrAlY (Bond coat)	2720	2240	165	800

Table. 2. *Optimum APS parameters*

Powder	Primary gas flow rate, scfh	Secondary gas flow rate, scfh	Current, amps	Voltage, V	Standoff distance, mm
Al_2O_3-ZrO_2	110	10	600	62-66	120
Mullite	110	8	500	60-62	120
Mullite+20 %YSZ	110	8	510	60-62	80
YSZ	110	12	600	65-68	75
Cr_3C_2-NiCr	90	12	510	64-68	65
NiCoCrAlY (Bond coat)	80	8	500	62-64	110

2.2 Property Evaluation of Coatings

The coating porosity was measured on the cross section of coatings in Leica optical microscope using image analysis software. The Vickers microhardness was measured by a digital microhardness tester by applying a load of 200 g for 13 seconds of dwell time. To simulate the abrasion caused to copper tuyere by falling burden material in the blast furnace, solid particle erosion testing was carried out using the angular silica particles of size 50-150 μm impacting the substrates at an impact velocity of 40 m/s (accelerated wear) and at two impact angles of 30° and 90°.

In hot corrosion testing, 50 wt.% $FeCl_3$ + 50 wt.% $FeSO_4$ chemical was uniformly applied over the coating surface to a coverage of 25 mg/cm^2. The specimens were then isothermally heated to 850°C in an air furnace for 40 h. The heating and cooling rate was maintained at 3.5°C/min. The specimens were analyzed for phase change using XRD. The thermal cycling test was conducted using a rapid heating furnace with a heating rate of 50°C/min, wherein, the specimens were subjected to cycles consisting of 14-20 minutes of heating to 1273K, soaking at 1273K for 5 min and followed by 5 min cooling through a forced air draft to reach about 573K. The number of cycles to failure is reported.

ΔT measurement was performed using a customized setup involving an oxy-acetylene torch, thermocouple, and a dedicated chart data-recorder. Temperature measurement was done using a thermocouple attached at the back end of the coated specimens. Initially, the flame conditions were

set for a temperature above 1273K, wherein the copper substrate became red-hot and started melting within 2 minutes. Similar flame setup was used to heat the coated specimens for a span of 5 minutes and the temperature drop was recorded.

3. Results & Discussion

The microhardness and porosity results are shown in Fig. 1. Al_2O_3-ZrO_2 and Cr_3C_2-NiCr coatings demonstrated highest hardness, mullite – intermediate, while YSZ showed the least. Porosity in coating decreases the microhardness of coating, as is evident from Fig. 1.

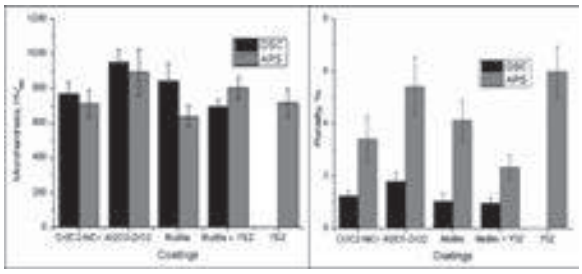

Fig. 1. *Microhardness and Porosity in coatings*

The erosion wear performance of the DSC and APS coatings is shown in Fig. 2. The data presented is in terms of volumetric loss incurred by the coating per gram of erodent impacting the coated surface. Results show that Cr_3C_2-NiCr provided better erosion resistance, mainly due to the presence of NiCr binder which acts as a toughening agent in absorbing the impact forces, followed by Al_2O_3-ZrO_2 and mullite based coatings.

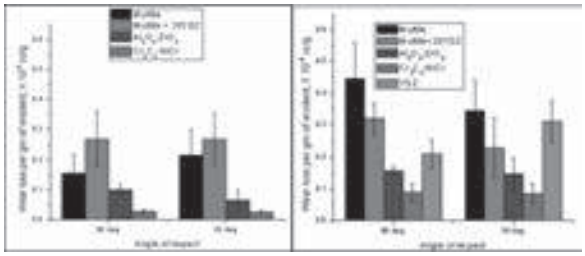

Fig. 2. *Erosion behaviour of DSC and APS coatings*

In hot corrosion testing, all the coatings exhibited inert behaviour except Cr_3C_2-NiCr. Cr-carbide reacted with oxygen to form chromium oxide resulting in disintegration of coating. The comparative XRD plots for Cr_3C_2-NiCr and YSZ are shown in Fig. 3.

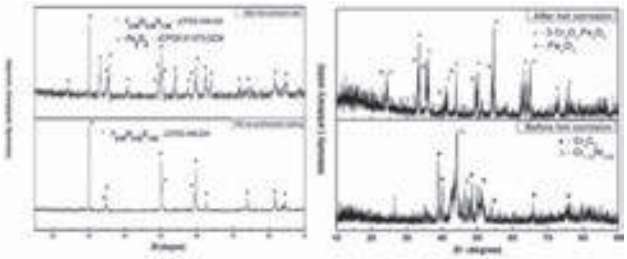

Fig. 3. *XRD of Air Plasma Sprayed YSZ and Cr_3C_2-NiCr before and after hot corrosion test*

The thermal cycling results are shown in Fig. 4. All the coatings except APS alumina containing coatings exhibited thermal cycling life in excess of 1000 cycles.

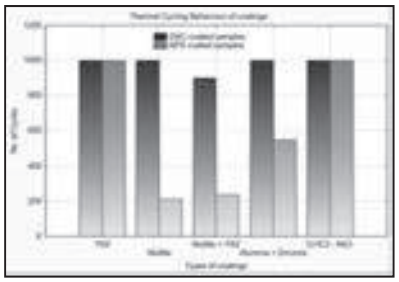

Fig. 4. *Thermal cycling behaviour of coatings*

ΔT results are shown in Fig. 5. Among the coatings assessed, the lowest back-surface temperature was observed for plasma sprayed YSZ and Cr_3C_2-NiCr coatings. Plasma sprayed Mullite coatings exhibited higher temperature values due to the more thermal conductivity from the Al_2O_3 and SiO_2 constituents. However, upon addition of YSZ into mullite, there is significant advantage with drop in temperature. DSC coatings demonstrated a similar trend.

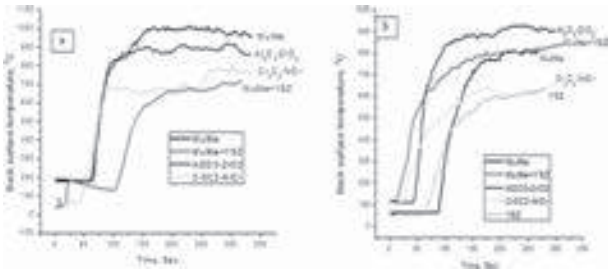

Fig. 5. *ΔT measurement for (a) DSC and (b) APS coatings*

4. Conclusion

Al_2O_3-ZrO_2 coating demonstrated high microhardness and moderate porosity. Its erosion resistance was next to Cr_3C_2-NiCr. Presence of Al_2O_3 makes the coating inert in hot corrosive environment. DSC coated Al_2O_3-ZrO_2 exhibited thermal cycling life in excess of 1000 cycles and moderate thermal conductivity in ΔT measurements. Based on the analysis of simulated tests for service conditions of tuyere, Al_2O_3-ZrO_2 shows the highest potential to mitigate the potential sources of tuyere failure. Cr_3C_2-NiCr also exhibited good results in all tests except in hot corrosion test rendering it un-favourable for tuyere application.

5 References

The references should be indicated in the following format:

[1] Charles Copeland and Stewart Street: Iron and Steel Technology. (2013） pp. 47-62.
[2] N. E. Shlykov and S. L. Livshits: Metallurgist. **25(4)** (1981) pp. 123-124.
[3]S. Matthews: Journal of Thermal Spray Technology. 19(6) (2010) pp. 1267-1276.
[4] Joseph R. Davis: *Handbook of Thermal Spray Technology*. (ASM International, 2004) pp. 169-175.

An Approach For Selection And Validation Of Thermal Spray Coating For Repair Of An Aero-engine Component

P S Ashwin Kumar[1], G Nithiyanantham[1,] V Sambasiva Rao[2]
[1]Senior Design Engineer, Cyient Ltd., Hyderabad-500 032, India
[2]Discipline Chief, Cyient Ltd., Hyderabad-500 032, India

Abstract
The aero-engine components are prone to various distresses including the erosion and wear due to the severe mechanical and thermal loading encountered during operation. There is a growing demand to repair such components to extend their service life. This paper describes an approach for the selection and validation of High Velocity Oxy Fuel (HVOF) coating for repair of a High Pressure (HP) Turbine Shaft, a critical component of a commercial aero-engine. The HP Turbine Shaft reported wear at the Bearing Nut mating area during the engine operation. The wear area is in contact with oil. The Original Equipment Manufacturer (OEM) part design does not specify any protective coating in this area. The approach for the selection of an appropriate coating involves the study of the materials of the component and the mating part, their function, the environment during engine operation and the coating thickness required to restore the part to OEM dimensional requirements. The validation process consists of a series of tests that include laboratory tests on test coupons, engine ground test and limited service trials. The worn out HP Turbine Shaft is restored to the design dimensions using the HVOF coating established through the validation process mentioned above.

1 Introduction

Aero-engine components are subjected to rigorous operating conditions of temperature and stress that may lead to various distresses viz., corrosion, erosion, wear, cracking, oxidation etc. There is an increasing demand to repair the components in order to extend their service life as well as to reduce the Life Cycle Cost (LCC). This paper describes an approach for selection and validation of thermal spray coating[1][5] for repair of High Pressure (HP) Turbine Shaft of a commercial aero-engine, that reported wear during operation.

2 Component and its distress

The High Pressure Turbine (HPT) in an aero-engine drives the High Pressure Compressor (HPC) via HP Turbine Shaft, which is supported by the bearings. HP Turbine Shaft is a critical, rotating and life limited component of the aero-engine as shown in **Fig. 1.**

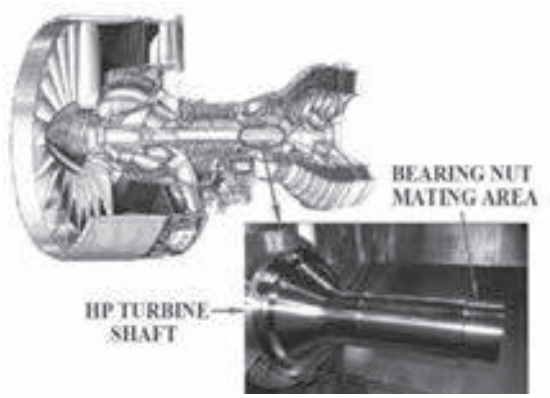

Fig. 1. *High Pressure Turbine Shaft*

A Bearing Nut is assembled onto the HP Turbine Shaft, with the specified tight fit, to arrest the axial movement of the hubs/disks. The region where the HP Turbine Shaft mates with the Bearing Nut is an oil wetted zone. A wear damage of 0.014 inch depth is reported on the HP Turbine Shaft at the Bearing Nut mating area, due to the engine operation. The parent material of the HP Turbine Shaft is a Nickel alloy (Waspaloy) and that of the mating part (Bearing Nut) is also a Nickel alloy (Inconel 718).

3 Repair feasibility assessment

A feasibility study for repair of this component has been undertaken by critically examining the location & accessibility to repair, extent of damage, parent material, operating environment and function of the part. The structural capability of the part is also assessed by considering the reduction in parent material thickness due to the reported wear.

4 Selection of repair method

4.1 Assessment of potential repair methods

The assessment of the suitability of various repair methods viz., welding, plating and coating to refurbish the component affected by the reported distress has been made. The welding method is not considered appropriate due to (a) its debit on the parent material properties considering that the component is subjected to fatigue loading during operation, (b) Weld Heat Affected Zone (HAZ) and (c) likely distortion of the part. Plating method is also not considered appropriate due to its thickness capability limitations, debit in the parent material properties and also the Environmental Health and Safety issues (EH&S) associated with this method. Thermal spray coating[2][6] methods are preferred, considering the advantages over the welding and the plating methods.

4.2 Identification of appropriate thermal spray coating method

The criteria for selection of an appropriate thermal spray coating method and also the coating material depends on various factors as depicted in **Fig. 2.** The Bearing Nut mating area on the HP Turbine Shaft is subjected to oil wetted environment during operation. The use of coating

processes that are prone to porosity are not recommended as the oil will tend to seep through the pores and degrade the coating and subsequently contaminate the oil itself. In view of the above and the part functional requirements, coating processes that produce more denser coatings with no porosity are the most appropriate for repair of HP Turbine Shaft. The widely used thermal spray processes that produce denser coatings[3] are High Velocity Oxy Fuel (HVOF) and Detonation Flame Spray.

Fig. 2. *Criteria for Selection of Thermal Spray Coating*

In HVOF[4][7] spraying, fuel and oxygen are fed into a combustion chamber with a continuous flow, producing a jet of combustion products at extremely high speed. The powdered coating material is injected into this gas steam and accelerated to a very high velocity. The high velocities provide kinetic energy required to produce coatings that are very dense and very well adhered to the part/substrate.

Detonation spray[3] process uses a cannon like device. The powdered coating material is fed into the chamber of the gun where a mixture of oxygen and acetylene is detonated. The coating material is heated and propelled at high velocity out of the gun onto the part. This process produces coatings with relatively high density.

While both the above coating processes produce denser coatings and also meet the component performance requirement, but considering the availability of the coating facility at the customer locations, HVOF spray process is selected for repair of HP Turbine Shaft. The coating material identified for HVOF spray is 95% Nickel - 5% Aluminum as it is compatible with the part material (Waspaloy) and also with the mating part material (Inconel 718).

5 Validation of HVOF coating

The selected procedure for validation of coating[5] takes into account the criticality of the component, its function and the debit in the parent material properties due to coating repair. The validation consists of simple laboratory tests, simulated environmental tests, wear test, engine ground test and limited service evaluation. The tests have been carried out on coated test coupons, dummy parts and on actual components. Standard test methods and test coupons have been used for validation, where applicable and feasible. The laboratory tests consisted of tests on coated test coupons for evaluation of microstructure, porosity, oxide inclusions, hardness, bond strength, wear test and mechanical properties viz., tensile, fatigue properties evaluation**.** The bond strength of the coating exceeded 10,000 psi. A coated component was assembled on an engine and subjected to engine ground test/test bed run. The condition of the coated component after engine ground test was satisfactory. In addition, a coated component has successfully undergone limited engine service evaluation. All the validation tests have been successfully carried out at customer facility. The coating process has been optimised for this application and documented to standardize the procedure and to ensure reproducibility.

6 Conclusions

A repair feasibility assessment of HP Turbine Shaft reported with wear damage during engine operation indicated that the part was repairable. The HVOF spray process using 95% Nickel - 5% Aluminum powder was identified as the appropriate coating repair method for restoration of this component, considering various factors. The coating was successfully evaluated on test coupons for microstructure, porosity, bond strength, wear resistance etc. The condition of the coated component after engine ground test and limited service evaluation was found to be satisfactory. This HVOF coat repair method is being used successfully for restoration of HP Turbine Shafts of a commercial aero-engine.

7 Acknowledgements

The authors would like to thank the management of Cyient and the Customer for their encouragement in preparing this manuscript.

9 References

[1] G.W. Meetham: *Use of Protective Coatings in Aero Gas Turbine Engines*. Mater. Sci. Technol., Vol. 2, March 1986, pp. 290-294.

[2] G.W. Meetham: *Coating Requirements in Gas Turbine Engines*, J. Vac. Sci. Technol., 1985, A3(6), pp. 2509-2515.

[3] B.G. Mellor: *Surface Coatings for Protection against Wear*; CRC Press: Boca Raton, FL, USA, 2006.

[4] K.A. Kowalsky, D.R. Marantz, and M.F. Smith, W.L. Oberkampf: *HVOF: Particle, Flame Diagnostics and Coating Characteristics*, Vol. 91, 1990, National Technical Information Service.

[5] V Sambasiva Rao, T Rangaraju and V Unnikrishnan: *Qualification of Indigenously Developed Special Coatings for Aero-engine Components*. Defence Science Journal, Vol. 49, No 4, August 1999, pp. 299-309.

[6] Lech Pawlowski: *The Science and Engineering of Thermal Spray Coatings, 2nd Edition.* March 2008, Publisher: John Wiley & Sons, Ltd.

[7] Mingheng Li, Panagiotis D. Christofides: *Modeling and Control of High-Velocity Oxygen-Fuel (HVOF) Thermal Spray: A Tutorial Review*. Journal of Thermal Spray Technology, December 2009, Vol. 18, Issue 5-6, pp. 753-768.

Thermal Spray Coatings and Laser Cladding for Oil & Gas and Steel industry

Michael Breitsameter
FW Gartner Thermal Spraying, USA

Laser Cladding technology is rapidly becoming an integral process within the surface technology business, alongside thermal spraying and PTA hardfacing. Recent developments in material technology, tailored specifically for the laser cladding process, expand the range of industries and applications utilizing this emerging technology. We will discuss two such developments that open up applications for Ti based hardfacing and a fully Martensitic Stainless Steel overlay, both with unique industrial applications.

Effect of colonization of *Escherichia coli* on the corrosion behavior of thermal sprayed Al-based coatings in artificial seawater

Leila Abdoli, Yaling He, Hua Li*

Key Laboratory of Marine Materials and Related Technologies, Ningbo Institute of Materials Technology and Engineering, Chinese Academy of Sciences, Ningbo 315201, China

Abstract

Corrosion of metallic alloys leads to serious problems. Particularly, the corrosion in the marine environment is the most remarkable issue influencing environment and economy. Although the electrochemical nature of corrosion remains valid for microbiologically influenced corrosion (MIC), the participation of microorganisms in the process nonetheless induces several unique features, the most significant being the modification of the metal-solution interface by biofilm formation. In this study, the corrosion behavior of thermal sprayed Al and Al/nano-Al_2O_3 composite coatings deposited on SS316L in artificial seawater (ASW) in the presence of E. coli bacteria was investigated. The analytical techniques including electrochemical impedance spectroscopy (EIS), Potentiodynamic polarization, and scanning electron microscopy (SEM) were employed for the investigation. The corrosion processes were simulated using equivalent circuit models, which provided electrochemical information on the liquid/surface interface.

1 Introduction

Thermal spray techniques, e.g. flame spraying, plasma spraying, arc spraying, and high-velocity oxygen fuel (HVOF) spraying, are successful in depositing both structural and functional coatings [1]. In general, the coatings usually exhibit high levels of interlamellar oxide and porosity, which could be detrimental to corrosion resistance, strength and machinability properties [2]. Corrosion occurs due to chemical or electrochemical reactions between the environment and metal. It can cause dangerous and expensive damage to a wide range of industries. However, it is difficult to evaluate the economic impact of corrosion, particularly when microorganisms are involved in the corrosion mechanism. If microorganisms are present in an aqueous solution, they first attach to the surface of the coatings and then grow, replicate and produce exopolymers (EPS), forming a cohesive structure known as biofilm [3]. Microorganisms change the electrochemical reaction at the biofilm/metal interface and either inhibit or accelerate the process of metal corrosion. The predictability of the results is not yet affirmed, as sometimes the same bacteria with an inhibitory property may induce corrosion.

2 Experimental

2.1 Deposition of the aluminum and nanocomposite coatings

Stainless steel 316L plate with dimensions of 2 cm × 2 cm × 0.2 cm was used as the substrate. Commercially available aluminum and alumina powder with the size range of +50-100 μm and 30 nm respectively was used. The coatings were deposited with high velocity arc spray (AS, TLAS-500C, China) and plasma spray (FS-4 system, Wuhan Research Institute of Materials Protection, China), respectively. The thickness of the coatings was ~200 μm.

2.2 Characterization of the coatings

The surface morphology was characterized by field emission scanning electron microscope (FESEM, FEI Quanta FEG 250, the Netherlands). To investigate the corrosion behavior of the coatings, the potentiodynamic polarization curves and electrochemical impedance spectroscopy (EIS) were carried out using a Solartron Modulab System. All tests were conducted in ASW solution prepared according to ASTM D1141-98 (2003) at room temperature. A traditional three-electrode cell was used, with 1cm^2 platinum as the counter electrode, saturated calomel electrode (SCE) as the reference electrode and a test specimen with an exposed area of 1 cm^2 as the working electrode.

EIS measurement was performed at an applied ac signal of 10 mV and a frequency ranging from 100 kHz to 0.01 Hz. Finally, the acquired data were fitted and analyzed using a ZSimpWin software based on equivalent circuit models. The equivalent circuits were chosen based on the number of time constants and the quality of fits. Potentiodynamic polarization studies were carried out in the potential range −500 mV to 500 mV versus E_{ocp} at a scan rate of 0.5mVs^{-1}.

2.3 Preparation of bacterial strains

Gram-negative E. coli bacteria (ATCC No. 25922) were selected for the adhesion testing. E. coli was grown in LB media. The medium was prepared by dissolving 10g NaCl, 5g yeast extract and 10g peptone in 1000ml deionized water. The media containing the bacterial strains were shaken for 24h at 37°C. The concentration of bacteria is diluted to 1 × 10^8cfu.ml^{-1}. Finally, 1.5 ml of the solution was added to 150 ml ASW that was richened by peptone.

3 Results and discussion

The specimens were immersed in the ASW in presence and absence of *E. coli* bacteria for 1 week and their corrosion behaviors were evaluated by electrochemical impedance spectroscopy and potentiodynamic polarization after the immersion. The Potentiodynamic polarization and Nyquist curves are shown in Fig. 1 and Fig. 2 respectively.

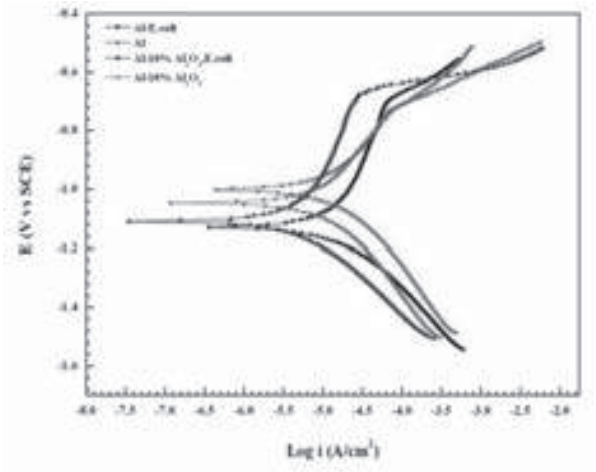

Fig. 1. *Potentiodynamic polarization curves of the Al and Al-10%Al_2O_3 coatings in presence and absence of E. coli in ASW.*

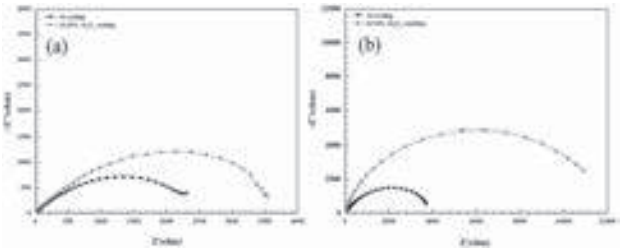

Fig. 2. *Nyquist plots for the Al & Al-10%Al_2O_3 coatings in ASW in (a) absence and (b) presence of E. Coli bacteria.*

As shown in Fig. 1, for the samples tested in presence of E. coli, the corrosion current density (i_{corr}) has decreased. From the Nyquist plot it is evident that the impedance offered by the Al-10% Al_2O_3 and Al coatings in presence of E. coli is higher than that exhibited by the coatings measured in absence of E. coli. Based on the above results, the EIS equivalent circuit for the coating is proposed, as shown in Fig. 3. The EIS results shows that the Al-10% Al_2O_3 and Al coatings tested in presence of E. coli provide better resistance (R_{ct}) than the coatings tested in absence of the bacteria. In addition, in comparison between the Al and the nanocomposite coatings, the nanocomposite coatings showed better corrosion resistance. This behavior of the Al-Al_2O_3 composite coatings could be due to their fine structure compared with the pure Al coating. The Al_2O_3 nanoparticles incorporated in the composite coatings also act as insulators on the coating surface.

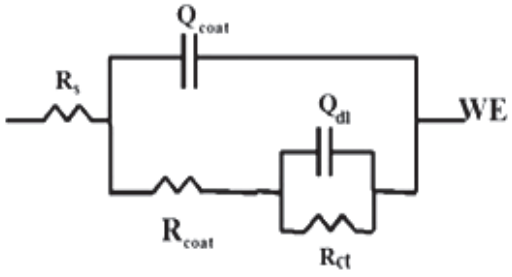

Fig. 3. *Equivalent circuit proposed to simulate the experimental impedance diagrams in the evaluation of the coatings immersed in ASW.*

Microorganisms are able to change the electrochemical conditions at the metal/solution interface. These changes can range from the acceleration of corrosion to corrosion inhibition. Microbial corrosion inhibition is usually accomplished through: i) a decrease in cathodic rate by microbial consumption of a cathodic reactant (e.g. oxygen consumption by respiratory activity); ii) decreasing the medium aggressiveness in restricted areas of the metal solution interface (e.g. by neutralizing acidity); iii) providing or stabilizing protective films on the metal (e.g. biofilm exopolymers with metal binding capacity) [4].

The SEM images shown in Fig. 4 clearly suggest that in the presence of *E. coli* bacteria, many bacteria attached on the surfaces of the coatings and triggered biofouling that can act as a protective layer. Especially, there are many pores that covered with bacteria. In the absence of the bacteria, the corrosive liquid penetrates more easily through the coating to the coating/substrate interface, causing corrosion of the steel substrate. Therefore, it could be concluded that presence of the bacteria enhances the anti-corrosion performances of the Al-based coatings in the marine environment.

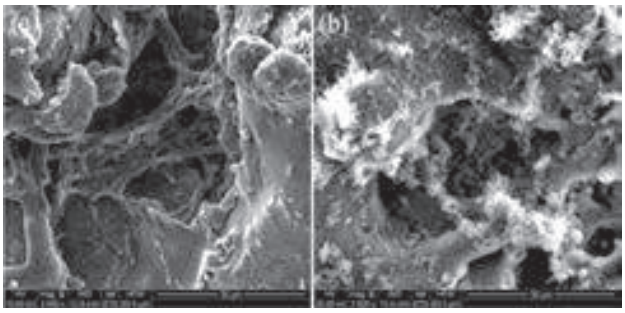

Fig. 4. *SEM topographical morphology of (a) the Al-10%Al_2O_3 coatings and (b) the Al coatings after 1week immersion in the ASW in presence of the E. coli bacteria.*

3 References

[1] L. Pawlowski:*The Science and Engineering of Thermal Spray Coatings*, (John Wiley & Sons, 2nd edition,2008).
[2] R. Molins, B. Normand, G. Rannou, B. Hannoyer, and H. Liao: Mater. Sci. Eng. A 351(2003) 325–333.
[3] J.W. Costerton, G.G. Geesey, and K.J. Cheng:Scientific American 238 (1978) 86–95.
[4] H. A. Videla: Rev. Metal. Madrid Vol. Extr. (2003) 256-264.

Splat Flattening Behavior and Coating Properties of NiCoCrAlYTa Powders Thermally Sprayed onto K4169 Substrates

Kun YANG, Changguang DENG, Min LIU
Guangdong General Research Institute of Industrial Technology (Guangzhou Research Institute of Non-ferrous Metals), Guangzhou, 510651, China

Abstract
NiCoCrAlYTa powders were thermally sprayed onto K4169 substrates by atmospheric plasma spraying (APS), low pressure plasma spraying (LPPS) and high velocity oxyfuel spraying (HVOF), respectively. The microstructures of splats and some fundamental properties of coatings were evaluated in detail. The results indicate that the coating performances have a close relation with the characteristics of the individual splat under different designations.

1 Introduction

MCrAlY coatings are often manufactured under inert gas conditions by low pressure plasma spraying (LPPS) [1], this however is expensive and sometimes inefficiency. Atmospheric plasma spraying (APS) and high velocity oxyfuel spraying (HVOF) are the appropriate alternatives due to the lower cost [2]. However, the controllability and reliability of these processes have not been established yet. In general, the flattening nature of the single splat could be treated as the fundamental process of the coating fabrication, the coating service properties depend strongly on the splat formation process. In this study, NiCoCrAlYTa powders were thermally sprayed onto Ni-based superalloy K4169 substrate by APS, LPPS and HVOF, respectively. The splat microstructure and its relation with the coating performances has been investigated.

2 Experiment procedural

The feedstock material was NiCoCrAlYTa alloy powder. The substrate material was Ni-based surperalloy K4169, which was mirror polished for the particle collection and grit blasted for the coating formation on its surface. The spraying works were conducted using APS, LPPS, and HVOF. The microstructures of the splats and cross sections of the coatings were observed by scanning electron microscope (SEM). The element analyses at splat top surface were performed by electron probe micro-analyzer (EPMA). Surface roughness (Ra) of as-sprayed coatings was measured by Protable Surface Finish Measuring Instrument. The image processing and analysis software, ImageJ was employed to measure the porosity. The oxygen content of the feedstock powder and coatings were measured using TC600 oxygen/nitrogen determinator.

3 Results and Discussion

3.1 Splat characterizations

The morphologies of the splats were indicated in Fig 1. Most of the particles sprayed by APS were fully melted, but exhibited as splash shape with ring-shaped splashings around the main solidification core. Splat curl up could be observed at the periphery of the splat. The relative unfavorable wetting between the molten droplet and substrate under atmospheric pressure, and the shrinkage during cooling leads to the curling of the splat. Un-molten and semi-molten particles exist in the depositions obtained by LPPS. However, the melted splats show less splashing with only few coarse fingers around the central disk-shaped core. The depositions prepared by HVOF method performed as disk-shaped splat with irregular geometric shapes. A part of the central solidification zone inhibited as oval shaped. In HVOF, the flame temperature was quite lower than the plasma source flame, while the combustion gas velocity reached supersonic at the gun exit, evident deformation of the droplet could be obtained and lead to the good adhesion with the substrate, however, the flattening is not sufficient enough before the solidification finish because of the poor fluidity of the droplet.

From the view at the bottom surface, amount of central pores with nano and micro-size could be frequently observed for most of the splats obtained by APS. The nano-sized pores might be generated by the desorption of adsorbed gas condensations on the substrate surface during the flattening of the molten droplet. Both the number and the diameter of the central pores decreased evidently for the splats collected under reduced ambient pressure. Meanwhile, only few splats achieved by HVOF could be obtained on the carbon tape after pulling off from the substrate, some splash fingers and fragmentations could be found on the carbon type, that is because the HVOF splat adheres quite well with the substrate.

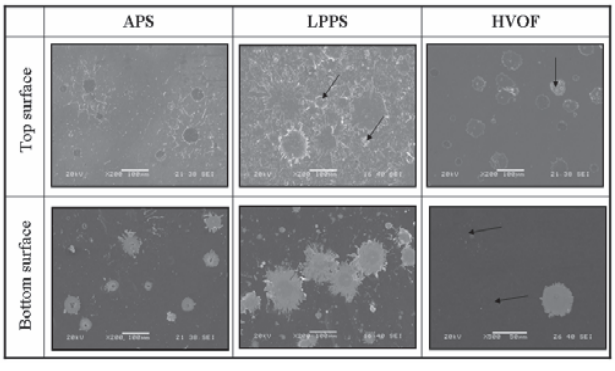

Fig.1 *Morphologies of NiCoCrAlYTa splats*

3.2 Coating characterizations

The micrographs in Fig. 2 show cross sectional views of coatings. The microstructure of APS coating is lamellar and contained pores within splats, typical interface composed by thin layer of voids resulting from poor contact between the lamellar could be found. On the other hand, the coating is dense and compact in the case of LPPS, un-melt particles with almost original sphere shape trapped between well-

molten particles could be found in the coating. In the case of HVOF, the microstructures comprised a combination of fully molten splats and sei-molten particles with obviously deformation, which might caused by the high velocity of the in-flight particles prior to the impacting onto the substrate, and a fraction of the feedstock powders was too large to be melted in the flame.

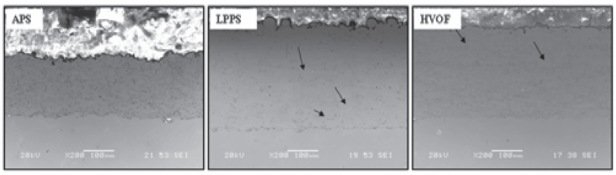

Fig.2 *Cross sections of NiCoCrAlYTa coatings*

The oxygen contents of feedstock powder, splats and coating was presented in Fig. 3. The oxygen content of NiCoCrAlYTa powders is 0.057wt. %. By APS, the oxygen contents of 3.8 wt.% could be achieved in the individual splat, and increased to 4.2 wt.% in the coating. When the spraying was conducted in the reduced inert gas using LPPS, the oxygen partial pressure is kept in constant and quite low, the oxygen contents in both splat and coating are lowest among the three spraying methods and approximately around 0.4-0.5 wt. %. In particular, the oxygen content of the HVOF sprayed splat was about 0.65 wt. %, but rapidly increased up to 4.3 wt. % in the coating. In general, the oxidation is highly dependent on the particle in-flight characteristics, environment gas and substrate temperature. The oxygen content of HVOF coating could be reduced through improving the combustion flame and controlling substrate temperature by further optimization of the substrate cooling system during spraying.

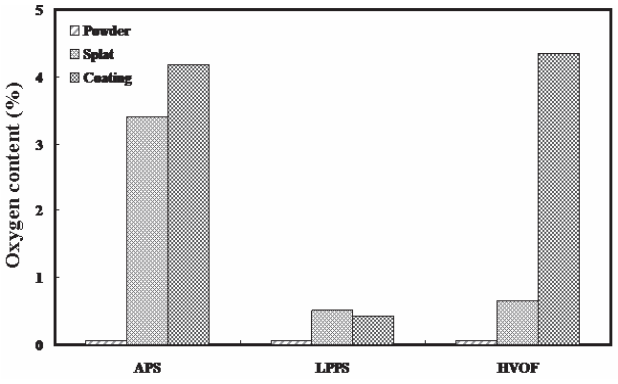

Fig.3 *Oxygen content of powder, splats and coatings*

The surfaces roughness and porosity of coatings deposited by the mentioned methods was summarized in Fig. 4, respectively. The roughness of LPPS coating is the highest, followed by the APS coating, and the HVOF coating is the lowest. Although most of the molten droplet sprayed by LPPS deposited as disk-shaped splat, the existence of the un-molten and semi-molten droplet formed as peaks on the substrate and previous deposited coatings, and raise the surface roughness accordingly. When the spraying was conducted by APS, most of the particles were deposited as splash splat and the fragmentation debris could enhance the roughness, however, the sufficient flattening of the particles due to the fully molten condition could result in the relatively lower surface roughness of the coating obtained. Partial of the HVOF sprayed particles looks insufficient melting, but largest plastic deformation could be achieved because the velocity of the in-flight particles is the highest, and also ramming the previous deposited coating and finally promote the coating with lowest surface roughness.

The desorption of the adsorbed gas condensation on the substrate surface, entrapped environmental gas during the in-flight process, and the fragmentation debris from the individual splash splats worked jointly and lead to the highest porosity in APS coating. In the case of LPPS coating, the porosity is quite low, because less environmental gas could be entrapped into the molten droplet and most of the adsorbed gas condensations on the substrate surface were removed, the favorable wetting promote the sufficient spreading of the molten droplet on the substrate and formed as regular disk-shaped splat, few fragmentation could occur. When the spraying was conducted by HVOF, the porosity is between APS and LPPS coatings. One reason might be that the particles were already cooling down prior to the impacting onto substrate, so that larger porosity was formed. In contrast, the hitting by the latter particles with supersonic in-flight velocity might ram the previous deposited coating down.

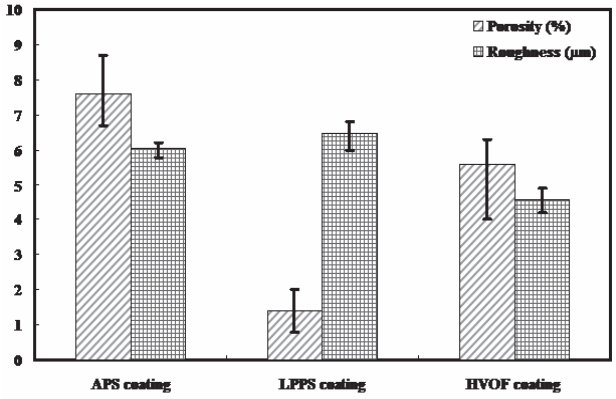

Fig. 4 *Porosity and roughness of NiCoCrAlYTa coatings*

4 Conclusion

The coating proprieties have a close relation with the flattening nature of the individual splat, a cost-effective method by investigating on the deposition behavior of the individual splat could be used to optimize the thermal spraying process.

Acknowledgments

This research was supported by the National Nature Science Foundation of China (No. 51301046), and National Key Basic Research Program of China (No. 2012CB625100).

References

1. W. Brandl, H.J. Grabke, D. Toma, et al.: Surf. Coat. Technol. 86–87(1996) 41-47.
2. M. D. Ferdinando, A. Fossati, A. Lavacchi, et al.: Surf. Coat. Technol. 204 (2010) 2499-2503.

Critical Interface temperature for plasma spray ceramic droplet to form bonding

Shu-Wei Yao, Guan-Jun Yang, Cheng-Xin Li, Xiao-Tao Luo, Chang-Jiu Li
State key Laboratory for Mechanical Behaviour of Materials, School of Material Science and Engineering, Xi'an Jiaotong University, Xi'an, Shaanxi 710049, China

Abstract
Controlling the lamellae bonding is essential to fulfill requirements of various coating applications, since the lamellae bonding of thermally sprayed coatings dominates coating mechanical, thermal and electrical properties. In this study the bonding state at the interfaces between plasma sprayed ceramic splats was examined to reveal the effect of deposition temperature on the bonding formation. The results show that the splat can be well bonded with the identical substrate only when substrate is preheated above a critical temperature. This critical bonding temperature influencing the formation of splat bonding during the plasma spray linearly increases with the melting point of splats. Thus, versatile coatings for different applications can be prepared by controlling the deposition temperature above or below the critical bonding temperature according to the melting point of splat material. A one-dimensional numerical model is used to obtain the interface temperature, which directly affects the bonding formation. The interface temperature corresponding to the critical bonding temperature is defined as the intrinsic bonding temperature. It was found that the intrinsic bonding temperature is closely realted to the glass transition temperature of molten droplet. The intrinsic bonding temperature will be used to explain the lamellar bonding formation during the plasma spray.

1 Introduction

With plasma-sprayed ceramic coatings, the investigation revealed the coatings exhibit a maximum bonding ratio of 32% when deposited following conventional routine [1]. The lamellae bonding of plasma sprayed coatings dominates their mechanical, thermal and electrical properties [2-5]. Thus, understanding the formation mechanism and factors controlling lamellar bonding formation is essentially important to prepare high performance coatings, which can fulfill the versatile requirements of different applications.

Depositing a ceramic coating at a high deposition temperature is an alternative approach to improve the bonding ratio between lamellae of coating. Our previous study revealed that there is a critical deposition temperature for droplets to form effective bonding by examining the bonding state from the cross-section morphology of Al_2O_3 and YSZ splats deposited at different deposition temperatures [6]. The critical temperatures are 300°C and 600°C for Al_2O_3 and YSZ, respectively. It can be suggested that the critical deposition temperature depends on the coating materials. However, how the materials properties and how certain property are related to the critical deposition temperature the is not clear.

In this study, the critical deposition temperatures for different ceramic materials, i.e. TiO_2, $La_2Ce_2O_7$ (LCO) and $La_2Zr_2O_7$ (LZO), were investigatyed by depositing splats on the identical polished substrate at different deposition temperatures. A one-dimensional numerical model is used to estimate the interface temperature corresponding to the critical deposition temperature for bonding formation to expore the factor dominating the lamellar bonding formation during plasma spray.

2 Experiment

An aggregated TiO_2 powder with a particle size range from 30 to 38 μm was used for the deposition of TiO_2 splat. Commercially available LCO and LZO with the same size distribution, varying from 10 to 45 μm with a mean particle size of 18 μm, were employed to deposit LCO and LZO splats. Sintered dense TiO_2, LCO and LZO bulks were used as substrates to deposit TiO_2, LCO and LZO splats, respectively. A commercial plasma spray system (80 kW class, Jiujiang China) was employed to deposit splats. Each type of splats was deposited on the substrate preheating to different deposition temperatures. To reveal the interface bonding state of splat with substrate deposited at different temperatures, after deposition of splats the samples were fratured and then the splat bonding was examined by SEM. The deposition temperature was carefully controlled by using a heated copper plate over which the sample substrate was placed. Based on the change of splat bonding state with the deposition temperature, the critical deposition temperature was determined.

3 Results

3.1 Critical bonding temperature of different splats

Fig. 1. shows the cross sectional morphology of the TiO_2 splats deposited on the TiO_2 substrates at different deposition temperatures of 115 °C, 200 °C, 300 °C and 400 °C. It was found that the TiO_2 splat can be well bonded with the substrate only when the substrate was preheated about 200 °C. It was confirmed that when the deposition was less than 200 °C as shown in Fig.1a for 115 °C TiO_2 splat did bond to TiO_2 substrate. The confirmed that the critical deposition temperature for splat bonding is 200 °C for TiO_2 splat.

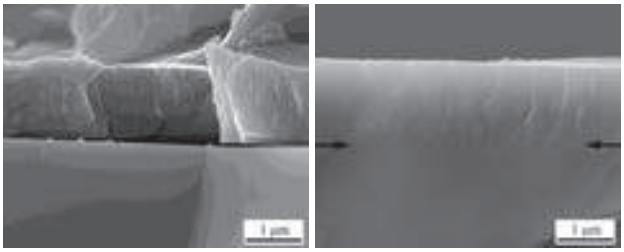

（a） (b)

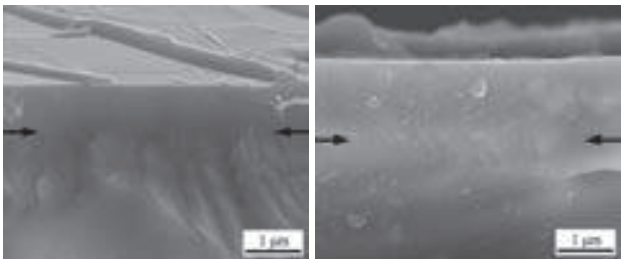

（c） (d)

Fig. 1. *Cross-sectional morphology of typical fractured TiO_2 splats deposited on the polished TiO_2 substrate: (a) 115 °C, (b) 200 °C, (c) 300 °C and (d) 400 °C.*

The investigation into the critical deposition of LCO and LZO yielded 400 °C for LCO splat and 500 °C for LZO splat.

3.2 Relationship between the critical deposition temperature and the melting point

In the previous study, it was revealed that the critical deposition temperatures for Al_2O_3 and YSZ are 300 °C and 600 °C, respectively. The bonding between splat and substrate can form only when the deposition temperature becomes higher than the critical deposition temperature. In this study, the systematic investigation indicates that the critical deposition temperature increases almost linearly with the melting point of splat material, as shown in Fig. 4.

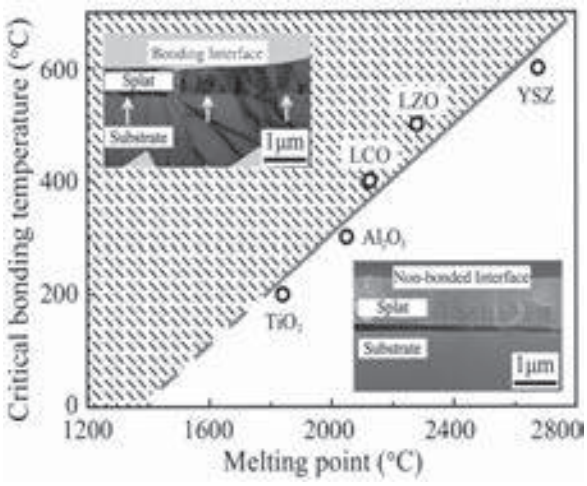

Fig. 2. *Critical deposition temperature for the bonding formation of ceramic splat against melting point.*

3.3 Interface temperature of splat at the critical deposition temperature for bonding formation

A one-dimensional heat transfer model was used to estimate the interface temperature corresponding to the critical bonding temperature. This temperature is defined as intrinsic bonding temperature. It was found out that as shows in Fig. 5., the intrinsic bonding temperature is linearly proportional to the glass transition temperature of splat material.

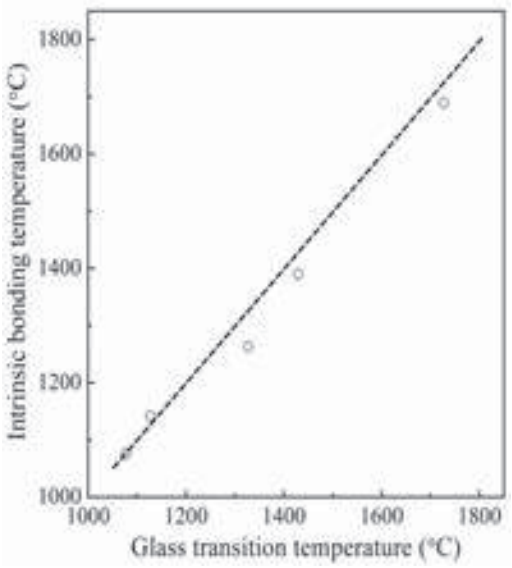

Fig. 3. *Relationship between the intrinsic bonding temperature and glass transition temperature.*

4 conclusions

The critical deposition temperatures for the bonding formation of TiO_2, LCO and LZO splats were experimentally determined. It was found that the critical deposition temperatures increase with the melting point of splat material. Moreover, it was revealed that the intrinsic splat bonding temperature is lineally proportional to the glass transition temperature of splat material.

References

[1] C.-J. Li, G.-J. Yang, C.-X. Li, Development of the Particle Interface Bonding in Thermal Spray Coatings: A Review, J. Therm. Spray Technol. 22 (2013) 192-206.
[2] C.-J. Li, A. Ohmori, Relationship between the structure and properties of thermally sprayed deposits, J. Therm. Spray Technol. 11 (2002) 365-37.
[3] C.-J. Li, W.-Z.Wang, Y. He, Dependency of fracture toughness of plasma sprayed Al_2O_3 coatings on lamellar structure, J Therm Spray Technol, 13 (2004) 425-431.
[4] R. McPherson, A model for the thermal conductivity of plasma-sprayed ceramic coatings, Thin Solid Films, 112 (1984) 89-95.
[5] Y.-Z. Xing, C.-J. Li, C.-X. Li, G.-J. Yang, Influence of through-lamella grain growth on ionic conductivity of plasma-sprayed yttria-stabilized zirconia as an electrolyte in solid oxide fuel cells, J. Power Sources, 176 (2008) 31-38.
[6] G.-J. Yang, C.-X. Li, S. Hao, Y.-Z. Xing, E.-J. Yang, C.-J. Li, Critical bonding temperature for the splat bonding formation during plasma spraying of ceramic materials, Surf. Coat. Technol. 198 (2005) 278-282.

Substrate melting and resolidification during impact of high melting point droplet material on a substrate

Rajesh Kumar Shukla, Arvind Kumar*
Department of Mechanical EngineeringIndian Institute of Technology Kanpur, Kanpur, 208016, India
* Corresponding author: Email: arvindkr@iitk.ac.in

Abstract
In this paper, impact, spreading and solidification of molten droplet on a substrate along with substrate melting and its resolidification are investigated numerically. The problem consists of tracking the free surface between droplet and air, solidification front in the droplet as well as melting/ resolidification front in the substrate with droplet and substrate are of different materials. Volume of fluid surface tracking method (VOF) coupled with the solidification model within a one-domain continuum formulation is used to model the transient flow during the droplet impact, its subsequent spreading and solidification, and melting front of the substrate. Numerical simulations are performed for impact of heated molybdenum droplet on aluminium substrate. The model predicts substrate melting with droplet and substrate are of different materials, which can give better insight of bonding between coating material and substrate. It is observed for the present case that melting in the substrate starts just after the impact of the heated droplet. Depth and width of the melting front in the substrate increases with the time and after reaching a maximum it tends to decrease because of start of resolidification from the melted edge.

1 Introduction

In thermal spray coating process, prior to the impact on the substrate, the molten particle can remain superheated during the in-flight and contains sufficient thermal energy that can locally melt the substrate after the impact. Substrate melting during droplet-substrate interaction substantially influence the metallurgical bonding between the flattened molten particle and the substrate surface. Therefore, understanding of melting and resolidification of the substrate is essential for appropriate bond coat selection as well as avoidance of substrate damage. Coating formed by high melting point metals and their alloys have been widely used in thermal spray process due to higher resistance to wear and corrosion. In refernces [1-5] experimental and numerical investigations were performed for various droplet and substrate combinations. It was reported experimentally that the material properties of droplet and substrate had great effects on the melting. Melting and re-solidification of a substrate caused by molten micro droplet impact was studied in [1] and the influence of the droplet fluid dynamics on the substrate melting is dicussed. Li et al. [2] developed a numerical model to study the integrated effect of droplet solidification, and melting of the substrate during thermal spray coating.

In the present study numerical simulations have been performed with high velocity impact of molybdenum droplet onto a solid aluminium surface with conditions typically found in a real thermal spray coating process. Two-dimensional axi-symmetric formulation has been considered, **Fig. 1**. The impact and boundary conditions are shown in **Fig. 1**. The problem consists of tracking the free surface between droplet and air, solidification front in the droplet as well as melting/ resolidification front in the substrate with droplet and substrate are of different materials. Volume of fluid surface tracking method (VOF) coupled with the solidification model within a one-domain continuum formulation is used to model the transient flow during the droplet impact, its subsequent spreading and solidification, and melting front of the substrate.

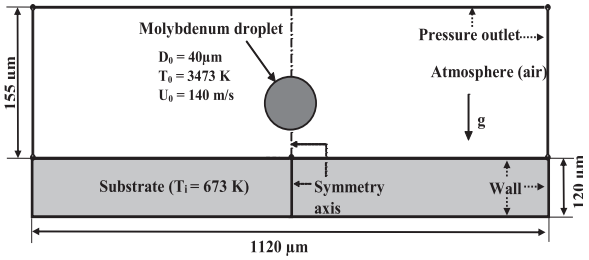

Fig. 1. *Computational domain and boundary condition*

2 Result

Figure 2 shows the evolution of the shape of the droplet during the droplet flattening process and the melted region in the substrate. As the droplet impacts the substrate, the droplet begins to deform during its flattening. It can be seen that the substrate melting starts at early stage of time, **Fig. 2** (t = 0.14 μs). The melting interface in the substrate propagates downward and reaches a maximum. At about t = 1.5 μs the maximum melting depth in the substrate is reached and after this time solidification at the edge of melted interface starts.

It is also observed that the temperature in the substrate just below the droplet impact point increases and after reaching a maximum value (2240 K) starts to decrease, **Fig. 3**. The maximum melting depth is the substrate is reached when the temperature in **Fig. 3** attains the maximum value. In the initial stage of the droplet flattening process large amount of heat transfer occurs from the droplet to the substrate due to high temperature gradient. This causes rapid increase in the temperature in the substrate as shown in **Fig. 3**. After reaching the maximum value this temperature decreases due to lowering in the droplet temperature by cooling from the surrounding atmosphere.

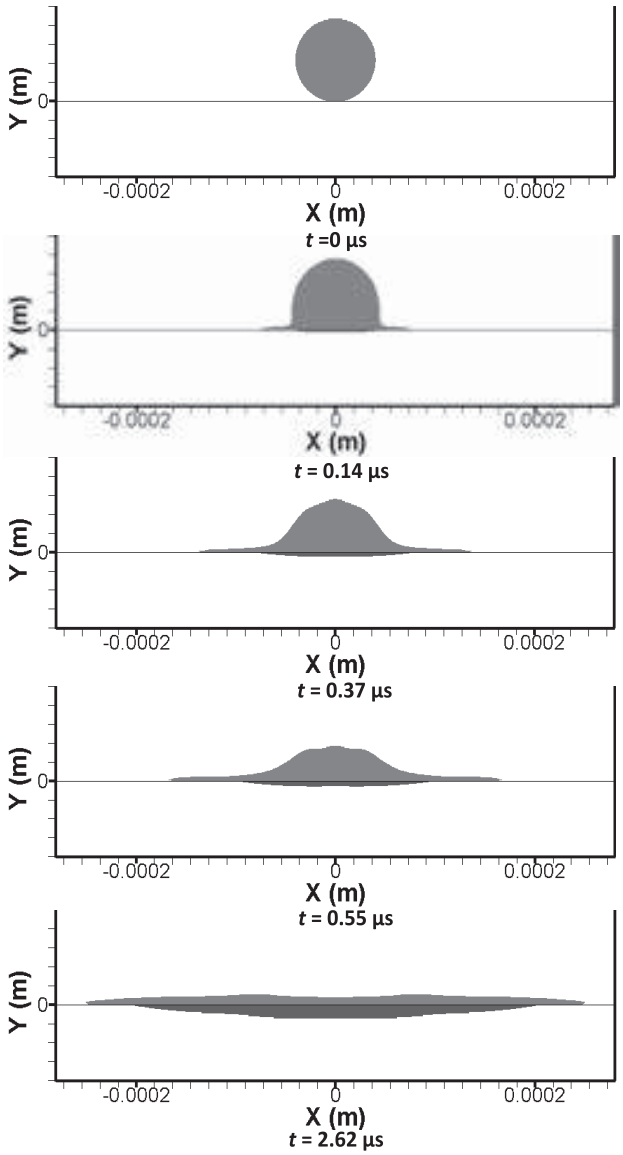

Fig. 2. *Droplet shape and substrate melting front as a function of time*

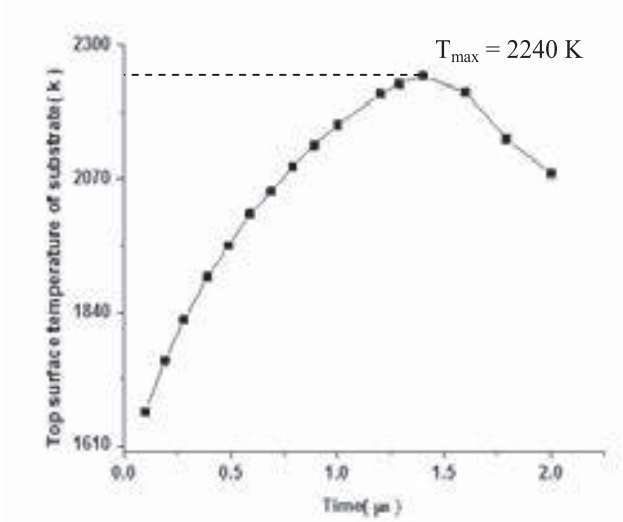

Fig. 3. *Temperature history of the top surface of the substrate during the course of impact process*

3 References

[1] D. Attinger and D. Poulikakos: Trans. ASME. **123** (2001) 1110-1122.
[2] L. Li, X. Y. Wang, G. Wei, A. Vaida, H. Zhang and S. Sampath: Thin Solid Films. **468** (2004) 113-119.
[3] L. J. Zarzalejo, K. S. Schmaltz, and C. H. Amon: Heat and Mass Transfer. **34** (1999) 477-485.
[4] K. S. Schmaltz, L. J. Zarzalejo, C. H. Amon: Heat and Mass Transfer. **34** (1999) 17-23.
[5] S. P. Wang, G. X. Wang, and E. F Matthys: Materials Science and Engineering A. **262** (1999) 25-32.

Structure-Property Correlation in Cold sprayed splats of Copper and Copper alloys with varying Stacking fault energies (SFE)

Naveen Manhar Chavan[1], Prita Pant[+] and G. Sundararajan[1]

[1]International Advanced Research Centre for Powder Metallurgy and New Materials, Balapur PO, Hyderabad, India.

[+]Indian Institute of Technology Bombay, Powai, Mumbai, India

It is well known that cold spray involves impact of micron sized powder particles at supersonic velocities to form thick and dense coatings. In general, cold sprayed coating consists of splats (erstwhile powder particles) that have a varying degree of deformation from centre to periphery. The extent of this heterogeneity depends on factors such as particle/substrate properties and incident particle velocity. In the present study, Copper and Copper-Aluminium alloy powders with varying stacking fault energies have been selected to evaluate the deformation behaviour under cold spray conditions involving high strain rates. Copper and Copper-Aluminium alloy powder particles (~38-44 μm) were used to generate single splats at four different velocities on polished SS 301 in order to study the above heterogeneity aspect at a single particle level. It was observed that as the particle velocity increased, the flattening ratio of individual splats also increased. The starting powder particles and splats were dissected using FIB to observe the microstructure. Hardness mapping across the powder and splat cross section was carried out using nanoindentation and correlated to the microstructures observed. An attempt was also made to repeat the above analysis for a copper-aluminum alloy with different stacking fault energy.

Correlation studies between in-flight particle characteristics, splat formation and microstructure of atmospheric plasma sprayed XPT 512 powder

M Jayamathy[1], Sivakumar G[2], S V Joshi[2] and Vikram Jayaram[3]

[1]TVS Motor Company Limited, India

[2]ARCI Hyderabad, India

[3]IISc, Bangalore, India

Automotive industries thrive to develop fuel efficient engines through various means, such as friction and weight reduction. Friction in the cylinder bore and piston ring assembly alone contributes about 30-40% of the overall friction losses in an engine. Thus, research in this area is being actively pursued all around the world to reduce friction. The desired reduction in frictional losses is being attempted through various surface modification routes. One among them is applying protective coating through plasma spray on the cylinder bore surfaces. A low alloy steel powder (XPT512) has been specifically developed for cylindrical bore applications and is reported to exhibit enhanced wear resistance as well as reduced friction. Preliminary studies under simulated tribological conditions revealed that the above coatings appear promising for the perceived applications.

Prior studies related to the role of microstructure, porosity, oxide content, phases present on the tribological characteristics are not available. In order to develop coating specific to the automotive engine operating conditions, a fundamental understanding on the role of process parameters on the coating characteristics can be beneficial in tailoring the coating microstructures. In view of the above, a detailed study was carried out in evaluating the role of plasma spray variables on in-flight particle characteristics and the splat formed. These were correlated with the deposited coatings. Initial efforts indicated that the plasma power and spray distance exhibited significant influence on the melting behaviour, deposition rate and the oxide content. A detailed parametric study by systematically varying the plasma power and spray distance was carried and the ensuing results will be presented.

1.0Material:

Chemical composition of the powder is steel with 1.4wt% Chromium, 1.4wt% Manganese and 1.2 Carbon. Particle size range: -38+15 microns (-400 mesh +15 microns) .Morphology of the powders is spheroid and obtained through gas atomized route from M/S Oerlikon METCO, Switzerland. These powders were observed using Scanning electron microscope, FEI Philips Quanta 200 to study the particle shape and morphology. The particles were found to be spherical.

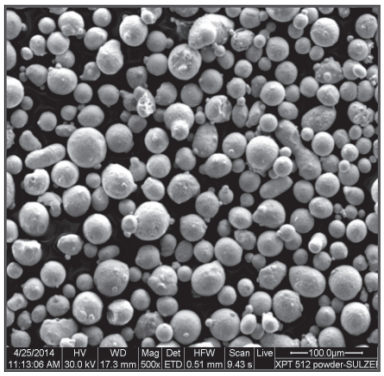

Fig.1 *Steel powder reveals spheroidal morphology*

In order to understand the effect of varying the spray process parameters on the splats being formed and **arrive at useful range of process spray conditions** which will contribute to the formation of oxides in the coating.

2.0Method of splat deposition:

Splats were deposited on stainless steel mirror polished coupons of surface roughness of 0.02 Ra. The splats were deposited on mirror polished samples to reduce the flattening splashing and also improve the reflectivity of the substrate onto which it is deposited to observe the splat morphology. Powders were injected perpendicular to the plasma plume. Powders were sprayed at a traverse speed of 1000 mm/second. Substrates are preheated to 100^{o}C for constant time period for the entire splat formation studies. The oxide layer composition remains same at a particular preheating temperature; however, with time the thickness of the oxide layer increases [1].

Table 1.*Plasma spray process parameters used for the study*

Sl. no	Process parameters	Values
1	Arc Current ,Amperes	340 - 500
2	Voltage, Volts	maintained at 65 V by controlling the H_2 gas flow rate
3	Primary gas flow Ar, LPM	45
4	Secondary gas flow H2 ,LPM	2.5
5	Powder feed rate, gm/min	2

2.1Splat observation using SEM:

A droplet flattening during thermal spraying influences significantly the coating structure and properties. The observations were done at the centre of the squared stainless steel coupons. The maximum particle velocity is found at the centerline because of the highest momentum transfer at the center [2], As the vertical position relative to

the flame centerline changes downward with particle injection from the top, particle velocity decreases as larger particles are found on the side opposite from the injection port [3].The formation of oxides and porosities in the form of coatings correlates well with the splat studies conducted.

3.0 Coating: Unetched microstructures-oxide content & porosity

Microstructure studies on the specimens for determining the oxide contents in the coatings were performed using SEM images image analysis.

XPT 512 powder is being used to form the splats and the splat morphology has been observed using SEM to understand the influence of change in plasma power and standoff distance.

Table 2.*Plasma spray process parameters used for the preparation of splats*

Sl. no	Arc current, Amperes	Standoff distance, mm
1	340	100
2	500	100
3	340	200
4	500	200
5	340	45

Increasing the arc current leads to higher particle temperatures and thus ensures complete melting of particles, leading to decrease in porosity content during coating. Absence of unmelted powders observed at higher plasma power (500A). Lower deposition rates at standoff distance of 200mm. Keeping the particle feed rates constant the number of splats deposited on the substrate at 200 mm standoff distance is lower compared to the number of splats deposited at a standoff distance of 100mm, indicative of the event of resolidification of the powder particles impinging on the substrate and falling down (Fig 2.)

From the above studies, it can be inferred that complete melting of powder particles occurs in the arc current range of 340 A to 500 A as few unmelted particles observed at 340 A. Also the standoff distance shall be in the range of 100 -150 mm, as at lower standoff distance of 45 mm unmelted particles observed and above 200 mm resolidification (lower deposition rate) of the particles observed.

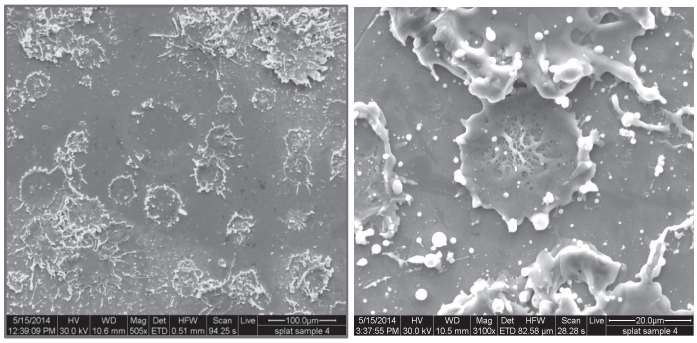

Fig.2 *Splats impinging and falling, observed as dents*

Table 3. *Oxide and Porosity contents in the coatings formed*

Sl. no	Arc current, Amperes	Spray distance, mm	Oxide content (%)	Porosity (%)
1	340	45	3-5	13-15
2	340	75	7-9	9-11
3	340	125	15-18	5-6
4	500	125	24- 26	7-9

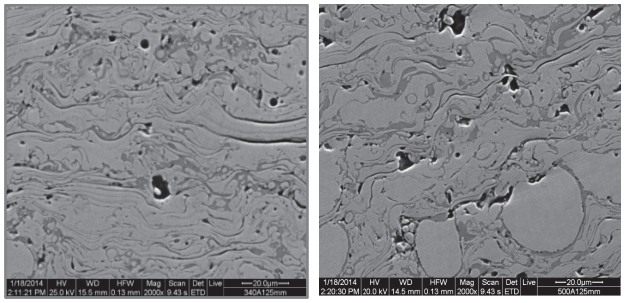

Fig.3 *Effect of spray distance on the oxide content*

When the spray distances are increased the in-flight time is increased thus allowing the particles to oxidize and thus increase the amounts of oxides in the coatings.

When the arc current is increased the particle temperatures increases, so that apart from melting , oxidation of the powders takes place, thus increasing the oxide formation.

In flight particle studies have been carried out. Characterization of the coatings has been performed to study their structure and correlate the same with the spray process parameters. The ensuing results will be shared .

References:

[1] P. Fauchais, M. Fukumoto, A. Vardelle, and M. Vardelle, J. of Thermal Spray Technology (2004)337 -343

[2] Y.J. Su, T.F. Bernecki, and K.T. Faber J. Therm. Spray.Technology(2002)11 52-61

[3] A. Elsebaei, J. Heberlein, M. Elshaer, and A. Farouk J. of Thermal Spray Technology,19(2010).

Hot corrosion stability of perovskites and pyrochlores in Na_2SO_4+50 wt.% V_2O_5 and Na_2SO_4+10 wt.% NaCl at 900 ºC

Gosipathala Sreedhar[1], T. Baskaran[2], S.B. Arya[2], L. John Berchmans[1]
[1] Electropyro Metallurgy, CSIR-Central Electrochemical Research Institute, Karaikudi- 630006, India
[2] Department of Metallurgical and Materials Engineering, NIT-Karnataka Surathkal, Mangalore – 575 025, India

Abstract
Perovskites, pyrochlores and double perovskites are have matching thermal expansion co-efficient with bond coat and can act as candidate materials for an intermediate layers between bond coat and top coat in Thermal Barrier Coatings. Hot corrosion stability of provskites and pyrochlores is also important for enhanced thermal cycle life. Based on these issues, systematic studies were conducted to determine the hot corrosion stability of perovskites, pyrochlores and double perovskites. The results revealed that, perovskites, pyrochlores and double perovskites were undergone destabilization in the Na_2SO_4+50 wt.% V_2O_5 and Na_2SO_4+10 wt.% NaCl environments at 900 ºC. The implications of these findings address the key issues related hot corrosion mechanism and give pathway for developing newer materials.

1. Introduction

Most recently, the perovskites (ABO_3), pyrochlores ($A_2B_2O_7$) and double perovskites ($Ln_2SrAl_2O_7$) type ceramic oxides have been fascinated owing to their matching CTE with bond coat material (~14 x 10^{-6} K^{-1}) (1400 ºC). In addition to this, their melting points are moderately more than 1940 ºC [1-3]. Hence, such type ceramics are considered as an intermediate layer between bond coat and ceramic top coat material. So that, this can effectively reduces the discontinuities in CTE between bond coat and top coat material. Besides, the porous top coats may permit the corrosive elements into the intermediate layer to experience the hot corrosion attack. Hence, there is a need in developing the newer materials with matching CTE with bond coat and stability against hot corrosion. But the review of the literature shows that the published work focused on zirconate based perovskites and pyrochlores. Notably these materials not have matching CTE with bond coat [4]. The materials with matching CTE with bond coat, like $SrTiO_3$, $Gd_2Ti_2O_7$ and $Sm_2SrAl_2O_7$ can be proposed as an intermediate layers in graded TBC. Surprisingly, the hot corrosion stability of above mentioned materials is scarce. Therefore, further studies are needed to understand the hot corrosion stability of these oxides to propose as an intermediate layer between bond coat and top coat in TBCs system. Hence, the intermediate coating materials were synthesized in our laboratory and studied their hot corrosion stability against corrosive environments.

In this regard, $SrTiO_3$, $Gd_2Ti_2O_7$ and $Sm_2SrAl_2O_7$ materials were tested in Na_2SO_4+50 wt.% V_2O_5 and Na_2SO_4+10 wt.% NaCl environments at 900 ºC. The testing temperature was preferred at 900 ºC, because it is the temperature generally an intermediate layer in the TBC can experience, if the TBC operate at 1200 ºC.

2. Experimental Methods

Perovskite $SrTiO_3$ and pyrochlore $Gd_2Ti_2O_7$, double perovskite $Sm_2SrAl_2O_7$ materials were synthesised by hydrothermal and molten flux methods, respectively. A mixture of Na_2SO_4 + V_2O_5 and Na_2SO_4 + NaCl in 1:1 and 9:1 weight ratio were used to conduct the hot corrosion test at 900 ºC for the period of 100 h.

3. Results and discussion

3.1. Perovskite $SrTiO_3$

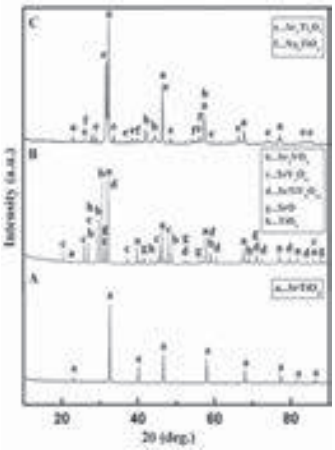

Fig. 1: *XRD patterns of the $SrTiO_3$, (A) before exposure to hot corrosion, after exposure to hot corrosion at 900 ºC in (B) Na_2SO_4+50wt.% V_2O_5 environment and (C) Na_2SO_4+10 wt.% NaCl environment.*

After hot corrosion, additional phases such as Sr_2VO_4, SrV_2O_6, $SrTiV_5O_{11}$ (JCPDS-81-0854, 28-1267 and 48-0540 respectively) and $Sr_3Ti_2O_7$ (JCPDS-78-2479), Na_4TiO_4 (JCPDS-42-0513), TiO_2 were identified in Na_2SO_4+50 wt.% V_2O_5 and Na_2SO_4+10wt.% NaCl environments, respectively (Fig. 1).

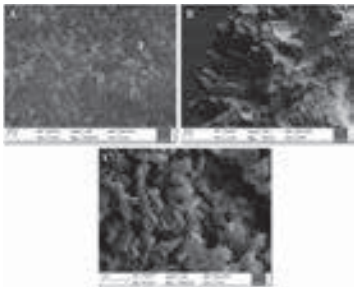

Fig. 2: *Surface morphology of the $SrTiO_3$, (A) before exposure to hot corrosion, after exposure to hot corrosion at 900 ºC in (B) Na_2SO_4+50wt.% V_2O_5 environment and (C) Na_2SO_4+10 wt.% NaCl environment.*

EDS analysis was demonstrated to identify the composition at region 1 in Figure 2 (A,B and C) which are composed of $SrTiO_3$, Sr_2VO_4 and $Sr_3Ti_2O_7$ respectively. These observations are well in agreement with XRD results.

3.2. Pyrochlore $Gd_2Ti_2O_7$

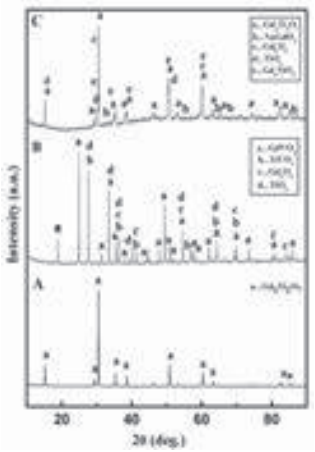

Fig. 3: *XRD patterns of the $Gd_2Ti_2O_7$, (A) before exposure to hot corrosion, after exposure to hot corrosion at 900 ºC in (B) Na_2SO_4+50wt.% V_2O_5 environment and (C) Na_2SO_4+10 wt.% NaCl environment.*

The $Gd_2Ti_2O_7$ sample, after exposure to hot corrosion in Na_2SO_4+50 wt.% V_2O_5 and Na_2SO_4+10 wt.% NaCl environments (Fig. 3), they have exhibited the additional phases, which corresponds to gadolinium vanadate, titanium vanadate, gadolinium oxide and titanium oxide. environment (Fig. 3).

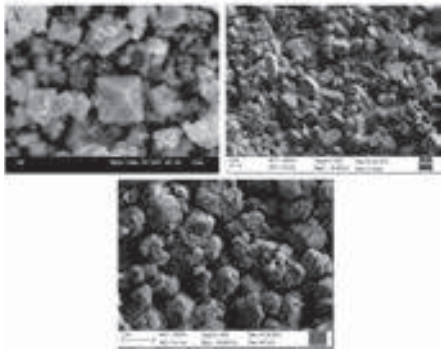

Fig. 4: *Surface morphology of the $Gd_2Ti_2O_7$, (A) before exposure to hot corrosion, after exposure to hot corrosion at 900 ºC in (B) Na_2SO_4+50wt.% V_2O_5 environment and (C) Na_2SO_4+10 wt.% NaCl environment*

EDS analysis was done at various regions of sample surface which showed that after hot corrosion $Gd_2Ti_2O_7$ phase has been changed into $GdVO_4$, $TiVO_4$, Gd_2O_3, TiO_2 and $NaGdO_2$ phases in respective environments. It is interesting to point out that $Gd_2Ti_2O_7$ phase is unstable in both environments at 900 ºC.

3.3. Double perovskite $Sm_2SrAl_2O_7$

The XRD (Fig. 5) and morphological analysis (Fig. 6) revealed that Sm2SrAl2O7 is quite stable in Na_2SO_4+10 wt.% NaCl but not in Na_2SO_4+50 wt.% V_2O_5 environment at 900 ºC. Destabilization rections were occured according to the lewis-acid base character of oxides and molten salt.

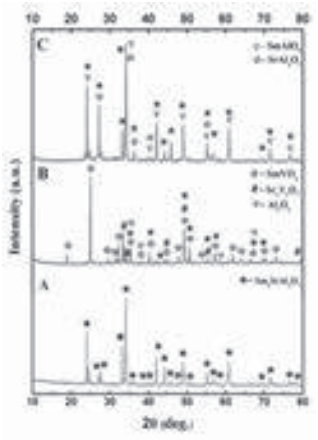

Fig. 5: *XRD patterns of the $Sm_2SrAl_2O_7$, (A) before exposure to hot corrosion, after exposure to hot corrosion at 900 ºC in (B) Na_2SO_4+50wt.% V_2O_5 environment and (C) Na_2SO_4+10 wt.% NaCl environment.*

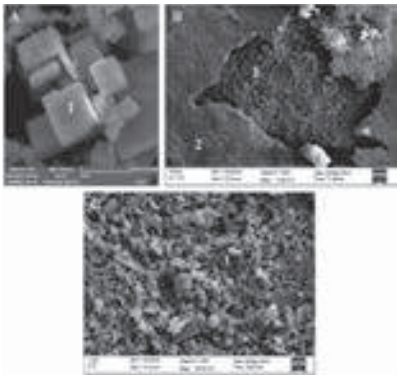

Fig. 6: *Surface morphology of the $Sm_2SrAl_2O_7$, (A) before exposure to hot corrosion, after exposure to hot corrosion at 900 ºC in (B) Na_2SO_4+50 wt.% V_2O_5 and (C) Na_2SO_4+10 wt.% NaCl environments.*

4. Conclusions

1. The perovskites, pyrochlores and double perovskites were undergone destabilization in the Na_2SO_4+50 wt.% V_2O_5 and Na_2SO_4+10 wt.% NaCl environments at 900 ºC.
2. In Na_2SO_4+50 wt.% V_2O_5 environment, the reactions between ceramic oxides and molten salt were observed.
3. The Na_2SO_4+10 wt.% NaCl environment also caused the leaching of elements from their own phase.

References

[1] S. Yamanaka, K. Kurosaki, T. Oyama, H. Muta, M. Uno: J. Am. Ceram. Soc. **88 (**2005) 1496-1499.
[2] Q. Zhixue, W. Chunlei, Weipan: Act. Mater. **60** (2012) 2939-2949.
[3] J. Feng, B. Xiao, R. Zhou, W. Pan and D. R. Clarke: Act. Mater. **60** (2012) 3380-3392.
[4] R. Vassen, X. Cao, F. Tietz, D. Basu, D. Stover, J. Am. Ceram. Soc. 83 (2000) 2023-2028.
[5] W. Ma, D. E. Mack, R. Vaben, D. Stover: J. Am. Ceram. Soc. **91** (2008) 2630-2635.

Improving Hot Corrosion Resistance of Ti-31 Alloys by Thermal Spray Deposition

Jegadeeswaran N.[1], Ramesh M.R.[2], Udaya Bhat K.[1]

[1] Deparment of Metallurgical & Materials Engg, NITK Surathkal, Srinivasnagar P.O., India, 575025
[2] Department of Mechanical Engg, NITK Surathkal, Srinivasnagar P.O., India, 575025

Abstract
Titanium alloys used in gas turbines of power plant sector undergo hot corrosion, when exposed to temperature in the range of 600-800 °C in presence of salts like Na_2SO_4 and V_2O_5. One way of overcoming this is to give a protective barrier coating. This paper reports the results of hot corrosion studies done on Ti-31 and stellite-6 coated Ti-31. Stellite-6 coating was deposited using high velocity oxy-fuel process. The coating was dense, lamellar in nature and thickness was about 280-300 micrometers. Uncoated Ti-31 and HVOF sprayed Ti-31 were subjected to cyclic hot corrosion tests for 50 cycles at 800 °C under the environment of Na_2SO_4+50 wt% V_2O_5. Each cycle consisted of heating at 800 °C for 1 hour followed by cooling for 20 minutes. It is observed that the oxide scale on the Ti-31 was spalling, whereas, the scale on the stellite-6 coating was intact. Thermogravimetric studies indicated that the weight gain and parabolic rate constant for stellite coated Ti-31 is one order less than uncoated Ti-31. Thickness of the oxide scale was very small compared to total stellite coating thickness. Hence, it is concluded that stellite-6 coating provides protection to Ti-31 alloy.

1 Introduction

Titanium alloys are a candidate material for structures of turbines used in power sector [1]. It is mainly due to improved specific strength, fatigue strength and strength at elevated temperatures. Major constraint for the use of Ti alloys comes from the possible damage due to hot corrosion [2]. Ti alloys when used for long duration near 800 °C, in presence of salts like Na_2SO_4, NaCl, V_2O_5 and others undergo accelerated mode of corrosion which is referred to as hot corrosion [3]. Providing a suitable coating to the substrate material is a method to overcome the hot corrosion problems, without sacrificing the benefits offered by the base material and in this context high velocity oxy-fuel spraying (HVOF) is a highly promising method [4]. From protection point of view the coating should have elements like Co, Cr and Al. Stellite-6 is a coating material which is rich in Co and Cr. To the best of our knowledge there is not much literature investigating the improvements in hot corrosion resistance of Ti-31 by coating with stellite-6 using HVOF process.

2 Experimental Procedure

2.1 Materials and coating spraying

Ti alloy, namely, Ti-31 (Ti-6Al-4V) was the substrate material and it was supplied by M/s Midhani, India. Specimens of 25 mmx25 mm and 5 mm (thickness) were cut, ground and cleaned by grit blasting. Commercially available stellite-6 (Make: M/s Shanghai Zhong Zhou Special Alloys, China) was used as the feedstock powder.
HVOF spraying of coating was done using a Metco DJ 2600 gun. Following are the parameters used for spraying-oxygen flow rate, 270 LPM; fuel (LPG) flow rate, 70 LPM; air flow rate, 700 LPM; spray distance, about 20 cm; powder feed rate, 50 g/min; fuel pressure,7 kg/cm^2; air pressure, 5.5 kg/cm^2; oxygen pressure,10 kg/cm^2; nitrogen gas (powder carrying gas) pressure, 5 kg/cm^2.

2.2 Hot corrosion studies

Hot corrosion studies were done in a silicon carbide furnace at 800 ± 5 °C on both uncoated Ti-31 and stellite-6 coated Ti-31, in a molten salt environment of Na_2SO_4+50% V_2O_5. Studies were done for 50 cycles where in each cycle consisted of heating at 800 °C for 1 hour followed by cooling in stagnant air for 20 minutes. Weight change values were measured at the end of each cycle. Visual observations were made after the end of each cycle with respect to colour, luster or physical condition of the oxide scales being formed. The corrosion products of the uncoated Ti-31 and HVOF coated Ti-31 were analyzed by using XRD, SEM and EDX to understand the hot corrosion behaviour.

3 Results and Discussion

3.1 Visual observations and thermogravimetric analysis

For both uncoated Ti-31 and stellite-6 coated Ti-31, there was indication of oxide formation from the first cycle itself. Colour changes during the studies indicated this change. The surface of uncoated Ti-31 became brownish in 23rd cycle and severe spalling was observed from 31st cycle onwards. The stellite-6 coating was dark grey in colour and it turned in to black in the first cycle and it remained as black throughout. There was visible cracks in the surface, otherwise coating was intact.

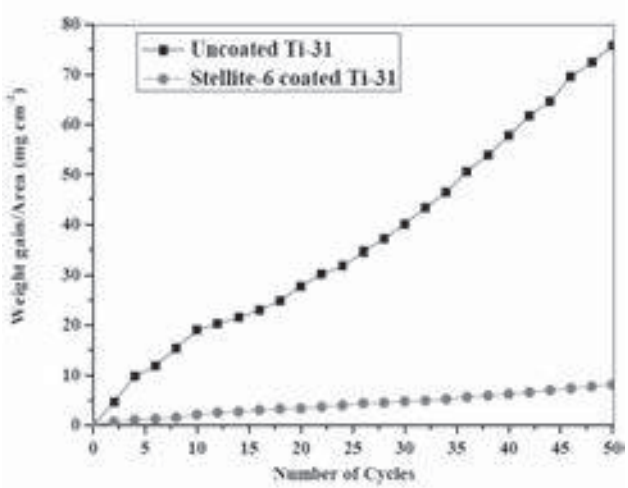

Fig. 1 *Weight gain plots for uncoated Ti-31 and stellite-6 coated Ti-31, after 50 cycles of hot corrosion.*

Plots of weight gain as a function of number of stress cycles is drawn (Fig. 1). Weight gains after 50 cycles are 75.8 and

8.1 g/cm^2 for Ti-31 and stellite-6 coated Ti-31, respectively. This clearly indicates that the oxide scale on Ti-31 is not protective and Ti-31 undergoes rapid weight gain under hot corrosion conditions.

3.2 XRD analysis

X-ray diffractograms of stellite-6 feedstock powder and after HVOF spraying is taken. It is observed that during HVOF process some amount of chromium oxide forms. But majority of the stellite-6 remains as it is without undergoing oxidation. Similarly, XRDs of samples after hot corrosion is obtained. XRD of uncoated Ti-31 show that the surface is rich in TiO_2, Al_2O_3 phases. Surface also has $V_3Ti_6O_7$, AlV_2O4, $AlVO_4$ and $TiVO_4$ as minor phases. Surface of stellite-6 coated Ti-31, after hot corrosion consists CoO and Cr_2O_3 as major phases and NiO, FeO, Na_2O, V_2O_5, $CoCr_2O_4$ and WO_3 as minor phases.

3.3 Microstructural analysis

The micrograph of the Ti-31 surface after hot corrosion for 50 cycles is given in Fig. 2. The surface shows a clear indication of sputtering in the form of independent oxide particles. EDS analysis shows that the surface is rich in TiO_2 and minor quantities of oxides of Al and V. The surface of stellite-6 coated Ti-31 shows a compact morphology without noticeable cracks. The EDS analysis shows that the surface as rich in oxides of Co and Cr. Small amounts of Na_2O, SO_3, V_2O_5, FeO and NiO are also observed.

Figure 3 shows cross-sectional micrograph of the stellite-6 coated Ti-31. Only a small portion of the coating is oxidised during hot corrosion studies. A good amount of coating did not undergo change. It is available for protection. The peeling off in the coating is in laminar way. This prevents the base material from being exposed to molten salt environment. The EDS also indicates that the top oxide layer is rich in oxides of cobalt and chromium.

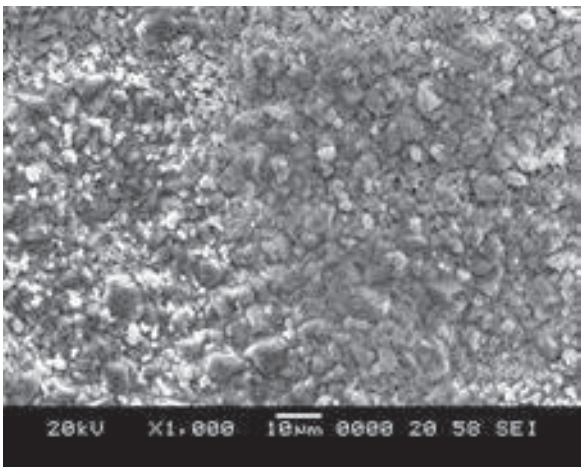

Fig. 2 *SEM micrograph showing morphology of Ti-31 after hot corrosion studies.*

The resistance to hot corrosion is poor for uncoated Ti-31 compared to stellite-6 coated sample. In the case of uncoated Ti-31, all three elements (Ti, Al and V) are prone to oxidation. Although Al can form a protective oxide scale, due to limited fraction in Ti-31, it cannot form a continuous layer. It is a minor fraction and Ti is the major fraction forming TiO_2 on exposure to hot corrosion environment. Wieght gain rate in this investigation is greater than 10 mg/cm$^{2.}$ The value is much higher compared to value reported by Stawiarski et al. [5]. It is attributed to peeling-off the scale and enhanced oxidation due to that. Deviation from parabolic graowth (Fig. 1) also supports this. A large difference in coefficient of thermal expansion is a source for mismatch stress, promoting cracking and peeling [6].

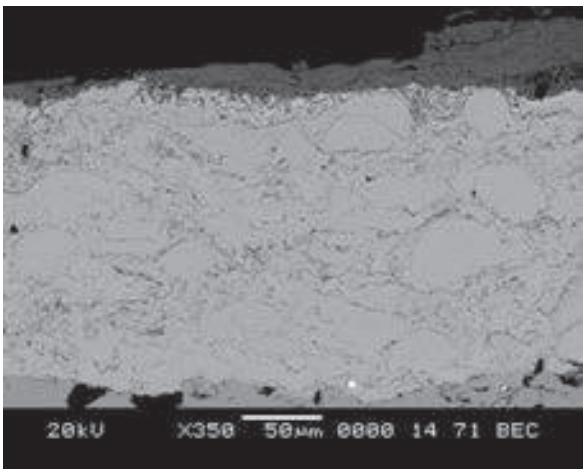

Fig. 3 *Cross sectional micrograph of stellite-6 coated Ti-31, after cyclic hot corrosion studies*

When Ti-31 is coated with stellite-6, cobalt and chromium are the major elements forming coating. They form CoO and Cr_2O_3 and they provide protection against hot corrosion. Formation of spinels like $CoCr_2O_4$ also helps in protection against hot corrosion. Rapid formation of these oxides at the splat boundaries and open pores in the HVOF sprayed coatings reduces penetration of the oxidising species. As a result, the formation of the oxide scale on the coating is limited mainly to the surface of the specimen.

4. Conclusions

The hot corrosion behaviour of Ti-31 alloy is compared with stellite-6 coated Ti-31. The weight gain of Ti-31 is almost one order more than coated Ti-31. The improved hot corrosion resistance of stellite-6 coated Ti-31 is attributed to formation of CoO and Cr_2O_3. The investigation clearly reveals that the cyclic hot corrosion resistance of Ti-31, could be improved by stellite-6 coating sprayed by HVOF process.

5. References

[1] Q. Jin, W. Xue, X. Li, Q. Zhu, and X. Wu: *J. Alloys and Compds*. **476** (2009) 356-359.
[2] I. Gurappa, *Mat. Sci. Engg. A*. **3(56)** (2003) 372-380.
[3] N. Eliaz, G. Shemish, R. M. Latenision: *Engg. Fail. Anal.* **9** (2002) 31-43.
[4] S. S. Chatha, H. S. Sidhu, B. S. Sidhu: *J Miner. Mater. Character. Engg*. **11(6)** (2012) 569-586.
[5] A. Stawiarski, Z. Zurek, W. Szkliniarz, and J. Sieniawski: www.korozja.pl/html/JCM/JCM_08-022. *pdf* date:17-06-13
[6] C. Boettcher: *Surf. Engg*. **16(2)** 2000 148-152.

Corrosion Response of Cold Sprayed IN625 and NiCr Coatings

A S S Balan[1], Vighnesh Chandrasekhar[2], Dheepa Srinivasan[1], Y.C. Lau[3], Eklavya Calla[1] and Vishwanathan Venkatachalapathy[1]

[1] GE Power and Water, GE India Technology Centre, Bangalore 560066, India
[2] Tata-AIG General Insurance Company, Mumbai 400012, India
[3] GE Power and Water, Schnectady - 12345-6000, New York, USA

Corrosion resistant coatings, of Inconel 625 (Trademark of Huntington alloys corporation) and NiCr, were deposited on 4130 steel substrates, using the cold spray coating process, as possible alternatives to bulk corrosion resistant forms. Cyclic potentiodynamic tests were carried out to establish the coating behavior as compared to the bulk as well as a weld clad alloy, in sea water environment. Static corrosion tests were carried out in a $FeCl_3$ environment, and comparisons were made between the as deposited and heat treated coatings, using different process gases, Helium and Nitrogen. The coatings were ranked based on their susceptibility to pitting corrosion, as compared to bulk IN625. Detailed characterization of the coating behavior, interdiffusion characteristics with the substrate, cohesive strength, and residual stress, enabled a selection of the optimum coating that could be used as a possible alternative for bulk corrosion resistant of IN625 on 4130 steel.

1. Introduction

Nickel based superalloy Inconel 625 (IN625) is widely used for corrosion protection applications, both aqueous as well as high temperature corrosion, in various industrial sectors [1]. The presence of Mo and Nb are attributed to the superior corrosion properties of this alloy [2]. With the prohibitive cost of Ni based alloys, it is often not feasible to use bulk forms for these corrosion applications and therefore several applications make use of the superior properties of IN625 as a surface layer, via weld cladding [3], on a steel or a less expensive bulk material, specific to the application. Cold spray technology has been proven to be well suited for obtaining thick, dense metallic coatings [4]. This study comprises a study of the corrosion behaviour of cold sprayed IN625 superalloy and NiCr coatings, and compares the pitting corrosion response IN625 and NiCr, with that of bulk IN625.

2. Experimental Details

Cold spray coatings of IN625 and Ni20wt%Cr (NiCr), of nominal thickness ~ 500 µm, were obtained using a CGT Kinetics 8000, 30 bar (IN625) and Kinetics 4000/47, 40 bar (NiCr), 500-600°C gas temperature, using Helium (He) and Nitrgen (N_2), process gases. The substrate was a low alloy steel AISI 4130 steel (~220 Hv). Microstructural characterization was performed using a Nikon Eclipse MA 200 optical microscope, Keyance VXF 2000, Shimadzu microhardness tester (0.3 H_v), SEM (Carl Zeiss EVO18) with EDS (Oxford, Link). Corrosion tests were performed as per ASTM G61, cyclic potentidynamic polarization, in 5% NaCl, to understand the aqueous corrosion response of these coatings. The pitting behaviour was also monitored in chloride environments, as per ASTM G48, in $FeCl_3$, on polished surfaces. Table 1 lists the corrosion DOE used in this study.

Table 1 : *Corrosion DOE used for this study (AS-As Sprayed), HT (350℃, 2.5h, air)*

	Bulk IN625	IN625 Coating He	IN625 Coating N_2	NiCr Coating He	NiCr Coating N_2
NaCl	-	AS, HT	AS,HT	AS, HT	AS
$FeCl_3$	-	AS	AS	AS	AS

3. Results and Discussion

Dense coatings of IN625 and NiCr (> 99.5%) were obtained using He gas. The NiCr coatings usign N_2 gas were marginally less dense (99%), as shown in Table 2, which lists the measured values of the coating thickness, porosity and hardness, pertaining to the coatings DOE used for this study. Fig. 1(a-b) and Fig.1 (c-d) shows representative SEM and optical micrographs of the cold sprayed IN625 and NiCr coatings, using He and N_2 respectively. The hardness and porosity remain invariant between the multicomponent IN625 coating and the binary NiCr, using He gas, measuring between 500-515 H_v, (< 0.5% porosity). However, there is a significant drop seen in the hardness for both types of coatings, using N_2 gas.

Table 2: *IN625 and NiCr cold sprayed coating properties*

Substrate	Coating	Coating thickness (µm)	Condition	Coating Porosity (%)	Microhardness (H_v0.3) AS	HT
4130 Steel	IN 625	525	Helium	< 0.2%	517	589
		510	Nitroge	0.4%	470	534
	NiCr	490	Helium	0.5%	510	553
		485	Nitroge	0.8%	282	340

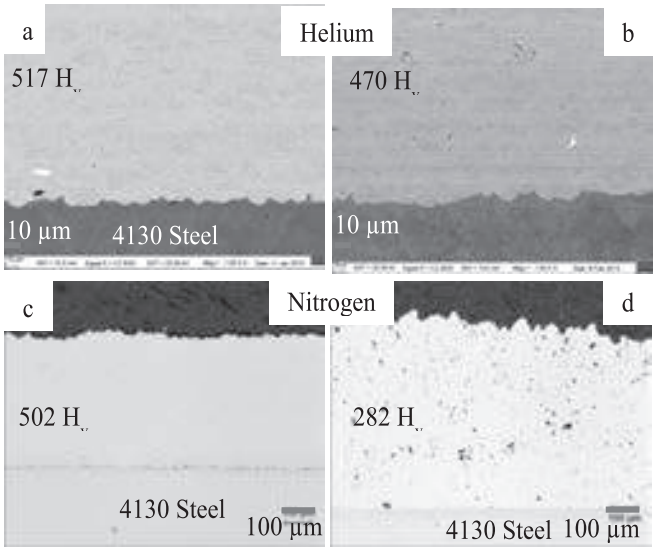

Fig. 1 : Representative micrographs from, (a-b) He coatings (SEM) and (c-d) Nitrogen coatings (optical), for IN625 (a,c) and NiCr (b,d), respectively.

Fig. 2 is a representative cyclic potentiodynamic curve from cold sprayed NiCr coating, using He gas, indicating the difference points on the curve that distinguish the corrosion potential (E_{corr}), breakdown potential (E_{br}) and the protection potential (E_{prot}). Fig. 3 is comparative cyclic potentidynamic plot of cold sprayed IN625 coating, using He and N_2 gases, with bulk IN625. The effective pitting resistance was evaluated and the coatings were ranked, by calculating E_{prot}-E_{br}, as shown in Fig. 4. The static corrosion to $FeCl_3$ response of the coatings is compared in Fig. 5.

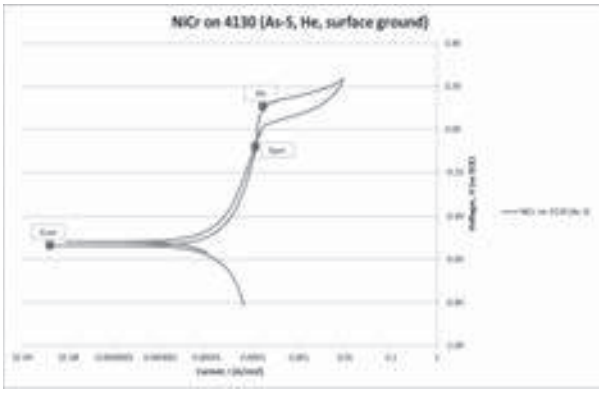

Fig. 2 : *Cyclic potentiodynamic curves (5% NaCl) solution, comparing bulk IN625, with cold sprayed IN625 coaitngs, using He and N_2 gas (in 5% NaCl)*

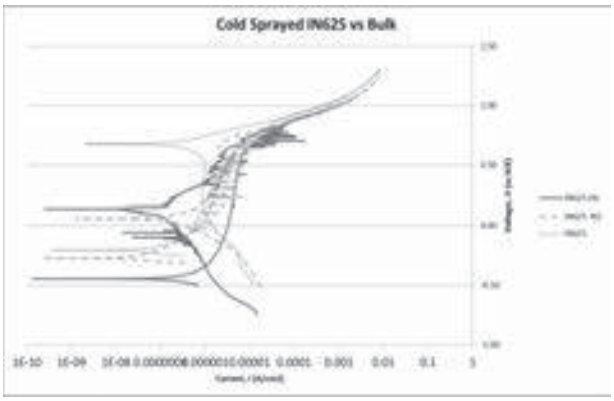

Fig. 3 : *Representative Cyclic potentiodynamic curves (5% NaCl) solution, IN625, with cold sprayed IN625 coaitngs, using He and N_2 gas (5% NaCl)*

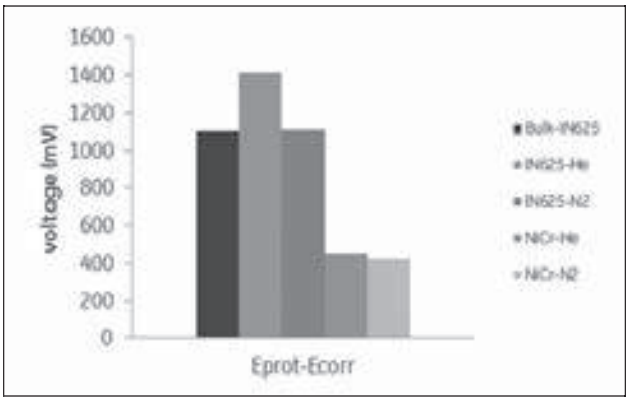

Fig. 4 : *Relative ranking of the pitting resistance of the as sprayed coatings, against bulk IN625(5% NaCl)*

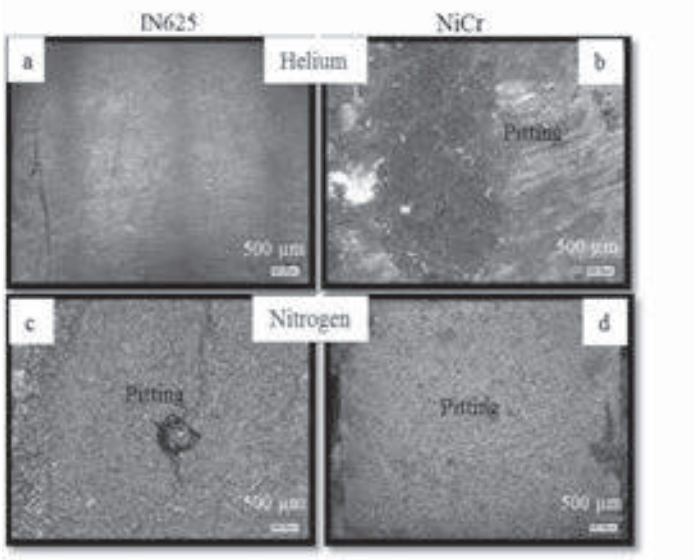

Fig. 5 *: Pitting response, under $FeCl_3$ environment, for cold sprayed coatings, IN625 (a,c) and NiCr (b,d), using He(a,b) and Nitrogen (c,d), process gas.*

4. Conclusions :

Dense IN625 and NiCr (0.5 mm) cold sprayed coatings were obtained using He and N_2 as the process gas, on 4130 steel substrates. Both types of alloy coatings measured between 500-520 H_v in the as sprayed condition, using He, however there was a significant reduction in the hardness seen on using N_2 gas, by 10% for IN625 and 50% for NiCr. Upon HT, at 350°C, all the coatings showed an increase in the hardness, by 10-15%, attributed to the formation of recrystallized fine grains (50-200 nm) [5]. IN625 (He) coatings stand out to be the best, even better than bulk IN625, in both NaCl and $FeCl_3$ environments. Inspite of having dense coatings, the polarization curves show a smaller slope and larger current for NiCr coatings, using both He and N_2 gas, as compared to IN625 coatings. The static $FeCl_3$ tests revealed the formation of pits in all the coatings, except the He sprayed IN625 coating. Overall, the corrosion tests on the as sprayed coatings indicate that the IN625 coatings sprayed using Helium gas, show the best resistance, to pitting corrosion, both under aqueous and chloride conditions, even better than bulk IN625.

5. Acknowledgements :

The authors thank Dr. Leonardo Ajdelsztajn, GE, Global research, Schnectady, for providing the IN625 coatings using N_2 gas, and Mr. Adam Drufke, program manager, GE, Oil and Gas, for financial support, for carrying out this study. Mr. Christopher Thompson, Dr. Sundar Amancherla and Dr. Kathleen Morey, GE Power and Water are acknowledged, for supporting this work.

6. References

[1] L. Thivillon, Ph. Bertrand, B. Lagel, I. Smurov, J. Nucl. Mater. **385 (2009) 236-241.**
[2] Inconel 625, Special Metals Publn. wspecialmetals.com
[3] H.L. Eiselstein, D.J. Tillack, in E.A. Loria (Ed.), Superalloy 718. 625 and various derivatives, (1991) 1-11.
[4] A.N. Papyrin, Cold spray technology, Elsevier, 2007.
[5] D. Srinivasan and R. Amuthan, *Superalloys* 718, 625 and 706 conference proceedings, Sept 2014.

High Temperature Exposure Studies of HVOF Sprayed Cr_3C_2-25(NiCr)/ (WC-Co) Coating

Manpreet Kaur[1], Harpreet Singh[2], Satya Prakash[3]
[1]Baba Banda Singh Bahadur Engineering College, Fatehgarh Sahib, India
[2] Indian Institute of Technology Ropar, Rupnagar, India
[3]Indian Institute of Technology Roorkee, Roorkee, India

Abstract
In this research, development of Cr_3C_2-25(NiCr)+25%(WC-Co) composite coating has been done and investigated. Cr_3C_2-25(NiCr)+25%(WC-Co) composite powder [designated as HP2 powder] was prepared by mechanical mixing of [75Cr_3C_2-25(NiCr)] and [88WC-12Co] powders in the ratio of 75:25 by weight. The blended powders were used as feedstock to deposit composite coating on ASTM SA213-T22 substrate using High Velocity Oxy-Fuel (HVOF) spray process. High temperature oxidation/corrosion behaviour of the bare and coated boiler steels was investigated at 700°C for 50 cycles in air, as well as, in Na_2SO_4-82[$Fe_2(SO_4)_3$] molten salt environments in the laboratory. Erosion-corrosion behavior was investigated in the actual boiler environments at 700±10°C under cyclic conditions for 1500 hours. The weight change technique was used to establish the kinetics of oxidation/corrosion/erosion-corrosion. X-ray diffraction (XRD), field emission-scanning electron microscopy/energy-dispersive spectroscopy (FE-SEM/EDS) and EDS elemental mapping techniques were used to analyze the exposed samples. The uncoated boiler steel suffered from a catastrophic degradation in the form of intense spalling of the scale in all the environments. The oxidation/corrosion/erosion-corrosion resistance of the HVOF sprayed HP2 coating was found to be the better in comparison with standalone Cr_3C_2-25(NiCr) or WC-Co coating. A simultaneous formation of protective phases such as Cr_2O_3, $NiCr_2O_4$ and $NiWO_4$ as strong phases might have contributed the best properties to the coating.

1 Introduction

High temperature oxidation/corrosion and erosion-corrosion of coal-fired boiler tubes are the key material issues in these plants since it affects the thermal efficiency and hence the electricity production [1]. The maintenance costs for replacing broken tubes in these installations are also high. One of the most economical and feasible approach to increase the resistance of the materials exposed to steam environments is the deposition of metallic coatings by thermal spraying techniques [2].

Although, a considerable work has been done to evaluate the performance of various thermal spray coatings in air and salt environments under laboratory tests, however there is a further need to develop high performance coating compositions. Literature reveals that the thermal spray WC-Co coatings have relatively good wear and erosion resistance, whereas Cr_3C_2-NiCr coatings have comparatively better hot corrosion resistance. Therefore, in the present research, mechanical mixing of Cr_3C_2-25(NiCr) [Cr_3C_2-NiCr] and WC-12Co [WC-Co] powder was done to obtain a suitable composition for the combined erosion-corrosion resistance. The in-depth characterization of the as-sprayed and the exposed specimens was done.

2 Coating Formulation, Characterisation and High-Temperature Exposure Studies

The substrate material selected for the study was a boiler steel, namely, ASTM SA213-T22 (T22), which was procured from Guru Gobind Singh Super Thermal Power Plant (GGSSTPP) (Ropar, Punjab, India). The composition of the steel is 0.15 C, 0.3-0.6 Mn, 0.03 max P, 0.03 max S, 0.5 Si, 1.9 to 2.60 Cr, 0.87 to 1.13 Mo, and 94.66 Fe. HP2 powder was prepared by mechanical mixing of Cr_3C_2-NiCr (particle size −45+15µm) and WC-12Co (particle size −45+15µm) powders in the ratio of 75:25 by weight. The specimens were grit blasted with Al_2O_3 (grit 60) before the deposition of the coatings. The coatings were then deposited on the steel specimens at Metallizing Equipment Company Private Limited (Jodhpur, India) with their commercial HVOF (HIPOJET-2100) apparatus operating with oxygen and liquid petroleum gas (LPG) as input gases. The spray parameters have been reported in the earlier publication of the authors [3]. The thickness of the coating was kept in a range of 225 ± 25 µm. The as-coated samples were characterised to investigate their surface and cross-sectional microstructures and compositions, as per the detailed procedures reported elsewhere [3]. High-temperature oxidation, corrosion and erosion-corrosion tests were conducted in the laboratory and in actual boiler environments on the coated and uncoated samples as per the procedures reported elsewhere [3].

3. Results and Discussion

3.1 Microstructure of As-sprayed coating

The blending of the two powders resulted into the formation of composite-like coatings, where the WC-Co phase was nearly uniformly distributed into the Cr_3C_2-NiCr matrix. The WC-Co phase was found to have a laminar splat-like distribution into the said matrix. The coatings seemed to be intact with the substrate

3.2 High Temperature Oxidation, Corrosion and Erosion-Corrosion Behaviour

During air oxidation studies, the oxide scale of the coated steel was intact with no cracks and spallation, whereas the oxide scales for the bare T22 steel showed intensive tendency towards cracking or spalling. From the weight change data of the uncoated and coated steels, HP2 coating showed the lowest weight gain values (0.26 mg/cm^2). Further, the XRD analysis of the coated steel showed the formation of Cr_2O_3, $NiWO_4$ and $NiCr_2O_4$ as strong intensity

phases after oxidation. The oxide particularly Cr_2O_3 may partially inhibit oxidation of the substrate steel by blocking the diffusion of reacting species towards the substrate alloys, as had been suggested by Nicoll and Wahl [4]. Surface and cross-sectional FE-SEM/EDS analysis further supported the formation of these phases in the coated T22 steel. The schematic diagram showing probable oxidation mode of attack for the HVOF spray HP2 coated T22 steel exposed to air at 700°C for 50 cycles is shown in Fig. 1.

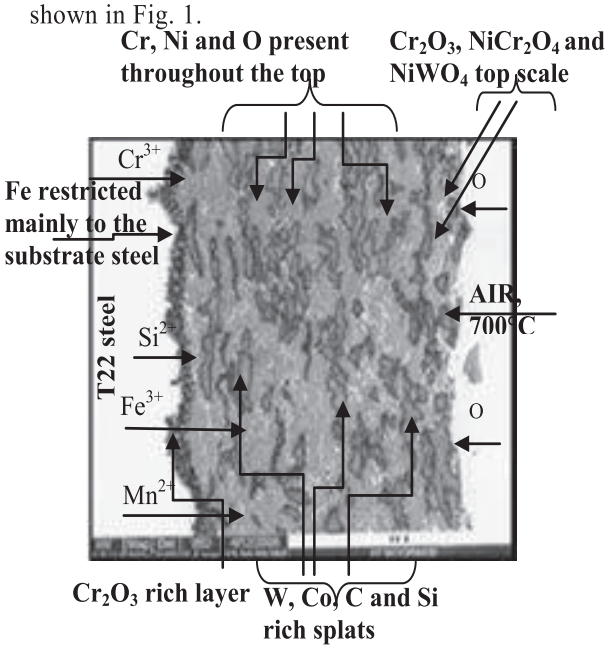

Fig. 1. *Schematic diagram showing probable oxidation mode for the HVOF spray HP2 [(Cr_3C_2-NiCr)+25%(WC-Co)] coated T22 steel*

In molten salt envirnments, the coated steel showed no major spallation and the oxide scale was intact. The weight change measurements showed the overall lower weight gain values for the HP2 coating. The corroded scale revealed the formation of $NiWO_4$ as a very strong phase, WC as a strong phase and $NiCr_2O_4$, Fe_2O_3, NiO, CoO and WC_{1-x} as the medium intensity phases.

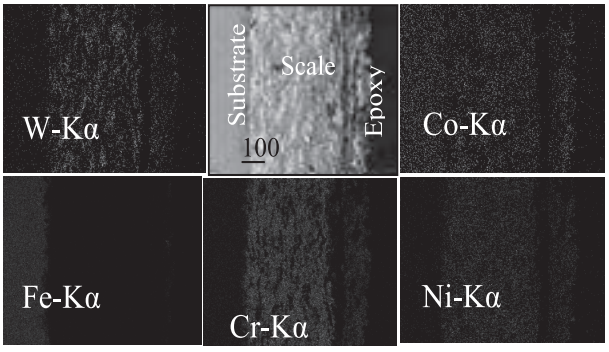

Fig. 2. *Composition image (SE) and X-ray mappings of the cross-section of HVOF sprayed HP2 [(Cr_3C_2-NiCr)+25%(WC-Co)] coated T22 boiler steel subjected to cyclic oxidation in Na_2SO_4-82%$Fe_2(SO_4)_3$ environments at 700°C after 50 cycles.*

The respective X-ray mappings analysis (Fig. 2) showed that the oxide scale is containing mainly Cr, Ni and W with significant amounts of Co. Nickel is nearly uniformly dispersed throughout the cross-section of the scale. Fe which is the basic element of the substrate steels is restricted to the substrate only.

In actual boiler environments, based upon the thickness lost data, again a minimum corrosion rate in the given environment was offered by HP2 coated T22 steel which was around 26% of that for the uncoated steel. The XRD analysis further revelaed the formation of Cr and CrNi as very strong phases and Cr_3C_2 as a strong phase. Ni, W_2C, WC, Co, Cr_2O_3 and Al_2O_3 are observed as medium intensity phases and Fe_2O_3 as a weak phase. The X-ray mapping analysis for HP2 coated case (Fig. 3) indicates that the oxide scale is containing mainly Cr, Ni and W with some amounts of Co. There are areas rich in W which are depleted of Cr and Ni and vice-versa. Co seems to be aligning in W-rich areas. Iron has been found to be restricted to the substrate steel only.

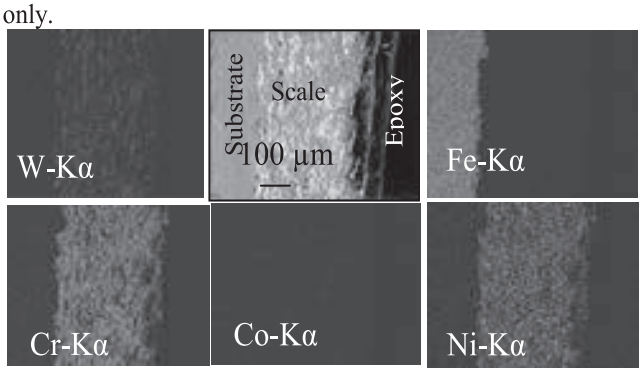

Fig.3. *Composition image (SE) and X-ray mappings of the cross-section of HVOF spray HP2 [(Cr_3C_2-NiCr)+25%(WC-Co)] coated T22 boiler steel subjected to low temperature superheater of the Stage-II Boiler of GGSSTPP at 700°C after 1500 hrs.*

4. Conclusions

The oxidation/corrosion/erosion-corrosion resistance of the HVOF sprayed HP2 coating was found to be the better in comparison with standalone Cr_3C_2-25(NiCr) coating. A simultaneous formation of protective phases such as Cr_2O_3, $NiCr_2O_4$ and $NiWO_4$ as strong phases might have contributed the best properties to the coating. The HP2 coating showed the ability to retain its microstructural features even after the exposure to air, molten salt and actual boiler environments.

Acknowledgement

Harpreet Singh et al thankfully acknowledge the research grant from Department of Science and Technology, New Delhi (India) under SERC FAST Scheme (File No. SR/FTP/ETA-06/06, Dated March 16, 2006) to carry out this R & D work, titled "Development of Erosion-Corrosion Resistant Thermal Spray Coatings for Power Plant Boilers."

References

[1] A.J. Lopez, M. Proy, V. Utrilla, E. Otero and J. Rams: Mat. and Design, 59 (2014) 94-102.

[2] V. R. S. Sa Brito, I.N. Bastos and H.R.M. Costa: Mat. and Design 41 (2012) 282-288.

[3] M. Kaur, H. Singh and S. Prakash: Mett. and Mat. Trans. A 43A (2012) 2979-2993.

[4] A. R. Nicoll and G. Wahl: Thin Solid Films, 95 (1983) 21-34.

A Study on Wear and Corrosion Resistant Cr_2O_3-Al_2O_3 Coating by Detonation Spray Technique

P Suresh Babu, D Srinivasa Rao, D Sen and S V Joshi
International Advanced research Centre for Powder Metallurgy and New Materials (ARCI)
Balapur P.O., HYDERABAD 500005, INDIA

Abstract

Thermal spray techniques have been widely used to deposit various ceramic composite coatings on different types of industrial components to impart high resistance to wear and corrosion for better performance in harsh environments. The detonation spray coating (DSC) process utilizes a higher particle velocity and lower flame temperature compared to air plasma spray (APS) and enables dense coatings to be generated. A variety of oxide, metal composite and cermet coatings has been deposited using the DSC technique. The present talk focuses on Cr_2O_3-Al_2O_3 cermet composite coatings deposited by the DSC technique on a Ti alloy substrate. The microstructure of the coatings was analysed using SEM and EDS. Phase formation in the coatings was studied by x-ray diffraction. Vickers Hardness of coatings was measured and three-body abrasive wear behaviour and electro-chemical corrosion tests in salt solution of the coatings were carried out. The material removal mechanism and degradation of detonation sprayed Cr_2O_3-Al_2O_3 coating will be discussed in terms of coating microstructure and compared against the plasma sprayed Cr_2O_3 coating popularly used in textile, marine and aerospace industries.

1 Introduction

A variety of materials like metals, cermets, and ceramics can be deposited using the detonation spray coating (DSC) technique. Generally, most of ceramic coatings are deposited by atmospheric plasma spray (APS). The advantage of the DSC process is that it uses higher particle velocities and lower particle temperatures. This helps retain the phases present in the initial feedstock powder in the final coatings, which may not necessarily be the case of plasma spray. For example, the formation of metastable γ-Al_2O_3 phase in plasma sprayed Al_2O_3 coating deteriorates the properties of the coating. However, the γ- Al_2O_3 phase formation is very limited in detonation sprayed Al_2O_3 coatings.

Chromium oxide (Cr_2O_3) is widely being used as a wear & corrosion resistant material on a variety of engineering components used in aerospace, marine, chemical, wire manufacturing, textile, pump and paper industries [1]. Similarly, Al_2O_3 coatings also exhibit good mechanical and anti-wear performance. In Cr_2O_3-Al_2O_3 coatings, Cr_2O_3 stabilizes the α-Al_2O_3 phase in the final coating [2]. It has been reported that plasma sprayed Cr_2O_3-Al_2O_3 coatings showed better mechanical properties when the Al_2O_3 content is in the range from 10-30 wt% compared to pure Cr_2O_3 and Al_2O_3 plasma sprayed coatings. However, very limited information is available on DSC deposited Cr_2O_3-Al_2O_3 coatings and even so in proprietary form.

The aim of present study is deposition and study of Cr_2O_3-Al_2O_3 coatings by the DSC technique. Detailed microstructural analysis was carried out along with a study of the mechanical, wear and corrosion properties, and a comparison was made with the atmospheric plasma sprayed Cr_2O_3 coating.

2 Experimental Details

Cr_2O_3-20%Al_2O_3 composite coatings were deposited by detonation spray, and Cr_2O_3 by atmospheric plasma spray, on Ti alloy using commercially available powders at optimum processing conditions. Coating thickness of around 300μm was maintained on all samples generated for microstructural, mechanical, corrosion and wear property studies. Surface roughness was measured using a contact stylus profilometer. Surface morphology and cross-sectional microstructures of the coated samples were examined using a scanning electron microscope (Hitachi, Japan) attached with an EDS detector. For phase identification, X-ray diffraction (XRD) patterns were recorded on a Bruker D8 diffractometer with Cu $K\alpha_1$ radiation in the range $20^o<2\theta<90^o$.

Three-body abrasive wear tests were carried out as per the ASTM G 65 standard with silica as the wear medium. Weight loss of the samples was measured after every 200 revolutions. SEM analysis was carried out on worn surfaces to understand the material removal mechanisms. Corrosion tests were carried out on coated samples of area $1cm^2$ exposed to 3.5% NaCl solution (pH=7) for 48hrs. A potentiodynamic polarization scan was obtained in the potential range –0.8V to +1.0V by using Corrware software.

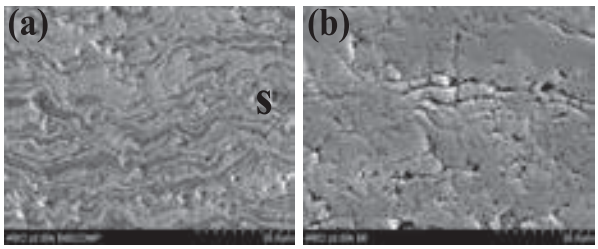

Fig.1 *Cross-sectional SEM images of* ***(a)*** *detonation sprayed Cr_2O_3-20%Al_2O_3 and* ***(b)*** *plasma sprayed Cr_2O_3.*

3 Results and Discussion

Cross sectional micrographs of detonation sprayed Cr_2O_3-20%Al_2O_3 (DSC) and plasma sprayed Cr_2O_3 (APS) coatings are shown in **Fig.1 (a-b)**. The micrograph of DSC coating exhibited a dense structure with alternate Cr and Al oxide layers and solid solution formation at some places (indicated by 'S' in the micrograph). In contrast, high

porosity, and cracks at splat boundaries and within the splats were noticed in APS coating.

Surface roughness (average R_a) of DSC and APS coatings was 0.06 µm and 0.04 µm respectively. Porosity of the coatings was measured using image analysis software and the average porosity values were found to be around 0.39% and 1.78% in DSC and APS coatings respectively while average Vickers Hardness values at 200g load measured on the coating cross-sections were $H_{V0.2}$1221 and $H_{V0.2}$1139. XRD phase analysis in the DSC coating revealed Cr_2O_3, Al_2O_3 and Cr-Al-oxide, and only Cr_2O_3 phase in the APS coating. Peak broadening was more in case of the APS coating as compared to the DSC coating, attributed to amorphous/ nanocrystalline phase content in the former due to increased melting of feedstock in the plasma spray and rapid solidification of splat immediately after deposition.

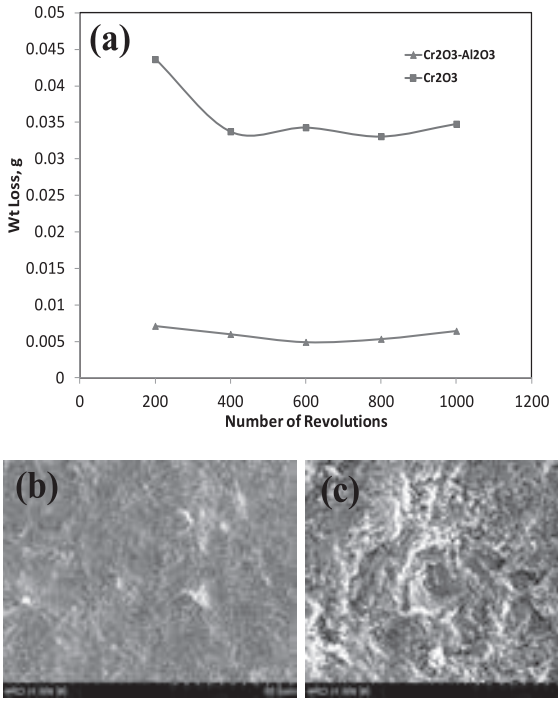

Fig.2 (a) *Abrasive wear loss of coatings. SEM images of* ***(b)*** *detonation sprayed Cr_2O_3-20%Al_2O_3 and* ***(c)*** *plasma sprayed Cr_2O_3 worn surface after testing using SiO2 abrasive medium.*

Three-body abrasion wear loss of both coatings is shown in **Fig. 2(a)**. Tests were carried out up to 1000 revolutions with 200 revolutions/lap. The wear loss became stable after the first lap. The average weight loss per revolution of DSC coating ($28X10^{-6}$ g/rev) is six times lower than that of APS coating ($181X10^{-6}$ g/rev). SEM images of worn surfaces are shown in **Fig. 2(b-c)**. It is clear from the SEM images that the worn surface of DSC coating is smoother and only micro chipping or micropolishing is the dominant material removal mechanism. In contrast, the worn surface of the APS coating shows higher roughness and also cracking, chipping, plucking of splats in the worn surface region and may be the dominant material removal mechanisms. The dense structure and alternative layers of Al and Cr oxides in the detonation sprayed Cr_2O_3-20%Al_2O_3 DSC coating resulted in superior abrasion wear resistance as compared to porous and cracked plasma sprayed Cr_2O_3 coating.

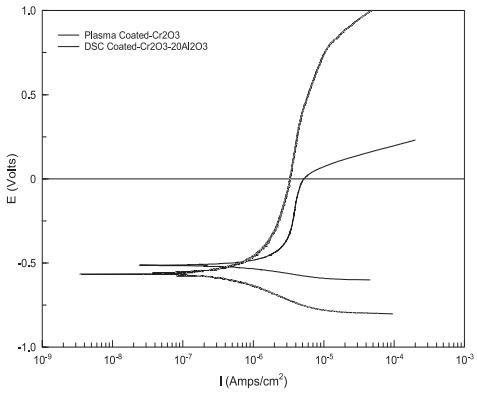

Fig.3*Potentiodynamic polarization curves for detonation sprayed Cr_2O_3-20%Al_2O_3 and plasma sprayed Cr_2O_3 coatings in 3.5%N NaCl electrolyte.*

Potentiodynamic polarization tests were carried out on coatings and results are shown in **Fig. 3**. A Tafel fit was employed to analyze the polarization curves, and corrosion rates were obtained by extrapolating the Tafel slopes. A corrosion rate of DSC coating is 0.24 mpy, which is one third of the corrosion rate of APS coating (0.75 mpy), indicating excellent corrosion resistance of DSC coating compared to APS coating.

4 Conclusions

The microstructure of detonation sprayed Cr_2O_3-20%Al_2O_3 coating is very dense and consists of alternative layers of Cr and Al rich oxides. Higher hardness was observed in the detonation sprayed Cr_2O_3-20%Al_2O_3 compared to plasma sprayed Cr_2O_3 coating. The detonation sprayed Cr_2O_3-20%Al_2O_3 coating exhibited superior abrasive wear and corrosion resistance properties as compared to plasma sprayed Cr_2O_3 coating.

5 Acknowledgements

Authors would like to thank The Director, ARCI, for permitting to present this work in the conference. Suresh Babu acknowledges the support provided by Centre for Engineered Coatings in coating deposition and the Centre for Materials Characterization and Testing for analysis.

6 References

[1] A. Cellard, V. Garnier, G. Fantozzi, G. Baret, P. Fort: Ceramics International. **35** (2009) 913–916.

[2] K. Yang, X. Zhou, H. Zhao, S. Tao: Surf. Coat. Technol., **206** (2011) 1362-1371.

Advancement in HP/HVOF Thermal Spray Equipment & Materials

Rakesh K Anand

Consultant (Thermal spray Equipment & materials), Praxair India Private Limited.
215, Atrium, unit 004, C wing, Andheri Kurla road, Andheri- East. Mumbai-400093

Abstract

Praxair Surface Technologies and TAFA Incorporated is a world leader in thermal spray equipment & materials, and coatings technology. As a primary contributor to the development and applications of High Pressure, High Velocity Oxygen-Fuel spraying, Praxair and TAFA has designed a complete family of HP/HVOF products reflecting years of equipment engineering and coatings expertise. With over 60 years of coatings experience, we apply hardware, materials, and technical expertise to HVOF products that produce the industry's most advanced coating solutions.

Safety:

Praxair and TAFA take thermal spray safety very seriously. All of our HP/HVOF® systems are engineered and built for productive and safe operation.

Powders:

Praxair and TAFA is a leading supplier of HVOF powders specifically designed for use with the JP-5000®, JP-8000™ HP/HVOF®, and other HVOF systems. A solid commitment and development, linked with state of-the-art manufacturing facilities, allow us to meet both small and large production requirements. We manufacture extensive lines of carbides, metal alloys, and ceramic powders designed for high deposition efficiency and unsurpassed coating quality.

Our Indianapolis, IN powder facility manufactures quality carbide and alloy powders specifically designed to produce exceptional HVOF coatings. The powder processes generate materials with the precise characteristics to allow HVOF systems to produce the hardest, thickest, most dense coatings .

Conclusion:

The continuous development in Thermal spray equipment & Materials has increased tremendously Scope of usage of Hp/ Hvof technology to resist different kinds of wear & increase life of components thus saving money for all type of industries.

Mechanisms Study Of High Hardness Wear Resistant Coating Onto Heat Susceptible Substrates Deposited By Low Power Microwave Plasma Spray

Ahmad Redza, Toshiaki Yasui, Masahiro Fukumoto
Department of Mechanical Engineering, Toyohashi University of Technology, 1-1 Hibarigaoka, Tempaku, Toyohashi, Aichi 441 8580, Japan.

Abstract
Microwave plasma spray requires relatively low power in comparison to other plasma spraying method and is operable under atmospheric pressure condition. However, the research of using microwave source as the plasma spray method is still few and the mechanisms are less known. Therefore, our research is focusing on the study of understanding the mechanisms in microwave plasma spray. Until now, we are able to generate plasma below 0.5 kW and high melting point material coatings deposition is possible. Furthermore, due to the low heat input, coatings are also able to be deposited onto heat susceptible substrates such as CFRP and high carbon steel. Generally, hard chrome plating is used to deposit high hardness coatings but this method has disadvantages such as it produces poisonous exhaust liquids. Such coatings deposition is also possible by conventional plasma spray but due to the excessive heat input, the microstructural change of the materials is occurred. By controlling the working gas flow rate and spraying distance as the important factors influencing the substrates temperature, we are able to deposit hard chrome coating onto heat susceptible substrates with the hardness higher than the ones produced by hard chrome plating and the mechanisms are also studied.

1 Introduction

Microwave plasma spraying is the method which needs relatively low power if compared to other plasma spraying method and operable under atmospheric pressure. Until now, microwave plasma spraying device is able to produce plasma using power below 0.5kW and able to deposit high melting point material coatings such as ceramics. Furthermore, due to the low heat input, coating can also be deposited onto CFRP[1]. On this study, we are focusing on the most well-known material used for high hardness coating which is chromium. Hard chrome plating is a conventional method to deposit hard chrome coating but this method has some disadvantages such as it produces poisonous liquid which are harmful to human and the low deposition speed. Therefore, from the previous research study mentioned beforehand, the deposition of coating by using microwave plasma spraying method is expected to overcome these problems. This is due to the facts that this method will not produce harmful exhaust materials and could contributes high deposition speed with relatively low power consumption comparing to other plasma spraying methods. We are able to deposit chrome coating onto heat susceptible subtrates with the hardness higher than the hard chrome plating[2]. However, the mechanisms is not studied well. Therefore, the objective of this study is to investigate the mechanisms involved in the deposition of the coating on high carbon steel and CFRP which are susceptible to heat.

2 Experimental procedure

Figure 1 shows the schematic diagram of the atmospheric pressure microwave plasma spraying device. As the plasma generation method, the micro wave oscillates from magnetron in frequency 2.45GHz, high electric field strength is generated to the tip of the antenna arranged on the center axis of the cylindrical resonator. Plasma is generated by dielectric break of the working gas supplied from the tip of the antenna. The spray particle was inserted inside the aerosol chamber, and supplied with the working mixture into plasma. Experimental conditions are shown in Table 1. In this experiment, the working gas flow rate, input power and substrate materials which are important parameters in the spraying process were investigated. The mechanisms were studied by the observation of coating morphologies as well as splat particles conditions by using scanning electron microscope (SEM). Hardness of the coatings were evaluated by Vickers micro-hardness test. X-ray diffraction test was performed for the composition of the coatings on SUS304 substrates.

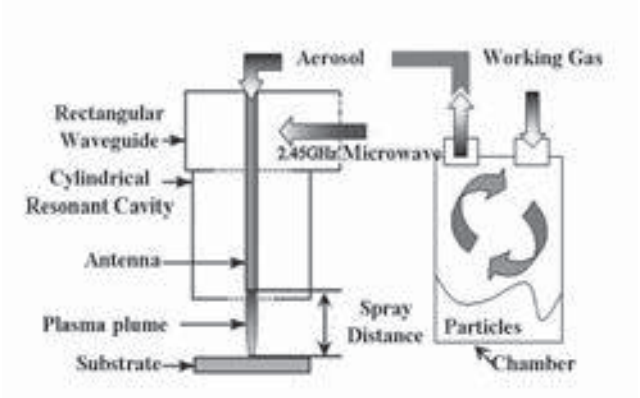

Fig. 1 *Schematic diagram of the atmospheric pressure microwave induced plasma spray.*

Table 1 *Experimental conditions*

Input power	0.5 kW
Working gas flow rate (W.G.)	Ar 11,15,19 L/min
Operation time	360 s
Spray distance (S.D.)	30,35,40 mm
Spray particle	Cr (10μm)
Substrate	SUS304 High Carbon Steel CFRP (T_g : 523K)

3 Results and discussions

X-ray diffraction test was conducted on the deposited coatings by changing the spraying distance from 30 to 40 mm at 19l/min of working gas flow rate which is considered as the optimum conditions. The results are

shown in Fig. 2. From the results, the peak of chromium (III) oxide which is an oxide of Cr was confirmed inside the coatings. From this, it can be considered that the emergence of high hardness chromium (III) oxide during spray is resulting the increase of the coating hardness. Moreover, it turned out that the peak intensity of chromium (III) oxide becomes higher with the increase of spraying distance. The oxidization of the Cr particles is considered to rise since the in-flight travelling time of the particles exposed into the atmosphere increased with the increment of spraying distance.

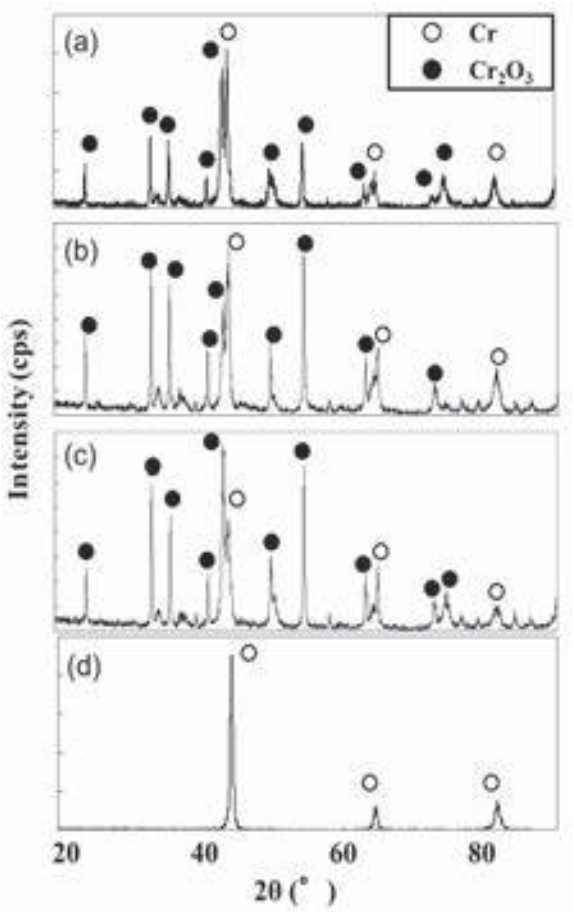

Fig. 2 *X-ray diffraction patterns of Cr coatings at spray distance (a) S.D. 30mm, (b) S.D. 35mm, (c) S.D. 40mm; (d) Cr feedstock powder*

Fig. 3 shows the SEM morphologies of splat collected on high carbon steel and CFRP substrates respectively at optimum condition which is at 19 l/min of gas flow rate and 30 mm of spray distance. The deposition rate of Cr coating is slower for the coating onto CFRP. This is due to the deposition mechanisms of the coating is different for the particular substrates type. From the observation, it is clear that the surface of high carbon steel substrate is not changed during the spray and the fully flattened splat as well as the half molten particles is adhered to substrate surface. While on CFRP, the polymer part of the surface is slightly melted and the spray particles is observed to be gathered at the area that is appeared to be the carbon fibre.

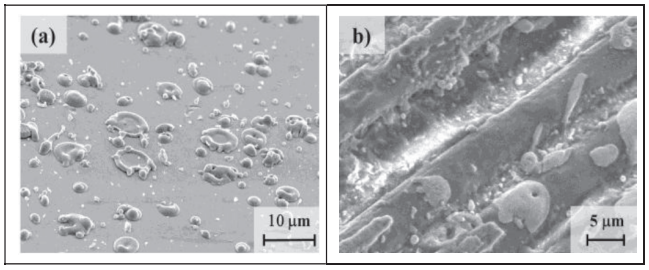

Fig. 3 *SEM surface morphologies of splat collected on (a) high carbon steel and (b) CFRP substrates.*

Fig. 4 shows the cross sectional morphologies of Cr coating deposited onto high carbon steel and CFRP respectively at optimum conditions. From the observation of the interface between the coating and the substrates, the bonding mechanism is considered to be physical bonding with mechanical interlocking in between the coating and the carbon fibre as seen in Fig. 4. In this observation, coating is seen to be adhered also to the polymer of CFRP rather than only onto carbon fibre means that there is also bonding between the Cr particles and the polymer. The particle temperature is also can be considered to be at the level that will slightly melt the polymer to increase the bonding between the coating and substrate's suface but will not ruin the structure of the polymer from the observation of the condition of the polymer that is still remain intact.

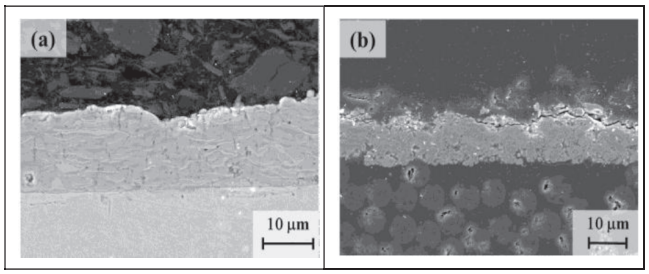

Fig. 4 *SEM Cross sectional morphologies of Cr coating deposited onto (a) high carbon steeland (b) CFRP substrates.*

3 Conclusions

It is clarified that high hardness chrome coating is able to be deposited on heat susceptible substrates by using microwave plasma spraying method. The excellent hardness of the coating obtained by microwave plasma spraying method is considered to be the result of the emergence of chromium (III) oxide. The bonding mechanisms of Cr coating onto the substrates is considered to be physical bonding with mechanical interlocking in between the coatings and the substrates.

4 References

[1] T. Kondo, T. Yasui and M. Fukumoto: "Fabrication and Evaluation of Ceramics Coatings by Atmospheric Microwave Plasma Spray", National Meeting of Japan Thermal Spray Scociety, pp. 206-207 (2010) (in Japanese)
[2] A. Redza, T. Yasui and M. Fukumoto: "Deposition of High Hardness Coating by Using Low Power Atmospheric Pressure Microwave Plasma Spray", Asian Thermal Spray Conference, pp. 147-148 (2012)

High performance wear resistance titanium coating on CFRP materials using high pressure warm spray system

Amirthan Ganesan[1], Okada Takuma[1], Motohiro Yamada[1], Masahiro Fukumoto[1]
[1] Department of Mechanical Engineering, Toyohashi University of Technology, Toyohashi 441-8580, Japan

Abstract
Use of polymer materials in engineering application has been gradually increased year by year. However, for the application of erosion critical area or the application where the surface performances are more desirable, then these polymers are stay behind. Recent days, the polymers and polymer based composite materials surface performances have remarkably been improved by thermal spray coating. Titanium is a low dense and high strength material and thus can be preferable used for surface production applications. So far deposition of titanium on the polymer substrate is considered as mirage. To our knowledge, no successful results have been reported on the thermal spray titanium coating on the polymer substrate. In our present work, a high dense and thick titanium coating was successfully deposited on the CFRP substrate using the newly developed high-pressure warm spray system. This technique is considered as a highly versatile, which can operate over wide range of temperature from 600° to 2000°C, and coined as very appropriate coating technique for the polymer substrates. The coating properties such as hardness (350 ± 50 HV) and the adhesion strength (5 ± 0.5 MPa) of the coating were evaluated and correlated with the tribological properties of the coating.

1 Introduction

Carbon fiber reinforced plastics (CFRP) are considered to be a potential material for fuel efficient aircrafts and automobiles despite their poor surface performance. The CFRP structures in aircrafts and automobiles are often subjected to erosion caused by sand, fine dust, volcanic ash, which most likely lead to massive materials losses [1]. Recently, the application of CFRP materials is also been extended to various heavy industries, where the components are most often subjected to relative motion and the phenomenon of sliding wear is very unambiguous. The matrix polymer types, the fiber content and fiber orientations are largely control the magnitude of the mass loss during erosion/sliding condition. When using CFRP in erosion critical areas such as leading edges of airplanes, turbine fans of aero engines, and the application where the components are in relative motion, the materials must be protected against erosion/sliding wear condition in order to avoid severe damage and high maintenance costs. Numerous ways have been proposed to protect CFRP surface, such as polymer based anti-erosion paints, metals or ceramics based coating by physical vapor deposition and chemical vapor deposition etc., [1, and 2]. However, those processes have their own hitches, the former process has very limited life-span and the latter processes have very low deposition rate and involves various toxic chemicals so on. Recently, the thermal spray process has been considered as a potential method for making coating on the CFRP surface with adequate bonding strength. Another advantage of using thermal spray is the coating with high deposition rate can be possible and therefore large area can be deposited without any special deposition requirements. The temperature involved in most of the thermal spray processes are incomparable with the glass transition temperature of the most of the polymer and hence stringent process control is necessary for thermal spray coating on the polymer based coating [2]. A cursory survey of the literature showed that the cold spray technique is viable method for polymer substrate since it has operated over low temperature. However, the process is not suitable for most of the thermosetting polymer where the severe erosion has been reported due to the brittle nature of the polymer. Those drawback pounded researcher to find a new method that more suitable for polymer substrate. The newly developed warm spray technique is considered as a highly versatile, which can operate over wide range of temperature from 600° to 2000°C, and coined as very appropriate technique for the polymer substrates. So far deposition of titanium on the polymer substrate is considered as mirage. To our knowledge, no successful results have been reported on the thermal spray titanium coating on the polymer substrate. Titanium is a low dense and high strength material and thus it is highly preferable for CFRP surface production without disturbing their high strength to weight ratio. Recently, using bi-process method, i.e., combining the plasma spray (inter layer) and warm spray (top layer) technique, we deposited high performance titanium coating on the carbon fiber reinforced polymer (CFRP) surface. The coating physical and mechanical properties were measured. In order to access the coating performance under the sliding motion, the required dimension of the sample was subjected to the ring-on-disc tribometer. The wear behavior of the coating was correlated with the coating process parameters and the coating mechanical and physical properties.

2 Experimental procedure

2.1 Materials

The Fig. 1 shows the schematic view of the warm spray system. The system is composed of four main regions called combustion chamber, mixing chamber, nozzle and barrel. By changing the nitrogen flow rate in the mixing chamber, the temperature of the flow gas and the temperature of the entrained particles are greatly controlled. The process condition of the warm spray coating is given in Table 1. In this study, a commercially available atmospheric plasma spray system (APS: 9MB, Sulzer Metco) was used. CFRP plate was used as a substrate, which was supplied by Mitsubishi Rayon, Co. Ltd, Japan. It was made up of airplane grade epoxy resin having heat resisting temperature of 180ºC, and PAN based carbon fiber as the reinforcement

(TR50S-6L). Properties of the CFRP composite are discussed elsewhere [2]. In this study, we used titanium (+10 to -45μm) and copper powders (-75μm) as a feedstock material. Here, copper powder was used to make an interlayer on the CFRP substrate using APS system.

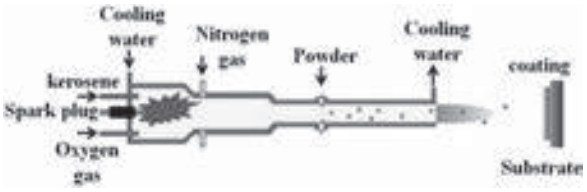

Fig. 1. *Schematic view of warm spray gun*

Table. 1. *Warm spray process conditions*

Fuel (ml/min)	O_2 (l/min)	N_2 (l/min)	Powder feed rate (RPM)	Spray distance (mm)
350	600	500	2	200
350	600	1000	2	200
350	600	1500	2	200

2.2 Characterization

The adhesion strength of the coating was measured by standard pull-out testing. The coating hardness was measured by Vickers hardness machine. Dry lubricated ring-on-disc wear tests were conducted. CFRP plate with the dimension of 30mm*30mm*3mm were used for the test. These samples were tested against commercial SUS304 ring. The sliding tests were conducted at room temperature under dry (normal atmospheric conditions with relative humidity of 50%) conditions, using normal applied loads of 15 N, 10 N and 5 N for desire time period. Before and after testing, the plates and the ring were cleaned in an ultrasonic bath of absolute ethanol for 5 min, dried under cold air for 5 min and weighted in a microbalance with an accuracy of ±0.1 mg. The wear rate (W_R) was calculated by using the following equation:

Wear rate = $W_v/W_d*L_{(Kgf)}$

Where W_v-wear volume, W_d-wear distance and $L_{(kgf)}$ load in kilogram force.

3 Results and Discussion

Generally, the microstructure of the warm spray coating is gravely changed due to the vast variation in the state of the sprayed particle, where it is being either in the state of completely molten or fully solid state depending on the nitrogen flow rate. Fig. 2a shows the bulk titanium coating on the CFRP substrate and Fig. 2b shows the cross-section of the titanium coating. As it can be seen in the micrograph, the titanium coating seems very porous and the value varies from 6 to 15% depending upon the warm spray process parameters. The measured oxygen content in the coating as well fairly varies according to the N_2 flow rate. However, under carefully controlled condition, a quality coating can be deposited on the CFRP substrate. The coating properties such as Vickers hardness and the adhesion strength were measured and the values were 350 ± 50 HV and 5 ± 0.5 MPa respectively.

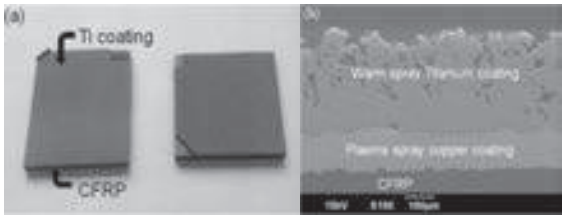

Fig. 2. *Warm spray titanium coating on CFRP substrate a) bulk titanium coating b) SEM micrograph of cross-section of titanium coating on CFRP*

Fig.3a shows the wear rate of the titanium coating on the CFRP substrate. The results show mammoth increase in the wear resistance of the CFRP materials after the titanium coating. As shown in the graph, the wear rate increases with increasing nitrogen flow rate, which signifies the increased coating porosity as the nitrogen flow rate increase. Interestingly, the tribo-film formation on the wear track, which is believed to be TiO_2, significantly changes the tribo-behavior of the coating after certain period of the rotation. Low nitrogen flow rate where the titanium particles are completely molten, thus resulting dense coating with high oxide content that would rather in turn help to improve the wear resistance. Whereas, the high porosity, due to the solid state deformation, could be associated with the high wear rate in the high nitrogen flow rate coating. Fig. 3b shows evident for the TiO_2 tribo-film formation on the surface of the low nitrogen flow rate titanium coating.

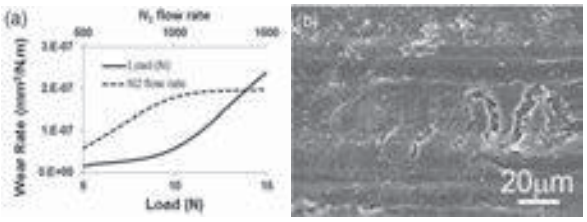

Fig. 3. *a) The wear rate of titanium coating as a function of load and nitrogen flow rate b) SEM micrograph of oxide tribo-film on the surface of titanium coating deposited at the 500 l/min nitrogen flow rate*

4 Conclusion

A thick, roughly of 600-700 μm, titanium based wear resistance coating was deposited on the CFRP surface using warm spray system. The wear resistance of the coating was studied by ring-on-disc tribo-meter. The preliminary study showed that the TiO_2 film, developed during the period of time, on the titanium surface dramatically changed the wear characteristic and resulted low wear rate. The coating porosity was also a controlling factor of the wear rate.

5 References

[1]C. Maurer and U. Schulz: Wear. **302** (2013) 937-945.
[2]A. Ganesan, H. Tokuyama, M. Yamada and M. Fukumoto: Proc. Int. Therm. Spray Conf., (DVS, 2014) pp. 157-161.

Depositing dense Ti and Ti6Al4V coatings by in-situ shot peening assisted cold spray

Xiao-Tao Luo, Ying-Kang Wei, Cheng-Xin Li, Guan-Jun Yang, Chang-Jiu Li
State Key Laboratory for Mechanical Behavior of Materials, School of Materials Science and Engineering, Xi'an Jiaotong University, Xi'an Shaanxi 710049 China

Abstract
In this study, stainless steel (SS) shot peening powder with diameters over 150 μm was blended with commercial pure titanium (CP Ti) and Ti6Al4V (TC4) powders. These mixtures were used as feedstocks. It is attempted that by the in-situ impact of those large sized shot peening powders, plastic deformation of the deposited Ti and TC4 particles can be greatly enhanced and thereby porosity of the deposit can be decreased and inter-particle bonding can be improved. Results show that some shot peening particle was incorporated into the deposited CP Ti coatings for their relatively low velocity. With the increasing of the shot peening fraction from 0% to 70 vol.%, porosity of CP Ti and TC4 coatings decreased from 18% to 0.6% and from 17.6% to 2.1%, respectively. Meanwhile, Remarkable work hardening induced by impact of the shot peening particles was detected for both CP Ti and TC4 coatings. With the content of the shot peening particles increasing from 10vol.% to 70 vol.%, Vickers microhardness of CP Ti and TC4 coatings increased from 143 to 203 $HV_{0.3}$ and from ~240 to 427 $HV_{0.3}$, respectively.

1 Introduction

Cold sprayed titanium and its alloy coatings always exhibit a porous microstructure and poor inter-particle bonding although they are easily deposited. This makes the corrosion resistance and mechanical properties much lower than their bulk counterparts [1]. To obtain dense titanium and its alloy coatings by cold spray, high temperature (>800°C) helium gas of high cost is usually used to accelerate the spray particles to high velocities [2]. However, due to their high activity, titanium and its alloys are easily oxidized at high gas temperature and thus lead to poor inter-particle bonding [3]. In our previous study on cold spraying titanium [4], it was found that former deposited particles are inevitably impacted and deformed by the following particles, which makes under-layer of the coating usually show denser microstructure than top-layer. This fact indicates that the shot peening effect is effective to modify the coating microstructure. In this study, large sized stainless steel powders were used as the shot peening particles and mixed with the Ti and TC4 powders. It is attempted that by the in-situ impact of those large sized shot peening powders, plastic deformation of the deposited Ti and TC4 particles can be greatly enhanced and thereby porosity of the deposit can be decreased.

2 Experimental procedures

Gas atomized Ti6Al4V and pure Ti powders with sizes ranging from 20 to 50 μm and 10 to 50 μm respectively were used as feedstocks. Spherical shaped 1Cr13 matensite stainless steel powder with sizes ranging from 150 to 180 μm was used as the shot peening particle. To clarify the effect of the shot peening particle content on microstructure and mechnical properties of the cold sprayed coatings, 10 vol.%, 30vol%, 50vol.% and 70vol.% 316 stainless steel plates with thickness of 3 mm were used as the substrates. Nitrogen with a pressure of 2.8 MPa and at a temperature of 550±10 °C was used as the accelerating gas. The powder feed rate was set to be 14 g/min. Scaning electron microscopy was carried out to characterize the cross sectional microstructure of the sprayed coatings. 10 Vickers microhardness indentations were made on the crosssection of each sample with a load of 300 g holding for 30 s. The average value is used as the coating hardness for each sample.

3 Results

It can be found from Fig.1 that the coating deposited by pure Ti powder exhibits a porous microstructure while the coating deposited by powders with 70vol.% shot peening particles shows a dense microstructure. Meanwhile, regions in bright contrast, identified to be 316 SS shot peening particles by energy disperse spectroscopy, were observed.

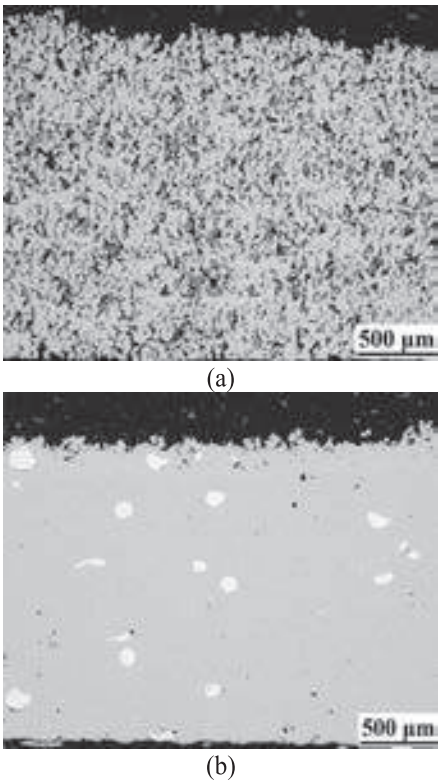

Fig.1 *Cross sectional microstructure of the CP Ti coatings deposited by (a) pure Ti and (b) powders with 70vol.% of shot peening particles*

As can be seen from Fig.2, similar result was observed in cold sprayed TC4 coatings. However, deposited 316 SS shot peening particle was not observed in TC4 coatings.

This is due to the higher hardness of TC4 powder as compared to the CP Ti powder. These results demonstrate that the in-situ shot peening is an effective approach to decrease the porosity of the cold sprayed Ti and its alloy coatings.

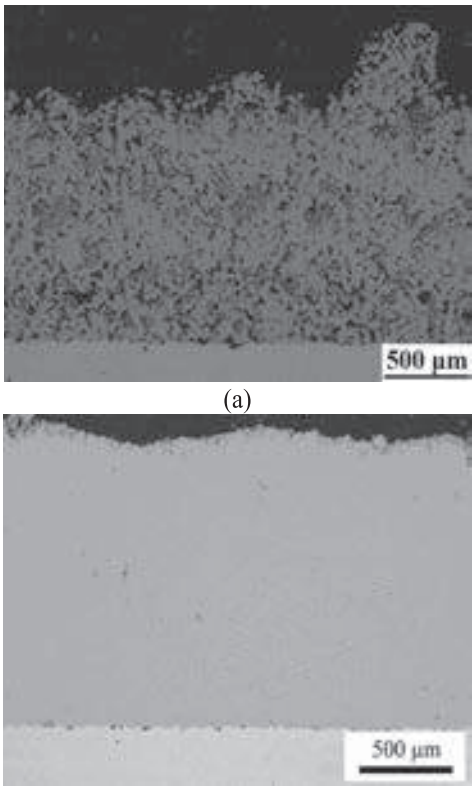

(a)

(b)

Fig.2 *Cross sectional microstructure of the TC4 coatings deposited by (a) pure TC4 powder and (b) powders with 70vol.% of shot peening particles*

Deposition efficiency (DE) and coating porosity as function s of the shot peening particle content are plotted in Fig.3. It can be found that with the increase in shot peening particle content, porosities of CP Ti and TC4 coatings gradually decrease. For CP Ti and TC4 coatings deposited by powders with 70vol.% shot peening particles, the porosities are 0.6% and 1.1%, respectively. Meanwhile, deposition efficiency does not change significantly with the shot peening particle content.

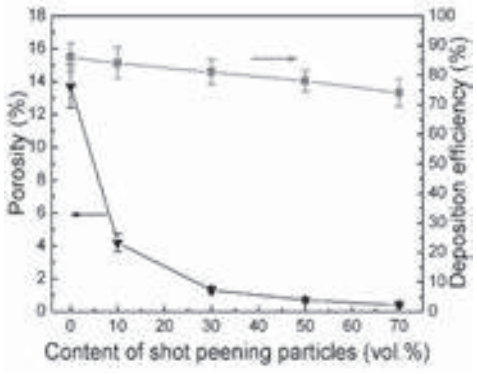

(a)

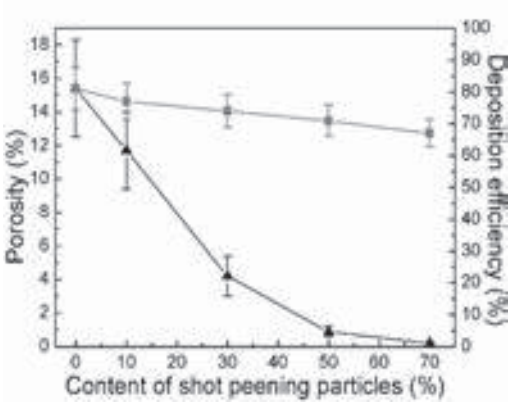

(b)

Fig.3 *Porosity and deposition efficiency of (a) the CP Ti and (b) TC4 coating as a function of the shot peening content*

Plastic strain and thus the work hardening of the deposited particles increase with the increasing shot peening particle content. As a result, it can be found from Fig.4 that the coating hardness increases significantly with the increase in shot peening particle content.

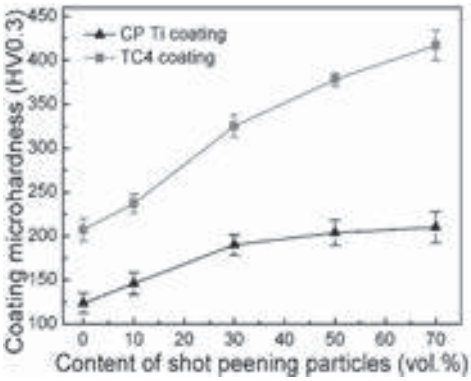

Fig.4 *Microhardness of CP Ti and TC4 coatings as a function of the shot peening particle content*

4 Conclusions

In-situ shot peening assisted cold spray is an effective approach to deposited dense Ti and TC4 coatings. Meanwhile, deposition of shot peening particles can be minimized/avoided by controlling their sizes. Deposition efficiency of the CP Ti and TC 4 powders does not change significantly with the shot peening content from 0 to 70vol.%.

Acknowledgement

This project was supported by the Natural Science Foundation of China (No.51401158).

References

[1] H.R. Wang and W.Y. Li: Surf. Coat. Technol. 201(2007) 5203-5206

[2] N.M. Chavan and P. S.Phani: Surf. Coat. Technol. **205** (2011) 4798-4807

[3] C-J Li and W.Y. Li: Surf. Coat. Technol. **167** (2003) 278-283

[4] K.Kim and S.Kuroda: Scripta Mater. **63** (2010) 215-218

Deposition of Nitrogen Doped Diamond/ Mo Hybrid Coating by APS with C_2H_2/O_2 combustion flame assisted Ar/N_2 plasma jet

Yasutaka Ando[1], Yoshimasa Noda[2]
[1] Division of Renewable Energy and Environment, Ashikaga Institute of Technology, Tochigi 326-8558, Japan
[2] Collaborative Research Center, Ashikaga Institute of Technology, Tochigi 326-8558, Japan

Abstract
In order to develop a high rate diamond and hard carbon nitride particle synthesis process for promotion of wear resistance of thermal spray coating, deposition of nitrogen doped diamond on thermal sprayed Mo coating was carried out. Consequently, by using twin torch type combustion flame diamond deposition equipment, superimposed combustion flame which had enough potential to deposit 20 micron large diamond particles for only 5 minutes. Besides, since diamond surface was abraded by argon/ nitrogen plasma in open air, some useful information for practical use of this technique using combustion flame assisted Ar/N2 plasma were obtained from these results.

1 Introduction

Combustion flame method is a high rate diamond synthesis process using acetylene/ oxygen combustion flame. This process has been hoped to be a low cost diamond production process because of its simple constitution and its working environment (that is atmospheric process). As for the utility of diamond particle in the field of thermal spray, since hard particle dispersion in the thermal sprayed coating was proved to be effective on promotion of its wear resistivity. Accordingly, high rate diamond synthesis process will be available as a hard particle dispersion method for coating deposition process. However, since diamond synthesis area is very small due to small cross-sectional area of the combustion flame in case of combustion flame method, traverse of the substrate or the combustion torch should be done during operation for conduction of large area diamond synthesis. In order to high rate diamond synthesis on the condition of the traversing substrate or torch, promotion of the diamond synthesis rate is mandatory. Therefore, a twin torch type combustion flame diamond deposition equipment which can generate super imposed combustion flame with high radical density was developed by our research group [1].

Regarding the hard particle, beta- C_3N_4 is hoped to have higher hardness than that of diamond [2]. In our research group, from the view point that the crystal structure of beta-C_3N_4 is the same as that of beta-Si_3N_4, beta-C_3N_4 synthesis was tried to conduct by diamond deposition by acetylene/ oxygen combustion flame with nitrogen addition [1]. Consequently, though difference the appearances between the synthesized particles and ordinary diamond particles appeared, beta- C_3N_4 could not be confirmed.

In this study, in order to establish high rate and large area synthesis process of diamond and hard carbon nitride by combustion flame method, deposition of nitrogen doped diamond/ molybdenum (Mo) hybrid coating by APS with C_2H_2/O_2 combustion flame assisted Ar/N_2 plasma jet was carried out.

2 Experimental procedure

Figs.1-2 show the schematic diagram of the atmospheric thermal spray equipment for Mo coating deposition and combustion flame equipment for diamond deposition. The APS equipment consisted of plasma torch, DC power source, feedstock supplying system and working gas supplying system. Except the feedstock supplying system, the constitution of this equipment was the same as the conventional high power thermal plasma spray equipment. In case of the conventional thermal spray equipment, the mechanically and electrically driven type powder feeder is generally used. On the other hand, since the powder feeder is very expensive, a suction type powder feeder, which can feed the powder into plasma jet by negative pressure generated by thermal plasma jet, was used in this study. As the feedstock, commercial molybdenum powder was used. In case of diamond deposition, as shown in Fig.2, twin torch type combustion flame equipment was used. Although nitrogen was fed into the combustion flame in our previous study [2], Ar/N_2 plasma and N_2 plasma were fed into the combustion flame in the present study. As the substrate, 15 mm x 15 mm x 1 mm 304 stainless steel plate with grit blasted surface was used in case of Mo coating deposition. In case of diamond deposition, Mo plate and above mentioned Mo thermal spray coating deposited 304 stainless steel plate were used as substrate. The substrate was horizontally set on the substrate holder and the central area of the sample was placed perpendicular to the axial center of the plasma jet. The spray distance (distance between the nozzle outlet of the plasma torch and the surface of the substrate was fixed at 20 mm. The input power for discharge was fixed at 40 A. The diamond

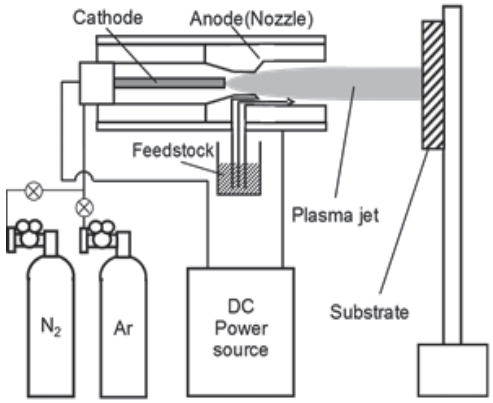

Fig. 1 Schematic diagram of the atmospheric thermal plasma spray equipment used in this study.

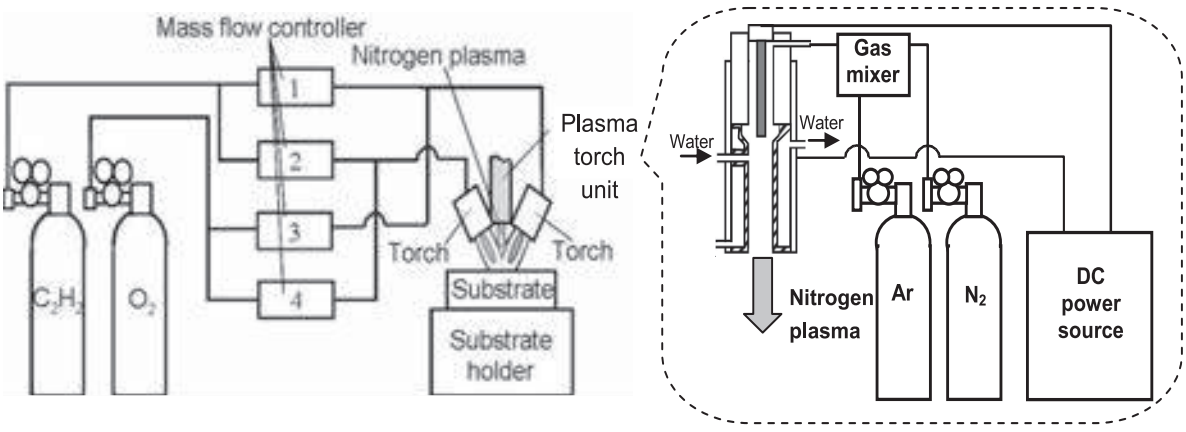

Fig. 2 Schematic diagram of the diamond deposition equipment used in this study.

Table 1 Film deposition conditions.

a) Molybudenum coating deposition

Substrate	304 stainless steel
Working gas (Flow rate)	Ar (10 l/min.)/ N_2 (1 l/min.)
Spray distance	20 mm
Discharge Current	40A, 25V
Deposition time	1 min
Feedstock material	Mo powder

b) Diamond synthesis

Substrate	Mo, Mo coated 304 stainless steel
Combustion gas (Flow rate)	C_2H_2 (1.45 l/min each) / O_2 (1.25 l/min each)
Spray distance	7 mm
Deposition time	5 min

c) Nitriding

Working gas (flow rate)	Ar (0-1 l/min.)/ N2(20 l/min.)
Spray distance	20 mm
Discharge Current	10A, 100V
Deposition time	3 sec.*10 times

synthesis was conducted along the same procedure as that in case of our previous study [3]. The nitriding of the diamond was conducted during diamond deposition or after diamond deposition. After carbon nitride particle synthesis, the microstructures were investigated by optical microscope and X-ray diffraction (CuKa, 40 kV, 100 mA). Table 1 shows the experimental consitions.

3 Experimental results

In this paper, the results of nitriding after the diamond particles synthesis on Mo substrate. Fig.3a) shows the optical microscope of the diamond particles before nitriding. As shown in this figure, it was confirmed that by using the superimposed combustion flame, 20 micron large diamond particles could be deposited for only 5 minutes. Fig.3b) shows the optical microscope of the diamond particles after nitriding using nitrogen working gas. Although the variation of crystal structure of the diamond particles due to nitriding could not be confirmed from the results of X-ray diffraction, it was confirmed that surfaces of diamond particles were hevily abraded by nitrogen plasma irradiation.

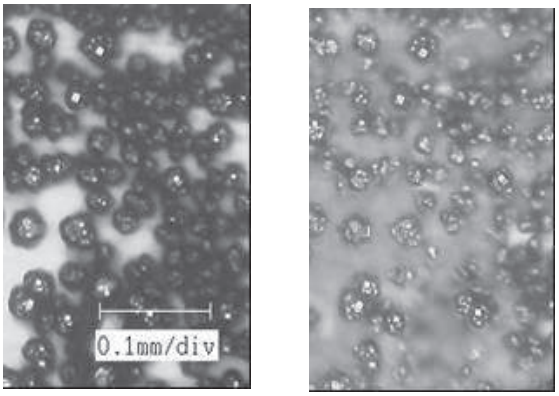

a) Before nitriding b) After nitriding

Fig.3 Optical micrograph of the diamond particles

4 Conclusion

In order to develop a high rate diamond and hard carbon nitride particle synthesis process, nitrogen doped diamond deposition by combustion flame assisted Ar/N_2 plasma was carried out. Consequently, it was proved that 20 micron large diamond particles could be synthesized for only 5minutes by using super imposed combustion flame generated by twin torch. Besides, it was confirmed that nitrogen plasma had enough reactivity to abrade diamond surfaces.

References

[1] Q. Yang and Y. Ando: Applied Plasma Science, 19,2 2011, pp.113-118.
[2] B. R. Marple, J. Voyer: Proc. 1st Int Thermal Spray Conf. (2000), pp. 909-918.

Adsorption of alginate and albumin mediates colonization of *Escherichia coli* on arc-sprayed aluminum coatings

Xiaoyan He, Yi Liu , Hua Li*
Key Laboratory of Marine Materials and Related Technologies, Ningbo Institute of Materials Technology and Engineering, Chinese Academy of Sciences, Ningbo 315201, China

Abstract
Thermal sprayed aluminum coatings have been extensively used as protective layers for steel structures against corrosion through anodic passivation of Al in the marine environment. The corrosion usually deteriorates resulting from marine biofouling and the mechanism of the accelerated corrosion of the coatings yet remains elusive. Here we report adsorption behaviors of typical protein and marine polysaccharide on arc-sprayed aluminum coatings and their influence on adherence of *Escherichia coli*. As the first stage participating in the biofouling process, adsorption of the molecules plays a key role in mediating formation of biofilm. Adsorption of alginate and albumin was evidenced by a MicroBCA protein assay reagent kit and total organic carbon, respectively. The adsorption of either alginate or albumin on the coatings inhibits effectively the adhesion of the bacteria by altering the properties of the coatings and the mechanism was elucidated through a brief energy model.

1 Introduction

Marine biofouling is an international problem of great economic waste due to accelerated corrosion, transport of non-native invasive species, increased operating costs and decreased fuel efficiency [1-3]. Corrosions caused by biofouling are more than 20% and related to direct economic damage of 30-50 billion annually worldwide [4, 5]. It is therefore essentially required to understand the biofouling mechanisms so that antifouling measures can be taken for the marine infrastructures.

Biofouling is a very complicated process which involves four major stages, namely adsorption of the organics such as polysaccharides and/or proteins, formation of microbial layer of cross-linked structure, colonization of spores of macroalgae or protozoa, and larvae of macrofoulers [6, 7]. Bacterial adhesion is usually affected by many factors, such as characteristics of bacteria, surface properties of target materials [8, 9], and environment factors for example ambient temperature, bacterial concentration, and the presence of protein or time of exposure [10, 11]. For target materials, their surface features, including chemical compositions [12, 13], hydrophobicity [14], surface charge [15], and surface morphology [7], are the focal points. All of the features are directly related to their surface free energy. Fig. 1 shows the schematic model describing the adhesion behaviors. After adsorption of the organics, the properties of the interfaces are changed. This study aims to elucidate the influence of alginate/albumin on *E. coli* adhesion by a simple energy model.

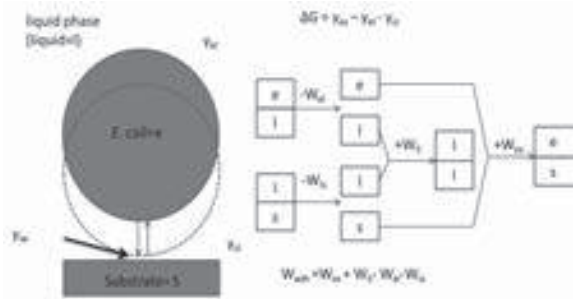

Fig. 1. *The model of E. coli adhesion.*

2 Materials and experimental procedures

2.1 Deposition and characterization of the coatings

High velocity arc spray (AS, TLAS-500C, China) was employed to deposit the aluminum coatings. The current and voltage of the arc were set at 80-100 A and 25 V, respectively. The spray distance was ~15 cm and the compressed air with the pressure of 0.5 MPa was used for the arc spraying. 316L plates with the dimension of 20×20×2 mm were used as the substrates to deposit the coatings with a thickness of ~150 μm. For comparison, some of the coatings were sealed by tetrafluoroethylene-hexafluoropropylene copolymer (FEP). Microstructural features of the coatings and the adhered *E. coli* were observed and characterized by field emission scanning electron microscope (FESEM, FEI Quanta FEG 250, the Netherlands)

2.2 Preparation of bacterials strains and bacterial adhesion testing

Artificial seawater (ASW) was prepared according to ASTM D1141-98. All the reagents and solvents were used as received without any further purification. Gram-negative *E. coli* bacteria (ATCC25922) were selected for the adhesion testing which was cultured in LB media. The media were prepared by dissolving 10 g NaCl, 5 g yeast extract and 10 g peptone in 1000 ml deionized water. The media containing the bacterial strains were shaken for 24 h at 37°C. The LB media on *E. coli* was removed by centrifugation with a rotational speed of 2000 r min^{-1} for 5 min 3 times.

The *E. coli* suspension with a concentration of 10^9 ml^{-1} was prepared in ASW. Coating samples were put into 6-well plates after sonication washing in ethanol and subsequent deionized water and then dried under a flow of dried air at 37°C. 4 ml of the *E. coli* suspension was added into each well for soaking at room temperature for 12 h, 24 h and 48 h, respectively. After the incubation, the samples were washed with ASW for 3 times to remove the bacteria that did not adhere onto the samples and then fixed by 2.5% glutaraldehyde. For SEM observation, dehydration of the

samples was carried out through the critical point drying using 25%, 50%, 75%, 90%, and 100% ethanol solution.

2.3 Quantitative analysis of alginate/albumin

The samples were soaked in 4 ml ASW containing 1 mg ml^{-1} sodium alginate (AR, Sinopharm Chemical Reagent Co. Ltd., China) and 1 mg ml^{-1} bovine serum albumin (BSA, 98% purity, Sigma-Aldrich). Then, Albumin adsorption was performed by using a MicroBCA protein assay reagent kit and alginate adsorption was analyzed by total organic carbon (TOC).

3 Results and discusion

After being soaked for 12 h, 24 h and 48 h, obvious adhesion of *E. coli* bacteria was observed on the surfaces of the samples. Statistical analysis of the *E. coli* adhered on the sample surfaces was made by counting the bacteria from the FESEM observations. Significant differences in the adhesion behaviors of the bacteria were realized for the samples tested under different conditions.

3.1 Hydrophibility/hydrophobicity - alginate

Adsorption of alginate decreases *E. coli* adhesion on the Al coating, while it shows no influence on their adhesion on the sealed Al coating (Fig. 2), indicating almost no interaction between alginate and the sealed Al coating. The TOC data suggests only a little bit of alginate adsorbed on the sealed Al coating, while a large amount of alginate was suggested on the Al coating.

According to the model shown in Fig. 1, at initial stage of the testing, the adhesion energy could be caculated by $W_{adh}=W_{se}-W_{sl}+W_{ll}-W_{el}$, while after the adsorption of alginate, $W_{adh}=W_{ae}-W_{al}+W_{ll}-W_{el}$.

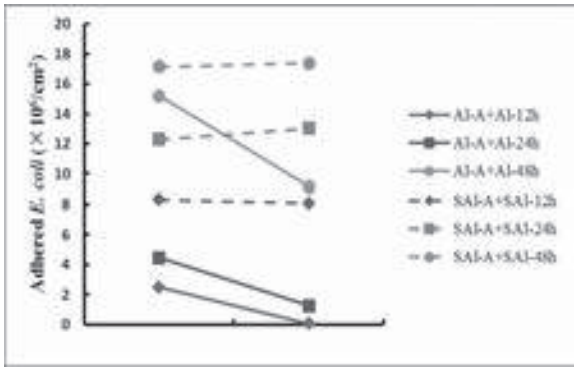

Fig. 2. *The influence of adsorption of alginate on E. coli adhesion.*

3.2 Hydrophibility/hydrophobicity – Albumin

Albumin interferes in *E. coli* adhesion on both the Al coating and the sealed Al coating (Fig. 2). The influence of albumin adsorption on the sealed Al coating is more significant than that on the as-sprayed Al coating. The mass of albumin adsorbed on the Al coating and the sealed Al coating is about 0.2 mg as determined by the MicroBCA protein assay reagent kit. This roughly equals 1.8×10^{15} of the molecule albumin overspreading over the coating surface. The *E. coli* bacteria at least intimately contact the interface formed by albumin, so the adhesion energy could be described as $W_{adh}=W_{be}-W_{bl}+W_{ll}-W_{el}$, regardless of the adhesion on the sealed Al coating or on the as-sprayed Al coating. The same adhesion energy could explain the similar density of *E. coli* on the surfaces of both the coatings.

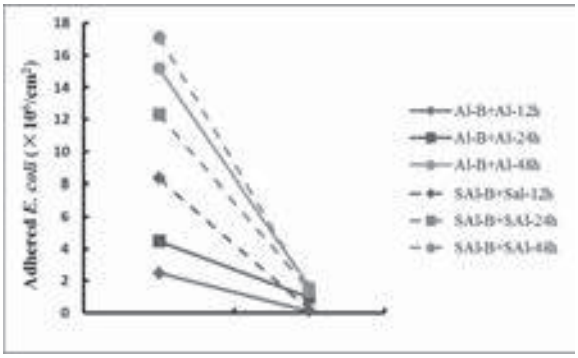

Fig. 3. *The influence of adsorption of albumin on E. coli adhesion.*

4 Conclusion

Adsorption of albumin and alginate on the surfaces of the arc-sprayed aluminum coating and the sealed Al coating was quantitatively investigated by a BCA kit and TOC methods. The results showed that alginate/albumin forms a conditioning layer on the coating surfaces, which alters colonization behaviors of *E. coli* bacteria. The conditioning layer hinders the adhesion of *E. coli* through modifying the surface properties and the adhesion energy.

5 References

[1] Stafslien S J, Bahr J, Daniels J, et al.:Journal of Adhesion Science and Technology. 25(2011) 2239-2253.
[2] Sundaram H S, Cho Y, Dimitriou M D, et al.:Biofouling. 27(2011) 589-602.
[3] Wang Y P, Pitet L M, Finlay J A, et al.:Biofouling. 27(2011) 1139-1150.
[4] Yuan S J, Pehkonen S O, Ting Y P, et al.:Langmuir. 26(2010) 6728-6736.
[5] Yuan S J, Xu F J, Pehkonen S O, et al.:Biotechnology and Bioengineering. 103(2009) 268-281.
[6] Buskens P, Wouters M, Rentrop C, et al.:Journal of Coatings Technology and Research. 10(2013) 29-36.
[7] Hong F, Xie L Y, He C X, et al.:Journal of Materials Chemistry B. 1(2013) 2048-2055.
[8] Lakshmi K, Muthukumar T, Doble M, et al.:Colloids and Surfaces B-Biointerfaces. 91(2012) 205-211.
[9] Vedaprakash L, Dineshram R, Ratnam K, et al.:Colloids and Surfaces B-Biointerfaces. 106(2013) 1-10.
[10] An Y H, Friedman R J:Journal of Biomedical Materials Research. 43(1998) 338-348.
[11] Katsikogianni M, Missirlis Y:Eur. Cell. Mater. 8(2004) 37-57.
[12] Jiang S, Cao Z:Adv Mater. 22(2010) 920-32.
[13] Andre R, Natalio F, Tahir M N, et al.:Nanoscale. 5(2013) 3447-3456.
[14] Wang C, Feng R, Yang F:Journal of Colloid and Interface Science. 357(2011) 273-279.
[15] Das S K, Khan M M R, Parandhaman T, et al.:Nanoscale. 5(2013) 5549-5560.

Gas and fuel Management in Thermal spray process

R.Bateriwala, Keepsake Engineering Consultancy Pvt. Ltd

Thermal Spraying, a surface coating technique, is utilised to enhance specific properties to counter wear on inferior base material. The coatings are produced using thermal & Kinetic energies. Major thermal spray process uses oxygen + fuel flame, electric arc & Plasma arc for deposition.

Thermal energy causes the spray material to melt, soften or fuse. Kinetic energy accelerates & imparts velocity to the sprayed particles.

Various gases are used to achieve sufficient thermal & Kinetic energy requirements of specific thermal spray process. Depending on the process, control of gas flow & pressure is essential to achieve consistent & desired coating properties.

Gases are supplied mostly in a pressurised container. Withdrawal of gas depends on tank & outlet valve design. The tank itself becomes pressurised based on ambient atmospheric considerations & gas property. The pressure & flow also change as more and more gas is withdrawn. The overall effect is difference in Thermal & Kinetic energies transferred to the spray material.

This paper is an effort to practically manage the pressure & flow variations inherent for gas based systems and achieve consistent energy transfer. Case study is based on WC 88/12 powder deposited using MEC hybrid HVOF system. The gases used were Oxygen & LPG (propane & butane). The tungsten carbide coatings produced the gas management system achieved bond strength, porosity & hardness nearing liquid fuel HVOF systems.

Repair Development For A Thermal Spray Coated Component Of An Aero-engine

V Krishnakanth[1], Ekshwaku N Srivastava[1] and V Sambasiva Rao[2]
[1]Senior Design Engineer, Cyient Ltd., Hyderabad - 500 032, India
[2]Discipline Chief, Cyient Ltd., Hyderabad - 500 032, India

Abstract
Aero-engine components operate under arduous conditions of temperature, stress and environment during engine operation, which limits its performance and durability. The appropriate selection and use of coatings can enhance the performance and durability of these components. While coatings by thermal spraying are widely used, these coatings gradually degrade when subjected to continued and prolonged operation. It would then need a repair of the coated components to avoid replacement with a new component to reduce the Life Cycle Cost (LCC). This paper describes the repair development for a Diffuser Air Seal that reported excessive wear of 0.014 inch depth at the seal land mating area during engine operation. As per the Original Equipment Manfacturer (OEM) design, the component is thermal spray coated to a thickness of 0.003-0.008 inch by plasma spray using Chromium Carbide–Nickel Chromium powder. Repair assessment indicates that coating repair using Dual Coat plasma spray or High Velocity Oxy Fuel (HVOF) spray is appropriate for restoration of the component. The repair procedure evolved includes removal of the existing coating, surface preparation prior to coating and application and finishing of the coating. The coating repair has been successfully validated and being used for repair of the Diffuser Air Seals.

1 Introduction

In the aerospace industry, there is an increasing interest in reducing the Life Cycle Cost (LCC) of the components. Further, the components are required to be designed to operate under severe conditions of temperature, stress and environment ensuring adequate life against wear, erosion, corrosion etc. While the durability of the components can be enhanced by application of coatings[1], the continued and prolonged operation of these components leads to degradation of the coatings. It is not economical to scrap such components to replace with new components. It is a general practice to perform coating replacement/repair on such components. However, if the reported damage exceeds the Original Equipment Manfacturer (OEM) coating limits, a thorough assessment is required in order to examine the feasibility of repairing the components. This paper describes the development of repair for a thermal spray coated Diffuser Air Seal, of a commercial aero-engine, with excessive wear reported at the seal land mating area, during engine operation.

2 Component and its distress

Diffuser Air Seal is a critical, rotating and life limited component in an aero-engine as shown in **Fig.1.** It is bolted to High Pressure Compressor (HPC) shaft and regulates the secondary air coming from the HPC to cool the High Pressure Turbine Blades.

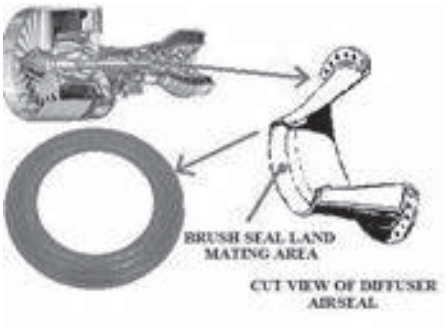

Fig. 1. *Diffuser Air Seal*

The Diffuser Air Seal mates with HPC (Rear) Exit Brush Seal at the seal land area. The seal land area is subjected to wear during engine operation. The OEM part print specifies a plasma spray coating (using Chromium Carbide –Nickel Chromium powder) of 0.003-0.008 inch thickness on the seal land area for protection against wear. The seal land is not located in the oil wetted zone. The wear damage reported is about 0.014 inch depth on the Diffuser Air Seal at the seal land mating area which is quite high needing feasibility studies of alternative repair methods to restore the component.. The parent material of Diffuser Air Seal is a Nickel Alloy (Waspaloy) and that of the mating part - Brush Seal is also a Nickel Alloy (Inconel 625).

3 Repair feasibility assessment

A feasibility study, to repair the component is undertaken by critically looking at various factors. The study indicated that coating replacement repair alone (i.e. removal of the existing coating and application of a new coating by plasma spray) cannot restore the component back to its OEM condition as the extent of wear damage is beyond the OEM coating thickness limits. Further, the OEM plasma spray coating i.e. Chromium Carbide –Nickel Chromium Coating cannot be sprayed to a thickness of 0.014 inch required for restoration of the Diffuser Air Seal. The higher coating thickness by plasma spray would likely develop high residual stresses within the coating that would adversely effects its integrity.

The structural capability of the component considering the reduction in parent material thickness due to excessive wear of 0.014 inch depth has also been assessed. The study indicated that it is feasible to go for repair of the part by application of a suitable coating repair method.

4 Potential thermal spray coatings

Thermal spray coatings are employed to restore the dimensions of the components that have been worn out. Although these coatings do not contribute to the strength of the component, it is a quick and economical way to restore the dimensions, functionality & performance of the components. The potential thermal spray coating processes identified for restoration of Diffuser Air Seal are plasma spray using Dual Coat and the High Velocity Oxy Fuel (HVOF) spray. While HVOF spray process is preferred

over Dual Coat plasma spray, but these two coating processes are proposed considering the availablity of coating equipment/facility at various Customer locations. The plasma spray process[2] uses a high intensity electric arc that heats inert gas or gaseous mixture to an ionized state. Powdered materials are injected into the hot, high velocity gas, melted and propelled on to the substrate. In the HVOF spraying, fuel and oxygen are fed into a combustion chamber in a continuous flow, producing a jet of combustion products at extremely high speed. The powdered coating material is injected into this gas steam and accelerated to a very high velocity. The extreme velocities provide kinetic energy which helps in producing coatings that are very dense and very well adhered to the part/substrate.

5 Dual coat plasma spray

The Dual Coat plasma spray involves application of two different coatings - a base coat and a top coat, one over the other by plasma spray. This is mainly used to achieve a higher total coating thickness for dimensional restoration of the component. While the top coat conforms to that specified in the OEM design i.e. Chromium Carbide – Nickel Chromium Coating of 0.003-0.008 inch thickness, the base coat needs to be selected based on its compatibility with the parent material and with the top coat. In view of the above, 94% Nickel Chromium - 6% Aluminum coating of 0.003-0.006 inch thickness by plasma spray has been identified as the appropriate base coat. The total combined thickness of base coat and top coat that can be achieved is 0.014 inch maximum which meets the repair requirement for restoration of Diffuser Air Seal.

6 HVOF spray coating

The coatings applied by HVOF spray process[3] can achieve higher coating thickness when compared to the other thermal spray processes such as plasma spray and flame spray. Considering the parent material of the component, mating component, hardness and the operating environment, HVOF coating using 50% Chromium Carbide - 50% Nickel Chromium is found to be appropriate for the present application. The HVOF coating can be sprayed to a thickness of 0.014 inch required for dimensional restoration of the Diffuser Air Seal.

7 Repair procedure development

A systematic and detailed repair procedure has been evolved for dimensional restoration of worn Diffuser Air Seal as shown in **Fig. 2.** It specifies the removal of the damaged coating using chemical & mechanical removal methods and high pressure water jet blasting. The component is required to be cleaned and inspected for surface and sub-surface defects by fluorescent penetrant inspection. The preparation of the component for coating application involves the masking of the areas, which do not require coating, followed by shot peening of the seal land area to reduce the fatigue debit associated with the coating process. Grit blasting will enhance the bonding of the coating with the part. This is followed by coating application and subsequent de-masking, finishing/grinding to achieve the required dimensions/coating thickness. The finished coating is inspected visually for presence of any defects.

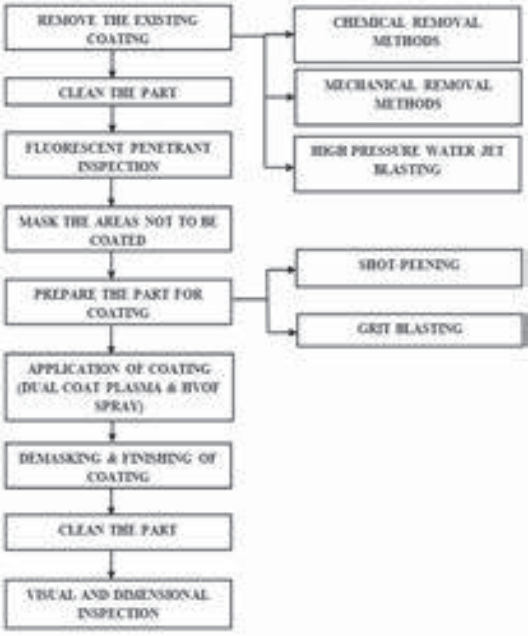

Fig. 2. *Repair Procedure for Dimensional Restoration*

8 Validation of coatings

The coating by both techniques - Dual Coat Plasma Spray and HVOF Spray were evaluated[4] on test coupons for microstructure, porosity, bond strength, oxide inclusions, hardness, mechanical properties, wear etc. The coating bond strength exceeded 4,500 psi for Dual Coat plasma spray and 10,000 psi for HVOF coat. A few coated components have successfully undergone engine ground test/test-bed run and also limited engine service evaluation. All the validation tests have been carried out at the customer facility.

9 Conclusions

The excessive wear damage reported on thermal spray coated Diffuser Air Seal during engine operation, has been assessed for its repair feasibility. Identified that Dual Coat Plasma Spray and HVOF Spray processes are appropriate for restoration of the component considering the coating thickness (0.014 inch) requirement and availability of the coating equipment. A systematic and detailed repair procedure has been evolved. The test coupons and the components coated with the proposed coatings/processes have undergone evaluation satisfactorily. The proposed coatings/processes are being used for restoration of worn out Diffuser Air Seals of a commercial aero-engine.

10 Acknowledgements

The authors would like to thank the management of Cyient and the Customer for their encouragement in preparing this manuscript.

11 References

[1] G.W.Meetham: *Coating requirements in Gas Turbine Engines*, J.Vac. Sci. Technol., A3(6), 1985, PP 2509-2515.

[2] B.J.Gill, R.C.Tucker,Jr.: *Plasma Spray Coating Processes*, Mat.Sci.Technol.,Vol. 2, 1986, PP 207-213.

[3] K.A.Kowalsky et al, *HVOF: Particle, Flame Diagnostics and Coating Characteristics*, Vol. 91, 1990, National Technical Information Service.

[4] V Sambasiva Rao, T Rangaraju and V Unnikrishnan: *Qualification of Indigenously Developed Special Coatings for Aero-engine Components*; Defence Science Journal, Vol 49, No. 4, August 1999, PP 299-309.

Thermal Spray Coating on Geothermal Turbine Blades by High Velocity Oxy-Liquid Fuel Gun MJP-5000 for Corrosion Protection

Rohit Upadhyaya**^, Dr Sharad Shrivastava**, S.C.Modi^, A. Modi^,

**Birla Institute of Technology and Science,Pilani,Rajasthan,INDIA

^Metallizing Equipment Company Pvt.Ltd JODHPUR INDIA

Authore email rnd@mecpl.com, rohit.upadhyaya@pilani.bits-pilani.ac.in

ABSTRACT

Geothermal energy is reusable clean energy, and its usage is expected to increase in the future to help prevent global warming. Geothermal steam contains large quantities of chloride, sulfate, hydrogen sulfide and carbon dioxide and other such corrosive chemicals. The majority of these corrosive substances are removed by a separator (water/steam separator), a flasher (reduced pressure evaporator), demister (moisture separator), and so on located upstream from the turbine. Nevertheless, the corrosive substances contained in the steam that enters the steam turbine are 100 to 1,000 times more plentiful than in steam turbines for fossil fuel power plants where the feed water has been chemically treated. Therefore, measures are needed to prevent general corrosion, stress corrosion cracking (SCC), corrosion fatigue and erosion corrosion of parts and materials. This paper discussing on salt spray test and acid dip test for corrosion on coated turbine blades used in geothermal steam turbines.

Parts such as the rotors and stationary blade holders that are exposed to highly corrosive geothermal steam are particularly susceptible to general corrosion and erosion corrosion, which may lead to the problem of dropout of the blades. A thermal spray coating technology for the parts surface has been developed. Basic tests like hardness, porosity and corrosion tests were conducted at R&D Laborartry of Metallizing Equipment Company Pvt. Ltd to establish a practical technology using a HVOLF (high-velocity oxygen-Liquied fuel thermal spray coating) process to apply a coating of WC-Co-Cr thermal spray material by MJP-5000. HVOLF coating was applied on the 8th stages blades of the turbine rotor at Metallizing Equipment Company Private Limited Company, Jodhpur.

Plasma spray coating as an alternative wear resistance to hard chrome on cast iron piston ring

Shailesh Mani Pandey[1], Qasim Murtaza[1]*, R. S Walia[1]
[1]Mechanical, Production & Industrial and Automobile Engineering Department, Delhi Technological University (formerly Delhi College of Engineering) Delhi, India.

Abstract
In recent times, piston rings require some form of coating to minimize abrasion and corrosion to enhance the service life of internal combustion engines. In this study, we investigate the used of plasma spray coating of a mixture of powders (Mo, NiCr, Cr3C2, Fe Alloy) for wear resistance as to hard chrome coating which is cryogenic in nature, on the plates with similar composition as the piston ring material. Pin on disc wear test on the coating with three counter bodies viz tungsten carbide (WC), high carbon steel (En-31), and nickel having pin diameter of 3mm at constant sliding distance of 12000m and at increasing load of 30N, 40N, and 50N were conducted under dry sliding conditions respectively. With increase in load the wear rate was found to be increased. The friction increased with the increase in load for the sometime and later became constant. The worn surfaces of the coating were examined with SEM micrographs and showed that the wear mechanism of the coating was accompanied by abrasion, micro cutting and adhesion. It was conculded that the plasma spray coating is much better than hard chrome and can be used as an alternative to it.

1 Introduction

The function of Piston rings is to stabilize the piston under combustion pressure. Hard chrome coating was used to enhance the piston ring life by increasing the wear resistance which is produced by electrolytic process of hard chrome baths containing the hexavalent chromium ion [1]. The nature of waste chrome electrolyte is cryogenic in nature and it can affect the health of worker, so nowadays, the chromium electroplating is worldwide banned. Alternate coatings and deposition methods were investigated by many authors to compensate hard chrome coating [2-8]. Piston ring surfaces are thermally (plasma) sprayed with molybdenum, metal composites, metal-ceramic composites or ceramic composites, as a uniform coating or an inlay coating material. Experimental work with new powder compositions for thermal spraying has included molybdenum-nickel-chromium alloys, chromium oxide (Cr2O3) with metallic chromium binder, alumina-titania (Al2O3-TiO2), tungsten carbide (WC) with metallic cobalt binder, MoSi2, CrC-NiCr. Hard chromium layers can be improved by plasma spraying of chromium ceramic on the ring face, thus increasing the thermal load capacity. A dense chromium carbide coating, produced by HVOF coating was found promising for piston ring applications. In this study, plasma spray coating of a mixture of four powders (Mo, NiCr, Cr3C2, Fe Alloy) as an alternative to hard chrome coating for wear reistance was investigated.

2 Experimental procedure

The plasma spray coating substrate was casted, similar to commercial piston ring material used so as to simulate the same piston ring environment. Then plasma spray coating plate made of Piston Rings material was plasma sprayed with a Sulzer-Metco PT F4 torch. Special attention was paid to the dependency of micro- structure and chemical composition of coatings on the nature of the plasma gas: Ar:H or Ar:He, the power of the plasma jet: 13–19.5 kW and the cooling device. For plasma spray powder, mixed the mixture of four commercial powders (Metco-350, Metco-63, Metco-70 &Metco-43F NS) and it can be called as Moly powder. These powders were mixed together with binder & slurry. Using this mixture a lump of 50µm size was prepared. A number of different mixtures were chosen and wear tested. After initial trials, the approximate final composition of one charge is represented below in the table 1. The charge amount prepared for the coating is of 6 Kg. To study the wear behaviour, pin on disc (WINDCUM 2008) wear test was used for plasma spray coating against three pins (3mm diameter) of En-31, nickel & tungsten carbide at loads - 40, 50 and 50 N and constant sliding speed 500 rpm for 2 Km distance, respectively.

Table. *Composition of the final mixture ready for coating.*

Sr. No	Elements	Material Type	Quantity (Kg)
1	(63)Mo	Hard material	1.2
2	(43)NiCr	binder	0.6
3	(70)Cr_3C_2	Hard material	0.6
4	(350)Fe Alloy	Base material	3.6

3 Results and disscusion

The microstructure of moly plasma coating shows a clear deposited splat and does not seem to form a continuous layer but at the cross section, it was observed that the coating was more homogeneous, regular with a few unmelted particles (Fig. 1).

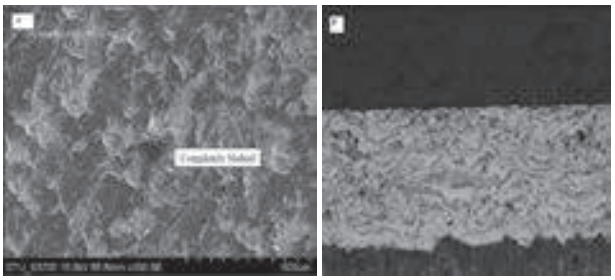

Fig.1. *Top and crosssection view of moly plasma spray coating.*

The wear rate of the air plasma coating was studied with different counter bodies – En-31, nickel & tungsten carbide at loads - 40, 50 and 60 N and constant sliding speed of 500 rpm. With all three counter bodies, the coating wear rate increased linearly where as counter body tungsten carbide

wear was almost constant at all loads (Fig.2). The wear rate of the coating at low load and with the counter body-nickel was found to be very low. The wear rate of coating increased to a lesser degree with increase of the loads with the counter body of nickel. The wear rate of the plasma spray coating was maximum with the counter body of the tungsten carbide. The wear rate increased more with increased load. The wear rate with the En-31 counter body was found to increase very rapidly for the initial increased load after which the increase became constant in manner. Thus it can be concluded that at lower load the wear is caused by adhesion and very less abrasion as wear rate of the coating was decreased by the tribolayer. The nickel pin at low load and high load showed high deformation and low wear rate of the plasma spray coatings because the micro hardness of coating used was large as compared to hardness of the nickel pin.

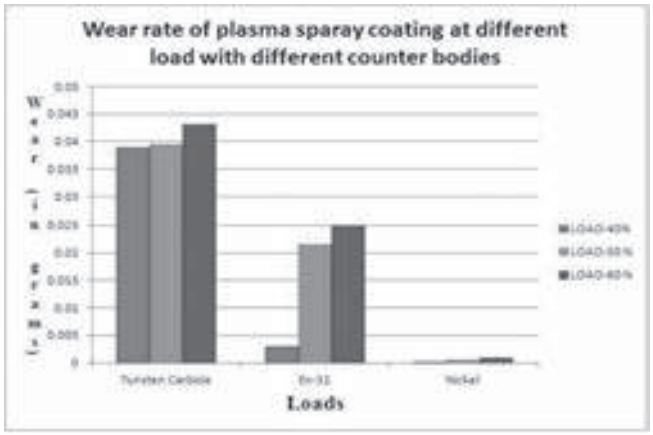

Fig.2.*The wear rate of the moly plasma spray coating at different loads with different counter bodies.*

To study the wear mechanism of moly plasma spray coating with En-31, nickel & tungsten carbide, the worn surfaces were examined. With En-31 pin, at lower load the wear was mainly due to abrasion (Fig. 3.A). When the load was increased to 50 N then adhesion also come into picture. Due to adhesion some deformation was also observed. The deformed particles were observed toget flattened over the coating surface.

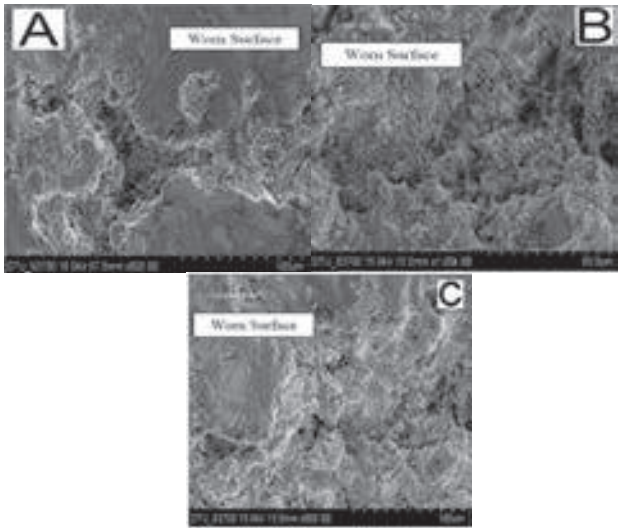

Fig.3.*SEM micrographs of the moly plasma spray coating.*

With further increased load of 60 N, long worn debris was generated. At higher loads and sliding speeds the occurrences of severe metallic wear by physical metallic failure are more dominating. With nickel pin, the coating showed wear at 40 N load and only some deformation as load increase to 50 N and adhere to the coating. Further increased in load to 60 N, the adhesion of the coating over the wear track and delamination occurred (Fig. 2.B). in the case of tungsten carbide pin at 40 N load, the coating showed some adhesion and as the load increased to 50 N wear pronounced with adhesion and with erosion (Fig.2.C). on furhter increase in load to 60 N, deformation of the coating was less, and directly microcutting was seen with more flattened over the wear track.

Commerically used hard chorme coating was prepared on the same substrate piston ring material and pin on disc wear tested at the same conditions of moly powder plasma spray coating. Moly powder plasma spray coating was found to impart better wear resistance at all loads (Fig. 4).

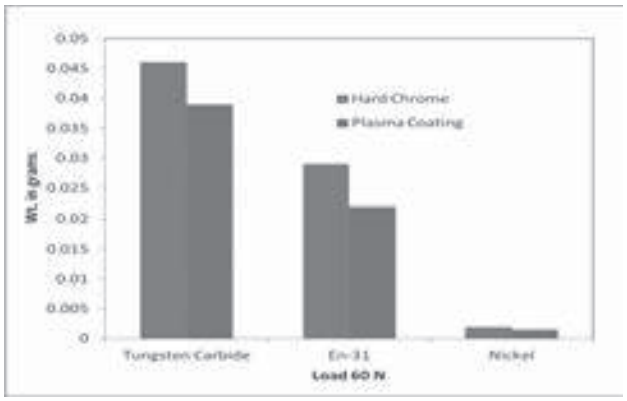

Fig. 4. *Comparsion of wear rate of hard chrome and plasma spray coating with different counter bodies.*

4 Conclusion

The Moly plasma spray coating was sucessfully preapared as wear resistance coating and can be used for piston ring applicaiton as an alternate to hard chome coating.

5 References

[1] S.M. Pandey, Q. Murtaza, S. S.Singh and M.S. Nirajan, Proc. 3rd Int. Conf. CPIE-2013, pp 1207-1212.
[2] F. Rastegar and D. E. Richardson, *Surface and Coatings Technology*, 90(1997)1–2, pp. 156–163
[3] S. Pandey, Q. Murtaza, and K. Gupta, *SAE Technical Paper* 2014-01-0946, 2014, doi:10.4271/2014-01-0946.
[2] B. Torres, et al., *Wear* 268 (2010) 828–836.
[5] C. Broszeit, C. Friedrich, and G. Berg, *Surface and Coatings Technology*, 11(1999)5, pp. 9–16.
[6] S. Zhuo et. al., *Surface and Coatings Technology*, 131 (2000)1–3, pp. 422–427
[7] R. Gonzalez, et al., Wear 262 (2007) pp 301–307
[8] J.A. Picas, A. Forn, G. Matthäus, *Wear*, vol.26, 2006 pp 477-484

Fabrication of Porous YSZ Coatings by Suspension Plasma Spray

Mohammed Shahien[1,2], Masato Suzuki[1]
[1] National Institute of Advanced Industrial Science and Technology, AIST, Tsukuba 305-8569, Japan.
[2] Central Metallurgical Research and Development Institute, CMRDI, Helwan 11421 Cairo, Egypt

Abstract
Yttria stabilized zirconia (YSZ) coatings considered to a promising candidate as thermal barrier coatings to protect and insulate metallic component in gas-turbine engines. It became a critical material for turbine efficiency, performance as well as overhaul and repair frequency. The microstructure is one of the most important challenges to increase the YSZ coatings efficiencies, due to its significant effects on coating properties and consequently on its applications and performance. The suspension plasma spraying (SPS) process has been developed to permit the injection of sub-micron particles into the plasma plume. This enables the deposition of novel microstructures as highly porous or segmented coatings (compared to the conventional atmospheric plasma spraying process). In this study, the approach of fabrication of porous YSZ coatings by suspension plasma spray system will be investigated. A unique an axial injection plasma spray system with low power and using one plasma gas was used.
It was possible to fabricate porous 8YSZ coatings and its microstructure, porosity was controlled by adjusting the spraying parameters. It was clear that, the spray distance and the suspension concentration are the most important parameters to control the particle size, which affects the coating structure significantly. Thus, through changing these parameters the coating microstructure changed from porous to dense structure and the most dominant factor is the splat size and the microstructure. It reveals that, the coating microstructure and porosity level can be controlled by appropriate changes in the solids amount in the suspension and the spraying parameters.

1 Introduction

The thermal barrier coatings (TBCs) have been used widely for the hot section parts in the stationary gas turbine engines for providing a thermal protection for the based superalloy components from the excessive thermal load of the hot gas.
The TBCs commercially consist of an oxidation resistant bond coat between the high temperature superalloy and a ceramic top-coating layer. The yttria stabilized zirconia (Y_2O_3-ZrO_2: YSZ); containing 7-8 wt% Y_2O_3, is a commercial ceramic top-coat material, which has been applied to the hot section areas of gas turbines for long time [1, 2].
Generally the top ceramic coating is usually applied either by air plasma spray (APS) or electron-beam physical vapour deposition (EB-PVD) process. Both these methods result in coatings with defective microstructures that help alleviate stresses arising from the thermo-mechanical mismatch between the metal and the ceramic (strain tolerance), and further reduce the thermal conductivity of the YSZ top-coat. Although EB-PVD process offers better coating mechanical properties due to the presence of columnar structure, its disproportionately high cost and low deposition rate limits its application to critical turbine components such as first stage of rotor blades. In contrast, the plasma spraying is a cost effective process with higher deposition rate and wider composition flexibility than EB-PVD process [3].
The conventional APS process is used to deposit TBCs in less critical areas within gas-turbine engines. The plasma-sprayed coating has porous microstructure with large "splat" boundaries/cracks that are parallel to the metal–ceramic interface. Although these "splat" boundaries/cracks are effective in reducing the thermal conductivities of APS TBCs. They leave the top-coat relatively less strain-tolerant and are the source of weakness in the TBCs that ultimately led to TBCs delamination and/or spallation. Furthermore, the adoption of the APS-YSZ coatings as TBCs should have concerns including sintering, phases transformation. Using the nanostructured feedstock material is one of the interesting approaches which have been explored to overcome the above concerns and to enhance the TBCs performance, it is due to its significant effect to control the coating microstructure and properties.

The suspension plasma spraying (SPS) process has been developed to permit the injection of nano/sub-micron particles into the plasma plume. The SPS process has received increasing interest in the thermal spray field due to its coating unique microstructure and properties. Thus, the injection of nano/sub-micron particles into the plasma plume enables the deposition of novel microstructures as highly porous or segmented coatings and also the columnar structure (compared to the conventional atmospheric plasma spraying process).
In this study, the approach of fabrication of porous YSZ coatings by suspension plasma spray will be investigated. A unique an axial-injection plasma spray system with low power and using one plasma gas was used to fabricate suspension plasma sprayed porous YSZ coatings.

2 Experimental Procedures

All experiments were carried out by using a twin-cathode type plasma spray gun (Aeroplasma Corporation, Japan) as shown schematically in Fig.1.

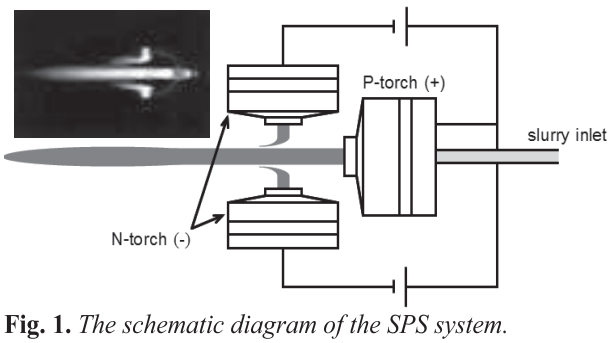

Fig. 1. *The schematic diagram of the SPS system.*

It is a unique system with three plasma torches; a P-torch (+) as main torch which has reversed polarity (with a cathode nozzle and an anode), and two N-torches (-) as sub-torches with normal polarity (with an anode nozzle and a cathode). During the operation, the electric power is supplied between an anode of P-torch and two cathodes of N-torches, so that the plasma jet can be maintained. This system makes it possible to vary operating parameters very widely, such as plasma gas flow rate, carrier gas flow rate, electric power inlet,.

Moreover, the electrode of the main torch (P-torch) is a hollowed anode, so that an axial feeding can be applied in this system. A commercial dual tube nozzle is inserted into the hollowed anode of the main torch to supply the mist of the suspension into the plasma jet as shown in Fig.2. Furthermore, the system requires only the argon gas as plasma gas (without H_2, N_2 or He), since the voltage (ie. enthalpy of plasma jet) is enough high with Ar for melting the ceramic powders with this system, which makes it as cost reduction system. All the spray parameters are shown in Table 1.

The cross-section and the surface microstructure of the fabricated coatings were observed by the FE-SEM (JSM-6300F, JEOL, Japan). The samples porosity were estimated and calculated by image analysis method with a conventional software for PC (Image-Pro Plus, Media Cybanetics, Inc., USA).

3 Results and Discussion

It was possible to fabricate suspension plasma spray 8YSZ coatings with low power and using only one plasma gas through using the twin cathode plasma spray system and the axial injection.

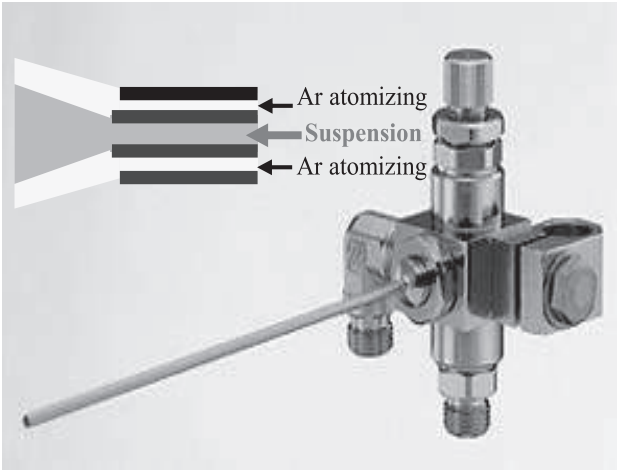

Fig. 2. *The Dual tube nozzle and its cross-section sketch.*

Table 1 The spray parameters

Plasma gas (Ar)	P: 40 l/min.
	$N_{A/B}$: 3.5 l/min.
Carrier gas (Ar)	5.5 l/min.
Power input	100A-160V*2 (32kW)
Sprayed suspension	8 YSZ+ EtOH
Suspension conc.	5-15 wt%
Feeding rate	35 ml/min
Spray distance	15-45 mm
Substrate	Blasted SUS304

The coating microstructure and porosity level can be controlled by appropriate changes in the solids amount in the suspension and the spraying distance. Thus, these two parameters are controlling the size/shape of deposit and porosity significantly. Figure 3 shows the SEM images of some the fabricated coatings indicating the effect of controlling the spray distance and the suspension concentration on changing the coating microstructure (porous/dense microstructure). It is clear that, by using high suspension concentration and/or short spray distance the fabricated coatings will have dense microstructure. On the other hand, using low solid content of the suspension and/or long spray distance the coatings will have porous microstructure.

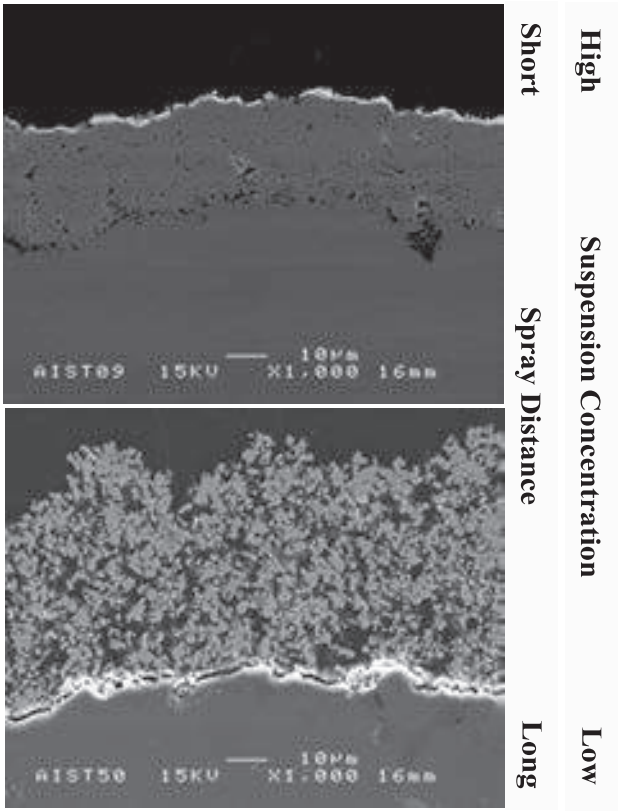

Fig. 3. *The SEM cross-section microstructure of the fabricated coatings with changing the spray distance and the suspension concentration.*

4 Conclusion

It was possible to develop a low cost suspension plasma spray system by using an axial-injection and a twin-cathode type plasma spray gun. A porous 8YSZ coatings were successfully fabricated and its microstructure, porosity was controlled by adjusting the spraying parameters.

5 References

[1] R.A.Miller: J. Therm. Spray Technol. **61-1** (1997) 35-42.

[2] C. U. Hardwicke and Y.-C. Lau: J. Therm. Spray Technol. **22-5** (2013) 564-576.

[3] A. Feuerstein, J. Knapp, T. Taylor, A. Ashary, A. Bolcavage and N. Hitchman: J. Therm. Spray Technol. **17-2** (2008) 199-213.

Process parameter studies to achieve phase pure α-Al_2O_3 coatings during solution precursor plasma spraying

G. Sivakumar[1], Rajiv O. Dusane[2], Shrikant V. Joshi[1]
[1]International Advanced Research Center for Powder Metallurgy and New Materials, Balapur P.O., Hyderabad, INDIA
[2]Department of Metallurgical Engineering & Materials Science, Indian Institute of Technology, Powai, Mumbai. INDIA

Abstract
The present paper describes the role of process conditions in developing phase-pure α-Al_2O_3 coatings using solution precursor plasma spraying (SPPS). Different precursor combinations were employed and two key parameters, namely the plasma power and substrate pre-heat temperature, were varied. Detailed studies of in-flight formed particles and splat characteristics were found to correlate well with the Al_2O_3 coating characteristics. The Al_2O_3-forming precursor formulation was also found to be crucial in determining the coating properties, including phase constitution.

1 Introduction

Thermally sprayed alumina coatings find wide-ranging industrial use in wear-resistant, dielectric, corrosion-resistant and diffusion barrier applications [1-2]. However, most of these applications ideally demand a thermally stable α-Al_2O_3 phase, which is often not achieved by conventional thermal spray variants including plasma spraying, even if the starting powder feedstock is phase-pure and comprises α- Al_2O_3 alone [2-4]. It is relevant to mention that conventional powder synthesis techniques, too, may not readily yield pure α-Al_2O_3 powders in a single step and necessitate process modifications, such as using high calorific value fuels during combustion spray pyrolysis or calcination after synthesis [5]. A recent report by the authors on the deposition of phase-pure, nanostructured and thick α-Al_2O_3 coating in the as-deposited condition using SPPS has provided useful insights and demonstrated the possibility of achieving the above by thermal spray processing [6]. This has encouraged the present detailed process parametric study to be carried out. SPPS coatings are known to be influenced by a wide range of variables, comprising plasma spray and liquid injection parameters as well as other external parameters. Based on preliminary trials, plasma power, substrate pre-heat temperature, standoff distance and precursor chemistry were found to be particularly significant. Among the above, the role of plasma power and substrate pre-heat temperature was investigated in detail for two different precursor combinations.

2 Experimental

Aluminum acetate mixed with 10 wt% acetic acid and aluminum nitrate (Sigma Aldrich, Germany) without any modification were specifically chosen as two extreme cases to understand conditions favoring the formation of phase-pure α-Al_2O_3. Aluminum salts were dissolved in DM water to prepare a 1 M solution and thoroughly mixed using a magnetic stirrer. Due to poor solubility, aluminum acetate was stirred for about 4 hours to form a clear transparent solution. SPPS coatings were deposited employing a 9MB plasma spray system (Sulzer Metco AG, Switzerland) equipped with a precursor delivery unit (Model: SPS-II; Inframat Corporation, USA). Plasma power was varied between 35 to 49 kW, by changing plasma current while keeping the voltage constant. All other relevant parameters that were kept constant, as well as the particle and splat collection methodologies, have already been provided in an earlier study [6]. The coatings were generated on substrates pre-heated to 500^{o}C.. The in-flight formed particles, splats and the resultant coatings were all extensively characterized through SEM, XRD and TEM analyses.

3 Results and discussion

The starting precursors were subjected to TG/DTA analysis to identify the possible pathways for transition to a stable alumina phase. In case of both precursors, the eventual Al_2O_3 formation starts with removal of water and nitrate/acetate ligands that successively result in amorphous Al_2O_3, followed by transition γ, θ, δ-Al_2O_3 phases which, upon further heating, lead to formation of α-Al_2O_3 around 1200^{o}C [7]. A continuous weight loss was observed over the entire temperature range in case of aluminium nitrate and also, absence of any DSC peak suggests that α-Al_2O_3 phase might not have formed within 1200^{o}C. In case of aluminium acetate, no significant change in mass occurs beyond 600^{o}C and shows a minor peak around 1055^{o}C. The organic ligands and additional presence of acetic acid might have been responsible for substantial heat of combustion, which plausibly accelerates the transformation to α–Al_2O_3 phase much earlier than with aluminium nitrate.

The unpyrolyzed mass content was found to be high at lower plasma power conditions and relatively higher when aluminium nitrate was used. This was apparent from lower mass loss observed when in-flight collected particles, from studies involving aluminium acetate based precursor, were subjected to TG/DTA analysis. Amorphous content was predominantly observed at low plasma power levels, along with boehmite phase on using aluminum nitrate. In case of modified aluminum acetate precursor, γ-Al_2O_3 phase was found to be present even at low power. With increase in plasma power, γ-Al_2O_3 content was found to progressively increase and an improvement in crystallinity also being noted in case of modified aluminum acetate. Although the Al_2O_3 particles collected mid-stream using various precursors appear dense, their inherent hollowness could be clearly seen from TEM analysis. The extent of hollowness is critical, as it can potentially influence the eventual coating microstructure. Upon careful Focused Ion Beam (FIB) milling, shell thickness was observed to be approximately 100 nm as shown in Fig. 1.

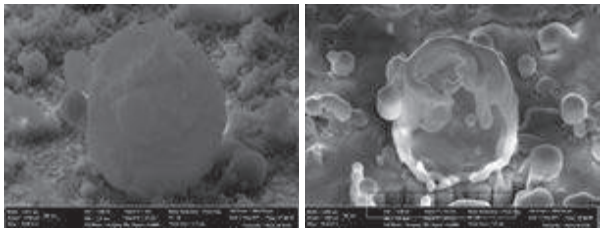

Fig. 1. *FIB milled Al_2O_3 particle clearly revealing its hollow nature*

The different particle and splat morphologies that can result during SPPS are summarized in Fig. 2, using micrographs from the exhaustive experiments conducted. It is clear from the these micrographs that the morphologies can vary over a wide range, depending upon the choice of process parameters.

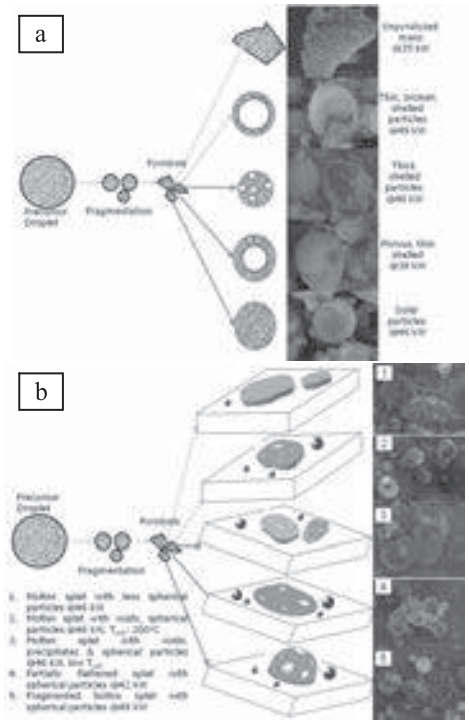

Fig. 2. *Summary of a) in-flight formed particles and b) splat morphologies at varied processing conditions*

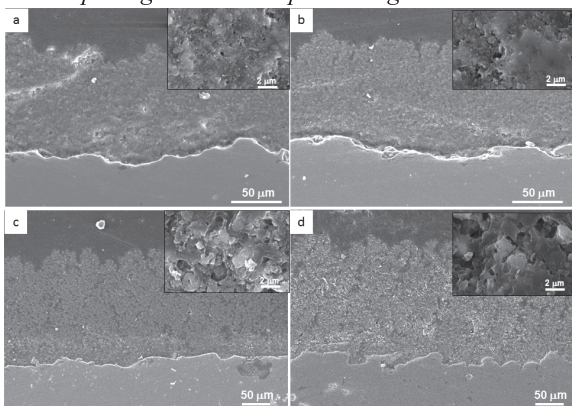

Fig. 3. *Cross-sectional microstructure of Al_2O_3 coatings generated at 35 and 49 kW plasma power using a-b) Al nitrate and c-d) Al acetate precursors*

The cross-sectional analysis of SPPS Al_2O_3 coatings deposited employing different plasma power levels shows that relative coating thickness was almost doubled to around 180-250 µm when aluminum acetate precursor was used, as compared to 90-120 µm in case of aluminum nitrate precursor, as shown in Fig. 3. Due to higher cation concentration in aluminum acetate (22.5%) than aluminum nitrate (7.2%), the effective conversion to the oxide was higher in case of the former. High magnification observation revealed that Al_2O_3 coatings (shown in inset) generated from both precursors exhibited significant amount of porosity along with distributed presence of unmelted, or partially melted, fine particles throughout the microstructure. There is an understandable influence of such defects, which resulted in substantial porosity and low microhardness values for the Al_2O_3 coatings.

Although the Al_2O_3 coatings exhibited only apparently minor differences in microstructure, there were distinct variations in phase constitution of the coatings formed using the two precursors (Fig. 4). In case of aluminum nitrate precursor, substantial amounts of transition phases were noted along with traces of α-Al_2O_3 phase at plasma power levels below 46 kW. In case of modified aluminum acetate precursor, α-Al_2O_3 phase was found to be the majority phase, even at the lowest plasma power of 35 kW. The retention of α-Al_2O_3 phases in thermally sprayed coatings is reported to occur under high solidification rates, which is provided by the intense plasma heat flux, heat of combustion from acetic acid and acetate ligands, which collectively contributed towards increased deposition temperature. Thereby, the use of a formulated precursor sprayed at high plasma power yielded phase-pure α-Al_2O_3 coatings.

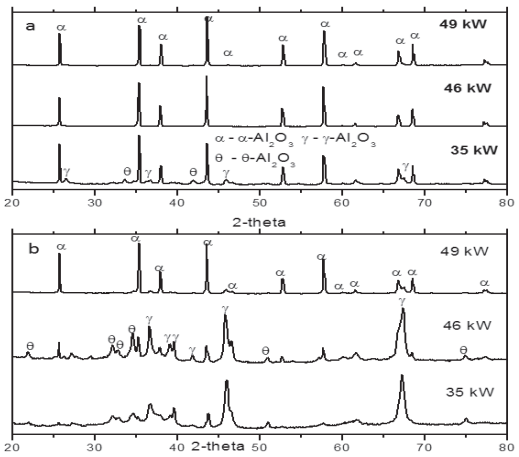

Fig. 4. *Phase analysis of Al_2O_3 coatings deposited at varied plasma power using a) Al acetate & b) Al nitrate*

4 References

[1] L. Pawlowski: Surf Coat Technol. **35** (1988) 285-298.
[2] C.-J. Li, G.-J. Yang and A. Ohmori: Wear **260** (2006) 1166-1172.
[3] C. C. Stahr, S. Saaro, L.-M. Berger *et al* :J Therm Spray Technol. **16** (2007) 822-830.
[4] R. McPherson: J Mater Sci. **15** (1980) 3141-3149.
[5] R. M. Laine, J. C. Marchal, H. P. Sun, X. Q. Pan: Nat Mater. **5** (2006) 710-712.
[6] G. Sivakumar, R.O. Dusane and S.V. Joshi: J Eur Cer. Soc. **33** (2013) 2823–2829.
[7] T. Sato, S. Ikoma, F. Ozawa: Thermochim Acta **75** (1984) 129-137.

Effects of Vanadates on High Temperature Degradation Behavior of Solution Precursor Plasma Sprayed Thermal Barrier Coatings

A. Ajay[1, 2], V. S. Raja[1], G. Sivakumar[2], S. V. Joshi[2]
[1] Department of Metallurgical Engineering and Materials Science, Indian Institute of Technology Bombay, Mumbai 400 076, India
[2] Centre for Engineered Coatings, International Advanced Research Center for Powder Metallurgy and New Materials, Hyderabad 500 005, India

Abstract
The degradation behavior of solution precursor plasma sprayed (SPPS) thermal barrier coatings (TBCs) in a molten salt mixture of 50 wt. % Na_2SO_4 + 50 wt. % V_2O_5 at 900 °C was studied. Scanning electron microscopy, energy dispersive x-ray spectrometry and x-ray diffraction results indicate that the formation of monoclinic ZrO_2 and YVO_4 phases along with a few non-protective oxides at the bond coat/top coat interface caused the degradation of SPPS TBCs. The salt appears to have an easy access to the bond coat/ top coat interface through the vertical cracks present in SPPS TBCs that are otherwise beneficial for resisting thermal strains induced during thermal cycling.

1 Introduction

Thermal barrier coatings (TBCs) are commonly deposited by electron-beam physical vapor deposition (EB-PVD) and air or atmospheric plasma spray (APS) techniques. TBCs produced by EB-PVD technique are advantageous over those produced by APS technique in terms of superior durability, but suffer from higher thermal conductivity and higher production costs [1-5]. A third method of making TBCs, namely, solution precursor plasma spray (SPPS) is gaining importance, in recent times, as the desire to produce highly durable coatings with the lower thermal conductivities economically is ever increasing. TBCs produced using SPPS technique are known to offer many inherent advantages over APS and EB-PVD techniques owing to their unique microstructure [1, 4, 6-8]. YSZ based TBCs are vulnerable to hot corrosion caused by molten Na, S and V salts [9-12]. To the authors' knowledge hot corrosion behavior of SPPS coatings is yet to be investigated and thus an attempt has been made in this study to address it.

2 Experimental

Inconel 718 discs of dimensions 10 mm Ø x 4 mm thickness, grit blasted with alumina particles (mesh 60) were used as substrates. These were coated with NiCoCrAlY powder of nominal composition (wt. %) 23Co - 17Cr - 12.5Al - 0.45Y –Ni(Bal.) as bond coat, using APS technique. The YSZ (with 8 wt. % Y_2O_3) top coat, coated using SPPS technique, was produced using a precursor solution, prepared by mixing zirconium acetate [$Zr(C_2H_4O_2)_4$] diluted in acetic acid with an appropriate stoichiometric amount of yttrium nitrate hexahydrate [$Y(NO_3)_3.6H_2O$] followed by continuous magnetic stirring. The plasma spray parameters adopted for the generation of coatings are shown in Table 1. The thicknesses of the TBCs were: (a) 100 ± 10 µm for the bond coat and (b) 250 ± 20 µm for the top coat.

A salt mixture of 50 wt. % Na_2SO_4 + 50 wt. % V_2O_5 was chosen as corrosive salt. This salt mixture was dissolved in distilled water to obtain a 50 wt. % salt slurry which was spread over the surface of coatings in the concentration of 5-7 mg cm^{-2}. These salt coated specimens were placed in a tubular furnace with air atmosphere at a temperature of 900 ± 1°C. The specimens were periodically examined and hot corrosion tests were interrupted at the first observation of visual chipping of the top coat from the specimen surface. Scanning electron microscopy (SEM), energy dispersive x-ray spectrometry (EDS) and x-ray diffraction (XRD) techniques were used to study microstructure, chemical composition and crystalline structure of the coatings and hot corrosion products.

Table. 1. *Plasma spray parameters*

Parameters	NiCoCrAlY	YSZ
Primary gas, Ar scfh @ 80 psi	90	140
Secondary gas, H_2 scfh @ 50 psi	10	12
Plasma arc current (A)	500	650
APS powder feed rate (g min^{-1})	30	-
SPPS precursor feed rate (mL min^{-1})	-	24
Spray distance (mm)	110	50

3 Results and Discussion

Fig. 1 shows the SEM surface morphology of SPPS TBC after hot corrosion testing (80 h). The surface of SPPS YSZ after hot corrosion testing was found to be porous and revealed the presence of rod shaped crystals which were composed of Y, V and O (Fig.1). XRD analysis (Fig. 2) showed that these rod shaped crystals to be YVO_4. In addition, monoclinic-ZrO_2 was also observed to have formed in coatings after hot corrosion testing.

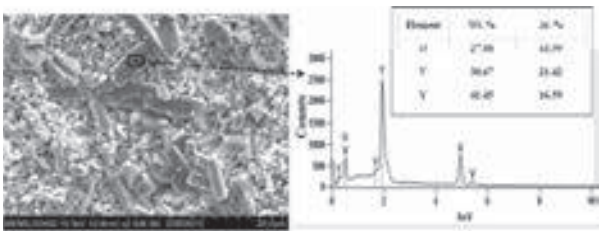

Fig. 1. *SEM image showing YVO_4 rod shaped crystals on the surface of SPPS TBCs after hot corrosion testing (80 h) along with EDS analysis data*

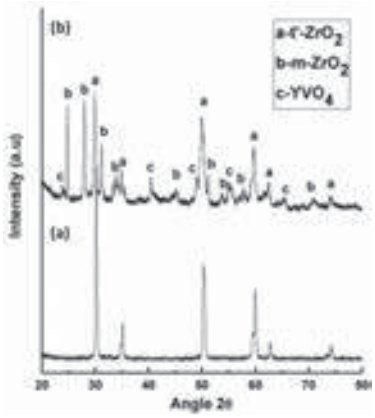

Fig. 2. *XRD patterns of SPPS TBCs in: (a) the as-sprayed condition and (b) after the hot corrosion testing (80 h)*

In as-sprayed condition, XRD pattern of the coating (Fig. 2) showed complete tetragonal structure. The hot corrosion mechanism leading to the formation of YVO_4 crystals and monoclinic-ZrO can be explained by following reactions [13-14]:

$$V_2O_5 + Na_2SO_4 \rightarrow 2\ NaVO_3 + SO_3 \quad (1)$$

$$ZrO_2\,(Y_2O_3) + 2\ NaVO_3 \rightarrow ZrO_2\,(\text{monoclinic}) + 2\ YVO_4 + Na_2O \quad (2)$$

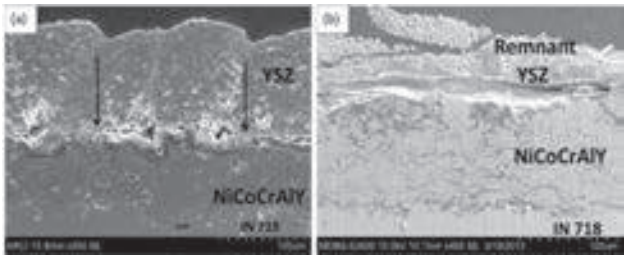

Fig. 3. *Cross-sections of coating: (a) after 40 h and (b) after 80 h of hot corrosion testing. Arrows in (a) indiacte crack intitaion with in YSZ along the inter-pass boundary*

The formation of monoclinic ZrO_2 and YVO_4 crystals results in volume expansion, generating stresses in the top coat [9-10, 13]. These stresses led to cracking in SPPS TBCs which initiated and propagated along inter-pass boundaries (Fig. 3a) due to the weaker bonding of the coating in this region resulting from the preferential distribution of unmelted particles and porosity [1].

After 80 h of hot corrosion testing YSZ layer has spalled and SEM and EDS analysis were carried out on the surface of remnant YSZ (Fig. 4). Irregular shaped crystals were observed on the surface of remnant YSZ. From EDS analysis (Fig. 4), it can be seen that these irregular shaped crystals were composed of Cr, Co, Ni-rich oxides. The formation of these oxides due to depletion of Al in the bond coat is a result of corrosive medium reacting with the bond coat [10]. This can be ascribed to the presence of vertical cracks in SPPS coatings, which enabled infiltration of the molten corrosive salt through the top coat towards the bond coat. The growth of such non-protective oxides are known to promote extensive cracking of these oxides [1]. These cracks were found to connect the already existing cracks within YSZ resulting in the top coat spallation (Fig. 3b).

In general, when the separation between the top coat and the bond coat becomes large enough in TBCs, either edge delamination or buckling (delamination over the entire specimen surface) (both lead to subsequent spallation) were found to occur. Literature indicates that buckling is favored when the stored energy in the coating is small and the preexisting cracks are large [15]. In the present case, low strain energy is expected due to the effectiveness of vertical cracks in lowering the stress in the TBC.

Thus SPPS TBCs exposed to 50 wt. % Na_2SO_4 + 50 wt. % V_2O_5 corrosive salt failed due to the synergic action of corrosion (formation of irregular shaped oxides) on the bond coat (Fig. 4) which exert stresses on the top coat and volumetric stresses generated in the top coat due the formation of monoclinic zirconia (as illustrated by Eqns. (1)-(2)) along with YVO_4 crystals.

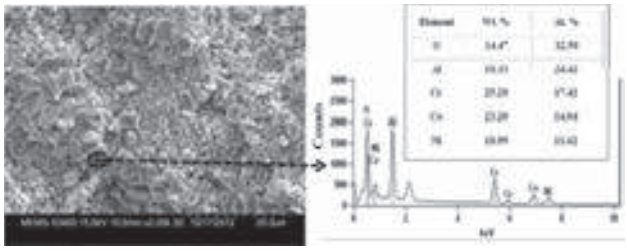

Fig. 4. *Surface morphology of remnant YSZ after hot corrosion testing (80 h)along with EDS analysis data*

3 References

[1] M. Gell, L. Xie, E. H. Jordan and N. P. Padture: Surf. Coat. Technol. **188-189** (2004) 101-106.

[2] E. H. Jordan, L. Xie, X. Ma, M. Gell, N. P. Padture, B. Cetegen, A. Ozturk, J. Roth, T. D. Xiao and P. E. C. Bryant: J. Therm. Spray Technol. **13** (2004) 57-65.

[3] L. Xie, X. Ma, E. H. Jordan, N. P. Padture, D. T. Xiao and M. Gell: J. Mater. Sci. **39** (2004) 1639-1646.

[4] L. Xie, D. Chen, E. H. Jordan, A. Ozturk, F. Wu, X. Ma, B. M. Cetegen and M. Gell: Surf. Coat. Technol. **201** (2006) 1058-1064.

[5] R. L. Jones: J. Therm. Spray Technol. **6** (1997) 77-84.

[6] M. Gell, E. H. Jordan, M. Teicholz, B. M. Cetegen, N. P. Padture, L. Xie, D. Chen, X. Ma and J. Roth: J. Therm. Spray Technol. **17** (2008) 124-135.

[7] F. Wu, E. H. Jordan, X. Ma and M. Gell: Surf. Coat. Technol. **202** (2008) 1628-1635.

[8] L. Xie, X. Ma, A. Ozturk, E. H. Jordan, N. P. Padture, B. M. Cetegen, D. T. Xiao and M. Gell: Surf. Coat. Technol. **183** (2004) 51-61.

[9] G. Sreedhar and V. S. Raja: Corros. Sci. **52** (2010) 2592-2602.

[10] G. Sreedhar, MD. M. Alam and V.S. Raja: Surf. Coat. Technol. **204** (2009) 291-299.

[11] Z. Chen, J. Mabon, J. G. Wen and R. Trice: J. Eur. Ceram. Soc. **29** (2009) 1647-1656.

[12] H. Liu, X. Xiong, X. Li, Y. Wang, , Corros. Sci. **85** (2014) 87–93.

[13] A. Afrasiabi, M. Saremi and A. Kobayashi: Mater. Sci. Eng., A **478** (2008) 264-269.

[14] R. Ahmadi-Pidanin, R. Shoja-Razavi, R. Mozafarinia and H. Jamali: Ceram. Int. **38** (2012) 6613-6620.

[15] S. R. Choi, J. W. Hutchinson, A. G. Evans: Mech. Mater. **31** (1999) 431-447.

Application of instrumented indentation and scratch methods for characterization of thermally-sprayed coatings.

Gregory Favaro[1], Nicholas Randall[1],Jiri Nohava[1], Kapil Joshi[2] , Hemant Gourkar[3] ,Shiva Tummalapalli[3]

[1] Anton Paar TriTec SA, Rue de la Gare 4, CH-2034 Peseux, Switzerland.
[2] Anton Paar India, Arcadia, 301, 3rd floor, Hiranandani Estate, Thane (W) INDIA.
[3] Anton Paar India, 501, Srivas Capital, Phase-V, K.P.H.B, Hyderabad, INDIA.

Abstract

In order to improve the knowledge on the use and significance of instrumented indentation and scratch testing on thermally-sprayed materials, a wide range of tests were performed on thermally-sprayed ceramic, cermet and metal coatings. A scale-dependent behavior of hardness was observed as a function of indentation depth for all coatings: At low penetration depths, the hardness value depends on the intralamellar material properties, whereas at larger depths it reflects the long-range cohesive strength of the coating. In all cases, hardness becomes independent of the indentation depth above a threshold value of ~2 µm. The elastic modulus is also scale-dependent, but it never stabilizes to a depth-independent value, probably on account of crack opening/closing mechanisms. Scratch testing on the cross-section has also been thoroughly investigated and identified as a comparative method to quantify the cohesion of the coatings. Visual matrix indentation & CMC mode are also useful to determine the variation of mechanical properties of the inhomogeneus samples at different depths in single experiment.

1 Introduction

Thermal spray coatings are used in Power plant turbines, aircraft engines, on pulp rolls in the paper industry for their enhanced wear, corrosion and thermal protection properties. This paper considered two type of thermal spray coating techniques namely-HVOF & WSP. Thermal Spray coatings of WC-Co, Cr_3C_2-NiCr, (Ti,Mo)(C,N)-NiCo are formed by HVOF-sprayed & Alumina, SS coatings on SS substrates by WSP spraying techniques. We have tested mechanical properties of thermal spray coatings by nano & macroindentation at different length scales using visual matrix method. Cohesion, Adhesion properties of the coating were studied using scratch tester on cross-section of the sample. Instrumented indentation gives more information about mechanical properties of the coatings such as elastic modulus, elastic/plastic work of indentation and creep or cyclic behavior [1-3].

2 Experimental

Thermal spray (TS) coatings namely-WC-Co, Cr3C2-NiCr and (Ti,Mo)(C,N)-NiCo formed by HVOF-sprayed & Alumina, (316L) SS coatings on SS substrates were formed by WSP-sprayed technique. In case of WSP feeding and spraying distances are essential parameters as they determine the mechanical properties of the material. All samples were cross-sectioned, embedded in resin and metallographically polished. CSM instruments NHT (0.1-500 mN, Berkovich indenter), MHT (0.03-10 N, Vickers indenter) & Revetest Scratch Tester (1-200 N, Rockwell C diamond indenter of 200 µm radius) setup were used to carry out the experiments in nano & micro scale domains. Few measurements were also done by the CMC method carried out from 1mN to 100 mN with 20 cycles and the indented areas were selected by Visual matrix technique [4]. On each sample five to seven measurements of the same type were performed and only average values are presented.

3 Results

Fig. 1 shows SEM image of typical microstructure of WC-17Co HVOF-sprayed coating showing WC grains and binding metal matrix. At very small loads of a few mN the properties of the individual grains or splats can be measured whereas increasing the load upto few N, larger volume is being involved which reveals a 'composite' value of mechanical properties.

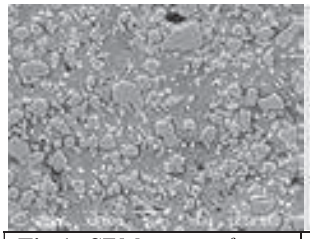

Fig.1: *SEM image of typical microstructure HVOF-sprayed coating*

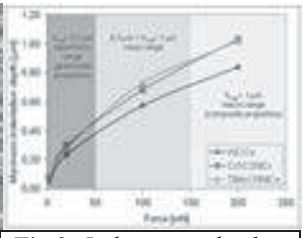

Fig.2*: Indentation depth (mm) vs Load (mN)*

Nanoindentation was carried out using (NHT) at four loads corresponding to different depth ranges as shown in fig.2. Indentation load values were selected such that the Indentation depth lie in one of these regions. In nano/micro range were indivisual grains/splat affects or determines the properties of the coatings (h_{max}<0.5 µm). In meso range (0.5 µm<h_{max}<1 µm) & macro range (h_{max} > 1 µm) composite properties of the coating were measured. It is observed that decrease in hardness with increase of the maximum indentation force for all samples thermal sprayed by HVOF technique. At small loads, the volume involved in the indentation is small so measurements are not influenced by pores or grain boundaries. With increasing indentation forces the volume of material influenced by indentation increases and comprises also the softer metallic matrix. This leads to the observed decrease in hardness with increasing indentation force. Elastic modulus remained rather constant for all coatings irrespective of the maximum indentation force.

We have also observed that parameter (η_{IT}) work of indentation which is the ratio of elastic work to total work of indentation. Since (η_{IT}) measures the elastic-plastic

response of the material to external load, it can be used for estimation of the ability of the material to resist wear or abrasive damage. The value of η_{IT} for all three tested TS coatings was much higher at lower loads and progressively decreased with increasing loads as shown in Table-1. Indenting at low loads in the relatively homogeneous microstructure of single grains composed of carbides results in a high ratio of elastic to total work of indentation. At higher loads (above 100 mN) however, increasing contribution of plastic deformation in the metallic matrix and formation of intergranular and intersplat cracks leads to dissipation of the indentation energy which is reflected in lower fraction of elastic work of indentation.

Table-1: *work of indentation η_{IT} at different loads.*

Force (mN)	2	20	100	200
WC-Co	48±7	34 ± 4	30 ± 2	29 ± 3
Cr_3C_2-NiCr	50 ±4	38 ± 3	31 ± 6	30 ± 3
(Ti, Mo)(C,N)-NiCo	37 ±11	34 ± 5	28 ± 4	28 ± 3

Fig. 3 shows SEM image of cross section of region on which constant load Scratch test carried out.

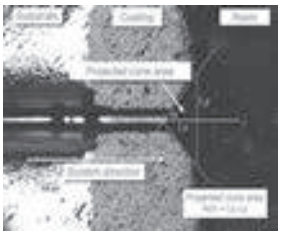

Fig.3: *Scratch test of cross-section of coating WC*

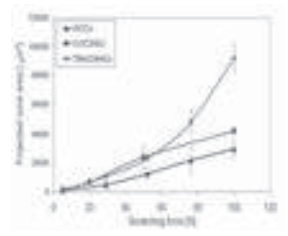

Fig. 4 : *Projected cone area vs scratching force.*

Fig. 4 shows that the projected cone area ($A_{cn}=L_x.L_y$) obtained from SEM increase with load was almost linear for samples WC-17Co and Cr_3C_2-NiCr whereas for sample (Ti,Mo)(C,N)-NiCo the increase showed a more parabolic trend. This indicates the existence of a different failure mechanism. WC-17Co showed the highest abrasion resistance followed by Cr_3C_2-NiCr whereas the (Ti,Mo)(C,N)-NiCo mixture showed the lowest abrasion resistance.use of scratch test for adhesion /cohesion was 1st proposed by Lopez et. al. [5].

Mechanical properties of WSP sprayed high quality alumina (Al_2O_3) and steel coatings were studied. **Alumina samples:** Almost similar trend observed for NHT & MHT measurements as rapid decrease of both hardness and elastic modulus at low depths and stabilization of the hardness and elastic modulus values above 2 µm depth. Above this depth the influence of load on the mechanical properties of plasma sprayed coatings can be considered as negligible. Samples are characterized by parameters (Feeding distance-Spraying distance) (80-500, 60-425, 40-350). The differences were observed at low loads likely due to the different local temperature history of the deposited layers. Hardness of the 80-500 was the highest, followed by the 60-425 coating and the 40-350 coating. Though the differences in the microstructure between the coatings were quite small [6]. In general, both the hardness and elastic modulus were higher at the top interface than at the substrate-coating interface. (cross-sectional samples). **Plasma sprayed stainless steel:** The samples were sprayed under different conditions to achieve different fraction of oxides (oxide % varied from 2.72 to 7.65 for samples 1408 to 1412 resptly) which are typical for metallic coatings sprayed in air.

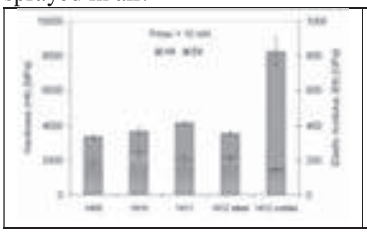

Fig. 5 *Hardness and elastic modulus of the steel coatings. (Note high hardness of the oxides in sample 1412).*

In case of sample 1412 (7.65%) where the fraction of oxides was sufficiently high and single indentations could be carried out on both metallic and oxide particles. The prevailing metallic particles in all coatings were easy to target for both cyclic indentation and single load indentations. The chart in Fig. 5 shows the results of single indentation at low load of 10 mN for all steel samples. There was little variation in hardness and elastic modulus of all coatings observed; elastic modulus of all metallic splats was close to 200 GPa, which is the known value for bulk steel. Low load indentation can therefore effectively measure single phases or constituents in heterogeneous material such as TS coating. Oxide particles on sample 1412 were clearly visible – though still relatively small – and their hardness was much higher than that of the surrounding metallic splats. On the other hand, the elastic modulus of the oxides (~150 GPa) is surprisingly lower than that of steel (~200 GPa). This could be explained by internal porosity of the oxide particles or intraparticular cracking [7].

4 Conclusion

In conclusion, Instrumented indentation and scratch testing methods give a new insight into understanding the mechanical properties on micro and nano scale of thermal sprayed coatings. A parameter (η_{IT}) was used for characterization of elastic-plastic properties i.e. coatings resistance to failure. The constant load scratch testing on the cross-sectioned coating is a very intuitive, fast and efficient method for characterization of cohesion.

5. Acknowledgement:

These coatings were received from Skoda Research, Ltd. in Plzen, Czech Republic & Institute of Plasma Physics (Prague, Czech Republic), respecivetly.

6 References

1. A. C. Fischer-Cripps: Nanoindentation. Springer Verlag, p. 198
2. ASTM E 2546 – 07 Standard Practice for Instrumented Indentation Testing.
3. ISO 14577 Metallic materials–Instrumented indentation test for hardness and material parameters.
4. N. X. Randall, R. Christoph, S. Droz, C. Julia-Schmutz: Thin Solid Films 290 -291 (1996) 348-354.
5. E. Lopez, F. Beltzung, G. Zambelli: Journal of Materials Science Letters 8, (1989) 346-348.
6. Musalek, R. Matejicek, J. Vilemova, M. Kovarik, JTST, Vol. 19(1-2) Jan 2010, p. 422-428.
7. Musalek, R. Kovarik, O. Matejicek, J.: Accepted for publication in Surface and Coatings Technology, 2010.

Characteristics of cold-sprayed Cu coatings with pretreated feedstock

J.O. Choi, K.H. Ko,H. Lee

Department of Energy Systems Research, Ajou university,Department of Energy Systems Research, Ajou university

Powder properties of the feedstock used for spray coatings, especially cold-spray coatings, have an influence on the coating properties such as deposition efficiency, morphology and hardness. The effects of pretreatment on Cu feedstock with dendritic morphologies used for cold spraying were investigated. The Cu powders were pretreated into air and vacuum in the temperature range of 50 - 200Â°C at dwell times of 1 and 6 hours. The deposition efficiency of the air-annealed feedstock shows an initial increase due to the stress relaxation till the oxidation begins and prevails in bringing about drop in the efficiency. The coatings produced from the vacuum-annealed feedstock had much higher deposition efficiency than the air-annealed feedstock, resulting from the combined effect of stress relaxation and reduction of Cu. Therefore, it was confirmed that the feedstock properties modified by a pretreatment had a significant influence on the properties of cold-sprayed coatings.

Residual Stress Behaviour of Cold Sprayed IN625 Coatings

Chintala V Manikantha[1], Dheepa Srinivasan [2]
[1] BHEL GE Gas turbine Services, Hyderabad 560 012, India
[2] GE Power and Water, GE India Technology Centre, Bangalore 560066, India

Abstract
A detailed experimental analysis of the residual stress behavior in cold sprayed coatings (IN625 (Inconel 625 is a Trademark of Huntington alloys corporation)), was able to reveal some insights about the compressibility as well as interfacial behavior, on a 4130 steel substrate. The X-Ray diffraction $Sin^2\psi$ technique was employed to obtain coating through thickness residual stresses, at different locations in the coating into the substrate. In the cold sprayed coating, the residual stress is always compressive, at around -300 to -400 MPa, and gradually decreases towards the substrate. Close to the coating substrate interface, 25-50 µm in the coating, the residual stress becomes less compressive until it levels off to a zero stress or a slightly tensile value in the substrate. The effect of, a. process gas (He vs N2), and, b. the coating relaxation behavior (As sprayed vs 350°C vs 650°C), on the evolution of residual stress in the coating has been evaluated in the present work.

1. Introduction

Residual stresses play an important aspect of cold sprayed coatings [1]. In many ways, cold spray is akin to shot peening in having a compressive residual stress, owing to the severe plastic deformation that takes place during processing [2]. The magnitude of residual stress in the coating and the substrate varies depending on the coating and substrate materials, in terms of the hardness and deformability [3]. In soft metals, such as Al and Cu, it is reported that the cold spray coatings actually impart a compressive stress to the substrate that enables a better fatigue response of the coated component [4]. In many ways, the bonding to the substrate is expected to be an outcome of the compressive residual stress, that tends to hold the cold sprayed coating to the substrate, without any significant metallurgical bonding [5]. The aim of this paper is to analyze the residual stress behavior of a Ni based cold spray coatings, IN625 on 4130 steel, sprayed using two different process gases Helium and Nitrogen. The thermal relaxation of the coatings has been studied, and the evolution of the coating residual stress has been mapped as a function of temperature, in order to assess the stability of these coatings, for potential applications.

2. Experimental Details

IN625 powder was cold sprayed on to a low alloy steel AISI 4130 steel substrate with a hardness of ~220 Hv, using various cold spray systems, CGT Kinetics 8000, Kinetics 4000/47 and Impact Innovation, using Helium (He) and Nitrogen (N_2) process gases. The nominal coating thickness was ~500 µm. Table 1 lists the coating process parameters, gas pressure and temperature. Helium sprayed coatings were sprayed at 30 bar pressure and Nitrogen at 50 bars 50 bars. The coatings were characterized using a Nikon

Eclipse MA 200 optical microscope, Shimadzu microhardness tester (0.3 H_v) and Rigaku Automate II micro area X-ray residual stress analyzer. Through thickness residual stress measurements were carried out using using the $Sin^2\psi$ method (CrK_α, λ=2.284°). The coatings were heat treated at 350°C and 650°C, for 2.5 h, in a Lindberg furnace, in air, to study the coating relaxation response.

Coating	Gas	Gas Pressure (bar)	Temperature °C
IN625 on 4130 Steel	Helium	30	500
	Nitrogen	50	800

Table 1: *Coating process parameters*

3. Results

Fig. 1 compares the optical microstructure (200X) of the IN625 coatings sprayed using Helium vs Nitrogen, in the, as sprayed condition (Fig. 1(a-b)), and after heat treatment, 2.5 h(air) at 350°C (Fig.1(c-d) and at 650°C (Fig.1(e-f), respectively. The legends in the figures indicate the coating hardness (H_v) and the coating porosity (%). Fig. 2 is a comparative plot of the coating microhardness. Fig. 3 shows the through thickness residual stress of the as sprayed coating, comparing the He vs. the N_2 sprayed one. Fig. 4 is a residual stress plot comparing the coaitng response in the as sprayed condition vs the heat treated condition.

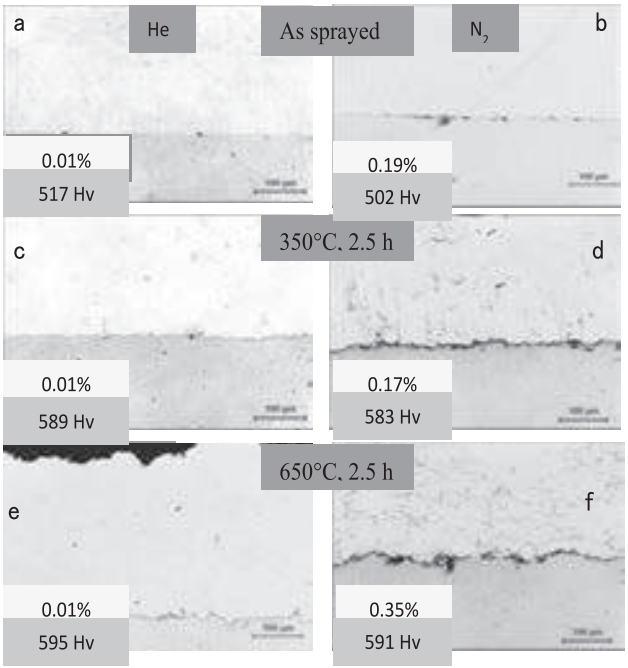

Fig. 1 : *Optical micrographs (200 X) comparing the Helium (a,c,e) vs Nitrogen (b,d,f), in the (a-b) As Sprayed, (c-d) 350°C, and (e-f) 650°C, conditions, respectively.*

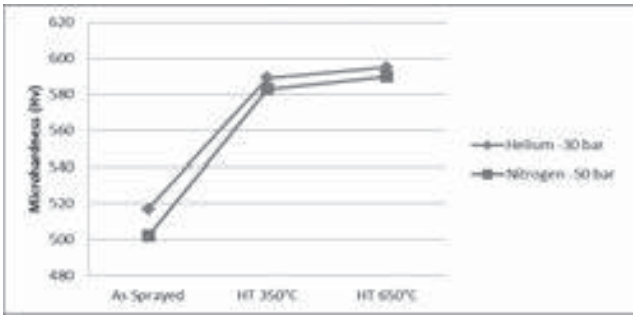

Fig. 2 : *Comparative microhardness plot of the Helium vs Nitrogen IN625 coating, in the as sprayed and heat treated condition*

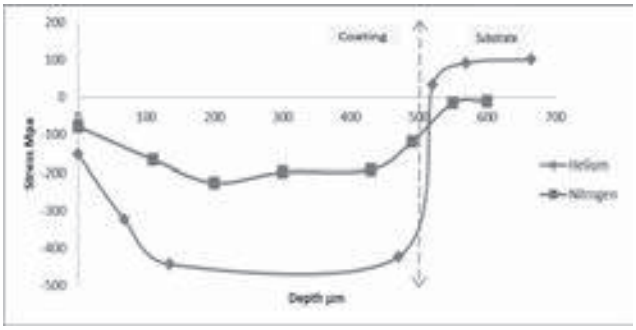

Fig. 3 : *Effect of process gas (He vs. N_2) on the residual stress of the IN625 cold sprayed coating*

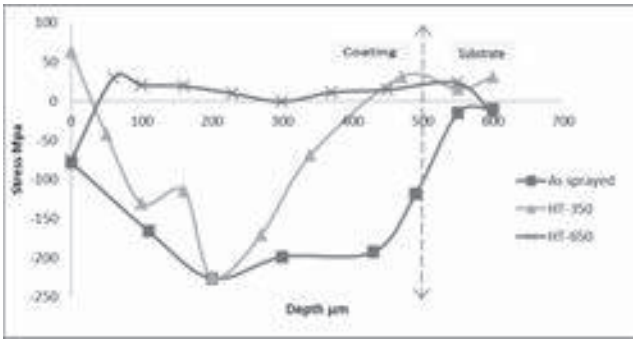

Fig. 4 : *Residual stress in the IN625 cold sprayed coating(N_2 gas) as a function of heat treatment*

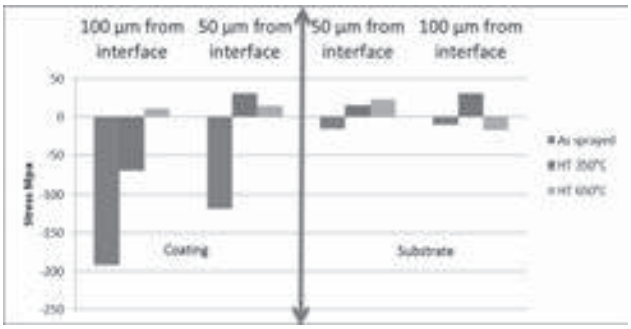

Fig. 5 : *Evolution of residual stress close to the coating substrate interface*

3. Discussion

Dense coatings (> 99.5%) were obtained using both He and N_2 process gases, measuring between 480-520 µm in thickness. The compressive residual stress was nearly 50% higher using He as the process gas as compared to N_2. The average coating hardness in the as sprayed condition (~500 H_v), using both gases, was found to increase with heat treatment. This is attributed to the recrystallization [6] leading to nanometer sized grains, inspite of recovery and dislocation free grains. The microstructure revealed coating delamination from the substrate, upon heat treatment, especially at the higher temperature (650°C). The residual stress was found to show a sharp decrease upon heat treatment, to completely becoming tensile at 650°C, thus corroborating the delamination seen at 650°C. Detailed analysis of the residual stress, closer to the coating substrate interface, to within 100 µn on either side, reveals the residual stress in the coating to be tensile even at 350°C, thereby correlating with the coating delamination.

4. Conclusion

1. Dense (< 0.5% porosity) IN625 coatings were obtained using He and N_2 process gas, on 4130 substrate.
2. The coatings microhardness ranged between 500-510 H_v for both the processs gases.
3. The hardness was found to increase by nearly 20% with heat treatment, up to 650°C, using both gases.
4. The coatings showed a compressive residual stress in the as sprayed condition, using both gases. However, the average residual stress measured through a 500 µm coating sprayed usign N_2 gas was roughly half that of the He sprayed coating.
5. Upon heat treatment, there is a sharp decrease in the compressive stress at 350°C, and a complete lack of any compressive stress at 650°C.
6. The residual stress close to the substrate is tensile, thereby reflecting the coating delamination that is seen to take palce.

5. Acknowledgements

The authors would like to thank, Dr. Y.C Lau, Dr. Eklavya Calla, Dr. Vishwanathan Venkatachalapahy, from GE, Power and Water, Materials and Process Engineering, and Dr. J. Karthikeyayan, ASB, Industries, Ohio, for processing the IN625 coatings and various discussions. This work was carried out as part of the Oil and gas coatings program, financial support from the program manager, Mr.Adam Drufke, is gratefully acknowledged. Mr. Christopher Thompson and Dr. Sundar Amancherla, GE Power and Water are thanked for support in carrying out the work.

6. References

[1] T.D. Phan, S. Masood, M. Jahedi and S. Zahiti, Trans. Tech. Publications, 2010.
[2] W.B. Choi, L. Li, V. Luzin, R. Neiser, T. Gnaupel-Herold, H.J. Prask, S. Sampaht, A. Gouldstone, **55** (2007) 857-866
[3] K. Spencer, V. Luzin, N. Matthews and M.X. Zhang, Surf. Coatings Tech. **206** (2012) 4249-4255.
[3] R. Gherifard and S. Bagherifard, AIAS-2011-141.
[4] Hassan Mahmoudi-Asl: *The effect of residual Stress induced by cold spray process on the fatigue life of Magnesium alloy, AZ31B* waterloo University, 2011.
[5] D. Zhang, P.H. Shipway and D.G. Mccartney, J. Thermal Spray Tech., **14** (2005) 109-116.
[6] D. Srinivasan and R. Amuthan, *Superalloys* 718, 625 and 706 conference proceedings, Sept 2014.

Advanced metallographic sample preparation techniques for Thermal spray coatings

Patrick Voos
Buehler, An ITW Company, In der Steele 2, 40599 Duesseldorf, Germany

Abstract
Thermally sprayed coatings are used to improve the resistance of substrate materials to oxidation, corrosion, surface wear and erosion. The accurate characterization of coated metal components requires metallographic examination of their microstructures. Coating thicknesses range from 0.002 to 0.060 inches (0.005 to 1.5mm) and are deposited on substrates using various spray techniques and parameters. The microstructural characteristics must be accurately determined using metallographic preparation techniques. Due to the brittle nature of some coatings and the occurrence of pores and constituents of widely different hardnesses in the layered structure, there is always a danger that metallographic preparation may either fail to expose the true microstructure or induce artifacts that will lead to a misinterpretation of the coating characteristics. Light optical microscopy provides a means by which a properly prepared coating specimen can be evaluated to determine the quality of the coating/substrate interface, the amount of porosity, unmelted particles and oxide distribution, coating thickness and other coating characteristics. Metallographic techniques used to prepare thermally coated specimens for microstructural evaluation vary from laboratory to laboratory. The variation often produces marginal to acceptable results. This presentation will give you the most advantaged sample preparation techniques by using mechanical sample preparation and latest consumable technologies to ensure excellent and repeatable results.

1. Introduction

Sample preparation for termally sprayed coatings is quite difficult, because the sample has to be handled very carefully. In general, no residual damage should be present at the end of the sample preparation. If there is still some residual damage on the sample surface, the image analysis can easily end in a misinterpretation of the material characteristic. One good example is the incorrect amount of porosity. If the sample preparation wasn't properly done, the spray coating will show pull outs, which means that the visible amount of porosity is higher compared with the true structure/ porosity **(Fig.1)** .

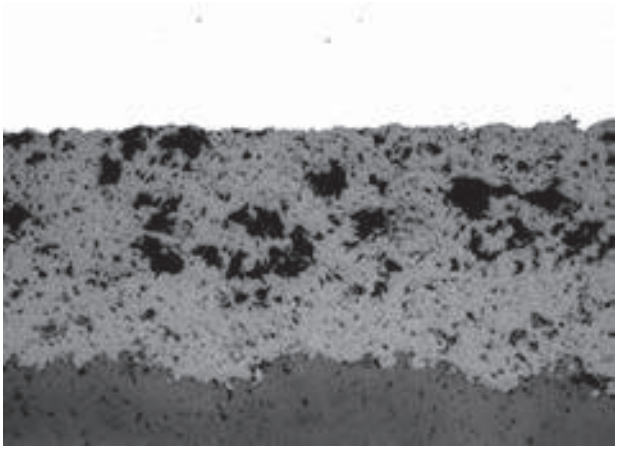

Fig. 1. Incorect amount of porosity due to improper sample preparation of an ZrO_2-Y_2O_3 coating.

For this reason, the mechanical sample preparation must be optimized to ensure the materials are without any artefacts. Current Buehler SumMet™ sample preparation methods are optimized by using latest methodology and combining state of the art equipment and consumables.

2. Sample Preparation Process

Sample preparation usually starts with a cutting process. The best method is to use a IsoMet precision saw with a 15HC IsoMet diamond blade. These blades are very thin and the damage introduced by sectioning is very low while the surface finish is excellent. The use of abrasive blades should be avoided, because the blades are too aggressive and often, the abrasive particles have the same hardness as the spray coating by itself. One important hint is the cutting direction. The most sensitive cuting method is to cut the coating under compression (blade cuts into the coating and coming out of the substrate/ other direction will end in delamination). Porous and brittle materials need to be impregnated prior to cutting **(Fig.2).**

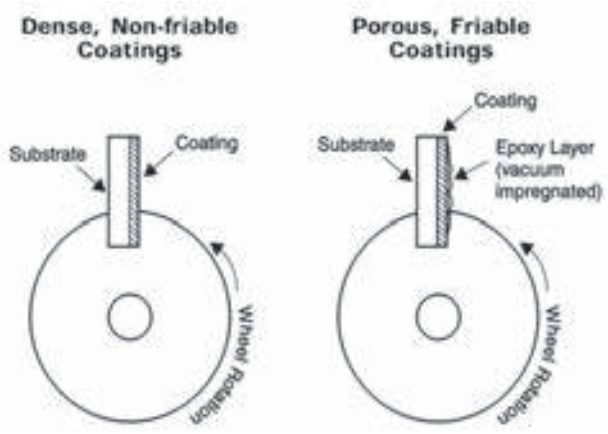

Fig. 2. Optimal cutting direction and protective epoxy layer.

Once the sample is cut, the sample needs to be cleaned in alcohol and dried afterwards. The mounting process should be done by using castable mounting and a low viscosity epoxy mounting compound such as EpoThin. Porous and friable coatings shall be mounted under vacuum. This process will close existing pores and stabilize the coating during the following sample preparation process.

The traditional sample preparation method for TSC and TBC samples are quite complex and not perfect in terms of repeatability and sufficient sample quality. The traditional and most common methods contain the use of SiC-paper starting from P180 and ending with P1200. After this, two or three additional polishing steps on hard polishing cloths were used to get a sufficient sample preparation quality. As mentioned before, the disadvantages are the variations in sample preparation quality and long polishing times.

Contemporary methods are able to produce excellent and repeatable results and finally without preparation artefacts. The main differences between the traditional and the contemporary method are the use of diamond grinding discs and state of the art polishing cloths. Buehler has developed two preparation methods for ceramic **(Table. 1.)** or metallic **(Table. 2.)** type coatings, which eliminate common preparation artefacts.

Table. 1. Contemporary SumMet™ preparation method for ceramic spray coatings.

4-Step Method for Ceramic TSC Coatings					
Surface	Abrasive/Size	Load lb. (N)/Specimen	Base Speed (RPM)	Relative Rotation*	Time (min:s)
Apex Color Red	75-µm Diamond water cooled	5 (22)	300	>>	Until Plane
Apex Hercules S rigid grinding disc	9-µm MetaDi Supreme Diamond*	5 (22)	150	><	4:00
Trident	3-µm MetaDi Supreme Diamond*	6 (27)	150	>>	3:00
ChemoMet	0.02 – 0.06-µm MasterMet colloidal Silica	6 (27)	150	><	2:00
*Plus MetaDi Fluid as desired >> = Complimentary (platen and specimen holder rotate in the same direction) >< = Contra (platen and specimen holder rotate in opposite directions)					

Table. 2. Contemporary SumMet™ preparation method for metallic spray coatings.

Alternate Four-Step Procedure for TSC and TBC Specimens with Metallic Coatings					
Surface	Abrasive/Size	Load lb. (N)/Specimen	Base Speed (RPM)	Relative Rotation*	Time (min:s)
Apex Hercules H rigid grinding disc	30-µm MetaDi Supreme Diamond*	6 (27)	300	>>	Until Plane
UltraPad	9-µm MetaDi Supreme Diamond*	6 (27)	150	><	4:00
TriDent	3-µm MetaDi Supreme Diamond*	6 (27)	150	>>	3:00
ChemoMet	0.02 – 0.06-µm MasterMet colloidal Silica	4 (18)	150	><	2:00
*Plus MetaDi Fluid as desired >> = Complimentary (platen and specimen holder rotate in the same direction) >< = Contra (platen and specimen holder rotate in opposite directions)					

The final examination can be done by using an upright microscope under bright field at 20x – 50x magnification.

The following images showing well prepared samples with the correct amount of porosity of a ceramic type spray coating (ZrO_2-Y_2O_3) **(Fig 3.)** and a metallic type coating (WCCo) **(Fig 4.)**

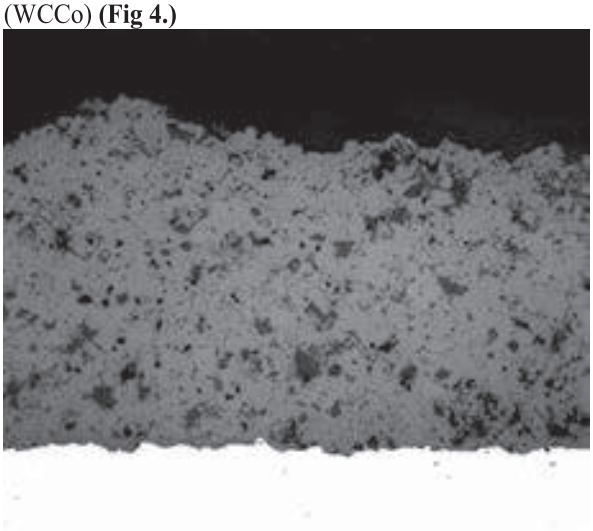

Fig. 3. ZrO_2-Y_2O_3 coating with filled pores (bright grey) and partially unfilled pores (dark grey) at 50x.

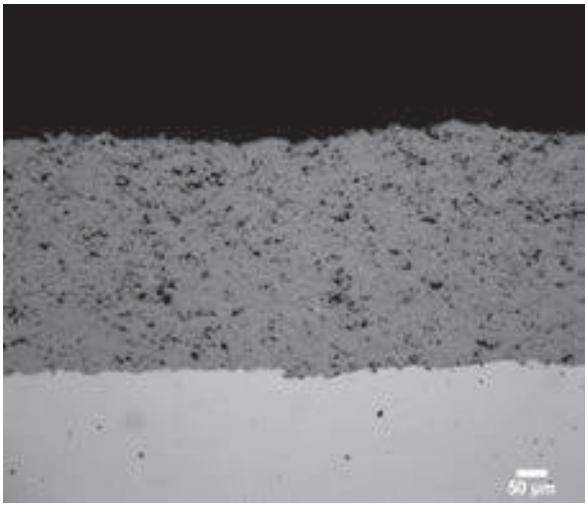

Fig. 4. Dense WCCo coating with open “real” porosity (dark grey) at 50x.

3 Summary

The mechanical sample preparation is very important to ensure a correct microstructure is shown. Improper sample preparation will cause linear cracks and incorrect amount of porosity which mislead in interpretation. Semi automatic sample preparation helps to get repeatable and consistent results compared with manual “hand” preparation on a grinding and polishing maschine. Use the latest developed preparation methods to ensure the given result is the “true” microstructure without any artefacts.

4 References

[1]Leistner, Elisabeth:Structural Atlas for the Preparation and Evaluation of Thermally Sprayed Coats (Fachbuchreihe Schweisstechnik 2001) pp.11-43
[2]Buehler: SumMet – A Guide to Materials Preparation and Analysis (2013).
[3] G. F. Vander Voort, Metallography: Principles and Practice, ASM International, Materials Park, OH, 1999; originally published by McGraw-Hill Book Co., NY (1984).

Quantification of Grit Entrapment in Thermal Sprayed Coatings

Hariharan S[1], Dheepa Srinivasan[1] and George Meng[2]
[1] GE Power and Water, GE India Technology Center, EPIP-II, Whitefield, Bangalore 560066, India
[2] GE Power and Water, 300 Garlington Road, Greenville, South Carolina, 29615-4614, USA

Abstract
Grit blasting is a mandatory step prior to any coating deposition, in particular, for thermal sprayed coatings, which require a mechanical interlocking of the coating on to the substrate. The ensuing surface roughness after grit blasting, is critical for subsequent adhesion of the coating. Many a time, inspite of optimizing the parameters for grit blasting, there is some grit entrapment at the coating substrate interface, which, if exceeds the specified limit, could result in coating spallation. The typical way of measuring the effectiveness of grit entrapment, is via metallography, using destructive metallurgical analysis. This however, may not be representative of the entire span of the coated surface, at all times. More importantly, this destructive inspection occurs after coating and cannot help identify or prevent excessive grit entrapment before the coating the parts. This paper presents a simpler method to quantify the extent of grit entrapment, via looking at planar sections of sample coupons, and thereby giving a true representation of the extent of grit entrapment. This non-destructive inspection method can effectively help to identify excessive grit entrapments and thus allow correction of the grit blasting problem before the grit blasted components get coated.

1 Introduction

Recent studies show that nearly 70% of all coating failures are attributed to improper surface preparation of the substrate [1]. Grit blasting of the substrate (hardware), prior to thermal spraying any coating, is an important and indispensible process step in order to ensure that the necessary surface roughness is created, for enabling good coating adhesion [2,3]. In addition, grit blasting also enables cleaning the surface of contaminants that could hamper good coating adhesion. There is a notable enhancement of the surface area, up to nearly 50% after grit blasting [2,3], and a large number of studies, both academic as well as industrial, have dealt with the practical aspects of 'proper' grit blasting, in order to ensure that there is a uniform surface roughness, on actual components having the required geometry. Typically there is a linear increase in the bond strength with increase in the surface roughness [3], with the preferred roughness for thermal sprayed coatings, being in the range 5-10 µm R_a. Grit blasting is usually done using relatively hard, friable. Al_2O_3 particles, and includes a number of variables, such as the pressure, particle size, shape, nozzle angle, stand off distance, etc. In order to get the correct roughness on the substrate to be coated [4]. In many a case, if any one or a combination of the variables is altered, this could result in excessive grit entrapment, which despite giving the desired surface roughness, may end up in coating delamination. Typical methods of assessing the grit entrapment, is to perform a destructive metallurgical analysis, after the coating has been sprayed, and assessing the number of grits entrapped at the coating-substrate interface in a qualitative manner based on visual examination (Fig. 1a), in a random linear cross section (Fig. 1b). This method however, cannot prevent the contaminated parts from being coated and may end up rejecting parts owing to excessive contamination, since the section selected is not representative of the area of the sample. This study presents a simpler way of analysing the overall extent of grit entrapment, in a larger cross section, in order to qualtify the extent of grit entrapment more precisely.

2. Experimental Details

4 samples were analysed in the as grit blasted condition, using, a. the destructive analysis of one section (Nikon Eclipse MA200, with a clemex image analysis, and b. using a digital microscope (Keyance, VHX 1000) and a Scanning electron microscope (SEM, Carl Zeiss, EVO18, Oxford Link), in the planar section, without cutting. Table 1 lists the DOE of samples that was analysed, using two different grits (white and borwn alumina, of different sizes, #20 and #90), and spray angles (45° and 60°). The coupons were marked into 4 quadrants, and the presence of grits were identified first using the SEM/EDAX, and thereafter analysed in the Optical microscope. Surface roughness measurements were made using a simple hand held roughness gauge, Mitutoyo SJ 210.

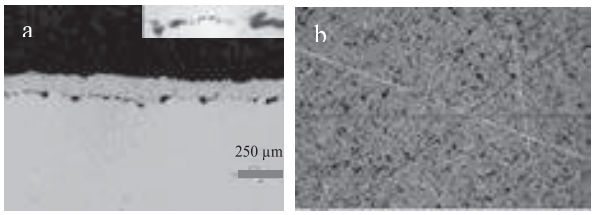

Fig. 1 : a. *Optical micrograph at 200X (insert at 400X), revealing an unacceptable extent of grit entrapment, (b) reference location in the planar section for the cross section in Fig.1a.(arrowed)*

Table 1 : List of Grit blasted samples used in this study

Sample No..	Mesh type	Spray Angle (Deg)	Pressure (MPa)
1	White Alumina # 20	45	280
2		90	280
3	Brown Alumina # 90	45	280
4		90	280

3 Results

Figs. 2a and 3b show representative SEM images, from Sample 1, identifying the embedded grit. This location is carefully marked and analysed via the optical digital microscope and the % of grit entrapment, quantified using image analysis, as shown in Fig. 3 (a-c). In this manner, different frames, at 50X, can be easily quantified, as to the

extent of grit entrapped. A sample coupon, 1“ (2.54 cm) diameter, is analysed, by diving it into four quandrants and measuring the extent of grit entrapped via representative optical images, as shown in Fig. 4 (a-e). The average grit content, is calculated by taking 4 frames from each quadrant. The grit size as well as as the % grits in each quadrant is measured as shown in Fig. 5, for Sample 1. This is compared with the conventional method of assessing the grit entrapment, via metallurgical samples, taken for representative frames showing the maximum entrapped grit, from the 4 samples, as shown in Fig. 6(a-d). Table 2 summarizes the measured % grit entrapment.

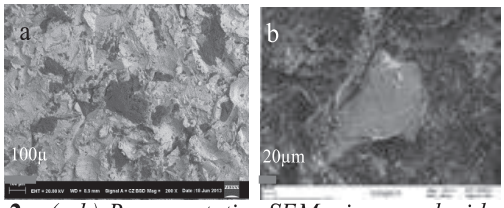

Fig. 2 : *(a-b) Representative SEM micrographs identifying the grit (Sample 1)*

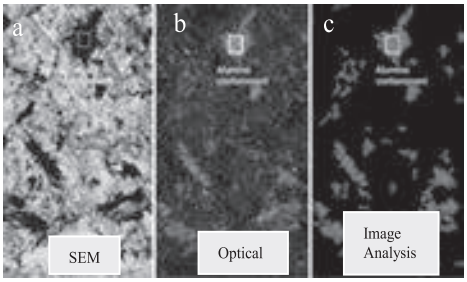

Fig. 3 : *Al_2O_3 contaminant identified via the, (a) SEM, (b) digital microscope,and quantified via (c) image analysis*

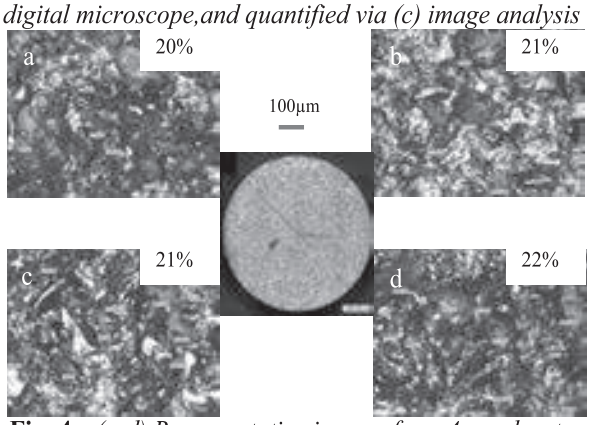

Fig. 4 : *(a-d) Representative images from 4 quadrants of a 2.54 cm diameter coupon, quantified using digital imaging for grit entrapment, Sample 1 (legends indicate the extent of grit present in each quadrant)*

4. Discussion and Conclusion

This analysis illustrates a quantifiction of the grit entrapment, via a non-destructive method of analysis. The existing method involving sample cut ups is fraught with uncertainty in terms of few random locations in the sampling set. In addition, it is not quantitative to indicate a maximum allowable limit for grit entrapment. In the present analysis, a systematic identification of the grits entrapped in the surface of the coupon is illustrated, via image analysis.. A surface area of 500 mm^2 is covered, via direct imaging of the grits, using an optical microscope. The SEM was used as a means to confirm the grits without any ambiguity. Not only a near exact quantification of the grit entrapment was made possible, but also distinctions between white and brown alumina and mesh size, was brought out. The surface roughness was half the value using brown alumina (#90) as compared to white alumina (#20). There was nearly double the entrapment while spraying at 90 degrees as compared to 45 degrees, using both while and brown alumina. This when compared to the conventional means of assessing grit entrapment using metallurgical cut ups, showed that there was no correlation whatsoever, with the image anlaysis showing a large uncertainty in the quantification of the entrapped grits (ranging between 10-50%), within the sampling set. This imples that during any new component coating or during qualifications, it is better and recommendable to make use of this simpler, more quantitative and accurate non-destructive technique to assess the extent of grit entrapment prior to thermal spray coating.

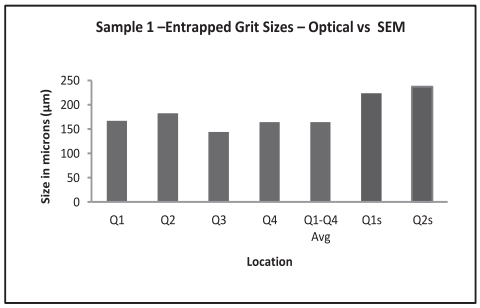

Fig. 5 : (a) *Comparison of average grit sizes, and (b) % grits in the 4 quadrants*

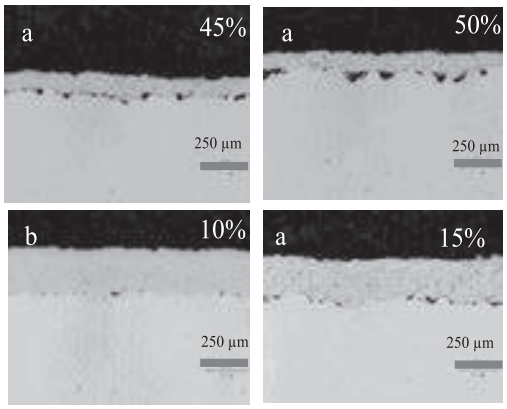

Fig. 6 : *(a-b) Optical micrographs (50X) with a representavie location from all the 4 samples, indicating the % grit entrapment*

Table 2 : % Grit entrapment in various samples

Mesh Type	Spray Angle	Roughness (µm R_a)	Grit Entrapped (%) Actual	Metallography
White Alumina # 20	45	6.44	5	45%
	90	7.87	20	50%
Brown Alumina # 90	45	4.28	10	10%
	90	3.85	24	15%

5. Acknowledgements

The grit blasted coupons were provided by two service centers, GEMTEC, Saudi Arabia and BGGTS. RDC managers, Dr. Sundar Amancherla and Mr. Christopher Thompson are acknowledged.

6. References

[1] Lydia Frenzel, Proc. Of the WJTA conference, 1999. Sept 2014.
[2] A.F. Harris and A. Beevers, Int. J. Adhesion and Adhesives, **19** (1999) 445-452.
[3] M.F. Bahbon, P. Nylen and J. Wigren, J. Therm. Spray Tech., **13** (2005) 508-514.
[4] J. Day, X. Huang and .L. Rishards, J. Therm. Spray Tech., **14** (2005) 471-478.

Oxidation and Protection of Graphite

Ariharan S,Pradyut Sengupta,Ankur Agnihotri,N. Balaji,S.T. Aruna,Kantesh Balani

Indian Institute of Technology Kanpur, India,Indian Institute of Technology Kanpur, India,Chhatrapati Shahu Ji Maharaj University, Kanpur, India,National Aerospace Laboratory, Bangalore, India,National Aerospace Laboratory, Bangalore, India,Indian Institute of Technology Kanpur, India

Graphite is an attractive material for high temperature (> 600Â°C) applications due to its high elastic modulus (10-15 GPa), thermal shock resistance and light weight (1.3-1.9 g/cc). But graphite is prone to oxidize and form CO and CO2 at elevated temperature (600-1000Â°C) under oxidizing atmosphere. Since it is difficult to ascertain reducing atmosphere in practical application, oxidation protective coating deposited over graphite substrate. In the current work, graphite was coated by SiC/ZrB2/Al2O3/CNT composites using atmospheric plasma spraying. The retention of CNT was confirmed by Raman spectroscopy analysis, which elicited increase in fracture toughness of SiC+20wt.% ZrB2+4wt.% CNT by up to 11% (from ~4.50 to ~4.95 MPa.m1/2). In order to characterize and analyse properties of composite materials, we made free standing dense (theoretical density of ~98%) free-standing pellets of SiC/ZrB2/CNT and Al2O3/CNT composite using spark plasma sintering (SPS). The oxidation studies (using thermo-gravimetric analysis) revealed weight gain, up to 17.4% at 1000Â°C for SiC+20wt.% ZrB2 due to formation of SiO2 in oxygen atmosphere, which was also confirmed via x-ray diffraction and transmission electron microscopy. Tribological studies have revealed and CNT addition in pellet reduced co-efficient of friction value from 0.18 to 0.11, using ball (Al2O3) on disc method.

Evaluation of Air Plasma Sprayed Alumina Coatings for DC Conduction Pump

R. Krishnan

Thin Films and Coatings Section, Surface and Nanoscience Division,
Materials Science Group, Indira Gandhi Centre for Atomic Research,
Kalpakkam – 603102, India

Electro Magnetic DC conduction sodium pump is for use in Failed Fuel Location Module. The pump works on the principle that when a current carrying conductor is placed in magnetic field it experiences a force. The DC Conduction Pump, even though less efficient than the other electromagnetic pumps, was chosen, because of its low voltage operation. The pump will be immersed in liquid sodium and will experience temperatures up to 550°C. The pump is fed from a low voltage high current DC source (2V, 2500 Amps). In order to provide electrical insulation between copper and sodium duct and iron pole pieces, a coating of alumina (Al_2O_3) is to be done on copper and iron. A 300 µm thick alumina ceramic coating was applied over OFHC copper and on soft iron Air Plasms Sprayed technique. This work deals with the analysis of these samples with regard to various parameters and the suitability of the coating for the present application. Apart from solid state characterization tools such as XRD, SEM, and SEM other analytical evaluation tests were carried out to measure the hardness, adhesion and thermal cycle fatigue and the results are presented. The objective of this study is to evaluate a commercially developed alumina coating on both soft iron and copper substrates to examine the suitability or otherwise in meeting the requirements of the targeted application.

Email: krish@igcar.gov.in

Plasma Sprayed Alumina Coating on Inconel 600 for Neutron Detector Application

A. Ravi Shankar[1], K. Thyagarajan[1], Chandra Kant Upadhyay[2], C. Mallika[1] and U. Kamachi Mudali[1]
[1] Corrosion Science and Technology Group, Indira Gandhi Centre for Atomic Research, Kalpakkam – 603102, India
[2] Reactor Design Group, Indira Gandhi Centre for Atomic Research, Kalpakkam – 603102, India

Abstract
High temperature fission chamber neutron detectors, made of Inconel 600 and operating at 923 K, need to be coated with high resistivity alumina ceramic which operates at a temperature of 923 K and should withstand 100 controlled thermal cycles. The insulation resistance should be $>10^{13}$ Ω at room temperature and $>10^{8}$ Ω at 923 K. In the present study Ni-50%Cr has been deposited as the bond coat by HVOF technique to achieve dense and adherent coating while the top alumina ceramic coat was deposited using plasma spray process. SEM examination indicated typical splat type of morphology with minimum porosity. XRD pattern revealed γ and α Al_2O_3 phases in the coating. Thermal cycling studies carried out at 923 K on coated samples and rings showed no weight loss and delamination of the coating after 100 cycles. The coating exhibited remarkable adhesion strength and a stable insulation resistance of ~10^{11} Ω at room temperature and ~10^{8} Ω at 923 K. The paper highlights the results of the present investigation.

1 Introduction

High purity alumina insulators in the form of discs, rings and tubes are used in gas-filled neutron and gamma detector applications [1]. Ceramic insulated discs/spacers used in nuclear reactors are prone to failure during seismic vibration and shock. Therefore, feasibility of using metallic parts coated with high-purity alumina by plasma spraying was explored and was found to be beneficial [1]. There is a need for using such ceramic insulated neutron detectors in the prototype fast breeder reactor (PFBR), under construction in Kalpakkam. High temperature fission chamber (HTFC) neutron detectors, whose outer shell/ring, made of Inconel 600 requires to be coated with insulating ceramic material. As per the specifications, the ceramic coated Inconel ring should withstand 100 controlled thermal cycles at a maximum temperature of 923 K in argon atmosphere. The desired value of insulation resistance is $>10^{13}$ Ω at room temperature and $>10^{8}$ Ω at 923 K. The ceramic insulators used in gas-filled neutron detectors also should exhibit very low leak rate. High pure alumina is one of the ceramic materials possessing high electrical resistivity. Plasma sprayed alumina coating, deposited initially on Inconel 600 rings with and without NiCrAlY bond coat failed during thermal cycling. The poor thermal cycle life of the coating was attributed to oxidation at the interface of sprayed coating and metallic substrate. Irisawa and Matsumoto [2] reported that Ni-50%Cr alloy and nickel-based self-fluxing alloy bond coats significantly improved the thermal shock resistance of alumina, coated on flake graphite iron specimens. On the other hand, bond coats deposited by high velocity oxygen fuel (HVOF) thermal spray coating technique produce dense coatings without much oxidation. Thus, deposition of oxidation resistant bond coat and coating technique are crucial to achieve maximum thermal cycling life and adhesion strength. The present study aims at improving the thermal cycling resistance combined with adhesion strength of alumina coatings.

2 Experimental Details

Inconel 600 samples of size 20 × 20 × 6 mm, and collars/ring components of neutron detectors were coated with Ni-50%Cr bond coat of 50 μm thickness by HVOF technique. Top alumina coating of 250 μm thickness was deposited by atmospheric plasma spray process in collaboration with M/s. Metallizing Equipment Co Pvt Ltd at Jodhpur. Surface morphology and cross section microstructures of the coated samples were examined using scanning electron microscope (SNE-3000M model, SEC, Korea) attached with EDS. For phase identification, X-ray diffraction (XRD) patterns were recorded using STOE diffractometer with Cu $K\alpha_1$ radiation in the range $10^{o}<2\theta<90^{o}$. Adhesion testing was done at M/s. Metallizing Equipment Co Pvt Ltd, Jodhpur on the as-sprayed sample and also after thermal cycling as per ASTM C 633–01 standard. Thermal cycling tests were conducted in air on two sets of coated samples and collars/rings at 923 K, holding for 60 min, followed by cooling to 473 K in 90 min, and again heating to 923 K in 30 min. The thermal cycle schedule as per the required specification and that was followed in the present study, along with the schedule reported by Irisawa and Matsumoto [2] is shown in **Fig. 1**. Weight loss of the samples was measured after every 10 cycles and visual examination was made to determine coating delamination. Insulating resistance at room temperature and at 923 K was measured on two sets of coated samples (after 100 thermal cycles) with high resistance meter (Agilent technologies) at 600 V.

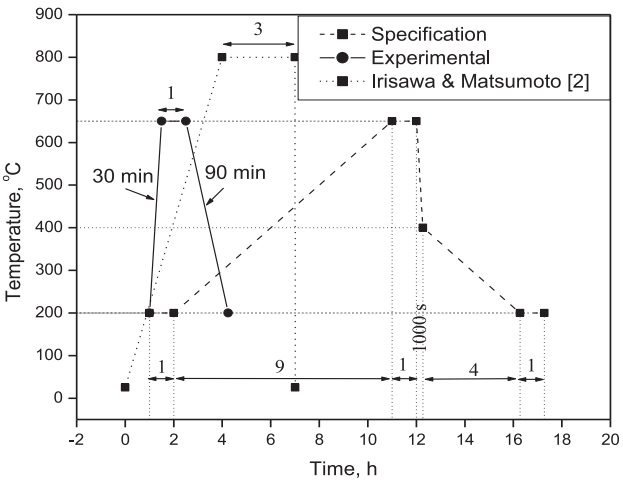

Fig. 1. *Thermal cycling schedule*

3 Results and Discussion

Plasma spraying is a well established coating technique for producing thick thermal barrier coatings. The surface morphology and cross section micrograph of plasma sprayed alumina coating over Inconel 600 with Ni-50%Cr bond coat are shown in **Figs. 2a&b** respectively. The micrograph exhibited relatively dense surface morphology with complete splat type of melting and solidification without any micro-cracks. The cross section micrograph also shows that the coating was relatively dense. XRD analysis revealed well-crystallized phases of γ-Al_2O_3 and α-Al_2O_3. Plasma sprayed alumina coatings usually contain metastable γ-Al_2O_3 and stable α-Al_2O_3 depending on the particle size and cooling rates achieved [3]. Oxidation of bond coat is one of the reasons for failure of coating and in order to minimize the oxidation of bond coat and to increase the adhesion strength of the coating, HVOF coating was used for bond coat which resulted in dense bond coat without oxidation. Alex et al. [1] evaluated the coating characteristics of plasma sprayed alumina coatings on copper, aluminium and stainless steel components for neutron and gamma detector applications. However, the adhesion strength and thermal cycling studies were not reported. The photograph of plasma sprayed alumina coated Inconel 600 rings after 25, 50 and 100 thermal cycles is shown in **Fig. 3**. No spallation or delamination of the coating from the substrates was observed. Similarly, plasma spray coated Inconel 600 samples performed well without any spallation. Weight change was not observed on coated samples and rings after thermal cycling.

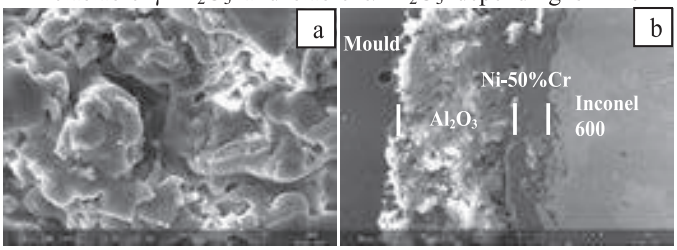

Fig. 2. *(a) Surface, and (b) cross section SEM micrographs of as- sprayed alumina coating on Inconel 600*

An improvement in the adhesion strength of plasma sprayed alumina coating over Inconel 600 was observed, compared to plasma sprayed alumina coating over flake graphite cast iron reported by Irisawa and Matsumoto [2] in the as-sprayed condition. The improved performance of the coating (as-sprayed: 38 MPa and after thermal cycling: 30 MPa) could be attributed to the presence of bond coat (Ni-50%Cr) deposited by HVOF technique with optimized parameters. The insulation resistance at room temperature was found to be ~10^{11} Ω while at 923 K it was ~10^{8} Ω. The insulation resistance at 923 K satisfied the acceptance criterion. However, the insulation resistance at room temperature was found to be lower than the specified value. Both temperature and humidity influence the insulation resistance of solid dielectric materials. Alex et al. [1] observed that moisture present on the coating from ambient atmosphere resulted in low electrical insulation and an improvement was achieved by using moisture-repellent coating on the ceramic surface which mitigates the effect of porosity [1]. Therefore, the low insulation resistance observed at room temperature can be improved by achieving dense ceramic coated surface and by using moisture-repellent coating. Earlier studies by Alex et al. [1] on plasma sprayed alumina coating on tube and rod samples irradiated for 40 h in Apsara reactor indicated no deterioration in the adhesion of the coating. Apart from insulation resistance, the plasma sprayed alumina coating on Inconel 600 exhibited good thermal cycle life and remarkable adhesion strength in the present study. Hence, plasma sprayed alumina coatings over Inconel 600 can be used for critical components like neutron detectors exposed to high temperature in fast breeder reactors. However, further thermal cycling tests as per specification and improvement in the coating are essential for achieving reproducible and reliable coatings.

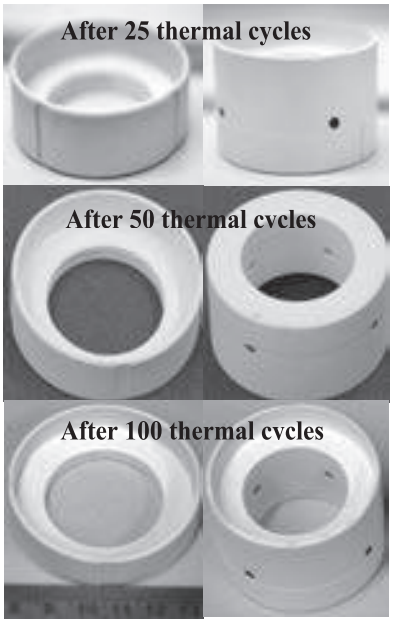

Fig. 3. *Photograph of as- sprayed alumina coated Inconel 600 collars/rings.*

4 Conclusions

Inconel 600 samples and rings for high temperature fission chamber neutron detector applications were coated with Ni-50%Cr bond coat by HVOF technique and top alumina coat by air plasma spray process. The results showed relatively dense surface with typical splat type of morphology and well-crystallized phases of γ-Al_2O_3 and α-Al_2O_3. Thermal cycling tests carried out at 923 K for 100 cycles in air on coated samples and rings revealed that the coating performed well without spallation or delamination. The adhesion test results showed remarkable improvement in adhesion strength while the insulation resistance at room temperature (600 V) was found to be ~10^{11} Ω and at 923 K it was ~10^{8} Ω.

5 Acknowledgements

The authors acknowledge the support provided by Shri Rohit Upadhyaya of M/s. Metallising Equipment Ltd, Jodhpur for coating and adhesion testing.

6 References

[1] M. Alex, V. Balagi, K.R. Prasad, K.P. Sreekumar and P.V. Ananthapadmanabhan: PRAMANA — J. Phys. **55** (2000) 927–932.

[2] T. Irisawa and H. Matsumoto: Thin Solid Films. **509** (2006) 141–144.

[3] McPherson: J. Mater. Sci. **8** (1973) 851-858.

Development of Tungsten Coating using Atmospheric Plasma Spraying for First Wall Applications in Fusion TOKAMAK

Shailesh Kanpara[1], G. Sivakumar[2], Kedar Bhope[1], S.S. Khirwadkar[1], S.V.Joshi[2]
[1] Divertor & First wall Technology Development Division, Institute for Plasma Research, Gandhinagar 382428, India
[2] International Advanced Research Center for Powder Metallurgy and New Materials, Hyderabad 500005, India

Abstract
Tungsten is one of the most promising candidate armour materials for plasma facing components (PFC) in the future fusion reactors. For the near term application, a possible convenient solution for W based PFC, especially for the first wall application is the coating of the heat sink or structural materials with the tungsten coating. Present work is focused on formation of tungsten coating on stainless steel substrate of grade SS304 using Atmospheric Plasma Spraying technique. Preliminary efforts in depositing tungsten coating revealed the possibility of achieving uniform thickness of about 60 microns. Further efforts will be focused on building further thickness and characterized for microstructural characteristics in terms of porosity and oxide presence. Ultrasonic Testing by immersion as well as contact method has been carried out to identify the defect within the tungsten like metallic coating using 2mm Flat Bottom Hole (artificial defect) also checked the bond quality of the coatings. In terms of performance studies, thermal load testing through a custom-made High Heat Flux (HFF) test facility and hydrogen permeation studies will be carried out to satisfy the technical specifications required for ITER-like First wall applications. The efforts carried out to optimize the process parameters for tungsten coatings will also be discussed in the paper.

1 Introduction

Tungsten (W) is promising plasma-facing armor material in the future fusion devices. The advantage of W is the high melting point, low tritium inventory and low erosion rate under plasma loading [1,2]. The main drawbacks of W are the high ductile to brittle transition temperature (DBTT, approximately 400 °C) and difficulties in machining. A possible solution for the utilization of tungsten at plasma-facing surfaces is the coating of the heat sink or structural material with a thin tungsten layer. As coating technologies,
vacuum plasma spray (VPS) [3], physical vapor deposition (PVD) [4,5] and chemical vapor deposition (CVD) [6], have been proposed and tested under high heat flux loading. As substrate materials for Wcoating, the following materials have been applied: copper or copper alloys foreseen in concern of water cooled system, graphite and/or CFC for inertially cooled system and reduced activation ferritic steel [7].
In the present paper, stainless steel of grades SS304 & SS316LN are selected to develope the tungsten coating techonlogy which can be used in IN-RAFM (India Specific Reduced Activation Ferritic Martensitic) steel for First Wall application in Fusion TOKAMAK.

2 Experimental Procedure

Tungsten powders with an average particle size of 6-20µm were used as starting materials as shown in Fig. 1. The purities of both materials are higher than 99.5%. Two substrate materials, SS304 steel with dimension of 30mm x 30mm x 5mm and SS316LN of Size 71mmx 10mm x 10mm used in the experiments. High purity argon gas was used for cooling the substrate and preventing the coatings from oxidation.
Stainless steel substrate was grit-blasted and ultrasonically cleaned in order to enhance the adhesion between the coating and the substrate. Tungsten coating was deposited via a 9MB-SULZER METCO Atmospheric Plasma Spray (APS) system at ARCI, Hyderabad. Argon acted as both the primary and carrier gas, while hydrogenwas used as secondary gas. The coating was deposited onto SS304 steel and SS316LN substrate under the conditions listed in Table 1.
The microstructure of the coatings was characterized by scanning electron microscopy (SEM). The ultrasonic testing of samples was done using OMNISCAN MX-OLYMPUS model by ultrasonic pulse-echo technique

Table. 1
Atmospheric plasma spraying parameters.

Parameters	APS-W
Plasma Power (kW)	35
Current (A)	500
Primary gas, Ar (l/min)	45
Secondary gas, H2 (l/min)	3.5
Spray distance (mm)	150
Powder feed rate (g/min)	40

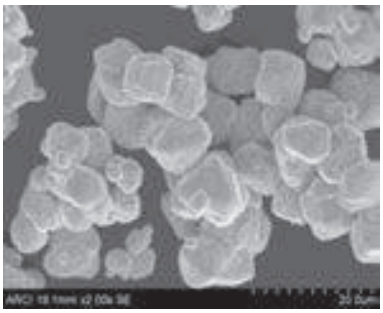

Fig. 1. *SEM image of Tungsten Powder morphology*

3 Results and discussion

3.1 Microstructure, Surface Roughness & Tungsten Oxidation

SEM image was taken of the interface between the coating and the substrate after coating. Fig. 2 show the cross-sections of the coatings having more than 200 micron coating thickness. As seen from SEM image, uniform coating layer obseved with well-melted particles. Surface

roughness of the tungsten coatings was measured by surface roughness tester of of model SJ-210.

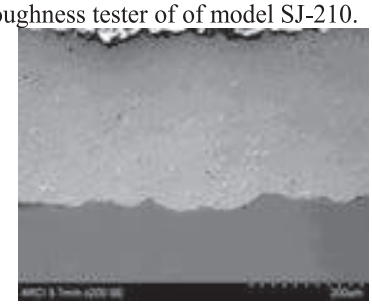

Fig. 2. *SEM image of Tungsten Coating on SS304 substrate*

Average roughness (Ra) measured is Ra=4.83. The oxygen content in the coatings, measured by EDS, was found to be 0.17%. Priliminary experiments gives significant control in the oxdiation % within the coatings using localised gas shrouding.

3.2 Ultrasonic Testing

Ultrasonic Testing of the W coating & SS304 substrate interface done by water- immersion technique as well as contact technique using Omniscan MX (UFD).For immersion testing, focused transducer with the center frequency of 20 MHz crystal diameters 6.35mm and the focus lengths 50 mm in water were used while for contact method, transducer with the center frequency of 10 MHz and crystal diameters 6.35mm were used. A 2mm flat bottom hole (FBH) were drilled to remove W coating from Substrate surface and perfect uncoat condition was created. Ultrasonic C-scan image is shown in Fig 3.In order to validate the technique; contact method has been employed to check the maximum amplitude response from uncoated region.

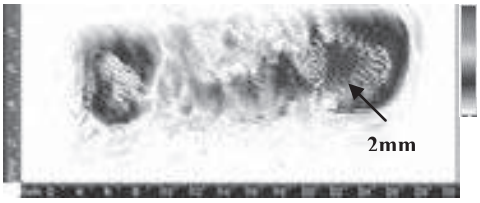

Fig. 3. *Ultrasonic C-Scan image with 2mm FBH*

Ultrasonic testing of W coating on SS316LN sample has been carried using OMNISCAN MX-OLYMPUS model by ultrasonic pulse-echo technique. For the ultrasonic testing, 20MHz probe (3.16mm-dia, F12.5mm) has been used with gain value of 72.00db with 0.1mm C-Scan index resolution. Ultrasonic C-scan image was obtained from side A to B on sample. Back wall response from uncoated side of sample has been used as defect reference condition for testing and it is kept 80% of Full Screen Height. Ultrasonic C-scan image represented in **Fig. 4** which shows the good bonding of the coatings on substrate material.

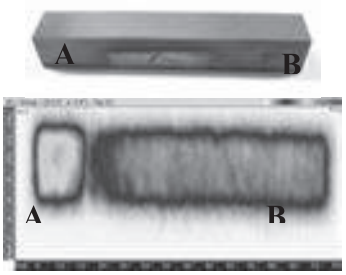

Fig. 4. *Image of W coating on SS316LN sample and Ultrasonic C-Scan of the sample*

3.3 High Heat Flux (HHF) testing and Thermal Cyclic Testing

After development of Tungsten Coating technology using Atmospheric Plasma Spray, following tests will be done to qualify the Tungsten coating to use for actual application.

(1) Tungsten coated (up to 500 micron) test mock-up of size 50mm (l) x 30mm (b) and substrate thickness = 30mm (with 12mm ID Hole for water channel) will be used for HHF testing up to 1 MW/m^2 heat load for 1000 thermal cycles using High Heat Flux Test Facility (HHFT) at IPR, Gandhinagar. **(2)** Thermal Cyclic testing of the tungsten coated samples up to 500 °C for 1000 cycles using HHFT and GLEEBLE 3800 system at IPR to see whether any delamination occurs or not **(3)** Permeation tests for Hydrogen and its isotopes with the help of DC-glow Discharge plasma loading for IN-RAFM (India Specific Reduced Activation Ferritic Martensitic Steel) substrate.

4 Summary

Preliminary efforts in depositing tungsten coating on two SS substartes revealed the possibility of achieving uniform tungsten coating thickness grater than 200 microns. Future efforts will be focused on building further thickness, the effect of interlayers and the effect of powder partical size & sape. Ultrasonic Testing methods has been established by immersion as well as contact method to identify the defect within the tungsten like metallic coating using 2mm Flat Bottom Hole (artificial defect) and also to check the bond quality of the coatings. Performance of the Tungsten coating for actual applications will be done in future experiments like High Heat Flux (HHF) testing, Themal Cyclic and hydrogen permeation studies will be carried out to satisfy the technical specifications required for ITER-like First wall applications.

5 References

[1] G. Federici, C.H. Skinner, J.N. Brooks, J.P. Coad, C. Grisolia, A.A. Haasz, et al., Nucl. Fusion 41 (2001) 1967.
[2] I. Smid, M. Akiba, G. Vieider, L. Ploechl, Journal of Nuclear Materials 258–263 (1998) 1602.
[3] S. Deschka, C. Garcia-Rosales, W. Hohenauer, R. Duwe, E. Gauthier, J. Linke, M. Lochter, W. Mallener, L. Plochl, P. Rodhammer, A. Salito, J. Nucl. Mater. 233–237 (1996) 645.
[4] H. Maier, J. Nucl. Mater. 335 (2004) 515.
[5] H. Maier et al., J. Nucl. Mater. 363–365 (2007) 1246.
[6] T. Hirai et al., Fus. Eng. Design 81 (2006) 175.
[7] H. Greuner, H. Bolt, B. Boeswirth, S. Lindig, W. Kuehnlein, T. Huber, K. Sato, S. Suzuki, Fus. Eng. Design 75–79 (2005) 333.
[8] Hyun.-Ki Kang, J. Nucl. Mater. 335 (2004) 1–4.
[9] Y. Zhao et. al. Measurements of coating density using ultrasonic reflection coefficient phase spectrum. Ultrasonics, 51 (2011) 596–601.
[10] T. KUBOHORI et al. Evaluation of thermal sprayed coating using ultrasonic inspection by means of bottom echo back reflection, Trans. Nonferrous Met. Soc. china 19(2009) 984-98.

Application of Thermal Spray Coating in Fusion Reactor Components

Samiran Mukherjee[1], Ranjana Gangradey[1], Jyoti Agarwal[1], Paresh Panchal[1], Pratik Nayak[1]
[1] Institute for Plasma Research, Bhat, Gandhinagar, Gujatrat 382428, India

Abstract
Thermal spray coatings are widely used in many industries and especially in aeronautical industry, automobile industry and space research. Since few decades this technology has found a broad area of application in the field of fusion research and cryo-vacuum industries. Recent research has already pointed out the potential of Al_2O_3/TiO_2 thermally sprayed coatings for diverse applications on components of fusion reactors such as cryo-adsorption Cryopump. In particular, plasma sprayed Al_2O_3/TiO_2 coating shows very high thermal emissivity (>0.95) which leads to the application of thermal radiation shielding in many cryogenic systems. Institute for Plasma Research, India, is pursuing a project on development of indigenous cryoadsorption cryopump for pumping a fusion reactor. In this regard found application of thermal spray coating in Ultra High Vacuum (UHV) because of its high emissivity, cryogenic compatibility and very low outgassing rates. An experimental system is developed to find the outgassing rate of Al_2O_3/TiO_2 thermally sprayed coatings and found to be acceptable in UHV application as the outgassing rate is ~ $1x10^{-9}$ mbar-ltr/s-cm^2 with cryogenic compatibility and are tested down to 4.2K..

1 Introduction

To meet the future energy demands high end research is ongoing to achieve the nuclear power through nuclear fusion. It is expected to develop various fusion technologies before realizing a commercial fusion reactor. The Crucial technologies needed are: devlopment of reactor grade materials, blanket technology, fuel system, plasma facing components for high heat flux, cryopumping system and superconduting magnets etc [1]. Therfore worldwide research is ongoing for the development of reactor grade materials, nobel coatings for the first wall, material compatible to tritium and other readiation, high heatflux materials.

Thermal spray coatings are widely used in many industries and especially in aeronautical industry, automobile industry and space research. Since few decades this technology hasbeen adopted for the development of coating compatible to the application of nuclear fusion technologies and hence found a broad area of application in the field of fusion research as well as cryo-vacuum industries.

Plasma spraying or plasma spray deposition is a process that combines particle melting, quenching and consolidation in a single operation with effective handling of process parameters [2,3]. Composites of alumina and titania are known for their high toughness, low thermal expansion, and low thermal conductivity. These properties make alumina-titania composites desirable materials of construction and coatings for high performance applications where thermal barriers are required. In particular, plasma sprayed Al_2O_3/TiO_2 coating shows very high thermal emissivity (> 0.95) which leads to the application of thermal radiation shielding in many cryogenic systems. In view of the above, the mentioned coating is used as a high emissivity coating for the radiation shield of cryopump components cooled down to 4.2K which is under development at Institute for Plasma Research India [4]. As the operating conditions of the cryopump is Ultra High Vacuum (UHV) hence the necessary outgassing rate of the coating was required to know. Outgassing is the evaluation of gas leaving per unit surface area per unit time at a specified temperature after the start of evacuation. Thus Outgassing gas load limits the lowest achievable pressure in a vacuum chamber and extends the time for high and ultrahigh vacuum to be reached [5].

Experiments were performed in two different experimental systems. For the measurement of outgassing rate experiments were performed in outgassing measuremnt facility and for the cryogenic compatibility experiments were performed on a test facility for cryogenic surface study at low trempereature.

2 Measurement of Outgassing rate

In Vacuum Science improper selection of material can test the nerves when it comes to operation in ultra high vacuum range. The relation Q (Gas Load) = S (Pumping Speed) x P (Pressure), shows that a lower Q will result in a lower P with any given S indicating the role of outgassing of material. As already described, outgassing rate defines the pumping speed at ultimate pressure requirement of the system. For a given material it depends on surface treatments like chemical treatment, prebaking, electro polishing, grinding, horning etc and also manufacturing processes including welding, brazing, polishing, alloying etc. Although literature reports outgassing rates of some standard materials but at times it is not available for specific material and at specific measurement conditions.

The basic parameter measured in the system is gas load. The gas load is determined by measuring the pressure different across a known conductance [6]. The system measures the flow of the gas evolving from the sample material due to Thermal Out-gassing and the specific Thermal Out-gassing rate Qth, is given by Qth = C ΔP/A, Where, C = Known conductance (l/s), ΔP = Pressure difference across the conductance (mbar) and A = Area of the desorbing surface – measureable physical area of the sample (cm^2)

2.1 Design of the system

The system comprises of two ultra high vacuum chambers (Pumping chamber and Sample chamber) separated by a known conductance as shown in fig.1. The gasload produced from the sample will pass through the know conductance and thus creates a differencial pressure. By measureing the differential pressure one can estimate the total gas load produced from the sample chamber with sample. Subtracting the gas load for the blank sample

chamber on can easily find out the gas loas due to the sample and hence the outgassing rate of the sample.

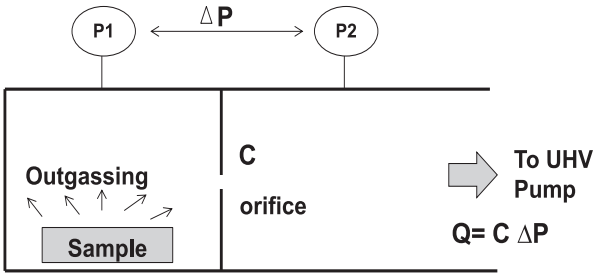

Fig. 1 *Basic Schematic of the outgassing measurement system*

2.2 Sample Details:

Substrate: SS304L plate
Dimention: 100mmx 50mm x 1.5mm thickness
Composition: 87% Al_2O_3 + 13% TiO_2
Sample shape: Rectangle in shape
Sample Area = 104.5 cm^2
Weight (sheet + coating) = 78.368 gm
Weight of coating (87% Al_2O_3 + 13% TiO_2) = 4.34 gm

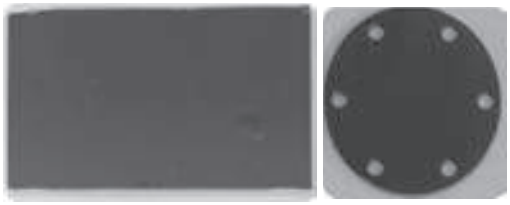

Fig. 2. *Sample used for the measurement of a) outgassing rate and b) for the cryogenic compatibility*

2.3 Experimental results

a) Total surface area of the UHV chamber: ~7600 cm^2
b) Aperture Area & Conductance (C): 0.21 cm^2, 2.46 l s^{-1}
c) Pressure in the measurement chamber: 3.7E-9 mbar
d) Outgassing rate of the blank system: 3.71E-12 mbar l/s-cm^2
e) Measured outgassing rate of Al_2O_3/TiO_2 thermally sprayed coatings
   i. at room temperature: 2.55E-8 mbar l/s-cm^2
   ii. at room temperature after 24hr baking at 150 degC: 1.32E-09 mbar l/s-cm2
f) Partial pressure: For H2: 3.38E-09 mbar
   For H2O: 4.83E-10 mbar
   For N2: 8.03E-10 mbar
   For CO2: 4.58E-10 mbar

3 Cryogenic compatibility experiments

For the cryogenic compatibility test the sample as shown in the fig.2.b was mounted on a GM cryocooler coldhead for the cooldown and thermal crack test. The ultimate achievable temperture of the cryocooler is less than 4K. Experiments were performed in the folowing manner

- SEM images and optical microscope images were taken, weight of the sample is measured before the experiment
- Sample is mounted on the 2nd stage of the GM cycle cryo cooler with the sensors
- Sample is cooled down up to 4 kelvin (K)and then is warmed up to 20 K then again it cooled down up to 4 K, the temperature cycle (4K-20K-4K) is given to the sample three times.
- After the experiment SEM and optical microscope images are taken.
- Weight of the sample is also measured

3.1 Experimental results

There were no physical crack found on the coating surface after the cryogenic performanc test.

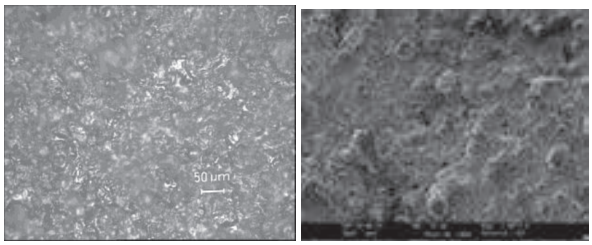

Fig.3 *Images after the cryogenic test cycle a)Optical microscope and b)SEM images*

4 Conclusion

Measurement of outgassing rate were carriedout for the Al_2O_3/TiO_2 thermally sprayed coatings and the coating is suitable for UHV appication as well as cryopump application.of any kind of coating. The coating also qualfies for the cryogeic application down to 4K. Henece a new area of research may be explored for the use of thermal spray coating on materials for fusion application.

5 References

[1] R.Srinivasan. R. Srinivasan and the Indian DEMO Team, Role of Fusion Energy in India. J.Pasma Fusion Res. Series,Vol.9(2010).
[2] H.Chen,S.W.Lee,Hao Du,Chuan X Ding and Chul Ho Dho ; Materials Letter Vol.58, Issues 7-8,March 2004 pp.1241-1245,Influence of feed stock & spraying arameters on the dep.eff.and microhardness of plasma sprayed zirconia coatings.
[3] G.Lalleman – Tallaron, Study of microstructure and adhesion of spinelles coatings formed by plasma spraying, Ph.D. Thesis No.96-58 (1996) E.C.Lyon, France.
[4] Ranjana Gangradey,Samiran Mukherjee et al. / Procedia Materials Science 6 (2014) 272 – 277
[5] P. A. Redhead, Extreme high vacuum, Proceedings of the CERN Acceleration School, Snekersten, Denmark, CERN report, edited
[6] Redhead, P.A .Recommended practices for measuring and reporting outgassing data'; J.Vac.Sc.Technol.A20,1667 (2002)

Plasma spray coating of Yttrium oxide coating on molybdenum and its thermal stability studies up to 800^{O}C.

Y.Chakravarthy[1], P.V.Ananthapadmanabhan[1]*, Vandana Chaturvedi[1], A .Pragatheeswaran[2].
[1]Laser and Plasma Technology Division, Bhabha Atomic Research Center, Trombay, Maharastra, India-400085
[2]Department of Physics, Karunya University, Coimbatore, Tamilnadu, India-641114
*Corresponding author. Tel.: +91-22-25595107; *E-mail address:* pvananth@barc.gov.in (P.V. Ananthapadmanabhan).

Abstract
Yttrium oxide (Y_2O_3) was coated on Mo substrates at 16, 20 and 24kW power levels using atmospheric plasma spray system (APS). Coating characterization was done using SEM, XRD and tensomter. The adhesion strength between coating and substrate was found to be around 8MPa. Molybdenum coated on all sides with Yttrium Oxide was heated to different temperatures up to 800^{O}C in air for 2 hrs and weight change measurements were observed after each thermal cycle. There is no weight gain/loss up to a temperature of 800^{O}C and above 800^{O}C coating delaminated from substrate. XRD results show that oxygen penetrated through the pores forming a volatile MoO_3 on substrate side which in turn reacts with yttria forming $Y_2Mo_4O_5$ on coating side. The two compounds forms a eutectic solution with low melting point, causes detachment of coating below 800^{O}C.

1. Introduction:

Molybdenum is a widely used refractory material because of its high melting point and superior strength properties at elevated temperatures [1-3]. However Mo forms a volatile oxide at low and elevated temperatures and therefore needs to be protected against oxidizing atmospheres [4]. Yttrium oxide (Y_2O_3) was proposed as a protective coating on molybdenum because of its high melting point, good thermal stability and chemical inertness towards variety of atmospheres [5]. Plasma spray technique was used for coating purpose because of its high enthalpy content; clean atmosphere and thick coatings [5, 6]. The present study focuses on plasma spray coating of yttria on molybdenum, characterization and interface reactions between coating and substrate at high temperatures (500^{O}C-800^{O}C).

2. Experimental methods

Yttrium oxide of spray grade quality was used as a raw powder for plasma spray coating. The coating was done using in-house 40 kW atmospheric plasma spray system at different power levels (16, 20, 24 kW). The operating parameters used for coating were given in Table [1]. The samples for adhesion test were coated on Mo with dimensions 1 inch dia x 1 inch length. Mo substrates coated on all sides with yttria was used for thermal stability studies Fig [1]. The coated samples were heat treated to different temperatures up to 800^{O}C in air for 2hrs (with an interval of 100^{O}C). The weight change measurements were done after each experiment. Coating characterization was done using SEM (Carl Zeiss EVO 40) and XRD (Rigaku Miniflex). The adhesion strength between coating and substrate was measured using tensile tensometer as per ASTM C-633 standard.

Table. 1. *Typical experimental parameters for Y_2O_3 coating*

Operating parameter	Experimental value
Input Power	16-24 kW
Plasma gas	30 SLPM
Plasma gas (N_2)	3 SLPM
Powder carrier gas	10 SLPM
Powder feed rate	~15 g/min
Particle size	15-40 micron

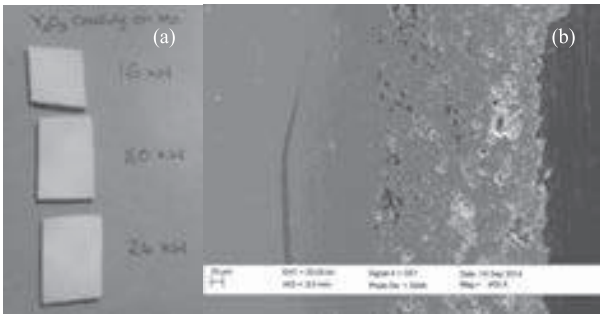

Fig. 1. *(a) Y_2O_3 coated Mo substrate (b) SEM image of coating/substrate interface.*

3. Results and Discussion

Figure 1(b) shows SEM microstructure of Mo/Y_2O_3 coating interface. The microstructure shows typical characteristic of plasma spray coating with coating thickness of around 300µm. XRD results of coated surface indicate that there is no phase change in yttrium oxide and cubic phase (JCPDS: 41-1105) is retained, **3(a)**. The adhesion strength between coating and substrate was found to be around 8MPa (average of five readings).

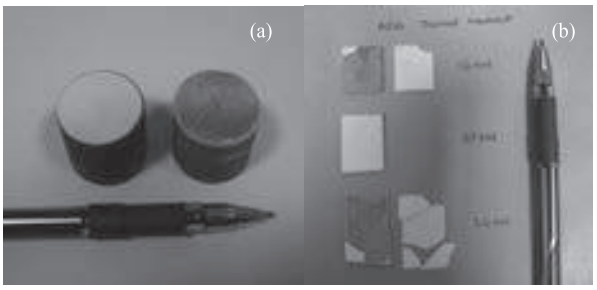

Fig. 2. *(a) Adhesion sample after testing (b) Coated sample after thermal treatment.*

Thermal studies of coated samples in air indicate that there is no weight gain/loss of the samples up to 800^{O}C and after 800^{O}C coating delaminated from substrate Fig [2]. Figure [3] shows XRD results of exposed surfaces (coating and

substrate) after heating to 800^{O}C. The results shows the formation of molybdenum trioxide (MoO_3) on the substrate side, **3(d)** and formation of $Y_2Mo_4O_{15}$ (Y_2O_3. $4MoO_3$) on coating side, **3(c)**.

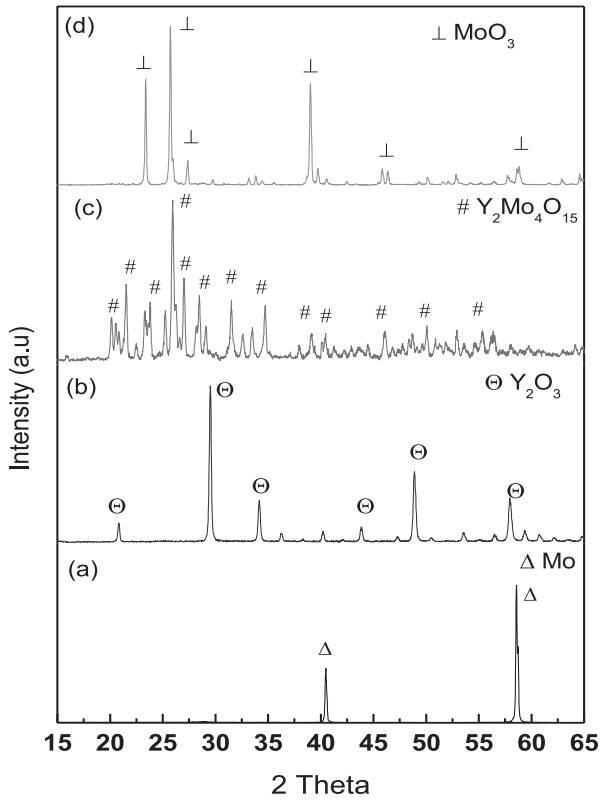

Fig. 3. *XRD results of (a) Mo Substrate before coating (b) Y_2O_3 coating (c)Y_2O_3 coating after experiment {substrate side} (d) Mo after experiment.*

It is observed that oxygen penetrated into the pores through coating, forming a MoO_3 on substrate side. Molybdenum trioxide is a volatile compound with a low melting point of 795^{O}C [4]. Molybdenum trioxide reacts with Y_2O_3 in the mole ratio of 1:4 forming yttria molybdenate ($Y_2Mo_4O_{15}$). Since the operating temperature is 800^{O}C, above the melting point of $Y_2Mo_4O_{15}$ (830^{O}C), it is understood that a eutectic mixture was formed between MoO_3 and $Y_2Mo_4O_{15}$ [7], which has a melting point of 740^{O}C. The formation of $Y_2Mo_4O_{15}$ on coating side indicates that coating was failed after formation of eutectic solution. Fig [3] shows coating peeled off completely without any formation of visible thermal cracks on coating surface. Therefore it is concluded that coating failed due to the formation of eutectic solution at the coating substrate interface.

5. Conclusions:

Yttium oxide was successfully coated on Mo substrate. A SEM and adhesion test shows good adhesion between coating and substrate. A single homogeneous cubic phase of yttria is retained after coating. Thermal studies indicate that plasma coating have interconnected pores which results in diffusion of oxygen through pores forming MoO_3 on molybdenum side. Coating was detached from substrate after formation of liquid phase eutectic solution. Further studies needs to be done to understand coating failure mechanism and remedies to contain diffusion of oxygen through yttrium oxide coating.

Acknowledgement

The authors express their gratitude to Dr. L.M. Gantayet, Group director, BTDG and Dr. K Dasgupta, Head, L&PT Division, BARC for their constant support.

References

[1] R.R. Freeman, the Metal Molybdenum, ASM, Cleveland, Ohio. 1958 pp. 10–30.
[2] S. Majumdar, G.B. Kale, I.G. Sharma, J. Alloys Compd. 394 (2005) 168-175.
[3] I.G. Sharma, S.P. Chakraborty, A.K. Suri, J. Alloys Compd. 393 (2005) 122–128.
[4] L.L.Y. Chang and B. Phillips, J. Am. Ceram. Soc. 53 (1969) 527-533.
[5] R.B. Hiemann, *Plasma-Spray Coating—Principles and Applications*, (VCH Publishers Inc, New York, USA, 1996).
[6] Pfdender E. *Plasma Chem Plasma Process* 19(1) (1999) 1–31.10.
[7] Fournier, J, Fournier, J, Kohlmuller, R., Bulletin de la Societe Chimique de France.12 (1970) 4277-83

Performance Evaluation of Yttria Coated High Density Graphite for Cathode Processor Applications

Ch. Jagadeeswara Rao, E. Vetrivendan, A. Ravi Shankar, C. Mallika, U. Kamachi Mudali
Corrosion Science and Technology Group, Indira Gandhi Centre for Atomic Research, Kalpakkam - 603102

Abstract
High density graphite (HDG) is proposed as a candidate material for process crucible and furnace liner in the pyrochemical reprocessing of spent metallic fuels. For protecting the HDG samples from the attack by molten salt and uranium, they were coated with yttria by atmospheric plasma spray process. To assess the integrity of the coating as well as its compatibility with molten uranium at high temperatures, uranium melting under UHP argon atmosphere was carried out in an induction heating system at 1300°C. Thermal cycling experiments were also carried out to check the durability of the coating. The coated samples were evacuated, sealed in quartz ampoules and were heated to either 1000 and 1100°C. After soaking for 1 h at these temperatures, the samples were furnace cooled. The coating failed after 36 and 20 thermal cycles at 1000 and 1100°C, respectively. The coated samples were characterised before and after thermal cycling and uranium melting experiments by SEM coupled with EDS and XRD techniques. The results of this study are discussed in the paper.

1 Introduction

The spent metallic fuel from future fast breeder reactors is proposed to be processed through the non-aqueous pyrochemical reprocessing. Pyrochemical reprocessing [1] involves several steps/processes such as salt purification, electrorefining, cathode processing, fuel casting process, etc., High density graphite (HDG) is considered as one of the candidate materials for salt purification vessel, lid, liners and cathode processor as well as casting process crucibles [2]. The HDG material reacts with molten chloride and Uranium and hence requires ceramic coating for the purpose of handling LiCl-KCl molten salt and molten uranium. Since pyrochemical reprocessing is a batch process, the structural materials with ceramic coatings require vigorous testing of several heating and cooling cycles to assess the durability and to predict the life of coating for applications at high temperatures.

The objective of the present study was to deposit yttria coating as top coat on HDG by plasma spray process after providing NiCrAlY bond coat and to evaluate the integrity of the yttria coating during thermal cycling studies. Yttria coating on HDG should also exhibit good compatibility with molten uranium for the applications in cathode processor; hence, uranium melting experiments were carried out.

2 Experimental

HDG disc samples (25 mm dia and 5.5 mm thick) with top flat and curved surfaces were coated on one side with 50 µm thick NiCrAlY bond coat and 250 µm thick yttria top coat using atmospheric plasma spray process. The coated samples were vacuum sealed in quartz tube for carrying out thermal cycling studies at 1000 and 1100°C. Mini SEM, Model SNE-3000M coupled with Energy Dispersive Spectroscopy (EDS), PAN alytical X'Pert diffractometer (40 kV, 30 mA, Cu K_α radiation, λ = 0.154 nm) and HR800 (Jobin Yvon) Raman spectrometer with argon ion laser of wave length 488 nm were used for characterizing the as-received and thermal cycled samples.

Uranium melting experiments were carried out in an induction melting setup [3] at 1300°C. The induction heating setup was housed in a glove box filled with UHP argon and heated at the rate of 75-80°C/min to reach 1300°C in about 15-20 min.

3 Results and Discussion

3.1 Surface morphology

The surface morphology of yttria coating on HDG (Figs. 1a and b) revealed that the coating was dense, with no cracks. The coating exhibited laminar morphology with splats all over the surface, which is a typical characteristic in plasma sprayed coatings. Elemental composition obtained by EDS analysis corresponded to Y: 46.1 wt% and O: 53.9 wt%.

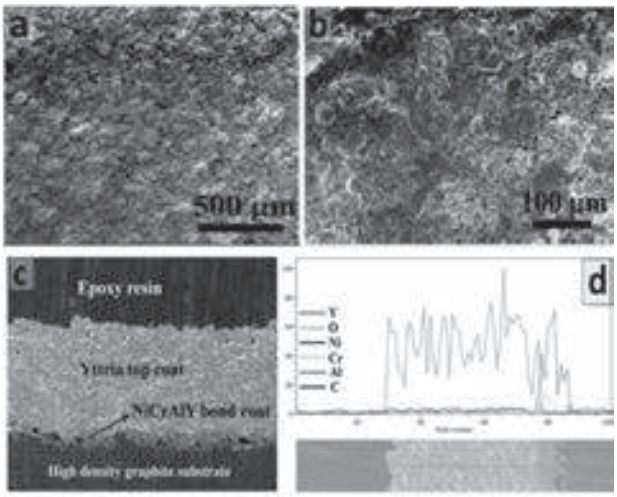

Fig. 1. *SEM micrograph of as-received yttria coating on HDG: (a) 50x magnification; (b) 200x magnification; (c) cross section image and (d) EDS line scan of cross section image.*

The coating thickness was found to be 50-60 µm of NiCrAlY bond coat and 250-300 µm of yttria top coat (Fig. 1c). The EDS line scan (Fig. 1d) indicates yttria top coat and NiCrAlY bond coat.

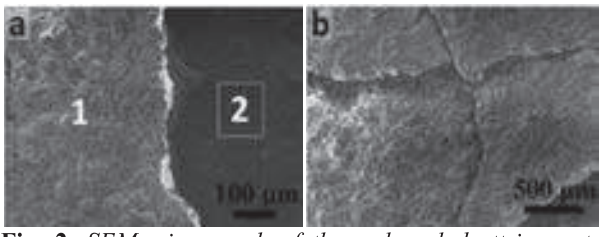

Fig. 2. *SEM micrograph of thermal cycled yttria coated HDG samples at 1000 (Fig.2a) and 1100°C (Fig.2b) after 36th and 20th cycles, respectively.*

Thermal cycling experiments at 1000°C revealed crack formation on the surface, which resulted in the coating failure after 36th cycle as shown in Fig. 2a. The EDS analysis of the region 1 in Fig. 2a corresponds to Y- 72.9wt%, O- 23.2wt%, Si- 3.9wt% and that of region 2 corresponds to Al- 4.4wt%, C- 17.6wt%, O- 32.8wt%, Cr- 1.0wt%, Ni- 3.0wt%, Y- 33.3wt%, Si- 5.1wt%, Ca- 3.0wt% and suggests that the region 2 corresponds to NiCrAlY bond coat. Hence, it is appeared that the coating got peeled off from the bond coat and top coat interface, but not completely from the HDG substrate. Thermal cycling studies at 1100°C revealed branched cracks all over the surface which led to the final failure of the coating after 20th cycle. Silicon on the coating surface could have originated from the quartz tube used for vacuum sealing of the sample due to high temperature. The cross sectional SEM examination of the thermal cycled sample at 1100°C after 20 cycles revealed the formation of vertical cracks throughout the interface of the coatings and HDG substrate.

3.2 Phase characterization

The X-ray diffraction (XRD) patterns of the as-received and thermal cycled (after 20 cycles at 1100°C) yttria coated HDG samples, shown in Fig. 3 confirmed the cubic phase (JCPDS No. 41-1105) of yttria present in the coated sample. No marked difference was observed between the XRD patterns of as-received and thermal cycled sample.

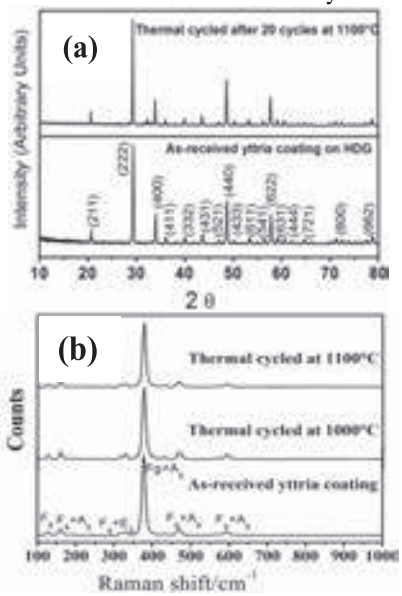

Fig. 3. XRD *pattern (a) and Laser raman spectra (b) of yttria coating on HDG before and after thermal cycling.*

The Laser Raman Spectra (LRS) of as-received and thermal cycled (at 1000 and 1100°C) samples of yttria coated HDG are reproduced in Fig. 3b. From the Raman shifts of as-received yttria coating, one dominant peak corresponding to Fg+Ag Raman active mode was observed at 377.9 cm^{-1}, in addition to other small peaks corresponding to Fg, Fg+Ag and Fg+Eg symmetry vibrations. These peaks correspond to the cubic phase of yttria [4]. No change in Raman shifts was observed in the thermal cycled samples. Retention of cubic phase of yttria after thermal cycling even at 1100°C, inferred from LRS studies validates the results of XRD analysis. The yttria coating failure after thermal cycling studies could be due to the thermal expansion mismatch between the substrate and coating.

3.3 Uranium melting

Figure 4a shows the photograph of yttria coated HDG sample after uranium melting experiments at 1300°C. Visual examination of the yttria coating showed the change in colour from white to black after uranium melting. The SEM image of yttria coating after uranium melting indicated the splat morphology of as-received coating. However, microcracks were generated on the surface of the coating due to fast heating and cooling (Fig. 4b). The EDS elemental analysis on selected regions of uranium melted coating showed the presence of U (48.3 wt%), Y (38.3 wt %) and O (13.4 wt %). The uranium content on the surface of yttria coating was low. The melting experiments were repeated on the same sample and the yttria coating was found to be intact until 3 melting experiments.

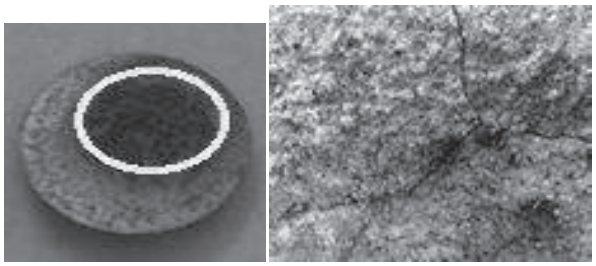

Fig. 4. *Photograph of yttria coated HDG disc and its SEM image after uranium melting experiments.*

4 Conclusions

1. Thermal cycling behaviour of HDG discs coated with NiCrAlY bond coat and yttria top coat using plasma spray process was investigated at 1000 and 1100°C under vacuum. The compatibility of yttria coating with uranium at 1300°C was also demonstrated.
2. Yttria coating was found to have good adherence until 35 and 19 cycles at 1000 and 1100°C, respectively. Visual examination of yttria coated HDG samples showed spallation during 36th cycle at 1000°C and 20th cycle at 1100°C.
3. XRD and LRS studies of yttria coated HDG confirmed only cubic phase of yttria in both as-received and thermal cycled samples.
4. The coating was intact for 3 uranium melting runs.

5 References

[1] K. Nagarajan, B.P. Reddy, S. Ghosh, G. Ravisankar, K.S. Mohandas, U. Kamachi Mudali, K.V.G. Kutty, K.V. Kasiviswanathan, C. Anand Babu, P. Kalyanasundaram, P.R. Vasudeva Rao and Baldev Raj, Energy Procedia, **7** (2011) 431–436.

[2] U. Kamachi Mudali, A. Ravi Shankar, C. Mallika, K. Thyagarajan, S. Ningshen, B.P. Reddy and K. Nagarajan, Internal Report: IGC/MMG/CSTG/2011, 2011, pp. 1-47.

[3] Jagadeesh Sure, Ch. Jagadeeswara Rao, P. Venkatesh, B. Prabhakara Reddy, C. Mallika, U. Kamachi Mudali, Ceramics International, **40** (2014) 6509–6523.

[4] M. Yashima, J.H. Lee, M. Kakihana and M. Yoshimura, J. Phys. Chem. Solids, **58** (1997) 1593-1597.

Microstructural Evolution of Stellite6 Coatings used in Gas turbines after Service Exposure and Heat Treatment

Apaar Shanker[1], Dheepa Srinivasan [2], Santhosh Bangera[2] and Vishwanathan Venkatachalapathy[2]
[1] Materials Engineering, Indian Institute of Science, Bangalore 560 012, India
[2] GE Power and Water, GE India Technology Centre, Bangalore 560 066, India

Abstract
HVOF Stellite6 coatings are used as wear coatings in several gas turbine components, such as the combustion liner, transition piece and related parts. The microstructural evolution and bond strength of Stellite6 coatings, present as a 100-200 µm coating on to Ni based superalloys, was studied after service exposure and different heat treatment. The coating microstructure undergoes a change, with the evolution of phases after the heat treatments, with the occurrence of Cr$_3$Si and M$_6$C phases, that result in a marginally lower hardness of the coating (500 H_v). The bond strength was found to be greater than 70 MPa, indicative of the good adhesion of the coating. Overall, based on comparison with a new coating, an assessment of the effect of service exposure enabled an assessment of the remnant life of the coating.

1. Introduction

Stellite6 is a well known popular material used in various structural applications, in a gas turbine. Belonging to the Cobalt based alloy category, it is used in applications that require superior, oxidation and hot corrosion resistance, including high temperature wear [1,2]. The alloy composition comprising Cr, Ni, Mo, W in a Co rich matrix [2], is used extensively for high temperature wear resistant applications, both as a weld cladding and as a thermal spray coating [3]. While the Cr is used for high temperature oxidation and corrosion, Mo and W are solid solution strengtheners as well as precipitation hardeners, in addition to forming intermetallics such as $Co_3(Mo,W)$. There are limited studies on the high temperature response of the Stellite6 coatings [3]. This paper presents a study of the microstructural evolution of Stellite6 HVOF coatings, after service exposure and compares the performance of the Stellite6 coatings subject to high temperature heat treatments.

2. Experimental Details

HVOF Stellite6 coatings, having a thickness range of 150-250 µm, sprayed using a DJ-2600 gun, on to a Ni based superalloy were evaluated, after being subject to 24000 h of service exposure, in a gas turbine component, made of a Ni based superalloy. New Stellite6 coatings were also evaluated as a reference, to the exposed coating. The nominal service exposure temperature ranged between 500-600°C. The coating roughness (Mitutoyo), microstructure (Optical-Nikon Eclipse MA 200, Scannning electron microscope-Carl Zeiss Evo18, Oxford Link), microhardness (Shimadzu-0.3 Hv) and bond adhesion strength (ASTM C633–Instron 8862, 100 KN), were evaluated. The bond tests were done using an EC2086 glue (glue strength of 90 MPa).The Stellite6 coatings were subjected to two different high temperature heat treatments, in vacuum at specified heating and cooling rates, as listed in Table 1.

Table 1: *Stellite6 coating heat treatment*

Coating	New	Service Exposed	Heat Treatment 1	Heat Treatment 2
HVOF Stellite6	As Coated – No HT	24000 h ~ 550°C	1150°C 30 mins	1100°C, 1.5 h 800°C, 8 h

3. Results and Discussion

Fig. 1 compares the optical microstructure (200X) of the Stellite6 coatings, in the (a) as sprayed, and (b) service exposed conditions, while Fig. 1(c-d), are the respective coating microstructures, after the heat treatments. In the as sprayed condition and after service exposure, the coating remains a complete solid solution, possibly due to the rapid solidification when the splats are formed. Fig. 2 has the corresponding microhardness of the service exposed and heat treated coating. There was no significant change in the hardness after service exposure and heat treatment. However, the coating microstructure shows a distinct phase evolution after the heat treatments as shown in Fig 3. The high temperature heat treatment results in the evolution of carbides (of the type $M_{23}C_6$/M_6C), along the splat boundaries, as shown in Fig. 4, via SEM-EDAX analysis. In addition, there are pockets that are enriched in Si and Cr, indicative of a Cr_3Si phase. Bond adhesion tests on the as spraeyd and heat treated coatings displayed adequate strength, with no deterioration in the bond strength after heat treatment, as shown in Fig. 5, with a value of 50 MPa (having a glue failure), in all the cases.

.

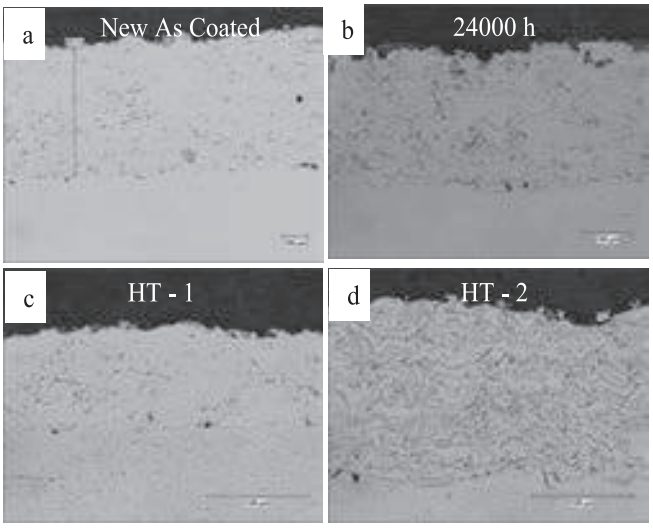

Fig. 1: *Optical micrographs (200 X) comparing the, (a) as sprayed, (b) Service exposed (24000 h), (c) HT 1, (d) HT 2, microstructures.*

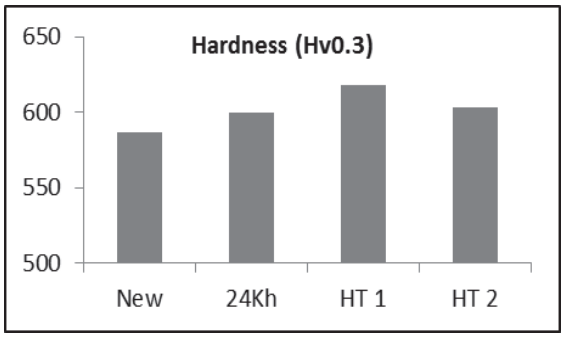

Fig. 2: *Comparative microhardness plot of the coatings subject to different conditions*

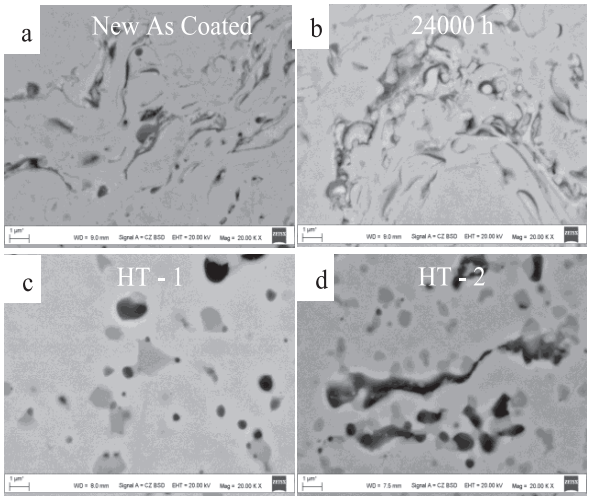

Fig. 3: *Scanning electron micrographs at 20KX, showing, representative microstructure of the Stellite6 coating, in the, (a) New, (b) Service exposed (after 24Kh), (c) after HT 1 and (d) after HT2.*

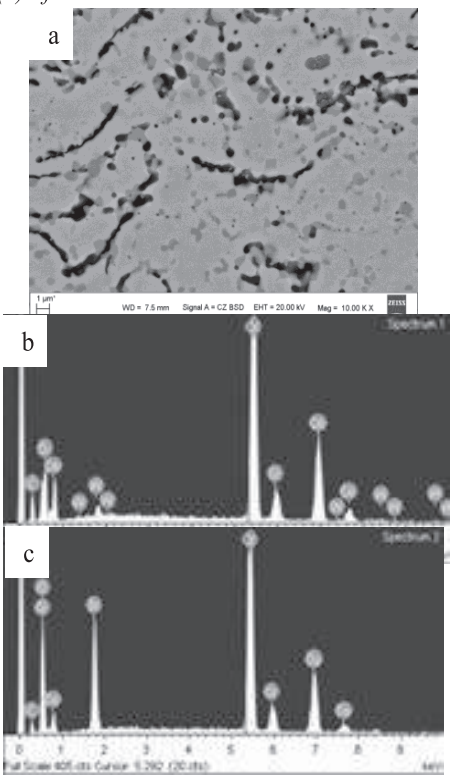

Fig. 4: *Representative SEM micrograph of the Stellit6 coating after HT 2.*

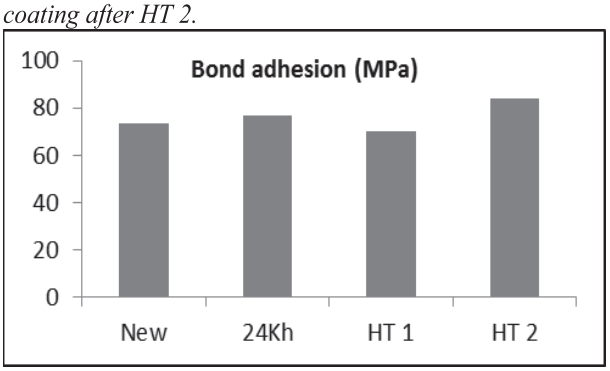

Fig. 5: *Comparative tensile bond adhesion strength of the stellite6 coating*

3. Conclusion

1. The Stellite6 coating was found to withstand the high temperature heat treatments without any deterioration to the functional properties.
2. There was no coating delamination after the heat treatment.
3. The microhardness (500 – 650 Hv) as well as the bond adhesion strength (70 MPa) were found to undergo no deterioration .
4. The coating microstructure is seen to undergo a phase evolution, with the occurrence of Cr_3Si and M_6C_3, along with the Co solid solution after Heat treatment.

4. Acknowledgements

The authors thank GEMTEC, Saudi Arabia and GTS, Abu Dhabi, for their help in carrying out the the coating trials. Mr. Christopher Thompson and Dr. Sundar Amancherla are acknowledged for their support of this work.

References

[1] P. Crook, Metals Handbook, **2**, 10th Edn. ASM International (1993).
[2] Journal of Metals, **39** (1983) 52-59.
[3] G. Kong, D. Zhang, P.D. Brown., Mater. Sci. Technol., **19** (2003) 1001-1011.

Poster Presentations

POSTER PRESENTATIONS

POSTER NO.	AUTHORS	TITLE
P01	R.Ishimura , Y.Sakai, M.Yamashita, K.Shiokawa, Izumi.K.Sato, Y.Ichikawa, K.Ogawa	Effect of Heat Treatment on the Microstructure and Mechanical Properties of Cold Sprayed WC-cermet Coatings
P02	Kesavan Ravi, Kazuhiro Ogawa,Yuji Ichikawa, Jean-Yves Cavaille, Tiana Deplanke, Olivier Lame	Development of Ultra High Molecular Weight Polyethylene Coatings by Cold Spray Technique
P03	Sateesh Kumar Yadav, Rajesh Kumar Shukla, Arvind Kumar	Numerical Modelling of Solid Spherical Particle Deposition on a Roughened Substrate during Cold Spraying
P04	S.Karthikeyan, V. Balasubramanian and R.Rajendran	Evaluation of Thermal Cyclic Performance of Rare Earth Oxide Based Thermal Barrier Coatings
P05	R.Sathiyamoorthy, K.Shanmugam, V.Balasubramanian	Tribological Behavior of SiC Reinforced Titanium di-oxide (TiO_2) Coating Deposited by High Velocity Oxy-Fuel (HVOF) Spraying
P06	M. Bharath Kumar, G. Krishna Mohana Rao, S. Gokul Laxmi, G. M. Reddy and Manish Roy	Comparison of Abrasive Wear of HVOF & D Gun Sprayed WC-Ni Coatings on Aluminium Alloy
P07	S. Sivakumar, K. Praveen and G. Shanmugavelayutham	Preparation and Characterization Study of Lanthanum Zirconate by Ball Milling Method for Plasma Spraying
P08	Mohammed Shahien, Motohiro Yamada, Masahiro Fukumoto, Kazumi Egota, Kenji Okamoto	Thermal Conductivity of the Atmospheric Aluminum Nitride Coatings
P09	Deepa Mudgal, Surendra Singh, Satya Prakash	Hot corrosion behaviour of Cr_3C_2-(NiCr)+0.2wt.%Zr Coated Superalloys Under Actual Medical Waste Incinerator Environment at 1050°C
P010	Arpan Katiyar, Prashant Kumar Singh and S. B. Mishra	Slurry Erosion Wear of Detonation Gun Sprayed Stellite-6 and WC-Co Coatings on AISI 201 and AISI 316 Stainless Steels
P011	K. Teja Swarup, S. Gokul lakshmi and Manish Roy	Elevated Temperature Erosion Behaviour of Thermal Sprayed Cr_2C_3-25(Ni20Cr)
P012	Sneha Goel, Ashish Ganvir, Nicolaie Markocsan	Image Analysis of Microstructural Features of Suspension Plasma Sprayed Coatings
P013	M.Raja, Gavisiddayya Hiremath, K. Ramachandran, P.V.A. Padmanabhan, T.K. Thiyagarajan	Prediction of Substrate Temperatures and Stresses During Plasma Spraying
P014	Gavisiddayya Hiremath, G Ravi, K. Ramachandran	Numerical Simulation of Heating and Melting of Materials by Thermal Plasma Jet
P015	R.Mahendran, S.P.Kumaresh Babu, S.Natarajan, P.Veerabalu, M.Kumarasamy	Electrochemical Corrosion Studies of HVOF Sprayed Nickel Based Self Fluxing Alloy Coating on Mild Steel in Mining Environment
P016	K. Praveen, S. Sivakumar, G. Shanmugavelayutham	Preparation and Characterization of Zirconia/Alumina Coatings by Atmospheric Plasma Spraying
P017	Roshan Jacob, R.Mahendran, A.Vallimanalan, S.P.Kumaresh Babu, S.Natarajan	Corrosion Studies of Twin Wire Arc Sprayed Duplex Stainless Steel Coatings on Mild Steel used in Mining Environment
P018	C.Thiruvikraman, V.Balasubramanian, S.Malarvizhi and K. Sridhar	Evaluating Micro – Mechanical Characteristics of HVOF Sprayed WC-CrC-Ni Coatings
P019	Praveen A. S., J. Sarangan, S. Suresh	Effect of HVOF Process Parameters on Porosity of NiCrSiB/WC-Co Coatings
P020	A.Pragatheeswaran, P V Ananthapadmanabhan, Y. Chakravarthy, Vandana Chaturvedi, Subhankar Bhandari, K Ramachandran	Plasma Spray Deposition of Lanthanum Phosphate and Phase Structure of the Resultant Coatings
P021	Mahrukh Mahrukh Hosein Torabmostaedi, Sai Gu	Numerical Simulation of the Solution Precursor High Velocity Oxygen Fuel Spray Process
P022	G. Vasanth, G. Siva Kumar, S.V. Joshi, Kantesh Balani, M. Geetha	Investigation on the Corrosion Behaviour of Plasma Sprayed Bi-layered and Mono-layered Ceramic Coatings on Ti-6Al-4V Alloy for Biomedical Application.
P023	Manoj Kumar, Harpreet Singh, Narinder Singh, S.V. Joshi, N. M. Chavan, S. Kumar	Development of Erosion-corrosion Resistant Cold-spray Nanostructured Ni-20Cr Coating for Coal Fired Boiler Applications
P024	Bhaskar Podeti, Oonnatie Deolankar, Mandira Bhattarcharyya, Gous Mohammed, Todd Wieland, Sachchidanand Velankar, S C Modi, Ankur Modi, Rohit Upadhyaya	Remanufacturing of Engine Connecting Rods using Twin Wire Arc Spray

Effect of heat treatment on the microstructure and mechanical properties of cold sprayed WC-cermet coatings

R.Ishimura[1] , Y.Sakai[2], M.Yamashita[2], K.Shiokawa [2], S.Izumi[2].K.Sato[3] ,Y.Ichikawa[1], K.Ogawa[1]
[1] Fracture and Reliability Research Institute, Tohoku University, Sendai, Miyagi 980-8579, Japan
[2]Fuji Electric Co.,Ltd. , Kawasaki, Kanagawa 210-9530, Japan
[3]Fujimi Incorporated, Kagamigahara, Gifu 509-0103, Japan

Abstract
In this study, two kinds of WC cermets (WC-FeCr , WC-FeNiCr) have been sprayed by cold spray process. It was investigated to confirm the influence of the powder chemical compositions on coating properties. Furthermore, microstructures and mechanical properties of the coatings were evaluated. In the CS process, there can be almost no phase transformation and high temperature oxidation during spraying. The cold sprayed WC cermet coatings were analyzed by SEM and XRD. As a result, it was confirmed that there was no decarburization and no brittle phases such as W_2C. And then, the both coatings were heat treated at a range of temperatures between 200 and 800°C in an air environment to improve coating properties. The properties of these coatings such as phase composition, microstructure, and coating hardness were investigated. Hardness of both coatings increased with heat treatment above 400°C. However, a phase transformation occurred over 600℃. It was thought that these are the oxide phase or intermerallic compound. Thus, heating temperature at around 600℃ is better than others. In this study, the improved properties were discussed in terms of the relationship between microstructure and microhardness.

1 Introduction

Tungsten carbide-cobalt(WC-Co) based materials are used for industry in sintered bulk as well as thermally sprayed forms for applications required in errosion, abrasion resistance. The high velocity oxy-fuel (HVOF) thermal spray technique has been applied to WC coatings. [1]

However, compared to sintered WC, WC coatings are inferior in fracture resistance, and it impedes the expansion of fields. These reasons are considered as follows (1) the decarburization and decomposition during spraying process leading to formation of brittleness phase such as W_2C, W, η phases[1] (2) weak bonding strength between WC and binder metals in layer particles. In other words, by solving these problems, it can be expected to improve the property of fracture resistance. Thus, in this study, WC feedstock powders were deposited by cold spray (CS) technique, which process temperature is lower than other coating techniques, to control the coating phase transformations. After that, post heat treatments were carried out to improve the bonding strength between WC and binder metals. In this paper, the results of the effect of post heat treatment for microstructures and hardness of the cold-sprayed coatings are reported.

2 Experimental procedure

Two types of WC cermets (WC-FeCr, WC-FeNiCr/ Fujimi Incorporated) were sprayed by CS process on 13% chromium alloy substrates with thickness of 500 μm. Table1 shows the spray condition. The coating samples were placed in the furnace with air environment and heated at a rate of 5 °C/min. After that, these were held for 1 hour at 200-800°C, and then cooled to room temperature in the furnace. The microstructures of coatings were observed by Scanning Electron Microscope (SEM). X-ray diffraction (XRD) analysis of the coatings was carried out with Cu-Kα radiation. The microhardness measurement was performed on the transverse section of the coatings with a Vickers indenter at loads of 2.9N with a 10 s dwell time. Ten hardness points were averaged.

Table 1 spray conditions

Parameters	
Working gas	N_2
Gas pressure	3MPa
Main gas temperature	800℃
Spray distance	20mm
Gun traverse speed	300mm/sec

3 Results and Discussion

SEM photographs of cold splayed coatings, post heated coating and HVOF sprayed WC-FeCr coating for comparison with CS coatings are shown in Fig.1. The feedstock powder, which WC size was lager than that of cold spray, was used for HVOF coatings to reduce phase transformation. There are some porosities of several μm in HVOF sprayed coating. On the other hand, there are less porosities and the size is smaller in cold sprayed coatings compared with the HVOF coating. Comparing as-sprayed coating with heat-treated (800°C) coating, there is dispersion of WC phase and binder metal (Fe) phase in as-sprayed coating. On the other hand, after heat treatment, the WC particles were a homogeneous distribution and the porosities were reduced.

Fig.2 shows the XRD patterns of the feedstock powders for the spray, as-sprayed and heat treated WC coating. It is seen that WC-FeCr feedstock powder is composed only of WC and Fe phases. In the cold sprayed coatings, the diffraction peak was also same as feedstock powder. Therefore, it is concluded that there is no phase transformation and decarburization during spraying, and the composition of the WC-FeCr, FeNiCr coatings by cold spraying is almost same with feedstock powders.

However, it was noticed that WC and Fe diffraction peaks of cold sprayed coating broadened significantly compared to the feedstock powder. It is known that a peak broadening can be attributed to either a strain effect or reduction in particle size. Therefore, a crystalline size and a lattice strain of both the feedstock and coating were estimated from the

peak broadenings with Halliamson-Hall methods[2]. As a result, as-sprayed coating was found to have a refined microstructure and added a more strain compared to feedstock powder. In the CS process, the particles traveled with high velocity. Consequently, it was thought that impact of incoming WC particles onto the underlying deposited layer of WC caused WC particles refinement. Thus, it was thought that cold sprayed WC coatings had compressive stresses and smaller crystal grains. In the case of high temperature, it was seen that the peak broadenings became narrow. It was thought that residual stress was decreased by heat treatment. On the other hand, a phase transformations were observed at over 600℃ heat treatment. It could not be identified in this study, however, it is believed that these are the oxide phase or intermerallic compound.

Fig.3 shows the microhardness of as-sprayed and heat treated WC coating. Comparing the binder composition, the hardness of WC-FeCr coating was higher than that of WC-FeNiCr, and was approximately 1300HV. For both coatings, the hardness decreased after heat treatment at 200℃. It was obsereved that the coating hardness increases with increasing temperature. Both the tendency of hardness WC-FeCr and WC-FeNiCr were almost same till 600℃ heat treatment. It is known that the hardness of an alloy, which is composed of only hard and soft phases, is decided whether the movement of hard phase (WC phase) is easy from an external force or not[3]. Therefore, it means that the hardness of cold sprayed WC coating depends upon the distance between WC particles and the strength of metal (Fe alloy) phase. The dispersion of WC particles in WC-FeCr coatings was narrower than that of WC-FeNiCr (Fig.1). As a result, the hardness of WC-FeCr was higher. And it is considered that high temperature promotes sintering action between WC and metal phase. Thus, the reason why increasing the hardness of coating with heat temperature is due to increasing the strength between WC and Fe alloy. According to the above results, a hardness of coatings increased with the heat treatment temperature. However, the temperature above 600℃, a phase transformation was observed and oxide phases or intermetallic compounds, which are brittleness phase, were generated. Thus, it is thought that heating temperature at around 600℃ is better than the others. It is important property for fracture resistance not only hardness but also fracture toughness. Thus, in order to evaluate correctly the influence of heat treatment for fracture resistance, the fracture toughness and coating strength should be evaluated by four-point bending test in near future.

4 Conclutions

In this study, in order to improvement of the WC coating properties, WC feedstock powders were deposited by CS technique. After that, post heat treatments were carried out to improve the bonding strength between WC and binder metals. Cold spayed coatings were so dense and there was no phase transformation and decarburization.

The hardness of coatings increased with the increasing heat treatment temperature. However, at temperatures above 600℃, phase transformation was confirmed. Thus, it is thought that heat temperature at around 600℃ is better.

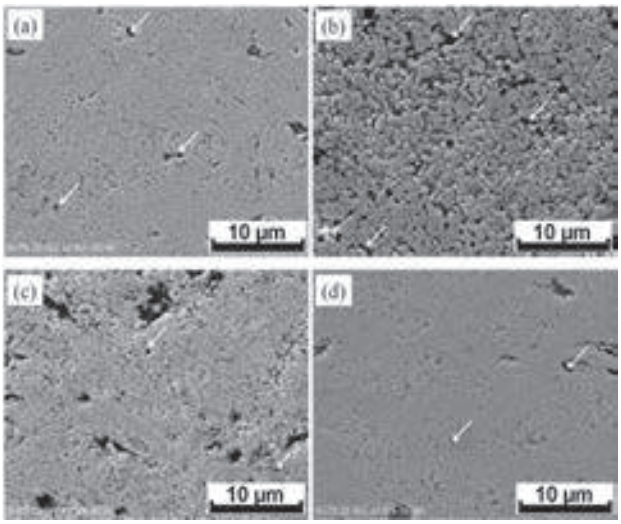

Fig. 1. SEM images for cross section of coatings (a)cold sprayed WC-FeCr (b) HVOF sprayed WC-FeCr (c)cold sprayed WC-FeNiCr (d) heat-treated WC-FeCr at 800℃

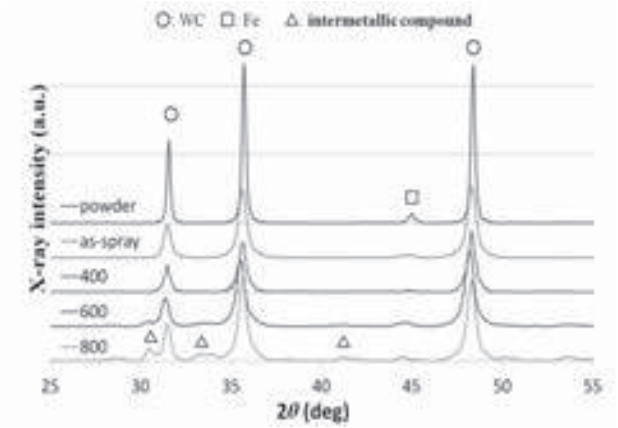

Fig. 2. The XRD patterns of the feedstock powders for the spray, as-sprayed and heat-treated WC-FeCr coating.

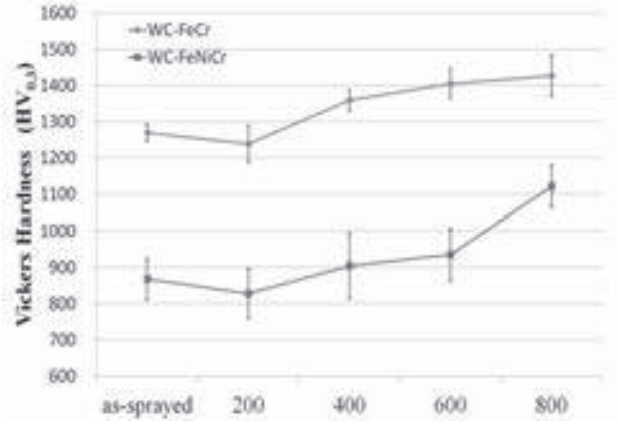

Fig. 3. Relationship between coatings hadness and heat treatment temperature

5 References

[1] C.J.Li and G.J Yang: J. Refractory Metals and hard matrrials. 39 (2013) pp.2-17.

[2]VD Mote, Y Purushotham and BN Dole: J.Theoretical and Applied Physics. 6(2012) 6;6

[3] J.Gurland and P.Bardzil:J.metals,7(1955)pp.311-315.

Development Of Ultra High Molecular Weight Polyethylene Coatings By Cold Spray Technique

Kesavan Ravi[1], Kazuhiro Ogawa[1],Yuji Ichikawa[1], Jean-Yves Cavaille[2], Tiana Deplanke[2], Olivier Lame[2]
[1]Fracture and Reliability Research Institute, Tohoku Univ.6-6-11, Aoba, Aramaki, Aoba-ku, Sendai, Japan
[2]Laboratory of Material Engineering and Science (MATEIS, France)

Abstract
The cold spray deposition of ultra high molecular weight polyethylene (UHMWPE) powder was attempted on two different substrates polypropylene (PP), aluminum (Al). The particles were accelerated at gas temperatures ranging from 150-350^{o}C and gas pressures ranging from 0.2-0.8MPa in air through a cylindrical nozzle of 200mm length, in order to develop sufficient thermally activated flow stress in the UHMWPE particles, and were deposited on to substrates. Thick and dense deposits were formed at temperatures substantially below the melt flow of the polymer. Deposition occurred readily on to polypropylene substrates at 170^{o}C gas temperature and on to Al at 350^{o}C gas temperature. Mechanical properties of the substrates affected the impact behavior oft he UHMWPE particles. Heat treatment also facilitated in significant reduction in pores and voids within the coating. Results of differential scanning calorimetry (DSC) results show the melt crystallisation in the UHMWPE during the cold spray.
Key words: Cold spray deposition, Ultra High Molecular Weight Polyethylene, Polymers, Coating

1 Introduction

The process known as cold spraying (CS) was developed in the 1980s by Dr. Papyrin and co-workers and involves the impact of metallic particles on to a target at very high speeds (500 to 1500 m/s) to form coatings or solid components [1]. The accelerating gas may be heated, mainly to achieve higher particle velocities. Figure 1 represents a schematic diagram of a cold spray system where the powder particles are accelerated to supersonic velocities through a De Laval nozzle and deposited onto a suitable substrate material.

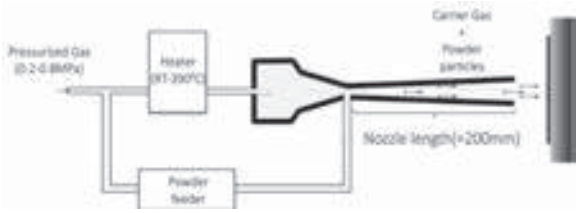

Fig. 1 Schematic of a cold spray apparatus.

Main idea behind this research work is the development of ultra high molecular weight polyethylene coatings with functional properties like wear resistance, impact resistance and cavitation erosion resistance.

2 Experimental

UHMWPE powder was hand mixed with 3.8 wt.% fumed nano alumina particles before the cold spray. The powder mixture was deposited on each of the substrates using low-pressure cold spray technique. Pressurized gas (air) from 0.2MPa to 0.8MPa was supplied from a compressor, which meets the powder particles at the nozzle region. The gas temperature was varied from room temperature to 500^{0}C. The powder particles were then fed through a vibrated powder feeder at a steady controllable rate. The air stream containing the polymer particles was then passed through a de Laval nozzle of length 200mm to deposit onto Aluminium (Al) and Polypropylene (PP) substrates.

3 Results and discussion

3.1 Effect of temperature and pressure

It was observed that deposition of the polymer-nanocomposite mixture of 4mm occurred when the temperature of the gas was close to 350^{o}C and gas pressure between 0.3-0.4MPa in the case of Al substrate.
On PP substrate, the deposition of 1mm thickness was observed at 170^{o}C gas temperature and 0.3-0.4MPa gas pressure. Figures 2 (a) and (b) represent the deposition behavior of the UHMWPE-nano alumina mixture at different gas temperature and pressure on Al and PP respectively.

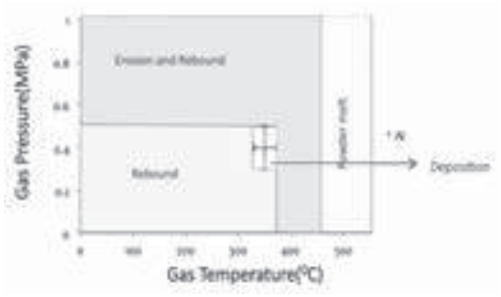

(a)

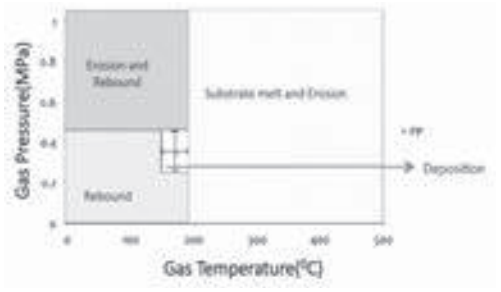

(b)

Fig. 2 Deposition behavior of the UHMWPE- fumed nano alumina mixture at different gas temperature and pressure on (a) Al (b) PP.

3.2 Effect of substrate properties

a) Aluminum Substrate

It was observed that, the particles broke in to smaller particles on impact with the Al substrate and tend to extensively deform plastically. Figure 3 shows the SEM image of the particles after the impact with the Al substrate.

The reason for such a behavior UHMWPE particles upon impact onto Al substrate, may be attributed to mechanical properties of the substrate and the UHMWPE particles.

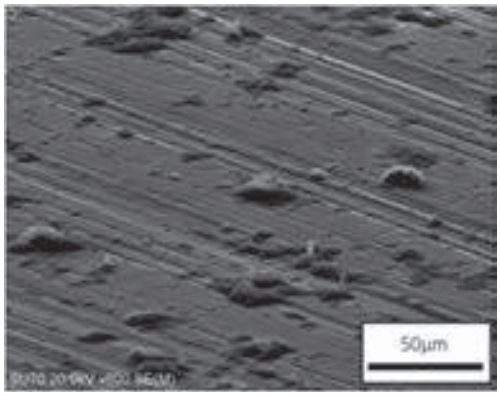

Figure. 3 SEM image of UHMWPE deposition on Al surface.

b) Polypropylene Substrate

It was observed that, the particles broke in to smaller particles on impact with the PP substrate. Deformation was observed in both particle and the substrate. Figure 4 shows the SEM image of the particles after the impact with the PP substrate.

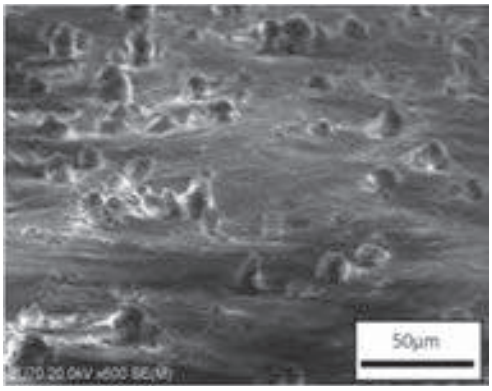

Figure. 4 SEM image of UHMWPE deposition on PP surface.

In the case of UHMWPE cold sprayed on Al substrate, particle breakage and the extensive plastic deformation in the particles may be due to the marginal difference in the hardness value of Al in comparison to UHMWPE. Under such conditions UHMWPE deforms extensively when impacted on Al substrate. On the other hand, the hardness of the PP is comparable to the UHMWPE particles. Hence, in the case of deposition on PP substrate, deformation was observed in the particle and the substrate. Jet formations are visible around the deposited UHMWPE particle (Fig. 4). Polypropylene allows itself to absorb the energy due to impact and plastically deform to very larger extent than Al.

3.3 Differential scanning calorimetry

The DSC curves for the deposited particles were observed to be markedly different from that of the nascent powder. The deposited particles, with all the different powder mixtures used, were observed to be melt crystallized (Fig. 5). The DSC curves of the rebound particles at all the gas temperatures were observed to be very similar to that of the nascent powder. Figure 6 represents the DSC curves for the rebound particles which is inherently highly crystalline and non-equilibrium.

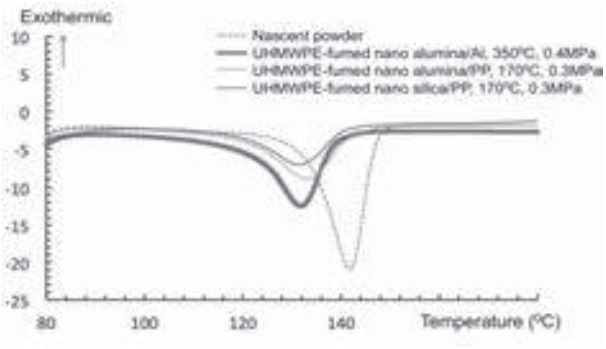

Figure. 5 DSC curves of the deposited particles.

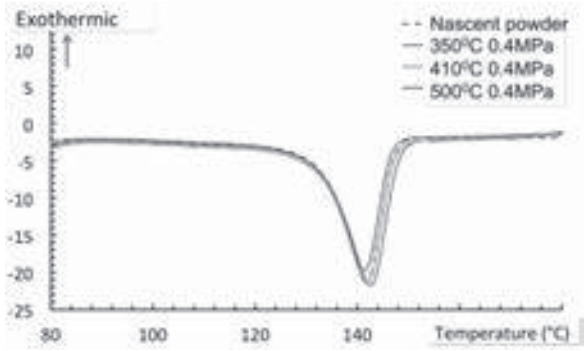

Figure. 6 DSC curves of the rebounded particles at various gas temperatures.

4 Conclusions

This study dealt with polymer coating by cold spray technique. The following can be concluded from the investigation,

1) UHMWPE coating of 4mm and 1mm thickness was achieved on Al and PP substrates respectively. Deposition occured at a small window of temperature and pressure conditions.

2) The mechanical properties of substrates have a profound impact on the deposition behavior of the UHMWPE particles.

3) Rebounding particles, due to insufficient thermal energy transfer from the carrier gas, remained similar to the nascent powder in its structure before the impact. Deposited particles were heated above its crystal melting temperature (>135^{o}C) by the carrier gas and made amorphous in structure before the impact.

5 Aknowledgement

Authors would like to thank JTSS internship program for financing and supporting the internship, carried out at Iwate Industrial Research Institute. This work was partly supported by the JSPS Core-to-Core Program, A. Advanced Research Networks, “International research core on smart layered materials and structures for energy saving”.

6 References

[1] McCune, R. C., W. R. Donlon, E. L. Cartwright, A. N.Papyrin, E.F.Rybicki and J.R.Shadley. Proceedings of the 1996 National Thermal Spray Conference, (1996) 7-11.

Numerical modelling of solid spherical particle deposition on a roughened substrate during cold spraying

Sateesh Kumar Yadav, Rajesh Kumar Shukla, Arvind Kumar*
Department of Mechanical Engineering Indian Institute of Technology Kanpur, Kanpur, 208016, India
* Corresponding author: Email: arvindkr@iitk.ac.in

Abstract
In this paper, a finite element analysis (FEA) of deposition mechanism of aluminum particle on a roughened copper surface in cold spray process has been performed. The particle deformation behavior is studied. The particle–substrate contact time, the contact temperature and the contact area upon impact have been estimated for different roughened substrates. Simulations indicate that the deformation and the resultant bonding were higher for the roughened substrates than that of smooth substrates.

1 Introduction

Cold spraying has been applied successfully in producing coating with higher density, superior bond strengths, and less particle surface reactions due to its unique advantage of high momentum and low thermal output. During cold spraying, heated solid powder particles impact on the substrate with high velocity. The kinetic energy of the solid particle is being converted to heat which soften the substrate and plastic deformation of the solid particle and substrate occurs. The plastic deformation depends on the material properties of feedstock and substrate, the impact particle velocity and the morphology of the substrate surface. The adhesion energy of the surface depends on contact area, contact temperature and contact time [1].

In the present study, a numerical modelling is performed study contact time, contact temperature and contact area during copper particle impact on smooth and roughened surfaces of aluminium. ABAQUS 6.13–1 finite element analysis software is used to model the deformation behavior. This model considers the strain hardening, strain-rate hardening, thermal softening and heating due to frictional, plastic and viscous dissipation. The strain rate-dependent and temperature-dependent constitutive description is required in finite element codes in order to simulate and analyze the deformability of the powder and the substrate under different impact conditions. The stress is expressed as a function of strain, strain rate, and temperature. The plastic flow of material is described by Johnson–Cook (J–C) model [2] to explain the mechanical behavior of metals at high strain rates and various temperatures. The equivalent flow stress is explained as:

$$\tau = \left(A + B\varepsilon_p^n\right)\left[1 + C\ln\left(\frac{\dot{\varepsilon}_p}{\dot{\varepsilon}_0}\right)\right]\left[1 - \left(\frac{T-T_0}{T_m-T_0}\right)^m\right] \quad (1)$$

$$T = T_0 + \frac{\beta}{\rho c_p}\int \tau\, d\varepsilon_p \quad (2)$$

where ε_p is the average plastic shear strain; $\dot{\varepsilon}_0$ is the reference shear strain rate; $\dot{\varepsilon}_p$ is the imposed shear strain rate; τ is the flow stress; T is the particle temperature; T_0 is the impact temperature; T_m is the melting temperature; β is the work to heat conversion factor (based on empirical assumption 90% of the kinetic energy is dissipated to heat allowing for heat conduction within the particle); $c_p$is the heat capacity; ρ is the density; A, B, C, m and n are material-dependent constants such as: static shear strength, strain-hardening modulus, strain rate sensitive coefficient, thermal-softening exponent and strain-hardening exponent, respectively.

The size of spherical particle is 40 μm. A smooth and two different kinds of roughened substrates were considered for simulation, **Fig. 1**. The material properties are shown in Table 1 [3,4]. Particle impact velocity of 400, 500 and 600 m/s, particle temperature of 400, 500, 600 K and surface roughness of 0, 1.25 and 3 μm were considered.

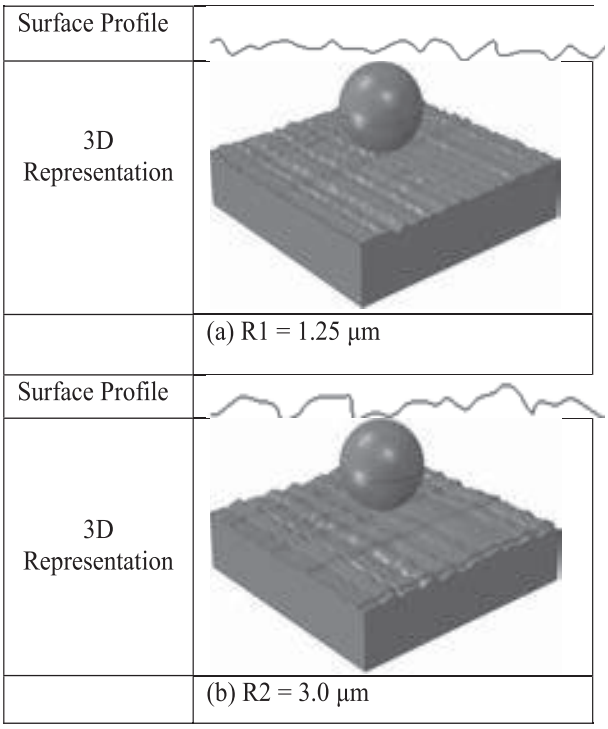

Fig. 1. *Randomly created substrate roughness profiles*

Table 1. Material Properties

Parameter/Material	Al	Cu
Density (kg/m^3)	2710	8960
Young's modulus (GPa)	68.9	124
Poison's ratio	0.33	0.34
Heat capacity (J/kg K)	904	383
Melting temperature (K)	916	1356
A (MPa)	148.4	90
B (MPa)	345.5	292
n	0.183	0.31
C	0.001	0.025
m	0.895	1.09
Reference temperature (K)	293	298
Reference strain rate (1/s)	1	1

2 Result

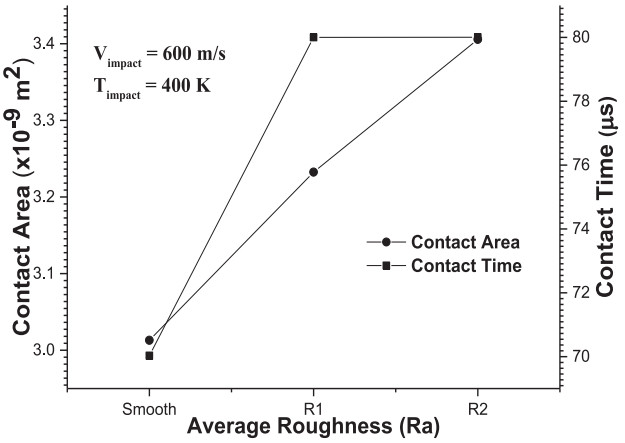

Fig. 2. *Effect of substrate roughness on particle impact time and contact area*

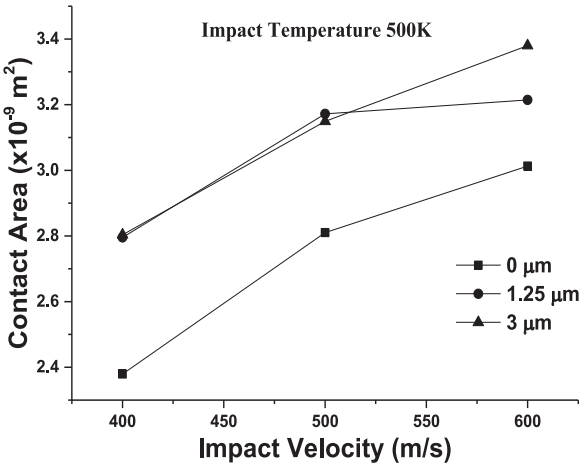

Fig. 3. *Effect of particle impact velocity on contact area*

The contact surface area, contact time and contact temperature influences the bonding strength and bonding mechanism. **Figure 2** shows the variation of contact area and contact time of particle impacting on smooth and roughened copper substrates. It can be observed that the contact area for roughened surfaces is higher than that of smooth surface. The contact time shows an increasing trend with the substrate roughness but for the two roughened surfaces considered there is not much difference. **Figure 3** shows the variation of contact area of particle impacting with different impact velocities on smooth and roughened substrates. It can be seen that increasing impact velocity increases the contact area values and the contact area is higher for roughened surfaces than the smooth surface. **Figure 4** shows the variation of contact area of particle impacting with different temperatures on smooth and roughened substrates. It is observed that there is negligible effect of particle impact temperature on the contact area on smooth and roughened surfaces.

From **Fig. 5**, it can be seen that the interface temperature at deformation increases as the substrate roughness increases. Since more internal energy is dissipated as heat for roughened surface, the interface temperature is observed to be more for the rough surface.

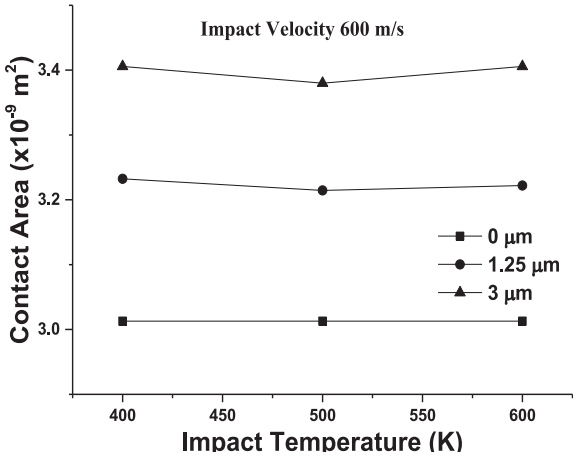

Fig. 4. *Effect of particle impact temperature on contact area*

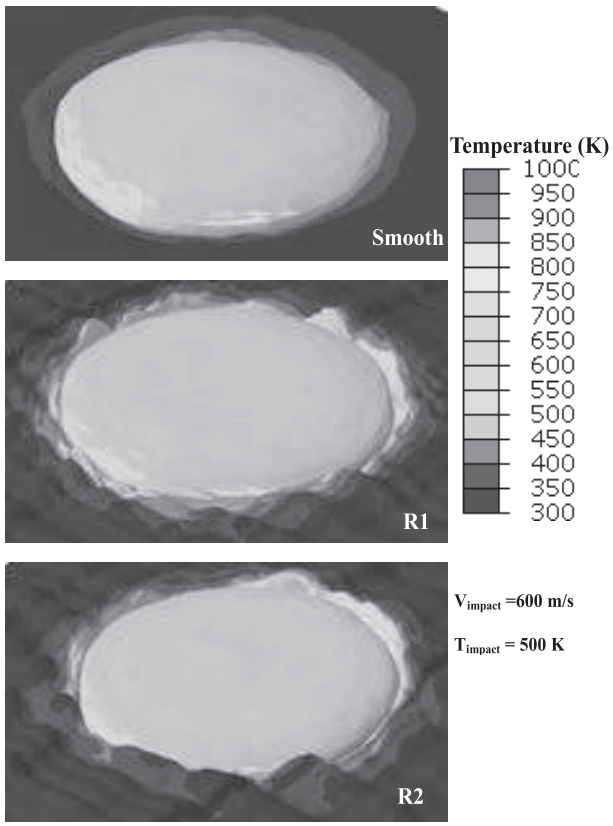

Fig. 5. *Effect of substrate roughness on temperature rise*

3 References

[1] J. Wu, H. Fang, S. Yoon, H. Kim, and C. Lee: Scripta Mater. **54** (2006) pp. 665–669

[2] G.R. Johnson and W.H. Cook: Proc. 7th Int. Symp. on Ballistics, (The Hague, The Netherlands, 1983) pp. 541–48..

[3] M. Fukumoto, H. Wada, K. Tanabe, M. Yamada, E. Yamaguchi, A. Niwa, M. Sugimoto, M. Izawa, J. Therm. Spray Technol. **16** (2007) 643–650.

[4] N.K. Gupta, M.A. Iqbal, G.S. Sekhon, Int. J. Impact Eng. **32** (2006) 1921–1944.

Evaluation of Thermal Cyclic Performance of Rare Earth Oxide Based Thermal Barrier Coatings

S.Karthikeyan[1], V. Balasubramanian[1] and R.Rajendran[2]
[1] Centre for Materials Joining and Research (CEMAJOR), Department of Manufacturing Engineering, Annamalai University, Annamalainagar 608002, India
[2] Gas Turbine Research Establishment, Bengaluru 560 093, India

Abstract
Ceramic based thermal barrier coatings (TBCs) are widely used as insulation materials protecting the underlying metallic structure of a gas turbine blade. A major disadvantage of present ceramic YSZ top coat is the limited operation temperature (1200 ^{0}C) for the long-term application. Zirconate-based TBCs are expected to be the candidate materials for the future application in aircraft, turbine and $La_2Zr_2O_7$ (LZ) is one of the candidate materials that can be used for TBCs. In this paper, single-ceramic-layer (SCL) 8YSZ, LZ and DCL LZ/8YSZ TBCs were fabricated by APS on nickel-based superalloy substrates with NiCrAlY as the bond coat and their thermal cyclic performance was investigated systematically. The results shows that the low thermal expansion coefficient of LZ leads to high thermal stress between the LZ coating and the metallic bond coat, resulting in a short thermal cycling life. The results indicate that the thermal cycling lifetime of LZ/8YSZ TBCs is longer than that of SCL 8YSZ TBCs due to the fact that the DCL LZ/8YSZ TBCs further enhance the thermal insulation effect, improve the sintering resistance ability and relieve the thermal mismatch between the ceramic layer and the metallic layer at high temperature. The failure patterns of the three as-sprayed coatings during thermal shock have been discussed in detail.
Keywords: Yttria stabilized zirconia; Lanthanum zirconate; Plasma spraying; Thermal barrier coatings; Thermal cycling life

1 Introduction

During the last decade, research efforts were devoted to the development and manufacturing of ceramic TBCs on turbine parts as the traditional turbine materials have reached the limits of their temperature capabilities. The typical TBC used in gas turbines consists of a MCrAlY bond coat and a top coat of yttria partially stabilized zirconia made by the atmospheric plasma spraying or electron beam-physical vapor deposition (EB-PVD) [1,]. A major disadvantage of YSZ is the limited operation temperature (1200 ^{0}C) for the long-term application. To overcome the disadvantages of YSZ, the search for candidate materials that can withstand higher gas-inlet temperature has been intensified in the past.

The number of materials that can be used as TBCs is very limited. Among the interesting TBCs candidates, especially those materials with pyrochlore structures and melting points, $La_2Zr_2O_7$ (LZ) shows promising thermo-physical properties. LZ has a lower thermal conductivity than YSZ, LZ has a cubic pyrochlore structure which is stable up to its melting point [2].The concept of multilayer is an effective way to overcome these shortcomings and drove the thermal shock life of TBCs [3]. Hence, this study was carried out to understand the effects of various coating architectures on the thermal cycling life of LZ based coatings, and to correlate the failure mechanism with tensile bond tested specimens. Furthermore, the DCL coatings developed based on TAP melted LZ powders with nickel based super alloy (C263) with an intermediate High velocity oxy fuel (HVOF) sprayed NiCrAlY bond coating system considered in the present investigation is truly unique in nature and has not been tried / reported by others.

2 Experimental

Lanthanum zirconate (LZ) powder with the desired composition was prepared by Transferred Arc Plasma (TAP) melting technique with La_2O_3 and ZrO_2 as the starting materials. The commercial grade 8YSZ powder was used to compare the performance laboratory prepared LZ powder. For the evaluation of thermal cycling behavior of coatings, the considered dimensions of the substrate superni C263 material coupons were 25.4 x 12.7 x 2 mm. After grit blasting NiCrAlY bond coat was deposited to a thickness of 150 µm by HVOF spraying technique.. The ceramic 8 YSZ and LZ coatings were deposited by atmospheric plasma (APS) spraying process. The total thickness of all the coatings, were kept constant at 500 µm. The porosity levels of the ceramic coatings were maintained at 14 vol. % by appropriately modifying the APS process parameters, which are given in Table 1.

Table 1 *APS and HVOF spray parameters*

Parameters	APS		HVOF
	YSZ	LZ	NiCrAlY
Power in kW	24	26	-
Standoff Distance in mm	124	110	210
Primary Gas flow rate (Argon / Oxygen) in lpm	30	30	250
Secondary gas flow rate (Nitrogen / LPG) in lpm	5	3	70
Powder feed rate in gpm	34	37	38
Carrier gas flow rate (Ar / Air) in lpm	5	5	15
Air flow rate in lpm	-	-	950

The thermal cycling test was carried out, using a 1700 ^{0}C automated thermal cycling furnace (Make: VBCC; India, Model: VBTCF-1). The test condition and procedures were followed as per the guidelines provided by the funding agency of this project (Gas Turbine Research Establishment, DRDO, Ministry of Defence, Govt. of India). The coupons for thermal cycling were placed on a zircar plate and inserted directly into the hot zone (150 X 150 mm) having a temperature of 1050 ^{0}C, in which the coupons were exposed to the aforesaid temperature for 45 minutes, followed by cooling the coupons for 15 minutes under forced air cooling arrangement leading to 50 ^{0}C temperature.

This one hour cycle was repeated until an area of 20% of the coating got peeled off and the corresponding number of cycle was recorded as the thermal cyclic life time of the coating.

3. Results and Discussion

The as deposited coatings cross-sectional micrographs of the coatings prepared for duplex and DCL coatings before thermal cycling test are presented in the **Figs. 1 (a-c)**.

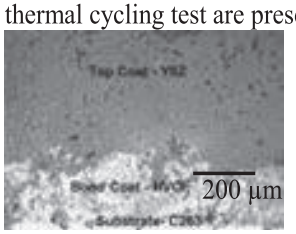

(a) *YSZ coating with bond coat*

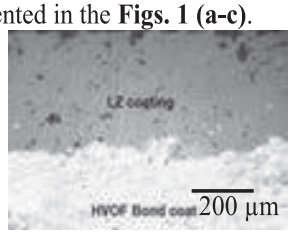

(b) *LZ coating with bond coat*

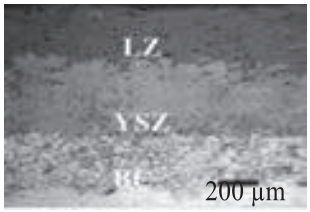

(c) DCL (LZ/YSZ coating with bond coat)

Fig. 1 *Cross sectional microstructure of duplexYSZ, LZ and DCL coatings.*

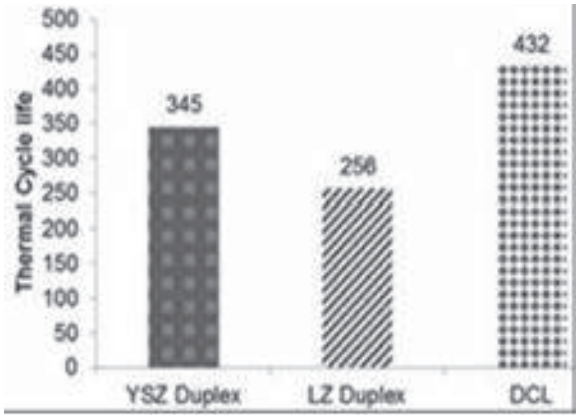

Fig. 2 *Thermal cyclic life of YSZ and LZ coatings*

The duplex YSZ and LZ coatings display a sharp and clear interface between the substrate, BC and the ceramic coat. The double ceramic layered coating also exhibits the same kind of clear interface between the LZ-YSZ interface and YSZ-BC interface as seen in figure.The thermal cyclic lifetimes of the duplex and duplex coatings are shown in **Fig. 2**. From the **Fig. 2,** it can be said that the LZ duplex coatings exhibited the lowest thermal cycling life of 256 cycles and the DCL coating exhibited the highest thermal cycling life of 432 cycles. The thermal cyclic lifetime of YSZ coating was limited due to three main reasons namely, the sintering of splats, phase transformation and thick TGO layer formation [4]. The low fracture toughness of LZ coating leads to the initiation and growth of micro-cracks even with lower stress levels and the low coefficient of expansion leads to the mismatch in coefficient of thermal expansion between the top ceramic layer and the BC [5].

This thermal expansion mismatch results in an increase of residual stresses that can cause the failure of coatings. The double ceramic layered coating survived more number of thermal cycles, compared to the LZ coating, which could be viewed in the graphical illustration shown in **Fig. 3**. Top surface of the thermally cycled double ceramic layered. coating has failed at the interface

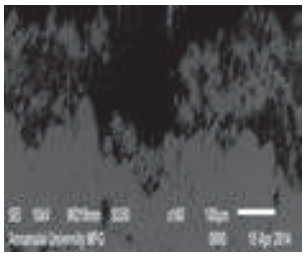

(a) *YSZ duplex coatings*

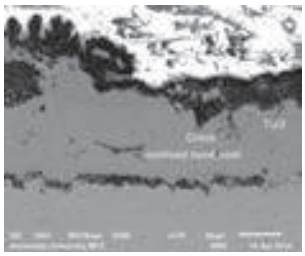

(b*) LZ duplex coatings*

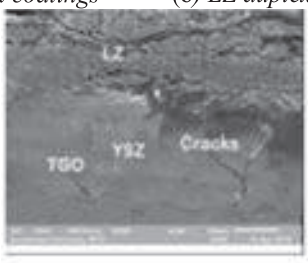

(c) *Duplex YSZ/ LZ coatings*

Fig. 3 *Cross sectional SEM image of thermal cycled coatings*

region of YSZ and LZ. The possible reason for the interface failure is that the top ceramic layer is subjected to a tensile stress during heating [6]. The tensile bond strength of 18 MPa was recorded in the case of the LZ duplex coating; 22 MPa and 28 MPa were the bond strengths of YSZ duplex and DCL coatings, respectively. However, DCL coating shows higher tensile bond strength this will help the coating system to get more intact during thermal cycling test.

4. Conclusions

(i) The double ceramic layered (DCL) coating with YSZ as the intermediate layer between the LZ coat and bond coat (BC) survived 432 thermal cycles, which is 176 cycles higher and 87 cycles higher than those of LZ and YSZ coatings respectively.

(ii) Within the considered coating architecture the DCL coatings provided sufficient toughness and bond strength during thermal cycling.

Acknowledgments

The authors wish to express their sincere thanks to the Aeronautics Research & Development Board (AR&DB), Ministry of Defense, Govt. of India, New Delhi for the financial support extended to carry out this investigation through the sponsored project Lr.No DARO/2031584/2011.

References

[1] W.A. Nelson and R.M. Orenstein: J Therm. Spr. Technlo. **6** (199) 176-180.

[2] X.Q. Cao, R.Vassen, E.Tietz, and D.Stover: J Euro.Cera. Soc. 26 (2006)] 247-251.

[3] Kenta Takagi, Daisuke Kudo, Akira Kawasaki and Yoshio Harada: Surf. Coat. Technolo. **205** (2011) .4411-4417.

[4] Guo Hongbo, Seiji Kuroda and Hideyuki Murakami: J Am. Cera. Soc., **89** (2006), 1432-1439.

[5] Xiaofang Bi, Huibin Xu and Shengkai Gong: Sur Coat. Technolo.**130** (2000) 122-127.

[6] X.Q. Cao, J.Y. Li, X.H.Zhong, J.F.Zhong, Y.F.Zhong: R.Vassen and D. Stover, Mate. Let., 62, (2008) 2667-2669.

Tribological behavior of SiC reinforced Titanium di-Oxide (TiO_2) coating deposited by High Velocity Oxy-Fuel (HVOF) spraying

*R.Sathiyamoorthy[1], K.Shanmugam[2], V.Balasubramanian[3]
[1]Research scholor, [2]Associate Professor, [3]Professor
Centre for Materials Joining and Research (CEMAJOR), Department of Manufacturing Engineering,
Annamalai University, Chidambaram, Tamil Nadu -608 002, INDIA.
*Email: rsmoorthy32@gmail.com

Abstract

Titania or titanium di-Oxide (TiO_2) is a multi functional material having many potential applications, such as medical technology, photo catalysis and wear protection. In this study, Titania and TiO_2+10% SiC coating was deposited on titanium substrate by High Velocity Oxy-Fuel (HVOF) spraying. The Microhardness and porosity of the coatings was measured using Vickers microhardness tester on coating cross section and bond strength was mesured as per ASTM C633. The XRD analysis identifies the rutile as major phase and presence of secondary phases in TiO_2-SiC coating. The tribological behavior of the coatings such as sliding and erosive wear behaviors were evaluated using Pin-on-disk, and Air-Jet Erosion tester respectively. Worn surface morphologies were analysed by SEM and found that the major wear mechanisms are plastic deformation, brittle fracture and micro cutting.

Key words: *Titania (TiO_2), High Velocity Oxy-Fuel (HVOF) Spraying, Sliding wear, Erosive wear*

1.Introduction

Titanium dioxide (TiO_2) or Titania is a very important industrial material attracts much research attention owning to their promising application to photocatalytical, electrical, optical and tribological coatings. Titania has moderate wear resistance mainly due to lower mechanical resistance to deformation, fracture toughness and hardness when compared with other ceramics [1-2]. However, the addition of titania with second phase ultrafine particles selected from the group consist of zirconia, tantalum oxide, boron carbide, silicon carbide(SiC), titanium carbide can improve the wear resistance. Among these SiC offers excellent wear resistane due to its mechanical and chemical stability. In this investigation an attempt has been made to develope Titania (TiO_2) with 10%SiC by High Velocity Oxy-Fuel (HVOF) spray process on titanium substrate and wear behavior of thus developed coatings has been analyased in detail.

2 Experimental

2.1 Thermal spraying

The fused and crushed TiO_2 and SiC powders with size ranging between 10-30µm was employed in this study. The coating was deposited by HVOF spraying on Titanium substrate. The substrate was grit blasted by corundum grits of size 320- 500µm and subsequently cleaned using acetone in an ultrasonic bath and dried. The spraying parameters employed during HVOF deposition were: oxygen flow rate -700 lpm, fuel flow rate- 262 lpm, powder feed rate- 33 gpm, spray distance -220 mm and air flow rate -700 lpm.

2.2 Coating characterization

The cross sectional morphology was analysed using optical microscope. The porosity of the coatings was analysed as per ASTM B276 standard on the polished cross-section of the coating, using optical microscope equipped with image analysing system. The microhardness measurement was made using a Vickers Microhardness tester at a load of 300 g and a dwell time of 15 s. A phase composition of as sprayed coating was characterized by X-ray diffraction (XRD) analysis. The tensile bond strength of the coatings was tested as per ASTM-C633. A commercially available heat-curable epoxy was used as an adhesive to test the coated specimens.

2.3 Wear test

Sliding wear test was carried out using Pin-on-disc configuration under dry sliding conditions as per ASTM G99-04. The Ø40 mm uncoated titanium and coated specimens are pressed on rotating wear disc acted as counter surface against WC pin with normal load 30 N. The total sliding distance and sliding speed was 500 m, 300 rpm respectively.

The solid particle erosion test was performed in air jet erosion test rig as per ASTM G76. In this rig Al_2O_3 particle size 50 µm was used as erodent. The particles hits the surface at an impact angle 60° with an impact velocity 60 m/s and particle flux 3 gpm. The 25x25 mm samples were cleaned in acetone, dried, weighed to an accuracy of 0.1mg using an electronic balance, eroded in the test rig for 120 s and then weighed after erosion to determine weight loss.

3 Results and Discussion

Fig 1 (a) shows the SEM morphology of TiO_2 with 10% SiC feed stock, which is irregular having some ultrafine particles. Fig 1(b) shows the cross section of the coating, which present the partially or unmelted particles embedded in the coating matrix. The melting point of the titania (1850 °C) is lower than SiC, therefore during spraying SiC particles were agglomerated with melted titania particles and deposited over the titanium substrate. The porosity, microhardness and bond stregnth of the coating are shown in Table 2. The coating has low porosity level (<2%), high hardness and bondstregnth. It is thought that high impact velocity of the sprayed particles is one of the main factors producing low porosity level, inter-splat cohesion and substrate adhesion [3]. The crystalline phases of SiC are evident from the XRD pattern shown in fig-3. XRD patter confirms presence of TiC and SiO_2 second phases exist in the XRD pattern [4].

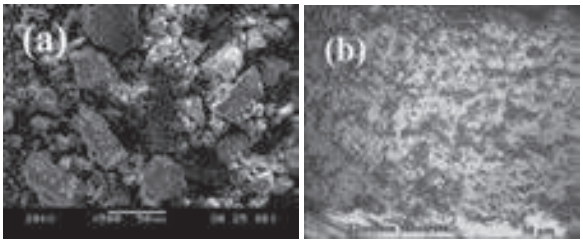

Fig.1. SEM Morphology of TiO_2+SiC feed stock and coating cross section

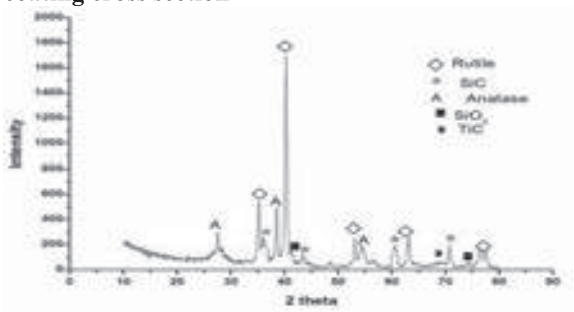

Fig.2. XRD Pattern of TiO_2+10% SiC coating

3.2 Tribological performance

Table 3 shows the sliding and erosive wear loss of titanium and coating. The wear resistance of TiO_2 has improved by incorporation of SiC with Titania coating matrix . The higher wear resistance of 10% SiC coating is due to higher hardness and bond stregnth of the coating. The observed difference of wear rates of TiO_2 with TiO_2 +10% SiC is the presence of hard phases such as SiC and TiC in the coating which act as load bearing component inhibit plastic deformation and wear. The wear surfaces were analysed by SEM, inorder to understand the wear mechanism of titanium substrate and coating. Fig 3(a) shows the worn surface morphology of titanium surface, The mechanism of wear in titanium is oxidative wear and adhesive wear, the uncoated Titanium shows very high wear rate which may be associated with the preferential transfer of titanium to WC counterface, this was typical adhesive wear [5]. Titanium is chemically active and have a high ductility which gives rise to the strong tendency to adhesion which is well suited with this study[6].

Fig 3(b) shows the SEM morphology of worn surface of coating, it appears to be smooth without many grooves. The wear track shows less wear mode, where plastic deformation and surface polishing are the preferred wear mechanism. It could also be seen that the well adhered tribofilm on the worn surface which is formed by strongly deformed wear debris generated during continuous sliding. These fine particles disperse between the ceramic coating and counterface and act as a bearing agent which can not only bear the applied load but also prevents direct contact results in a decrease in wear rate [7]. Fig 4 (a) shows the SEM morphology of titanium eroded surface, at the impact location, a hard erodedent cuases plastic flow and material removal by microcutting and microploughing. Very high level of shear strain might have produced in the material at the impact location. When shear strain exceeds the elastic strain limits, the particle penetrates the surface of material and plough along the surfaces removing materials. The mechanism of wear in titanium surface is plastic deformation and subsequently removed by cracking [8]. SEM examination of the coating eroded surface (Fig 4b) shows the lateral cracking which results in grain ejection. So the material removal at isolated impact sites is primarily by grain ejection and chipping at the edge of the craters [9].

Table.2. Porosity, microhardness and bond stregnth

Coating	Micro-hardness ($HV_{0.3kg}$)	Porosity (%)	Bond stregnth	
			Tansile	Lapshear
TiO_2 + 10%SiC	958	1.12±0.2	29±3	54±4
TiO_2	858	1.86±0.3	19±2	41±4

Table.3.Wear rate

Wear testing	Titanium (mg/s)	TiO_2+SiC (mg/s)	TiO_2 (mg/s)
Dry sliding	$4.3\ E^{-3}$	$1.4\ E^{-3}$	$3.1\ E^{-3}$
Erosion	$5.3E^{-5}$	$2.8E^{-5}$	$4.2\ E^{-5}$

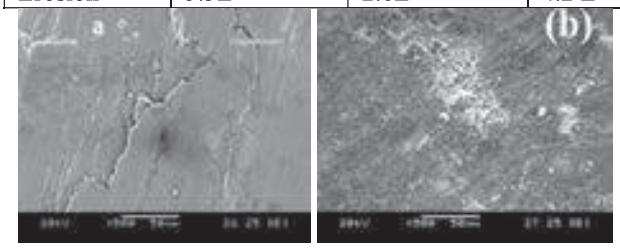

Fig.3. SEM morphology of worn surface

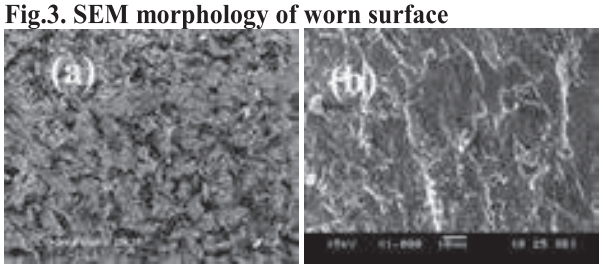

Fig.4.SEM morphology of eroded surface

3 Conclusions

Titania and SiC reinforced Titania coating was deposited by HVOF spraying on Ti substrate. The addition of SiC in TiO_2 coating matrix enhances mechanical properties and wear resistance of coating. On titanium substrate, adhesive wear is predominant mechanism under sliding wear conditions, where as coatings, plastic deformation and brittle fractrue are dominant. The erosive wear mechanism in titanium is plastic deformation and in coating is plastic deformation, plastic grooving and brittle failure.

4 References

[1] R.S. Lima, Materials and Design 29 (2008) 1845–55.
[2] Kim GE, Walker J. Jounnal of Therm Spray Technology 2007;16(1):34–39.
[3] B.R. Marple, ASM International, JTTEE5 12:360-369.
[4] S.H. Alavi, Int. J of Modern Physics:5 (2012) 598–606.
[5] S.M.Hsu. Tribology International 1997;30: 377–383.
[6] H. Dong, T. Bell, Wear 238 (2000) 131–137.
[7] C.S. Ramachandran, V. Balasubramanian, Materials and Design 39 (2012) 234–252.
[8] G. Sundararajan, Wear 149 (1991) 111–127.
[9] P.Bansal, , Acta Materials: 51 (2002) 2959-2970.

Comparison of Abrasive Wear of HVOF & D Gun Sprayed WC-Ni Coatings on Aluminium Alloy

M. Bharath Kumar, G. Krishna Mohana Rao, S. Gokul Laxmi*, G. M. Reddy* and Manish Roy*

Jawaharlal Nehru Technological University,
Kukutpally, Hyderabad: 500085, India

Defence Metallurgical Research Laboratory
PO: Kanchanbagh, Hyderabad: 500058, India

ABSTRACT

An important ongoing programme is to develop light weight clutch plate for aeronautical applications. In order to achieve this objective present work is undertaken to develop Al alloy based clutch plate with suitable surface modification. In this investigation the surface of aluminium alloy is coated with thermal sprayed WC-CO coating one by using "HVOF" and other using "D Gun" system. The microstructural features and mechanical properties of the modified surfaces are characterised extensively. The abrasive wear rates of the modified surfaces are determined for different applied load. The worn surfaces are examined under scanning electron microscopes. The abrasive wear rates of the modified surfaces are correlated with various mechanical properties. The results show that abrasion action takes place by both particle rolling and particle sliding. Fracture of particles during abrasion increases wear rate. In general, the abrasive wear rates of both types of modified surfaces are nearly equal. At a given abrasion mechanism abrasive wear rate correlates well with the hardness of the modified surfaces.

Introduction: Thermal spray is a processes where metals, ceramic, cermet and selected polymeric materials are fed in the form of powder, wire and rods to a torch where fed materials get heated or melted, accelerated in the gas stream towards a substrate and form a splat on the substrate. Thermal spraying is an important technique to modify the surfaces especially by laying a hard coating in relation to degradation of surfaces due to action related to tribology. An important ongoing programme is to develop light weight clutch plate for aeronautical applications. In order to achieve this objective present work is undertaken to develop Al alloy based clutch plate with suitable surface modification. In this investigation the surface of aluminium alloy is coated with WC-Ni layer by using high velocity oxy fuel (HVOF) and detonation spraying (D Gun) system.

Experimental: Aluminium alloy 7017 was coated with WC-Ni layer employing HVOF and D-Gun spraying. The microstructural features of the modified surfaces are characterised extensively with the help of optical microscopy and X-ray diffractometer. The mechanical properties were determined using a microhardness tester. The abrasive wear rates of the modified surfaces are determined for different applied load employing a commercially available dry sand, rubber wheel (DSRW) abrasion test apparatus as per ASTM standard (G65). The abrasive wear rate is defined as the ratio of the mass loss suffered by the test specimen to the mass of the abrasive responsible for the mass loss of the test specimen. The test was conducted till the abrasive wear rate reached a constant value with respect to the mass of abrading particle. The worn surfaces are examined under scanning electron microscopy. Transverse sections of the worn surfaces are also observed under SEM.

Results and discussion: The variation of the incremental abrasive wear rate as function of cumulative mass of abrasives is presented in Fig. 1. For both varieties of coatings the abrasive wear rate reaches the steady state value from initial high value. It is also clear that the abrasive wear rate of detonation sprayed WC-Ni coating is higher than that of HVOF sprayed coating. The influence of load on the abrasive wear rate is illustrated in Fig. 2. As expected abrasive wear rate increases with increase of applied load. This increase is linear and moderate in case of HVOF sprayed coating. In contrast, such increase is quite abrupt in case of detonation sprayed coating particularly at high load. Such change of load dependence of abrasive wear rate can be attributed to the fact that there is particle fracturing in case of detonation sprayed coating at higher load. The morphology of the surfaces worn at 13 kg load for HVOF and detonation sprayed coating are given in Fig. 3. Abrasion marks can be seen of detonation sprayed coating but not on HVOF sprayed coating.

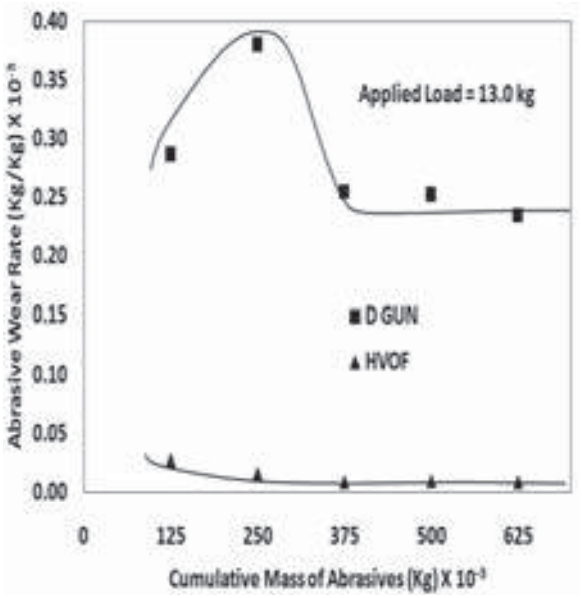

Fig.1: *Variation of the incremental abrasive wear rate as function of cumulative mass of abrasives*

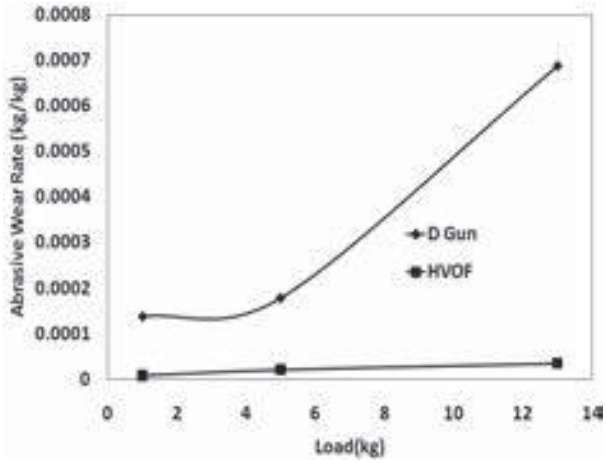

Fig. 2: *Influence of load on the abrasive wear rate*

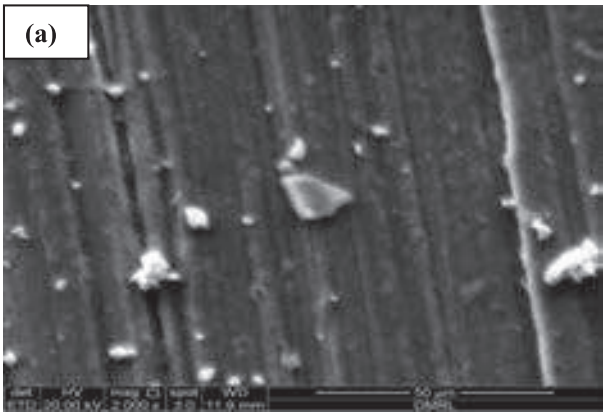

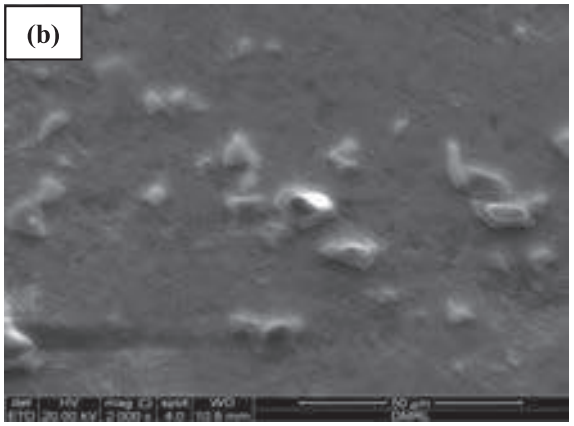

Fig. 3: *Morphology of abraded surfaces of a) detonation sprayed coatings and b) HVOF coating*

Conclusions:

1) HVOF sprayed coating has lower abrasion rate than detonation sprayed coating.
2) Particle fracturing is responsible for higher abrasion rate and abrupt increase of abrasion rate of detonation sprayed coating.

PREPARATION AND CHARACTERIZATION STUDY OF LANTHANUM ZIRCONATE BY BALL MILLING METHOD FOR PLASMA SPRAYING

S. Sivakumar, K. Praveen, and G. Shanmugavelayutham*
Plasma Physics Laboratory, Department of Physics, Bharathiar University,
Coimbatore – 641 046, India
*E-mail: velu1976@yahoo.co.in

Abstract

Thermal barrier coatings (TBCs) are one of the most advanced high temperature protective coatings and being widely used in aeronautics, astronautics, motor industry and heat power station for their good performance like thermal barrier and oxidation resistance. Recently yttria partially stabilized zirconia (8YSZ) is used as the commercial materials for TBCs applications. However, the major disadvantage of YSZ is the limited operation temperature about 1200°C for the long-term application. It is terminate us to identify new and novel materials that can work at higher temperature. Among the interesting candidates for TBCs, Lanthanum Zirconate ($La_2Zr_2O_7$, LZ) has been proposed as a promising TBCs material for its high melting point, more stable structure and lower thermal conductivity than YSZ. In the present work, Lanthanum Zirconate ($La_2Zr_2O_7$) was synthesized by the method of planetary ball milling. For typical synthesis, the mixture of La_2O_3 and ZrO_2 powders with 1:2 mole ratio were ball milled for 24 h. Subsequently, the structural, phase formation and morphological features were analyzed by XRD and FE-SEM. Further analysis will be carried to optimize the suitable reaction condition for TBCs applications.

Keywords: DC plasma torch, $La_2Zr_2O_7$, High temperature protective coatings

Introduction

Pyrochlore-type $La_2Zr_2O_7$ is one of the rare earth zirconate and well-known of its catalytic properties, high melting point (2300 ºC), good phase stability, low thermal conductivity (1.56 W m^{-1} K^{-1}), not oxygen-transparent and very low sintering ability [1,2]. It has a cubic pyrochlore structure which allows operation temperature up to 2200 ^{0}C before any phase transformation occurs [3,4]. In view of these remarkable properties, this rare earth oxide has recently found many interesting industrial applications including thermal barrier coating (TBC) [5]. The synthesis of $La_2Zr_2O_7$ has been achieved by many methods.

Experimental Procedure

In this work, commercially available lanthanum oxide (La_2O_3) and zirconium oxide (ZrO_2) were used as raw materials to prepare lanthanum zirconate. The mixture of La_2O_3 and ZrO_2 in the mole ratio of 1: 2 was milled for 24 h with corundum ball mill media by using planetary mill (Insmart, India). The ball to powder weight ratio was maintained at 10:1. The volume of the jar was around 250 ml. The milled powder were sintered at various temperatures 1100 ^{0}C and 1400 ^{0}C for 4 h using an electric furnace.

$$La_2O_3 + 2ZrO_2 \rightarrow La_2Zr_2O_7$$

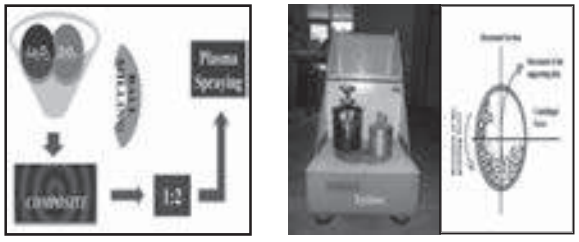

Fig. 1 Experimental set-up in a planetary ball milling

Characterization

The crystal structure and phase purity of the LZ powders were examined by X-ray Powder Diffraction (XRD). The overview of the morphology was analysed by using Field Emission Scanning Electron Microscope (FE-SEM).

Results and discussion

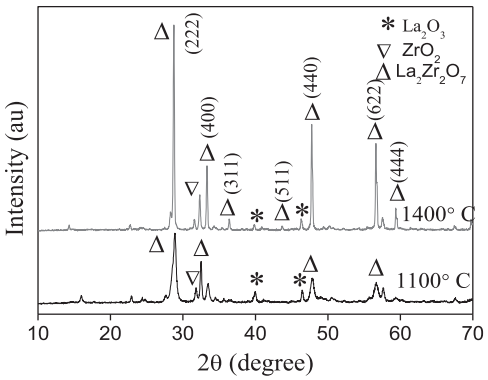

Fig. 2 XRD profiles of the powders after sintering at 1100 ^{0}C and 1400 ^{0}C for 4 h

Fig. 2 shows the XRD patterns of the samples prepared at1100 ^{0}C and 1400 ºC for 4 h, to determine the crystalline phases. It is reported in Ref. [4] that the binary oxides of rare earths with zirconia have two types of structures, i.e. pyrochlore and fluorite. The fully crystallized LZ as a pyrochlore structure which is very similar to that of the fluorite structure and the two weak peaks of 2θ between 36º peak of [3 3 1] and 46º peak of [5 1 1] are the indication of pyrochlore structure [5,6]. Which implied that LZ powders had a phase-transition when the temperature reached to 1400 ºC. The diffraction peaks can be readily indexed to the pyrochlore crystal system $La_2Zr_2O_7$ (JCPDS: 73-0444). As shown in the magnified peak of [2 2 2] and [4 0 0] the peaks of LZ powders shift

to the low degree side with the increase of temperature, implying that the lattice parameter increases with the increase of the nano-grain size.

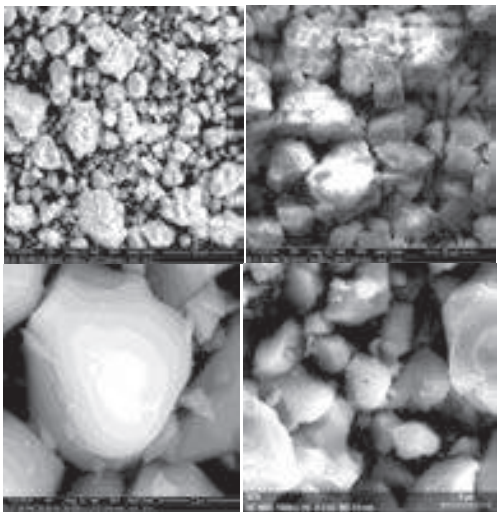

Fig.3 SEM image of $La_2Zr_2O_7$ powders sintering at 1400 ºC for 4 h

The morphology of as-prepared $La_2Zr_2O_7$ particles has a blocky irregular shape (Fig. 3). It is also interesting to see that each particle surface contains a large number of pores [7].

Conclusions

Lanthanum zirconate was successfully synthesized by ball milling method. This method is easier, low cost and simplicity which is dominant the other methods of synthesis. The synthesis condition for Lanthanum zirconate is optimized and its morphological analysis implies that after milling the size of the particles are reduced greatly. By further processing, the process parameters can be optimized such that it can be used for the application of thermal barrier coating using the same method. We can use this composite which acts as a good thermal barrier on the coated material.

The $La_2Zr_2O_7$ powders were successfully prepared by Ball Milling method at a relatively low temperature. The mixture of La_2O_3 and ZrO_2 was believed as flux in the reaction, which could decrease activation energy of the reaction. SEM results indicate the obtained $La_2Zr_2O_7$ nano-crystals were polycrystals. The procedure is facile and suitable for the synthesis of $La_2Zr_2O_7$ powders, and the most important thing is that it will be an excellent method for the preparation of other pyrochlore type of rare earth zirconate ($Re_2Zr_2O_7$, Re = rare earth).

Acknowledgement

This work was financially supported by the project of the Department of Science and Technology (DST-SERB), New Delhi, India.

References

[1]. Zhenhua Xu, Xinghua Zhong, Jiangfeng Zhang, Yanfei Zhang, Xueqiang Cao, Limin He, Surf. Coat. Technol. 202 (2008) 4714-4720.

[2]. L. Wang, Y. Wang, X.G. Sun, J.Q. He, Z.Y. Pan, L.L. Yu, Powder Technol. 212 (2011) 267-277.

[3]. S. Yugeswaran, Akira Kobayashi, P.V. Ananthapadmanabhan, L. Lusvarghi, Current Applied Physics, 11 (2011) 1394-1400.

[4]. M.A. Subramanian, G. Aravamudan, G.V.S. Rao, Prog. Solid State Chem. 15 (1983) 55.

[5]. G. Shanmugavelayutham, V. Selvarajan, S. Yugeswaran, M. Vijay K. Suresh, S. Vijeyakumar, L. Markkandan and P.V.A. Padmanabhan, Composite Interfaces, 19 (2012) 239–249.

[6]. X.Q. Cao, R. Vassen, W. Fischer, F. Tietz, W. Jungen, D. Stoever, Adv. Mater. 15 (2003) 1438.

[7]. H.M. Zhou, D.Q. Yi, Z.M. Yu, L.R. Xiao, J. Alloys Compd. 438 (2007) 217.

[8]. S.T. Aruna, C. Sanjeeviraja, N. Balaji, N.T. Manikandanath, Surf. Coat. Technol. 219 (2013) 131-138.

Thermal Conductivity of the Atmospheric Aluminum Nitride Coatings

Mohammed Shahien[1,3], Motohiro Yamada[1], Masahiro Fukumoto[1], Kazumi Egota[2], Kenji Okamoto[2]
[1] Department of Mechanical Engineering, Toyohashi University of Technology, Toyohashi 441-8580, Japan
[2] Fuji Electric Co.,Ltd., Hino 191-8502 , Japan
[3] Currently Central Metallurgical Research and Development Institute, CMRDI, Helwan 11421 Cairo, Egypt

Abstract
Reactive plasma spraying (RPS) is a promising technology for *in-situ* formation of aluminum nitride (AlN) thermal spray coatings. Recently, thick AlN/Al_2O_3 (Alumina) composite coatings were successfully fabricated through RPS of Al_2O_3/AlN mixture powders in N_2/H_2 plasma under the atmospheric ambient. This study will focus on the evaluation of the thermal conductivity of the fabricated AlN coatings. The thermal conductivity of the caotings were low compared to the AlN value. It is related to the phase composition of the coatings, oxide content and porosity. Thus, the presence of Al_2O_3, Al_5O_6N and the high coating porosity decreased the thermal conductivity. Furthermore, the coating density is lower than the AlN value, which suppressed the coatings thermal condutivity. In addition, although the N_2 gas flow improved the nitride content, it suppressed the thermal conductivity gradually, due to the further decrease in the coating density and increasing its porosity with the N_2 gas.

1 Introduction

Aluminum nitride (AlN) is outstanding ceramic material for several electrical and electronic applications. It is attributed to its high thermal conductivity, dielectric properties and unique mechanical properties [1]. On the other hand, thermal spraying is a versatile technique for producing abradable and protective thick ceramic coatings. However, it has been impossible to fabricate AlN coating by conventional thermal spray processes directly from AlN feedstock powder due to the thermal decomposition of AlN particles during spraying without a stable melting phase.
In order to fabricate AlN thermal sprayed coatings, the solution was using the reactivity of thermal plasma which is usually used to melt and accelerate the spray materials. Reactive plasma spraying (RPS) has been considered as a promising technique for *in-situ* formation of AlN thermal sprayed coatings [2-4]. The process is based on the reaction of molten particles (metallic or non-metallic materials) with the surrounding active species in the plasma such as atom, ion and radical. In our previous studies [4], it was possible to fabricate AlN based coatings with high nitride content through the RPS of Al_2O_3/AlN mixture and controlling the reaction process. This study will focus on the evaluation of the thermal conductivity of the reactive plasma sprayed AlN coatings and studying the effect of process parameters on the thermal conductivity.

2 Experimental Procedures

All the spray experiments were carried out by the atmospheric plasma spray system (APS: 9MB, Sulzer Metco, Switzerland), using N_2 and H_2 as plasma gasses. The spray conditions are shown in details in the previous sudy [4], the flow rate of the N_2 plasma gas varied from 100 to 160 SCFH (standard cubic feet per hour) with keeping its pressure at the standard conditions of 330.9 kPa. The H_2 plasma gas was kept at the standard condition of 5 SCFH and 344.7 kPa. The spray distance was kept at 150 mm from the gun exit. The feedstock powder is spray-dried fine 60 wt.% Al_2O_3 and 40 wt.% AlN mixture, its details are described before [4].
The thermal conductivity sample was prepared on pure copper (Cu) substrate, in a disk shape with a diameter of 10 mm and thickness about 0.5 mm. The thermal conductivity, thermal diffusivity and specific heat of the coatings were measured by Laser Flash method using the LFA 447 Nanoflash® instrument, (NETZSCH, Inc., Germany). Figure 1 shows the schematic diagram of the measurement process. The measurement is basically done through the following equation:

$$\lambda = \alpha \rho Cp \quad (1)$$

where:
λ= thermal conductivity (W/m.K), ρ= density (Kg/m^3)
α = thermal diffusivity (m^2/s), Cp = specific heat (J/Kg.K)

The specific heat capacity or specific heat, Cp, was measured using a differential scanning calorimeter (Perkin-Elmer Co., DSC-7) comparative method, in the temperature range of 100-1000 ºC with increasing rate of 10 ºC/min in dry N_2 atmosphere. The specific heat of the material is defined as:

$$Cp = Q/m\Delta T \quad (2)$$

Where: Cp = specific heat (J/Kg.K),
m = mass, ΔT = change in the temperature.

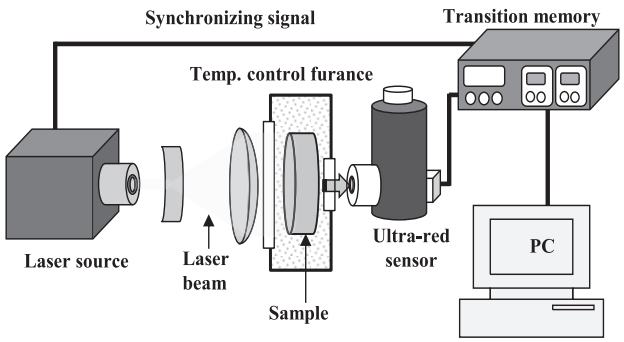

Fig. 1. *Thermal conductivity measurment sketch.*

The specific heat was measured by comparing the temperature rise of the sample to the temperature rise of a reference sample (sapphire: α-Al_2O_3) of known specific heat tested under the same conditions. The sample bulk density is normally calculated from the measured sample volume (calculated from the measured sample dimensions) and mass by using the Shimadzu Co. electronic balance (AuW120D) at 25ºC. The phase compositions of the fabricated coatings were verified by X-ray diffraction

(XRD: RINT-2500, Rigaku, Japan). A scanning electron microscope (SEM: JSM-6390, JEOL, Japan) was used to observe the cross-section microstructure of the fabricated coatings. The coating porosity was estimated by image analysis of SEM cross-sections.

3 Results and Discussion

Figure 2 shows the thermal conductivity and density of the fabricated coatings as function of the N_2 plasma gas flow rate. It is clear that, the thermal conductivity of the coatings is very low compared to the AlN sintered compacts. Moreover, the further increase in the N_2 gas flow rate suppressed the coatings thermal conductivity. The low thermal conductivity of the fabricated coatings is mainly attributed to several factors; the coating phase composition, oxide content and porosity. Thus, the fabricated coating consists of cubic-AlN (*c*-AlN), hexagonal-AlN (*h*-AlN), aluminum oxynitride (Al_5O_6N), γ-Al_2O_3 and small content of α-Al_2O_3 phases as shown in details in the previous study [4]. The presence of such large amount of alumina significantly lowered the AlN thermal conductivity due to its low conductivity. Furthermore, the formation of relatively large amounts of oxynitride phase in the Al_2O_3-AlN system, which has lower thermal diffusivity compared even with the Al_2O_3 itself, leads to further decrease in the fabricated coating thermal conductivity. Thus, the presence of oxygen is the principle impurity in the AlN industry, which may leads to phonon scattering and therefore a decrease in thermal conductivity of the polycrystalline AlN.

Furthermore, Fig.2 also shows the measured values of the coatings density. It is clear that, the values are lower than the AlN value (3.16 g/cm^3) and gradually decreased with the N_2 gas flow. This can also clarify the extreme low thermal conductivity of the fabricated RPS AlN coatings and its further decrease with the N_2 gas flow rate.

On the other hand, Figure 3 shows the the SEM cross-section microstructure of the fabricated coating at N_2 gas flow of 100 SCFH. It is clear that, the coating is approximately 500 μm thick with a uniform and porous structure. The porosity of the coating was estimated by image analysis of SEM cross-section. The coating has about 20 % porosity, which led to further decrease in the coating thermal conductivity.

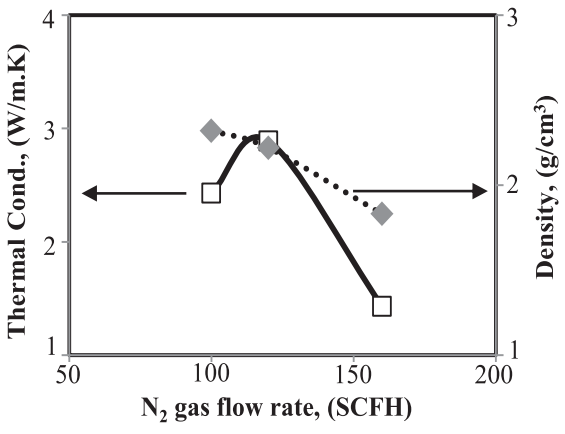

Fig. 2. *Thermal conductivity and Density Vs N_2 gas flow.*

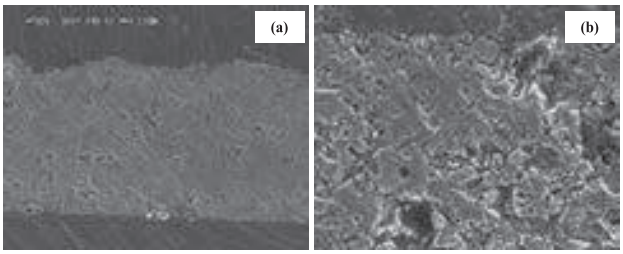

Fig. 3. *The fabricated coating cross-section microstructure.*

Thus, it is well known that, the plasma sprayed coating thermal conductivity is significantly lower than that of the corresponding bulk material. It is attributed to, the higher thermal resistance due to interlamellae boundaries, porosity, and microcracks parallel to the coating plane. Thus, the plasma sprayed coating consists of highly anisotropic layered structure with individual splats oriented parallel to the substrate surface, which lowered the thermal conductivity. It is related to the interfacial thermal contact caused by pores or secondary phases. Thus, the crystal lattice wave and heat wave are the main media through which the heat is transported in the ceramic materials, and dispersion as well as interference of the wave result from the pores and cracks in the coating lower its thermal conductivity.

The further decrease in the coatings thermal conductivity with increasing the N_2 gas flow rate can be explained as follow: Although the N_2 gas flow improved the nitriding conversion and therefore the AlN content in the coatings [3, 4], the coating porosity gradually increases with increasing N_2 gas flow rate, as shown before [4]. Therefore, the thermal conductivity decreased with the further increase in N_2 gas flow rate. Increasing the porosity with the N_2 gas is related to the increasing particle velocity with the N_2 gas. Thus, increasing particle velocity shortened the particle residence time in the plasma and leads to worse melting behavior of the powder in the plasma, which significantly affects the coating porosity. Besides that, increasing the N_2 gas flow in the RPS process enhanced the reaction tendency between the particles and the surrounding plasma, which leads to increasing the coating porosity. Further studies are under progress to increase the coating thermal conductivity based on theses current results.

4 Conclusions

The RPS AlN coating thermal conductivity was investigated as function of the N_2 plasma gas. It was clear that, not only the AlN content and its distribution are the required to get high thermal conductivity coatings. But also adjusting the oxide content and the coating porosity are required.

5 References

[1] H. O. Pierson, *Handbook of Refractory Carbides and Nitrides*, Noyes Publications, New Jersey, USA, 1996, pp. 237-239.

[2] M. Shahien, M. Yamada, T. Yasui and M. Fukumoto: J. Therm. Spray Technol. **20-3** (2011) 580-589.

[3] M. Shahien, M. Yamada, T. Yasui and M. Fukumoto: Surface and Coatings Technol. **216** (2013) 308-317.

[4] M. Shahien, M. Yamada, T. Yasui and M. Fukumoto: J. Therm. Spray Technol. **22-8** (2013) 1283-1293.

Hot corrosion behaviour of Cr_3C_2-(NiCr)+0.2wt.%Zr coated Superalloys under actual medical waste incinerator environment at 1050°C

Deepa Mudgal, Surendra Singh, Satya Prakash
Department of Metallurgical and Materials Engineering Indian Institute of Technology, Roorkee, Uttrakhand, India 247667

Abstract
Incineration techniques are widely used to dispose of various types of waste which lead to formation of very corrosive environment. Such corrosive environment leads to the degradation of the alloys in the incineartor. To obviate this problem, zirconium doped Cr_3C_2-(NiCr) coating powder has been deposited on three superalloys namely Superni 718, Superni 600 and Superco 605 using Detonation gun technique. Corrosion test were conducted in actual medical waste incinerator environment. The samples were hung inside the secondary chamber operated at 1050°C for 1000h under cyclic condition. Corrosion kinetics was monitored using the weight gain measurements and thickness loss. Corrosion products were characterized using scanning electron microscopy, energy dispersive spectroscopy and X-ray diffraction technique. It was observed that coating is found to be successfull in impeding the corrosion problem of superalloys in the incinerator environment.

1 Introduction

In last 20 years, developing countries have adopted incineration technique to dispose off the high volume of industrial, medical and municipal waste because of its advantage of being one of the effective and hygienic methods of disposal. For example, in Western Europe, the number of incinerators are constantly increasing apart from having almost 600 running plants [1]. However, the degradation of boiler material due to the usage of different types of waste such as biomass and solid waste fuels has been frequently encountered during the operation which is one of the major causes of unwanted shut down. The major species responsible for the corrosion problems are presence of chlorine and hydrogen chloride gases either as reactants, products, by-products or as contaminants. These problems generally arise in chemical and metallurgical industries such as coal-fired boilers, waste incinerators, plastic/polymer decomposition mills, vinyl chloride monomer mills, and recuperators[2-4]. The complex and corrosive nature of the incinerator environment coupled with high temperatures can lead to premature failure of various metallic components in an incinerator[5]. Hence in the present study, zirconium incorporated chromium carbide nickel chromium coating which was deposited using D-gun technique on different alloys were tested under the actual medical waste incinerators environment. The most corrosive area of incinerator was chosen for the study. The specimens were hung inside the secondary chamber of the incinerator where the temperature was 1050C±50°C. The specimens were exposed for 1000h where each cycle consists of 100h heating followed by 1h cooling.

2 Experimentation

Three superalloys viz. Supeni 718, Superni 600 and Superco 605 were procured from MIDHANI, Hyderabad, in hot rolled and annealed condition in the form of plates. The specimens of size 20×15×5 mm were cut down from the plates. The specimens were coated with 0.2wt.%Zr doped Cr_3C_2-NiCr coating power using Detonation gun technique at SVX Powder M Surface, Greater Noida, India. The specimens were coated from all the six surfaces. The specimens were drilled with a hole to hang inside the incinerator using Kanthal wire. For corrosion test the specimens were hung inside the secondary chamber of medical waste incinerator for 1000h under cyclic condition. Each cycle consisted of 100h heating followed by 1h cooling in ambient air. After 1000h, thickness loss measurments were done to know the corrosion rate in mpy.

2.1 SEM/EDS

Scanning electron microscopy analysis showed the morphology of oxide on the surface of the coating after 1000h exposure. EDS has been done to know the elements present in the oxide scale. In case of Cr_3C_2-(NiCr) +0.2wt.%Zr coated Superni 718 (Fig.1),spongy type massive oxide was observed on the surface of corroded specimen. EDS analysis indicated the existence of chromium and oxygen in major amount along with minor amount of sodium, sulphur, calcium, iron and zinc. Traces of aluminium, chlorine and potassium were also detected. Whereas in case of Cr_3C_2-(NiCr) +0.2wt.%Zr coated Superni 600 (Fig.2), dense and compact oxide was seen along with the cracked melted particles on the surface. EDS analysis indicated the presence of chromium, nickel and oxygen throughout the surface of the corroded coating. EDS analysis detected the presence of chlorine at the sites of melted particles. In case of Cr_3C_2-(NiCr) +0.2wt.%Zr coated Superco 605 (Fig.3), two different type of morphology were observed. White colour clustsres morphology showed the presence of sodium, sulphur, calcium, chromium and oxygen. Whereas platelet like spongy morphology indicated the presence of chromium and oxygen in major amount with minor amount of nickel and zinc. Traces of sulphur were also detected.

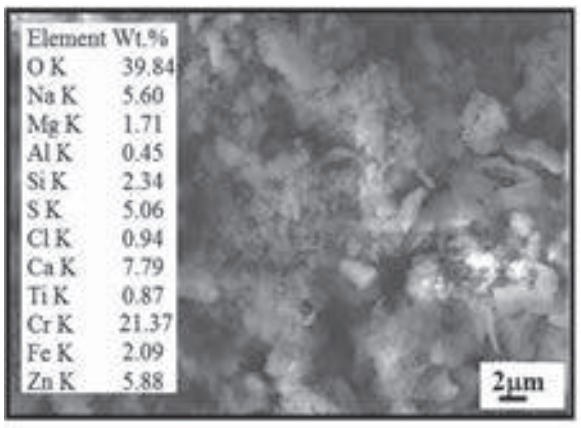

Fig. 1. SEM/EDS for Cr3C2-NiCr+0.2wt.%Zr coated Superni 718 after corrosion under medical waste incinerator.

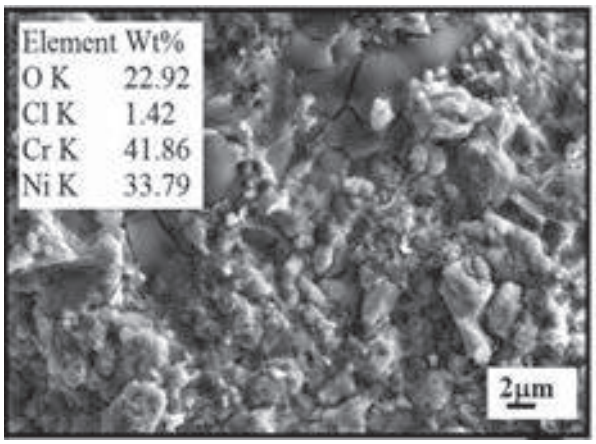

Fig.2 SEM/EDS for Cr_3C_2-NiCr+0.2wt.%Zr coated Superni 600 after corrosion under medical waste incinerator.

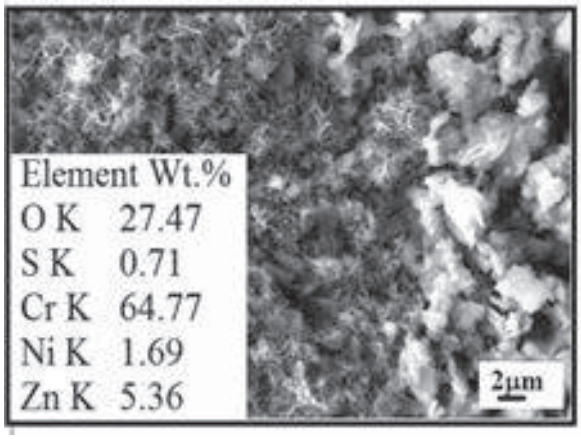

Fig. 3. SEM/EDS for Cr_3C_2-NiCr+0.2wt.%Zr coated Superco 605 after corrosion under medical waste incinerator.

2.2 XRD analysis

The XRD profiles for the scale of Cr_3C_2-(NiCr) +0.2wt%Zr coated Superni 718, Superni 600 and Superco 605 are shown in Fig.4. In case of Cr_3C_2-(NiCr) +0.2wt%Zr coated Superni 718 and Superni 600, the common major peaks identified after hot corrosion under incinerator environment are Cr_2O_3, $ZnCr_2O_4$, K_2ZnCl_4, $NiCr_2O_4$, $CaAl_2SiO_6$, $NiCl_2$ and $CaSO_4$. Whereas in case of Cr_3C_2-(NiCr) +0.2wt%Zr coated Superco 605, the peaks identified after hot corrosion in the actual incinerators environment are Cr_2O_3, $NiCr_2O_4$, $CaAl_2SiO_6$ and $NiCl_2$.

3. Discussion

Visual analysis clearly showed that the coating remain intact to the substrate even after 1000h of exposure. Brownish layer observed on the surface indicates the presence of ash on the coated alloys because of the sticky behaviour of the fly ash. SEM micrograph of all the three corroded coated substrates indicated the formation of irregular morphological structure. SEM micrograph of corroded Cr_3C_2-(NiCr) +0.2wt%Zr coated Superni 600 showed the presence of cracked oxide mainly consisting of chromium, nickel, oxygen and chlorine. Li et al.[1] discussed that presence of chlorine in the environment produces significant growth stresses and cause the oxide scale to become less compact and protective. This occurs because of the volatile nature of chloride which occurs due to the phenomena known as Active Oxidation. EDS analysis of the surface morphology of three coated superalloys showed almost same type of elemental composition present on the surface. Chromium , nickel and oxygen were found in major amount which shows that chromium oxide and $NiCr_2O_4$ might have formed on the surface of the coated specimen which protect the coating from degradation. Presence of various elements such Na. Mg, Al, Si, S, Cl, Ca, K and Zn were also indicated by EDS analysis. As these elements neither present in the coating nor in the substarte. Hence it was assumed that these elements are from the deposition of fly ash present in the secondary chamber of the incinerator. Composition of the fly ash depends upon the type of fuel burnt in the incinerator in primary chamber. Such as the most abundant elements found in Municipal waste incinerator are Si, Al, Fe, Ca, Mg, K, Na and Cl along with heavy metal such as Pb and Zn[6].

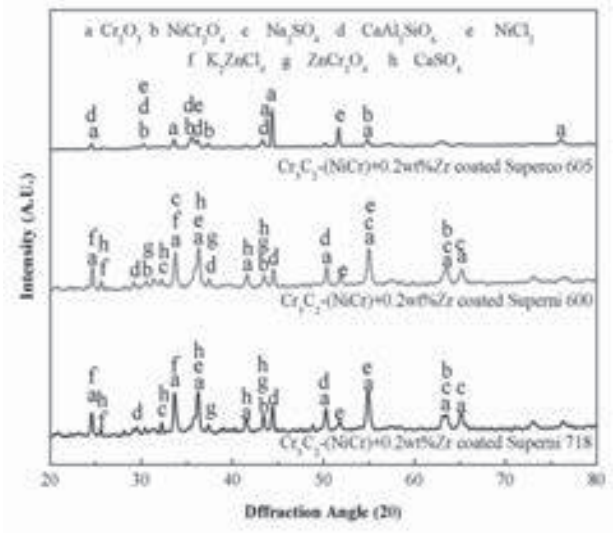

Fig.4 XRD analysis for Cr_3C_2-NiCr+0.2wt.%Zr coated Superni 718, Superni 600 and Superco 605.

4. Conclusion

All the three coatings remain intact on the surface of superalloys even after 1000h of exposure and found to be succefully in imaprting corrosion resistance to the alloys under the given environment.. Deposition of ash containing massive and nodular oxides mainly consisting of Na_2SO_4, CaO, SiO_2 and $MgSiO_3$ were observed on the surface of all the coated alloys.

3 References

[1] Y.S. Li, Y. Niu, W.T. Wu: Materials Science and Engineering: A,345(1–2),(2003)64–71.

[2] M. A. Uusitalo, P. M. J. Vuoristo, and T. A. M¨antyl¨a: Surf. Coat. Tech. **161(2-3)** (2002) 275–285.

[3]D.Mudgal, S.Singh, S.Prakash: Inter. J. of Corro., Vol. 2014 (2014), Article ID 505306, 14 pages.

[4] Y.-N. CHANG, F.-I. WEI: J. of Mat. Sci. **26** (1991) 3693 3698.

[5] George Lai, Hira Ahluwalia, ISBN: 97162 1997 CP, Corrosion.

[6]E. Bontempi, A. Zacco, L. Borgese, A. Gianoncelli, R. Ardesi and L. E. Depero: J. Environ. Monit. **12** (2010) 2093–2099.

Slurry erosion wear of Detonation gun sprayed Stellite-6 and WC-Co coatings on AISI 201 and AISI 316 Stainless steels

Arpan Katiyar[1], Prashant Kumar Singh[1] and S. B. Mishra[1]
[1] Department of Mechanical Engineering, Motilal Nehru National Institute of Technology Allahabad, Allahabad-211 004, India

Abstract
Slurry erosion wear of engineering components is encountered in large variety of industries. To combat this problem, the protective coatings are used. In the present investigation, Stellite-6 and WC-Co coatings on AISI 201 and AISI 316 stainless steel using detonation gun method. The effects of impingement angles and slurry concentrations have been studied using slurry erosion pot tester. Taguchi's orthogonal arrays approach was used to determine an optimal parameter combination with the aim to minimize the erosion rate. SEM was used to analyse the surface morphologies of the as-sprayed and eroded coatings. Amongst the tested samples, WC-Co coating deposited on AISI 316 stainless steel has shown lowest erosion rate.

1.Introduction

Materials loss due to slurry erosion is a serious problem in many industrial applications like hydraulic turbines, slurry pumps, pipe lines etc. where the ideal choice of engineering materials is a real challenge [1-6]. The turbine blades, needles pumps, valves, and nozzles in the hydraulic machinery, and ship propellers have to tolerate perpetual high-speed water (with or without solid particles) impingement, and hence they must have excellent strength, toughness and erosion resistance [7].

Stainless steel have adequate mechanical strength at different parameters such as impingement angle, slurry concentration and size of erodent particles they often lack resistance to erosion environments. Protective coatings of a wide variety of materials are often applied to improve resistance to erosion. Coating systems are designed to provide a more optimized environmental protection capability without the constraints of high strength that are normally placed on structural alloys for load bearing components [8]. The selection of a suitable treatment or coating for a given application depends on a complex interplay of surface, coating, and substrate related properties that are defined by the specific application [9].

Detonation-gun (D-gun) spray coating process is a thermal spray process, which gives an extremely good adhesive strength, low porosity, and coating surfaces with compressive residual stress [10]. In the present work, stellite 6 and WC-Co coatings were deposited by D-gun technique on the AISI 201 and AISI 316 stainless steels and were investigated for their erosion performance using slurry pot tester at the impingement angles of 30^o, 60^o and 90^o and slurry concentration of 10%, 20% and 30%.

2. Experimental Details

2.1 Materials and Coating Development

In the present work, AISI 201 and AISI 316 stainless steels have been selected as substrate materials as they are used in hydroelectric power plants, marine sectors and chemical containers due to their good mechanical properties and corrosion resistance. Two coating powders (Stellite-6 and WC-12Co) were deposited on the substrate materials by detonation gun spray method at SVX Powder M Surface Engineering Pvt. Ltd., Noida (India). The parameters used during coating deposition are reported in the Table 1.

Erosion wear tests of the coated steels were carried out using Slurry Erosion Pot Tester the pot tester reported in Desale et al. [11-12]. Taguchi's parameter design [13-15] has been adopted in this study to investigate the effect of various parameters and their interactions. The analysis of variance (ANOVA) is carried out to identify the most significant control factors and their interactions.

Table 1 - Coating deposition Parameters

Parameters	Stellite-6	WC-12%Co
Oxygen flow rate (SLPH)	3120	2960
Acetylene flow rate (SLPH)	2400	2400
Nitrogen flow rate (SLPH)	720	720
Spray distance(mm)	150	165

3. Results and discussion

3.1 Taguchi design

The erosion rate of the two coatings is influence by a large number of process parameters (factors) such as impact velocity, impingement angle, slurry concentration, erodent size and hardness of the erodent and target material. Table 2 and 3 shows the orthogonal array and associated experimental results for the erosion wear with calculated Signal to Noise (S/N) ratios of coatings on AISI 201 and AISI 316 stainless steel respectively. The analysis is made using the MINITAB 16 software specifically used for design of experiment.

Table 2 Erosion rate of coatings on AISI 201 stainless steel:

S.No	Type of coating	Impingement Angle	Slurry Concentration	Erosion Rate (mg/kg)	S/N ratio
1	WC-Co	30 º	20%	0.78182	2.1379
2	WC –Co	60 º	30%	0.36364	8.7867
3	WC -Co	90 º	10%	1.16364	-1.3163
4	Stellite 6	30 º	30%	0.92727	0.6559
5	Stellite 6	60 º	10%	2.03636	-6.1771
6	Stellite 6	90 º	20%	0.72727	2.7661

Table 3 Erosion rate of coatings on AISI 316 stainless steel:

S.No	Type of coating	Impingement Angle	Slurry Concentration	Erosion Rate (mg/kg)	S/N ratio
1	WC-Co	30 º	20%	0.56364	4.98002
2	WC –Co	60 º	30%	0.32727	9.70180
3	WC -Co	90 º	10%	0.92727	0.65585
4	Stellite 6	30 º	30%	0.59394	4.52516
5	Stellite 6	60 º	10%	1.54545	-3.78112
6	Stellite 6	90 º	20%	0.66364	3.56140

From the S/N ratio response, it can be concluded that among all the factors such as types of coating, impingement angle and slurry concentration, slurry concentration is the

most significant factor where as types of coating has significance on the erosion rate of AISI 201 and 316 stainless steels. The S/N ratios are the indicators of the relative significance of control factors and their interaction. The optimized combination of levels for all the three control factors from the analysis which provides the best result is found to be WC-12%Co coatings–90^o impingement angle–30% slurry concentration on both the substrates. The S/N ratios are confirmed by performing analysis of variance (ANOVA). The percentage contribution obtained from the ANOVA has indicated that types of coatings (15.22 %), impingement angle (14.79 %) and slurry concentration (69.58 %) have the significant influence on the erosion rate of AISI 201 stainless steel. The percentage contribution obtained from the ANOVA has indicated that types of coatings (11.19 %), impingement angle (9.09 %) and slurry concentration (77.387 %) have the significant influence on the erosion rate of AISI 316 stainless steel.

3.2 Scanning Electron Microscope Analysis

SEM analysis of the eroded samples has been carried out to study the surface morphology. Fig.1 shows the SEM micrographs of stellite 6 coating on AISI 201 steel after erosion at different impingement angle and slurry concentrations. SEM images indicated the deformed surface with interact coating phases. Fragments of coatings are visible in the SEM images. Fig. 2 shows the SEM images of eroded WC-12%Co coating on AISI 201 steel substrate. Very little effect of erosion on WC-12%Co coating is visible from the SEM micrographs of eroded WC-12%Co coating.

4. Conclusion

WC-12Co and Stellite 6 coatings have been succesfully deposited on AISI 201 and 316 stainless steels. Slurry erosion wear of the coatings were evaluated by using slurry pot tester. Following conclusions are drawn:

- All the three coatings have shown higher erosion rate at 30^o impingement angle as compared to that a 60^o and 90^o impingement angles.
- WC-12%Co coating has shown the minimum erosion wear among the two coatings deposited on the stainless steels.
- Slurry Erosion wear rate of the coating is found higher during the initial cycles followed by study state erosion rate.
- Slurry erosion rate of both the coating is found decreasing with the increase in slurry concentration.
- Both the coatings have shown lower erosion rate on AISI 316 stainless steels than that on AISI 201 stainless steel.
- SEM analysis of the eroded samples have also indicated the higher erosion of coatings on AISI 201 stainless steel as several fragments and loose particles can be seen on the surface of the samples.

References

[1] R. Hamzah, D.J. Stephenson, J.E. Strutt, Wear, **Vol.186**; (2004) pp-493–496.

[2] F. Aiming, L. Jinming, T. Ziyun, ,Wear, **Vol. 181**, (1995),pp-876–882.

[3] K. Haugen, O. Kvernvold, A. Ronold, R. Sandberg, Wear, (1995), pp179–188.

[4] Finnie I; Wear, **Vol.3,** (1960).

[5] A.G. Bain, S.T. Bonnington, First ed., Pergamon Press, (2004), pp-592–599.

[6] J.G.A. Bitter, Wear **6**, 5–21, (1962), pp-169–190.

[7] S.V. Joshi and R. Sivateumar, Coat. Technol **50**, (1991) pp- 67-74.

[8] Lin, H. C., Wu, S.K., and Yeh, C. H., Wear, **Vol. 249**, (2001), pp. 557-565.

[9] Nicholls J.R., JOM; (2000), pp-28.

[10] Sundararajan G, Roy, Manish,Tribol Int; **30(5)**: (1997),pp-339–59.

[11] G. R. Desale, B. K. Gandhi, S.C. Jain, (2006), Wear, vol. 261, pp- 914-921.

[12] G. R. Desale, B. K. Gandhi, S.C. Jain, (2009), W wear, vol. 266, pp- 1066-1071.

[13] Taguchi G. "*Introduction to quality engineering". Tokyo*: Asian Productivity Organization, (1990).

[14] Nalbant M, Gokkaya H, Sur G.,Mater Des; **vol 28**,pp-1379–85, (2007).

[15] Koksal S, Ficici F, Kayikci R, Savas O.,Mater Des; **vol.(42)**,pp-124–30, (2012).

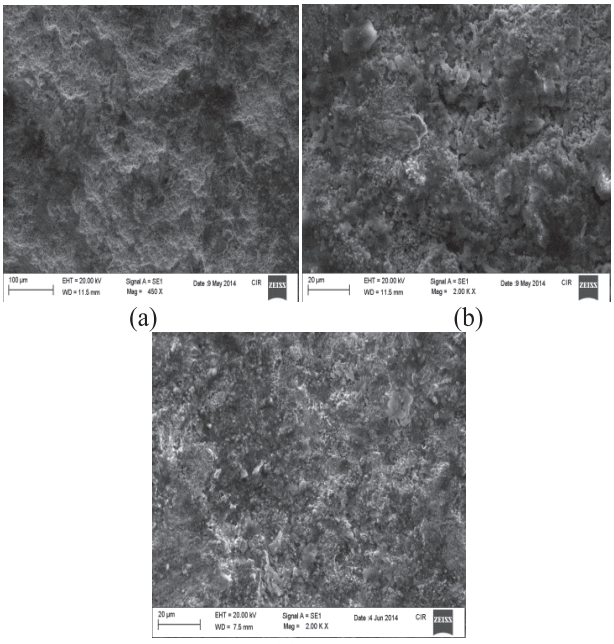

(a) (b) (c)

Fig. 1 SEMs of the eroded surfaces of the D-Gun sprayed stellite 6 coating on AISI 201 steel at (a) 30^o angle with 30% conc. (b) 60^o angle with 10% conc. (c) 90^o angle with 20% conc.

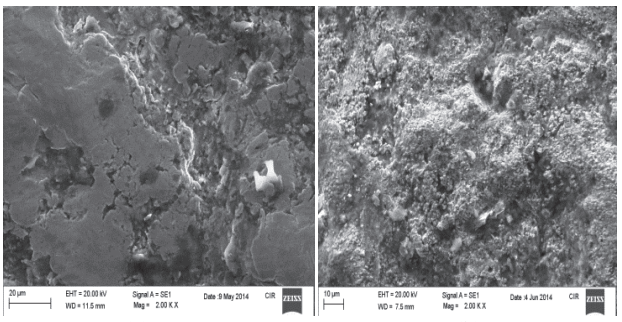

(a) (b)

Fig. 2 SEM of the eroded surfaces of D-gun sprayed WC-12Co coating on AISI 201 steel at (a) 30^o angle with 20% conc. (b) 60^o angle with 30% conc.

Elevated temperature erosion behaviour of thermal sprayed Cr_2C_3-25(Ni20Cr)

K. Teja Swarup[1], S. Gokul lakshmi[2] and Manish Roy[2]
[1]Andhra university, Visakhapatnam, India
[2]Defence Metallurgical Research Laboratory, Kanchanbagh, Hyderabad, India

Abstract
Cr_xC_y-NiCr coating is commonly used in the industry for protection against wear at elevated temperature. At elevated temperatures number of industrial components such as compressor blades of gas turbine, burner nozzles, super heater in combustion systems, turbines, lock hopper valves in coal gasification systems etc. are subjected to erosive wear leading to materials degradation at elevated temperature. Cr_xC_y-NiCr coating is considered to be potential layer for protection against solid particle erosion (SPE) at elevated temperature. With an aim to investigate the solid particle erosion behaviour of this layer at elevated temperature, Cr_3C_2-25(Ni20Cr) coating is deposited on Ni base super alloy employing D-gun system. Solid particle erosion rate of this coating has been determined with the help of high temperature erosion rig at five different test temperatures and at two different impact angles and two different impact velocities for each test temperatures. Erosion rate initially decreases with temperature and beyond some temperature it increases with temperature. Material removal mechanisms near ambient conditions and at elevated temperatures were found to different.

1 Introduction

Degradation of components in hot sections of gas turbine, boilers, industrial waste incinerators are due to high temperature oxidation, hot corrosion and erosion. Nickel based superalloys have been developed for high temperature turbine applications. Coatings provide a way of extending the limits of use of materials by maintaining the mechanical properties of the substrate and protecting them against wear and corrosion. Protection of the metallic components by cermet is an effective method to reduce erosion and corrosion. Cr_3C_2-NiCr coatings offer greater erosion and oxidation resistance and also have high hardness and wear resistance up to 800°C [1,2]. They are being deposited by high velocity spray processes like high velocity oxy-fuel (HVOF), detonation gun spray and high velocity air-fuel (HVAF) processes to minimize decarburisation of carbides during the spray process and to produce dense coatings [3,5]. In the present study, the high temperature erosion behavior of D-gun coated Cr_3C_2-25(Ni20Cr) coatings have been reported.

2 Experimental procedure

Nickel base nimonic alloy of dimension 20 mm x 20 mm x 3 mm has been used as the substrate material. The substrates were grit blasted using alumina and coated with Cr_3C_2-25(Ni20Cr) using D-gun process. The spray parameters used are given below. Oxygen flow rate of 2800 slph, C_2H_2 flow rate of 2240 slph and N_2 flow rate of 1040 slph. The spray distance was maintained at 165 mm. The coating powder, surface morphology and cross-sectional microstructure of the coating observed using a Quanta 400 scanning electron microscope (SEM) coupled with an energy dispersive X-ray (EDAX) analyser. The phases constituting the coating was determined using a Philips 3020 diffractometer. The microhardness measurements of the coating were determined using Leica microhardness tester. The roughness (R_a) of the coated surface for all the samples was measured using a Mitutoyo profilometer. The solid particle high temperature erosion test were conducted using air jet erosion test rig using silica erodent at impact velocities of 65 and 110 m/s under normal and oblique impact conditions.

3 Results and discussion

The cross-sectional microstructure of Cr_3C_2-25(Ni20Cr) coating is shown in Fig. 1. The coating was uniform and thickness was found to be about 100 μm. The hardness across the coating varied in the range 1100-1200 Hv. The surface roughness of the coating was found to be about 4 μm.

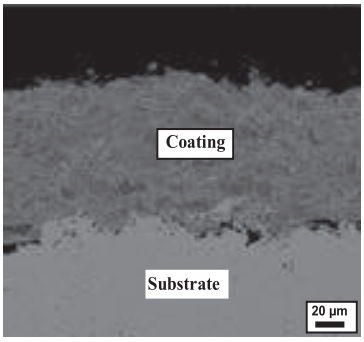

Fig. 1: *Cross sectional microstructure of Cr_2C_3-25(Ni20Cr) coating*

Erosion rates curves are plotted against cumulative weight of erodent and shown in Fig. 2. It is seen that steady state erosion rates are achieved. Variation of erosion rate as function of test temperature is shown in Fig. 3. The erosion rate initially decreases with increase of test temperature and beyond some intermediate temperature in increases again. Initially at low and intermediate temperature oxidation of the coating is negligible. Erosion rate decreases as the toughness of the coating improves with temperature. Beyond 673 K, oxidation of the coating influences erosion rate and hence erosion rate increases on further increase of test temperature. The morphologies of the surfaces eroded at room temperature and at 873 K are shown in Fig. 4. It is clear that brittle chipping of the coating governs erosion rate at ambient condition whereas propagation of cracks resulting in removal of chunk of materials from a surface layer containing coating oxide scale and erodent is responsible for erosion rate at 873 K.

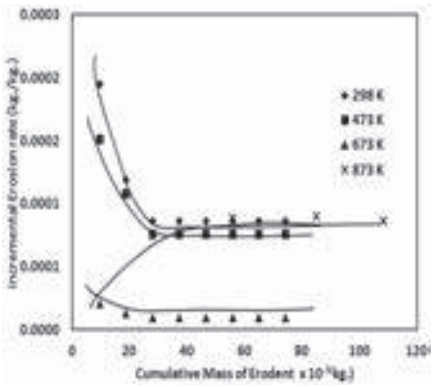

Fig. 2: *Variation of incremental erosion rate as function of cumulative mass of erodent.*

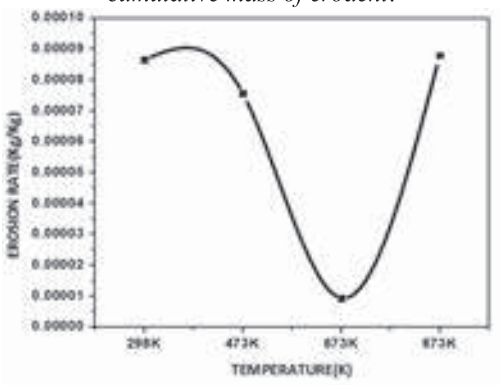

Fig. 3*: Influence of test temperature on steady state erosion rate.*

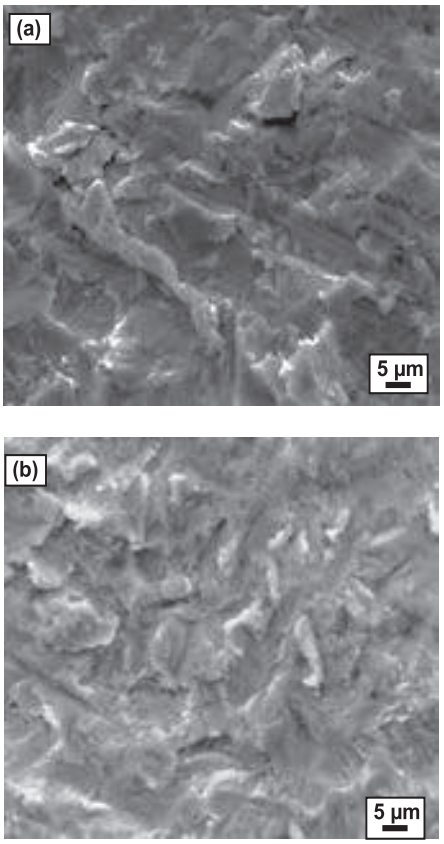

Fig. 4: *Morphology of eroded surfaces at 110 m/s impact velocity under normal impact, a) RT, b) 873 K.*

4. Conclusions

1) Erosion rate initially decreases with temperature and beyond some temperature it increases with temperature.
2) Material removal mechanisms near ambient conditions and at elevated temperatures are different.

Reference

[1] T.N. Rhys-Jones, Surf. Coat. Technol. 43/44 (1990) 1.
[2] R.V. Hillery, J. Vac. Sci. Technol. A 4 (6) (1986) 2624.
[3] G. Barbezat, A.R. Nicoll and A. Sickinger, Wear 162–164 (1993) 529.
[4] Kevin J. Stein, Brian S. Schorr and Arnold R. Marder, Wear 224 (1999) 153.

Image analysis of microstructural features of Suspension Plasma Sprayed coatings

Sneha Goel, Ashish Ganvir, Nicolaie Markocsan, University West, Trollhattan, Sweden

Abstract

Suspension Plasma Spray (SPS) is known for many years but problems in spraying uniform coating inhibited reliable research. This issue was overcome by the Axial Injection System which produces lamellar structures with trivial vertical cracks. In the comparative study, SPS has produced enhanced results on thermal insulation. Laminations (horizontal cracks) as in Atmospheric Plasma Spraying (APS) were absent in SPS pertaining to improved adherence of coating with the substrate. The present study is a pioneering work for image analysis using high magnification SEM images for nano-scale porosity. Porosity of thermal barrier coating (TBC) is vital for its thermal insulating properties. The current study reports the porosity measurements of the TBC structures produced by axial suspension plasma spraying (ASPS) under various spraying conditions. The IA results were compared also to the results obtained with Archimedes method.

1 Introduction

SPS is a plasma spraying process where the suspension of micron or sub-micron ceramic feedstock precursor is injected into the plasma jet. It offers the possibility of producing thin and dense and finely structured sprayed coatings [1]. The coatings were highly porous as compared to the literature [2].

2 Research Question

Effectiveness of IA for porosity measurement of TBCs? If no, what improvements can be done?

3 Experimental Methods

3.1 SEM-Aphelion

SEM images at 4000x magnification were taken and processed in Aphelion. Conventional Threshold Korrection Factor (TKF) is 0.84 (used in APS), but here it gave over estimation of porosity. Hence various TKFs values were tried until appropriate one, i.e., 2-2.2, was reached; on the basis that the features should be mostly similar in gray scale image and binary image, see **fig. 1-5**.

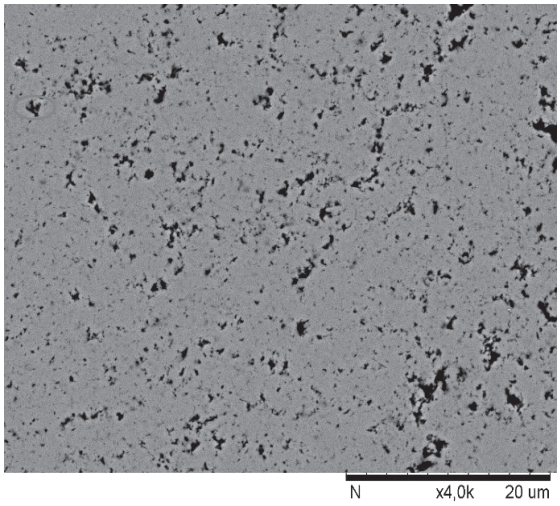

Fig. 1. *Original gray scale image with highlighted feature*

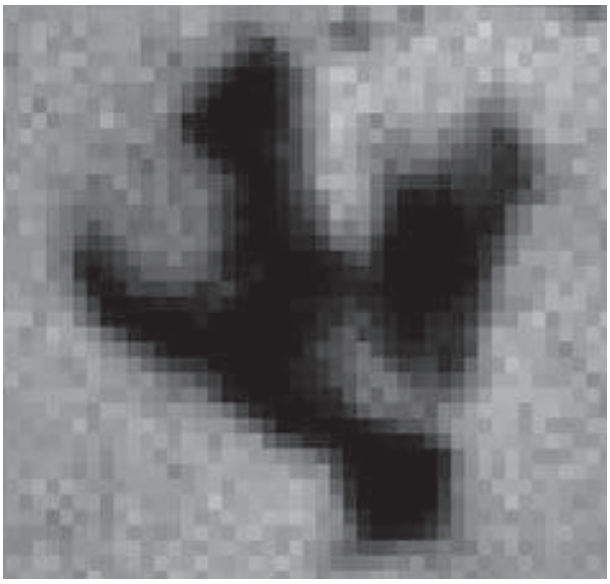

Fig. 2. *Original Big feature*

Fig. 3. *Magnified black and white image at 0.84 threshold*

Fig. 4. *Magnified black and white image at 0,22 threshold*

Fig. 5. *Magnified black and white image at 0.1 threshold*

It was observed that most of the pores were < 1µm but there was a limit to the resolution of the SEM, hence such features were neglected by setting up the pixel limit in Aphelion. Setting up the minimum pixel limit to #24 (whereas conventionally #2), we can neglect the features below 1µm. Pixel limit is calculated by counting total number of pixels a 1µm pore occupies and total number of pixels for the whole image at 4K).

3.2 Archimedes Method

Standard procedure was followed. As the bond coat got dissolved in Aqua Regia, color change of solution from yellow to dark green was observed.

4 Calculations:

Bulk Density of YSZ = $\left(1 - \frac{\Phi}{100}\right) * \rho)$

Given, Weight Gain (Wg) = Wet wt. – Dry wt.

Density of water (ρw) = 1 g/cm^3 (25°C)

Density of 8% YSZ (ρ) = 6.1 g/cm^3

% Porosity (Φ) = $\left[\frac{\frac{Wg}{\rho w}}{\left\{\left(\frac{Wg}{\rho w}\right)+\left(\frac{Wd}{\rho}\right)\right\}}\right] * 100$

Graph. 1. *Porosity values calculated by various techniques*

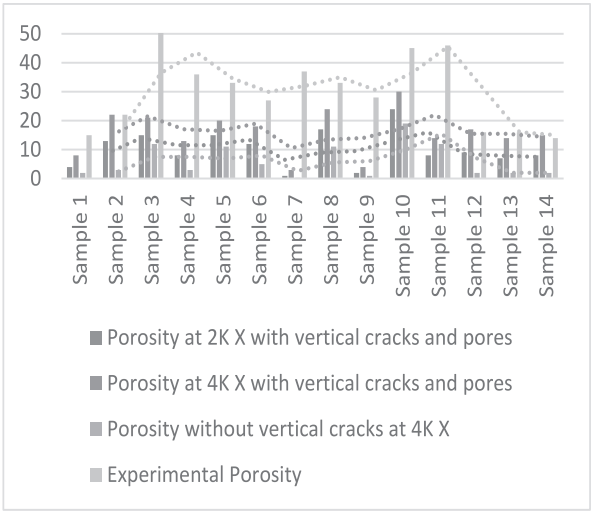

5 Conclusion:

Comparison of IA and experimental results reveals that the nano pores might be contributing significantly to the overall porosity than large pores (greater than 1um).

6 Future Scope:

Image Analysis using high resolutionary images which can capture nanoscale pores, and then setting up maximum pixel limit we can neglect features larger than 1µm. Coupling this value with the above results would yield practical values of the porosity of the SPS coatings.

7 References:

[1] Y.Whang, J.-G. Legoux, R. Neagu, S.Hui, B.R. Marple: Journal of Thermal Spray Technology (2011)

[2] O.Racek, C.C. Berndt, D.N. Guru, J. Heberlein: Surface & Coatings Technology (2005) 338-346

Prediction of substrate temperatures and stresses during plasma spraying

M.Raja[1,2], Gavisiddayya Hiremath[1], K. Ramachandran[3], P.V.A. Padmanabhan[4], T.K. Thiyagarajan[4]
[1]CRMS & TM, School of Mechanical Sciences, Karunya University, Coimbatore-641114, India
[2]Department of Biotechnology, Karunya University, Coimbatore-641114, India
[3]Department of Physics, Bharathiar University, Coimbatore – 641046
[4]L & PT Division, Bhabha Atomic Research Centre, Mumbai-400085, India

Abstract
A numerical model is developed to predict the temperature distribution in coating/substrate during plasma spraying. Further an analytical model is developed to predict the distribution of quenching, cooling and residual stresses in coating-substrate region. The predicted temperature distribution in coating-substrate region is used as an input for analytical model. Temperatures on the surface of the coating and substrate with spraying time as well as temperature and stress distributions along the thickness of the coating and substrate are predicted. Effect of micro-cracks in the coating on residual stress is illustrated by considering the mechanical properties of as-sprayed and dense materials.

1 Introduction

The temperature distribution both in substrate and coating during spraying has significant effect on adhesion and properties of coatings. However, the relationship between the temperature history, adhesion and properties of plasma sprayed coatings is still unclear. In this connection, researchers have taken efforts to study both substrate and coating temperatures during spraying and the residual stress formed on the coating. The substrate and / or coating temperatures during spraying have been measured [1-3] and predicted [1,2,4] by several authors. Residual stress that causes spallation, distortion and cracks in thermal spray coatings. Thermal stresses in the coating have been found numerically and experimentally [5, 6]. It is proposed to predict thermal stress in the coating with considering temperature distribution in coating and substrate during spraying.

2 Model description

2.1 Modelling of temperature distribution

A model for predicting the coating and/or substrate temperatures during plasma spraying is shown in Fig. 1.

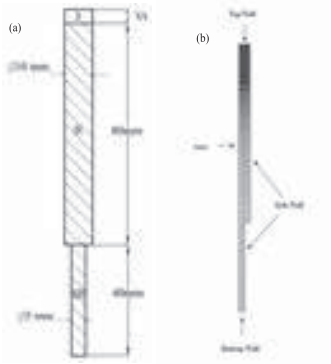

Fig. 1. *(a) Schematic of the coating(I-Al_2O_3)-substrate(II-Cu)-support system(III-SS) & (b) Computational geometry.*

The governing equation for heat conduction in the coating, substrate and substrate support/holder is given as

$$\rho\, C_p \frac{dT}{dt} = \propto \frac{d^2T}{dx^2} \qquad (1)$$

Where $\propto$ is temperature (T) dependent thermal diffusivity. The boundary conditions used to solve this equation are as follows. The top surface of the coating (top wall) receives heat flux from plasma and particles. The plasma jet deposits the heat on the substrate/built coating through convection and radiation. Particle heat flux is due to particle's solidification and cooling on the substrate/built coating. The total heat flux to the top wall is given by [1]

$$q = q_{conv} + q_{rad} + q_{sol} + q_{cool} \qquad (2)$$

2.2 Modelling of Thermal stresses

An analytical model, similar to the model developed by Ravichandran [7] is developed to predict the cooling stress in coating-substrate system and is given as

$$\sigma_{cool} = E(x)\left[\alpha(x) - \frac{A_1}{E_1} - \frac{\left\{A_2 - \frac{A_1}{E_1}E_2\right\}\{xE_1 - E_2\}}{\{E_1E_3 - {E_2}^2\}}\right](T - T_a) \text{ (3a)}$$

To obtain the quenching stress distribution in the coating, the equation (3a) is modified with ΔT as (T-T_m). The various parameters present in the equation 3a & 3b can be found elsewhere[7].

$$\sigma_{que} = E(x)\left[\alpha(x) - \frac{A_1}{E_1} - \frac{\left\{A_2 - \frac{A_1}{E_1}E_2\right\}\{xE_1 - E_2\}}{\{E_1E_3 - {E_2}^2\}}\right](T - T_m) \text{(3b)}$$

3 Results and Discussion

3.1 Temperature distribution

Fig. 2 shows the variation of both substrate and coating temperatures for a spraying time. Temperatures predicted by using pervious and present models are lower than that measured. Further, temperatures predicted by using present model is lower than that obtained from previous model. The possible reasons for the same could be explained as follows: previous model did not include the deposition of the coating on the substrate and the effect of coating on heat transfer from the plasma and particles to the substrate/built coating. Since heat flux from plasma and particles was assumed to be deposited on the substrate throughout the time, coating surface temperature was calculated from the substrate temperature using Fourier's law of heat conduction. Hence, heat stored by the coating material was omitted in the previous model. Since present model overcomes above mentioned issues, the predicted coating surface temperatures are lower than that of previous model. Since the emissivity involved in the temperature measurements depends on temperature, thickness and roughness of the coating, it is difficult to assume the suitable emissivity during the measurements. This may lead to determination of incorrect temperature from the experiments especially at higher coating temperatures. This was confirmed by Pawlowski et al. [1], who measured the

coating temperatures. This is the reason for deviation between measurements and predictions.

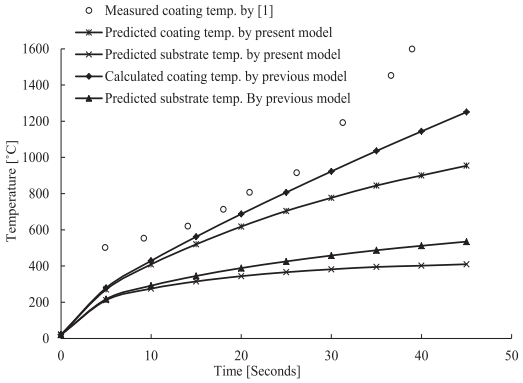

Fig. 2. *Variation of the coating and substrate temperatures with spraying time for τ = 57μm/s at S = 10cm.*

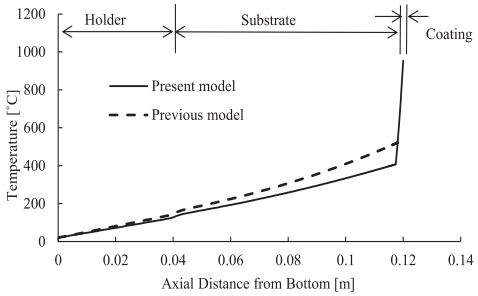

Fig. 3. *Axial temperature distributions along the axis of coating-substrate-substrate holder system.*

Fig. 3 compares the temperature distributions obtained from present and previous models along the axis of the system. The temperature predicted from the previous model varies linearly from the bottom of the substrate holder to top of the coating, which is not realistic. Since alumina has thermal conductivity much lower than the copper, there should be a larger temperature gradient in the coating than substrate. It is interesting to note that the present model predicts larger temperature gradients in the coating than the same in the substrate as anticipated. This is because the heat flux boundary condition is applied on the built coating surface not on the substrate surface when $t > 0$ in the present model.

3.2 Stress distribution

Fig. 4 shows the thermal stress distribution along the axis of coating-substrate-substrate holder system (Fig. 1) when the coating thickness reaches 2.57 mm during spraying. To calculate the thermal stress distributions, the temperature distribution obtained from present model for and dense/bulk mechanical properties (E_0 & α) are used. There are no significant thermal stresses produced in substrate and its holder. Thermal stresses rise sharply at the interface between substrate and coating and they diminish from the bottom to top of the coating. Residual stress at interface is 8 times larger than that at the top of the coating. A steep change in the temperature gradient at the interface causes a large change in the thermal stresses. As expected, quenching and cooling stresses in the coating are in tensile and compressive respectively. The sum of these stresses yields a tensile residual stress along the coating thickness. The predicted temperature distribution and dense material properties (E_0 & α) as well as as-sprayed material properties (E_d & α) for coating are used as inputs to predict the thermal residual stress distributions. From Fig. 5, It is interesting to note that residual stress on the top surface of an as-sprayed alumina is five times lower than that on the same of dense alumina.

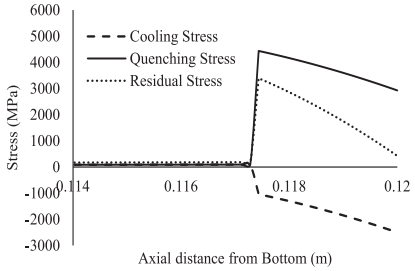

Fig. 4. *Thermal stress distributions along the axis for a coating thickness of 2.57 mm.*

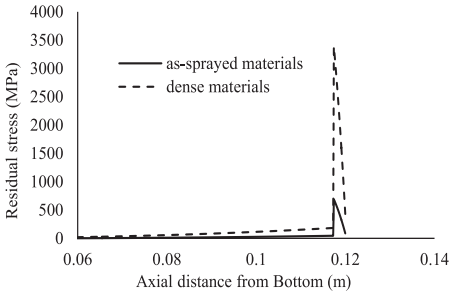

Fig. 5. *Residual stress distribution in as-sprayed and dense alumina for a coating thickness of 2.57 mm.*

4 Conclusion

Though present results deviate more from measured ones compare to previous results, it could be concluded that incorporation of the coating growth in the model is important to predict realistic temperature distribution around coating-substrate interface. For a coating thickness of 2.57 mm, cooling stress in the coating is compressive whereas both quenching and residual stresses in the same are tensile. Both residual and quenching stresses decrease from the interface to the top of the coating whereas cooling stress decreases from top of the coating to interface. The effect of micro-cracks in the coating on the residual stress in the coating can be simulated by considering the mechanical properties of as-sprayed material in the calculation.

5 References

[1] L. Pawlowski, M. Vardelle, P. Fauchasis: Thin Solid Films **94** (1982) 307-319.
[2] Y. Bao, T. Zhang, D.T. Gawne: Surface and Coatings Technology **194** (2005) 82-90.
[3] L. Moulla, P. Gougeon, C. Coddet: Infrared Physics & Technology **46** (2005) 364–369.
[4] L. Pawlowski: Thin Solid Films **81** (1981) 79-88.
[5] X.C. Zhang, B.S. Xu, H.D. Wang, Y.X. Wu, Materials and Design 27 (2006) 308 – 315.
[6] T.C. Totemeier, R.N. Wright, W.D. Swank: Metallurgical and Materials Transactions A **35A** (2004) 1807 – 1814.
[7] K.S. Ravichandran: Materials Science and Engineering **A201** (1995) 269 – 276.

6 Acknowledgement

The research grant provided by BRNS, DAE, India for this study is greatly acknowledged.

Numerical simulation of heating and melting of materials by thermal plasma jet

Gavisiddayya Hiremath, G Ravi[1], K. Ramachandran

Bharathiar University

[1]IPR Gandhinagar

It is important to control the interaction of plasma jet with materials exposed since the substrate melting is to be avoided in plasma spraying whereas complete melting is expected in ore processing and industrial waste treatment etc. With this in mind, a two-dimensional axi-symmetric computational fluid dynamics model is developed to simulate the heating and melting characteristics of materials exposed to plasma jet. Plasma jet is simulated from the nozzle exit with different gas compositions (Ar, Ar+H2 & Ar+N2) and powers (10, 12 & 15 kW). Global mass-energy relation is used to derive the input boundary condition to simulate the plasma jet. The jet is impinged on the material with different stand-off distances (80, 100 & 120 mm) in air at an atmospheric pressure. Evaporation from the molten pool is not considered in this work. Effects of gas composition, effective power of the plasma torch and stand-off distance on plasma heating and melting of the material are studied. Also, the influence of the viscosity of molten pool and Marangoni convection in the molten pool on thermal behavior of the material exposed to plasma jet is visualized.

Electrochemical Corrosion studies of HVOF sprayed Nickel based self fluxing alloy coating on mild steel in mining environment

R.Mahendran[1] S.P.Kumaresh Babu[1] S.Natarajan[1] P.Veerabalu[2] M.Kumarasamy[2]
[1] Department of Metallurgical and Materials Engineering, NIT,Tiruchirappalli,Tamilnadu 620 015, India
[2] CARD, Neyveli Lignite Corporation, Neyveli, India

Abstract
In this study, NiCrMoFeW were deposited onto mild steel using High Velocity Oxy Fuel (HVOF) spraying process. Potentio-dynamic Polarization (PDP) and Electrochemical Impedance Spectroscopy (EIS) studies were done at different pH conditions of water similar to the actual condition of the mines. The bare substrate and coated substrate after corrosion experiments were examined using Optical microscope and Scanning Electron Microscope (SEM) to access the corrosion behavior. As the electrolyte becomes more and more acidic (low pH) there is a tremendous decrease in the corrosion resistance of the bare substrate where as only a minimal decrease is observed in case of the coating. Coated samples were found to have a more noble E_{corr} value when compared to that of the uncoated substrate at all pH conditions.

1 Introduction

Low carbon steel possesses high strength with relatively low cost, which makes them to be used in mining industry for dewatering operations from underground mines. However they suffer from severe corrosion problem while ~~put~~ in service. During operations they are exposed to various mining environment which includes wide pH range, and the presence of many corrosive species in solution contributes to the corrosion-related difficulties which limit their applications.[1]

Several attempts have been made to improve the corrosion property by several surface modification techniques. Thermally sprayed coatings are widely used in areas where high wear and corrosion resistance are required.In the family of thermal spray coatings, HVOF thermal spray techniques are promising in producing dense structure with low porosity. Spray can be achieved by means of combustion of gases such as oxygen and a gaseous fuel such as propylene or kerosene to produce an extremely high speed flame capable of heating and accelerating the powder feedstock. [2,3]

In the present study, corrosion behavior of IS 3589 Fe 410 Grade and thermally sprayed Ni based coating were investigated by potentiodynamic scanning and EIS. Experiments were done at different water pH levels similar to that of actual condition in mines

Experimental materials and procedures

IS 3589 Fe 410 Grade carbon steel was used as substrate material which was cut from a plate of dimension 50 mm x 10 mm x 15 mm. The substrate was sand-blasted prior to coating with 30 meshes Alumina and degreased in acetone. Commercially available NiCrMoWFe thermal spray powder was sprayed on the treated surface to an approximately coating thickness of 200µm by HIPOJET 2700(MEC, Jodhpur, India make) . The particle size is around 45/15 microns. The **chemical composition** of Fe 410 Grade and the powder, given in **Table 1**. During coating the substrate temperature was maintained below 150 deg Celsius by continuous supply of air. The **coating parameters** were listed in **Table 2**.

Table. 1. *Chemical composition(wt%)*

Sl. No.	C	Mn	S	P	Fe	Ni	Cr	Mo	W
Fe 410	0.20	1.3	0.04	0.04	Bal.	-	-	-	-
Powder	-	-	-	-	5.5	Bal.	15.8	16.5	4.0

Table.2. *Coating Parameters*

Oxygen	270 SLPM
Lpg	50-55 SLPM
Air	550-600 SLPM
Nitrogen	20 SLPM
Spray distance	7 inch
Powder feed rate	40g/min
Particle velocity	300-350 m/s

Microstructural examination of the powders and coatings was carried out by using SEM. XRD analysis were used for the identification of evolved phase in the coatings with CuKα radiation.

Prior to corrosion test all coated samples and substrates were mechanically polished with 200 – 1200 grit SiC paper and then washed with distilled water and acetone followed by drying in air.The electrochemical tests were performed using ACM GILLAC three-electrode cell setup consisting of platinum wires as a counter electrode and standard calomel electrode as a reference.The working electrode was mounted in the electrochemical cell with an area of 1.0cm^2 exposed to the electrolyte.The electrolyte used in this study were mining water with pH level of 3.0,4.0 & 5.0. The Tafel analysis was performed with a potential range from Erest −150 mV to 1.0V (vs. SCE) and the scan rate was 1 mV/s. The OCP was determined after 30 min of immersion until stabilization.

Electrochemical impedance Spectroscopy measurements were performed in the frequency range of 100kHz–10mHz. The potential amplitude applied was 10mV. The number of Points per decade in the EIS test was 51.The EIS spectra were analyzed using Zview software.

Results and Discussion

Fig.1. obtained showed a well-bonded structure with low porosity and poor oxide content.

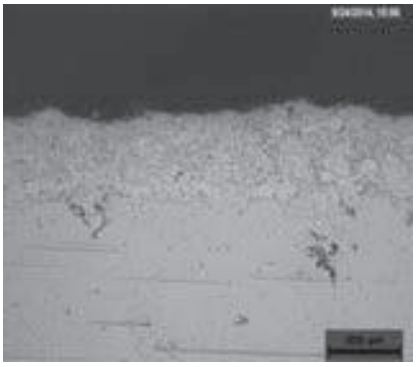

Fig.1. *OM cross section of HVOF coated substrate*

Potentiodynamic Polarisation curves

Fig. 2-4. represents the **Potentiodynamic Polarisation curves** for NiCrMoFeW caoted and Bare substrate at various pH levels.From this is evident that the NiCrMoWFe coated exhibits lower corrosion densities in all cases.

Fig.2 *PDP curve for coated and Bare substrate @ pH 3*

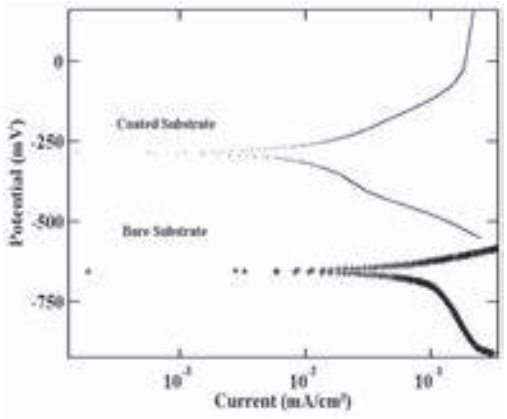

Fig.3. *PDP curve for coated and Bare substrate @ pH 4*

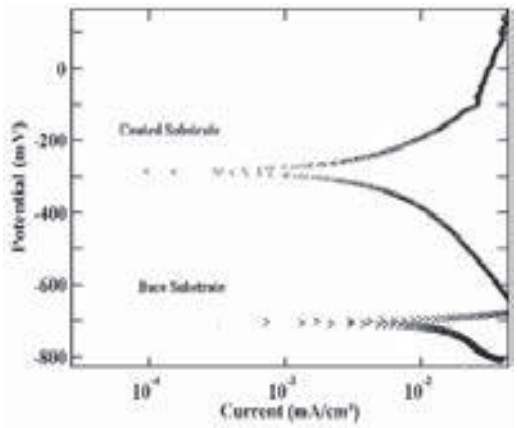

Fig.4. *PDP curve for coated and Bare substrate @ pH 5*

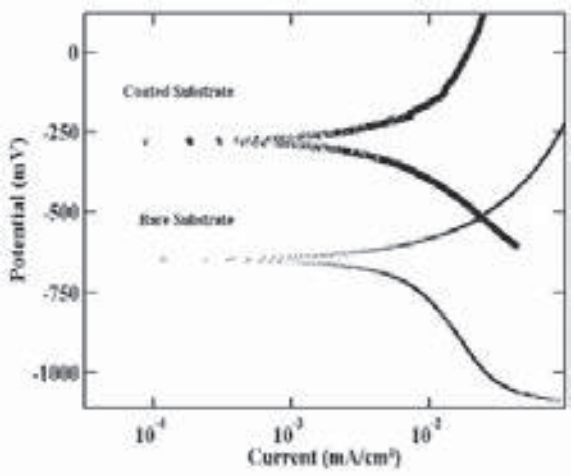

The corrosion potential, E_{corr} and corrosion current density, i_{corr} , values estimated by Tafel extrapolation method are indicated in **Table 3.**

Table 3. Corrosion potential *E_{corr} and Current Densities i_{corr}*

pH	Ecorr (mV)		Icorr (µA/Sq. Cm.)		Cor. Rate mm/year	
	Bare Substrate	NiCrMoWFe Coated	Bare Substrate	NiCrMoWFe Coated	Bare Substrate	NiCrMoWFe Coated
3	-653.55	-269.67	25.92	3.27	0.30014	0.04177
4	-708.24	-286.17	8.909	2.17	0.10317	0.02781
5	-655.83	-273.32	3.583	1.15	0.04149	0.01476

The corrosion potential of bare substrate at different pH levels (Ecorr = -653.55,-708.24 & -655.83) was higher than that of coated substrate which is -269.67,-286.17 & -273.32 respectively.

Conclusion

NiCrMoWFe coated sample Shifts the corrosion potential toward anodic values and leads to a decrease in the corrosion current density,which improves the corrosion resistance of the coatings.

3 References

[1] Peng-zhu Wang a, Yuan-sheng Yang b, Gang Ding ", Jing-xin Qu a, He-sheng Shao "Laser cladding coating against erosion-corrosion wear and its application to mining machine parts wear 209 (1997) 96-100 .

[2] W. Hume-Rothery, R. E. Smallman and C. W. Haworth: *The Structure of Metals and Alloys*, （The Metals and Metallurgy Trust of the Institute of Metals and Institution of Metallurgists, London, 1969） pp. 336-342.

[3]K. Abe and Y. Sato: Proc. 4th Int. Conf. on Rapidly Quenched Metals, （The Japan Inst. Metals, 1982） pp. 19-25.

PREPARATION AND CHARACTERIZATION OF ZIRCONIA/ALUMINA COATINGS BY ATMOSPHERIC PLASMA SPRAYING

K. Praveen[1], S. Sivakumar[1], G. Shanmugavelayutham[1]
[1]Plasma Processing Laboratory, Department of Physics, Bharathiar University, Coimbatore- 641046.

Abstract

Zirconia based coatings were proposed for the protection of turbine components from high temperature oxidation and high temperature corrosion. Several stabilizers were used for TBCs. In this present study, alumina, zirconia/alumina composite and double-layered zirconia/alumina coatings were prepared in stainless steel surface through atmospheric plasma spraying. Composites of zirconia/alumina were prepared by ball milling. Phase constituents and transformation of the ball milled powders and coatings were investigated by X-ray diffraction technique, Field Emission Scanning Electron Microscopy (FE-SEM) equipped with Energy Dispersive Spectroscopy (EDS) is to analysis the microstructure of the coatings. Microcracks and micropores of coatings leads to the degradation and spallation of coatings.

Keywords: corrosion, oxidation, microcracks, plasma spraying

1. Introduction

Currently thermal barrier coatings are used hot section of the turbines and vanes, to protect them from oxidation and hot corrosion and increase of efficiency [1]. Due to the usage of low grade fuels the formation of Na_2SO_4 and V_2O_5 occur, which get deposited on the blades causes severe damage to the blades. To protect the hot section components thermal spray coatings of zirconates, oxides are deposited. Several materials were proposed for them, among them zirconia based coatings shows better resistance. The state of art YSZ, which is limited due to phase transformation, so a new stabilizer which alternate Y_2O_3 is needed. Hence the present study investigates the plasma spray deposition of zirconia/ alumina composite and double-layered zirconia, alumina coatings over SS316 substrate.

2. Experimental procedure

2.1. Materials

Stainless steel (SS316) is used as the base material with 20 mm x 20 mm x 2 mm dimensions. Chemical compositions of base material contains: Cr- 16% to 18%, Ni-10% to 14%, Mn-2% (max), Mo-2% to 3%, Fe- balance and trace amount of C, Si, S, P and N. Commercially available aluminium oxide and zirconium oxide from Sigma-Aldrich were used as feedstock material.

2.2. Preparation of composites and coatings

50wt%Al_2O_3+50wt%ZrO_2 were made composite using planetary balling for four hours. The formation of Al_2O_3/ZrO_2 composite is confirmed from XRD data (fig.1a) and it is confirmed by EDS, the morphology of coating shown in figure 2. The prepared powder sprayed on sand blasted SS base material using 40kW atmospheric plasma spray (APS) torch, spray parameter were shown in table 1. Phase constituents and the microstructure of the coatings were investigated by using X-ray diffractometry (XRD), field emission scanning electron microscopy (FESEM), with energy-dispersive spectroscopy (EDS).

3. Results and discussion

3.1. XRD analysis

XRD pattern of Alumina(c), Zirconia (b) and Zirconia/alumina composite (a) used for plasma spraying are shown in figure 1. The Xrd pattern conforms the formation of composites through ball milling in fig. 1(a). The feedstock powder contains the α-alumina peaks, whereas the coatings

spray

Table.1: Optimized operating parameter

Parameters		
Arc current (A)		42
Arc voltage (V)		420
Plasma gas (lpm)	Ar	25
	N	2.5
Carrier gas (lpm)		5
Standoff distance (mm)		130

contains the γ-alumina peaks which is formed due to high rate of solidification and heat conduction at the coating/substrate, some α-alumina are also seen in coatings which is due to incomplete melting or partial-melting of larger particles during spraying [2].

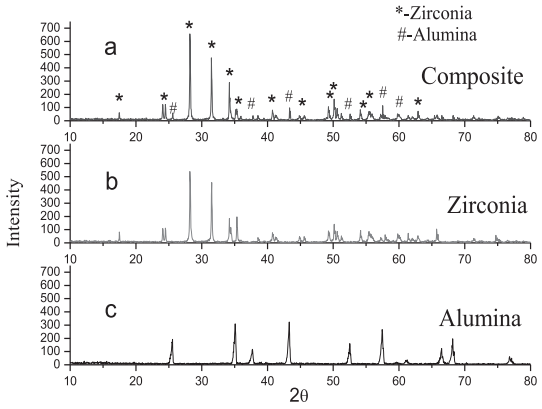

Fig.1. XRD pattern of feedstock powders a) Al_2O_3/ ZrO_2 Composite, b) ZrO_2, c) Al_2O_3

3.2 Microstructure analysis

The microstructure of alumina and zirconia/alumina composites are shown in fig 2. The

surface area clearly shows the formation of Alumina 2a, zirconia/alumina coatings 2b, EDS conforms the presence of alumina and zirconia/alumina in the coatings respectively. The surface of the coated samples shows molten, semi-molten particles and also contains the open pores. Open pores are formed due to splats and semi-molten particles. The splats and semi-molten are formed, the reason is before approaching the substrate the molten powder get solidified which increases the pores. Due to thermal stress and rapid cooling the formation of cracks occur, the presence of crack increases the strain tolerance and enhances the thermal shock resistance for TBCs [3].

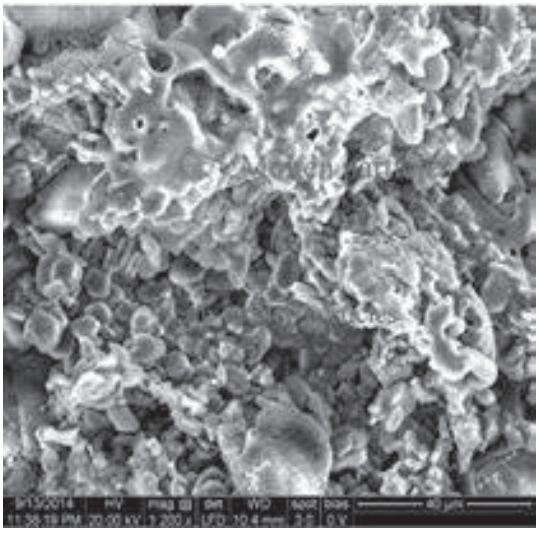

Input power and powder flow rate play an important role in melting of particles. Molten particles shows better coating than the semi-molten particles (which forms voids and cracks).

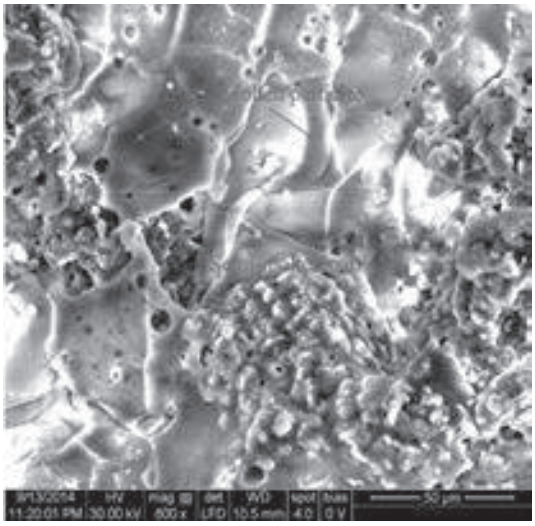

Fig.2. **a**) alumina coating **b**) alumina/zirconia composite with coatings.

4. Conclusion

Composite of 50wt%Al_2O_3+50wt%ZrO_2 is successfully prepared by ball milling and it is conformed from XRD and EDS analysis.

Alumina and alumina/zirconia composite coatings were successfully prepared. The coating were prepared over sand blasted SS316 surface. In addition the surface roughness play an important role in adhesion of the coatings.

Open pores and microcracks were seen throughout the coatings which is due to un-molten particles, which is responsible for degradation of coatings.

We also observed that the increase of torch to base distance there is a poor adhesion of coatings and increase of pores.

5. References

[1] X. Q. Cao, R. Vassen and D. Stoever, J. Eur. Ceram. Soc. 24 (2004) 1–10.

[2] S. Yugeswaran, V. Selvarajan, D. Seo, K. Ogawa, Surface & Coatings Technology 203 (2008) 129–136.

[3] G. Shanmugavelayutham, S. Yano, A. Kobayashi, Vacuum 80 (2006) 1336–1340.

Corrosion studies of twin wire arc sprayed duplex stainless steel coatings on mild steel used in mining environment

Roshan Jacob, Roshan Jacob,R.Mahendran,A.Vallimanalan,S.P.Kumaresh Babu,S.Natarajan

National Institute of Technology, Tiruchirappalli-620015,National Institute of Technology, Tiruchirappalli-620015,National Institute of Technology, Tiruchirappalli-620015,National Institute of Technology, Tiruchirappalli-620015,National Institute of Technology, Tiruchirappalli-620015

Duplex Stainless Steel (DSS) possessing higher PERN were coated on mild steel pipe substrate using simple twin wire arc spraying technique. Potentio-dynamic Polarization (PDP) and Electrochemical Impedance Spectroscopy (EIS) studies under different pH conditions of mine water were carried out. Optical microscopy was used to evaluate surface porosity on the coating and Scanning Electron Microscope (SEM) to reveal the morphology of the sprayed coating. Immersion corrosion testing were performed on DSS coated samples and were compared with bare samples under different mining conditions to support the polarization data. X-ray diffraction analysis confirms the phases present in the coating and precipitate that resulted from thermal degradation of DSS. The results show that the DSS coating exhibit better corrosion resistance than the bare substrate under mining condition.

Evaluating Micro – Mechanical Characteristics of HVOF Sprayed WC-CrC-Ni Coatings

C.Thiruvikraman[1], V. Balasubramanian[2], S.Malarvizhi[3] and K. Sridhar[4]
[1]Research Scholar, [2]Professor, [3]Asso. Prof. Dept. of Manufacturing Engg, Annamalai University, Annamalainagar – 608 002,
[3]Scientist'F', Marine Materials Department, NMRL, Ambernath, India

Abstract
High Velocity Oxygen Fuel (HVOF) sprayed cermet coatings are extensively used to combat erosion - corrosion in naval applications and in slurry environments. Major problem encountered in producing HVOF sprayed coatings is the selection of optimum combination of process parameters which influences the coating characteristics. This problem can be resolved by optimizing the combination of process parameters such oxygen flow rate, fuel flow rate, powder feed rate, carrier gas flow rate and spray distance which have significant influence on coating characteristics like adhesion bond strength, shear strength, porosity & hardness. In this study WC-CrC-Ni was sprayed on AISI 304L stainless steel substrates using High Velocity Oxy Fuel (HVOF) technique. HVOF sprayed coatings were characterized for their different properties such as tensile bond strength, lap shear bond strength, porosity & micro hardness. The microstructure of the coatings were characterized by optical microscope and SEM. Vickers's micro hardness tester was used to find the hardness. X ray diffraction and EDS Analysis were carried out to determine various elements present in the powder material and coated material. Tensile bond strength was determined by adopting ASTM C633 standard. Porosity analysis of the coating was done following ASTM B276 standard. Characterization results of the coatings for different combination of HVOF spray process parameters were compared and reported.
Keywords: *AISI 304L stainless steel, WC-CrC-Ni powder, HVOF, Bond strength, Porosity & Micro hardness*

1.0 Introduction

High velocity oxygen fuel (HVOF) spraying has proved to be effective thermal spraying technique particularly in industries to deposit WC-based cermet coatings, producing very dense coatings with greater adhesion to the substrate and higher hardness **[1].** Due to the high velocity associated with a relatively low flame temperature, HVOF process is suitable for producing cermet coatings of low porosity content (about 1%) with denser and less oxidized cermet coatings than other thermal spray methods with no significant thermal and mechanical alterations of the substrate [**2**]. Fang et al., studied the effect of HVOF process parameters on the wear behaviour of WC-CrC-Ni coatings using Taguchi technique. Maria et al., discussed different techniques of optimisation and characterization of HVOF coatings, and they opined that a deeper understanding of the spray process including starting material, spray process and particle-substrate interactions is required to produce good coating quality with suitable properties and required performance for specific applications [**3**]. Application of thermal spray coatings in industries greatly depends upon the quality of coatings such as lower porosity, higher hardness and higher bond strength (determines the adherence) of the coating to the substrate. Thus it was decided to study these micro – mechanical properties in our investigation.

2.0 Experimental

2.1 HVOF Thermal spraying

In this present investigation, at each condition, three specimens were coated as prescribed by the design matrix. To evaluate the coating properties, substrates with the dimensions of 25.4 X 25.4 mm were used for metallographic examination and microhardness measurement. Surface preparation was done by grit blasting before the spraying. Grit blasting was carried out using corundum grits of size of 500 ± 320 µm and subsequently degreased using acetone in an ultrasonic bath and dried. After grit blasting, the average surface roughness (5 µm)was measured using the surface roughness tester. (Make: Mitutoyo, Japan)

2.2 Metallographic preparation

Metallographic cross sections of the coatings were prepared for the porosity and microhardness measurements. The samples were first carefully cut to the specific dimensions (25X10X5 mm^3) using low speed metallurgical sample saw (Make: Ducom Instruments Pvt. Ltd, Bangalore, India). They were then mounted with low viscosity epoxy resin under vacuum environment. The mounted samples were successively ground with 600, 800, 1000 and 1500 grit SiC papers and eventually polished using diamond slurries of 10-8, 8-5,5-2, 2-0.5, 0.5-0 mm for a duration of 5, 5,7, 10 and 10 min, respectively.

2.3 Porosity Analysis

Porosity measurements were carried out following the procedures prescribed by the ASTM B276 standard on the polished cross-section of the coating, using optical microscope (Make: MEIJI, Japan, Model: MIL-7100) equipped with image analyzing system (Metalvision Version.6). In this investigation 400 X magnification was chosen for porosity analysis. Initially, an area of interest (AoI) of 200 µm square area was selected on the polished cross-section of the coating, and the image was analyzed. The same procedure was repeated at five random locations to find out the average percentage volume of porosity.

2.4 Microhardness measurements

Microhardness measurement was done by indenting a diamond indenter on the coating cross section of metallographically prepared specimen under 300 g load for 15 s using a Vickers microhardness tester (Make: Shimadzu, Japan; Model: HMV-2T). In each coated specimen, the measurement series comprised 20 indentations. Distance between indentations was kept three times longer than the indentation diagonal to prevent the effects of the stress field of nearby indentations.

2.5 Bondstrength measurements

The adhesion bond strength test was carried out as per ASTM C 633 standard, and the lap shear bond strength test were
carried out as per EN 1465 standard using a universal testing machine (Make: FIE Blue Star, India; Model: UNITEK-94100). For each experimental condition, three coated specimens were prepared and tested to minimize

experimental errors. A special purpose heat curable epoxy, HTK ULTRA BOND – 100, Supplied by Metallizing Equipment Corporation (MECPL), Jodhpur, India Scanned images of the failed specimens during the adhesion bond test and lap shear bond strength test are shown in (Fig. 1). From Fig. 1, it could be inferred that a few of the bond test specimens present partial (combined adhesive and cohesive) coating failures. The basic bond strength was evaluated by the degree of coverage of the remaining particles which remain bonded even after the testing of bonding strength .

3.0 Results & Discussion

Fig 1 shows the characterization results of HVOF sprayed WC-CrC-Ni coatings for various spray conditions. Max. bond strength, higher hardness & lower porosity is obtained for the spray condition of O –250,L–60,S–228, F –38, C–13.

3.1 Effect of spray parameters on microstructure

Improper oxygen/fuel ratio results in poor melting of the WC hard particles which affects the splat formation eventually poor deposition of the coating. Higher powder feed rate, carrier gas flow rate and lower standoff distance results in shorter dwell time of the powder in the flame causes improper melting characterised with large amount of unmelted particles in the coating as shown in **Fig 1(b).**

3.2 Effect of spray parameters on porosity & hardness

Insuffiecient oxygen/fuel ratio and excessive powder feed rate, carrier gas flow rate and increased stand off distance results in large number of unmelted particles in the coating and vice versa which obviously forms inter and intra splat voids which increases the porosity content of the coatings as evident from **Fig 1.** Porosity and hardness have an inversely proportional relationship and hence if the porosity is high the the hardness is low and vice versa.

3.3 Effect of spray parameters on bond strength

Inadequate oxygen/fuel ratio & excessive powder feed rate, carrier gas flow rate & increased stand off distance results in large number of unmelted and partially melted particles in the coating and vice versa which eventually have a poor adherence of the coating to the substrate (adhesion) and between the splats (cohesion). Due to poor adhesive and cohesive forces the mechanical interlocking between the coating and substrate becomes weak providing room for adhesive failure in tension and shear load and vice versa. This phenomenon is evident from the failed adhesion and shear specimens in **Fig 1**.

4.0 Conclusions

In this paper micro – mechanical characterization of HVOF sprayed WC-CrC-Ni coatings at various spray conditions were studied. The following conclusions are arrived from the above study.

1. Insufficient oxygen/fuel ratio results in improper melting of the powder particles leading to large number of unmelted particles with poor splat formation and microstructure.
2. Increase in powder feed rate, stand off distance and carrier gas flow rate increases the porosity which in turn reduces the hardness.
3. Presence of unmelted particles in the splat boundaries near the coating substrate interface reduces the mechanical interlocking between the splats and substrate resulting in weak tesile bond strength and shear strength.

Acknowledgements

The authours wish to thank the Naval Research Board (NRB – DRDO, GoI) for sponsoring this work through a funded project No. DNRD/05/4003/NRB/212.

References

1. Mostaghimi et al., 'Modelling thermal spray coating processes: a powerful tool in design & optimization', Surf. Coat. Technol., 2003,163–164, 1–11
2. L.Pawlowski: 'The Science Engg. of Thermal Spray Coatings', 2008, London, John Wiley & Sons Ltd.
3. Maria et al., Optimization and Characterization of High Velocity Oxy-fuel Sprayed Coatings: Techniques, Materials, and Applications', Coatings, 2011,1, 17 – 52.

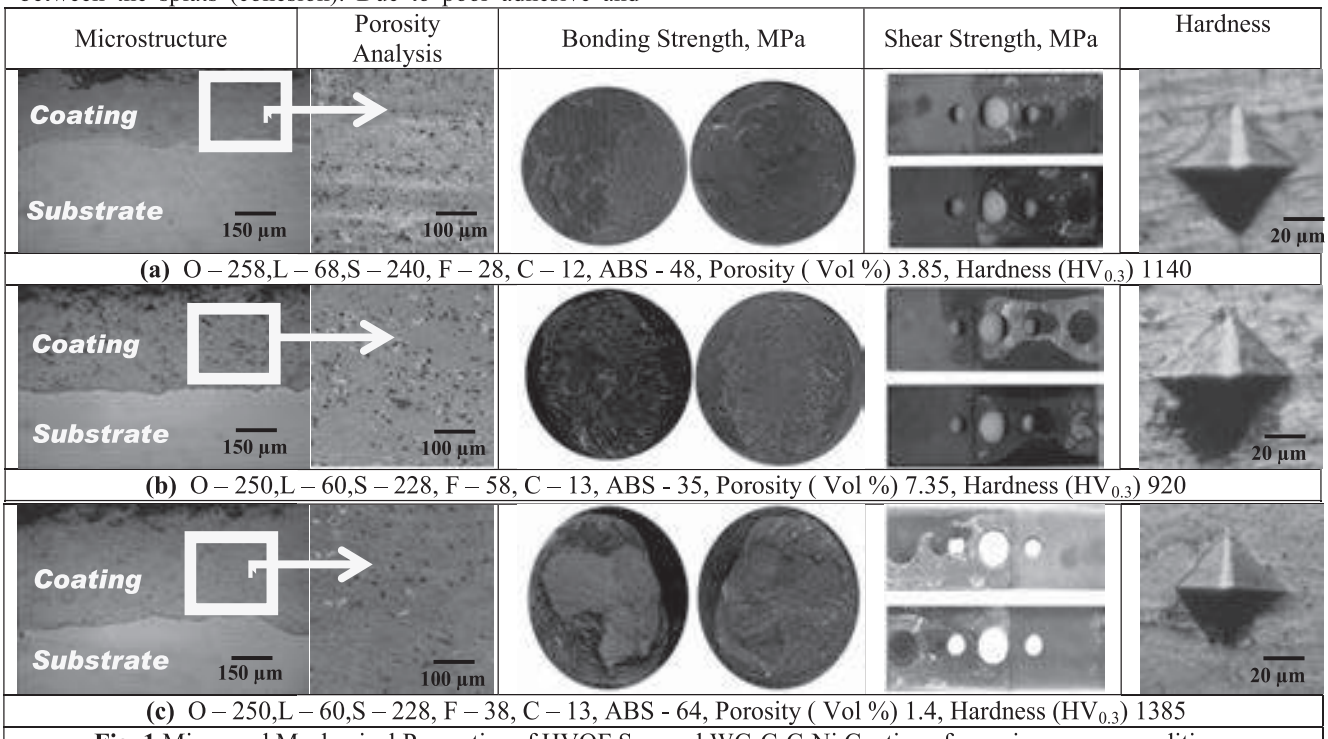

Fig. 1 Micro and Mechanical Properties of HVOF Sprayed WC-CrC-Ni Coatings for various spray conditions

Effect of HVOF Process Parameters on Porosity of NiCrSiB/WC-Co Coatings

Praveen A. S.[1], J. Sarangan[1], S. Suresh[1]
[1]Department of Mechanical Engineering, National Institute of Technology, Tiruchirappalli, 620015, Tamil Nadu, India

Abstract
High Velocity Oxygen Fuel (HVOF) spray process is a promising thermal spray process to deposit coatings with low porosity, high density, high hardness and higher bond strength. These coatings are extensively used to deposit cermet, metals and alloy coatings for protecting the components against wear and corrosion. Coating process parameters such as composition of working gas, standoff distance, powder feed rate, carrier gas flow rate have significant influence on the coating characteristics. In this work, HVOF technique was used to develop NiCrSiB/WC-Co coatings on AISI 304 substrate. Taguchi method was taken to optimize the spray parameters like LPG flow rate, oxygen flow rate, feed rate and standoff distance to obtain the lowest porosity. The porosity of the coatings were measured using an optical microscope with an image analyzing software. The result indicates that the standoff distance is the most significant factor affects the porosity of NiCrSiB/WC-Co coating.

1 Introduction

High Velocity Oxygen Fuel (HVOF) coating process is used to deposite NiCrSiB alloys for enhancing the wear and corrosion resistance of steels [1]. Even though NiCrSiB having excellent wear and corrosion resistant properties, it is not used as the primary material in the industry because of lower hardness in comparison to other materials (carbides and ceramics) [2]. But it was incessantly proved that Ni based alloy NiCrSiB coating reinforced with additives giving good results in the field of erosion-corrosion resistance. Various hard phases used as reinforcing additives along with NiCrSiB are WC, Al_2O_3, Cr_3C_2, Cr_2O_3, TiC, TiO, SiC, TiN etc.[3].The HVOF coating process parameters, such as the fuel flow rate, oxygen flow rate, feed rate, standoff distance, the incidence angle, the gun geometry, the substrate temperature and the property of original powder particles in terms of its chemical composition, morphology and size distribution will play an important role in the microstructure and interns affect the properties of sprayed coatings[4]. In order to achieve a good coating, it is very essential to find out the optimum process parameters.

In this work, the HVOF NiCrSiB/WC-Co coating parameters are optimized using Tagichi method. The fuel flow rate, oxygen flow rate, feed rate and standoff distance were considered for optimization of the coating process. The microstructure and porosity of coating developed using optimal process conditions were investigated.

2 Experimentation

2.1 Substrate and Coating material

AISI 304 having the nominal composition (in wt.): 0.023% C, 1.440 % M, 0.366 % Si, 0.006% S, 0.029% P, 18.736% Cr, 8.288% Ni and Fe as the balance, was used as the substrate material in this study. Prior to coating, the substrate material was grit blasted using corundum grits of size ranged from 300 to 150 µm in order to improve the coating adhesion. After grit blasting the samples were cleaned in acetone medium using an ultrasonic bath. The surface roughness of the blasted samples were measured using the surface roughness tester (Mitutyo, SJ 401) and it was found to be approximately 8-10 µm. In this work, NiCrSiB (MEC-335) and WC-Co (MEC-740) powders were used. The chemical composition and particle size are tabulated in the table 1.

Table 1. *Powder composition and nominal particle size*

Powder	Composition, wt.%	Nominal particle size
NiCrSiB	Ni-72, Cr-16, Si-5, B-3	-53+10 µm Gas atomized
WC-Co	WC-88, Co-12	-45+15 µm Agglomerated, sintered

The composite powder of 65 wt.% NiCrSiB and 35 wt.% WC-Co was used as the feedstock powder for the HVOF spraying process. The two powders were blended in a turbo-mixer for one hour in order to obtain homogeneous mixing. The SEM morphology of NiCrSiB and WC-Co powders are shown in Fig.1. It can be observed that the NiCrSiB powder is in spherical shape, whereas the WC-Co powder is in near spherical with micropores on the surface. These micro-pores will favour homogenous heating of the powder in the plume [5].

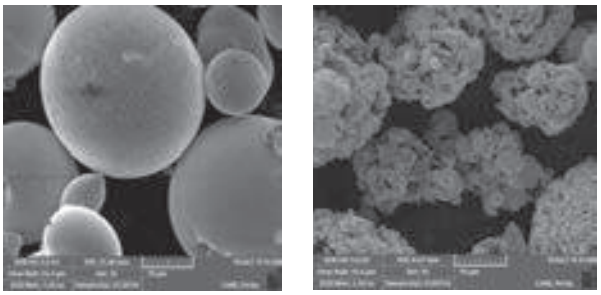

(a) (b)

Fig. 1. *SEM images of (a) NiCrSiB (b) WC-Co powders*

2.2 HVOF coating

NiCrSiB/WC-Co coatings are prepared by nine different processes generated by Taguchi design of experiment. In the experimentation process, four parameters at three levels were selected for the optimum process condition. The coating process parameters are LPG flow rate, oxygen flow rate, feed rate and standoff distance. The thickness of the coating was kept as constant for all the coating conditions as 250±20 µm.

Table 2. *HVOF process parameters and their levels*

Symbol	Parameter	Level 1	Level 2	Level 3
A	Oxygen flow rate (lpm)	220	240	260
B	Fuel flow rate (lpm)	55	60	65
C	Feed rate (gm/s)	28	32	36
D	Standoff distance (mm)	200	250	300

2.3 Porosity Measurement

Porosity of the coating was investigated by analyzing the cross sectional optical microscopic (OM) images [6]. The OM images were further processed using ImageJ processing and analysis software. The measurement was carried at five different locations and their average value was calculated.

3 Results and Discussions

3.1 Analysis of the signal-to-noise (S/N) ratio

In this work, the smaller-the-better performance characteristic for porosity was taken for obtaining optimal process conditions [7]. The signal to noise (S/N) ratio (η) is defined as:

$$\eta = -10\log\left[\frac{1}{n}\sum_{i=1}^{n} P_i^2\right]$$

where n is the number of observations and P_i is the value of porosity for the ith observation.

To analyse the effect of factors influencing porosity, the S/N ratio for all the experiment runs are calculated using the statistical tool Minitab 16 are as shown in Table 3.

Table 3. *Experimental results for porosity and corresponding S/N ratio*

Test Run	Oxygen Flow rate	Fuel Flow Rate	Particle Feed Rate	Standoff distance	Porosity	S/N ratio
1	220	55	28	200	2.2	-6.8485
2	220	60	32	250	2.4	-7.6042
3	220	65	36	300	1.5	-3.5218
4	240	55	32	300	1.9	-5.5751
5	240	60	36	200	3.3	-10.3703
6	240	65	28	250	1.7	-4.6090
7	260	55	36	250	2.8	-8.9432
8	260	60	28	300	1.6	-4.0824
9	260	65	32	200	3.1	-9.8272

Table 4. *S/N response for porosity (smaller is the better)*

Parameter	Mean S/N ratio				Rank
	Level 1	Level 2	Level 3	Max-Min	
Oxygen Flow rate	-5.992	-6.851	-7.618	1.626	3
Fuel Flow Rate	-7.122	-7.352	-5.986	1.366	4
Particle Feed Rate	-5.180	-7.669	-7.612	2.489	2
Standoff distance	-9.015	-7.052	-4.393	4.622	1

The stand off distance has the highest differnce amoung the values of the three levels (Table 4), 4.622 dB. Based on taguchi prediction, larger differnce between values of S/N ratio is the most influential factor ie. standoff distance. The important sequences of parameters affecting the porosity are as follows: standoff distance > particle feed rate > oxygen flow rate > fuel flow rate. It is observed from the main effect plot for porosity given in fig.2 that to get minimum porosity, the optimal process paramters should be low level of oxygen flow rate (220 lpm), high level of fuel flow rate (65 lpm), low level of feed rate (28 gm/s) and high level of stand off distance (300 mm).

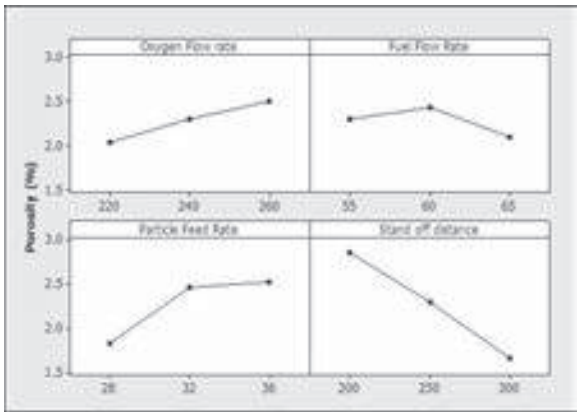

Fig. 2. *Main effect plot for porosity*

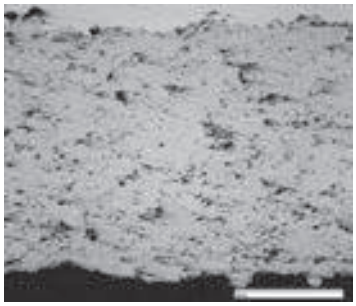

Fig. 3. *OM image of coating sprayed at run no. 3*

4 Conclusions

The spray parameter of NiCrSiB/WC-Co coating are optimized for porosity by Taguchi method based on L9 orthogoanl array. The important sequence of papramter is standoff dstance>feed rate>oxygen flow rate>fuel flow rate. The optimized conditions to obtain lower porosity, 220 lpm oxygen flow rate, 65 lpm fuel flow rate, 28 gm/s particle feed rate and 300 mm stand off distance has to be adopted.

5 References

[1] W. Zhao, Y. Wang, T. Han, K. Y. Wu, J. Xue: Surf. Coat. Technol 183 (2004) 118-125.
[2] H.S. Grewal, H. Singh, A. Agrawal: Surf. Coat. Technol. 216 (2013) 78–92.
[3] M. Oksa, E. Turunen, T. Suhonen, T. Varis, S. Hannula: Coatings ISSN 2079-6412 (2011) 17-52.
[4] X. Guo, M. Planche, J. Chen, H. Liao: J. of Materials Processing Technol. 214 (2014) 456– 461.
[5] Wang Q., Chen Z.H., Li L.X., Yang G.B.: Surf. Coat. Technol. 206 (2012) 2233–2241.
[6] ASTM Standard E2109-01(2007)
[7] S. Hong, Y. Wu, B. Wang, Y. Zheng, W. Gao, G. Li: Materials and Design 55 (2014) 286–291.

Plasma spray deposition of Lanthanum Phosphate and phase structure of the resultant coatings

A.Pragatheeswaran[1], P V Ananthapadmanabhan[2], Y. Chakravarthy[2], VandanaChaturvedi[2], SubhankarBhandari[2], K Ramachandran[3]

[1]Department of Physics, Karunya University, Coimbatore, Tamilnadu, India-641114
[2]Laser and Plasma Technology Division, Bhabha Atomic Research Center, Trombay, Maharastra, India-400085
[3]Department of Physics, Bharathiar University, Coimbatore, Tamilnadu, India-641046
Corresponding author- pvapadmanabhan@gmail.com

Abstract
Plasma spray deposition of lanthanum phosphate was carried out at different power levels of 16, 20 and 24 kW using the 40 kW atmospheric plasma spray system. $LaPO_4$ (monazite) powder with 75-106 μm particle size was used for the experiments. Phase structure of lanthanum phosphate coatings was studied by x-ray diffraction technique. XRD patterns of plasma spray coated samples at different power levels revealed that polyphosphate and oxy-phosphate could be formed apart from the monazite phase during plasma spraying. Heat treatment of the spray deposited samples resulted in recombination of the ploy-phosphate phase and oxy-phosphate phase to form the monazite phase of lanthanum phosphate having monoclinic structure. SEM analysis of plasma spray-coated specimen showed microstructures typical of plasma sprayed coatings with molten, partially molten lamellae and porosity. Large number of cavities, horizontal cracks and voids were observed on coatings deposited at lower power levels.

1. Introduction

The as-synthesized lanthanum phosphate ($LaPO_4.1/2\ H_2O$), known as rhabdophane, has a hexagonal structure and is stable upto about 550 ^{0}C. At temperatures beyond 550 ^{0}C, it loses the water of hydration and forms the monazitic phase with monoclinic structure, which is a potential candidate for thermal barrier applications in view of its high melting point and low thermal conductivity value. The rhabdophane-monazite phase change is irreversible [1,2]. Plasma spraying is a well-established and extensively used technique to address a host of surface engineering problems from simple abrasive wear to complex multifaceted corrosion issues. Plasma spraying utilizes the high temperature and high enthalpy of the thermal plasma medium to heat the coating material to a molten or semi-molten state and propel the molten particles onto a substrate, where they solidify to produce adherent coatings. A major advantage of plasma spray processes is that virtually any material that melts without decomposing can be deposited [3,4].

The main objectives of the present study include plasma spray deposition of in-house developed lanthanum phosphate and characterization of the coatings. Lanthanum phosphate synthesized by the chemical route was converted into thermal spray-grade powder by sintering, crushing and sieving and used for plasma spray deposition. X-ray diffraction, Fourier transformation Infra-red spectrometer (FTIR) and scanning electron microscopy were used for phase and microstructural characterization of the deposits.

2. Synthesis of plasma spray grade of lanthanum phosphate and experimental methods

2.1. Synthesis of $LaPO_4$

Lanthanum oxide powder with 85% orthophosphoric acid was used to prepare lanthanum phosphate. The oxide was converted to phosphate by reaction with 85% ortho-phosphoric acid in a glass beaker. Sufficient quantity of the acid was used to ensure total conversion of the oxide to phosphate. The reaction mixture was continuously stirred and the beaker was allowed to cool in an atmosphere to control the temperature resulting from the highly exothermic nature of the reaction. The white precipitated gel was collected in a glass beaker (shown in figure 1). The precipitate was repeatedly washed with demineralized water until it was free of acid and then dried at 373 K.

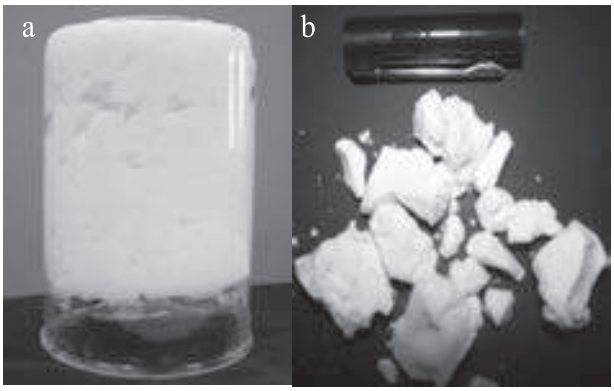

Fig.1. (a,b): *(a) As-precipitated lanthanum phosphate gel in glass beaker. (b) Lanthanum phosphate chunks dried at 100 ^{0}C and sintered at 1400 ^{0}C.*

2.2. Method of powder production for plasma spray experiments

The $LaPO_4$ precipitate was washed and dried and the resulting dried soft chunks were fired at 1400 ^{0}C to convert the hydrated lanthanum phosphate to the anhydrous monazite phase. The fired chunks were broken and crushed into smaller chunks, pounded using a pestle and mortar. The crushed powder was sieved and graded into different size fractions. The coarser powder mass left behind was again crushed and sieving operation was repeated. The powder fraction having particle size in the range of 75–106 μm was used for plasma spray deposition.

2.3 Plasma spray deposition

Plasma spray deposition was carried out using 40 kW atmospheric plasma spray facility developed at the Laser & Plasma Technology Division. The torch consists of a thoriated-tungsten cathode (10 mm diameter) and a conical tipped copper anode nozzle, 7 mm diameter. The electrodes are cooled by water and a Teflon insulator separates the electrodes. A mixture of argon and nitrogen was used as the plasma gas, which was injected through a side inlet in the

insulator segment. Experimental parameters for plasma spray deposition are given in the table 1.

Table-1. *Plasma spray deposition experiments parameters.*

Parameters	Values
Torch input power (kW)	16, 20 and 24
Primary gas flow Ar (SLPM)	30
Secondary gas flow N_2 (SLPM)	3
Carrier gas flow (SLPM)	8-10
Powder feed rate (g/m)	10
Standoff distance (mm)	100
Powder size distribution(μm)	75-106

3. Results and discussion

3.1. X-ray diffraction

Figure 2 shows the x-ray diffraction patterns of the starting powder and the coated specimens. It is evident from the figure that the diffraction patterns of the plasma spray coated samples are the same as that of the feedstock powder showing the monazite phase. X-ray diffraction pattern of the spray-grade powder showed that it consisted of a single homogeneous phase identical with anhydrous $LaPO_4$ (monoclinic phase) having monazite structure. The plasma spray deposited coatings showed $LaPO_4$ (monazite) as the major phase with additional diffraction peaks. The plasma spray coated at 16 kW showed the major monoclinic phase corresponding to orthophosphate ($LaPO_4$). Diffraction peaks at the two-theta values of 13.0, 22.5, 23.7, 27.3,29.1, 30.1 and 30.9 correspond to La-poly phosphate and La-oxy phosphate. The peak intensity of poly and oxy-phosphates were found to increase with plasma input power. The poly phosphate phase, $La_2P_4O_{13}$ has been reported [5] to be stable up to 755^0 C.

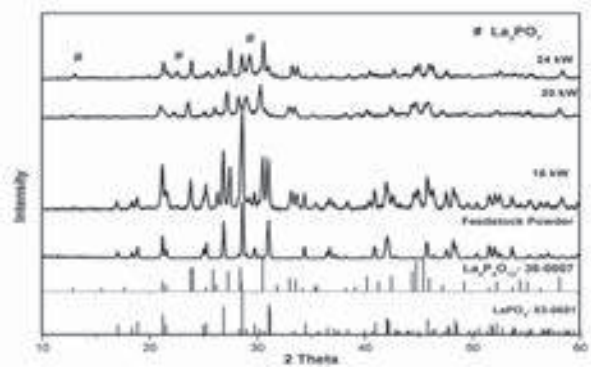

Fig 2. *XRD patterns of feedstock powder and plasma deposited $LaPO_4$ with JCPDS cards ($LaPO_4$- 83-0651 and $La_2P_4O_{13}$- 38-0007).*

Post-spray thermal treatment of the coatings to 1100 ^{0}C for two hours showed interesting results. The XRD patterns of all the heat-treated samples showed that they consisted of a single homogeneous phase corresponding to the monoclinic orthophosphate with JCPDS card number 83-0651 identical with the starting material. The poly-phosphate, and oxy-phosphate are formed during melt-quenching of the ortho phosphate by following equations.

$$5LaPO_4 \longrightarrow La_2P_4O_{13} + La_3PO_7 \quad \text{---- (1)}$$

$$La_2P_4O_{13}+La_3PO_7 \xrightarrow{1100\ ^0C} 5LaPO_4 \quad \text{---- (2)}$$

3.2 Scanning Electron Microstructure (SEM)

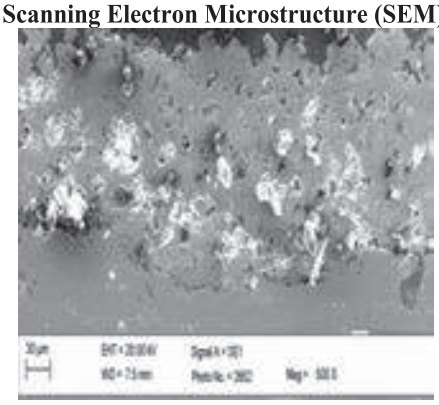

Fig 3. *Cross section SEM image of plasma spray deposited at 20 kW.*

Subsequent heat treatment of the samples result in the recombination of the poly-phosphate and oxy-phosphate to form $LaPO_4$. The SEM photo of $LaPO_4$ plasma spray deposited at 20 kW is shown in figure 3. Plasma spray-coated specimen showed microstructures typical of plasma sprayed coatings with molten, partially molten lamellae and porosity. Large number of cavities, horizontal cracks and voids were observed on coatings deposited at lower power levels. The surface of interface between the coating and substrate did not show any detachment or de-lamination showing good adhesion with the substrate.

4. Conclusions

Free flowing $LaPO_4$ powder was prepared from chemically synthesized $LaPO_4.1/2\ H_2O$ and used for plasma spray deposition. Partial conversion of $LaPO_4$ to La-polyphosphate and La-oxy phosphates was observed in the coatings. However, post-spray heat treatment of the coatings at 1100 ^{0}C resulted in recombination of the oxy and poly-phosphates to $LaPO_4$. SEM analysis of the coatings showed microstructures typical of plasma sprayed coatings with molten, partially molten lamellae and porosity.

Acknowledgement

The Authors AP and KR gratefully acknowledge funding from Board of Research in Nuclear Sciences (BRNS), Department of Atomic Energy, Mumbai through the research project No: 2010/34/6-BRNS/632, dated: 23.07.2010.

References

[1] Y. Hikichi, T. Nomura: J. Am. Ceram. Soc. 70 (1987) C252–C253.
[2] P.V. Ananthapadmanabhan, K.P. Sreekumar, T.K. Thiyagarajan: j.mat.chem.phys.113 (2009) 417–42..
[3] X.Q. Cao, R. Vassen, D. Stoever, J. Eur. Ceram. Soc. 24 (2004) 1-10.
[4]. P Fauchais, J. Phys D: Appl Phys 37 (2004) R86–R108
[5] H D Park and Eric R. Kreidler: J. Am. Ceram. Soc 67 (1983) 23-26.

Numerical Simulation of the Solution Precursor High Velocity Oxygen Fuel Spray Process

Mahrukh Mahrukh[1], Hosein Torabmostaedi[1], Sai Gu[1*]
[1] School of Energy, Environment and Agrifood, Cranfield University, Cranfield, Bedfordshire MK43 0AL, UK
E-mail: s.gu@cranfield.ac.uk

Abstract

The feasibility of a new processing method—Solution precursor high velocity oxygen fuel spray (SP-HVOFS)—is presented for production of dense ZrO_2-based nanostructured coatings, in which organometallic chemical precursor droplets are injected into a HVOF spray system. This study is aimed at understanding the influence of some key SP-HVOFS process variables on in situ generated particles to augment the current level of understanding. A two-dimensional computational fluid dynamics model is developed accounting for supersonic combustion and particle dynamics by an Eulerian continuum approach coupled with Lagrangian description of multicomponent spray droplet atomization, transport, break-up and evaporation. The time-temperature history of the droplets/particles in the HVOF flame is shown to control the size of resultant particulate deposits (i.e. primary particle and agglomerate size). Overall the results show that by controlling the oxy-fuel gas flow rate, single scale nanometre particles (~1-5 nm) can be fabricated without any agglomeration.

1 Introduction

SP-HVOFS process removed the barriers of using micro/nano-sized particles in conventioanl/suspension flame spraying and also eliminated the cumbersome process of micro/nano-sized powder manufacturing (see Fig. 1). The coating generated by this approach is denser, and no cracks are observed in the as-sprayed coating, also it is well bonded to the substrate [1, 2]. Compared to suspension and conventional powder flame spraying, solution precursor are mixed at molecular level, therefore more uniform phase composition and properties are expected in the sprayed coatings [3]. Droplets disintegration is dependent on the liquid precursor preparation; the main parameters required to maintain during precursor preparation process are precursor viscosity, surface tension, boiling point of liquid solvent, solute chemistry and its solubility.

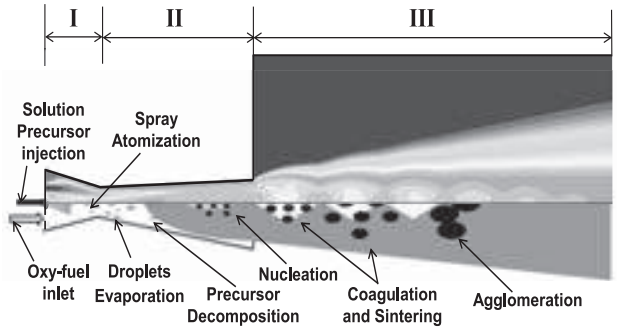

Fig. 1. *CFD temperature contours (Top) with schematic representation of nanoparticles synthesis inside SP-HVOFS process (Bottom); (I-Combustion chamber (CC), II-Barrel, III-Free jet region)*

The behaviour of nanoparticles generated during the SP-HVOFS process depends mainly on precursor evapration and the residence time of the particles in the high temperature zone of the flame. These problems must be restrained by optimizing the process parameters and it can be achieved by numerical modelling. To date, no work has been done to study the formation and growth of nanostructured materials during the SP-HVOFS process. The process includes complex steps of droplets fragmentation, precursor/solvent evaporation, chemical reactions, formation and growth of nanoparticles while transferring heat, mass and momentum with the surrounding hot gas [2]. In this work a CFD-based model for SP-HVOFS process is proposed to analyse the interaction between precursor droplets with combustion flame and to capture the aerosol dynamics during the course.

2 Modelling of SP-HVOFS process

The modelling of particle formation and growth in the SP-HVOFS process involves coupling of the gas dynamics with the droplet/particle dynamics (See Fig. 1). The gas dynamics in SP-HVOFS process is a compressible reacting flow, contained with turbulence and subsonic/sonic/supersonic transitions. The solution of gas dynamics together with the droplet dynamics provide detailed information for the gas flow field that is required to predict the particle dynamics. Similar to our previous studies [4,5], the liquid solution used in this study is the mixture of 0.5 M zirconium n-propoxide (ZnP) 70% wt in n-propanol diluted with ethanol for ZrO_2 nanoparticle production. The monodisperse aerosol model developed by Torabmostaedi et al. [4] is modified here for the synthesis of ZrO_2 nanoparticles in SP-HVOFS process. In this work, the equations of total particle number concentration, surface area concentration and volume concentration undergo convection and diffusion in addition to being generated and depleted.

2.1 Gas dynamics

The HVOF gun geometry used in this study is DJ2700 torch [6, 7]. To analyse the effect of oxy-fuel gas flow rate on combustion gas and particle dynamics inside SP-HVOFS process, four different levels of oxy-fuel gas flow rates (i.e. 0.005, 0.01, 0.02, 0.03 kg/s-case 1-4, respectively) were considered for constant oxy-fuel ratio and zirconia production rate of O/F=2.333 and 100 g/h, respectively.

Fig. 2 shows the calculated centerline flame velocities at different oxy-fuel gas flow rate across the domain (i.e. from gun inlet to the free jet section-III). As the oxy-fuel gas flow rate is increased, the velocity and enthalpy of the HVOF flame is increased. The former reduces the particle residence time in the HVOF flame while the latter favors the sintering.

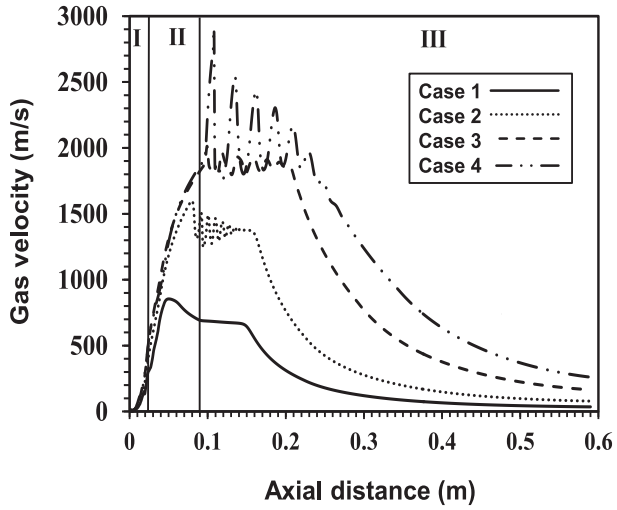

Fig. 2. *Variation of gas velocity along centreline axis for different gas flow rates, Case 1(solid line), Case 2 (dotted line), Case 3(dashed line), and Case 4(dash-dot-dot line)*

2.2 Droplet and particle dynamics

Fig. 3 shows the contours of precursor evaporation and ZrO_2 nanoparticle formation inside the HVOF gun (zone I and II). As the oxy-fuel gas flow rate increased from case 1 to case 3, the precursor droplets evaporated faster (i.e. due to higher temperatures) which favored the particle formation rate. This behavior is slightly different in case 4 because the high gas velocities in case 4 has reduced the residence time for some of the droplets and hindered the evaporation rate. It can be clearly seen that some of the droplets has escaped from zone I and is evaporated in Zone II. This will have a direct effect on the nanoparticle formation rate which can be seen in Fig. 3.

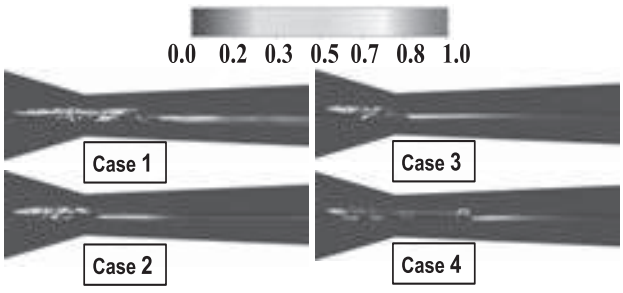

Fig. 3. *Normalized contour plot of ZnP droplets evaporation rate (top) and ZrO_2 nanoparticles formation rate (bottom) for Case 1-to- Case 4, respectively.*

As discussed, the formation and growth of nanoparticels are totally dependent on the precursor evaporation rate and particles residence time in the flame. This can be clearly seen in Fig. 4 which shows the contours of primary particle and agglomerate collision diameter for case 1 and case 4. The size of primary particle diameter is decreased by a factor of 2 when the oxyfuel gas flow rate is increased from case 1 to case 4. This is due to higher gas velocities which reduced the residence time of particles inside the high temperature zone of the flame. Also in case 4, the the precursor droplets evaporated later in Zone II, which means the the particles formed later in the gun and has not experienced the high temperatures of the flame in Zone I. Further, the values of d_p and d_c varied for Case 1, whereas in Case 4 the agglomerates has the similar size as that of primary particles; only 1% increase is detected in section-III. This can be explained by higher temperatures acheived in Case 4 which favoured the sintering. Overall by controlling the oxy-fuel gas flow rate, single scale nanosize particles (~1-5 nm) can be fabricated without any agglomeration.

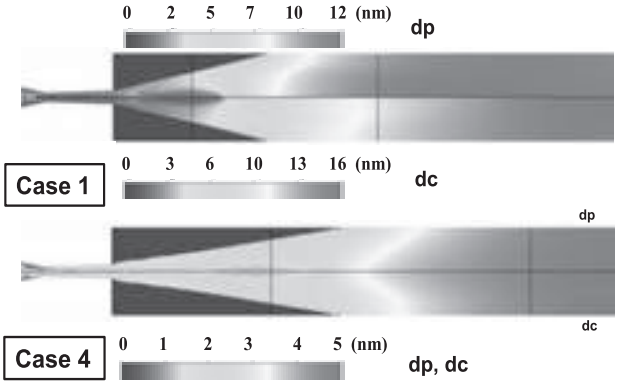

Fig. 4. *Contours of Primary (d_p-top), and Collision (d_c-bottom) particle diameter for (a) Case 1 and (b) Case 4*

The SP-HVOFS method, which offers some unique advantages over the conventional particle fed HVOF coating, can be potentially used to deposit a wide variety of ceramic coatings for diverse applications. In the future investigations, more parameters will be studied to fulfil all aspects of nanostructured coatings in SP-HVOFS process.

3 References

[1] P. Fauchais, and G. Montavon: *Journal of Thermal Spray Technology*. **19** (2009) 226–239.
[2] B. M. Cetegen and S. Basua: *Journal of Thermal Spray Technology*. **18** (2009) 769-793.
[3] J. Puranen, J. Laakso, M. Kylmalahti, P. Vuoristo: *Journal of Thermal Spray Technology*. **22** (2013) 622–630.
[4] H. Torabmostaedi, T. Zhang, P. Foot, S. Dembele, C. Fernandez: *Powder Technology*. **246** (2013) 419–433.
[5] H. Torabmostaedi, T. Zhang: *Journal of Thermal Spray Technology*. **2014**) DOI: 10.1007/s11666-014-0148-4.
[6] E. Gozali, S. Kamnis, and S. Gu: *Surface & Coatings Technology*. **228** (2013) 176–186.
[7] E. Gozali, M. Mahrukh, S. Gu, S. Kamnis: *Journal of Thermal Spray Technology*. **23** (2014) 940-949.

Investigation on the corrosion behaviour of plasma sprayed bi-layered and mono-layered ceramic coatings on Ti-6Al-4V alloy for biomedical application.

G. Vasanth[1], G. Siva Kumar[2], S.V. Joshi[2], Kantesh Balani[3], M. Geetha[1*]
[1] School of Advanced Sciences, VIT University, Vellore 632 014, India
[1*]Centre for BioMaterials Science & Technology, School of Mechanical & Building Sciences, VIT University, Vellore 632 014, India
[2] International Advanced Research Centre for Powder Metallurgy and New Materials ARCI, Hyderabad 500 005, India
[3] Biomaterials Processing & Characterization Lab, Department of Materials Science & Engineering, IIT Kanpur, Kanpur 208016, India

Abstract
In the present work, nanostructured bi-layered $Al_2O_3/13TiO_2$-$7Y_2O_3$ stabilized ZrO_2 (AT/YSZ) and mono-layered $Al_2O_3/13TiO_2$- 40wt%$7Y_2O_3$ stabilized ZrO_2 (AT40YSZ) were successfully deposited on biomedical grade Ti-6Al-4V alloy using atmospheric plasma spraying technique. The microstructure and elemental composition of the coatings were characterized using SEM and EDAX technique respectively. The corrosion behaviour of the coatings was performed using potentiostat under Stimulated Body Fluid environment (Hank's solution). In addition, micro-indentation hardness measurements and scratch test were also performed. Results showed that the coating AT/YSZ has high corrosion resistant than the AT40YSZ coating.

1 Introduction

Due to their high specific strength, low density, high strength to weight ratio and excellent biocompatibility, Titanium and its alloys are found to be a promising material in the field of aerospace, naval and biomedical applications. Ti-6Al-4V is the most commonly used titanium materials in the orthopaedic implant applications, such as hip and knee replacement. However their poor tribological properties have lead to release of Aluminium and vanadium which leads to osteolysis [1-6]. Many coating techniques such as ion implantation, magnetron sputtering, plasma spraying etc have been employed to achieve coating on titanium implants. Among these, plasma spraying is a commercial viable technique and widely employed in implant industries. Hydroxyapatite coating on Titanium implants using plasma spraying has been approved by Food and Drug Administration (FDA) USA [7]. Superior wear resistance, spallation resistance, higher toughness has been achieved by plasma sprayed nanostructured Al_2O_3-$13TiO_2$ over the conventional micron sized Al_2O_3-$13TiO_2$ [8]. Enhancement of hardness, scratch and wear resistance of bilayered coated nanostructured $Al_2O_3/13TiO_2$-ZrO_2 composite ($Al_2O3/13TiO_2$ as top layer and ZrO_2 as the base layer) was observed by Satish et al [9]. Recently, Perumal et al. reported that the wear resistance of micron sized Al_2O_3-40wt% $8Y_2O_3$ stabilized ZrO_2 composite coating has showed 8 times higher than Al_2O_3 coating and more than 60 times higher than Y_2O_3 stabilized ZrO_2 coating [10]. Hence, in this present work we made an attempt to compare the corrosion behaviour of plasma sprayed nanostructured bilayered coated $Al_2O_3/13TiO_2$-$7Y_2O_3$ stabilized ZrO_2 (AT/YSZ) and monolayered coated $Al_2O_3/13TiO_2$-40wt%$7Y_2O_3$ stabilized ZrO_2 (AT40YSZ) using atmospheric plasma spraying technique.

2. Experimental Methods

Commerically available nanostructured $Al_2O_3/13TiO_2$ and 7wt% Y_2O_3 stabilized ZrO_2 (7YSZ) was procured from Inframat Corporation, USA. The procured powders are in the form of spheroids and has trace amount of additives such as CeO_2 to reduce the sintering temperature and increasing the densification process. Composite powder for monolayer was obtained by blending 60wt% $Al_2O_3/13TiO_2$ and 40wt% 7YSZ in double cone blender for 10 hrs. Metco 9MB Gun plasma spray (80KW) was employed to develop the coatings. All the coatings were deposited on Ti-6Al-4V alloy.

2.1 Microstructures of plasma sprayed coating

Scanning electron microscope images and EDX spectrum of plasma sprayed bi-layered AT/YSZ and mono-layered AT40YSZ were shown in, Fig. 1. Presence of fully melted splats were observed in the case of bilayered AT/YSZ, while a mixture of partially melted, unmelted and completely melted were observed in the case of AT40YSZ.

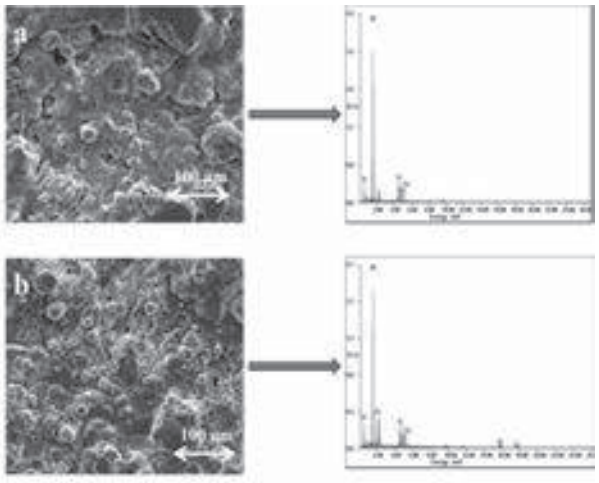

Fig. 1. *SEM images of a) bi-layered AT/YSZ and its corresponding EDX spectrum, b) mono-layered AT40Z and its corresponding EDX spectrum.*

2.2 Potentiodynamic polarization studies

Fig. 2. Shows the potentiodynamic polarization plots for bi-layered AT/YSZ and mono-layered AT40YSZ. The polarization behavior of the two different coatings were not showing much difference, however, amongst the two the

corrosion rate of AT/YSZ was lesser when compared to the bilayered AT/YSZ coatings.

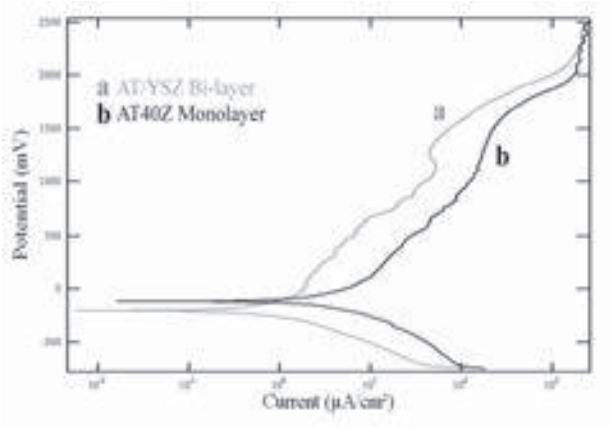

Fig. 2 *Potentiodynamic polarization plots*

2.3 Scratch Testing

Fig. 3 Shows the scratch track of bi-layered AT/YSZ and mono-layered AT40YSZ. The track width was found to be very less for the bilayed coating, with many tensile cracks observed at the side of the scratch tracks.

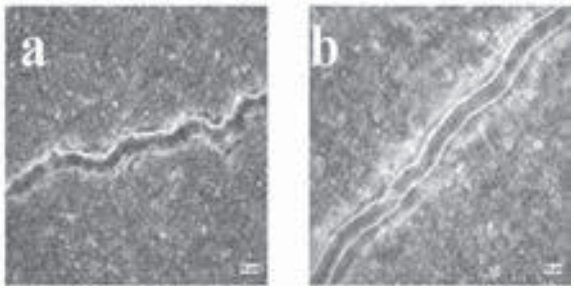

Fig. 3 *Scratch track of a) bi-layered AT/YSZ, b) mono-layeredAT40YSZ*

Conclusions:

- Plasma spraying parameters were optimized to obtain a thick adherent coating of bi-layered AT/YSZ and mono-layered AT40YSZ
- The formation of fully melted splats in bilayered coating resulted in superior corrosion resistance and high scratch resistance.

2.4 Plasma spray process parameters

Table. 1 *Plasma spray process parameters of the feedstock*

Parameters	AT	YSZ	AT40YSZ
Current (A)	500	600	600
Voltage (V)	65-70	65	65
Primary (Ar) gas flow rate (LPM)	42	48	48
Secondary (H_2) gas flow rate (LPM)	6.5	5.5	5.5
Powder feed rate (g/min)	40	40	40
Standoff distance (mm)	100	100	100

2.5 Corrosion test results

Table. 2 *Corrosion test results*

Sample	Ecorr (mV)	Icorr (mA/cm^2)
AT/YSZ	-204	0.021616
AT40YSZ	-117	0.026528

3. Reference

[1] M. Geetha , A.K. Singh , R. Asokamani , A.K. Gogia : Progress in Materials Science 54 (2009) 397–425.
[2] Mitsuo Niinomi, Masaaki Nakai, Junko Hieda: Acta Biomaterialia 8 (2012) 3888–3903.
[3] J.P. Simon and G. Fabry: Acta Orthopaedica Belgica vol 57-1-1991.
[4] A.H. De Azaa, J. Chevaliera,*, G. Fantozzia,*, M. Schehlb, R. Torrecillasb: Biomaterials 23 (2002) 937−945.
[5] C. Suryanarayana , Nasser Al-Aqeeli: Progress in Materials Science 58 (2013) 383–502.
[6] Giulio Maccauro, Pierfrancesco Rossi Iommetti, Luca Raffaelli and Paolo Francesco Manicone: InTech.
[7] Kantesh Balani, Yao Chen, Sandip . Harimkar, Narendra B. Dahotre, Arvind Agarwal*: Acta Biomaterialia 3 (2007) 944–951.
[8] George E. Kim: INTERNATIONAL THERMAL SPRAY & SURFACE ENGINEERING 2012 VOL 7 ISSUE 1.
[9] S. Sathish, M. Geetha*, S.T. Aruna, N. Balaji, K.S. Rajam, R. Asokamani: Wear 271 (2011) 934– 941.
[10] G. Perumal, M.Geetha, R.Asokamani, N.Alagumurthi: Wear 311(2014)101–113.

Development of erosion-corrosion resistant cold-spray nanostructured Ni-20Cr coating for coal fired boiler applications

Manoj Kumar[1], Harpreet Singh[2], Narinder Singh[3], S.V. Joshi[4], N. M. Chavan[5], S. Kumar[6]
[1,2]School of Mechanical, Materials & Energy Engineering, Indian Institute of Technology Ropar, Rupnagar, Punjab, India
[3]Department of Chemistry, Indian Institute of Technology Ropar, Rupnagar, Punjab, India
[4,5,6]International Advanced Research Centre for Powder Metallurgy & New Materials (ARCI), Hyderabad 500005, India.

Abstract
The erosion-corrosion (E-C) behavior of cold-spray nanostructured Ni-20Cr coating was studied under cyclic conditions in a coal fired boiler. This study was done for 15 cycles (1500 hours), where each cycle comprised 100 hours of exposure to the boiler followed by 1 hour of cooling under ambient air conditions. The E-C extent was evaluated in terms of thickness loss data of the samples. The eroded-corroded samples were characterized using XRD, SEM/EDS, and X-ray mappings analyses. The nanostructured coating offered excellent E-C protection to boiler tube material (SA 516 steel) in the coal fired boiler. This E-C resistance offered by the coating may be attributed to the presence of protective NiO and Cr_2O_3 phases in its oxide scale and its superior as-sprayed micro hardness.

1 Introduction

Rupturing of the boiler tubes of the coal fired water tube boilers due to high temperature erosion-corrosion phenomenon is most common and is responsible for 50% to 75% arrest time of the boilers [1-2]. So, to increase the working life of boiler tubes in the coal fired boilers is the area of great importance [3]. Thermal sprayed coatings have the potential to provide suitable protection to boiler steels from the aggressive fireside corrosion. These coatings possess many advantages such as versatility, on-site applications and has relatively lesser impact on the environment in comparison with other techniques [4].

Recently, cold spraying has emerged as a promising new coating process, which was developed by A. Papyrin and colleagues [5]. This process has gained quite popularity since this process uses high velocity rather than high temperature to deposit coatings, and thereby avoid/minimize many harmful high temperature reactions. In this process, the powder particles are accelerated to supersonic levels through a de Laval nozzle with the help of the carrier gas such as He, N_2 or air. These powder particles get plastically deformed by momentum transfer principle, when come in contact with substrate material and hence form interlinked splats. The temperature of spray particles prior to impact is much lower than the melting point, so no phase transformation occurs during the process [5]. That is why cold-spray is a promising spray process to develop nano-structured coatings. The fine-grained nanostructured coatings have received a considerable attention in the recent times [7] due to their excellent properties in comparison to their conventional coarse grained counterpart coatings, such as hardness, ductility, corrosion and wear resistance. Moreover, mechanical milling of powders is known as the recently developed method to synthesize nano-structured coating materials in bulk [8].

Nickel based alloys, having high chromium content, are widely used corrosion resistant coating materials, since they offer good resistance to oxidation/corrosion [4]. Furthermore the nanostructured Ni-Cr alloys offer excellent resistance to oxidation/corrosion, due to formation of high density Cr_2O_3 oxide layer by selective oxidation. Cr_2O_3 is a thermodynamically stable phase upto very high temperature due to its very high melting point and forms a dense, continuous and adherent layer that inhibits interaction of oxygen with the underlying coating/substrate [9].

The authors have already reported detailed synthesis and deposition process of the same coating on SA 516 steel by cold-spray process [10]. The present study is an incremental and novel attempt to study the behavior of this deposited coating (Ni-20Cr nanocrystalline coating) in an actual boiler environment. The outcome of the study shall be useful to explore the possibilities of use of the developed coatings for enhancing the working life of boiler tubes used in coal fired power plant boilers.

2 Experimental details

The boiler tube material SA 516-Grade 70 (SA 516), was procured from Cheema Boilers (Pvt.) Limited (a boiler manufacturing industry) Kurali (India). The details of synthesis and deposition of Ni-20Cr nanocrystalline powder on SA 516 steel has been already reported by the authors [30]. The uncoated and cold-sprayed specimens were exposed in low temperature superheater zone of the Boiler-I (740 ± 10°C) of Guru Gobind Singh Super Thermal Power Plant (GGSSTPP), Ropar (India). This particular location was chosen based on the reported failures of the boiler tubes. The detailed procedure of E-C study in coal fired boiler, along with coal analysis data, chemical analysis of ash and flue gases inside the boiler has already been reported elsewhere [10].The kinetics of E-C was established based on the thickness loss data. The surface and cross sectional microstructural examination of eroded-corroded samples was done by using XRD, SEM/EDS, and X-ray mapping as per the standard metallurgical procedure.

3 Results and discussion

The average microhardness of cold-sprayed coating was found to be 456 ± 20 Hv, which is 115% higher than its conventional counterpart (212 Hv) [11]. Weight change per unit area versus number of cycles' plots for the uncoated and coated steel specimens exposed to actual boiler environment are shown in Fig. 1. The uncoated and coated SA 516 steel have shown a continuous weight loss upto 15th cycle, with overall weight change of 38.27 mg/cm^2 and 20 mg/cm^2 respectively. The thickness loss of bare SA 516 steel was found to be 0.38 mm and that of coated sample 0.17 mm after 1500 hours of boiler exposure. The corrosion rate (mil per year) calculated based on this thickness loss data was 87 mpy and 39 mpy respectively for uncoated and

coated sample, which indicates that the investigated coating is useful to reduce the E-C rates of the steel.

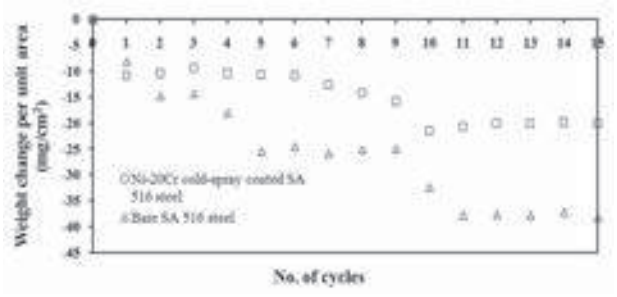

Fig. 1 Weight change per unit area vs. number of cycles plots for uncoated and cold-spray Ni-20Cr coated SA 516 boiler steels subjected to actual boiler environment at 750°C for 15 cycles.

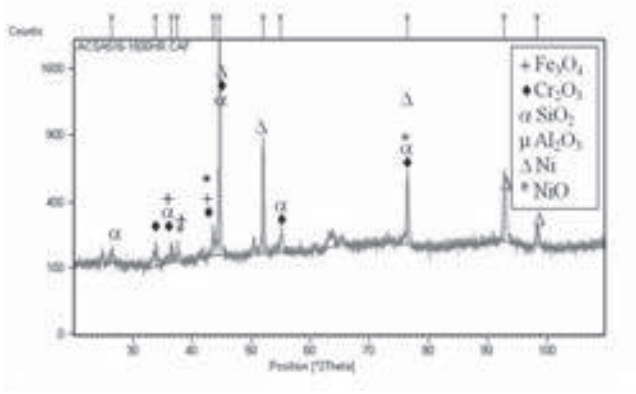

Fig. 2 X-ray diffraction profiles of cold-spray Ni-20Cr coated SA 516 steel, subjected to actual boiler environment at 750°C for 1500 h

X-ray diffraction analysis of the coated samples subjected to cyclic E-C study in actual boiler environment at 740 ± 10 °C for 15 cycles is shown in Fig. 2. Cr_2O_3, Al_2O_3, SiO_2, NiO and Ni phases have been observed for the scale of Ni-20Cr coating as depicted in Fig. 2. SEI image of Ni-20Cr coated SA 516 steel after exposure to actual boiler environment is shown in Fig. 3 along with X-ray elemental mappings. The scale substrate interface is perfectly intact, and the scale has dense morphology, which mainly contains Ni and Cr. Relatively denser layer of Oxygen is present on the top most portion of the exposed coating, however the diffusion of Fe is restricted mainly to the scale-substrate interface area. These observations indicate that the coating is able to act as a diffusion barrier to the elements of base steel.

Conclusions

The investigated coating on SA 516 steel was found to have 115% more hardness in comparison with their conventional counterparts. The coating was successful to reduce the thickness loss of SA 516 steel by 55% in actual boiler environment, thus offered better erosion-corrosion resistance under actual boiler conditions, which might be attributed to the presence of protective Cr_2O_3 phases in their oxide scales. The governing mechanism of E-C for SA 516 steel may be dictated by erosion. The higher hardness of the coatings may also have helped to enhance the erosion-corrosion resistance of the coating.

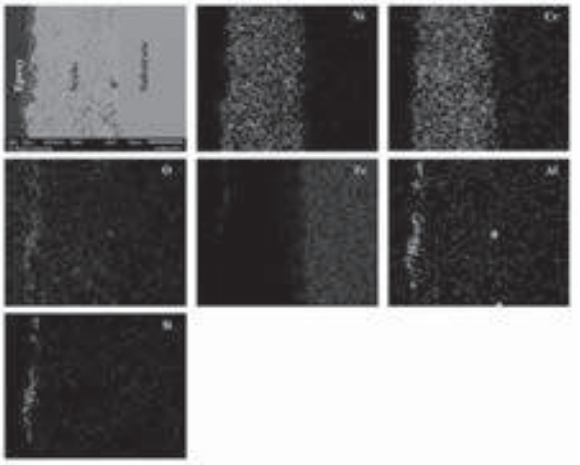

Fig. 3 Back Scattered electron image (BSEI) and X-ray mapping of the cross-section of cold-spray Ni-20Cr coated SA 516 boiler steel subjected to actual boiler environment at 740 ± 10°C for 15 cycles

References

[1] R. A. Rapp and Y.S. Zhang: JOM **46(12)** (1994) 47-55.

[2] V. H. Hidalgo, F. J. B. Varela and E. F. Rico: Trib. Int. **30(9)** (1997) 641-649.

[3] A. S. Khanna: *Introduction to High Temperature Oxidation and Corrosion,* (ASM International, Materials Park, Ohio, 2002).

[4] J. R. Davis: *Handbook of Thermal Spray Technology*, (TSS/ASM International, Materials Park, OH, 2004).

[5] A. Papyrin, V. Kosarev, S. Klinkov, A. Alkimov and V. Fomin: *Cold Spray Technology,* (Elsevier 2007).

[6] J. Karthikeyan: *Cold Spray Technology: International Status and USA Efforts*, (ASB Industries, 2004).

[7] Guozhong Cao: *Nanostructures and Nanomaterials – Synthesis. Properties and Applications*, (Imperial College Press, London, 2004).

[8] C. C. Koch: *Nanostructured Materials Processing, Properties, and Applications,* (William Andrew Publishing, Norwich, NY, USA, 2007).

[9] F.H. Stott: *Principles of Growth and Adhesion of Oxide Scales*, in: E. Lang (Ed.), *The Role of Active Elements in the Oxidation Behavior of High Temperature Metals and Alloys*, E. Lang, Ed., (Elsevier Applied Science, London, 1998).

[10] M. Kumar, H. Singh and N. Singh: Surf. Eng. **29(6)** (2013) 419-426.

[11] N. Bala, H. Singh, and S. Prakash: J. Therm. Spray Technol. **19(1)** (2010) 110-118.

Remanufacturing of engine connecting rods using Twin Wire Arc spray

Bhaskar Podeti [1], Oonnatie Deolankar [1], Mandira Bhattarcharyya [1], Gous Mohammed [2], Todd Wieland [2], Sachchidanand Velankar [3], S C Modi [4], Ankur Modi [4], Rohit Upadhyaya [4]

[1] Cummins Technologies India Limites, New & ReCon Parts India, Product Engineering Group, India Office Campus (IOC), Balewadi, Pune - 411045, India
[2] Cummins Inc., USA, New & ReCon Parts Manufacturing.
[3] Cummins Research & Technology India Ltd., India Office Campus (IOC), Balewadi, Pune - 411045, India
[4] Metallizing Equipment Company Pvt. Ltd., Jodhpur, India

Abstract
This paper provides details of application of thermal spray technology for remanufacturing of engine connecting rod having ovality or damage at big end ID. Twin Wire Arc thermal spray was used to regain connecting rod big end ID, ***back to print specifications*** and circularity. Fatigue testing and computational analysis was carried out to validate the process.

1 Introduction

It is observed that connecting rod that has been used on an engine for several cycles, develops an ovality in the big end region. The traditional remanufacturing standard advocates use of lapping of mating face to regain the circularity. However, this method is useful for only straight connecting rods and does not work for angle split/***serrated/fracture split*** connecting rods, where the parting plane of the cap and the rod is angled with respect to the vertical axis.
In this project, trials were taken to regain connecting rod big end ID and circularity using Twin Wire Arc (TWA) thermal spray.

Fig. 1. *Connecting Rod (big end highlighted)*

2 Process

2.1 Material Properties

The base material of connecting rod is forged medium carbon steel. The material chosen to spray over the big end was phosphor bronze alloy. Initially trials were taken on different sets of materials and based on the characterization report, phosphor bronze alloy was chosen owing to the high bonding strength exhibited.

2.2 Method

The Twin Wire Arc thermal spray technique was selected for this process.
The trials and proto-development was done at Metallizing Equipment Company (MEC), Jodhpur.
The connecting rod big end ID was initially ***honned*** to make it oversize by 250 microns post which the material spraying was carried out. Post machining (honing) was done to obtain the print ***specifications and*** surface finish.

2.3 Characterization

It was observed that the deposit was uniform throughout the base material. The interface bond showed no porosity or voids that may be of concern. The bond is good and dilution is homogenous. Interlocking bond is seen at certain placed assuring that bond strength will be good. No porosity is observed at the deposited material.

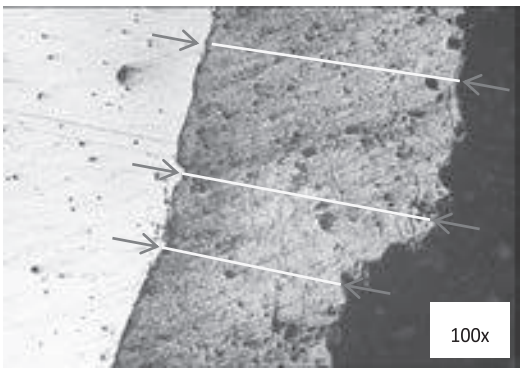

Fig. 1. *Microstructural analysis (100X)*

2.4 Fatigue Testing

The prototypes were sent for fatigue testing at Cummins Technical Center, Columbus. The staircase fatigue testing method was used to test each rod at a frequency of 20Hz to reach 10 million cycles. Test results for six connecting rods indicate that none of the rods failed at the thermal coating or big end region. The test will be carried out further for ***six*** more connecting rods as per recommendation of test.

2.5 Computational Analysis

To validate the results of the trials, a computational structional analysis was carried out for this process. The connecting rods were analysed as per the Cummins Engineering Standard Work guidelines. The stress and strain values of the thermally coated component were found to be close to the baseline component.

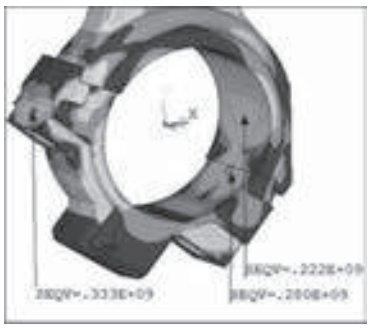

Fig. 3. *Von Mises Stress Contour for thermal coated big end*

The maximum principal stress at 150% intermittent over speed was found to be in the acceptable zone.

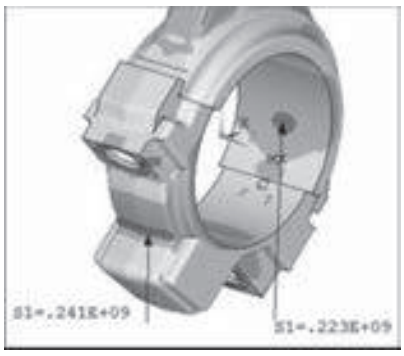

Fig. 4. *Principal Stress S1 at thermal coated big end at overspeed condition*

The directional strain at TDC at 125% overspeed was analyzed and found to be within accpetable limits.

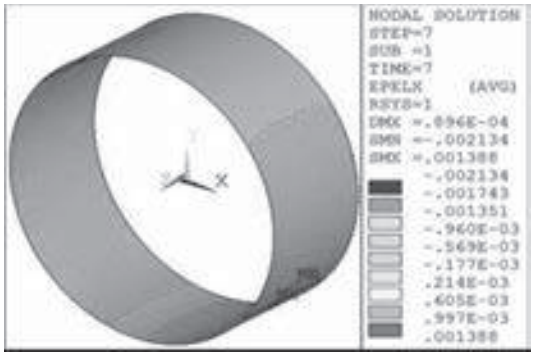

Fig.5. *Direction strain at TDC for thermal coating material inner surface*

The results of the analysis concludes that the thermal coated connecting rod is as good as the baseline component from structural point of view.

3 References

[1] ESW95036 Cummins Engineering Standard Work (Confidential)
[2] ESW95033 Cummins Engineering Standard Work (Confidential)
[3] FEP00007029 Cummins Confidential
[4] FEP00029076 Cummins Confidential

Sponsors and Exhibitors

Our Sponsors

PLATINUM SPONSOR	Metallizing Equipment Company Private Limited, Jodhpur, India
OTHER SPONSORS	Sai Surface Coating Technologies, Hyderabad, India GE Power and Water Praxair Surface Technologies, Mumbai, India Industrial Processors & Metallizers Private Limited, Delhi, India
SUPPORTED BY	Society for Advancement of Heat Treatment and Surface Engineering (SAHTSE) Science and Engineering Research Board (SERB) Govt. of India Board of Research in Nuclear Sciences (BRNS) Govt. of India Defence Research and Development Organization (DRDO) Govt. of India Council of Scientific and Industrial Research (CSIR) Govt. of India

List of Exhibitors

Stall No.	Exhibitor	Stall No.	Exhibitor
1	Metallizing Equipment Company Private Limited, Jodhpur	14	ATS Techno Pvt.Limited , Ahmedabad
2	Metallizing Equipment Company Private Limited, Jodhpur	15	Chennai Metco Pvt.Limited, Chennai
3	Metallizing Equipment Company Private Limited, Jodhpur	16	Innomet Powders, Hyderabad
4	Metallizing Equipment Company Private Limited, Jodhpur	17	International Aerospace Manufacturing Private Limited, Bangalore
5	Oerlikon Metco, Singapore	18	Globe Metal Inc., Canada
6	Oerlikon Metco, Singapore	19	Andritz Hydro Private Limited, Palwal, Haryana
7	Censico International Private Limited, Agra	20	Andritz Hydro Private Limited, Palwal, Haryana
8	Ducom Instruments Private Limited, Bangalore	21	Polymet Corporation, USA
9	Saint Gobain Coating Solutions, Bangalore	22	Camfil Air Filtration India Pvt Limited, Gurgaon
10	Anton Paar India Private Limited, Delhi	23	C&M Technologies GmbH, Germany
11	Anton Paar India Private Limited, Delhi	24	Fujimi Incorporated, Japan
12	Sai Surface Coating Technologies, Hyderabad	25	Spraymet Surface Technologies Private Limited, Bangalore
13	Carborundum Universal Limited, Kochi	26	Nanjing AnTie Anticorrosion Technology Company Limited, China

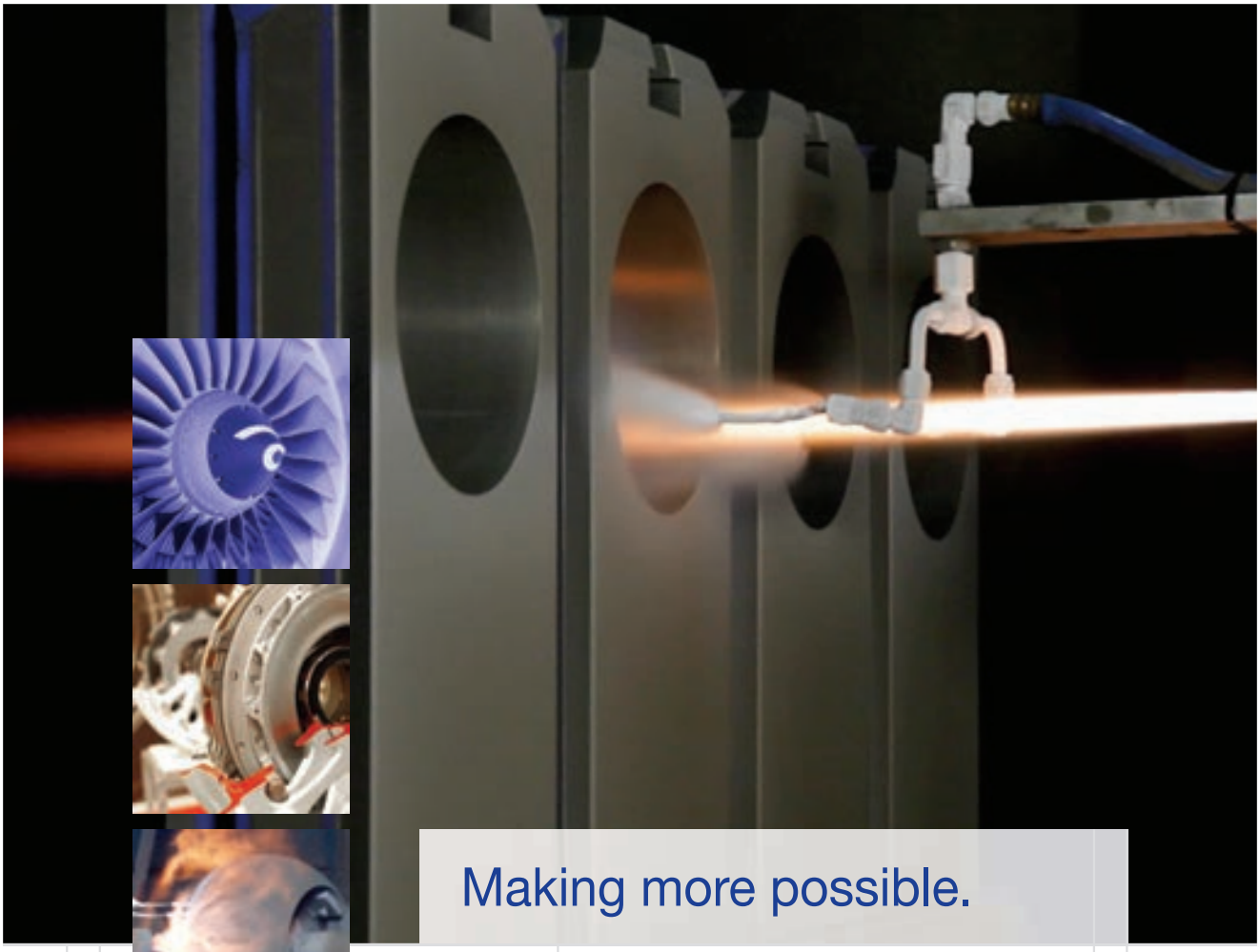

Making more possible.

At Praxair Surface Technologies, we protect what drives your industry.

High-performance coatings available from Praxair's Coimbatore, India location reduce harmful effects of abrasion, corrosion, oxidation, wear, and extreme heat on oilfield gate and ball valves and aircraft engines and airframe parts.

These coatings extend product life, decrease energy consumption, and reduce operating costs by using innovative coating processes including high-velocity oxy-fuel (HVOF) and plasma spray.

Praxair protects your critical components from our more than 35 coating service centers in 12 countries including China, India, Japan, Korea, and Singapore.

Call +0091.422.268.7376 for information on how we can help your business.

www.praxairsurfacetechnologies.com

PRAXAIR
SURFACE TECHNOLOGIES

DUCOM

Material Characterization Systems

Erosion tester

Bio-tribometer

Metal forming tribometer

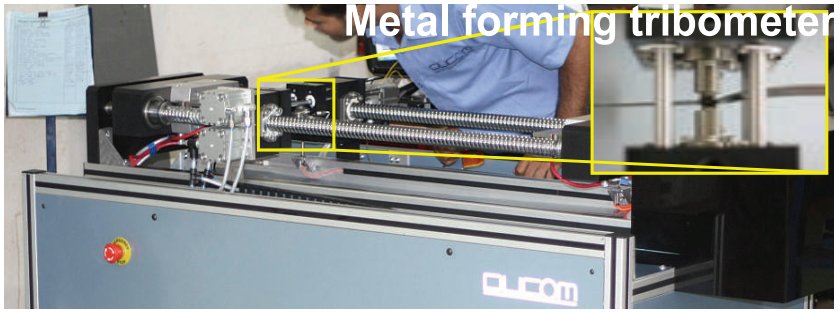

Bearing tester

High temperature tribometer

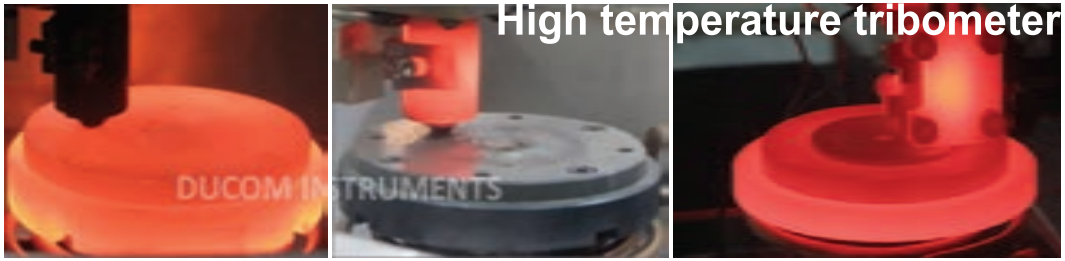

Lubricant tester

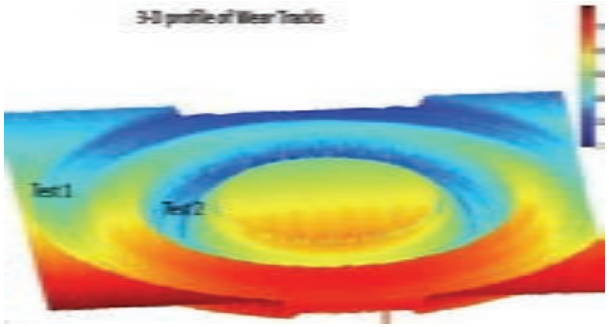

Extensive post-test analyses

Advanced reporting software

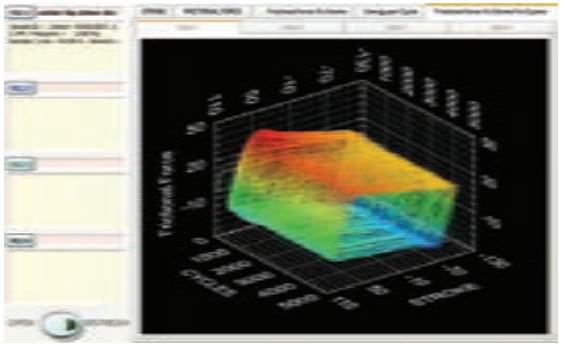

www.ducom.com | info@ducom.com | America: +1 (847) 737-1590 | Asia, Africa: +91 (80) 4080-5555 | Europe, A-Pac: +31 (50) 363-3295

Anton Paar Nano Tribometers (NTR2)

Designed to investigate surface interactions at low contact pressures

::: Features

- Unique dual beam cantilever with normal applied load up to1000 mN (resolution 5 nN)
- High resolution capacitive sensors combined with piezo actuator
- Rotative and/or linear reciprocating motion
- 2 independent high resolution capacitive sensors for normal load and friction force
- Low noise floor for microtribological measurements

::: Options

- Adhesion measurements
- Atomic force microscope
- Temperature and humidity sensors
- Continuous wear depth measurement
- Mirau interferometer

Anton Paar

Anton Paar® India Pvt. Ltd.
582, Phase V,
Udyog Vihar Industrial Area,
Gurgaon - 122 016 (Haryana), India
Tel.: + 91 - 124 - 4361057
Fax: + 91 - 124 - 4361058
info.in@anton-paar.com
www.anton-paar.com

ATS
Engineering long life Components

Services provided by ATS,

Component Manufacturing	Thermal Spraying	Surface Repairs	Plant Facility
➢ Steel Mill Rolls ➢ Rolls for Offset Machine ➢ Piston Rod ➢ Steam Turbine Valve Spindle ➢ Steam Turbine Guide Bush ➢ Steam Turbine Valve Cone ➢ Steam Turbine Threaded Ring ➢ Hydro Turbine Labyrinth Ring ➢ Hydro Turbine Needle Cone ➢ Hydro Turbine Seat Ring ➢ Ceramic coated Sleeve ➢ Carbide Coated Sleeve	➢ In-Situ Coating ➢ On-site TSA Coating ➢ Job shop Coating	➢ Re-babbiting ➢ Reclamation ➢ Refurbishing ➢ Spot repairing ➢ Dynamic balancing ➢ In-situ grinding ➢ Machining	➢ State of Art Acoustic Spray Booth (13x4.5x4.3) mtr ➢ Spray Booth for Heavy Duty compoments. (9x8x4.5) mtr ➢ 6 +1 axis Robot Automatic Grit Blasting Unit (6x3.5x4) mtr ➢ Heating Furnace (Ø1.2 X 3.5) mtr ➢ Cylindrical Grinding Machine (Ø1.05 X 6) mtr ➢ Cylindrical Grinding Machine (Ø 400 X 2000) mm

OUR VALUED CUSTOMERS

BHEL	SIEMENS
TATA STEEL	ALSTOM
KIRLOSKAR	VOITH HYDRO
JK PAPER	GAIL
JSW STEEL	BHEL -HARIDWAR,VARANASI
GNFC	BHEL -BHOPAL,TRICHY
TNPL	IOCL

ATS TECHNO PVT. LTD.
Plot No.419-420, Phase-II, Road No. 10,
Kathwada G.I.D.C., Ahmedabad Guj.-382430
Telefax : 079- 2290 0931/32
e-mail : mkt@atstechno.in Visit us : www.atstechno.in

ANDRITZ Hydro

ANDRITZ HYDRO

Your Indian partner for renewable and clean energy

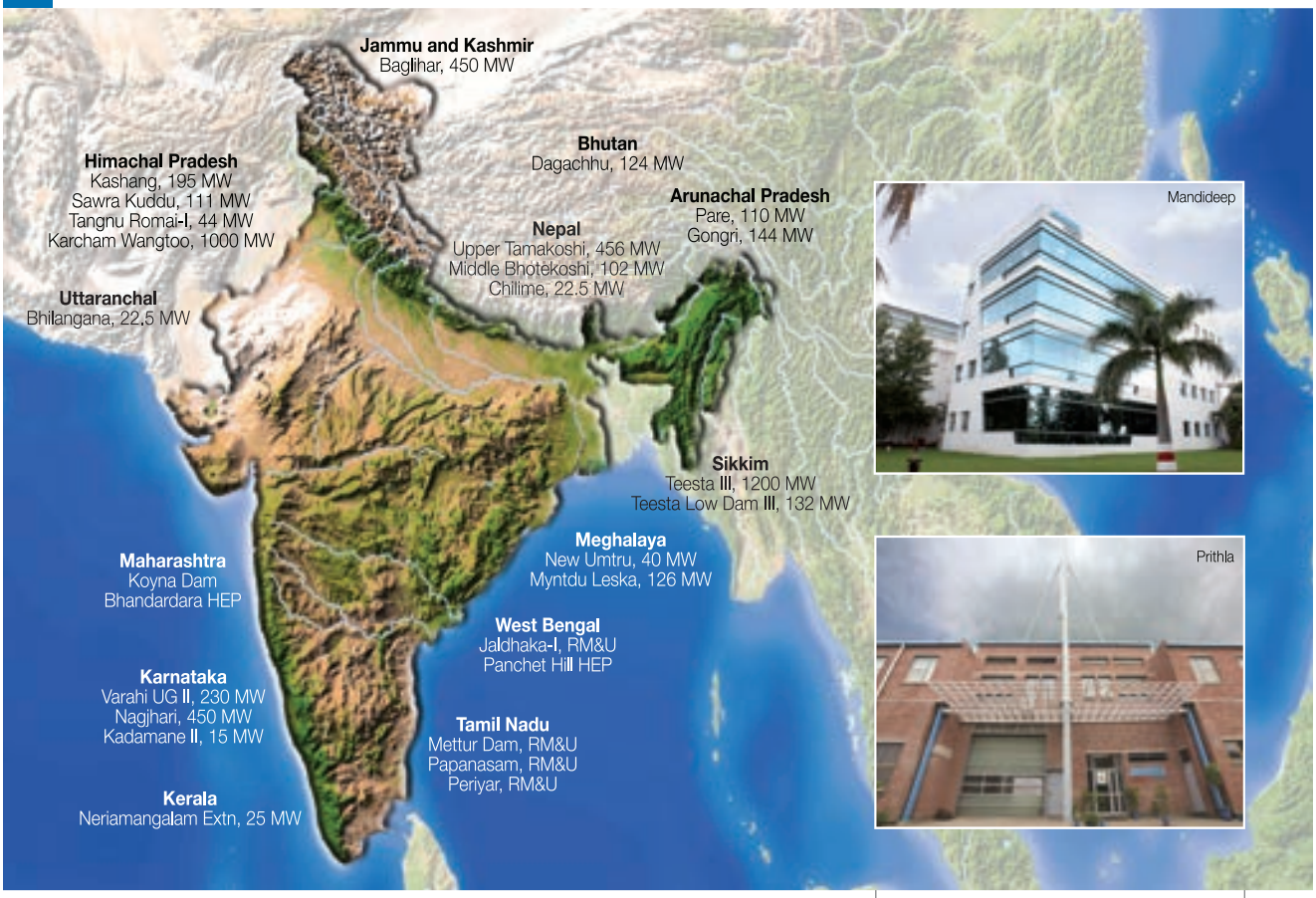

ANDRITZ HYDRO is a global supplier of E&M systems and services for hydropower plants and a leader in the hydraulic power generation market. With over 170 years of experience and more than 30,000 turbines (400,000 MW) installed globally, we cater to the complete range up to more than 800 MW.

Catering to over 14,000 MW, ANDRITZ HYDRO is committed to the hydropower sector of India. With our modern manufacturing facilities in Mandideep and Prithla, we offer turnkey solutions for greenfield and rehabilitation projects.

We focus on the best solution – from water to wire.

ANDRITZ HYDRO Pvt. Ltd.
D-17, MPAKVN Industrial Area
Mandideep 462 046
District Raisen, Bhopal, India
Phone: +91 7480 400 400
Fax: +91 7480 403 393
E-mail: contact-hydro.in@andritz.com

www.andritz.com

AT-QDI ANTI BREAK ARC SPRAYING MACHINE

Technological innovation:

- Since 2003, through 10 years research with great concentration,AT-QDI anti break arc metal electric arc spraying machine (push wire type) can thoroughly solve the problems such as breaking arc often , buring electric conduction mouth during the process of spraying zinc, aluminum and its alloys, so the equipments can improve spraying efficiency and spraying quality Greatly.

The patent technology :

- Have our own patents in the key technologies. Patent numbers: ZL201310431080.1、ZL201320583298.4

Technical indicators:

- The practical spraying efficiency(Spraying wire⌀3mm, kg/h):
  Al 10 ~ 15 ; Zn 25 ~ 30;
  Zn85Al15 25 ~ 30; Stainless steel 30
- The actual break arc rate: ≤1time/2coil (Shaft mounted wire)
- The life of wearing parts (take zinc aluminum alloy spraying as an example, h) The life of electric conduction mouth ≥20,Can spray over 600kg wire;The life of electric conduction assembly ≥40,Can spray over 1200kg wire.

A full range of quality services:

- The company provides one free test machine, The test time: 8 hours of continuous spraying;
- The company provides 2 operators training for customers by free;
- The company provides 2 pieces of job protection clothes by free;
- 1 year free replacement and repairing services (wearing parts are not included)

seeking cooperation ,seeking agents all over the world.
welcome you to come to consult、negotiate and visit.

Contact way: Nanjing AnTie Anticorrosion Technology Co.,Ltd Ms Cai
Address: Technological Entrepreneurship Park, No. 625 Geguan Road Chemical Industry Park, Nanjing,China.
Telephone number: (0086 025) 5839 8490 Fax: (0086 025) 5701 1235
Website: www.njat.cn Post number: 210048

ए आर सी आई
ARCI

International Advanced Research Centre for Powder Metallurgy and New Materials (ARCI), Hyderabad

Translating Research into Technology

- Development of unique, novel and techno-commercially viable technologies in the area of advanced materials
- Demonstration of related technologies at prototype/ pilot plant scale
- Transfer of technologies to companies in various industry sectors

ARCI at a Glance

- Industry Centric, major thrust areas include Surface Engineering, Nano Materials, Sol-Gel Coating, Carbon Materials, Solar Energy Materials, Fuel Cells, Automotive Materials, Laser Materials Processing and Ceramics.
- Transferred 14 technologies to more than 26 companies with major contribution from Centre for Engineered Coatings. Many new technologies are available currently for adaptation/transfer.
- Collaborations with a large number of Indian and foreign Companies/Universities/R&D institutions, Undertakes sponsored/contract projects from various government/industrial organizations to develop specific products and/or associated technologies.

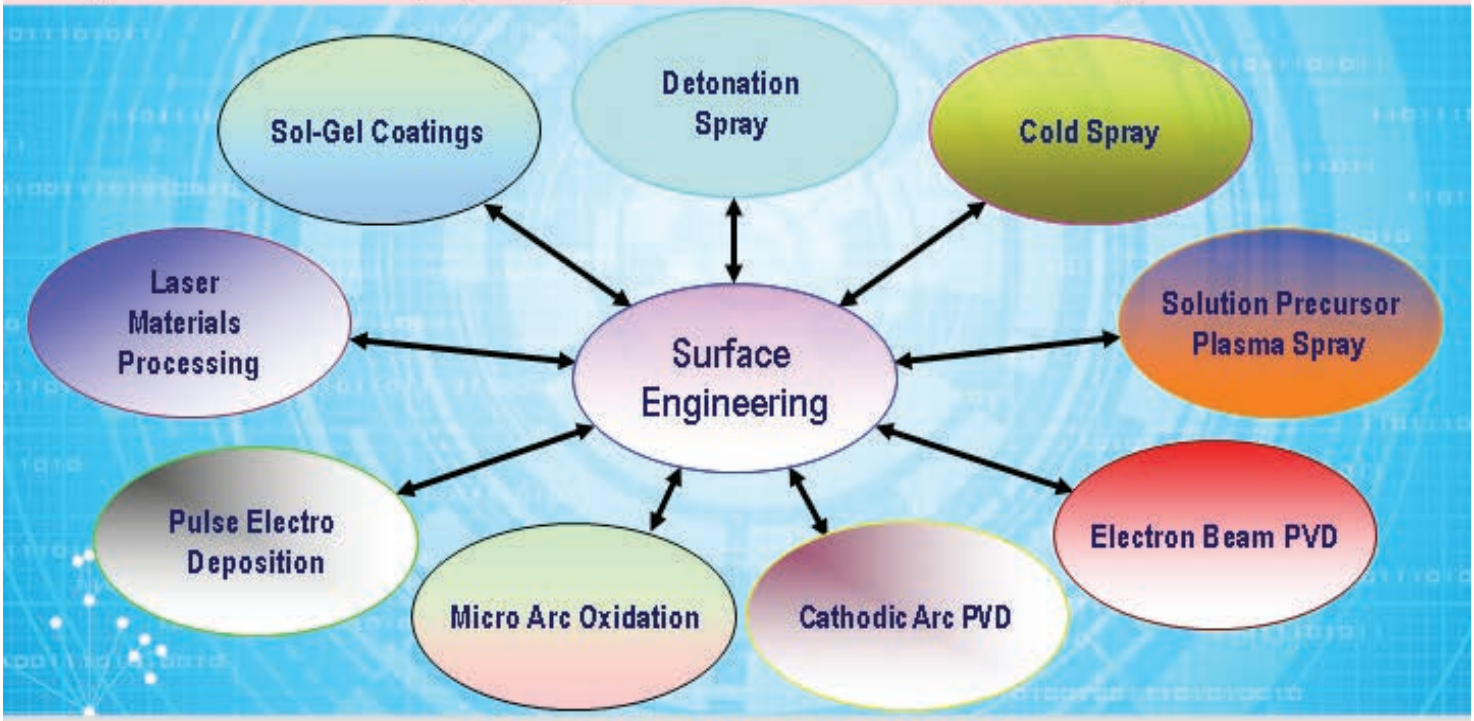

FOR FURTHER DETAILS, PLEASE CONTACT:
International Advanced Research Centre for Powder Metallurgy and New Materials (ARCI)
Balapur PO, Hyderabad - 500 005, India
Phone: (0091) (040) 24441077, 24452470, 24457106, 24452374, **Fax:** (0091) (40) 2444 2699, 2444 3168
E-mail: svjoshi@arci.res.in, raods@arci.res.in, info@arci.res.in; **Website:** www.arci.res.in

ISO 9001:2008

NEW ARRIVAL

MJP - 6000™

ANGULAR HVOLF GUN

MEC INTRODUCE MJP-6000™ GUN FOR APPLYING HARD COATING IN INTERNAL DIAMETER & DIFFICULT TO REACH AT AREA. THIS GUN CAN BE ATTACHED WITH ANY STANDARD HVOF (LIQUID FUEL) SYSTEM SUCH AS XPOJET®-5000, JP-5000 OR EQUIVALENT.

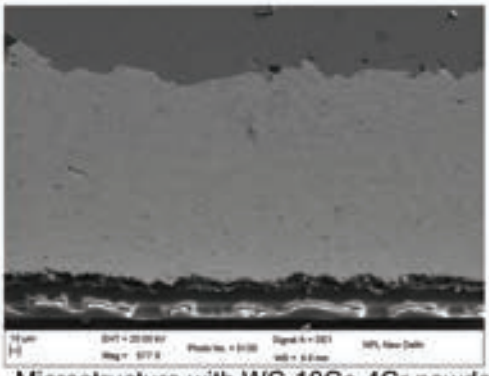

Microstructure with WC-10Co-4Cr powder, (Particle size +5 -30 microns)

A TYPICAL HVOF (LIQUID FUEL) SYSTEM

SPRAY GUN'S DIMENSIONS L – 40cm , H – 9cm
GROSS WEIGHT 7.40 KG
SHIPPING VOLUME 47cm(L) x 22cm(H) x 43cm(W)

SPECIFICATIONS

INTERNAL COATING DIAMETER	180 mm minimum
SPRAYING ANGLES	45° & 70°
NET WEIGHT (WITHOUT HOSES & MOUNTING BRACKETS)	4.70 kg. approx.
SPRAY RATE	60 gm/min maximum
COATING THICKNESS	2.0 mm maximum
HVOF CARBIDE POWDERS	Particle size +5 –30 MICRONS

COATING PROPERTIES *

HARDNESS	Upto 1200 VHN
POROSITY	<0.9%
BOND STRENGTH	>10,000 PSI
DEPOSITION EFFICIENCY	Upto 41%
COATING ROUGHNESS	2–4 Ra

** For WC-10Co-4Cr (+5 -30) with 70◦ angular head*

API Spec Q1 Registered

MEMBER OF ASM

ICRA Ltd. (Moody's service) The High Credit Quality rating assigned is an SME

CE

METALLIZING EQUIPMENT CO. PVT. LTD.

E-101, M.I.A., Phase-II, Basni, Jodhpur-342005 (India)

Ph. : +91 291 2747601 Fax : 2746359

E-Mail : marketing@mecpl.com / sales@mecpl.com / trade@mecpl.com

Web : www.mecpl.com